Quantum Phase Transitions in Multi-Impurity and Lattice Kondo Systems

Dissertation
zur
Erlangung des Doktorgrades (Dr. rer. nat.)
der
Mathematisch-Naturwissenschaftlichen Fakultät
der
Rheinischen Friedrich-Wilhelms-Universität Bonn

von
Ammar Nejati
aus
Schiraz, Iran

Bonn, 10.11.2016

Dieser Forschungsbericht wurde als Dissertation von der Mathematisch-Naturwissenschaftlichen Fakultät der Universität Bonn angenommen und ist auf dem Hochschulschriftenserver der ULB Bonn http://hss.ulb.uni-bonn.de/diss_online elektronisch publiziert.

1. Gutachter:	Prof. Dr. Johann Kroha
2. Gutachter:	Prof. Dr. Ralf Bulla
Tag der Promotion:	16.01.2017
Erscheinungsjahr:	2017

Summary of the Dissertation

The main purpose of this dissertation is to provide a detailed development of a self-consistent perturbative renormalization group (RG) method to investigate the quantum phases and quantum phase transitions of multi-impurity Kondo systems (e.g., two impurities or a lattice of impurities). The essence of the RG method is an extension of the standard "poor man's scaling" by including the dynamical effects of the magnetic fluctuations in the Kondo vertex. Such magnetic fluctuations arise due to the indirect carrier-mediated exchange interaction (RKKY interaction) between the impurities and compete with the Kondo effect to determine the ground-state. The aim is to take the most 'economic' route and avoid intensive numerical computations as far as possible. In general, it is shown in detail how a relatively small amount of such magnetic fluctuations can suppress and ultimately, destroy the Kondo-screened phase in a universal manner, and without incurring a magnetic instability in the system.
The renormalization group method and its extensions are further applied to several distinct experimental realization of the multi-impurity Kondo effect; namely, Kondo adatoms studied via scanning tunneling spectroscopy, a highly-tunable double-quantum-dot system based on semiconducting heterostructures, and finally, the heavy fermionic compounds as Kondo lattices. We will demonstrate the qualitative and quantitative agreement of the RG theory with the experimental findings, which supports the validity of the method.
In the case of Kondo lattices, we further include the possibility of a magnetic ordering in the lattice to see whether a magnetic ordering can happen simultaneously with or before the Kondo breakdown (or even prevent it altogether).
In the last chapter, we consider the fate of the local moments in the absence of full Kondo screening while Kondo fluctuations are still present. This partially-screened phase needs itself an extensive study since it can support other phases besides a simple magnetic ordering (e.g., quantum spin glass or exotic non-Fermi-liquid phases).
Finally, the dissertation is concluded with a summary of findings and future research prospects.

Contents

CHAPTER 1

Foreword

One may say that theorists "diverged" on their own, leaving the experimental realities way behind. The justification for such a theoretical game has only come recently, with the fancy theories yielding in the end very simple physical ideas.

P. Nozières (1975) [1]

The Kondo effect is a long but marvelous story of puzzlement, surprise, intuition, breakdown, discovery and advancement in condensed matter physics. The essence of the Kondo effect is the strong correlations due to the interaction between a localized, degenerate degree-of-freedom (like the magnetic moment of an impurity) and a delocalized continuum (like the conduction electrons).[1]

It is a genuine many-body quantum phenomenon which can be observed even at room temperature, although typical Kondo temperatures are of the order 10–100 K [7]. Usually, at sufficiently low temperatures, it causes a significant change in the transport and thermodynamics properties of a system [8].

The Kondo effect was originally considered as an 'anomalous behavior' observed in a non-magnetic metallic host containing small traces of magnetic impurities.[2] The story of the Kondo effect begins in 1930, when Meissner and Voigt [10] observed a rise in the resistivity of "pure gold"[3] below 10 K, in contrast to what is expected for simple normal metals for which the resistivity is dominated by electron-phonon scattering and tends toward a residual constant value at low temperatures, which is due to defects or static impurities in the sample [11].[4]

Later, in 1930s, de Haas, de Boer and van der Berg [12] observed a resistance minimum in the resistivity of copper, gold, silver, and many other metals at low temperatures.

[1] Two-fold degeneracies in degrees-of-freedom other than spin can also produce a Kondo effect (e.g., Refs. [2–5]). These are called 'exotic' Kondo systems [6].

[2] The host can be a simple metal like copper or aluminium, or a transition metal like palladium; atomic impurities should have unfilled localized d- or f- shells which leads to formation of a magnetic moment at relatively high temperatures and a related Curie-Weiss susceptibility [7, 9]

[3] In fact, the gold samples had small traces of iron impurities from the preparation process, and these played the role of magnetic (Kondo) impurities. However, at that time, with the experimental precision available, it was difficult to separate the effect of such a low concentration of impurities from spurious anomalies.

[4] Deviations from the expected behavior of resistivity can happen also in a superconducting material in which, below a certain transition temperature, the electrical resistivity suddenly drops to zero.

Further experimental characteristics of the single-impurity Kondo effect are relatively sharp peaks in the linear coefficient of specific heat, as well as a flattening in the magnetic susceptibility and particular signatures in the magneto-resistance, thermopower, and the excess entropy extracted from the specific heat [8] (for an early experimental review, consult Ref. [13]).
The origin of this "anomalous behavior" (the low-temperature minimum in resistivity) was not understood for three decades, until at last, the effect was related to the presence of magnetic impurities in the samples (Ref. [14] and references therein). Jun Kondo [15, 16] was the first to provide a theoretical explanation of such 'anomalies' as caused by the presence of magnetic impurities and their interaction with the conduction electrons. He described the system with an antiferromagnetic exchange interaction between a local moment and the conduction electrons (the *s-d* model [17]). Later, it was found that the *s-d* model can be obtained from the more general Anderson Hamiltonian via the Schrieffer-Wolff transformation [18]. Kondo's lowest-order perturbative analysis showed that the antiferromagnetic exchange leads to a singular behavior (divergence) in the scattering rate of conduction electrons near the Fermi level. However, although Kondo's calculation could explain the experimental observations (of resistivity), the perturbation theory broke down at low temperatures (below a certain energy scale, T_K) due to logarithmic divergences and therefore, the method had to be improved. This pioneering work evoked a fervent interest from the physics community to resolve or eliminate the divergence, leading to a huge research effort focused on the "Kondo problem" to find a proper description of the low-temperature behavior of "Kondo systems". Later calculations showed that a logarithmic divergence appears in other physical quantities such as magnetic susceptibility, entropy, and specific heat (for a detailed review, consult Refs. [7, 9, 14, 19–22]) below the same exponential energy scale (Kondo scale, T_K), regardless of the method applied.
Continuous efforts to treat and solve the Kondo Hamiltonian and to eliminate this puzzling divergence actually led to significant advances, in general, in condensed matter physics and in particular, strongly-correlated electronic systems (like the 'polished pearls' of numerical renormalization group (NRG) [23] or perturbative renormalization group (pRG) [24]).
The 'root of evil' had been found to be the multiple spin-flip scattering of conduction electrons from the impurity [25], which makes the problem fundamentally different from the usual single-particle scattering from a static potential – inherently, a many-body problem involving all the conduction electrons plus the impurity.
A further novel insight into this plaguing divergence came with Anderson's idea of "scaling" [26–28]. Via a 'scaling' method, Anderson and coworkers provided a way to eliminate the excitations with higher-energy while keeping their contribution in a modified set of couplings of a low-energy Hamiltonian. This was one of earliest appearance of the powerful idea of renormalization group (RG) in condensed matter which indicates how a physical system behaves as it is probed in different energy and length scales. The scaling method too, leaves one ultimately with a divergent coupling, yet it yields a vital clue to low-energy physics of the Kondo problem.
Generally, it turns out that for the *antiferromagnetic* single impurity (or dilute) case, there are two distinct phases; (i) asymptotically-free local moment at high temperatures, which is weakly interacting with the conduction electrons, and (ii) a fully-screened moment at low temperatures, which forms a spin singlet with conduction electrons and acts as a strong scattering center for the itinerant electrons.
The *ferromagnetic* Kondo problem is much simpler; the local moment only couples weakly to the conduction electrons allowing a perturbative treatment.
The findings of the poor man's scaling — the increase in the coupling strength upon reducing the energy scale and the expected singlet ground-state — was ultimately confirmed by the

'exact' result produced by Wilson's numerical renormalization group (NRG) analysis [29]. NRG is a non-perturbative iterative numerical procedure which uses the fact that the Kondo model can be mapped to a 1-dimensional chain of conduction electrons where the impurity is coupled to only one conduction electron at the edge of the chain. The number of electrons in the chain is increased in each step and the Hamiltonian is diagonalized, retaining only the states with the lowest energies. Ultimately, the spectrum of the Hamiltonian converges when the RG reaches a fixed point [23]. Wilson's NRG results confirmed that below a characteristic Kondo temperature T_K, a magnetic impurity forms a spin-singlet with the surrounding sea of conduction electrons. Later, NRG techniques were developed to calculate the transport properties such as resistivity [30].
The quantum state of the Kondo system in the whole range of temperatures, above and below the Kondo scale, was later obtained by analytical exact methods, like Bethe-Ansatz [31–34]. The analytical solution is very complicated and cannot be expressed in closed form, although it provides a rigorous support for the results from other perturbative or numerical methods.
As a consequence of the above-mentioned results, the zero-temperature phase of a single-impurity Kondo problem turns out to be a Fermi liquid fixed point [35] where the magnetic moment of the local electron is quenched by the conduction electrons near the Fermi energy. Therefore, the quasi-particles of this phase are fermions corresponding to heavily-renormalized itinerant electrons (with a resistivity $\sim T^2$).
Besides the methods mentioned above, other notable approaches were also pursued to 'solve' the Kondo problem:

(i) Nagaoka's method [36–38] was based on the hierarchy of the Heisenberg's equations-of-motion for the Green's functions and their decoupling at a certain level to yield a closed set of equations. This method leads to singular integral equations which then can be solved by appropriate techniques. A general exact solution to these equations were given by Zittartz and Müller-Hartmann [39].

(ii) Suhl's 'dispersion relation' method [40, 41] used the close relation of the Kondo problem to the meson-nucleon scattering which was then investigated in high-energy physics by a method due to Chew and Low who had derived a closed set of equations for the scattering amplitude.

(iii) Resummation of perturbative series was performed by many authors (e.g., Refs. [42–46]) who considered the parquet diagrams and derived and solved the equations for the scattering amplitudes or self-energies up to logarithmic accuracy.

It was further shown that the above approaches, i, ii and iii, are exactly equivalent in the sense that these theories retain essentially the same class of diagrams (the most divergent ones) [1, 7].

(iv) Variational approaches has been also used to obtain the ground-state as a spin singlet bound-state of the conduction electrons and impurity. These calculations, however, did not make an improvement over the previously mentioned methods [47, 48].

(v) Large-N expansion methods [49] which are essentially a mean-field treatment of the Anderson or Kondo Hamiltonian in the limit of large number of levels for the local moment(s) and conduction electrons [14]. In such methods, auxiliary bosons ('slave bosons') are introduced in order to facilitate the calculation for large Coulomb repulsions. These method

are composed of two parts: a mean-field approximation (Gaussian approximation), and inclusion of fluctuations beyond the mean-field solution. These slave-boson methods can be extended to multiple impurities and a lattice [14, 21, 50–54]. Although the mean-field character of these theories leads to an incorrect prediction of a *first-order* phase transition, these methods provide the first insights into such complicated strongly-interacting physical systems [14, 22, 55].

(vi) Boundary conformal field theory methods [56–58] which are an important class of non-perturbative theoretical technique adapted from high-energy theory, were also employed to study condensed matter systems in general, and Kondo problem in particular. These methods benefit from the fact that the Kondo model can be mapped to an effective 1-dimensional problem. Hence, (1+1)-dimensional boundary conformal field theories can be applied to provide exact solutions to different Kondo models (single impurity, two-impurity, and multi-channel).

One can generalized the single-impurity Kondo problem to a case in which there are M (finite) 'channels' or 'flavors' of conduction electrons. Such channels of conduction electrons can arise, e.g., in presence of crystalline electric fields [6], and orthogonal sets of electrons can be considered as distinct 'flavors'. According to an analysis by Nozières and Blandin [59], for a *single-impurity* system in which the spin of the impurity equals the total spin of conduction electron channels, a Kondo effect will emerge at low temperatures and the ground-state will be a 'local' Fermi liquid with fermionic quasi-particles that are 'Kondo' spin-singlets formed by anti-alignment of the spin of conduction electrons and impurities. If the spin of the impurity is less than the net spin of conduction electron flavors, then a partial Kondo effect will occur (under-screened case). Finally, if the net spin of conduction electron flavors exceeds the spin of the impurity (over-screened case), the ground-state will be an non-Fermi liquid. This over-screened case has been treated by Bethe Ansatz [32], NRG [60], and $1/N$-expansion [61] methods.
Therefore, for a single-impurity Kondo model with a single channel of conduction electrons, the ground state is indeed a Fermi liquid. In the ground-state, a composite fermion is formed out of the conduction electrons and the local moment which will play the role of a fermionic quasi-particle at low energies.
When the number of impurities N is increased (even for $N = 2$), the complexity of the problem increases drastically. This is due to the fact that when the distance between the impurities is small enough, they can interact via a carrier-mediated indirect exchange interaction, called the RKKY interaction [48, 62–65]. The magnetic fluctuations arising from the RKKY interaction then compete with the Kondo effect, leading to a significant change in the ground-state; namely, at a vanishing RKKY interaction, the Kondo effect prevails and the impurities are screened at low temperatures by the conduction electrons via formation of 'Kondo' spin-singlets; but as the strength of the RKKY interaction is increased, then at a certain ratio of RKKY interaction to the Kondo scale, the ground-state changes to a 'molecular singlet' (or 'dimer') formed from the spins of the impurities. Since these two ground-states are inherently different, then the question arises whether there exists a phase transition point in between, which is actually an instance of a quantum phase transition. We will discuss this problem in detail in chapter 4.
Another major Kondo problem arises when a lattice ($N \to \infty$) of impurities is embedded in a see of conduction electrons. Hence, at each lattice site, a local moment interacts via an exchange coupling with the conduction electrons and due to the high concentration of impurities, the magnetic correlations between them can not be neglected anymore; the RKKY interaction

therefore plays a substantial role. This picture provides the heart of the physical model for heavy-fermionic systems, the Doniach's picture [66]. Doniach considered the competition of the Kondo effect and the RKKY interaction to explain the appearance of the antiferromagnetic and Kondo liquid phases in these compounds. This picture is essentially based on a comparison of energy scales corresponding to the Kondo singlet formation, T_K, and antiferromagnetic ordering via the RKKY interaction, J_{RKKY}. For a small exchange coupling, the RKKY interaction dominates and an antiferromagnetic ground-state is preferred below the ordering temperature, T_c; above the transition temperature, the system is in a paramagnetic phase with local moments. With increasing the exchange coupling J, the Kondo screening becomes stronger, eventually winning over the RKKY interaction, and the system enters the heavy Fermi liquid regime. In between the two phases, when the two energy scales are comparable, a quantum phase transition is expected (see chapter 5 for a more detailed discuss).

The Kondo effect was at first observed in a metallic host with a concentration of impurities, yet today, manifold realizations of the Kondo effect have been found in a variety of systems (adatoms on surfaces, molecules, and quantum dots).

The single-impurity Kondo effect was first observed in an STS study of magnetic Co atoms on a non-magnetic Au(111) surface and for Ce atoms on a Ag(111) surface [67, 68], where the Kondo effect reveals itself as a sharp peak in differential conductance (dI/dV) at zero bias (see section 3.5 for a more detailed discussion).

The realization of the Kondo effect is much more controllable by nanostructures. One the most promising approaches is based on GaAs/AlGaAs heterostructures, containing a high-mobility two-dimensional electron gas (2DEG) which is confined by electrostatic gates. This confinement leads to formation of puddle(s) of electrons called a "quantum dot" or "artificial atom" [69] (for a review, consult Refs. [11, 70]). The quantum dots can be 'connected' to other dots or extended reservoirs of electrons ('source' or 'drain') via 'quantum point contacts' which are electrodes with some electrostatic potential. These point contacts can be used to vary the strength of the tunneling between a dot and the surrounding dots or electrodes ('leads'). The number of electrons in a quantum dot can be also varied by applying a voltage to the dot (via a 'plunger gate') [71]. The first experiments on single-impurity Kondo effect in quantum dots were performed by several groups in 1998 [72–75]. This led a sudden rise in the attention to (or a 'revival' [76] of) the Kondo effect. Besides GaAs-based heterostructures, it is possible to realize the Kondo effect by using various types of nanomaterials, such as carbon nanotubes [5], semiconductor self-assembled nanostructures [70] and molecular devices [77].

Since the realization of Kondo effect in quantum dots, another important connection has emerged to the highly active field of quantum computing. An approach to quantum computing using coupled quantum dots was suggested by Loss and DiVincenzo in which the two levels of the spin of the electron on the quantum dot, play the role of a 'quantum bit' ('qubit') [78]. This is an scalable approach since one can, in principle, increase the number of quantum dots, and manipulate the properties of each quantum dot and the intra- or inter-dot interactions precisely with electrostatic gates [79]. So to follow this promising approach, there is a vital need to understand the physics of single and double, or multiple quantum dot systems including their strongly-correlated regimes at low temperatures. Upon such a knowledge, a quantum computation operation can be performed through a proper series of qubit operations [79].

Beyond its place in condensed matter, the Kondo model is one of the physical systems which exhibits the notion of 'asymptotic freedom' that is a remarkable property of (3+1)-dimensional non-Abelian Yang–Mills gauge theories which provide the fundamental theory of the strong interactions, or quantum chromodynamics. This 'freedom' appears in the renormalization group

flow of the Kondo coupling which is weak at large energy scales and grows logarithmically at low energies. This implies that at energies higher than the Kondo scale, T_K, the impurity and the electrons are essentially decoupled, while at energy scales below T_K, the electrons and the impurity are strongly bound into a spin-singlet ('infra-red slavery'). This is quite analogous to the scenario for quark confinement where the same behavior is observed for the coupling strengths between gluons and quarks (i.e., at high energy scales, quarks are approximately free whereas they are confined at low-energy scales[5] [80]. Therefore, although the form of the Kondo Hamiltonian is utterly different from the Yang–Mills theories, this interesting link may potentially lead to a general understanding of the class of strongly-interacting theories which show asymptotic freedom [81].

In this work, we shall apply a perturbative renormalization group analysis to a multi-impurity (either 2-impurity or an impurity lattice) Kondo problem. We tend to take the 'most economical' route and avoid intensive numerical computations as far as possible. We seek the leading corrections to the original single-impurity 'scaling' or RG flow. The single-impurity scaling then becomes a first-order or leading approximation. Such corrections will arise due to the presence of the RKKY interaction and lead to contributions which compete with the Kondo screening. We will apply this RKKY-modified RG method to several cases of interest; namely, (i) scanning tunneling spectroscopy of two adatoms on a surface (section 3.5), (ii) double quantum dot systems (chapter 4), and finally (iii) a Kondo lattice (chapter 5).
In the first chapter, we prepare the scene by beginning with the simplest case, the single-impurity Kondo problem, and provide a detailed renormalization group analysis. After this long introduction, we establish the RKKY-modified renormalization group analysis for a multi-impurity Kondo system in chapter 3. We provide a comparison with experimental results (from a scanning tunneling spectroscopy of two magnetic atoms) at the end of this chapter. Chapter 4 provides a slight generalization of the RKKY-modified RG method to the case of a double-quantum dot system with unequal ('asymmetric') Kondo couplings for each dot. We will compare the RG results with the experimental observations at the latter part of this chapter.
The next chapter, 5, is focused on the Kondo lattices and their magnetic instabilities which compete with the Kondo effect. In this chapter, we will concisely discuss the major scenarios for quantum criticality in heavy fermionic systems. Then, we will incorporate the possibility of a magnetic instability in the RKKY-modified RG analysis to see its competition with the Kondo liquid phase. We will find that there is a possibility of an intermediate phase in which the local Kondo screening has collapsed but still no long-range magnetic order is present in the system. The last chapter, 6, is devoted to this partially-screened disordered phase and its possible magnetic instability. At last, we will summarise the RG method and its results and provide a conclusion.

[5] In quantum chromodynamics, the energy scale corresponding to the quark confinement is $\mathcal{O}(1)$ GeV, the mass of the proton, and the length scale is $\mathcal{O}(1)$ fm. In contrast, the Kondo length scale, ξ_K, is typically $\mathcal{O}(0.1-1)$ μm and the energy scale is $\mathcal{O}(1-10)$ meV.

CHAPTER 2

Single-Impurity Kondo Problem

In its magnetic manifestation, the Kondo effect appears when a free magnetic ion is immersed in a non-magnetic host metal. At high temperatures, the magnetic moment of the ion exhibits a Curie magnetic susceptibility ($\chi \sim \frac{1}{T}$) corresponding to *uncorrelated* moments in a paramagnetic phase. When the temperature is decreased below a certain scale, called the "Kondo temperature" (T_K), the local moment gets screened (or "quenched") collectively by the spins of the conduction electrons so that ultimately, at lower temperatures, it reduces to a strong spinless elastic-scattering center for conduction electrons [14]. This local scattering center leads to an increase in the resistivity of the conduction electrons. The Kondo temperature is a small scale which is generated *dynamically* and is smaller than any other energy scale in the *bare* Hamiltonian. Kondo screening is a result of build-up of strong correlations between conduction electrons and the impurity. In this regard, it has become a paradigm in strongly-correlated electronic systems.

2.1 Kondo effect as a scattering problem

Kondo [15] introduced the minimal model for such (quantum) impurity systems by assuming an *antiferromagnetic* (AFM) exchange interaction (with a strength of $J > 0$) between a localized magnetic moment and the conduction electron spins, with the following *s-d* Hamiltonian [17][1]

$$H_{sd} = \sum_{\mathbf{k},\mathbf{k}'} J_{\mathbf{k},\mathbf{k}'}(S^+ c^\dagger_{\mathbf{k}\downarrow} c_{\mathbf{k}'\uparrow} + S^- c^\dagger_{\mathbf{k}\uparrow} c_{\mathbf{k}'\downarrow}) + S^z(c^\dagger_{\mathbf{k}\uparrow} c_{\mathbf{k}'\uparrow} - c^\dagger_{\mathbf{k}\downarrow} c_{\mathbf{k}'\downarrow}) \ , \tag{2.1}$$

in which $S^z, S^\pm$ are the spin operators for the magnetic impurity with spin S, and $c^\dagger_{\mathbf{k}}, c_{\mathbf{k}}$ are creation and annihilation operators for the conduction electrons. Assuming a perturbatively small J, and by a straight-forward (yet elaborate) perturbative calculation of electrical resistivity beyond the Born approximation and up to the third order in J, Kondo was able to reproduce the experimentally observed minimum in the resistivity of dilute alloys(see, e.g., Fig. 2.1). He showed that — in case of an antiferromagnetic coupling, $J > 0$ — the scattering rate of conduction electrons is

$$\frac{1}{\tau} \propto \left(\mathcal{N}J + 2(\mathcal{N}J)^2 \ln(\frac{D}{T})\right)^2 \tag{2.2}$$

[1] This model was originally introduced by Zener [17], who used that to describe the exchange interaction of electrons in *s*- and *d*- orbitals in ferromagnets [7, 9].

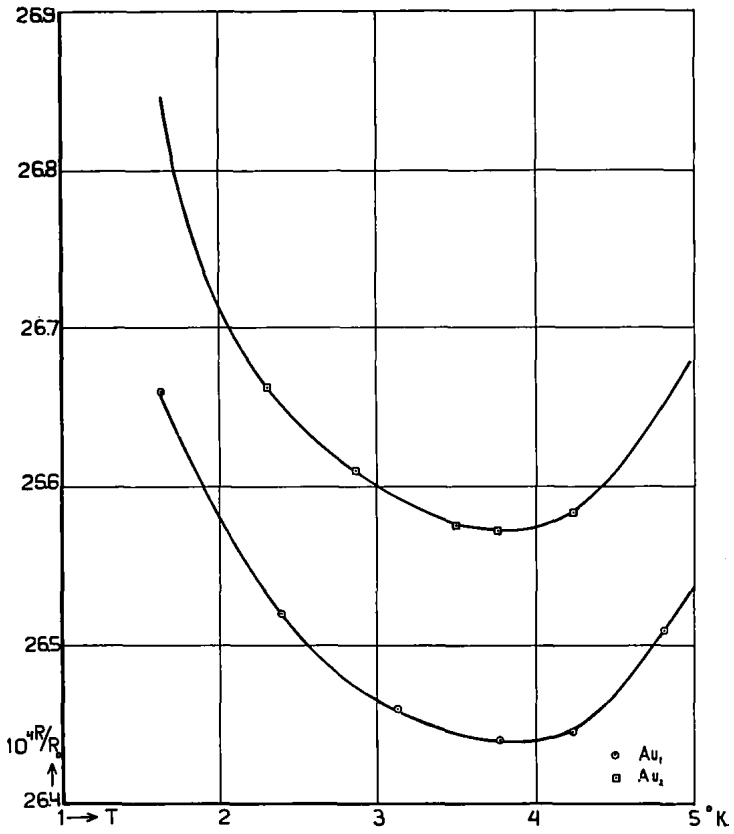

Figure 2.1: Resistance of gold samples with traces of iron impurities between 1 K and 5 K, as measured in Ref. [12].

in which $\mathcal{N}$ is the density of states of the conduction electrons and D is their bandwidth [14]. The experimentally observed dip in electric resistivity was obtained by combining the logarithmic Kondo resistivity with the contributions of phonons ($\sim T^5$) and the non-magnetic static defects (using the Matthiessen's rule[2]):

$$\rho(T) = \rho_0 + a\,T^2 + b\,T^5 + c\left(J^2 + J^3\mathcal{N}(\varepsilon_F)\ln(\frac{D}{T}))\right) \ , \tag{2.3}$$

where ρ_0 is the resistivity due to non-magnetic static disorder, T^2 is the characteristic contribution of the Fermi liquid regime, and T^5 is the contribution of phonons [81] (a, b and c do not depend on J). Hence, lowering the temperature leads to a growth of the logarithmic term, and in turn, to an increase of the scattering rate and resistivity.

Despite its success, perturbation theory breaks down below a certain "Kondo scale", T_K, due to appearance of divergent logarithmic contributions, and the behavior below the Kondo scale, is inaccessible by a weak-coupling perturbation theory [22]. The same logarithmic divergence is

[2] Matthiessen's rule is an empirical rule of thumb which states that the total resistivity of a metallic system is the sum of the contributions from different sources of resistivity (e.g., thermal vibration of lattice ions or imperfections in the crystal) [82].

obtained for other physical quantities, like specific heat, magnetic susceptibility, entropy [22].[3] The underlying reason is the multiple spin-flip scattering of conduction electrons from the impurity which becomes the dominant scattering channel as the energy or temperature scale is decreased, culminating in a *spurious* divergence in a perturbative analysis. The situation is utterly different compared to scattering from a *static* potential, since, in a Kondo system, an *active* impurity is embedded in the conduction electron bath, which can change its spin orientation in each scattering event; therefore, the state of the impurity is correlated with the state of conduction electrons, leading to a genuine interacting many-body problem. All the electrons near the Fermi level— in a certain width of T_K — are collectively involved in the process, and the logarithmic divergence in the perturbatively calculated observables is the result of a 'coherent' superposition of such spin-flip scattering events.

Although the perturbative series diverges at the Kondo scale, this does *not* correspond to a phase transition but a "cross-over scale"[4] which indicates a smooth change from a high-temperature phase (with a Curie-law magnetic susceptibility, $\chi_C \sim \frac{1}{T}$) to a low-temperature phase (with a paramagnetic Pauli susceptibility, $\chi_P \sim \frac{1}{T_K}$) without any divergence in the free energy or its higher derivatives.[5]

Besides other fundamental complications, there is another methodological difficulty if one pursues a systematic perturbative approach via the usual diagrammatic methods. The problem is related to the operator nature of the quantum spin. The usual diagrammatics is based on the Wick's theorem which is applicable only to operators which have a simple algebra like the creation and annihilation operators; that is, their commutator/anticommutator is a simple number (c-number). It becomes immediately clear that one has to go beyond the usual form of the Wick's theorem when spin operators are present, since they obey an $\mathfrak{su}(N)$ algebra, and their commutator is again an *operator* instead of a c-number.[6] This problem which hinders attempts to go to higher orders or to resum diagrams, can be resolved by devising a faithful representation of spin operators in terms of creation/annihilation operators. In this regard, several valid representations has been introduced (e.g., [43, 86, 87]).

In a seminal paper on the single-impurity Kondo problem, Abrikosov [42] provided an exact representation of spin operators in terms of pseudo-fermions and a projection method. A corrected version of the Abrikosov's pseudo-fermion method [44, 88] forms the basis of the perturbative method used in the current work (see Appendix C). With this pseudo-fermion representation, Abrikosov attempted to construct a perturbative resummation of leading logarithmic terms ("up

[3] The presence of a low-energy ("infra-red") divergence is an indication of an incorrectly chosen reference ground-state. This ground-state is orthogonal to that of the non-interacting system and therefore, is unreachable by a perturbative method. The simplest example of such a divergence happens in superconductivity of normal metals. In contrast, high-energy ("ultra-violet") divergences are not a significant problem in condensed matter. Their presence indicates that the continuum description is incomplete at shorter length scales or higher energy scales [83].

[4] A cross-over is a smooth change of phase (without a phase transition), or in renormalization-group language, going continuously from the vicinity of a fixed point to the vicinity of another without an identifiable phase transition point (see, e.g., Refs. [84, 85]).

[5] Note that this absence of phase transitions is only true for the *single-impurity* or *very dilute* case (impurity concentration lower than 1% [7, 9]).

[6] For instance, $S = 1/2$ operators obey an $\mathfrak{su}(2)$ algebra,

$$[S_i, S_j] = \mathrm{i}\epsilon_{ijk}\, S_k \quad \text{for } i, j, k \in \{x, y, z\} \ .$$

to logarithmic accuracy")[7] which dresses the vertex in the conduction electron self-energy in order to eliminate the logarithmic divergence which appeared in Kondo's original perturbative calculations. Although even this elaborate resummation could not remove the logarithmic divergence at the Kondo scale, it provided further insight into the nature of the divergence which involved the so-called "intermediate states" (or virtual excitations of the conduction electrons and impurity). The significance of such intermediate states implies the excitation of a large number of particle-hole pairs which has vanishing energy cost at lower energies.[8]

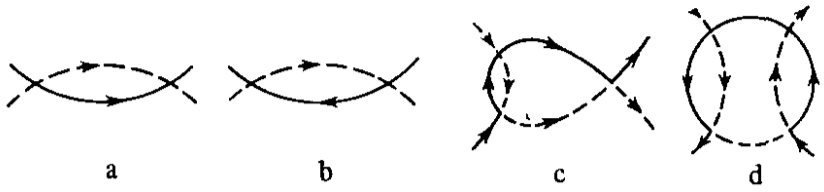

Figure 2.2: Abrikosov's vertex corrections: Note that the diagrams in this set separate into two pieces by cutting one electron and one pseudo-fermion line (adopted from Ref. [25]).

From the form of the resummed diagrams, it is clear that those processes involving a single excited particle (electron or hole) in the 'intermediate state' are taken into account in the dressed vertex. This class of diagrams is called 'parquet diagrams' and are calculated up to logarithmic accuracy.

For a low concentration of impurities, Abrikosov obtained the following form for the renormalized vertex

$$\Gamma = \frac{J}{1 - J\frac{k_F m}{\pi^2}\ln(\frac{\varepsilon_F}{|\omega|})} \ , \tag{2.5}$$

and the conduction electron self-energy,

$$\Sigma_c = -\frac{\mathrm{i}}{2\tau_0}\,\mathrm{sign}(\omega)\left[1 - \frac{3J}{2\varepsilon_F}\ln(\frac{\varepsilon_F}{\omega})\right]^{-2} \ , \tag{2.6}$$

in which τ_0 is the scattering time is absence of the Kondo interaction. The *real* part of the scattering amplitude at the Fermi level was obtained by Abrikosov as [7]

$$t(\epsilon = 0) = \frac{J}{1 + 2\mathcal{N}_0 J\,\ln(T/D)} \ , \tag{2.7}$$

[7] A quantity is said to be calculated "to logarithmic accuracy" when in an expansion like

$$F(\varepsilon) = c\sum_{n=2}^{\infty} A^n \sum_{m=2}^{n} a_{n,m}\ln^{n-m}(\varepsilon/E) \ , \tag{2.4}$$

only the coefficients $a_{n,m}$ associated with the *most divergent* terms are calculated exactly while the coefficients for $m > 2$ are determined by an approximation procedure [89] (consult Refs. [90, 91])

[8] Such a low-energy or "infra-red" divergence appears also in a related problem, the "X-ray absorption edge" [82, 92]. Nozières *et al.* have applied a parquet resummation technique to this problem [93, 94]; for a renormalization-group approach, see Ref. [95].

and the resistivity [7],

$$R(T) \sim \frac{S(S+1)\,J^2}{(1+2\mathcal{N}_0 J\,\ln(T/D))^2}\ . \tag{2.8}$$

An important aspect of these results is that the behavior of ferromagnetic and antiferromagnetic cases are utterly different. Notice that in the ferromagnetic case, the logarithmic expression in the scattering amplitude or resistivity *decreases* upon lowering temperature; in constrast, in the antiferromagnetic case, the expressions diverges as T reaches the Kondo temperature T_K,

$$T_K/D_0 = \exp(-\frac{1}{2\mathcal{N}_0 J}) \ll 1\ , \tag{2.9}$$

since the expression has a pole. This emergent dynamical energy scale has a non-analytic dependence on the coupling J, which is a remininisce of the superconducting transition temperature in the BCS theory [7], although there is no phase transition is this single-impurity Kondo problem. Similarly, the magnetic susceptibility of the impurity, χ_{imp}, is obtained as [7]

$$\chi_f(T) = c\frac{S(S+1)\mu_{\mathit{eff}}(T)^2}{3T}(1-2\mathcal{N}_0 J) + \text{Pauli polarization}\ , \tag{2.10}$$

where

$$\mu_{\mathit{eff}}(T) = \mu\left(1+\frac{1}{2}\frac{(2\mathcal{N}_0 J)^2\,\ln(T/D)}{1-2\mathcal{N}_0 J\,\ln(T/D)}\right)\ , \tag{2.11}$$

and c is the impurity concentration. The first term suggests that the effective magnetic moment decreases as the temperature is lowered. The impurity spin is screened by a 'compensation cloud' surrounding it. This screening cloud is collectively produced by the conduction electrons (in a layer of width T_K near the Fermi level) which align their spin anti-parallel to the magnetic moment. The spatial extent of the cloud is roughly given by [7]

$$\xi_K \sim \frac{v_F}{T_K}\ , \tag{2.12}$$

where v_F is the Fermi velocity. This is a coherence length in the Kondo effect.
Abrikosov [42] and Suhl [41] suggested that the spurious infra-red divergence in the logarithmic approximation actually implies the formation of a resonance, the "Abrikosov-Suhl resonance" (Fig. 2.3), in the conduction electron–impurity scattering amplitude, centered at the Fermi level. This resonance is the hallmark of the Kondo effect.
It turns out that going beyond the logarithmic approximation with a full inclusion of the imaginary parts is a tremendously difficult (or impossible) task (e.g., see the attempts in Refs. [96–99]).

2.2 A "poor man's" scaling

A thoroughly novel approach, along with a new perspective to physics of interacting systems in general, and to the Kondo effect in particular, was introduced by Anderson and coworkers [24, 26–28, 100]. In this method, one successively eliminates the high-energy modes (or excitations) of the system and retains their effect in a set of energy-dependent 'running' couplings which

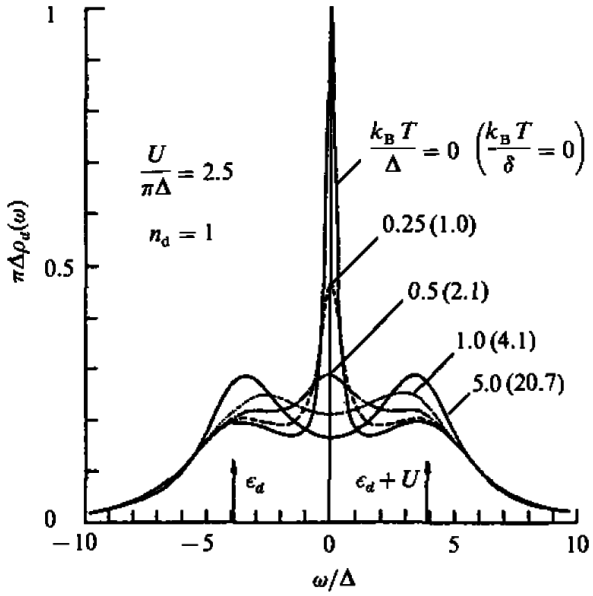

Figure 2.3: Local spectral density for the symmetric Anderson model for various temperatures (adopted from Ref. [22]). The sharp Abrikosov-Suhl resonance at the Fermi level is obtained at low temperatures. The width of the central resonance, $\delta \sim T_K$.

describe the low-energy behavior of the system. This 'down-folding' of high-energy states is performed such that the normalized scattering amplitude remains invariant, so that the physical properties of the system does not change. In this way, at each step, as the energy/temperature scale, D, is reduced, one obtains a Hamiltonian equivalent to the original one at the 'bare' coupling $J(D_0)$, but with the energy cut-off, D, reduced; so, one obtains a trajectory in the "space of Hamiltonians" with the couplings becoming energy-dependent, $J = J(D)$. In case of the Kondo problem, reducing the energy cut-off (the bandwidth D), tames the logarithmic singularities at a cost of increasing couplings. Note that in this case, as we integrate out the high-energy modes, other forms of interactions (like potential scattering) are also produced; however, it turns out that they do not play a significant role compared to the Kondo interaction and therefore, are neglected [18, 101].[9]

Anderson's "poor man's scaling" is essentially the simplest perturbative renormalization-group analysis applied to the Kondo problem. It yields an insight into the low-energy behaviour of the problem, and the infra-red divergence in the perturbation theory. It transpires that the physics, or more precisely, the properties of the ground-state, changes qualitatively when the energy cut-off crosses the Kondo scale. Therefore, this scale plays a crucial role in the problem. Furthermore, the bare coupling is only important at the beginning of the flow; the initial conditions are 'forgotten' as one gets away from the original energy cut-off, D_0.[10]

[9] Neglecting such non-Kondo terms is only justified *a posteriori* when the results are confirmed by exact or numerical methods.

[10] The details of the calculations are provided in Appendix D.

$$\frac{\mathrm{d}J_z}{\mathrm{d}\ln D} = -2\mathcal{N}(\varepsilon_F)\, J_\pm^2 \ ,$$
$$\frac{\mathrm{d}J_\pm}{\mathrm{d}\ln D} = -2\mathcal{N}(\varepsilon_F)\, J_\pm J_z \ , \tag{2.13}$$

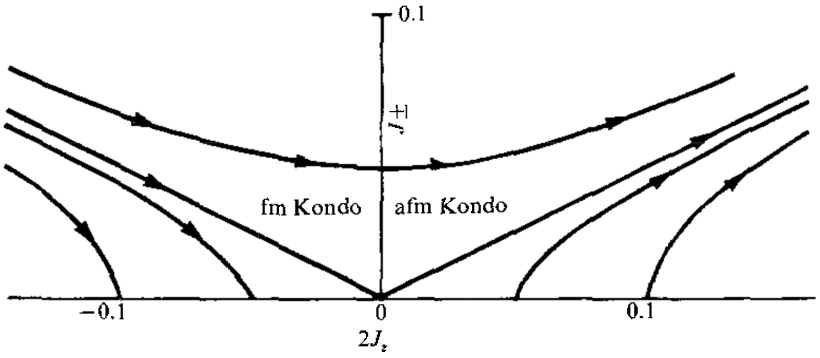

Figure 2.4: RG flow (or 'scaling curves') for the anisotropic Kondo problem (adopted from Ref. [22]). The arrows indicate the direction of the flow as the conduction electron bandwith is reduced. The straight lines correspond the isotropic situation ($J_\pm = J_z$). The most significant consequence of this RG flow is that the coupling strength grows indefinitely for the antiferromagnetic case (RG flow to the 'strong-coupling' fixed point). For the ferromagnetic case, the couplings flow towards zero (the J_z-axis) indicating that a perturbative treatment suffices to calculate the physical observables.

One of the important pieces of information in the RG flow is the structure and character of the fixed points (see Fig. 2.4). The fixed points are those points on the RG flow where the couplings do not change upon reducing the high-energy cut-off (for a detailed discussion, consult, e.g., Ref. [102]).

Ferromagnetic coupling For the ferromagnetic case, there is only a single 'weak-coupling' fixed point at which $J = 0$. The conduction electrons and the impurity are not entangled and a perturbative expansion in J will be sufficient to describe the properties of the system. Hereafter, we will not consider this case in the present work.

Antiferromagnetic coupling For the antiferromagnetic single impurity (or dilute) case, there are two distinct fixed points which are two asymptotic limits separated by the Kondo scale:
(i) a fixed point at $J = 0$ ("weak-coupling fixed-point"), which corresponds to asymptotically-free conduction electrons and uncorrelated local moments. Therefore, at $T \gg T_K$, the impurity spin is disentangled from the conduction electrons and weakly coupled to them so that it can fluctuate almost freely due to external fields or temperature. This is reflected in the corresponding Curie susceptibility. Hence, in this limit, the Kondo interaction can be treated perturbatively.
(ii) a fixed point at $J \to \infty$ ("strong-coupling fixed-point") which corresponds to a fully-screened moment which acts as a strong scattering center for conduction electrons which scatter at the *unitary limit*; that is, scattering phase-shift is $\frac{\pi}{2}$ for both up and down spin channels. Using Friedel's sum rule [103], this implies that effectively, one conduction electron has been removed

from the system to make a spin-singlet with the local moment and screen it.[11] So, at $T \ll T_K$, the impurity and the conduction electrons are locked into a spin-singlet state. The polarization of this singlet by the conduction electrons induces an effective indirect interaction between the electrons themselves: an electron polarizes the singlet, and another electron is affected subsequently by this polarization. This mechanism is reminiscent of the phonon-mediated interaction in superconductivity [1]. Near $T = 0$, a phenomenological Fermi liquid approach due to Nozières provides the physical properties of the system (*'local' Fermi liquid*).
These limiting phases are relatively simple, but the intermediate cross-over range is indeed very complicated and does not yield itself to a perturbative treatment.
When the flow reaches T_K from above, perturbative scaling diverges and breaks down. Actually, at this scale, saturation mechanisms come into play to prevent the system from becoming unstable; so that the spurious divergence is eliminated (for first attempts at such a theory, see Refs. [104, 105] and a more detailed discussion in Ref. [106]).

2.3 Orthogonality catastrophe and the ground-state of the antiferromagnetic Kondo problem

As pointed out first by Anderson [107], the divergence in the perturbative treatment can be traced back to the "orthogonality catastrophe" (or "infra-red catastrophe"). Anderson showed that the ground-state of the an electron gas in presence of an impurity is orthogonal to ground-state in absence of the impurity. This vanishing overlap between the two ground-states is the reason for the failure of the perturbation theory (since 'adiabaticity' is destroyed), and the nature of Fermi sea has fundamentally changed.
The ground-state of the Kondo Hamiltonian is not two-fold degenerate (like the atomic limit of a single spin-1/2 degree-of-freedom). It is instead a spin-singlet formed by anti-alignment of spins of a conduction electron and that of an impurity to yield a vanishing net spin. This is called "Kondo screening". This screening is performed collectively by the conduction electrons near the Fermi level; however, on average, only one electron is bound to compensate the impurity spin [70]. The "Kondo screening cloud" is depicted schematically in Fig. 2.5.
The formation of this cloud leads to the characteristic signature of a narrow Kondo (Abrikosov-Suhl) many-body resonance formed at (or very close to) the Fermi level causing an enhancement in physical quantities such as the specific heat or susceptibility. The binding energy of the Kondo singlet is roughly equal to the Kondo scale, *not* the Kondo coupling J. The spatial dimension of the Kondo cloud is roughly given by $\xi_K \sim v_F/T_K$, where v_F is the Fermi velocity [108–110].[12]
Measuring the Kondo cloud has been very difficult since it involves measuring the dynamic local spin density without destroying the Kondo effect [108, 110, 111]. Furthermore, the Kondo energy scale cannot be sharply defined [11] and several valid conventions are used which can differ by a constant multiplicative factor.
Although the Kondo effect is a genuine many-body problem, it can be described as an scattering of conduction electrons from the impurity, as described before. Due to the localized nature of the scattering potential, only $l = 0$ component or s-wave scattering need to be considered. The

[11] This is essentially the point of view of numerical renormalization group (NRG) [1, 23].
[12] A theoretical estimation for this length scale is $\xi_K \sim 0.1$ to 1 μm [110] for metals and typical semiconductor quantum dots in the Kondo regime, which gives an estimate of the spatial extent of Kondo correlations. However, such relatively large length scales has not been observed in experiments so far — perhaps due to the roughness of the estimate.

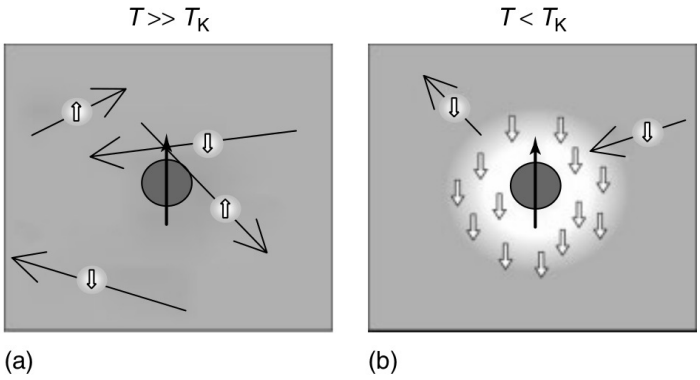

Figure 2.5: A magnetic impurity in a sea of conduction electrons, (a) above the Kondo temperature, T_K, and (b) below the Kondo temperature. Above the Kondo temperature (a), the conduction electrons scatter weakly from the magnetic impurity, while below the Kondo temperature (b), the scattering becomes 'resonant' and the conduction electrons form a spin-singlet with the impurity, making a cloud to quench the local moment (adopted from Ref. [11]).

formation of the Kondo singlet leads to a scattering phase-shift of $\pi/2$ (*unitary limit*) for the electrons in the Fermi sea. This is the reason behind the increase in resistance. The resistivity saturates finally as the temperature vanishes [1].
Using this scattering analogy and via a phenomenological approach analogous to Landau's Fermi liquid theory, Nozières [35, 59] provided the essential physical properties of the ground-state at the strong coupling fixed point (when $J \to \infty$) where the impurity is bound to the conduction electrons and forms a singlet state with them. This strongly-bound singlet is decoupled from the rest of the system and serves only as a very strong scattering center for the conduction electrons. Therefore, the conduction electrons acquire a maximum phase shift $\delta\phi = \frac{\pi}{2}$ due to this strong scattering. From this scattering phase-shift, and using the Friedel sum rule, one can obtain the number of electrons bound into the Kondo singlet, $N_{bound} = 2\frac{1}{\pi}\delta\phi = 1$, which implies that effectively one electron has been captured by the impurity. This is the first step in Nozières' "local Fermi liquid" theory [35, 59]. In fact, since the coupling is large but not infinite, the conduction electrons can polarize the singlet. This polarization will affect another electron and thus, leads to an indirect interaction between electrons much like the case in superconductivity with phonons. In this way, an interacting Fermi liquid is formed where the origin of the electron-electron interaction is 'local'. Such an analysis can be extended to the case where multiple 'channels' or 'flavors' of conduction electrons are present (e.g., with different angular momentum quantum numbers) and the impurity has a higher spin. The ground-state of such a multi-channel single impurity Kondo problem is determined by two parameters, the spin, S, of the impurity and the number of channels of conduction electrons, M [59]:
(1) When $2S = M$, the ground-state of the impurity is a singlet and the low-temperature properties are those of a 'local' Fermi liquid.
(2) When $2S > M$, there are not enough channels to completely screen the impurity spin and form a singlet, and the impurity remains 'under-screened'. At low temperatures, the impurity behaves effectively like a free spin of magnitude $S - M/2$.
(3) When $2S < M$, the number of channels are more than enough to screen the impurity spin, and the impurity becomes 'over-screened'. The ground-state will be a non-Fermi liquid.
For a detailed discussion of Fermi and non-Fermi liquid behaviour, consult section 5.1.2.

2.4 Universality in the Kondo effect

A notable aspect of Kondo effect is the universal nature of the physical properties. It turns out that there is only a single parameter, the dynamically-generated Kondo energy scale[13], which determines the thermodynamic or transport properties via a universal functional dependence. Indeed the Kondo scale itself will depend on the microscopic non-universal properties of the system (the impurity and the metallic host), but beyond this, there is not any non-universal parameters in the physical observables (see Fig. **??**). In the experiments, this universality can be verified by the collapse of the experimental curves on a *single* curve (denoting a single functional dependence) when one scales the parameters with the Kondo scale. There is finally no explicit reference to the high-energy ("ultra-violet") properties of the system.

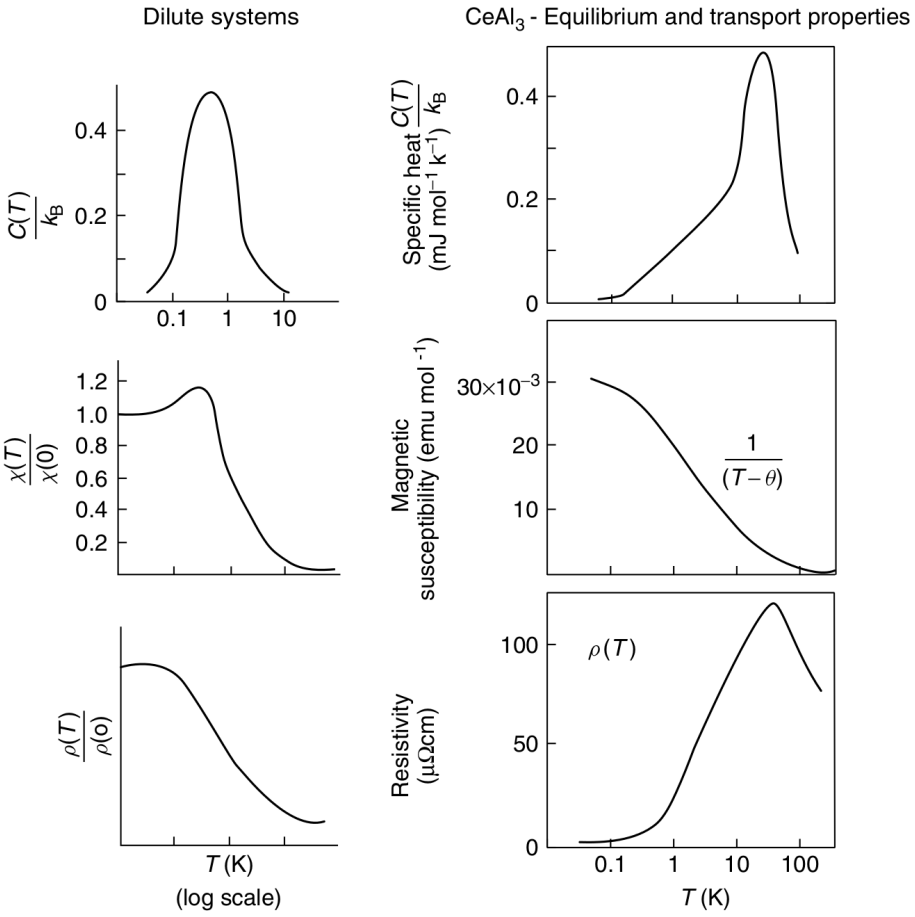

Figure 2.6: Schematic universal functional forms for the spin-1/2 Kondo systems: specific heat, magnetic susceptibility, and resistivity. For comparison, the same properties are given for a typical Kondo lattice system, $CeAl_3$ (adopted from Ref. [8]).

[13] The crucial aspect of the dynamically-generated scales is that they cannot be estimated or predicted from a mere dimensional analysis of the bare parameters of a system.

2.5 Origin of local moments

In his theoretical description, Kondo had *assumed* the presence of magnetic moments in the metallic host. But it was not clear at all why it should be the case, especially when it was later found that Kondo model can be obtained by a canonical transformation performed on the more general Anderson model (see section 4.6). Schrieffer-Wolff transformation is itself a simple instance of the perturbative renormalization group idea to obtain the effective low-energy Hamiltonian for a system. In the case of Anderson model at low energies, when the hybridization between the conduction band and the local level is small relative to the Coulomb energy, charge fluctuations are suppressed leaving the system with only spin degrees-of-freedom.[14]

Therefore, a more fundamental microscopic description is necessary to understand the origin of the moments and their antiferromagnetic interaction with the conduction electrons.

Friedel was the first to consider this problem using a simple scattering theory which predicted the emergence of *virtual bound-states* in the continuum [112–114]. In Friedel's work, the impurity was modelled by a static potential well in which a bound-state of finite width can be formed (near the Fermi level). The condition for the formation of a impurity magnetic moment was unequal (non-degenerate) resonance levels for the different spin directions.

In 1961, Anderson [115] proposed a microscopic model for the formation of magnetic moments in metals informed by an earlier work by Blandin and Friedel [116] who had observed that localized d-states form resonances in the electron sea.[15]

The main contribution of the Anderson was incorporating a simplified local (or 'on-site') Coulomb interaction between the localized d-electrons (see chapter 4) Anderson performed a Hartree-Fock mean-field analysis on the model and showed that a local moment can form when the strength of Coulomb interaction U becomes larger than the hybridization strength (see below).

The simplest case of the Anderson Hamiltonian is obtained for a single band of Bloch electrons interacting with a single local level[16] (where the d-state is a 'Kramers doublet'[17])

$$H = \sum_{\mathbf{k}\sigma} \varepsilon_{\mathbf{k}} c^\dagger_{\mathbf{k}\sigma} c_{\mathbf{k}\sigma} + \sum_{\sigma} \varepsilon_d \, d^\dagger_\sigma d_\sigma + V \sum_{\mathbf{k}\sigma} \left(c^\dagger_{\mathbf{k}\sigma} d_\sigma + d^\dagger_\sigma c_{\mathbf{k}\sigma} \right) + U \hat{n}_{d\uparrow} \hat{n}_{d\downarrow} \, . \tag{2.14}$$

The essential ingredients of the model are the localized d-electrons of the (magnetic) ion which 'feel' a large Coulomb repulsion (due to their spatially-constrained d-orbitals), and the spin-conserving hybridization (V) of these d-electrons with the delocalized Bloch (conduction)

[14] The exchange (Kondo) coupling J can be, generally, positive or negative. Yet, when the model is derived via a Schrieffer-Wolff transformation on the Anderson Hamiltonian, it turns out to be positive (antiferromagnetic), as it is observed experimentally in many systems.

[15] Such localized moments can be found in $4f$ (rare earth, like Ce, Gd, Tb, Dy, Eu), $5f$ (actinide, like U), and $3d$ (transition metals, like Fe) atomic shells.

[16] The 'crystal fields' present in real metals, destroy the spherical symmetry of the atomic orbitals, and produce a level-splitting. Their effect is usually negligible for d-electrons, but not for the narrower f-orbitals [7].

[17] Kramers degeneracy theorem states that in a time-reversal-invariant system with an *odd* number of fermions, all the energy levels must be doubly degenerate; that is, for an eigenstate $\psi_{n\mathbf{k}\sigma}$ of the Hamiltonian, there must be another time-reversed state, $\psi^*_{n,-\mathbf{k},-\sigma} \equiv \mathcal{T}\psi_{n\mathbf{k}\sigma}$ which has the same energy ($\mathcal{T}$ is the time-reversal operator). This holds true especially for a 'Kramers ion', an ion with an odd number of electrons (hence, a half-integral spin) [117].

electrons which tends to 'deconfine' the d-electrons to form a renormalized electronic band.[18, 19] The contention between these two effects are clearly seen even in the mean-field picture. The two asymptotic limits are apparently irreconcilable: In the atomic limit where the Coulomb interaction wins over the hybridization and prevents double-occupation of the localized level, the ground-state would correspond to a singly-occupied state and a local moment, with the low-lying excitation being related to moment fluctuations (spin waves); in the adiabatic limit where the Coulomb interaction is relatively small, the impurity is partially occupied with spin-up and spin-down electrons and the ground-state is a *paramagnetic* Fermi liquid, with particle-hole excitations. The original mean-field treatment by Anderson yields an approximate condition for the moment formation [92],

$$U \geq \pi \mathcal{N}(\varepsilon_F) V^2 \ . \tag{2.15}$$

However, the mean-field picture cannot reconcile the two different adiabatic and atomic ground-states mainly because the spin fluctuations are neglected in this simplified picture. These are in fact the fluctuations which originate the Kondo effect. At low enough energy scales, such 'coherent' fluctuations dominate the quantum dynamics of the system and lead to a formation of a new bound-state very close to to the Fermi surface. This is observed as a resonance in the density-of-states of the conduction electrons and is called the Abrikosov-Suhl [41, 42] or the Kondo resonance. The width of the resonance is approximately given by the Kondo energy scale [7, 9],

$$T_K = \sqrt{\frac{2U\Delta}{\pi^2}} \exp(-\frac{\pi U}{8\Delta}) \ , \tag{2.16}$$

for the symmetric Anderson model where $\varepsilon_d = -U/2$, and Δ is the hybridization strength, $\Delta = \pi \mathcal{N}(\varepsilon_F) V^2$ [14].
So far, we have introduced the renormalization-group ideas qualitatively and provided the major results. In the following, we will obtain explicitly the RG flow equation for a single-channel single-impurity Kondo model in detail.

2.6 Renormalization group analysis for the single-impurity Kondo problem

The idea of renormalization group was briefly sketched in the section on "poor man's scaling" (section 2.2). To lay the foundations for the RG analysis for the multi-impurity Kondo problem, we begin by applying a diagrammatic RG method to the single impurity Kondo problem in order to reproduce the Anderson's "poor man's scaling" results in a diagrammatic language which is suited for extention to more elaborate cases. This section serves also as a general introduction to the methods used in the RG analysis (e.g., Abrikosov's pseudo-particle method or one-loop

[18] More precisely, there is problem with this simplified picture of two fermion types (s and d). The conduction electron states (Bloch waves) constitute a complete set, and therefore, any orbital (like d-orbitals) can be decomposed in terms of these Bloch waves, and hence is *not* orthogonal to them. However, this would be a serious problem only for real material calculations (*ab-initio* methods) and will not concern us in the present context.

[19] As a rough estimate, the strength of the Coulomb interaction is $\sim$ 5–10 eV (further reduced due to screening), the hybridization is $\sim$ 0.5–1 eV, and the bandwidth is $\sim$ 2–3 eV [7].

RG).[20]
The Kondo Hamiltonian[21] for a single impurity immersed in a sea of conduction electrons is

$$H = \sum_{\mathbf{k}\sigma} \varepsilon_{\mathbf{k}} c^{\dagger}_{\mathbf{k}\sigma} c_{\mathbf{k}\sigma} + J\, \mathbf{S}(\mathbf{x}) \cdot \mathbf{s}(\mathbf{x}) \tag{2.17}$$

where J is the Kondo coupling, $\mathbf{S}$ is the spin operator for the impurity and $\mathbf{s}$ represents the spin operator for the conduction electrons; the impurity is assumed to be at position $\mathbf{x}$. The *bare* Kondo interaction (i.e., the interaction vertex without any renormalization or dressing from other interactions) is

$$H_K = J\, \mathbf{S}(\mathbf{x}) \cdot \mathbf{s}(\mathbf{x}) \ . \tag{2.18}$$

In order to make use of conventional diagrammatic methods, we use the pseudo-particle representation fot the impurity spin operator (see Appendix C),

$$\mathbf{S}(\mathbf{x}) = \frac{1}{2} \sum_{\nu\nu'} f^{\dagger}_{\nu'}(\mathbf{x})\, \boldsymbol{\sigma}_{\nu'\nu}\, f_{\nu}(\mathbf{x}) \,, \tag{2.19}$$

where $f^{\dagger}_{\nu'}(\mathbf{x})$ ($f_{\nu'}(\mathbf{x})$) creates (annihilates) a localized fermion with spin ν at site $\mathbf{x}$, and $\boldsymbol{\sigma}$ denotes the Pauli matrices. The conduction-electron spin operator can also be re-written as

$$\mathbf{s}(\mathbf{x}) = \frac{1}{2} \sum_{\nu\nu'} c^{\dagger}_{\nu'}(\mathbf{x})\, \boldsymbol{\sigma}_{\nu'\nu}\, c_{\nu}(\mathbf{x}) \,. \tag{2.20}$$

Therefore, the Kondo interaction can be re-written as

$$H_K = \frac{J}{2} \sum_{\substack{\mathbf{k}\mathbf{k}' \\ \mu\alpha,\mu'\alpha'}} f^{\dagger}_{\mu'} f_{\mu}\, \boldsymbol{\sigma}_{\mu'\mu} \cdot \boldsymbol{\sigma}_{\alpha',\alpha}\, c^{\dagger}_{\mathbf{k}'\alpha'} c_{\mathbf{k}\alpha} \ , \tag{2.21}$$

which can be represented diagrammatically as in Fig. 2.7. Obviously, the spin interaction conserves neither the momentum, nor the spin, but it conserves the energy.

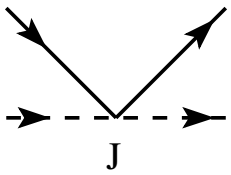

Figure 2.7: Bare Kondo vertex. The solid (dashed) line represents the conduction electrons (f-pseudo-fermions).

As explained previously, the idea of renormalization is to obtain an effective low-energy Hamiltonian by eliminating the high-energy modes while keeping their effect in a set of renormalized couplings which depend on the energy scale, and obey an RG flow equation which determines the change in the couplings as the energy scale is reduced. This flow equation contains the

[20] Details of poor man's scaling calculations are provided in Appendix D.
[21] From here onwards, anisotropy in the Kondo coupling J will be neglected since it does not play a vital role in the results and the final physical picture. The anisotropic case is discussed in detail in Appendix D.

essential information about the low-energy physics of the system.

In this work, we use a perturbative RG method and obtain the flow equation as a perturbative series for the Kondo coupling. In such a perturbative analysis, mode elimination is performed in infinitesimal steps and its effect on the couplings is described in terms of 'corrections' to the Green's functions and interaction vertices. The general method is known due to the work of Wegner and Houghton [118] who derived a formally exact functional differential equation for the change of action (to all orders) as the high-energy cut-off is reduced infinitesimally. However, this formal differential equation has little practical use since it cannot be solved directly (usually, heavy numerical computation is necessary). Therefore, one has to keep only the most important terms in the perturbative series to be able to perform an analytic calculation; yet, this truncation should be done without compromising the essential physics of the problem.

In a perturbative analysis, the emergence of the Kondo effect is revealed in the divergence of the scattering amplitude of the conduction electrons from the impurities; thus, the quantity which should be considered is the Γ_{c-f} (or Kondo) vertex. We will consider the change of this vertex under the RG flow.

In the following perturbative analysis, it turns out that keeping only one-loop corrections is enough to have the Kondo physics (especially, Kondo-screened fixed point). Up to one-loop order in RG (second order in J), one obtains two contributions: the 'direct' and 'exchange' RG diagrams. We will elaborate on these two contributions in the following sections.

2.6.1 Direct diagram

The direct RG diagram is depicted in Fig. 2.8.

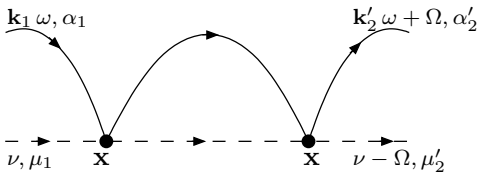

Figure 2.8: Direct RG diagram for the single-impurity Kondo model.

The operator product plus contractions are

$$\mathcal{D}_{dir} = \frac{J^2}{2!} \sum_{\substack{\mathbf{k}_1,\mathbf{k}_1' \\ \mu_1\alpha_1 \\ \mu_1'\alpha_1'}} \sum_{\substack{\mathbf{k}_2,\mathbf{k}_2' \\ \mu_2\alpha_2 \\ \mu_2'\alpha_2'}} \overbrace{f^\dagger_{\mu_1'} f_{\mu_1} \boldsymbol{\sigma}_{\mu_1'\mu_1} \cdot \boldsymbol{\sigma}_{\alpha_1'\alpha_1} c^\dagger_{\mathbf{k}_1'\alpha_1'} c_{\mathbf{k}_1\alpha_1} f^\dagger_{\mu_2'} f_{\mu_2} \boldsymbol{\sigma}_{\mu_2'\mu_2} \cdot \boldsymbol{\sigma}_{\alpha_2'\alpha_2} c^\dagger_{\mathbf{k}_2'\alpha_2'} c_{\mathbf{k}_2\alpha_2}} \tag{2.22}$$

So the overall sign of the diagram due to Wick theorem is $+1$ and this complies to the Feynman rules for two-body Green's functions [119].

The expression can be divided into two parts and considered separately: the diagrammatic part which involves the Green's functions and the Pauli-matrix part which involves the Pauli matrices and the sums over spins.

Spin summations The summations over spin indices leads to the following expressions

$$\begin{aligned}\mathcal{P}_{dir} &= \sum_{a,b=x,y,z} \sum_{\mu_2\alpha_2} \sigma^a_{\mu_2\mu_1}\sigma^a_{\alpha_2\alpha_1}\sigma^b_{\mu_2'\mu_2}\sigma^b_{\alpha_2',\alpha_2} \\ &= \sum_{a,b=x,y,z} \sum_{\mu_2\alpha_2} \left(\sigma^b_{\mu_2\mu_1}\sigma^a_{\mu_2\mu_1}\right)\left(\sigma^b_{\alpha_2',\alpha_2}\sigma^a_{\alpha_2,\alpha_1}\right) \ . \end{aligned} \tag{2.23}$$

Using the Pauli matrix algebra (Appendix A), one obtains

$$\begin{aligned}\sum_{\mu_2}\sigma^b_{\mu_2'\mu_2}\sigma^a_{\mu_2\mu_1} &= (\sigma^b\sigma^a)_{\mu_2'\mu_1} \\ &= \delta_{ab}\delta_{\mu_2'\mu_1} + \mathrm{i}\sum_c \epsilon_{bac}\sigma^c_{\mu_2'\mu_1} \ , \\ \sum_{\alpha_2}\sigma^b_{\alpha_2'\alpha_2}\sigma^a_{\alpha_2\alpha_1} &= (\sigma^b\sigma^a)_{\alpha_2'\alpha_1} \\ &= \delta_{ab}\delta_{\alpha_1\alpha_1'} + \mathrm{i}\sum_c \epsilon_{bac}\sigma^c_{\alpha_2'\alpha_1} \ ; \end{aligned} \tag{2.24}$$

therefore, the spin sum becomes

$$\begin{aligned}&\sum_{ab}\left(\delta_{ab}\delta_{\mu_1\mu_2'} + \mathrm{i}\sum_c \epsilon_{bac}\sigma^c_{\mu_2'\mu_1}\right)\left(\delta_{ab}\delta_{\alpha_1\alpha_2'} + \mathrm{i}\sum_d \epsilon_{bad}\sigma^d_{\alpha_2'\alpha_1}\right) \\ &= \sum_{ab}\left\{\delta_{ab}\delta_{\mu_1\mu_2'}\delta_{\alpha\alpha_2'} - \sum_{cd}\epsilon_{bac}\epsilon_{bad}\sigma^c_{\mu_2'\mu_1}\sigma^d_{\alpha_2'\alpha}\right\} \ , \end{aligned} \tag{2.25}$$

where ϵ_{ijk} are the Levi-Civita symbols which obey $\sum_{mn}\epsilon_{imn}\epsilon^{jmn} = 2\delta_{ij}$. This allows the simplification

$$\sum_{bac}\epsilon_{bac}\epsilon_{bad} = 2\delta^{cd} \ , \tag{2.26}$$

and thereupon, the spin sum reduces to

$$\begin{aligned}\mathcal{P}_{dir} &= 3\,\delta_{\mu_1\mu_2'}\delta_{\alpha_1\alpha_2'} - 2\sum_{cd}\delta_{cd}\sigma^c_{\mu_2'\mu_1}\sigma^d_{\alpha_2'\alpha_1} \\ &= 3\,\delta_{\mu_1\mu_2'}\delta_{\alpha_1\alpha_2'} - 2\,\boldsymbol{\sigma}_{\mu_2'\mu_1}\cdot\boldsymbol{\sigma}_{\alpha_2'\alpha_1} \ . \end{aligned} \tag{2.27}$$

2.6.2 Exchange diagram

The exchange RG diagram is depicted in Fig. 2.9.
The operator product plus contractions are

$$\mathcal{D}_{ex} = \frac{J^2}{2!}\sum_{\substack{\mathbf{k}_1,\mathbf{k}_1'\\ \mu_1\alpha_1\\ \mu_1'\alpha_1'}}\sum_{\substack{\mathbf{k}_2,\mathbf{k}_2'\\ \mu_2\alpha_2\\ \mu_2'\alpha_2'}} \overbrace{f^\dagger_{\mu_1'} f_{\mu_1}\,\boldsymbol{\sigma}_{\mu_1'\mu_1}\cdot\boldsymbol{\sigma}_{\alpha_1'\alpha_1}\,c^\dagger_{\mathbf{k}_1'\alpha_1'}c_{\mathbf{k}_1\alpha_1}\,f^\dagger_{\mu_2'}f_{\mu_2}\,\boldsymbol{\sigma}_{\mu_2'\mu_2}\cdot\boldsymbol{\sigma}_{\alpha_2'\alpha_2}\,c^\dagger_{\mathbf{k}_2'\alpha_2'}c_{\mathbf{k}_2\alpha_2}} \tag{2.28}$$

The overall sign of the diagram due to Wick ordering is +1.
Similar to the direction diagram, we can divide the expression into a spin summation and a

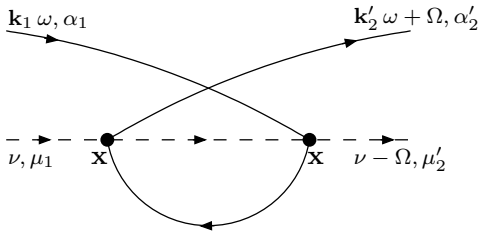

Figure 2.9: Exchange RG diagram for the single-impurity Kondo model.

summation over Green's functions.

Spin summation The spin summation can be performed using the algebra of Pauli matrices (Appendix A):

$$
\begin{aligned}
\mathcal{P}_{ex} &= \sum_{\mu_2\alpha_1} (\boldsymbol{\sigma}_{\mu_1'\mu_1}\cdot\boldsymbol{\sigma}_{\alpha_1'\alpha_1})(\boldsymbol{\sigma}_{\mu_2'\mu_2}\cdot\boldsymbol{\sigma}_{\alpha_2'\alpha_1}) \\
&\overset{\mu_1'=\mu_2,\alpha_2'=\alpha_1}{=\!=\!=} \sum_{ab}\sum_{\mu_2\alpha_1} (\sigma^b_{\mu_2'\mu_2}\sigma^a_{\mu_2\mu_1})(\sigma^a_{\alpha_1'\alpha_1}\sigma^b_{\alpha_1\alpha_2}) \\
&= \sum_{ab} (\sigma^b\sigma^a)_{\mu_2'\mu_1}(\sigma^a\sigma^b)_{\alpha_1'\alpha_2} \\
&= \sum_{ab}\left\{(\delta_{\mu_2'\mu_1}\delta_{ab} + \mathrm{i}\sum_c \epsilon_{bac}\sigma^c_{\mu_2'\mu_1})(\delta_{\alpha_1'\alpha_2}\delta_{ab} + \mathrm{i}\sum_d \epsilon_{abd}\sigma^d_{\alpha_1'\alpha_2})\right\} \\
&= \sum_{ab}\Big\{(\delta_{\mu_2'\mu_1}\delta_{ab}\delta_{\alpha_1'\alpha_2} + \underbrace{\mathrm{i}\,\delta_{ab}\delta_{\mu_2'\mu_1}\sum_d \epsilon_{abd}\sigma^d_{\alpha_1'\alpha_2}}_{=0} \\
&\quad + \underbrace{\mathrm{i}\,\delta_{ab}\delta_{\alpha_1'\alpha_2}\sum_c \epsilon_{bac}\sigma^c_{\mu_2'\mu_1}}_{=0} - \sum_{d,c}\epsilon^{bac}\epsilon_{abd}\sigma^c_{\mu_2'\mu_1}\sigma^d_{\alpha_1'\alpha_2})\Big\} \\
&= \sum_a \delta_{\mu_2'\mu_1}\delta_{\alpha_1'\alpha_2} - \sum_{d,c}\Big\{\sigma^c_{\mu_2'\mu_1}\sigma^d_{\alpha_1'\alpha_2}\underbrace{\sum_{a,b}\epsilon_{bac}\epsilon_{abd}}_{=-\sum_{ab}\epsilon_{abc}\epsilon_{abd}=-2\delta_{cd}}\Big\}\,.
\end{aligned}
\tag{2.29}
$$

Hence, the spin sum yields

$$
\begin{aligned}
\mathcal{P}_{ex} &= \sum_{a=x,y,z}\delta_{\mu_1\mu_2'}\delta_{\alpha_1'\alpha_2} + 2\sum_c \sigma^c_{\mu_2'\mu_1}\sigma^c_{\alpha_1'\alpha_2} \\
&= 3\,\delta_{\mu_1\mu_2'}\delta_{\alpha_1'\alpha_2} + 2\,\boldsymbol{\sigma}_{\mu_2'\mu_1}\cdot\boldsymbol{\sigma}_{\alpha_1'\alpha_2}
\end{aligned}
\tag{2.30}
$$

2.6.3 Diagrammatic parts

2.6.3.1 Direct diagram

The Green-function part of the direct diagram reads

$$\mathcal{D}_{dir} = \sum_{\mathbf{q}} \frac{1}{\beta} \sum_{\mathrm{i}\Omega = \mathrm{i}(2\mathbb{Z}+1)\frac{\pi}{\beta}} G_f(\mathrm{i}\omega + \mathrm{i}\nu - \mathrm{i}\Omega) G_c(\mathrm{i}\Omega_n) \ . \tag{2.31}$$

We perform the Matsubara summation over the frequencies, and drop the sum over the momentum $\mathbf{q}$ (which will be performed at the end). The branch cuts are at $z = \varepsilon \in \mathbb{R}$ and $z = \mathrm{i}\omega + \mathrm{i}\nu - \varepsilon$ (see a schematic depiction in Fig. 2.10); therefore,

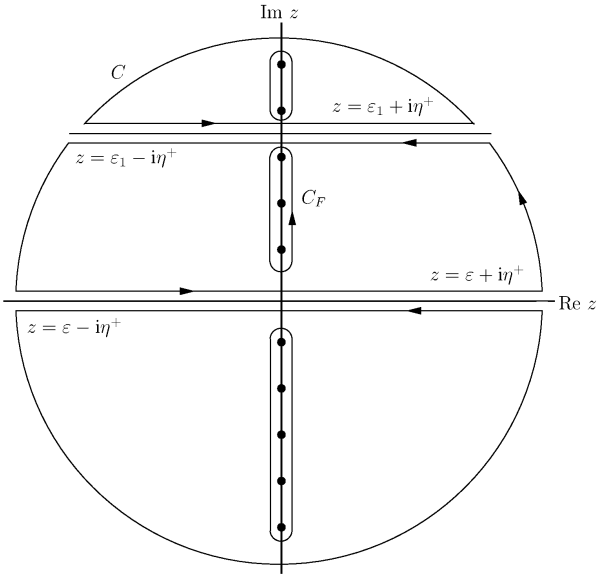

Figure 2.10: Branch cuts in a Matsubara summation (at $z = \varepsilon$ and $z = \varepsilon_1$). The contour C encompasses the whole comlex plane, and C_F is a contour around the fermionic Matsubara frequencies on the imaginary axis.

$$\frac{1}{\beta} \sum_{\mathrm{i}\Omega = \mathrm{i}(2\mathbb{Z}+1)\frac{\pi}{\beta}} G_f(\mathrm{i}\omega + \mathrm{i}\nu - \mathrm{i}\Omega_n) G_c(\mathrm{i}\Omega_n) = -\frac{1}{2\pi\mathrm{i}} \oint_{C_F} \mathrm{d}z \, n_F(z) \, G_f(\mathrm{i}\omega + \mathrm{i}\nu - z) G_c(z) \ , \tag{2.32}$$

where C_F is the contour around the fermionic Matsubara frequencies. Taking C to be a contour encompassing the whole complex plane, we obtain

$$\frac{1}{2\pi\mathrm{i}} \oint_{C} \mathrm{d}z \, n_F(z) G_f(\mathrm{i}\omega + \mathrm{i}\nu - z)) G_c(z) = 0 \ ; \tag{2.33}$$

thus,

$$\begin{aligned}
&\frac{1}{2\pi\mathrm{i}}\int_{-\infty}^{+\infty}\mathrm{d}\varepsilon\, n_F(\varepsilon)G_f(\mathrm{i}\omega+\mathrm{i}\nu-\varepsilon)[G_c(\varepsilon+\mathrm{i}\eta^+)-G_c(\varepsilon-\mathrm{i}\eta^+)]\\
&\quad+\frac{1}{2\pi\mathrm{i}}\int_{-\infty}^{+\infty}\mathrm{d}\varepsilon\, n_F(\underbrace{\mathrm{i}\omega+\mathrm{i}\nu-\varepsilon}_{\text{bosonic}})[G_f(\varepsilon-\mathrm{i}\eta^+)-G_f(\varepsilon+\mathrm{i}\eta^+)]G_c(\mathrm{i}\omega+\mathrm{i}\nu-\varepsilon)\\
&\quad-\frac{1}{2\pi\mathrm{i}}\oint_{C_F}\mathrm{d}z\, n_F(z)G_f(\mathrm{i}\omega+\mathrm{i}\nu-z)G_c(z)=0\ ;
\end{aligned}\tag{2.34}$$

therefore,

$$\begin{aligned}
\mathcal{D}_{dir}&=\frac{-1}{2\pi}\int_{-\infty}^{+\infty}\mathrm{d}\varepsilon\, n_F(\varepsilon)G_f(\mathrm{i}\omega+\mathrm{i}\nu-\varepsilon)[2\mathrm{Im}\,G_c^R(\varepsilon)]\\
&\quad-\frac{-1}{2\pi}\int_{-\infty}^{+\infty}\mathrm{d}\varepsilon\, n_F(-\varepsilon)[-2\mathrm{Im}\,G_f^R(\varepsilon)]G_c^R(\mathrm{i}\omega+\mathrm{i}\nu-\varepsilon)\\
&=\frac{1}{2\pi}\int\mathrm{d}\varepsilon\, n_F(\varepsilon)G_f(\mathrm{i}\omega+\mathrm{i}\nu-\varepsilon)A_c(\varepsilon)\\
&\quad-\frac{1}{2\pi}\int\mathrm{d}\varepsilon\, n_F(-\varepsilon)A_f(\varepsilon)G_c(\mathrm{i}\omega+\mathrm{i}\nu-\varepsilon)\ .
\end{aligned}\tag{2.35}$$

The 'retarded branch' of the vertex[22] which obtains via the transformations

$$\begin{aligned}
\mathrm{i}\nu&\mapsto\nu+\mathrm{i}\eta^+\\
\mathrm{i}\omega&\mapsto\omega+\mathrm{i}\eta^+\\
\mathrm{i}\Omega&\mapsto\Omega+\mathrm{i}\eta^+\ ,
\end{aligned}\tag{2.36}$$

that obtains

$$\begin{aligned}
\mathcal{D}_{dir}^R&=\frac{1}{2\pi}\int\mathrm{d}\varepsilon\, n_F(\varepsilon)G_f^R(\omega+\nu-\varepsilon)A_c(\varepsilon)\\
&=-\frac{1}{2\pi}\int\mathrm{d}\varepsilon\, n_F(-\varepsilon)A_f(\varepsilon)G_c^R(\omega+\nu-\varepsilon)\ .
\end{aligned}\tag{2.37}$$

One has to perform the transformation, $\nu\mapsto\nu+\lambda$, as in the Abrikosov's pseudo-particle method (Appendix C), so that

$$\begin{aligned}
\hat{\mathcal{D}}_{dir}^R&=\frac{1}{2\pi}\int\mathrm{d}\varepsilon\, n_F(\varepsilon)G_f^R(\omega+\nu-\varepsilon+\lambda)A_c(\varepsilon)\\
&\quad-\frac{1}{2\pi}\int\mathrm{d}\varepsilon\, n_F(-\varepsilon)A_f(\varepsilon)G_c^R(\omega+\nu-\varepsilon+\lambda)\ .
\end{aligned}\tag{2.38}$$

Furthermore, applying the transformation $\varepsilon\mapsto\varepsilon+\lambda$ yields

$$\begin{aligned}
\hat{\mathcal{D}}_{dir}^R&=\frac{1}{2\pi}\int\mathrm{d}\varepsilon\, n_F(\varepsilon)\hat{G}_f^R(\omega+\nu-\varepsilon)A_c(\varepsilon)\\
&\quad-\frac{1}{2\pi}\int\mathrm{d}\varepsilon\, n_F(-\varepsilon-\lambda)\hat{A}_f(\varepsilon)G_c^R(\omega+\nu-\varepsilon)\ ,
\end{aligned}\tag{2.39}$$

[22] For a detailed discussion of the analytical properties of the vertices, consult Ref. [120].

which allows the simplification

$$\lim_{\lambda\to\infty} n_F(-\varepsilon-\lambda) = \lim_{\lambda\to\infty} \frac{1}{e^{-\beta(\varepsilon+\lambda)}+1} = 1 \ .$$

Finally,

$$\hat{\mathcal{D}}^R_{dir} = \frac{1}{2\pi}\int \mathrm{d}\varepsilon\, n_F(\varepsilon)\hat{G}^R_f(\omega+\nu-\varepsilon)A_c(\varepsilon) - \frac{1}{2\pi}\int \mathrm{d}\varepsilon\, \hat{A}_f(\varepsilon)G^R_c(\omega+\nu-\varepsilon) \ . \tag{2.40}$$

Using the explicit expressions for the Green's functions,

$$\begin{aligned} G^R_c(\mathbf{k},\omega) &= \frac{1}{\omega-\xi_{\mathbf{k}}+\mathrm{i}\eta^+} \ , \\ \hat{G}^R_f(\omega) &= \frac{1}{\omega-\xi_d+\mathrm{i}\eta^+} \ , \end{aligned} \tag{2.41}$$

the previous expression becomes

$$\begin{aligned} \mathcal{D}^R_{dir} &= \frac{1}{2\pi}\int \mathrm{d}\varepsilon\, n_F(\varepsilon)\frac{1}{\omega+\nu-\varepsilon-\xi_d+\mathrm{i}\eta^+}\,2\pi\delta(\varepsilon-\xi_{\mathbf{q}}) \\ &\quad - \frac{1}{2\pi}\int \mathrm{d}\varepsilon\, 2\pi\delta(\varepsilon-\xi_d)\,\frac{1}{\omega+\nu-\varepsilon-\xi_{\mathbf{q}}+\mathrm{i}\eta^+} \\ &= \frac{n_F(\xi_{\mathbf{q}})-1}{\omega+\nu-\varepsilon_{\mathbf{q}}-\varepsilon_d+\mathrm{i}\eta^+} \ . \end{aligned} \tag{2.42}$$

2.6.3.2 Exchange diagram

The Green-function part of the exchange diagram reads

$$\mathcal{D}_{ex} = \sum_{\mathbf{q}} \frac{1}{\beta} \sum_{\mathrm{i}\Omega=\mathrm{i}(2\mathbb{Z}+1)\frac{\pi}{\beta}} G_f\left(\mathrm{i}\Omega+\mathrm{i}\nu-\mathrm{i}(\omega+\Omega_n)\right)\, G_c(\mathrm{i}\Omega_n) \tag{2.43}$$

We will perform the Matsubara summation over the frequencies, and drop the sum over the momentum $\mathbf{q}$ to be performed at the end. The branch cuts are at $z=\varepsilon\in\mathbb{R}$ and $z=\varepsilon+\mathrm{i}(\omega+\Omega)-\mathrm{i}\nu$ (see Fig. 2.10). Therefore,

$$\begin{aligned} \mathcal{D}_{ex} &= \frac{1}{\beta}\sum_{\mathrm{i}\Omega_n} G_f\left(\mathrm{i}\Omega+\mathrm{i}\nu-\mathrm{i}(\omega+\Omega_n)\right) G_c(\mathrm{i}\Omega_n) \\ &= -\frac{1}{2\pi\mathrm{i}}\oint \mathrm{d}z\, n_F(z)\, G_f\left(\mathrm{i}\Omega+\mathrm{i}\nu-\mathrm{i}\omega-z\right) G_c(z) \end{aligned} \tag{2.44}$$

Using the contours in the complex plain (analogous to the direct case), one obtains

$$0 = \frac{1}{2\pi\mathrm{i}}\oint_C \mathrm{d}z\, n_F(z)G_f(z+\mathrm{i}\nu-\mathrm{i}(\omega+\Omega))G_c(z) \ ; \tag{2.45}$$

hence,

$$\frac{1}{2\pi\mathrm{i}}\int_{-\infty}^{+\infty} n_F(\varepsilon)G_f(\varepsilon+\mathrm{i}\nu-\mathrm{i}(\omega+\Omega))[G_c(\varepsilon+\mathrm{i}\eta^+)-G_c(\varepsilon-\mathrm{i}\eta^+)]$$
$$+\frac{1}{2\pi\mathrm{i}}\int_{-\infty}^{+\infty} n_F(\underbrace{\varepsilon+\mathrm{i}(\omega+\Omega)-\mathrm{i}\nu}_{\text{bosonic}})[G_f(\varepsilon+\mathrm{i}\eta^+)-G_c(\varepsilon-\mathrm{i}\eta^+)]G_c(\varepsilon+\mathrm{i}(\omega+\Omega)-\mathrm{i}\nu)$$
$$-\frac{1}{2\pi\mathrm{i}}\oint_{C_F}\mathrm{d}z\, n_F(z)G_f(\varepsilon+\mathrm{i}\nu-\mathrm{i}(\omega+\Omega))G_c(z)=0\ . \tag{2.46}$$

Therefore,

$$\mathcal{D}_{ex}=-\frac{1}{2\pi}\int_{-\infty}^{+\infty}\mathrm{d}\varepsilon\, n_F(\varepsilon)G_f(\varepsilon+\mathrm{i}\nu-\mathrm{i}(\omega+\Omega))[-A_c(\varepsilon)]$$
$$-\frac{1}{2\pi}\int\mathrm{d}\varepsilon\, n_F(\varepsilon)[-A_f(\varepsilon)]G_c(\varepsilon+\mathrm{i}(\omega+\Omega)-\mathrm{i}\nu)\ . \tag{2.47}$$

The 'retarded branch' of the diagram[23] is obtained from the transformations

$$\begin{aligned}\mathrm{i}\omega&\mapsto\omega+\mathrm{i}\eta^+\\ \mathrm{i}\nu&\mapsto\nu+\mathrm{i}\eta^+\\ \mathrm{i}\Omega&\mapsto\Omega+\mathrm{i}\eta^+\ ,\end{aligned} \tag{2.48}$$

so that

$$\mathcal{D}^R_{ex}=\frac{1}{2\pi}\int\mathrm{d}\varepsilon\, n_F(\varepsilon)G^A_f(\varepsilon+\nu-(\omega+\Omega))A_c(\varepsilon)$$
$$+\frac{1}{2\pi}\int\mathrm{d}\varepsilon\, A_f(\varepsilon)G^R_c(\varepsilon+\omega+\Omega-\nu)\ . \tag{2.49}$$

As in Abrikosov's pseudo-particle method (Appendix C), the transformation $\nu\mapsto\nu+\lambda$ yields

$$\hat{\mathcal{D}}^R_{ex}=\frac{1}{2\pi}\int\mathrm{d}\varepsilon\, n_F(\varepsilon)G^A_f(\varepsilon+\nu+\lambda-(\omega+\Omega))A_c(\varepsilon)$$
$$+\frac{1}{2\pi}\int\mathrm{d}\varepsilon\, n_F(\varepsilon)A_f(\varepsilon)G^R_c(\varepsilon+\omega+\Omega-\nu-\lambda)\ . \tag{2.50}$$

Using the mapping $\varepsilon\mapsto\varepsilon+\lambda$, the expression becomes

$$\hat{\mathcal{D}}^R_{ex}=\frac{1}{2\pi}\int\mathrm{d}\varepsilon\, n_F(\varepsilon)\hat{G}^A_f(\varepsilon+\nu-(\omega+\Omega))A_c(\varepsilon)$$
$$+\frac{1}{2\pi}\int\mathrm{d}\varepsilon\, n_F(\varepsilon+\lambda)\hat{A}_f(\varepsilon)G^R_c(\varepsilon+\omega+\Omega-\nu)\ , \tag{2.51}$$

which allows the simplification

$$\lim_{\lambda\to+\infty} n_F(\varepsilon+\lambda)=\lim_{\lambda\to+\infty} e^{-\beta\lambda}=0\ ,$$

[23] For a detailed discussion of the analytical properties of the vertices, consult Ref. [120].

so that

$$\hat{\mathcal{D}}^R_{ex} = \frac{1}{2\pi}\int \mathrm{d}\varepsilon\, n_F(\varepsilon)\hat{G}^A_f(\varepsilon+\nu-(\omega+\Omega))A_c(\varepsilon)\ . \tag{2.52}$$

Using the explicit expressions for the Green's functions as above, Eq. (2.41), one finds

$$\begin{aligned}\hat{\mathcal{D}}^R_{ex} &= \frac{1}{2\pi}\int \mathrm{d}\varepsilon\, n_F(\varepsilon)\frac{1}{\varepsilon+\nu-(\omega+\Omega)-\xi_d-\mathrm{i}\eta^+}\,2\pi\delta(\varepsilon-\xi_{\mathbf{q}}) \\ &= \frac{n_F(\xi_{\mathbf{q}})}{\xi_{\mathbf{q}}+\nu-(\omega+\Omega)-\xi_d-\mathrm{i}\eta^+}\ .\end{aligned} \tag{2.53}$$

2.6.4 RG contributions in one-loop order

Putting together the pieces, one obtains the contributions of the direct and exchange RG diagrams,

$$\begin{aligned}\hat{\mathcal{D}}^R_{dir} &= \underbrace{(-2)}_{\text{spin sum}}\ \underbrace{(+1)}_{\text{Wick ordering}}\ \frac{J^2}{2!}\frac{1}{V}\sum_{\mathbf{q}}\frac{1-n_F(\xi_{\mathbf{q}})}{\xi_{\mathbf{q}}-(\omega+\nu-\xi_d+\mathrm{i}\eta^+)} \\ \hat{\mathcal{D}}^R_{ex} &= \underbrace{(+2)}_{\text{spin sum}}\ \underbrace{(+1)}_{\text{Wick ordering}}\ \frac{J^2}{2!}\frac{1}{V}\sum_{\mathbf{q}}\frac{n_F(\xi_{\mathbf{q}})}{\xi_{\mathbf{q}}-(\omega+\Omega-\nu+\xi_d+\mathrm{i}\eta^+)}\ ;\end{aligned} \tag{2.54}$$

hence, the one-loop RG contribution to the Kondo vertex will be

$$\delta J = -J^2\frac{1}{V}\sum_{\mathbf{q}}\left\{\frac{1-n_F(\xi_{\mathbf{q}})}{\xi_{\mathbf{q}}-(\omega+\nu-\xi_d+\mathrm{i}\eta^+)}-\frac{n_F(\xi_{\mathbf{q}})}{\xi_{\mathbf{q}}-(\omega+\Omega-\nu+\xi_d+\mathrm{i}\eta^+)}\right\} \tag{2.55}$$

At low temperatures, $T\to 0^+$, for conduction electrons on the Fermi surface, $\omega \stackrel{!}{=} 0$ [24], assuming a very small 'frequency exchange', $\Omega \stackrel{!}{=} 0$, and neglecting the imaginary parts of the Green's functions[25], with a 'wide-band' density-of-states (per spin per volume),

$$\mathcal{N}(\xi) = \mathcal{N}(\varepsilon_F)\Theta(D-|\xi|)\ , \tag{2.56}$$

[24] Note that the Schrödinger equation,

$$\mathrm{i}\frac{\mathrm{d}}{\mathrm{d}t}|\psi\rangle = H|\psi\rangle\ ,$$

for a single-particle eigen-state $|\psi_k\rangle$ becomes

$$\omega\,|\psi_k\rangle = H|\psi_k\rangle = (\varepsilon_k-\mu)|\psi_k\rangle\ ,$$

in frequency representation. One observes that, via the identification

$$\omega+\mu \stackrel{!}{=} \varepsilon_k\ ,$$

the frequency, ω, can be understood as the excitation energy of the particle above the chemical potential which for electrons, will be the excitation energy above the Fermi level.

[25] Notice that energy dissipation is proportional to the imaginary part of the susceptibility which vanishes linearly near the Fermi surface.

one obtains

$$\delta J = -J^2 \int_{-\infty}^{+\infty} \mathrm{d}\xi\, \mathcal{N}(\xi) \left(\frac{1 - n_F(\xi)}{\xi - \underbrace{(\nu - \xi_d)}_{:=\bar{\nu}}} - \frac{n_F(\xi)}{\xi + (\nu - \xi_d)} \right) . \tag{2.57}$$

Changing the variable $\xi \mapsto -\xi$ in the second term on RHS, leads to

$$\begin{aligned} \delta J &= -J^2 \mathcal{N}(\varepsilon_F) \int_{-D}^{+D} \mathrm{d}\xi\, \frac{1 - n_F(\xi) + n_F(-\xi)}{\xi - \bar{\nu}} \\ &= -J^2 \mathcal{N}(\varepsilon_F) \int_{-D}^{+D} \mathrm{d}\xi\, \frac{2 n_F(-\xi)}{\xi - \bar{\nu}} , \end{aligned} \tag{2.58}$$

where, in the last line, we have used

$$\begin{aligned} n_\zeta(-z) &= -(\zeta + n_\zeta(z)) \quad \text{with } \zeta = \pm 1 \text{ for bosons/fermions} \\ \rightarrow n_F(-z) &= 1 - n_F(z) . \end{aligned} \tag{2.59}$$

Note that the Fermi-Dirac distribution function can be re-written in terms of tanh function,

$$\begin{aligned} n_F(z) &= \frac{1}{2}(1 - \tanh(\frac{\beta z}{2})) , \\ n_F(-z) &= \frac{1}{2}(1 + \tanh(\frac{\beta z}{2})) , \end{aligned} \tag{2.60}$$

and the tanh function can be approximayed as

$$\tanh(\frac{\beta\xi}{2}) \approx \begin{cases} -1, & \xi < -2T \\ \beta\frac{\xi}{2}, & -2T \leq \xi \leq 2T \\ +1, & \xi > 2T \end{cases} ,$$

to obtain

$$\begin{aligned} \delta J &= -J^2 \mathcal{N}(\varepsilon_F) \Big\{ \underbrace{\int_{-D}^{-2T} \mathrm{d}\xi\, \frac{1-1}{\xi - \bar{\nu}}}_{=0} + \int_{-2T}^{+2T} \mathrm{d}\xi\, \frac{\beta\xi/2}{\xi - \bar{\nu}} + \int_{2T}^{+D} \mathrm{d}\xi\, \frac{1+1}{\xi - \bar{\nu}} \Big\} \\ &= -J^2 \mathcal{N}(\varepsilon_F) \Big\{ 2 + \frac{\beta}{2}\bar{\nu} \ln|\frac{2T - \bar{\nu}}{2T + \bar{\nu}}| + 2\ln|\frac{D - \bar{\nu}}{2T - \bar{\nu}}| \Big\} \end{aligned} \tag{2.61}$$

2.6.5 RG flow equations for the single-impurity Kondo problem

The RG flow equations are obtained from the relation

$$\frac{\partial J}{\partial \ln D} = \beta(J) , \tag{2.62}$$

which describes the change in the coupling J as the energy cut-off D (here, the electronic bandwidth) is reduced. For the single-impurity Kondo model,

$$\frac{\partial J}{\partial \ln D} = -2J^2\mathcal{N}(\varepsilon_F)\left(\frac{\partial}{\partial \ln D}\ln|D-\bar{\nu}|\right) . \tag{2.63}$$

Using the relation[26]

$$\frac{\partial}{\partial \ln D}\ln|D-\bar{\nu}| = 1+\frac{\bar{\nu}}{D}+\mathcal{O}\left((\frac{\bar{\nu}}{D})^2\right) \quad ; \quad \frac{\bar{\nu}}{D} \ll 1 ,$$

one obtains

$$\frac{\partial J}{\partial \ln D} = -2\mathcal{N}(\varepsilon_F)J^2 + \mathcal{O}(\frac{\bar{\nu}}{D}) . \tag{2.65}$$

By defining the *dimensionless* coupling,

$$g := \mathcal{N}(\varepsilon_F)J , \tag{2.66}$$

one can re-write the flow equation as

$$\frac{\partial g}{\partial \ln D} = -2\,g^2 \Rightarrow -\frac{\partial g}{g^2} = 2\,\partial \ln D ; \tag{2.67}$$

the Kondo temperature is obtained as

$$\begin{aligned} &\frac{1}{g}\Big|_{g=g_0}^{\infty} = 2\ln D\Big|_{D=D_0}^{T_K} \\ &\Rightarrow -\frac{1}{g_0} = 2\ln(\frac{T_K}{D}) \rightarrow \ln(\frac{T_K}{D_0}) = -\frac{1}{2g_0} \\ &\rightarrow \frac{T_K}{D_0} = \exp[-\frac{1}{2g_0}] \equiv \exp[-\frac{1}{2\mathcal{N}(\varepsilon_F)J}] . \end{aligned} \tag{2.68}$$

It is important to recognize the role of the spin algebra and the Fermi surface in producing the Kondo effect.

---

[26] Notice that

$$\frac{\partial}{\partial \ln D}\ln|D-\bar{\nu}| = \frac{\partial}{\partial \ln D}\ln|D(1-\frac{\bar{\nu}}{D})| = \frac{\partial}{\partial \ln D}(\ln D + \ln|1-\frac{\bar{\nu}}{D}|) .$$

Define $x := \frac{\bar{\nu}}{D}$ so that $\frac{x}{\ln D} = -\frac{\bar{\nu}}{D} = -x$; therefore,

$$\begin{aligned} \frac{\partial}{\partial \ln D}\ln|1-\frac{\bar{\nu}}{D}| &= \frac{\partial x}{\partial \ln D}\frac{\partial}{\partial x}\ln|1-x| \\ &= \underbrace{-x\frac{\partial}{\partial x}\ln|1-x|}_{\sim\mathcal{O}(x)} = \frac{x}{1-x} \overset{x\ll 1}{=} x\,(1+x+\cdots) \\ &= x+\mathcal{O}(x^2) . \end{aligned} \tag{2.64}$$

2.6.5.1 Applying the Leibniz integral rule

One can obtain the RG flow equation *without* performing the last integrations on ξ, Eq. (2.58), since what we ultimately need is the result of the differentiation $\frac{\partial}{\partial \ln D}$ to determine the flow equation, Eq. (2.62). Therefore, one can use the *Leibniz integral rule* (Appendix H):

When

$$F(x) = \int^x \mathrm{d}t\, f(t) \ ,$$

i.e., if $F(x)$ is the anti-derivative of f, then

$$\frac{\partial}{\partial D}\left(\int_{-D}^{D} \mathrm{d}\varepsilon\, f(\varepsilon)\right) = \frac{\partial}{\partial D}\Big(F(D) - F(-D)\Big) = f(D) - (-f(-D)) = f(D) + f(-D) \ ,$$

where we have used

$$\begin{aligned} \frac{\partial}{\partial D}F(D) &= \frac{\partial}{\partial x}F(x)\Big|_{x=D} = f(x)\Big|_{x=D} = f(D) \\ \frac{\partial}{\partial D}F(-D) &= \frac{\partial(-D)}{\partial D}\frac{\partial F(x)}{\partial x}\Big|_{x=-D} = -f(x)\Big|_{x=-D} = -f(-D) \ . \end{aligned} \tag{2.69}$$

Therefore,

$$\frac{\partial}{\partial D}\left(\int_{-D}^{D} \mathrm{d}\varepsilon\, f(\varepsilon)\right) \equiv D\frac{\partial}{\partial D}\left(\int_{-D}^{D} \mathrm{d}\varepsilon\, f(\varepsilon)\right) = D(f(D) + f(-D)) \ . \tag{2.70}$$

Now, using the above result for δJ, Eq. (2.58), one obtains

$$\frac{dJ}{d\ln D} = -\mathcal{N}(\varepsilon_F)J^2\frac{\partial}{\partial \ln D}\left(\int_{-D}^{D} \mathrm{d}\varepsilon\, \frac{2n_F(-\xi)}{\xi - \bar{\nu}}\right) = D\left(\frac{2n_F(-D)}{D-\bar{\nu}} + \frac{2n_F(D)}{-D-\bar{\nu}}\right) \ . \tag{2.71}$$

At low temperatures, the fact that $D \gg T \equiv \beta D \gg 1$ provides the simplifications

$$\begin{aligned} n_F(D) &= \frac{1}{e^{\beta D}+1} \to 0 \\ n_F(-D) &= \frac{1}{e^{-\beta D}+1} \to 1 \ , \end{aligned}$$

and finally, the RG flow is obtained as

$$\begin{aligned} \frac{\partial J}{\partial \ln D} &= -2\mathcal{N}(\varepsilon_F)J^2\frac{D}{D-\bar{\nu}} \\ &= -2\mathcal{N}(\varepsilon_F)J^2\frac{1}{1-\bar{\nu}/D} = -2\mathcal{N}(\varepsilon_F)J^2\left(1 + \mathcal{O}(\frac{\bar{\nu}}{D})\right) \\ &= -2\mathcal{N}(\varepsilon_F)J^2 \ , \end{aligned} \tag{2.72}$$

which is the same as the equation obtained before, Eq. (2.65).

2.6.5.2 Effect of the imaginary parts of the Green's functions

In this section, we provide the simplest justification for neglecting the imaginary parts of the Green's functions in the previous RG analysis. At low temperatures, and in the wide-band limit with a conduction electron density-of-states (per spin per volume) as before,

$$\mathcal{N}(\xi) = \mathcal{N}(\varepsilon_F)\Theta(D - |\xi|) \ ,$$

the renormalization to the Kondo vertex, explicitly including the imaginary parts of the Green's functions, will be

$$\begin{aligned}
\delta J &= -J^2\mathcal{N}(\varepsilon_F)\int_{-D}^{D} \mathrm{d}\xi \ \Big(\frac{1-n_F(\xi)}{\xi - (\omega+\nu-\xi_d+\mathrm{i}\eta^+)} - \frac{n_F(\xi)}{\xi-(\omega+\Omega-\nu+\xi_d+\mathrm{i}\eta^+)}\Big) \\
&= -J^2\mathcal{N}(\varepsilon_F)\int_{-D}^{D} \mathrm{d}\xi \ \Big(\frac{1-n_F(\xi)}{\xi - (\omega+\nu-\xi_d)} - \frac{n_F(\xi)}{\xi-(\omega+\Omega-\nu+\xi_d)}\Big) \\
&- \mathrm{i}\pi J^2\mathcal{N}(\varepsilon_F)\int_{-D}^{D} \mathrm{d}\xi \ \Big([1-n_F(\xi)]\delta(\omega+\nu-\xi_d-\xi) - n_F(\xi)\delta(\omega+\Omega-\nu+\xi_d-\xi)\Big) \ .
\end{aligned} \tag{2.73}$$

Therefore, using the Leibniz integral rule (section 2.6.5.1),

$$\begin{aligned}
\frac{\partial J}{\partial \ln D} &= -J^2\mathcal{N}(\varepsilon_F)\, D\Big(\frac{1-n_F(D)}{D-(\omega+\nu-\xi_d)} - \frac{n_F(D)}{D-(\omega+\Omega-\nu+\xi_d)} \\
&+ \frac{1-n_F(-D)}{-D-(\omega+\nu-\xi_d)} - \frac{n_F(-D)}{-D-(\omega+\Omega-\nu+\xi_d)}\Big) \\
&- \mathrm{i}\pi J^2\mathcal{N}(\varepsilon_F)\, D\Big([1-n_F(D)]\delta(\omega+\nu-\xi_d) - n_F(D)\delta(\omega+\Omega-\nu+\xi_d-D) \\
&+ [1-n_F(-D)]\delta(\omega+\nu-\xi_d+D) - n_F(-D)\delta(\omega+\Omega-\nu+\xi_d+D)\Big) \ .
\end{aligned} \tag{2.74}$$

Since D is the largest energy scale in the problem (or the high-energy cut-off),

$$\begin{aligned}
&D \gg |\omega|, |\nu|, |\xi_d|, |\Omega| \ , \\
&D \gg T \equiv \beta D \gg 1 \ ,
\end{aligned} \tag{2.75}$$

and

$$n_F(D) \to 0 \quad n_F(-D) \to 1 \ ,$$

so that

$$\begin{aligned}
\frac{\partial J}{\partial \ln D} &= -J^2\mathcal{N}(\varepsilon_F)\, D\Big(\frac{1}{D-(\omega+\nu-\xi_d)} - \frac{1}{-D-(\omega+\Omega-\nu+\xi_d)}\Big) \\
&- \mathrm{i}\pi J^2\mathcal{N}(\varepsilon_F)\, D\Big(-\delta(\omega+\Omega-\nu+\xi_d+D)\Big) \\
&= -J^2\mathcal{N}(\varepsilon_F)\Big\{\frac{1}{1-(\frac{\omega+\nu-\xi_d}{D})} + \frac{1}{1+(\frac{\omega+\Omega-\nu+\xi_d}{D})}\Big\} \\
&+ \mathrm{i}\pi J^2\mathcal{N}(\varepsilon_F)\,\delta(1+\frac{\omega+\Omega-\nu+\xi_d}{D}) \ .
\end{aligned} \tag{2.76}$$

The δ-function on the RHS will be non-vanishing only if $\omega + \Omega - \nu + \xi_d = D$, which contradicts our assumption that D is the largest energy-scale in the problem, Eq. (2.75). Thus, the imaginary part vanishes when the frequencies and energies are lying *inside* the reduced band and are not close to the edges — which always holds true in the present work. Therefore,

$$\begin{aligned}\frac{\partial J}{\partial \ln D} &= -\mathcal{N}(\varepsilon_F)\, J^2 \left\{1 + \frac{\omega+\nu-\xi_d}{D} + 1 - \frac{\omega+\Omega-\nu+\xi_d}{D} + \mathcal{O}(\frac{1}{D^2})\right\} \\ &= -2\mathcal{N}(\varepsilon_F) J^2 \left(1 + \frac{\nu - \xi_d - \Omega/2}{D}\right) + \mathcal{O}(\frac{1}{D^2}) \ . \end{aligned} \tag{2.77}$$

The main contribution to $G_f(\nu)$ comes from the 'on-shell' value of ν; i.e., $\nu \approx \xi_d$; therefore,

$$\frac{\nu - \xi_d - \Omega/2}{D} \approx -\frac{\Omega}{2D} \approx -\frac{\Omega}{D} \ ,$$

and

$$\frac{\partial J}{\partial \ln D} = -2\,\mathcal{N}(\varepsilon_F)\, J^2\, (1 - \frac{\Omega}{D}) \ , \tag{2.78}$$

which is the flow equation obtained previously, Eq. (2.65), if we neglect the term $\mathcal{O}(\frac{\Omega}{D})$.

2.6.6 RG flow equations in position representation

To prepare for the multi-impurity RG analysis in the following chapters, we provide a derivation of the RG flow equation using the Green's functions in *position* representation.

The one-loop diagrams are the same as before (the 'direct' and 'exchange' RG diagrams), but they are evaluated in position representation (the direct space) instead of the momentum representation (the reciprocal space). The spin summations remain the same as before, and will not be repeated here.

The direct RG diagram yields (see Figs. 2.8 and 2.9)[27]

$$\begin{aligned}\hat{\mathcal{D}}^R_{dir} &= \frac{1}{2\pi}\int \mathrm{d}\varepsilon \left\{ n_F(\varepsilon)\hat{G}^R_f(\omega+\nu-\varepsilon)A_c(\varepsilon) - A_f(\varepsilon)G^R_c(\omega+\nu-\varepsilon)\right\} \\ &\overset{\text{Re}+\text{Im}}{=} \frac{1}{2\pi}\int \mathrm{d}\varepsilon \left\{ n_F(\varepsilon)\hat{G}^{R\prime}_f(\omega+\nu-\varepsilon)A_c(\varepsilon) - \hat{A}_f(\varepsilon)G^{R\prime}_c(\omega+\nu-\varepsilon)\right\} \\ &\quad + \frac{\mathrm{i}}{2\pi}\int \mathrm{d}\varepsilon \left\{ n_F(\varepsilon)\hat{G}^{R\prime\prime}_f(\omega+\nu-\varepsilon)A_c(\varepsilon) - \hat{A}_f(\varepsilon)G^{R\prime\prime}_c(\omega+\nu-\varepsilon)\right\} . \end{aligned} \tag{2.79}$$

The exchange diagram yields

$$\begin{aligned}\hat{\mathcal{D}}^R_{ex} &= \frac{1}{2\pi}\int \mathrm{d}\varepsilon\, n_F(\varepsilon)\hat{G}^A_f(\varepsilon+\nu-(\omega+\Omega))A_c(\varepsilon) \\ &\overset{\text{Re}+\text{Im}}{=} \frac{1}{2\pi}\int \mathrm{d}\varepsilon\, n_F(\varepsilon)\hat{G}^{A\prime}_f(\varepsilon+\nu-(\omega+\Omega))A_c(\varepsilon) \\ &\quad + \frac{\mathrm{i}}{2\pi}\int \mathrm{d}\varepsilon\, n_F(\varepsilon)\hat{G}^{A\prime\prime}_f(\varepsilon+\nu-(\omega+\Omega))A_c(\varepsilon) \ . \end{aligned} \tag{2.80}$$

[27] The Green's functions are local (at the position of the impurity), so position dependence is dropped. The symbol 'Re+Im' denotes a decomposition into real and imaginary parts.

Defining

$$\begin{aligned}\bar{\omega} &:= \omega + \nu \ , \\ \bar{\nu} &:= \omega + \Omega - \nu \ ,\end{aligned} \tag{2.81}$$

to simplify the notation and adding the factors from spin sums (as derived before in section 2.6.4), one obtains

$$\begin{aligned}\delta J &= -2\,\frac{J^2}{2!}\hat{\mathcal{D}}^R_{dir} + 2\,\frac{J^2}{2!}\hat{\mathcal{D}}^R_{ex} = -J^2(\hat{\mathcal{D}}^R_{dir} - \hat{\mathcal{D}}^R_{ex}) \\ &= -J^2\Big(\frac{1}{2\pi}\int \mathrm{d}\varepsilon\,\Big\{n_F(\varepsilon)\hat{G}^{R\prime}_f(\bar{\omega}-\varepsilon)A_c(\varepsilon) - \hat{A}_f(\varepsilon)G^{R\prime}_c(\bar{\omega}-\varepsilon) - n_F(\varepsilon)\hat{G}^{A\prime}_f(\varepsilon-\bar{\nu})A_c(\varepsilon)\Big\} \\ &+ \frac{\mathrm{i}}{2\pi}\int \mathrm{d}\varepsilon\,\Big\{n_F(\varepsilon)\hat{G}^{R\prime\prime}_f(\bar{\omega}-\varepsilon)A_c(\varepsilon) - \hat{A}_f(\varepsilon)G^{R\prime\prime}_c(\bar{\omega}-\varepsilon) - n_F(\varepsilon)\hat{G}^{A\prime\prime}_f(\varepsilon-\bar{\nu})A_c(\varepsilon)\Big\}\Big) \\ &=: -J^2\,\left(\int \mathrm{d}\varepsilon\, g_1(\varepsilon) + \mathrm{i}\int \mathrm{d}\varepsilon\, g_2(\varepsilon)\right)\ .\end{aligned} \tag{2.82}$$

Using the Leibniz integral rule (section 2.6.5.1),

$$\frac{\partial J}{\partial \ln D} = -J^2\,D\Big(g_1(D) + g_1(-D) + \mathrm{i}\,(g_2(D) + g_2(-D))\Big)\ . \tag{2.83}$$

The expression involving g_1 is explicitly obtained as

$$\begin{aligned}g_1(D) + g_1(-D) = \frac{1}{2\pi}\Big[&n_F(D)\hat{G}^{R\prime}_f(\bar{\omega}-D)A_c(D) - \hat{A}_f(D)G^{R\prime}_c(\bar{\omega}-D) \\ &- n_F(D)\hat{G}^{A\prime}_f(D-\bar{\nu})A_c(D) \\ &+ n_F(-D)\hat{G}^{R\prime}_f(\bar{\omega}+D)A_c(D) - \hat{A}_f(D)G^{R\prime}_c(\bar{\omega}+D) \\ &- n_F(-D)\hat{G}^{A\prime}_f(-D-\bar{\nu})A_c(-D)\Big] \\ \overset{\beta D\gg 1}{=}\ &\frac{1}{2\pi}\Big[-\hat{A}_f(D)G^{R\prime}_c(\bar{\omega}-D) + \hat{G}^{R\prime}_f(\bar{\omega}+D)A_c(D) \\ &- \hat{A}_f(D)G^{R\prime}_c(\bar{\omega}+D) - G^{A\prime}_f(-D-\bar{\nu})A_c(-D)\Big]\ ;\end{aligned} \tag{2.84}$$

in the last line, we have used

$$\begin{aligned}n_F(D) &\overset{\beta D\gg 1}{\to} 0\ , \\ n_F(-D) &\overset{\beta D\gg 1}{\to} 1\ .\end{aligned} \tag{2.85}$$

Inserting the explicit expressions for G_c and $\hat{G}_f$, Eq. (2.41), we obtain

$$\hat{G}_f(\mathbf{x}-\mathbf{x},\nu) = \hat{G}_f(\mathbf{x}=0,\nu) = \frac{1}{V}\sum_{\mathbf{k}} \underbrace{\hat{G}_f(\mathbf{k},\nu)}_{=\hat{G}_f(\nu)\ :\ \text{no } \mathbf{k}\text{-dependence}} e^{\mathrm{i}\mathbf{k}\cdot(\mathbf{x}-\mathbf{x})} = \hat{G}_f(\nu)\delta_{\mathbf{x},\mathbf{x}} = \hat{G}_f(\nu)\ ;$$

$$\hat{A}_f(\nu) = 2\,\mathrm{Im}\,\hat{G}_f^A(\nu) = 2\pi\,\delta(\nu-\xi_d)\ ;$$

$$\begin{aligned}\hat{G}_c^{R,A}(\mathbf{x}-\mathbf{x},\omega) &= \frac{1}{V}\sum_{\mathbf{k}}\frac{1}{\omega-\xi_{\mathbf{k}}\pm\mathrm{i}\eta^+}e^{\mathrm{i}\mathbf{k}\cdot(\mathbf{x}-\mathbf{x})} = \int_{-\infty}^{+\infty}\mathrm{d}\xi\,\mathcal{N}(\xi)\frac{1}{\omega-\xi\pm\mathrm{i}\eta^+}\\ &= \mathcal{N}(\varepsilon_F)\int_{-D}^{+D}\mathrm{d}\xi\,\frac{1}{\omega-\xi}\mp\mathrm{i}\pi\mathcal{N}(\varepsilon_F) = \mathcal{N}(\varepsilon_F)\ln\left[\frac{1+\frac{\omega}{D}}{1-\frac{\omega}{D}}\right]\mp\mathrm{i}\pi\mathcal{N}(\varepsilon_F)\ . \quad (2.86)\end{aligned}$$

Notice that all the Green's functions above are 'local' in position representation. Therefore,

$$\begin{aligned}g_1(D)+g_1(-D) = \frac{1}{2\pi}\Big(&-2\pi\delta(D-\xi_d)\mathcal{N}(\varepsilon_F)\ln\left[1+\frac{\bar{\omega}-D}{D}\right]\\ &+\frac{2\pi\mathcal{N}(\varepsilon_F)}{\bar{\omega}+D-\xi_d}\\ &-2\pi\delta(D-\xi_d)\mathcal{N}(\varepsilon_F)\ln\left[\frac{1+\frac{\bar{\omega}+D}{D}}{1-\frac{\bar{\omega}+D}{D}}\right]\\ &-\frac{2\pi\mathcal{N}(\varepsilon_F)}{-D-\bar{\nu}-\xi_d}\Big)\ . \quad (2.87)\end{aligned}$$

Using the fact that

$$\xi_d \ll D \rightarrow \delta(D-\xi_d) = 0\ ,$$

one obtains

$$\begin{aligned}g_1(D)+g_1(-D) &= \frac{\mathcal{N}(\varepsilon_F)}{\bar{\omega}+D-\xi_d}+\frac{\mathcal{N}(\varepsilon_F)}{D+\bar{\nu}+\xi_d}\\ &= \frac{\mathcal{N}(\varepsilon_F)}{D}\Big[\frac{1}{1+\frac{\bar{\omega}-\xi_d}{D}}+\frac{1}{1+\frac{\bar{\nu}+\xi_d}{D}}\Big]\\ &= 2\frac{\mathcal{N}(\varepsilon_F)}{D}+\mathcal{O}(\frac{\varepsilon}{D})\ , \quad (2.88)\end{aligned}$$

where in the last line, ε can be ν, ω, or Ω; that is, smaller energy scales. Analogous steps for

the expression including g_2 yields

$$\begin{aligned}
g_2(D) + g_2(-D) = \frac{1}{2\pi}\Big[& n_F(D)\hat{G}_f^{R\prime\prime}(\bar{\omega}-D)A_c(D) - \hat{A}_f(D)G_c^{R\prime\prime}(\bar{\omega}-D) \\
& - n_F(D)\hat{G}_f^{A\prime\prime}(D-\bar{\nu})A_c(D) \\
& + n_F(-D)\hat{G}_f^{R\prime\prime}(\bar{\omega}+D)A_c(-D) - \hat{A}_f(-D)G_c^{R\prime\prime}(\bar{\omega}+D) \\
& - n_F(-D)\hat{G}_f^{A\prime\prime}(-D-\bar{\nu})A_c(-D)\Big] \\
= \frac{1}{2\pi}\Big[& - \hat{A}_f(D)G_c^{R\prime\prime}(\bar{\omega}-D) \\
& - \hat{G}_f^{R\prime\prime}(\bar{\omega}+D)A_c(-D) - \hat{A}_f(-D)G_c^{R\prime\prime}(\bar{\omega}+D) \\
& - \hat{G}_f^{A\prime\prime}(-D-\bar{\nu})A_c(-D)\Big] \\
= \frac{1}{2\pi}\Big[& - 2\pi\delta(D-\xi_d)G_c^{R\prime\prime}(\bar{\omega}-D) \\
& - \pi\delta(\bar{\omega}+D-\xi_d)2\pi\mathcal{N}(\varepsilon_F) - \delta(-D-\xi_d)(-\pi\mathcal{N}(\varepsilon_F)) \\
& - 2\pi\delta(-D-\bar{\nu}-\xi_d)2\pi\mathcal{N}(\varepsilon_F)\Big] \\
= 0 \ , &
\end{aligned} \tag{2.89}$$

where the expression is identically zero due to vanishing δ-functions. Therefore, finally,

$$\frac{\partial J(D)}{\partial \ln D} = -DJ^2\frac{2\mathcal{N}(\varepsilon_F)}{D} + \mathcal{O}(\frac{\varepsilon}{D}) \ , \tag{2.90}$$

where ε can be ω, Ω, or ν; i.e., small energy scales. Neglecting the $\mathcal{O}(\frac{\varepsilon}{D})$ term, one obtains an RG flow equation similar to the one obtained before using the momentum representation, Eq. (2.65),

$$\frac{\partial J(D)}{\partial \ln D} = -2\mathcal{N}(\varepsilon_F)J^2 \ , \tag{2.91}$$

which confirms that one can also perform the RG analysis in the position representation. Based on the experience gained with the single-impurity problem in this chapter, we can now begin to establish the RG flow for the multi-impurity case.

CHAPTER 3

Multi-Impurity Kondo Problem

Increasing the number of impurities in the Kondo problem brings up a much higher level of complexity. This is made clearer by the fact that, in contrast to the single-impurity case, no Bethe-ansatz solution has been provided to the 2-impurity problem so far (although, conformal field theory solutions at the critical point, and numerical renormalization group solutions exist). The origin of the complexity is in the fact that when the distance between the impurities is small enough, they can interact with each other via the carrier-mediated Ruderman–Kittel–Kasuya–Yosida (RKKY) interaction [48, 62–65][1] (see chapter 6 for a detailed discussion). The RKKY interaction is produced by the fact that the local moments polarize the spin of the conduction electrons around them, and due to the non-locality of the conduction electrons, this magnetic effect is 'carried' to the other impurity. The existence of the Fermi level leads to an oscillatory behaviour (with the wavelength of $2k_F$) in the RKKY interaction, leading to a change in its sign as a function of distance. So, the RKKY interaction will crucially depend on the details of the band structure of the host metal. At any case, in its most general form, the RKKY interaction can be obtained in second-order perturbation in terms of the Kondo coupling J (see section 6.1). It decays as $\cos(k_F R)/(k_F R)^3$ for a large impurity separation, R.

Thus, there are essentially (at least) two energy scales in the problem, the Kondo scale $T_K/D_0 \sim \exp[-\frac{1}{\mathcal{N}(\varepsilon_F)J_0}]$ and the RKKY scale, $I_{\mathrm{RKKY}} \sim \mathcal{N}(\varepsilon_F)J_0^2$. In general, magnetic correlations (like RKKY) compete with the Kondo effect. For instance, in the simplest case of two Kondo impurities, if RKKY effect prefers an antiferromagnetically-ordered ground-state with a 'molecular' spin-singlet (a 'dimer') made of the two impurities, while Kondo effect prefers a paramagnetic ground-state made of the conduction electrons and each impurity (Kondo singlets). In simple words, the RKKY interaction tends to keep the spins fixed in some direction, while the Kondo effect tries to flip the spins continuously [22]. This causes an intriguing competition between the two effects which can lead to a quantum phase transition between the two different ground-states and in turn, exotic phases at the critical point.

In the previous chapter, we obtained the RG flow equation for the single-impurity Kondo problem in detail. We can now obtain the RG flow for the multi-impurity case where RKKY interaction is present. The derivation is indeed much more detailed and hence, divided into several parts. In the first part, we obtain the modifications of the Kondo vertex due to presence of the RKKY interaction with other impurities and in the second part, one-loop RG flow equations for this

[1] One can also qualitatively understand that in terms of Kondo clouds: When the impurity separation is small enough, individual Kondo clouds begin to significantly overlap so that an indirect interaction is induced between the impurities.

RKKY-modified vertex will be obtained. Finally, we will solve the RG equation to obtain the RKKY-modified Kondo scale, and compare it with some experimental observations.

3.1 Multi-impurity or Kondo lattice model

A set of Kondo impurities or a lattice of magnetic impurities embedded in a sea of conduction electrons is described effectively at low temperatures by the *Kondo lattice model* (KLM) of localized spins exchange-coupled to a sea of conduction electrons with dispersion $\varepsilon_{\mathbf{k}}$:

$$H_{\mathrm{KLM}} = \sum_{\mathbf{k},\nu} \varepsilon_{\mathbf{k}}\; c^{\dagger}_{\mathbf{k}\nu} c_{\mathbf{k}\nu} + \mathtt{J} \sum_{l} \mathbf{S}(\mathbf{x}_l) \cdot \mathbf{s}(\mathbf{x}_l)\,; \quad \mathtt{J} > 0\;, \tag{3.1}$$

where $\mathbf{k}$ and ν are the momentum and spin of a conduction electron, respectively, and the local spin of the conduction electrons on the lattice site $\mathbf{x}_l$ is denoted by $\mathbf{s}(\mathbf{x}_l)$, and that of the localized impurities by $\mathbf{S}(\mathbf{x}_l)$.
In order to make use of conventional diagrammatic methods, the impurity spin operator $\mathbf{S}(\mathbf{x}_l)$ can be represented in terms of the pseudo-fermion creation and annihilation operators (see Appendix C),

$$\mathbf{S}(\mathbf{x}_l) = \frac{1}{2} \sum_{\nu\nu'} f^{\dagger}_{\nu'}(\mathbf{x}_l)\, \boldsymbol{\sigma}_{\nu'\nu}\, f_{\nu}(\mathbf{x}_l)\,, \tag{3.2}$$

where $f^{\dagger}_{\nu'}(\mathbf{x}_l)$ ($f_{\nu'}(\mathbf{x}_l)$) creates (annihilates) a localized fermion with spin ν at site $\mathbf{x}_l$, and $\boldsymbol{\sigma}$ denotes the Pauli matrices. The pseudo-fermions obey the constraint $\hat{Q} = \sum_{\nu} f^{\dagger}_{\nu} f_{\nu} \overset{!}{=} 1$. The conduction-electron spin operator can also be re-written as

$$\mathbf{s}(\mathbf{x}_l) = \frac{1}{2} \sum_{\nu\nu'} c^{\dagger}_{\nu'}(\mathbf{x}_l)\, \boldsymbol{\sigma}_{\nu'\nu}\, c_{\nu}(\mathbf{x}_l)\,. \tag{3.3}$$

Hence, the spin interaction can be finally recast as

$$\frac{J}{2} \sum_{l} \sum_{\mu\mu',\nu'\nu} f^{\dagger}_{\nu'}(\mathbf{x}_l) f_{\nu}(\mathbf{x}_l)\; \boldsymbol{\sigma}_{\nu'\nu} \cdot \boldsymbol{\sigma}_{\mu'\mu}\; c^{\dagger}_{\mu'}(\mathbf{x}_l) c_{\mu}(\mathbf{x}_l), \quad J > 0. \tag{3.4}$$

Obviously, the spin interaction conserves neither the momentum, nor the spin, but it conserves the energy.
It is well established that, through the antiferromagnetic exchange coupling $J > 0$, this model encompasses both the formation of local singlets of f-spins and conduction spins via the Kondo effect as well as long-range magnetic ordering. The latter is induced by the RKKY interaction which is mediated in $\mathcal{O}(J^2)$ by the conduction electron density correlations (see section 6.1 for more details). This effect of neighboring impurities due to RKKY interaction can be accounted by modifying the original bare Kondo vertex (say, at site $\mathbf{x}$) with RKKY corrections; i.e.,

$$J \overset{\mathrm{RKKY}}{\longmapsto} \tilde{J} = J + \delta J_{\mathrm{RKKY}}\,,$$

where the RKKY-corrected coupling $\tilde{J}$ includes the perturbative effect of all neighboring impurities. Here, we investigate the conditions for realization of the Kondo effect, i.e., complete spin screening of a local f-spin, to be realized in the Kondo lattice model. In particular, we

calculate the temperature scale below which the Kondo singlet is formed. In the language of the perturbative renormalization group this is the following question: Under which conditions the *full* spin-scattering vertex Γ_{f-c} between conduction electrons and an f-spin at an arbitrarily chosen, but fixed site, $\mathbf{x}$, diverges during the RG flow. It is important to notice that even though the bare spin coupling of the KLM is local, the full vertex Γ_{f-c} acquires non-local contributions, since conduction electrons can scatter from surrounding f-spins at sites $\mathbf{x}_l \neq \mathbf{x}$ and the effect of the flip of an f-spin on site $\mathbf{x}_l$ can be transferred to the f-spin on site $\mathbf{x}$ via the RKKY correlations.

Notation At the beginning of the calculation, we provide the notational conventions as a reference and for consistency. Throughout the calculations, J denotes the Kondo coupling at the reference site $\mathbf{x}$. We denote the *bare* Kondo coupling at neighboring impurity sites $\mathbf{x}_l \neq \mathbf{x}$ with J_0. The *bare* single-impurity Kondo temperature (when RKKY interaction vanishes) is denoted by T_K^0, and the RKKY-renormalized lattice Kondo temperature by $T_K(y)$, where y parameterizes the strength of RKKY fluctuations (defined explicitly in section 3.4). The superscript R (A) denotes a retarded (advanced) correlation function. The energies are measured from the Fermi energy ε_F (or the chemical potential μ). The full bandwidth of the conduction electrons is denoted by $D_0 \sim \varepsilon_F$ and the running energy scale (in the RG flow) by D. Density-of-states of the conduction electrons is denoted by $\mathcal{N}(\varepsilon)$. The Bose-Einstein distribution is denoted by n_B, and the Fermi-Dirac distribution by n_F; at low temperatures, they can be approximated by[2]

$$\begin{aligned} n_F(\varepsilon) &\approx \Theta(-\varepsilon) \ , \\ n_B(\varepsilon) &\approx -\Theta(-\varepsilon) \approx -n_F(\varepsilon) \ . \end{aligned} \tag{3.5}$$

The susceptibility (particle-hole bubble) of the conduction electrons is denoted by χ_c and that of the localized fermions by χ_f. The real and imaginary parts of a function $\mathcal{F}$ are denoted by $\mathcal{F}'$ and $\mathcal{F}''$ respectively. We have used the natural units in which $\hbar = 1$ and $k_B = 1$; hence the inverse temperature, $\beta = \frac{1}{T}$.

Green's function of conduction electrons The non-interacting Green's function of the conduction electrons reads

$$\begin{aligned} G_c^{R/A}(\mathbf{k},\omega) &= \frac{1}{\omega - \xi_{\mathbf{k}} \pm \mathrm{i}\eta^+} \ ; \quad \text{with } \eta^+ \to 0^+ \ , \\ G_c^{R/A}(\mathbf{x},\omega) &= -\frac{m}{2\pi}\frac{\exp(\pm \mathrm{i}\, k[\varepsilon_F + \omega]\, r)}{r} \ ; \quad \text{with } r := |\mathbf{x}| \ , \end{aligned} \tag{3.6}$$

for a quadratic dispersion, $\varepsilon_{\mathbf{k}} = \frac{k^2}{2m}$. Furthermore, order-of-magnitude estimations yield

$$\begin{aligned} \mathrm{Re}\, G_c^{R/A}(\mathbf{x},\omega) &\sim \frac{\omega}{D_0^2} \ , \\ \mathrm{Im}\, G_c^{R/A}(\mathbf{x},\omega) &\sim \mp\frac{1}{D_0} \ . \end{aligned} \tag{3.7}$$

[2] The Heaviside function is defined as $\Theta(-x) = 1 - \Theta(x)$, and $\Theta(0) = \frac{1}{2}$.

Green's function of pseudo-fermions The non-interacting *local* Green's function of the pseudo-fermions is

$$G_f^{R/A}(\omega) = \frac{1}{\omega - \xi_d \pm i\eta^+} \; ; \quad \text{with } \eta^+ \to 0^+ \; , \tag{3.8}$$

where ξ_d is the energy of the local level of the impurity measured from the chemical potential, $\xi_d = \varepsilon_d - \mu$.

Spectral functions Finally, the spectral function is defined as $A(\varepsilon) = \mp\frac{1}{\pi}\mathrm{Im}\, G^{R/A}(\varepsilon)$. Therefore, for non-interacting conduction electrons,

$$A_c(\mathbf{x}, \omega) = \frac{m}{2\pi}\frac{\sin(k[\varepsilon_F + \omega]\, r)}{r} \; . \tag{3.9}$$

3.2 Local impurity susceptibility

Throughout the explicit calculations, an expression for the local impurity susceptibility is required. This local susceptibility can be obtained from the Bethe-ansatz solution of the single-impurity Kondo problem [31] (Fig. 3.1). By using this solution, the f-susceptibility will include the *full* effects of the *on-site* (*local*) interaction of impurities with conduction electrons. Therefore, Kondo coupling J_0 at the neighboring sites remains unrenormalized and does not flow under the RG. Although the original Bethe-ansatz result is too complicated to be used straightly, one can model it with a function which analytically connects the asymptotic behaviour at $T \ll T_K$ and $T \gg T_K$. Ultimately, it turns out that merely the main qualitative features of the f-susceptibility are essential for the final RG equation, which implicates that it is merely a soft cut-off at T_K in the RG flow.[3]
The real part of $\chi_f^R(\omega)$ can be modelled with

$$\mathrm{Re}\,\chi_f^R(\omega) = \frac{(g\mu_B)^2 W}{\pi}\frac{1}{\sqrt{\omega^2 + T_K^2}} \; , \tag{3.10}$$

where W is the Wilson ratio, μ_B is the Bohr magneton and g is the gyromagnetic ratio of the electron[4]. The imaginary part of the susceptibility can be consistently obtained from the Kramers-Kronig relations (see, e.g., Ref. [121]),

$$\begin{aligned} \mathrm{Re}\,\chi^R(\omega) &= \mathrm{pv}\int_{-\infty}^{+\infty}\frac{\mathrm{d}\varepsilon}{\pi}\,\frac{\mathrm{Im}\,\chi^R(\varepsilon)}{\varepsilon - \omega} \; , \\ \mathrm{Im}\,\chi^R(\omega) &= -\mathrm{pv}\int_{-\infty}^{+\infty}\frac{\mathrm{d}\varepsilon}{\pi}\,\frac{\mathrm{Re}\,\chi^R(\varepsilon)}{\varepsilon - \omega} \; , \end{aligned} \tag{3.11}$$

[3] If we choose another function to model the local impurity susceptibility, it will lead merely to a change in values for quantities, such as the Kondo temperature; that is, it will not alter the overall result for the RG flow (section 3.4).

[4] Note that frequency, ω, and temperature, T, appear symmetrically in the expression for f-susceptibility, as it should be in the Fermi liquid regime.

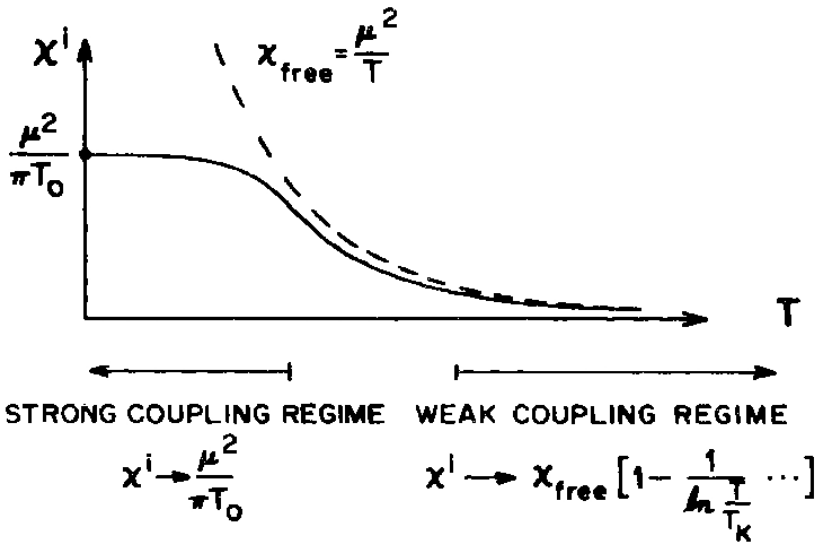

Figure 3.1: Bethe-Anstaz solution for the impurity susceptibility (adopted from Ref. [31]). Notice the soft cut-off at $T \sim T_K$.

since $\chi_f^R(\omega)$ is analytic in the upper half-plane[5]; therefore,

$$\chi_f^R(\omega) = \frac{(g\mu_B)^2 W}{\pi} \frac{1}{\sqrt{\omega^2 + T_K^2}} \left(1 + \frac{2\mathrm{i}}{\pi} \operatorname{arsinh} \frac{\omega}{T_K}\right) . \tag{3.12}$$

Notice that in the relevant energy interval, $\Omega \sim \mathcal{O}(T_K) \ll D_0$, where the RG β-function is non-vanishing (see section 3.4), the real and imaginary parts obey $|\mathrm{Im}\,\chi_f / \mathrm{Re}\,\chi_f| \sim \frac{T_K}{D_0} \ll 1$, and therefore, the imaginary part of χ_f can be safely neglected. Moreover,

$$\frac{(g\mu_B)^2 W}{\pi} \sim \mathcal{O}(1)\,, \tag{3.13}$$

and most importantly,

$$\chi_f^{R\prime}(\omega) \sim \frac{1}{T_K} . \tag{3.14}$$

This behaviour, Eq. (3.14), is of utmost importance in the final self-consistent RG equation as we will see in the section devoted to the flow equation (section 3.4).

3.3 RKKY modifications to the Kondo vertex

RKKY interaction is an effective long-range interaction between the localized impurity spins mediated by the delocalized conduction electrons (see section 6.1).
The leading RKKY contributions to the Kondo vertex (up to the second order in coupling to

[5] 'pv' denotes the Cauchy principal value of the integral.

the neighboring impurity lattice sites, J_0) are represented by the two diagrams which we call 'direct' and 'exchange' vertex corrections (not to be confused with the 'direct' and 'exchange' RG diagrams) (Fig. 3.2).

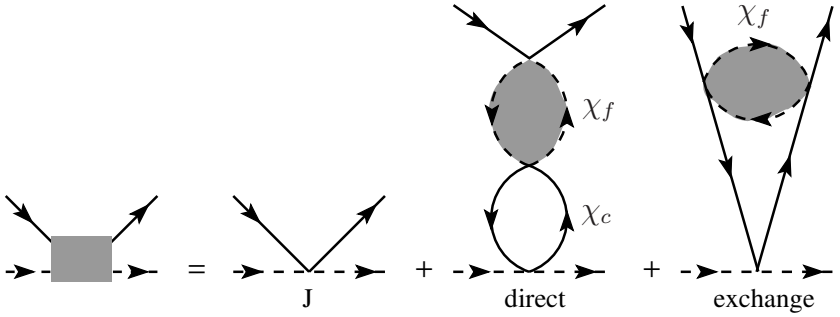

Figure 3.2: RKKY modifications to the Kondo vertex (up to $\sim \mathcal{O}(J_0^2)$)

In this following, we will explicitly derive the explicit expressions for the RKKY modifications to the Kondo vertex.

3.3.1 Direct vertex correction

The direct RKKY vertex correction is depicted in detail in Fig. 3.3.

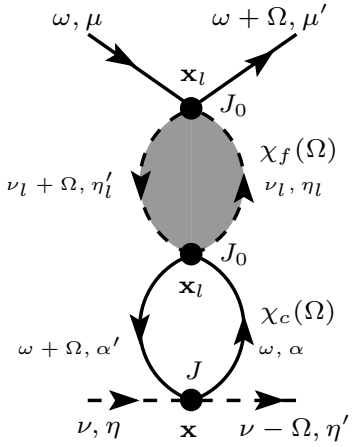

Figure 3.3: Direct RKKY vertex correction in detail.

The direct diagram Γ_{dir} corresponds to the following term[6]

[6] The operator contractions are

$$f^\dagger_{\eta_l'} f_{\eta_l}\, \boldsymbol{\sigma}_{\eta_l'\eta_l} \cdot \boldsymbol{\sigma}_{\mu'\mu}\, c^\dagger_{\mathbf{k}'\mu'} c_{\mathbf{k}\mu} \quad f^\dagger_{\eta_l} f_{\eta_l'}\, \boldsymbol{\sigma}_{\eta_l\eta_l'} \cdot \boldsymbol{\sigma}_{\alpha'\alpha}\, c^\dagger_{\mathbf{p}'\alpha'} c_{\mathbf{p}\alpha} \quad f^\dagger_{\eta'} f_{\eta}\, \boldsymbol{\sigma}_{\eta'\eta} \cdot \boldsymbol{\sigma}_{\alpha\alpha'}\, c^\dagger_{\mathbf{p}\alpha} c_{\mathbf{p}'\alpha'}\,, \tag{3.15}$$

with a plus sign for the Wick ordering.

$$\begin{aligned}
\Gamma_{dir} &= +J\, J_0^2\, \mathcal{P}_{dir}\, \mathcal{G}_{dir}\ ; \\
\mathcal{P}_{dir} &= \sum_{\substack{\eta_l',\eta_l \\ \alpha',\alpha'}} \boldsymbol{\sigma}_{\eta_l'\eta_l}\cdot\boldsymbol{\sigma}_{\mu'\mu}\,\boldsymbol{\sigma}_{\eta_l\eta_l'}\cdot\boldsymbol{\sigma}_{\alpha'\alpha}\,\boldsymbol{\sigma}_{\eta'\eta}\cdot\boldsymbol{\sigma}_{\alpha\alpha'}\ , \\
\mathcal{G}_{dir} &= \chi_f(i\Omega)\,\chi_c(\mathbf{x}-\mathbf{x}_l,i\Omega)\ ,
\end{aligned} \tag{3.16}$$

where $\mathcal{P}_{dir}$ and $\mathcal{G}_{dir}$ represent the spin and Green-function part of the direct RKKY vertex correction. Since the Green's functions are spin-independent, one can consider the Pauli-matrix part $\mathcal{P}$ and the Green-function part $\mathcal{G}$ of a diagram separately. The Pauli-matrix part of the diagram can be evaluated by a proper re-arrangement of the terms and using the general properties of the Pauli matrices (see below for a full calculation):

$$\mathcal{P}_{dir} = 4\,\boldsymbol{\sigma}_{\eta'\eta}\cdot\boldsymbol{\sigma}_{\mu'\mu}\ , \tag{3.17}$$

which has the same spin structure as the original bare Kondo interaction. The Green-function part includes the susceptibilities of the conduction and f-electrons. Finally, by the mapping $i\Omega \mapsto \Omega + i\eta^+$, Eq. (3.16) and Eq. (3.17) obtain the contribution of the direct vertex correction to the Kondo coupling as

$$\Gamma_{dir}(\Omega) = 4\ J\, J_0^2\ \chi_f^R(\Omega)\,\chi_c^R(\mathbf{x}-\mathbf{x}_l,\Omega)\ , \tag{3.18}$$

where χ_c represents the non-interacting susceptibility of the conduction electrons.

3.3.1.1 Spin part of the direct vertex correction

The spin part of the direct diagram reads

$$\begin{aligned}
\mathcal{P}_{dir} &= \sum_{\eta_l'\eta_l,\alpha'\alpha} \boldsymbol{\sigma}_{\eta_l'\eta_l}\cdot\boldsymbol{\sigma}_{\mu'\mu}\,\boldsymbol{\sigma}_{\eta_l\eta_l'}\cdot\boldsymbol{\sigma}_{\alpha'\alpha}\,\boldsymbol{\sigma}_{\alpha\alpha'}\cdot\boldsymbol{\sigma}_{\eta'\eta} \\
&= \sum_{\alpha'\alpha}\left(\boldsymbol{\sigma}_{\eta'\eta}\cdot\boldsymbol{\sigma}_{\alpha\alpha'}\ \sum_{\eta_l'\eta_l}\boldsymbol{\sigma}_{\alpha'\alpha}\cdot\boldsymbol{\sigma}_{\eta_l\eta_l'}\,\boldsymbol{\sigma}_{\eta_l'\eta_l}\cdot\boldsymbol{\sigma}_{\mu'\mu}\right)\ .
\end{aligned} \tag{3.19}$$

Recall that in Pauli-matrix expressions, the terms can be reshuffled since they are only c-number elements of the Pauli matrices. Furthermore,

$$\begin{aligned}
&\sum_{\eta_l'\eta_l}\boldsymbol{\sigma}_{\alpha'\alpha}\cdot\boldsymbol{\sigma}_{\eta_l\eta_l'}\,\boldsymbol{\sigma}_{\eta_l'\eta_l}\cdot\boldsymbol{\sigma}_{\mu'\mu} = \sum_{a,b=1,2,3}\sum_{\eta_l'\eta_l}\sigma^a_{\alpha'\alpha}\sigma^a_{\eta_l\eta_l'}\,\sigma^b_{\eta_l'\eta_l}\sigma^b_{\mu'\mu} \\
&= \sum_{ab}\left(\sigma^a_{\alpha'\alpha}\sigma^b_{\mu'\mu}\sum_{\eta_l'\eta_l}\sigma^a_{\eta_l\eta_l'}\sigma^b_{\eta_l'\eta_l}\right) \\
&= \sum_{ab}\sigma^a_{\alpha'\alpha}\sigma^b_{\mu'\mu}\ \mathrm{Tr}[\sigma^a\sigma^b]\ ,
\end{aligned} \tag{3.20}$$

which, by using the general properties of the Pauli matrices (Appendix A), i.e.,

$$\mathrm{Tr}[\sigma^a\sigma^b] = \mathrm{Tr}[\delta_{ab}\mathbb{1}_2 + \mathrm{i}\sum_c \epsilon_{abc}\,\sigma^c] = \delta_{ab}\mathrm{Tr}[\mathbb{1}_2] = 2\delta_{ab}\ , \tag{3.21}$$

and

$$\mathrm{Tr}[\sigma^a] = 0\ , \tag{3.22}$$

becomes

$$\begin{aligned}\sum_{ab}\sigma^a_{\alpha'\alpha}\sigma^b_{\mu'\mu}\,\mathrm{Tr}[\sigma^a\sigma^b] &= 2\sum_{ab}\delta_{ab}\,\sigma^a_{\alpha'\alpha}\sigma^b_{\mu'\mu} = \\ &= 2\,\boldsymbol{\sigma}_{\alpha'\alpha}\cdot\boldsymbol{\sigma}_{\mu'\mu}\ .\end{aligned} \tag{3.23}$$

Thus, $\mathcal{P}_{dir}$, Eq. (3.19), simplifies to

$$\begin{aligned}\mathcal{P}_{dir} &= 2\sum_{\alpha'\alpha}\boldsymbol{\sigma}_{\eta'\eta}\cdot\boldsymbol{\sigma}_{\alpha\alpha'}\,\boldsymbol{\sigma}_{\alpha'\alpha}\cdot\boldsymbol{\sigma}_{\mu'\mu} = 2\sum_{ab}\sum_{\alpha\alpha'}\sigma^a_{\eta'\eta}\sigma^a_{\alpha\alpha'}\,\sigma^b_{\alpha'\alpha}\sigma^b_{\mu'\mu} \\ &= 2\sum_{ab}\Big(\sigma^a_{\eta'\eta}\sigma^b_{\mu'\mu}\,2\delta_{ab}\Big) \\ &= 4\,\boldsymbol{\sigma}_{\eta'\eta}\cdot\boldsymbol{\sigma}_{\mu'\mu}\ .\end{aligned} \tag{3.24}$$

3.3.1.2 Real and imaginary parts of the direct diagram

The explicit form of Γ_{dir} can be calculated by decomposing it into its real and imaginary parts. First, we consider the conduction electron susceptibility χ_c:

$$\begin{aligned}\mathrm{Re}\,\chi^R_c(\mathbf{x},\Omega) &= -\int \mathrm{d}\varepsilon\Big(n_F(\varepsilon)A(\mathbf{x},\varepsilon)G^{R'}(\mathbf{x},\varepsilon+\Omega) + n_F(\varepsilon+\Omega)A(\mathbf{x},\varepsilon+\Omega)G^{R'}(\mathbf{x},\varepsilon)\Big) \\ &= -\int \mathrm{d}\varepsilon\, n_F(\varepsilon)A(\mathbf{x},\varepsilon)\Big(G^{R'}(\mathbf{x},\varepsilon+\Omega) + G^{R'}(\mathbf{x},\varepsilon-\Omega)\Big)\ .\end{aligned} \tag{3.25}$$

Using the explicit form of the conduction electron Green's functions, Eq. (3.6), one obtains

$$\mathrm{Re}\,\chi^R_c(\mathbf{x},\Omega) = \frac{1}{\pi}(\frac{m}{2\pi})^2\frac{1}{r^2}\int_{-D}^{0}\mathrm{d}\varepsilon\,\sin(k[\varepsilon_F+\varepsilon]r)\Big(\cos(k[\varepsilon_F+\varepsilon+\Omega]r) + \cos(k[\varepsilon_F+\varepsilon-\Omega]r)\Big)\ . \tag{3.26}$$

Finally, the integrations can be performed explicitly to obtain

$$\mathrm{Re}\,\chi^R_c(\mathbf{x},\Omega) = \frac{mk_F^4}{(2\pi)^3}\,\frac{1}{\varrho^4}\Big(\sin(2\varrho) - 2\varrho\cos(2\varrho)\Big) + \mathcal{O}(\Omega^2)\,, \tag{3.27}$$

where we have introduced the dimensionless variables $\varrho := k_F\, r$ with $r = |\mathbf{x}|$, and kept only the leading order in Ω. The imaginary part can be obtained similarly as

$$\begin{aligned}\operatorname{Im}\chi_c^R(\mathbf{x},\Omega) &= \pi\int \mathrm{d}\varepsilon\Big(n_F(\varepsilon)-n_F(\varepsilon+\Omega)\Big)A(\mathbf{x},\varepsilon)A(\mathbf{x},\varepsilon+\Omega)\\ &= \frac{1}{\pi}(\frac{m}{2\pi})^2\frac{1}{r^2}\int_{-\Omega}^{0}\mathrm{d}\varepsilon\,\sin(k[\varepsilon_F+\varepsilon]r)\sin(k[\varepsilon_F+\varepsilon+\Omega]r)\\ &= \frac{1}{2}\frac{mk_F^4}{(2\pi)^3}\frac{1+\cos(2\varrho)}{\varrho^2}\,\frac{\Omega}{\varepsilon_F}+\mathcal{O}(\Omega^3)\ .\end{aligned} \tag{3.28}$$

Notice that an order-of-magnitude estimation yields

$$\begin{aligned}\operatorname{Re}\chi_c^R(\mathbf{x},\Omega) &\sim \frac{1}{D_0}\ ,\\ \operatorname{Im}\chi_c^R(\mathbf{x},\Omega) &\sim \frac{\Omega}{D_0}\ .\end{aligned} \tag{3.29}$$

Therefore, in the relevant energy interval, $\Omega \sim \mathcal{O}(T_K) \ll D_0$, where the RG β-function is non-vanishing (see section 3.4), the real and imaginary parts satisfy $|\operatorname{Im}\chi_c/\operatorname{Re}\chi_c| \sim \frac{T_K}{D_0} \ll 1$, and thus, the imaginary part can be safely neglected. The explicit form of the f-susceptibility is discussed in section 3.2.
The c-electron susceptibility is represented diagrammatically as in Fig. 3.4,

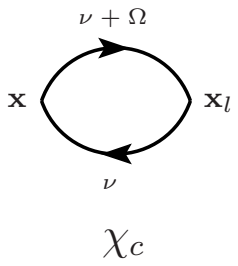

Figure 3.4: Susceptibility ('particle-hole bubble') diagram for the conduction electrons.

corresponding to the expression

$$\begin{aligned}\chi_c(\mathbf{x}-\mathbf{x}_l,\Omega) &= \frac{1}{\beta}\sum_{\mathrm{i}\nu=\mathrm{i}(2\mathbb{Z}+1)\frac{\pi}{\beta}} G_c(\mathbf{x}-\mathbf{x}_l,\mathrm{i}\nu)G_c(\mathbf{x}_l-\mathbf{x},\mathrm{i}\nu+\mathrm{i}\Omega)\\ &= \frac{1}{2\pi\mathrm{i}}\oint_{C_F}\mathrm{d}z\ n_F(z)\int\frac{\mathrm{d}\varepsilon}{2\pi}\frac{A_c(\mathbf{x}-\mathbf{x}_l,\varepsilon)}{z-\varepsilon}\int\frac{\mathrm{d}\varepsilon'}{2\pi}\frac{A_c(\mathbf{x}_l-\mathbf{x},\varepsilon')}{z+\mathrm{i}\Omega-\varepsilon'}\ ,\end{aligned} \tag{3.30}$$

where C_F is a counter-clockwise contour around the fermionic poles. The retarded component is

$$\begin{aligned}\chi_c^R(\mathbf{x}-\mathbf{x}_l,\Omega) &= \int\frac{\mathrm{d}\varepsilon\,\mathrm{d}\varepsilon'}{(2\pi)^2}\left(n_F(\varepsilon)-n_F(\varepsilon')\right)\frac{A_c(\mathbf{x}-\mathbf{x}_l,\varepsilon)A_c(\mathbf{x}_l-\mathbf{x},\varepsilon')}{\varepsilon-\varepsilon'+\Omega+\mathrm{i}\eta^+}\\ &= \int\frac{\mathrm{d}\varepsilon\,\mathrm{d}\varepsilon'}{(2\pi)^2}\left(n_F(\varepsilon)-n_F(\varepsilon')\right)\frac{A_c(\mathbf{x}-\mathbf{x}_l,\varepsilon)A_c(\mathbf{x}_l-\mathbf{x},\varepsilon')}{\varepsilon-\varepsilon'+\Omega}\\ &\quad-\mathrm{i}\pi\int\frac{\mathrm{d}\varepsilon}{(2\pi)^2}\left(n_F(\varepsilon)-n_F(\varepsilon')\right)A_c(\mathbf{x}-\mathbf{x}_l,\varepsilon)A_c(\mathbf{x}_l-\mathbf{x},\varepsilon+\Omega)\ ,\end{aligned} \tag{3.31}$$

Therefore,

$$\mathrm{Re}\,\chi_c^R(\Omega) = \int \frac{\mathrm{d}\varepsilon\,\mathrm{d}\varepsilon'}{(2\pi)^2}\,(n_F(\varepsilon) - n_F(\varepsilon'))\,\frac{A_c(\mathbf{x}-\mathbf{x}_l,\varepsilon)A_c(\mathbf{x}_l-\mathbf{x},\varepsilon')}{\varepsilon-\varepsilon'+\Omega}\ , \tag{3.32}$$

$$\mathrm{Im}\,\chi_c^R(\Omega) = \frac{1}{4\pi}\int \mathrm{d}\varepsilon\ (n_F(\varepsilon+\Omega) - n_F(\varepsilon))\,A_c(\mathbf{x}-\mathbf{x}_l,\varepsilon)A_c(\mathbf{x}_l-\mathbf{x},\varepsilon+\Omega)\ . \tag{3.33}$$

Real part of c-electron susceptibility The real part of the c-electron susceptibility reads

$$\begin{aligned}
\mathrm{Re}\,\chi_c^R(\mathbf{x},\Omega) &= -\int \mathrm{d}\varepsilon\,\Big[n_F(\varepsilon)A(\mathbf{x},\varepsilon)G'(\mathbf{x},\varepsilon+\Omega) + n_F(\varepsilon+\Omega)A(\mathbf{x},\varepsilon+\Omega)G'(\mathbf{x},\varepsilon)\\
&= -\int \mathrm{d}\varepsilon\ \underbrace{n_F(\varepsilon)}_{\approx\Theta(-\varepsilon)}\Big[A(\mathbf{x},\varepsilon)G'(\mathbf{x},\varepsilon+\Omega) + A(\mathbf{x},\varepsilon)G'(\mathbf{x},\varepsilon-\Omega)\Big]\\
&= -\int_{-D_0}^{0} \mathrm{d}\varepsilon\,A(\mathbf{x},\varepsilon)\,(G'(\mathbf{x},\varepsilon+\Omega) + G'(\mathbf{x},\varepsilon-\Omega))\\
&= \frac{1}{\pi}(\frac{m}{2\pi})^2\frac{1}{r^2}\int_{-D_0}^{0}\mathrm{d}\varepsilon\ \sin(k[\varepsilon_F+\varepsilon]r)\Big[\cos(k[\varepsilon_F+\varepsilon+\Omega]r) + \cos(k[\varepsilon_F+\varepsilon-\Omega]r)\Big]\ .
\end{aligned} \tag{3.34}$$

By introducing the dimensionless variables,

$$\begin{aligned}
x &:= \frac{\varepsilon}{\varepsilon_F}\ ,\\
\nu &:= \frac{\Omega}{\varepsilon_F}\ ,\\
\varrho &:= k_F r > 0\ ,
\end{aligned} \tag{3.35}$$

we obtain an integral,

$$I_{sc} = \int \mathrm{d}\varepsilon\ \sin(\varrho\sqrt{1+x})\left(\cos(\varrho\sqrt{1+x+\nu}) + \cos(\varrho\sqrt{1+x-\nu})\right)\ . \tag{3.36}$$

Upon a Taylor expansion, the term in the parenthesis yields

$$\begin{aligned}
&\cos(\varrho\sqrt{1+x+\nu}) + \cos(\varrho\sqrt{1+x-\nu})\\
&= 2\cos(\varrho\sqrt{1+x}) + \varrho\nu^2\left(\frac{-\varrho\sqrt{1+x}\cos(\varrho\sqrt{1+x}) + \sin(\varrho\sqrt{1+x})}{4(x+1)^{\frac{3}{2}}}\right) + \mathcal{O}(\nu^3)\ .
\end{aligned} \tag{3.37}$$

Therefore,

$$\begin{aligned}
I_{sc} &= 2\int \mathrm{d}x\ \sin(\varrho\sqrt{1+x})\cos(\varrho\sqrt{1+x})\\
&\quad - \frac{\varrho\nu^2}{4}\int \mathrm{d}x\ \sin(\varrho\sqrt{1+x})\frac{\cos(\varrho\sqrt{1+x})}{1+x}\\
&\quad + \frac{\varrho\nu^2}{4}\int \mathrm{d}x\,\frac{\sin(\varrho\sqrt{1+x})^2}{(1+x)^{\frac{3}{2}}}\ .
\end{aligned} \tag{3.38}$$

The first integration on the RHS of I_{sc} can be performed by a change of variable,

$$y = \varrho\sqrt{1+x} \rightarrow y^2 = \varrho^2(1+x) \rightarrow 2y\mathrm{d}y = \varrho^2\mathrm{d}x\,, \tag{3.39}$$

as

$$\begin{aligned}\int \mathrm{d}x\, \sin(\varrho\sqrt{1+x})\cos(\varrho\sqrt{1+x}) &= \frac{2}{\varrho^2}\int \mathrm{d}y\, y\sin(y)\cos(y) = \frac{1}{\varrho^2}\int \mathrm{d}y\, y\sin(2y)\\ &= \frac{1}{4\varrho^2}\left(\sin(2y) - 2y\cos(2y)\right)\ .\end{aligned} \tag{3.40}$$

The second integration on the RHS of I_{sc} can be performed by the same variable change to y,

$$\begin{aligned}\int \mathrm{d}x\, \sin(\varrho\sqrt{1+x})\frac{\cos(\varrho\sqrt{1+x})}{1+x} &= \int \mathrm{d}y\, \frac{2\sin y\cos y}{y}\\ &= \int \mathrm{d}y\, \frac{\sin(2y)}{y} = \mathrm{Si}(2y)\ ,\end{aligned} \tag{3.41}$$

where $\mathrm{Si}(z) := \int_0^z \mathrm{d}x\, \frac{\sin x}{x}$ is the *sine integral*.

The third integral on the RHS of I_{sc} can be performed by the same change of variable to y, Eq. (3.39), as

$$\begin{aligned}\int \mathrm{d}x\, \frac{\sin(\varrho\sqrt{1+x})^2}{(1+x)^{\frac{3}{2}}} &= 2\varrho\int \mathrm{d}y\, \frac{\sin(y)^2}{y^2}\\ &= \varrho\frac{\cos(2y) + 2y\,\mathrm{Si}(2y) - 1}{y}\ .\end{aligned} \tag{3.42}$$

Finally,

$$\begin{aligned}I_{sc} = &\frac{1}{2\varrho^2}\left(\sin(2y) - 2y\cos(2y)\right) - \frac{\varrho^2\nu^2}{4}\,\mathrm{Si}(2y)\\ &+ \frac{\varrho^2\nu^2}{4}\frac{\cos(2y) + 2y\,\mathrm{Si}(2y) - 1}{y} \quad ; \quad y = \varrho\sqrt{1+x}\ .\end{aligned} \tag{3.43}$$

Due to the distribution functions in the integrand, Eq. (3.34), the limits of integration will be

$$\varepsilon \in [-D_0, 0] \rightarrow x \in [-D_0/\varepsilon_F, 0] \approx [-1, 0] \rightarrow y \in [0, \varrho]\ ;$$

therefore,

$$\begin{aligned}I_{sc} = &\frac{1}{2\varrho^2}\left(\sin(2\varrho) - 2\varrho\cos(2\varrho)\right) - \frac{\varrho^2\nu^2}{4}\mathrm{Si}(2\varrho)\\ &+ \frac{\varrho^2\nu^2}{4}\left(\frac{\cos(2\varrho) + 2\varrho\mathrm{Si}(2\varrho) - 1}{\varrho}\right) - \lim_{y\to 0}\frac{\cos(2y) - 1}{y}\ .\end{aligned} \tag{3.44}$$

Noting that

$$\lim_{y\to 0}\frac{\cos(2y) - 1}{y} = \lim_{y\to 0}\frac{-2\sin(y)^2}{y} = 0\ ,$$

the integral yields

$$I_{sc} = \frac{1}{\varrho^2}\left(1 - \varrho\cos(2\varrho) + \frac{1}{2}\sin(2\varrho)\right) + \frac{\varrho\nu^2}{4}\left(\cos(2\varrho) - 3\varrho\,\mathrm{Si}(2\varrho) - 1\right) + \mathcal{O}(\nu^4)\ . \tag{3.45}$$

Therefore, we obtain,

$$\begin{aligned}\mathrm{Re}\,\chi_c^R(\mathbf{x},\Omega) &= \frac{1}{\pi}(\frac{m}{2\pi})^2\frac{1}{r^2}\frac{\varepsilon_F}{\varrho^2}\left(-\varrho\cos(2\varrho) + \frac{1}{2}\sin(2\varrho)\right) + \mathcal{O}(\nu^2)\\ &= \frac{1}{2\pi}m(\frac{{k_F}^3}{2\pi})^2\frac{1}{\varrho^2}\left(-\varrho\cos(2\varrho) + \frac{1}{2}\sin(\varrho)\right) + \mathcal{O}(\Omega^2)\ .\end{aligned} \tag{3.46}$$

Imaginary part of *c*-electron susceptibility The imaginary part of the c-electron susceptibility is simpler compared to the real part,

$$\mathrm{Im}\,\chi_c^R(\mathbf{x},\Omega) = \pi\int \mathrm{d}\varepsilon\left[n_F(\varepsilon) - n_F(\varepsilon+\Omega)\right]A(\mathbf{x},\varepsilon)A(\mathbf{x},\varepsilon+\Omega)\ . \tag{3.47}$$

At low temperatures, $T \to 0^+$, the imaginary part can be calculated explicitly. First note that

$$n_F(\varepsilon) - n_F(\varepsilon+\Omega) \overset{T\to 0^+}{\approx} \Theta(-\varepsilon) - \Theta\left(-(\varepsilon+\Omega)\right) = \Theta(\varepsilon+\Omega) - \Theta(\varepsilon)\ , \tag{3.48}$$

which limits the $\varepsilon-$integration range. Using the explicit form of the conduction-electron Green's functions, Eq. (3.6),

$$\begin{aligned}\mathrm{Im}\,\chi_c^R(\mathbf{x},\Omega) &= \frac{1}{\pi}\int_{-\Omega}^{0}\mathrm{d}\varepsilon\,\mathrm{Im}\,G^A(\mathbf{x},\varepsilon+\Omega)\\ &= \frac{1}{\pi}(\frac{m}{2\pi})^2\frac{\sin\left(k[\varepsilon+\mu]r\right)}{r}\frac{\sin\left(k[\varepsilon+\Omega+\mu]r\right)}{r}\\ &= (\frac{m}{2\pi})^2\frac{1}{\pi}\frac{1}{r^2}\int_{-\Omega}^{0}\mathrm{d}\varepsilon\,\sin\left(\sqrt{2m(\varepsilon+\mu)}\,r\right)\sin\left(\sqrt{2m(\varepsilon+\Omega+\mu)}\,r\right)\ ,\end{aligned} \tag{3.49}$$

where we have used a parabolic dispersion, $k[\varepsilon] = \sqrt{2m\varepsilon}$.[7] By introducing the dimensionless variables as in Eq. (3.35), the integration is re-written as

$$I_1'' = \int \mathrm{d}x\,\sin(\varrho\sqrt{1+x})\sin(\varrho\sqrt{1+x+\nu})\ . \tag{3.50}$$

At low frequencies $\Omega \ll \varepsilon_F \equiv \nu \ll 1$, one can Taylor-expand the integrand as

$$\sin(\varrho\sqrt{X+\nu})\Big|_{\nu=0} = \sin(\varrho\sqrt{X}) + \frac{\varrho\nu}{\sqrt{X}}\cos(\varrho\sqrt{X}) + \mathcal{O}(\nu^2)\ ; \tag{3.51}$$

[7] Notice that the condition $\varepsilon+\mu > 0 \equiv \varepsilon > -\mu$ ($\mu = \varepsilon_F$) is satisfied for the energies inside the band, and this prevents the square roots from being ill-defined.

then,

$$I_1'' = \int \mathrm{d}x\, \sin(\varrho\sqrt{1+x}\,)\left(\sin(\varrho\sqrt{1+x}\,) + \frac{\varrho\nu}{\sqrt{1+x}}\cos(\varrho\sqrt{1+x}\,)\right) . \tag{3.52}$$

This integration can be performed using the following integrals; first,

$$I_{ss} := \int \mathrm{d}x\, \sin(\varrho\sqrt{1+x}\,)\sin(\varrho\sqrt{1+x}\,) , \tag{3.53}$$

which, with the change of variable,

$$y := \varrho\sqrt{1+x}\,\rightarrow y^2 = \varrho^2(1+x) \rightarrow 2y\mathrm{d}y\, = \varrho^2\mathrm{d}x$$

yields

$$I_{ss} = \frac{2}{\varrho^2}\int \mathrm{d}y\, y\sin(y)^2 = \frac{2}{\varrho^2}(\frac{y^2}{4} - \frac{1}{8}\cos(2y) - \frac{1}{4}y\sin(2y)) , \tag{3.54}$$

and second,

$$I_{sc} := \int \mathrm{d}x\, \underbrace{\sin(\varrho\sqrt{1+x}\,)}_{=:y}\underbrace{\cos(\varrho\sqrt{1+x}\,)}_{=:\frac{\mathrm{d}y}{\mathrm{d}x}} = \int \mathrm{d}y\, y = \frac{1}{2}y^2 \equiv \frac{1}{2}\sin(\varrho\sqrt{1+x}\,)^2 . \tag{3.55}$$

Therefore,

$$I_1'' = \frac{2}{\varrho^2}\Big(\frac{1}{4}y^2 - \frac{1}{8}\cos(2y) - \frac{1}{4}y\sin(2y)\Big) + \frac{\nu}{2}\sin(y)^2 \quad ; \quad y = \varrho\sqrt{1+x}\,. \tag{3.56}$$

Using $\sin^2(y) = \frac{1}{2}\left(1-\cos(2y)\right)$, one obtains

$$I_1'' = \frac{1}{4\varrho^2}\Big(2y^2 + \nu\varrho^2 - (1+\varrho^2\nu)\cos(2y) - 2y\sin(2y)\Big) . \tag{3.57}$$

From Eq. (3.48), the integration bounds are

$$\varepsilon \in [-\Omega, 0] \rightarrow x \in [-\nu, 0] \rightarrow y \in [\varrho\sqrt{1-\nu}\,, \varrho] ,$$

and the proper integration will yield

$$\begin{aligned} I_1'' = \frac{1}{4\varrho^2}\Big[&2\nu\varrho + (1+\nu\varrho^2)\left(\cos(2\varrho\sqrt{1+\nu}\,) - \cos(2\varrho)\right) \\ &+ 2\varrho\left(\sqrt{1+\nu}\,\sin(2\varrho\sqrt{1+\nu}\,) - \sin(2\varrho)\right)\Big] . \end{aligned} \tag{3.58}$$

Using the Taylor expansions

$$\begin{aligned}\cos(2\varrho\sqrt{1+\nu}) - \cos(2\varrho) &= -\varrho\nu\sin(2\varrho) + \mathcal{O}(\nu^2) \ , \\ \sqrt{1+\nu}\sin(2\varrho\sqrt{1+\nu}) - \sin(2\varrho) &= \nu\left(\varrho\cos(2\varrho) + \frac{1}{2}\sin(2\varrho)\right) \\ &\quad + \frac{1}{8}\Big(2\varrho\cos(2\varrho) - (1+4\varrho^2)\sin(2\varrho)\Big)\nu^2 + \mathcal{O}(\nu^3) \ , \end{aligned} \tag{3.59}$$

the integral becomes

$$\begin{aligned} I_1'' &= \nu\left[\frac{\varrho^2}{2} - \frac{1}{4\varrho}\sin(2\varrho) + \frac{1}{2}\cos(2\varrho) + \frac{1}{4\varrho}\sin(2\varrho)\right] \\ &= \frac{\nu}{2}\left[1+\cos(2\varrho)\right] + \mathcal{O}(\nu^2) \ . \end{aligned} \tag{3.60}$$

Therefore,

$$\begin{aligned} \mathrm{Im}\,\chi_c^R(\mathbf{x},\Omega) &= \frac{1}{2\pi}(\frac{m}{2\pi})^2\frac{1}{r^2}\left(1+\cos(2k_Fr)\right)\Omega + \mathcal{O}(\Omega^3) \\ &= \frac{mk_F{}^4}{4\pi^3}\frac{1+\cos(2k_Fr)}{(2k_Fr)^2}\frac{\Omega}{\varepsilon_F} + \mathcal{O}(\Omega^3) \ . \end{aligned} \tag{3.61}$$

Summary of results for c-electron susceptibility Summarizing the calculations, we obtain

$$\mathrm{Re}\,\chi_c^R(\mathbf{x},\Omega) = \frac{mk_F{}^4}{(2\pi)^3}\frac{1}{\varrho^4}\left(-\varrho\cos(2\varrho) + \frac{1}{2}\sin(2\varrho)\right) + \mathcal{O}(\nu^2) \ , \tag{3.62}$$

$$\mathrm{Im}\,\chi_c^R(\mathbf{x},\Omega) = \frac{1}{2}\frac{mk_F{}^4}{(2\pi)^3}\frac{1+\cos(2\varrho)}{\varrho^2}\frac{\Omega}{\varepsilon_F} + \mathcal{O}(\Omega^3) \ . \tag{3.63}$$

Using the properties of non-interacting conduction electrons with a parabolic dispersion relation, $\varepsilon = \frac{k^2}{2m}$,

$$\begin{aligned} \mathcal{N}_\sigma(\varepsilon) = \frac{4\pi mk[\varepsilon]}{(2\pi)^3} \to \mathcal{N}(\varepsilon_F) \equiv \mathcal{N}_\sigma(\varepsilon_F) &= \frac{4\pi mk_F}{(2\pi)^3} \ , \\ n_e = \frac{N_e}{V} = \frac{k_F{}^3}{3\pi^2} \quad &: \text{average density of electrons} \ , \end{aligned} \tag{3.64}$$

one obtains

$$\mathrm{Re}\,\chi_c^R(\mathbf{x},\Omega) = \frac{3\pi}{4}\,n_e\,\mathcal{N}(\varepsilon_F)\,\frac{1}{\varrho^4}\left(-\varrho\cos(2\varrho) + \frac{1}{2}\sin(2\varrho)\right) + \mathcal{O}(\nu^2) \ , \tag{3.65}$$

$$\mathrm{Im}\,\chi_c^R(\mathbf{x},\Omega) = \frac{3\pi}{8}\,n_e\,\mathcal{N}(\varepsilon_F)\,\frac{1+\cos(2\varrho)}{\varrho^2}\frac{\Omega}{\varepsilon_F} + \mathcal{O}(\Omega^3) \ . \tag{3.66}$$

Finally,

$$\Gamma_{dir}(\Omega) = 4\,J\,J_0^2\,\chi_f^{R\prime}(\Omega)\,\chi_c^{R\prime}(\mathbf{x}-\mathbf{x}_l,\Omega) \ . \tag{3.67}$$

Therefore, having the result for the susceptibility, one can obtain the explicit expression for the direct vertex correction, Eq. (3.16). As it was justified above, the imaginary part of the

c-electron and f-susceptibilities can be ignored.

3.3.2 Exchange vertex correction

The exchange RKKY vertex correction, Γ_{ex}, is depicted diagrammatically in Fig. 3.5,

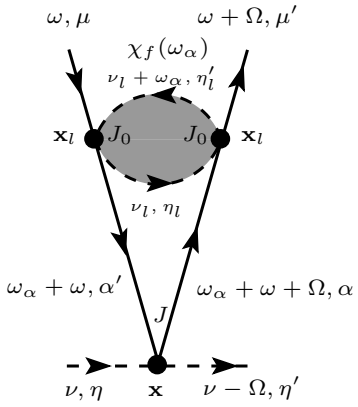

Figure 3.5: Exchange RKKY vertex correction in detail.

and corresponds to the following term[8]

$$\begin{aligned}
\Gamma_{ex} &= -J\, J_0^2\, \mathcal{P}_{ex}\, \mathcal{G}_{ex}\ , \\
\mathcal{P}_{ex} &= \sum_{\substack{\eta_l', \eta_l \\ \alpha', \alpha}} \boldsymbol{\sigma}_{\eta_l \eta_l'} \cdot \boldsymbol{\sigma}_{\alpha' \mu}\, \boldsymbol{\sigma}_{\eta_l' \eta_l} \cdot \boldsymbol{\sigma}_{\mu' \alpha}\, \boldsymbol{\sigma}_{\eta' \eta} \cdot \boldsymbol{\sigma}_{\alpha \alpha'}\ , \\
\mathcal{G}_{ex} &= \frac{1}{\beta} \sum_{i\omega_\alpha} \chi_f(i\omega_\alpha)\, G_c(\mathbf{x} - \mathbf{x}_l, i\omega_\alpha + i\omega) G_c(\mathbf{x}_l - \mathbf{x}, i\omega_\alpha + i\omega + i\Omega)\,,
\end{aligned} \tag{3.69}$$

in which both ω and Ω are bosonic, and ω_α is a fermionic Matsubara frequency. The -1 factor is the overall sign due to the Wick ordering.

Analogous to the direct diagram, the Pauli-matrix part of the exchange diagram yields

$$\mathcal{P}^{(ex)} = -2\, \boldsymbol{\sigma}_{\eta' \eta} \cdot \boldsymbol{\sigma}_{\mu' \mu}\,. \tag{3.70}$$

Again, the spin structure is identical with the bare Kondo interaction.

[8] The operator contractions are

$$f^\dagger_{\eta_l'} f_{\eta_l}\ \boldsymbol{\sigma}_{\eta_l' \eta_l} \cdot \boldsymbol{\sigma}_{\alpha' \mu}\ c^\dagger_{\mathbf{p}' \alpha'} c_{\mathbf{k} \mu} \quad f^\dagger_{\eta} f_{\eta'}\ \boldsymbol{\sigma}_{\eta_l \eta_l'} \cdot \boldsymbol{\sigma}_{\mu', \alpha}\ c^\dagger_{\mathbf{k}' \mu'} c_{\mathbf{p} \alpha} \quad f^\dagger_{\eta'} f_{\eta}\ \boldsymbol{\sigma}_{\eta' \eta} \cdot \boldsymbol{\sigma}_{\alpha \alpha'}\ c^\dagger_{\mathbf{p} \alpha} c_{\mathbf{p}' \alpha'}\ , \tag{3.68}$$

with a minus sign for Wick ordering.

3.3.2.1 Spin part of exchange diagram

The spin part of the exchange diagram yields

$$\begin{aligned}\mathcal{P}_{ex} &= \sum_{\eta_l'\eta_l,\alpha'\alpha} \boldsymbol{\sigma}_{\eta_l'\eta_l}\cdot\boldsymbol{\sigma}_{\alpha'\mu}\,\boldsymbol{\sigma}_{\eta_l\eta_l'}\cdot\boldsymbol{\sigma}_{\mu'\alpha}\,\boldsymbol{\sigma}_{\eta'\eta}\cdot\boldsymbol{\sigma}_{\alpha\alpha'} \\ &= \sum_{\alpha'\alpha}\left(\boldsymbol{\sigma}_{\eta'\eta}\cdot\boldsymbol{\sigma}_{\alpha\alpha'}\sum_{\eta_l'\eta_l}\boldsymbol{\sigma}_{\alpha'\mu}\cdot\boldsymbol{\sigma}_{\eta_l'\eta_l}\,\boldsymbol{\sigma}_{\eta_l\eta_l'}\cdot\boldsymbol{\sigma}_{\mu'\alpha}\right)\ ; \end{aligned} \tag{3.71}$$

moreover,

$$\begin{aligned}\sum_{\eta_l'\eta_l}\boldsymbol{\sigma}_{\alpha'\mu}\cdot\boldsymbol{\sigma}_{\eta_l'\eta_l}\,\boldsymbol{\sigma}_{\eta_l\eta_l'}\cdot\boldsymbol{\sigma}_{\mu'\alpha} &= \sum_{ab}\sum_{\eta_l'\eta_l}\sigma^a_{\alpha'\mu}\sigma^a_{\eta_l'\eta_l}\sigma^b_{\eta_l\eta_l'}\sigma^b_{\mu'\alpha} \\ &= \sum_{ab}\Big(\sigma^a_{\alpha'\mu}\sigma^b_{\mu'\alpha}\underbrace{\mathrm{Tr}[\sigma^a\sigma^b]}_{=2\delta_{ab}}\Big) \\ &= 2\,\boldsymbol{\sigma}_{\alpha'\mu}\cdot\boldsymbol{\sigma}_{\mu'\alpha}\ . \end{aligned} \tag{3.72}$$

Thus, $\mathcal{P}_{ex}$, Eq. (3.71), simplifies to

$$\begin{aligned}\mathcal{P}_{ex} &= 2\sum_{\alpha'\alpha}\boldsymbol{\sigma}_{\eta'\eta}\cdot\boldsymbol{\sigma}_{\alpha\alpha'}\,\boldsymbol{\sigma}_{\alpha'\mu}\cdot\boldsymbol{\sigma}_{\mu'\alpha} = 2\sum_{ab}\sum_{\alpha\alpha'}\sigma^a_{\eta'\eta}(\sigma^a\sigma^b)_{\alpha\mu}\,\sigma^b_{\mu'\alpha} \\ &= 2\sum_{ab}\left(\sigma^a_{\eta'\eta}\sum_{\alpha}\sigma^b_{\mu'\alpha}\,\left(\delta_{ab}\delta_{\alpha\mu}+\mathrm{i}\sum_c\epsilon_{abc}\sigma^c_{\alpha\mu}\right)\right) \\ &= 2\sum_{ab}\sigma^a_{\eta'\eta}\sigma^b_{\mu'\mu}\delta_{ab} + 2\mathrm{i}\sum_{abc}\sigma^a_{\eta'\eta}\epsilon_{abc}\underbrace{\sum_{\alpha}\sigma^b_{\mu'\alpha}\sigma^c_{\alpha\mu}}_{=(\sigma^b\sigma^c)_{\mu\mu'}=\delta_{bc}\delta_{\mu\mu'}+\mathrm{i}\sum_d\epsilon_{bcd}\sigma^d_{\mu'\mu}} \\ &= 2\,\boldsymbol{\sigma}_{\eta'\eta}\cdot\boldsymbol{\sigma}_{\mu'\mu} + 2\mathrm{i}\underbrace{\sum_{abc}\sigma^a_{\eta'\eta}\,\epsilon_{abc}\,\delta_{bc}\delta_{\mu\mu'}}_{=0} + 2\mathrm{i}\cdot\mathrm{i}\sum_{abcd}\sigma^a_{\eta'\eta}\,\epsilon_{abc}\,\epsilon_{bcd}\sigma^d_{\mu'\mu}\ , \end{aligned} \tag{3.73}$$

which by using the identity (Appendix A),

$$\sum_{bc}\epsilon_{abc}\epsilon_{bcd} = \sum_{bc}\epsilon_{abc}\epsilon_{dbc} = 2\delta_{ad}\ ,$$

yields

$$\begin{aligned}\mathcal{P}_{ex} &= 2\,\boldsymbol{\sigma}_{\eta'\eta}\cdot\boldsymbol{\sigma}_{\mu'\mu} - 2\sum_{ad}2\delta_{ad}\,\sigma^a_{\eta'\eta}\sigma^d_{\mu'\mu} \\ &= 2\,\boldsymbol{\sigma}_{\eta'\eta}\cdot\boldsymbol{\sigma}_{\mu'\mu} - 4\,\boldsymbol{\sigma}_{\eta'\eta}\cdot\boldsymbol{\sigma}_{\mu'\mu} \\ &= -2\,\boldsymbol{\sigma}_{\eta'\eta}\cdot\boldsymbol{\sigma}_{\mu'\mu}\ . \end{aligned} \tag{3.74}$$

3.3.2.2 Real and imaginary parts of the exchange diagram

The real and imaginary parts of the exchange diagram can be obtained by decomposing the Green's functions and the f-susceptibility into their imaginary and real parts and collecting factors of the real and imaginary parts of the impurity susceptibility. A detailed but straight-

forward calculation using the explicit form the Green's functions and f-susceptibility, yields the result

$$\Gamma_{ex} = JJ_0^2 \frac{(g\mu_B)^2 W}{\pi} \frac{1}{\pi} (\frac{mk_F}{2\pi})^2 \frac{\varepsilon_F}{T_K} \frac{\sin(2\varrho)\,\nu + 2\mathrm{i}\,\sin^2(\varrho)\,|\nu|}{\varrho^2}\,\Theta(T_K - |\Omega|)\ , \tag{3.75}$$

where $\nu = \Omega/\varepsilon_F$. One observes that in the relevant energy interval, $\Omega \sim \mathcal{O}(T_K) \ll D_0$, where the RG β-function is non-vanishing (see section 3.4), the direct and exchange vertex corrections satisfy $|\Gamma_{ex}/\Gamma_{dir}| \sim \frac{T_K}{D_0} \ll 1$, and thus, the exchange vertex correction can be safely neglected.[9]

Explicit Calculations The explicit form of the exchange vertex correction is obtained by performing the Matsubara summation,[10]

$$\begin{aligned}\Gamma_{ex} = +2J\,J_0^2 \int \mathrm{d}\varepsilon \Big[& n_F(\varepsilon+\omega)\,A_c(\mathbf{x}-\mathbf{x}_l,\varepsilon+\omega)\,G_c^R(\mathbf{x}_l-\mathbf{x},\varepsilon+\omega+\Omega)\,\chi_f^A(\varepsilon) \\ & + n_F(\varepsilon+\omega+\Omega)\,G_c^R(\mathbf{x}-\mathbf{x}_l,\varepsilon+\omega)\,A_c(\mathbf{x}_l-\mathbf{x},\varepsilon+\omega+\Omega)\,\chi_f^A(\varepsilon) \\ & + n_B(\varepsilon+\omega+\Omega)\,G_c^R(\mathbf{x}-\mathbf{x}_l,\varepsilon+\omega)\,G_c^R(\mathbf{x}_l-\mathbf{x},\varepsilon+\omega+\Omega)\,\frac{1}{\pi}\chi_f^{A\prime\prime}(\varepsilon)\Big]\ . \end{aligned} \tag{3.77}$$

To reduce the notational clutter, we drop the position coordinates in the following so that

$$\begin{aligned}\Gamma_{ex} = 2JJ_0^2 \int \mathrm{d}\varepsilon \Big\{ & n_F(\varepsilon+\omega)A_c(\varepsilon+\omega)G_c^R(\varepsilon+\omega+\Omega)\chi_f^A(\varepsilon) \\ & + n_F(\varepsilon+\omega+\Omega)G_c^A(\varepsilon+\omega)A_c(\varepsilon+\omega+\Omega)\chi_f^A(\varepsilon) && (3.78) \\ & + n_B(\varepsilon)G_c^R(\varepsilon+\omega)G_c^R(\varepsilon+\omega+\Omega)\frac{1}{\pi}\chi_f^{R\prime\prime}(\varepsilon)\Big\}\ . && (3.79)\end{aligned}$$

By decomposing χ_f into its real and imaginary parts, we can further expand the relation for Γ_{ex}:

$$\begin{aligned}\chi_f^{A\prime}(\varepsilon) &\equiv \chi_f^{A\prime}(\varepsilon) + \mathrm{i}\chi_f^{A\prime\prime}(\varepsilon) \\ &= \chi_f^{R\prime}(\varepsilon) - \mathrm{i}\chi_f^{R\prime\prime}(\varepsilon)\ , \end{aligned} \tag{3.80}$$

[9] This can be compared to the Migdal's theorem in the context of electron-phonon interaction, which states that phonon correction (renormalization) to the electron-phonon vertex is suppressed at least by a factor $\sqrt{\frac{m_e}{M_i}} \sim 10^{-2}$, where m_e and M_i represent the mass of an electron and an ion (for a detailed discussion, consult, e.g., Ref. [122, 123]). Here the impurity vertex correction to the electronic vertex is suppressed by a factor $\frac{T_K}{D_0} \sim 10^{-3}$.

[10] Note that the following relations are used

$$\begin{aligned}\mathrm{Re}\,\chi_f^A(\varepsilon) &= \mathrm{Re}\,\chi_f^R(\varepsilon)\ , \\ \mathrm{Im}\,\chi_f^A(\varepsilon) &= -\mathrm{Im}\,\chi_f^R(\varepsilon)\ . \end{aligned} \tag{3.76}$$

so that

$$\begin{aligned}\Gamma_{ex} = 2JJ_0^2 \int \mathrm{d}\varepsilon \Big[&\Big(n_F(\varepsilon+\omega) A_c(\varepsilon+\omega) G_c^R(\varepsilon+\omega+\Omega) + n_F(\varepsilon+\omega+\Omega) G_c^A(\varepsilon+\omega) A_c(\varepsilon+\omega+\Omega) \Big) \chi_f^{R\prime}(\varepsilon) \\ &- \mathrm{i} \Big(n_F(\varepsilon+\omega) A_c(\varepsilon+\omega) G_c^R(\varepsilon+\omega+\Omega) + n_F(\varepsilon+\omega+\Omega) G_c^A(\varepsilon+\omega) A_c(\varepsilon+\omega+\Omega) \Big) \chi_f^{R\prime\prime}(\varepsilon) \\ &+ n_B(\varepsilon) G_c^R(\varepsilon+\omega) G_c^R(\varepsilon+\omega+\Omega) \frac{1}{\pi} \chi_f^{R\prime\prime}(\varepsilon) \Big] \ . \end{aligned} \tag{3.81}$$

Therefore, the expression for Γ_{ex} can be decomposed into two major terms

i) A factor of $\mathrm{Re}\,\chi_f^R$ which reads

$$\begin{aligned}\mathcal{F}' := \int \mathrm{d}\varepsilon \Big[&n_F(\varepsilon+\omega) A_c(\varepsilon+\omega) G_c^R(\varepsilon+\omega+\Omega) \\ &+ n_F(\varepsilon+\omega+\Omega) G_c^A(\varepsilon+\omega) A_c(\varepsilon+\omega+\Omega) \Big] \chi_f^{R\prime}(\varepsilon) \ . \end{aligned} \tag{3.82}$$

By decomposing the Green's functions into their real and imaginary parts,

$$\begin{aligned} G^R(\varepsilon) &= G^{R\prime}(\varepsilon) + \mathrm{i} G^{R\prime\prime}(\varepsilon) = G^{R\prime}(\varepsilon) - \mathrm{i}\pi A(\varepsilon) \\ G^A(\varepsilon) &= G^{A\prime}(\varepsilon) + \mathrm{i} G^{A\prime\prime}(\varepsilon) = G^{A\prime}(\varepsilon) + \mathrm{i}\pi A(\varepsilon) \ , \end{aligned} \tag{3.83}$$

and applying the transformation $\varepsilon \mapsto \varepsilon - \omega$, the factor becomes

$$\begin{aligned}\mathcal{F}' = \int \mathrm{d}\varepsilon \Big[&n_F(\varepsilon) A_c(\varepsilon) G_c^{R\prime}(\varepsilon+\Omega) \\ &+ n_F(\varepsilon+\Omega) G_c^{R\prime}(\varepsilon) A_c(\varepsilon+\Omega) \\ &- \mathrm{i}\pi (n_F(\varepsilon) - n_F(\varepsilon+\Omega)) A_c(\varepsilon) A_c(\varepsilon+\Omega) \Big] \chi_f^{R\prime}(\varepsilon-\omega) \ . \end{aligned} \tag{3.84}$$

This is so far exact.

ii) A factor of $\mathrm{Im}\,\chi_f^R$ which reads

$$\begin{aligned}\mathcal{F}'' = -\mathrm{i} \int \mathrm{d}\varepsilon \Big[&n_F(\varepsilon+\omega) A_c(\varepsilon+\omega) G_c^R(\varepsilon+\omega+\Omega) \\ &+ n_F(\varepsilon+\omega+\Omega) G_c^A(\varepsilon+\omega) A_c(\varepsilon+\omega+\Omega) \\ &+ \mathrm{i} n_B(\varepsilon) G_c^R(\varepsilon+\omega) G_c^R(\varepsilon+\omega+\Omega) \frac{1}{\pi} \Big] \chi_f^{R\prime\prime}(\varepsilon) \ . \end{aligned} \tag{3.85}$$

By decomposing the Green's functions to their real and imaginary parts as before, and applying the transformation $\varepsilon \mapsto \varepsilon - \omega$, the factor becomes

$$\begin{aligned}\mathcal{F}'' = -\mathrm{i} \int \mathrm{d}\varepsilon \Big[&\left(n_F(\varepsilon+\omega) + n_B(\varepsilon-\omega) \right) A_c(\varepsilon) G_c^{R\prime}(\varepsilon+\Omega) \\ &+ \left(n_F(\varepsilon+\Omega) + n_B(\varepsilon-\omega) \right) G_c^{R\prime}(\varepsilon) A_c(\varepsilon+\Omega) \\ &+ (-\mathrm{i}\pi) \left(n_F(\varepsilon) - n_F(\varepsilon+\Omega) + n_B(\varepsilon-\omega) \right) A_c(\varepsilon) A_c(\varepsilon+\Omega) \\ &+ \frac{\mathrm{i}}{\pi} n_B(\varepsilon-\omega) G_c^{R\prime}(\varepsilon) G_c^{R\prime}(\varepsilon+\Omega) \Big] \chi_f^{R\prime\prime}(\varepsilon-\omega) \ . \end{aligned} \tag{3.86}$$

This is exact up to here.

The integrations above cannot be performed analytically. In order to make progress, we need to use the asymptotic form of the impurity susceptibility, χ_f. Furthermore, we will let the energy of the incoming electron to be on the Fermi level, $\omega \stackrel{!}{=} 0$.

Dimensionless variables Before the actual calculation, we introduce the dimensionless variables used in this section:

$$\begin{aligned} x &:= \frac{\varepsilon}{\varepsilon_F} \ , \\ \nu &:= \frac{\Omega}{\varepsilon_F} \ , \\ \varrho &:= k_F r \ , \\ \tau_K &:= T_K/D_0 \ll 1 \ , \\ d_0 &:= \frac{\varepsilon_F}{T_K} \approx \frac{D_0}{T_K} \gg 1 \ . \end{aligned} \tag{3.87}$$

3.3.2.3 Asymptotic form of the impurity susceptibility

The susceptibility for the f-pseudo-fermions was given before, in section 3.2. The real part of the impurity susceptibility reads

$$\operatorname{Re}\chi_f^R(\varepsilon) \equiv \chi_f^{R\prime} = \frac{(g\mu_B)^2 W}{\pi} \frac{1}{T_K} \frac{1}{\sqrt{1+(\varepsilon/T_K)^2}} \ ,$$

where W is the Wilson ratio, g is the Landé g-factor and μ_B is the Bohr magneton. Let us define

$$a' := \frac{(g\mu_B)^2 W}{\pi} \ , \tag{3.88}$$

to absorb the constants and reduce the notational clutter. Then, the asymptotic approximation to the real part reads

$$\operatorname{Re}\chi_f^R(\varepsilon) \approx \begin{cases} \frac{a'}{T_K} & ;|\varepsilon| \ll T_K \\ \frac{a'}{T_K}\frac{1}{|\varepsilon/T_K|} & ;|\varepsilon| \gg T_K \end{cases} \ . \tag{3.89}$$

The corresponding imaginary part (which can be obtained from the real part by the Kramers-Kronig relations) reads

$$\operatorname{Im}\chi_f^R(\varepsilon) \equiv \chi_f^{R\prime\prime}(\varepsilon) = \left(\frac{2}{\pi}\frac{(g\mu_B)^2 W}{\pi}\right) \frac{1}{T_K} \frac{\operatorname{arcsinh}(\varepsilon/T_K)}{\sqrt{1+(\varepsilon/T_K)^2}} \ .$$

We can absorb the constant factors in a'',

$$a'' := \frac{2}{\pi}\frac{(g\mu_B)^2 W}{\pi} = \frac{2}{\pi} a' \ . \tag{3.90}$$

The asymptotic approximation for $\mathrm{Im}\,\chi_f$ is[11]

$$\mathrm{Im}\,\chi_f^R(\varepsilon) \approx \begin{cases} \frac{a''}{T_K}\frac{\varepsilon}{T_K} & ;|\varepsilon| \ll T_K \\ \frac{a''}{T_K}\frac{\ln|\varepsilon/T_K|}{\varepsilon/T_K} & ;|\varepsilon| \gg T_K \end{cases} . \tag{3.95}$$

We need these asymptotic approximations in the explicit calculations in the next part.

[11] The asymptotic form of arcsinh function can be obtained as below:

$$x := \sinh^{-1}(y) \Rightarrow y = \sinh(x) = \frac{e^x - e^{-x}}{2} . \tag{3.91}$$

If $z \geq 0$ is defined as $z := e^x \Leftrightarrow x = \ln z$, then

$$\begin{aligned} z = y \pm \sqrt{1+y^2} &\overset{z\geq 0}{\Rightarrow} z = y + \sqrt{1+y^2} \\ &\rightarrow x = \ln z = \ln(y + \sqrt{1+y^2}) . \end{aligned} \tag{3.92}$$

If $y \to 0$,

$$\begin{aligned} &\lim_{y\to 0} y + \sqrt{1+y^2} =\rightarrow 1 + y \\ &\rightarrow \ln(y + \sqrt{1+y^2}) \rightarrow \ln(\underbrace{1+y}_{>0}) = y + \mathcal{O}(y^2) \\ &\rightarrow x \equiv \sinh^{-1}(y) \approx y . \end{aligned} \tag{3.93}$$

If $y \to +\infty$,

$$\begin{aligned} &\lim_{y\to +\infty} y + \sqrt{1+y^2} =\rightarrow 1 + |y| \overset{y\geq 0}{=} 2y \approx y \\ &\rightarrow x \equiv \sinh^{-1}(y) \rightarrow \ln(2y) \approx \ln(y) . \end{aligned} \tag{3.94}$$

If $y \to -\infty$,

$$\begin{aligned} &\lim_{y\to -\infty} y + \sqrt{1+y^2} =\rightarrow 1 + |y|(1+\frac{1}{y^2})^{\frac{1}{2}} \approx y + |y|(1+\frac{1}{2y^2}) \\ &= \underbrace{y + |y|}_{\overset{y\leq 0}{=} y-y=0} + \frac{1}{2|y|} = \frac{1}{2|y|} \\ &\rightarrow x = \sinh^{-1}(y) \rightarrow \ln(\frac{1}{2|y|}) = -\ln(2|y|) \approx -\ln|y| . \end{aligned}$$

Therefore,

$$\lim_{y\to\pm\infty} \sinh^{-1}(y) = \pm\ln|y| = \frac{|y|}{y}\ln|y| .$$

Finally,

$$\frac{\mathrm{arcsinh}(y)}{\sqrt{1+y^2}} = \begin{cases} y & ;y \to 0 \\ \frac{\frac{|y|}{y}\ln|y|}{|y|} & ;y \to \pm\infty \end{cases} .$$

3.3.2.4 Factors of the real part of f-susceptibility

The factor of the real part of the impurity susceptibility reads

$$\begin{aligned}\mathcal{F}' = \int \mathrm{d}\varepsilon \Big[& n_F(\varepsilon) A_c(\varepsilon) G_c^{R\prime}(\varepsilon+\Omega) \\ & + n_F(\varepsilon+\Omega) G_c^{R\prime}(\varepsilon) A_c(\varepsilon+\Omega) \\ & - \mathrm{i}\pi (n_F(\varepsilon) - n_F(\varepsilon+\Omega) A_c(\varepsilon) A_c(\varepsilon+\Omega)\Big] \chi_f'(\varepsilon) \ . \end{aligned} \tag{3.96}$$

First integral The first integral on the RHS of Eq. (3.96) is

$$\int \mathrm{d}\varepsilon \, n_F(\varepsilon) A_c(\varepsilon) G_c^{R\prime}(\varepsilon+\Omega) \chi_f'(\varepsilon) \ . \tag{3.97}$$

At low energies, the factor containing statistical distribution in the integrand merely determines the range of integration:

$$n_F(\varepsilon) \overset{T\to 0+}{\approx} \Theta(-\varepsilon) \ ; \tag{3.98}$$

therefore, $\varepsilon \in [-D_0, 0] \to x \in [-1, 0]$. The first integral will be

$$-\frac{1}{\pi} (\frac{m}{2\pi})^2 \frac{a'}{T_K} \frac{\varepsilon_F}{r^2} I_1' \ , \tag{3.99}$$

with

$$I_1' := \int_{-1}^{0} \mathrm{d}x \, \sin(\varrho \sqrt{1+x}) \left(\cos(\varrho \sqrt{1+x}) - \frac{1}{2} \varrho \nu \frac{\sin(\varrho \sqrt{1+x})}{\sqrt{1+x}} \right) \frac{1}{\sqrt{1+(d_0 x)^2}} \ , \tag{3.100}$$

where we have used the dimensionless variables defined in Eq. (3.87). The integral cannot be performed analytically. We have to use the asymptotic form of the impurity susceptibility, introduced in section 3.3.2.3, and consider all the possible cases

i) When $\Omega > 0 \wedge \Omega > T_K \to \varepsilon \in [-D_0, 0]$:

$$I_1' = -\frac{1}{2} \sin(2\varrho) \tau_K \ln \tau_K + \mathcal{O}(\tau_K) \ . \tag{3.101}$$

ii) When $\Omega > 0 \wedge \Omega < T_K \to \varepsilon [-D_0, 0]$:

$$I_1' = -\frac{1}{2} \sin(2\varrho) \tau_K \ln \tau_K + \mathcal{O}(\tau_K) \ . \tag{3.102}$$

iii) When $\Omega < 0 \wedge |\Omega| > T_K \equiv \Omega < -T_K \to \varepsilon \in [-D_0, 0]$:

$$I_1' = -\frac{1}{2} \sin(2\varrho) \tau_K \ln \tau_K + \mathcal{O}(\tau_K) \ . \tag{3.103}$$

iv) When $\Omega < 0 \wedge |\Omega| < T_K \equiv \Omega > -T_K \rightarrow \varepsilon \in [0, -\Omega]$:

$$I_1' = -\frac{1}{2}\sin(2\varrho)\tau_K \ln \tau_K + \mathcal{O}(\tau_K) \ . \tag{3.104}$$

Second integral The second integral on the RHS of Eq. (3.96) is

$$\int \mathrm{d}\varepsilon \, n_F(\varepsilon + \Omega) G_c^{R\prime}(\varepsilon) A_c(\varepsilon + \Omega) \chi_f'(\varepsilon) \ . \tag{3.105}$$

At low energies, the factor containing statistical distribution in the integrand merely determines the range of integration:

$$n_F(\varepsilon + \Omega) \overset{T \to 0+}{\approx} \Theta(-(\varepsilon + \Omega)) \ ; \tag{3.106}$$

therefore, $\varepsilon \in [-D_0, -\Omega] \rightarrow x \in [-1, -\nu]$. Then the integral will be

$$-\frac{1}{\pi}(\frac{m}{2\pi})^2 \frac{a'}{T_K} \frac{\varepsilon_F}{r^2} I_2' \ , \tag{3.107}$$

with

$$\begin{aligned} I_2' &:= \int_{-1}^{-\nu} \mathrm{d}x \, \cos(\varrho \sqrt{1+x}) \sin(\varrho \sqrt{1+x+\nu}) \frac{1}{\sqrt{1+(d_0 x)^2}} \\ &= \int_{-1}^{-\nu} \mathrm{d}x \, \cos(\varrho \sqrt{1+x}) \left(\sin(\varrho \sqrt{1+x}) + \frac{1}{2}\varrho\nu \frac{\cos(\varrho \sqrt{1+x})}{\sqrt{1+x}} \right) \frac{1}{\sqrt{1+(d_0 x)^2}} \ , \end{aligned} \tag{3.108}$$

where in the second line a Taylor-expansion is performed with respect to $\nu \ll 1$. The integral cannot be performed analytically. We have to use the asymptotic form of the impurity susceptibility, introduced in section 3.3.2.3, and consider all the possible cases

i) When $\Omega > 0 \wedge \Omega > T_K \rightarrow \varepsilon \in [-D_0, -\Omega]$:

$$I_2' = \mathcal{O}(\tau_K) \ . \tag{3.109}$$

ii) When $\Omega > 0 \wedge \Omega < T_K \rightarrow \varepsilon[-D_0, -\Omega]$:

$$I_2' = -\frac{1}{2}\sin(2\varrho)\nu + \mathcal{O}(\nu^2) + \mathcal{O}(\tau_K) \ . \tag{3.110}$$

iii) When $\Omega < 0 \wedge |\Omega| > T_K \equiv \Omega < -T_K \rightarrow \varepsilon \in [-D_0, -\Omega]$:

$$I_2' = -\sin(2\varrho)\tau_K \ln \tau_K + \frac{1}{2}\sin(2\varrho)\tau_K \ln \nu + \mathcal{O}(\tau_K) \ . \tag{3.111}$$

iv) When $\Omega < 0 \wedge |\Omega| < T_K \equiv \Omega > -T_K \rightarrow \varepsilon \in [0, -\Omega]$:

$$I_2' = -\frac{1}{2}\sin(2\varrho)\tau_K \ln \tau_K - \frac{1}{2}\nu \sin(2\varrho) + \mathcal{O}(\tau_K) \ . \tag{3.112}$$

Third integral The third integral on the RHS of Eq. (3.96) is

$$\int \mathrm{d}\varepsilon \; (n_F(\varepsilon) - n_F(\varepsilon+\Omega))\, A_c(\varepsilon) A_c(\varepsilon+\Omega) \chi_f'(\varepsilon) \; . \tag{3.113}$$

At low energies, the factor containing statistical distribution in the integrand merely determines the range of integration:

$$n_F(\varepsilon) - n_F(\varepsilon+\Omega) \overset{T\to 0^+}{\approx} \Theta(\varepsilon+\Omega) - \Theta(\varepsilon) \; ; \tag{3.114}$$

therefore, for $\Omega > 0$,

$$\varepsilon \in [-\Omega, 0] \to x \in [-\nu, 0] \; ,$$

and for $\Omega < 0$,

$$\varepsilon \in [0, -\Omega] \to x \in [0, -\nu] \; .$$

Then the proper integral will be

$$(\frac{m}{2\pi})^2 \frac{a'}{T_K} \frac{\varepsilon_F}{r^2} \, I_3' \tag{3.115}$$

with

$$\begin{aligned} I_3' &:= \int \mathrm{d}x \; \sin(\varrho\sqrt{1+x}\,) \sin(\varrho\sqrt{1+x+\nu}\,) \frac{1}{\sqrt{1+(d_0 x)^2}} \\ &= \int \mathrm{d}x \; \sin(\varrho\sqrt{1+x}\,) \left(\sin(\varrho\sqrt{1+x}\,) + \frac{1}{2}\varrho\nu \frac{\cos(\varrho\sqrt{1+x}\,)}{\sqrt{1+x}} \right) \frac{1}{\sqrt{1+(d_0 x)^2}} \; , \end{aligned} \tag{3.116}$$

where in the second line a Taylor-expansion is performed with respect to $\nu \ll 1$. The integral cannot be performed analytically. We have to use the asymptotic form of the impurity susceptibility, introduced in section 3.3.2.3, and consider all the possible cases:

i) When $\Omega > 0 \wedge \Omega > T_K \to \varepsilon \in [-\Omega, 0]$:

$$I_3' = \sin^2(\varrho)\tau_K \ln|\nu/\tau_K| + \mathcal{O}(\tau_K) \; . \tag{3.117}$$

ii) When $\Omega > 0 \wedge \Omega < T_K \to \varepsilon[-\Omega, 0]$:

$$I_3' = \sin^2(\varrho)\nu + \mathcal{O}(\nu^3) \; . \tag{3.118}$$

iii) When $\Omega < 0 \wedge |\Omega| > T_K \equiv \Omega < -T_K \to \varepsilon \in [0, -\Omega]$:

$$I_3' = \sin^2(\varrho)\tau_K \ln|\nu/\tau_K| + \mathcal{O}(\tau_K) \; . \tag{3.119}$$

iv) When $\Omega < 0 \wedge |\Omega| < T_K \equiv \Omega > -T_K \to \varepsilon \in [0, -\Omega]$:

$$I_3' = -\sin^2(\varrho)\nu + \mathcal{O}(\nu^3) \; . \tag{3.120}$$

Final result for factors of real part of f-susceptibility Putting the integral pieces together, one obtains

$$\begin{aligned}\mathcal{F}' = &-\frac{1}{\pi}(\frac{m}{2\pi})^2\frac{a'}{T_K}\frac{\varepsilon_F}{r^2}I_1' \\ &-\frac{1}{\pi}(\frac{m}{2\pi})^2\frac{a'}{T_K}\frac{\varepsilon_F}{r^2}I_2' \\ &-\mathrm{i}\pi(\frac{1}{\pi})^2(\frac{m}{2\pi})^2\frac{a'}{T_K}\frac{\varepsilon_F}{r^2}I_3' \\ &= -\frac{1}{\pi}(\frac{m}{2\pi})^2\frac{a'}{T_K}\frac{\varepsilon_F}{r^2}\underbrace{(I_1' + I_2' + \mathrm{i}I_3')}_{:=\mathcal{I}'}\end{aligned} \tag{3.121}$$

i) When $\Omega > 0 \wedge \Omega > T_K \to \varepsilon \in [-\Omega, 0]$:

$$\mathcal{I}' = -\frac{1}{2}\sin(2\varrho)\tau_K \ln\tau_K + \mathrm{i}\sin^2(\varrho)\tau_K \ln|\nu/\tau_K| \ . \tag{3.122}$$

ii) When $\Omega > 0 \wedge \Omega < T_K \to \varepsilon[-\Omega, 0]$:

$$\mathcal{I}' = -\frac{1}{2}\sin(2\varrho)\tau_K \ln\tau_K - \frac{1}{2}\sin(2\varrho)\nu + \mathrm{i}\sin^2(\varrho)\nu \ . \tag{3.123}$$

iii) When $\Omega < 0 \wedge |\Omega| > T_K \equiv \Omega < -T_K \to \varepsilon \in [0, -\Omega]$:

$$\mathcal{I}' = \frac{1}{2}\sin(2\varrho)\tau_K \ln|\nu/\tau_K| + \mathrm{i}\sin(2\varrho)\ln|\nu/\tau_K| \ . \tag{3.124}$$

iv) When $\Omega < 0 \wedge |\Omega| < T_K \equiv \Omega > -T_K \to \varepsilon \in [0, -\Omega]$:

$$\mathcal{I}' = -\sin(2\varrho)\tau_K \ln\tau_K - \frac{\nu}{2}\sin(2\varrho) - \mathrm{i}\nu\sin^2(\varrho) \ . \tag{3.125}$$

3.3.2.5 Factors of the imaginary part of χ_f

The factor of $\chi_f^{R\prime\prime}$, at low temperatures ($T \to 0^+$) and low frequencies ($\omega \to 0$), is

$$\begin{aligned}\mathcal{F}'' = -\mathrm{i}\int \mathrm{d}\varepsilon \Big[&(n_F(\varepsilon+\Omega) - n_F(\varepsilon))\, G_c^{R\prime}(\varepsilon)A_c(\varepsilon+\Omega) \\ &-\mathrm{i}\pi(-n_F(\varepsilon+\Omega))A_c(\varepsilon)A_c(\varepsilon+\Omega) \\ &-\frac{\mathrm{i}}{\pi}n_F(\varepsilon)G_c^{R\prime}(\varepsilon)G_c^{R\prime}(\varepsilon+\Omega)\Big]\chi_f^{R\prime\prime}(\varepsilon) \ .\end{aligned} \tag{3.126}$$

The three integrations will be considered separately.

First Integral The first integral on the RHS is

$$\int \mathrm{d}\varepsilon\ (n_F(\varepsilon+\Omega) - n_F(\varepsilon))\, G_c^{R\prime}(\varepsilon)A_c(\varepsilon+\Omega)\chi_f^{R\prime\prime}(\varepsilon) \ . \tag{3.127}$$

At low temperatures, the factor containing the Fermi-Dirac distributions merely limits the range

of integration:

$$n_F(\varepsilon+\Omega)-n_F(\varepsilon)=\Theta(\varepsilon)-\Theta(\varepsilon+\Omega)\equiv-(\Theta(\varepsilon)-\Theta(\varepsilon+\Omega))\ ; \tag{3.128}$$

thus, if $\Omega\geq 0$,

$$\varepsilon\in[-\Omega,0]\rightarrow x\in[-\frac{\Omega}{\varepsilon_F},0]\equiv[-\nu,0]\ , \tag{3.129}$$

otherwise, $\Omega<0$, and

$$\varepsilon\in[0,-\Omega]\rightarrow x\in[0,-\frac{\Omega}{\varepsilon_F}]\equiv[0,-\nu]\ . \tag{3.130}$$

In the proper integration range, we have to consider the integral

$$\begin{aligned}&\int \mathrm{d}\varepsilon\, G_c^{R\prime}(\varepsilon)A_c(\varepsilon+\Omega)\chi_f^{R\prime\prime}(\varepsilon)\\&=\frac{-1}{\pi}(\frac{m}{2\pi})^2\frac{\varepsilon_F}{r^2}\int \mathrm{d}x\,\cos(\varrho\sqrt{1+x}\,)\sin(\varrho\sqrt{1+x+\nu}\,)\chi_f''(d_0\,x)\ ,\end{aligned} \tag{3.131}$$

where the previously-defined dimensionless variables, Eq. (3.87), are used. Regarding Eq. (**??**), we should consider the dimensionless integral,

$$I_1'':=\int \mathrm{d}x\,\cos(\varrho\sqrt{1+x}\,)\sin(\varrho\sqrt{1+x+\nu}\,)\chi_f''(d_0x)\ . \tag{3.132}$$

At low frequencies, $\nu\ll 1$, one can Taylor-expand the integrand in ν to obtain

$$I_1''\overset{\nu\ll 1}{=}\int \mathrm{d}x\,\cos(\varrho\sqrt{1+x}\,)(\sin(\varrho\sqrt{1+x}\,)+\frac{1}{2}\varrho\nu\frac{\cos(\varrho\sqrt{1+x}\,)}{\sqrt{1+x}}\chi_f''(d_0x)\ . \tag{3.133}$$

The integral cannot be performed analytically. We have to use the asymptotic form of the impurity susceptibility, introduced in section 3.3.2.3, and consider all the possible cases:

i) When $\Omega>0\wedge\Omega>T_K\rightarrow\varepsilon\in[-\Omega,0]$:

$$I_1''=-\frac{1}{2}\sin(2\varrho)\tau_K\ln|\nu/\tau_K|+\mathcal{O}(\tau_K)\ . \tag{3.134}$$

ii) When $\Omega>0\wedge\Omega<T_K\rightarrow\varepsilon[-\Omega,0]$:

$$I_1''=\frac{-\sin(2\varrho)}{4\tau_K}\nu^2+\mathcal{O}(\nu^3)\ . \tag{3.135}$$

iii) When $\Omega<0\wedge|\Omega|>T_K\equiv\Omega<-T_K\rightarrow\varepsilon\in[0,-\Omega]$:

$$I_1''=\frac{1}{2}\sin(2\varrho)\tau_K\ln|\nu/\tau_K|+\mathcal{O}(\nu^3)\ . \tag{3.136}$$

iv) When $\Omega < 0 \wedge |\Omega| < T_K \equiv \Omega > -T_K \rightarrow \varepsilon \in [0, -\Omega]$:

$$I_1'' = \mathcal{O}(\tau_K) - \frac{1}{2}\sin(2\varrho)\tau_K \ln|\nu/\tau_K| \ . \tag{3.137}$$

Second Integral The second integral on the RHS of Eq. (3.126) is

$$\int \mathrm{d}\varepsilon \ (-n_F(\varepsilon+\Omega))\, A_c^{R\prime}(\varepsilon) A_c(\varepsilon+\Omega)\chi_f^{R\prime\prime}(\varepsilon) \ . \tag{3.138}$$

At low temperatures, the factor containing the Fermi-Dirac distributions merely limits the range of integration:

$$-n_F(\varepsilon+\Omega) = -\Theta(-(\varepsilon+\Omega)) \ ; \tag{3.139}$$

thus, for any Ω,

$$\varepsilon \in [-D_0, -\Omega] \rightarrow x \in [-1, -\nu] \ . \tag{3.140}$$

In the proper integration range, we have to consider the integral

$$\begin{aligned} &\int \mathrm{d}\varepsilon \, A_c^{R\prime}(\varepsilon) A_c(\varepsilon+\Omega)\chi_f^{R\prime\prime}(\varepsilon) \\ &= (\frac{m}{2\pi^2})^2 \frac{a''\,\varepsilon_F}{r^2} \int \mathrm{d}x \ \sin(\varrho\sqrt{1+x}\,)\sin(\varrho\sqrt{1+x+\nu}\,)\chi_f''(d_0 x) \ , \end{aligned} \tag{3.141}$$

where previously defined dimensionless variables are used. Consider the dimensionless integral,

$$I_2'' := \int \mathrm{d}x \ \sin(\varrho\sqrt{1+x}\,)\sin(\varrho\sqrt{1+x+\nu}\,)\,\chi_f''(d_0 x) \ . \tag{3.142}$$

At low frequencies, $\nu \ll 1$, one can Taylor-expand the integrand in ν to obtain

$$I_2'' \overset{\nu\ll 1}{=} \int \mathrm{d}x \ \sin(\varrho\sqrt{1+x}\,)\left(\sin(\varrho\sqrt{1+x}\,) + \frac{1}{2}\varrho\nu\frac{\cos(\varrho\sqrt{1+x}\,)}{\sqrt{1+x}}\right)\chi_f''(d_0 x) \ . \tag{3.143}$$

The integral cannot be performed analytically. We have to use the asymptotic form of the impurity susceptibility, introduced in section 3.3.2.3, and consider all the possible cases:

i) When $\Omega > 0 \wedge \Omega > T_K \rightarrow \varepsilon \in [-D_0, -\Omega]$:

$$I_2'' = -\frac{1}{2}\sin(2\varrho)\tau_K \ln|\nu| + \mathcal{O}(\tau_K) \ . \tag{3.144}$$

ii) When $\Omega > 0 \wedge \Omega < T_K \rightarrow \varepsilon[-D_0, -\Omega]$:

$$I_2'' = -\frac{1}{2}\left(1-\cos(2\varrho)\right)\tau_K \ln\tau_K + \mathcal{O}(\tau_K) \ . \tag{3.145}$$

iii) When $\Omega < 0 \wedge |\Omega| > T_K \equiv \Omega < -T_K \rightarrow \varepsilon \in [-D_0, -\Omega]$:

$$I_2'' = -\frac{1}{2}\left(1-\cos(2\varrho)\right)\tau_K \ln|\nu| + \mathcal{O}(\tau_K) \ . \tag{3.146}$$

iv) When $\Omega < 0 \wedge |\Omega| < T_K \equiv \Omega > -T_K \rightarrow \varepsilon \in [0, -\Omega]$:

$$I_2'' = \mathcal{O}(\tau_K) - \frac{1}{2}\left(1 - \cos(2\varrho)\right)\tau_K \ln \tau_K \ . \tag{3.147}$$

Third integral The third integral on the RHS of Eq. (3.126) is

$$\int \mathrm{d}\varepsilon \ (-n_F(\varepsilon))\, G_c^{R\prime}(\varepsilon) G_c^{R\prime}(\varepsilon+\Omega)\chi_f^{R\prime\prime}(\varepsilon) \ . \tag{3.148}$$

At low temperatures, the factor containing the Fermi-Dirac distributions merely limits the range of integration:

$$n_F(\varepsilon) = \Theta(-\varepsilon) \ ; \tag{3.149}$$

thus, for any Ω,

$$\varepsilon \in [-D_0, 0] \rightarrow x \in [-D_0, 0] \ . \tag{3.150}$$

In the proper range, we have to consider the integral

$$\begin{aligned} &\int \mathrm{d}\varepsilon\, G_c^{R\prime}(\varepsilon) A_c(\varepsilon+\Omega)\chi_f^{R\prime\prime}(\varepsilon) \\ &= \left(\frac{m}{2\pi}\right)^2 \frac{\varepsilon_F}{r^2} \int \mathrm{d}x \ \cos(\varrho\sqrt{1+x}\,)\cos(\varrho\sqrt{1+x+\nu}\,)\,\chi_f''(d_0 x) \ , \end{aligned} \tag{3.151}$$

where we have used the previously defined dimensionless variables, Eq. (3.87). Consider the dimensionless integral,

$$I_3'' := \int \mathrm{d}x \ \cos(\varrho\sqrt{1+x}\,)\cos(\varrho\sqrt{1+x+\nu}\,)\chi_f''(d_0 x) \ . \tag{3.152}$$

At low frequencies, $\nu \ll 1$, one can Taylor-expand the integrand in ν to obtain

$$I_3'' \overset{\nu\ll 1}{=} \int \mathrm{d}x \ \cos(\varrho\sqrt{1+x}\,)\left(\cos(\varrho\sqrt{1+x}\,) - \frac{1}{2}\varrho\nu\frac{\sin(\varrho\sqrt{1+x}\,)}{\sqrt{1+x}}\right)\chi_f''(d_0 x) \ . \tag{3.153}$$

The integral cannot be performed analytically. We have to use the asymptotic form of the impurity susceptibility, introduced in section 3.3.2.3, and consider all the possible cases:

i) When $\Omega > 0 \wedge \Omega > T_K \rightarrow \varepsilon \in [-D_0, 0]$:

$$I_3'' = \frac{1}{2}\left(1 + \cos(2\varrho)\right)\tau_K \ln \tau_K + \mathcal{O}(\tau_K) \ . \tag{3.154}$$

ii) When $\Omega > 0 \wedge \Omega < T_K \rightarrow \varepsilon[-D_0, 0]$:

$$I_3'' = \frac{1}{2}\left(1 + \cos(2\varrho)\right)\tau_K \ln \tau_K + \mathcal{O}(\tau_K) \ . \tag{3.155}$$

iii) When $\Omega < 0 \wedge |\Omega| > T_K \equiv \Omega < -T_K \rightarrow \varepsilon \in [-D_0, 0]$:

$$I_3'' = \frac{1}{2}\left(1 + \cos(2\varrho)\right) \tau_K \ln \tau_K + \mathcal{O}(\tau_K) \ . \tag{3.156}$$

iv) When $\Omega < 0 \wedge |\Omega| < T_K \equiv \Omega > -T_K \rightarrow \varepsilon \in [0, -\Omega]$:

$$I_3'' = \frac{1}{2}\left(1 + \cos(2\varrho)\right) \tau_K \ln \tau_K + \mathcal{O}(\tau_K) \ . \tag{3.157}$$

Final result for the factors of the imaginary part of f-susceptibility Putting all the integral pieces together, one obtains

$$\begin{aligned} F'' &= -\frac{1}{\pi}(\frac{m}{2\pi})^2 \frac{\varepsilon_F}{r^2} \frac{a''}{T_K}(-\mathrm{i})(-I_1'') \\ &+ (-\mathrm{i})(-\mathrm{i}\pi)(\frac{m}{2\pi^2})^2 \frac{\varepsilon_F}{r^2} \frac{a''}{T_K} I_2'' \\ &+ (-\mathrm{i})(\frac{-\mathrm{i}}{\pi})(\frac{m}{2\pi})^2 \frac{\varepsilon_F}{r^2} \frac{a''}{T_K} I_3'' \\ &= \frac{a''}{\pi}(\frac{m}{2\pi})^2 \frac{\varepsilon_F}{T_K} \frac{1}{r^2} \underbrace{\left(-I_2'' - I_3'' - \mathrm{i}I_1''\right)}_{:=\mathcal{I}''} \ . \end{aligned} \tag{3.158}$$

Now we can obtain $\mathcal{I}''$ for different ranges of Ω:

i) When $\Omega > 0 \wedge \Omega > T_K \rightarrow \varepsilon \in [-D_0, 0]$:

$$\mathcal{I}'' = \sin(2\varrho)\tau_K \ln \nu + \mathcal{O}(\nu^2) \ . \tag{3.159}$$

ii) When $\Omega > 0 \wedge \Omega < T_K \rightarrow \varepsilon[-D_0, 0]$:

$$\mathcal{I}'' = \mathcal{O}(\nu^2) \ . \tag{3.160}$$

iii) When $\Omega < 0 \wedge |\Omega| > T_K \equiv \Omega < -T_K \rightarrow \varepsilon \in [-D_0, 0]$:

$$\mathcal{I}'' = \mathcal{O}(\nu^2) \ . \tag{3.161}$$

iv) When $\Omega < 0 \wedge |\Omega| < T_K \equiv \Omega > -T_K \rightarrow \varepsilon \in [0, -\Omega]$:

$$\mathcal{I}'' = \mathcal{O}(\nu^2) \ . \tag{3.162}$$

3.3.2.6 Explicit expression for the exchange vertex correction

Ultimately, we have obtained an approximate expression for the exchange diagram, Γ_{ex},

$$\Gamma_{ex}(\Omega) = 2JJ_0^2 \left(\text{factors of } \chi_f^{R\prime} + \text{factors of } \chi_f^{R\prime\prime}\right) \ . \tag{3.163}$$

By defining a constant to simplify the notation,

$$c_0 := \frac{1}{\pi}(\frac{m}{2\pi})^2 \frac{1}{r^2}\frac{\varepsilon_F}{T_K} \ , \tag{3.164}$$

we obtain

i) When $\Omega > 0 \wedge \Omega > T_K$:

$$\Gamma_{ex} = \mathcal{O}(\nu^2) \ . \tag{3.165}$$

ii) When $\Omega > 0 \wedge \Omega < T_K$:

$$\Gamma_{ex} = 2JJ_0^2 \frac{1}{2} c_0 a' \left(\sin(2\varrho) - 2\mathrm{i}\sin^2(\varrho)\right)\nu + \mathcal{O}(\nu^2) \ . \tag{3.166}$$

iii) When $\Omega < 0 \wedge |\Omega| > T_K$:

$$\Gamma_{ex} = \mathcal{O}(\nu^2) \ . \tag{3.167}$$

iv) When $\Omega < 0 \wedge |\Omega| < T_K$:

$$\Gamma_{ex} = 2JJ_0^2 \frac{1}{2} c_0 a' \left(\sin(2\varrho) + 2\mathrm{i}\sin^2(\varrho)\right)\nu + \mathcal{O}(\nu^2) \ . \tag{3.168}$$

Therefore, the ultimate result of the previous calculation is the simple expression

$$\Gamma_{ex} = JJ_0^2 \frac{3\pi}{2} n_e \mathcal{N}(\varepsilon_F) \frac{1}{\varrho^2}\frac{1}{T_K}\, a' \left(\sin(2\varrho)\nu + 2\mathrm{i}\sin^2(\varrho)|\nu|\right) \cdot \Theta(T_k - |\Omega|) \ , \tag{3.169}$$

where $n_e = \frac{N_e}{V}$ is the average density of the electrons and

$$n_e \mathcal{N}(\varepsilon_F) = \frac{m{k_F}^4}{6\pi^4} \ . \tag{3.170}$$

Therefore, ultimately, we reach the expected expression,

$$\Gamma_{ex} = JJ_0^2 \frac{(g\mu_B)^2 W}{\pi}\frac{1}{\pi}(\frac{mk_F}{2\pi})^2 \frac{\varepsilon_F}{T_K}\frac{\sin(2\varrho)\,\nu + 2\mathrm{i}\,\sin^2(\varrho)\,|\nu|}{\varrho^2}\,\Theta(T_K - |\Omega|) \ . \tag{3.171}$$

One observes that in the relevant energy interval, $\Omega \sim \mathcal{O}(T_K) \ll D_0$, where the RG β-function is non-vanishing (see section 3.4), the direct and exchange vertex corrections satisfy $|\Gamma_{ex}/\Gamma_{dir}| \sim \frac{T_K}{D_0} \ll 1$, and thus, the exchange vertex correction can be safely neglected.[12]

[12] This can be compared to the Migdal's theorem in the context of electron-phonon interaction and superconductivity, which states that phonon correction (renormalization) to the electron-phonon vertex is suppressed at least by a factor $\sqrt{\frac{m_e}{M_i}} \sim 10^{-2}$, where m_e and M_i represent the mass of an electron and an ion (for a detailed discussion, consult, e.g., Ref. [122, 123]). Here the impurity vertex correction to the electronic vertex is suppressed by a factor $\frac{T_K}{D_0} \sim 10^{-3}$.

3.4 Renormalization group analysis for the RKKY-modified Kondo vertex

In the previous sections, the perturbative effect of the neighboring impurities on the one at the reference site was obtained and included in the RKKY corrections to the Kondo vertex at the reference site. Hence, now one can obtain one-loop RG flow equations for the RKKY-modified Kondo vertex which is *spatially non-local*. In the perturbative RG, one begins at an energy scale above the Kondo temperature, a region where perturbative methods can be used (above Kondo T_K, lattice coherence T_{coh}, and Néel temperature T_N), and reduces the bandwidth of the conduction electrons through successive RG steps. The energy scale at which the coupling flows to infinity (strong-coupling fixed point) yields the Kondo temperature for the lattice, $T_K(y)$.

Besides the simple contribution of the bare Kondo vertex, Eq. (2.65), the diagrams contributing to one-loop RG equations are (for a definition of variables, see below) shown in Fig. 3.6.

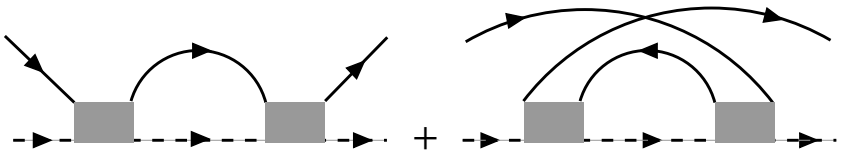

Figure 3.6: One-loop RG diagrams with the RKKY-modified Kondo vertex: 'direct' (left) and 'exchange' (right) RG diagrams.

The direct RG diagram corresponds to the expression,

$$\begin{aligned}\mathcal{K}_{dir} = (-2)\,\frac{J}{2}\int_{-D}^{D} \mathrm{d}\varepsilon\, \{ & n_F(\varepsilon)\, A_c(\varepsilon)\, G_f^R(\omega+\nu-\varepsilon)\, \Gamma_{dir}(\omega,\varepsilon,\nu) \\ & - G_c^R(\omega+\nu-\varepsilon)\, A_f(\varepsilon)\, \Gamma_{dir}(\omega,\omega+\nu-\varepsilon,\nu)\} \\ & + (-2)\,\frac{J}{2}\int_{-D}^{D} \mathrm{d}\varepsilon\, \{ n_F(\varepsilon)\, A_c(\varepsilon)\, G_f^R(\omega+\nu-\varepsilon)\, \Gamma_{dir}(\varepsilon,\omega+\Omega,\varepsilon,\omega+\nu-\varepsilon) \\ & - A_f(\varepsilon)\, G_c^R(\omega+\nu-\varepsilon)\, \Gamma_{dir}(\omega+\nu-\varepsilon,\omega+\Omega,\varepsilon)\}\ , \end{aligned} \tag{3.172}$$

where the -2 factor originates from the Pauli-matrix algebra;

The exchange RG diagram yields

$$\begin{aligned}\mathcal{K}_{ex} = (+2)\,\frac{J}{2}\int_{-D}^{D} \mathrm{d}\varepsilon\, n_F(\varepsilon)\, A_c(\varepsilon)\, G_f^A(\omega+\nu-(\omega+\Omega))\, \Gamma_{dir}(\varepsilon,\omega+\Omega,\nu) \\ + (2)\,\frac{J}{2}\int_{-D}^{D} \mathrm{d}\varepsilon\, n_F(\varepsilon)\, A_c(\varepsilon)\, G_f^A(\varepsilon+\nu-(\omega+\Omega))\, \Gamma_{dir}(\omega,\varepsilon,\varepsilon+\nu-(\omega+\Omega))\ , \end{aligned} \tag{3.173}$$

where $+2$ factor is again from the Pauli-matrix algebra.

After finding the RKKY-modified Kondo coupling, $\tilde{J}$, the RG flow equation can be obtained via a logarithmic differentiation,

$$\frac{\mathrm{d}\tilde{J}(D)}{\mathrm{d}\ln(D)} \equiv D\frac{\mathrm{d}\tilde{J}(D)}{\mathrm{d}D}\ , \tag{3.174}$$

which gives

$$\frac{\mathrm{d}\mathcal{K}_{dir}}{\mathrm{d}\ln(D)} = -4J^2 J_0^2\, \chi_f^{R\prime}(D) \sum_{\mathbf{x}_l \neq \mathbf{x}} A_c(\mathbf{x}-\mathbf{x}_l, D)\, \chi_c^{R\prime}(\mathbf{x}-\mathbf{x}_l, D)\ , \tag{3.175}$$

and

$$\frac{\mathrm{d}\mathcal{K}_{ex}}{\mathrm{d}\ln(D)} = -4J^2 J_0^2\, \chi_f^{R\prime}(D) \sum_{\mathbf{x}_l \neq \mathbf{x}} A_c(\mathbf{x}-\mathbf{x}_l, D)\, \chi_c^{R\prime}(\mathbf{x}-\mathbf{x}_l, D)\ . \tag{3.176}$$

Notice that while the conduction-electron Green's functions, G_c, and susceptibility, χ_c, vary on a scale of Fermi energy ε_F, the f-susceptibility varies on a scale of Kondo temperature $T_K \ll \varepsilon_F$, which implies that on a change of order $\delta D \ll D_0$, the conduction electron properties will remain unchanged and their energy dependence can be neglected.

Finally, the RG equations can be re-written in terms of the dimensionless couplings

$$J \mapsto \mathcal{N}(\varepsilon_F)\, J \quad , \quad J_0 \mapsto \mathcal{N}(\varepsilon_F)\, J_0\,,$$

and a dimensionless *energy-independent* parameter y,

$$y := -\frac{4(g\mu_B)^2 W}{\pi}\, \frac{1}{D_0\, \mathcal{N}(\varepsilon_F)^3} \sum_{\mathbf{x}_l \neq \mathbf{x}} A_c(\mathbf{x}-\mathbf{x}_l)\, \chi_c^{R\prime}(\mathbf{x}-\mathbf{x}_l)\,, \tag{3.177}$$

which includes the non-universal properties of the conduction electrons. This parameter can be 'tuned' as in the actual experiments (e.g., Ref. [124]), for instance, by chemical doping or pressure. For a lattice of impurities, using the translational invariance, the parameter y can further be re-written as

$$y = \text{const.} \sum_{\mathbf{x}_l \neq 0} \rho_c(\mathbf{x}_l)\, I_{\mathrm{RKKY}}(\mathbf{x}_l)\ , \tag{3.178}$$

where $\rho_c(x) = \frac{1}{\pi} A_c(x)$ is the local density-of-states of the conduction electrons and I_{RKKY} is the RKKY coupling [125] which depends on the details of the band structure and lattice properties of the conduction electrons. The parameter y is essentially an average of the strength of the RKKY interaction over the set of impurities. An order-of-magnitude estimation indicates a *positive* y which results in a term which *competes* with the Kondo effect.

Therefore, ultimately, putting all the relations together, the RG flow for the Kondo lattice is found to be

$$\frac{\mathrm{d}J(D)}{\mathrm{d}\ln D} = -2\, J(D)^2 \Big(1 - y\, J_0^2 \frac{D_0}{T_K(y)}\, \frac{1}{\sqrt{1+(D/T_K(y))^2}}\Big)\ , \tag{3.179}$$

which can be integrated to obtain the RKKY-modified Kondo temperature (see section 3.4.4).

In this section we will explicitly derive the RG flow equations for the RKKY-modified Kondo vertex. The resulting RG diagrams resemble those for the single-impurity, but with the bare Kondo vertices replaced by the RKKY-modified vertex. Note that the RKKY-modification results solely from the direct vertex correction, Γ_{dir} since, as shown explicitly before, Γ_{ex} can be neglected in comparison to the direct one. Therefore, henceforth, we denote the modified vertex simply with $\Gamma \equiv \Gamma_{dir}$.

3.4.1 Direct RG diagram

The contribution to the direct RG diagram (not to be confused with the direct vertex correction) to the RG flow is shown in Fig. 3.19:

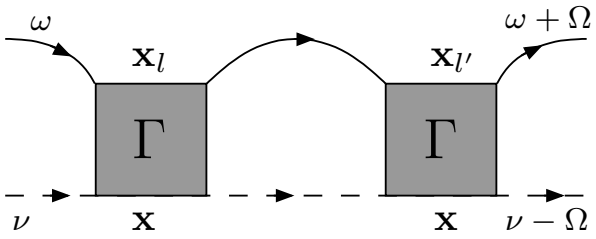

Figure 3.7: Direct RG diagram with the RKKY-modified Kondo vertex.

Note that we need the contributions only up to $\mathcal{O}(y)$, since the RKKY modifications appear at this order in the perturbative expansion. Therefore, one of the vertices can be left as bare (not modified by the RKKY interaction).

First direct contribution The first contribution (up to $\mathcal{O}(y)$) to the direct term is shown in Fig. 3.8

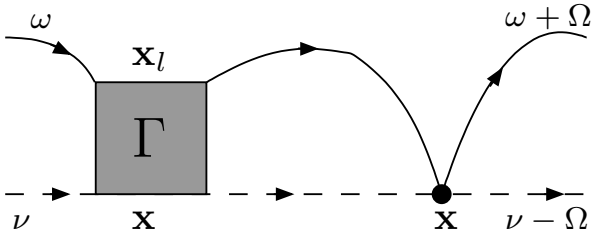

Figure 3.8: First direct contribution (up to $\mathcal{O}(y)$) to the RG.

and corresponds to the expression,

$$\mathcal{K}_{dir,1} := \frac{1}{\beta} \sum_{\substack{\mathrm{i}\Omega= \\ \mathrm{i}(2\mathbb{Z}+1)\frac{\pi}{\beta}}} \Gamma(\mathbf{x}_l, \mathrm{i}\omega; \mathrm{i}\Omega_n; \mathbf{x}, \mathrm{i}\nu) G_c(\mathbf{x} - \mathbf{x}_l, \mathrm{i}\Omega_n) G_f(\mathbf{x} - \mathbf{x}, \mathrm{i}\nu_n) \ , \tag{3.180}$$

where the RKKY-modified vertex Γ is defined as in Fig. 3.9.
We drop the position coordinates to simplify the notation and restore them only at the end of the calculations; thus,

$$\mathcal{K}_{dir,1} = \frac{1}{\beta} \sum_{\mathrm{i}\Omega} \Gamma(\mathrm{i}\omega, \mathrm{i}\Omega_n, \mathrm{i}\nu) G_c(\mathrm{i}\Omega_n) G_f(\mathrm{i}\omega + \mathrm{i}\nu - \mathrm{i}\Omega_n) \tag{3.181}$$

We perform the Matsubara summation over the frequencies taking into account the branch-cuts.

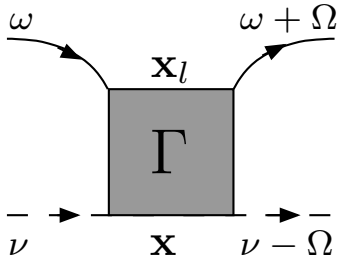

Figure 3.9: RKKY-modified Kondo vertex, $\Gamma(\mathbf{x}_l, \omega; \omega + \Omega; \mathbf{x}, \nu)$.

The integral over the large contour C is

$$0 = \frac{1}{2\pi \mathrm{i}} \oint_C \mathrm{d}z\, n_F(z) \Gamma(\mathrm{i}\omega, z, \mathrm{i}\nu) G_c(z) G_f(\mathrm{i}\omega + \mathrm{i}\nu - z) \;, \tag{3.182}$$

with the branch-cuts at

$$\begin{aligned} z &= \varepsilon \in \mathbb{R} \\ z &= \mathrm{i}\omega + \mathrm{i}\nu - \varepsilon \;. \end{aligned} \tag{3.183}$$

Therefore,

$$\begin{aligned} &\frac{1}{2\pi \mathrm{i}} \int_{-D}^{+D} \mathrm{d}\varepsilon\, n_F(\varepsilon) \Gamma(\mathrm{i}\omega, \varepsilon, \mathrm{i}\nu) [G_c(\varepsilon + \mathrm{i}\eta^+) - G_c(\varepsilon - \mathrm{i}\eta^+)] G_f(\mathrm{i}\omega + \mathrm{i}\nu - \varepsilon) \\ &+ \frac{1}{2\pi \mathrm{i}} \int_{-D}^{+D} n_F(\underbrace{\mathrm{i}\omega + \mathrm{i}\nu - \varepsilon}_{\text{bosonic}}) \Gamma(\mathrm{i}\omega, \mathrm{i}\omega + \mathrm{i}\nu - \varepsilon, \mathrm{i}\nu) G_c(\mathrm{i}\omega + \mathrm{i}\nu - \varepsilon) [G_f(\varepsilon - \mathrm{i}\eta^+) - G_f(\varepsilon + \mathrm{i}\eta^+)] \\ &- \frac{1}{2\pi \mathrm{i}} \oint_{C_F} \mathrm{d}z\, n_F(z) \Gamma(\mathrm{i}\omega, z, \mathrm{i}\nu) G_c(z) G_f(\mathrm{i}\omega + \mathrm{i}\nu - z) = 0 \;, \end{aligned} \tag{3.184}$$

which gives $\mathcal{K}_{dir,1}$ as

$$\begin{aligned} \mathcal{K}_{dir,1} &= -\frac{1}{2\pi \mathrm{i}} \int_{-D}^{+D} \mathrm{d}\varepsilon \Big\{ n_F(\varepsilon) \Gamma(\mathrm{i}\omega, \varepsilon, \mathrm{i}\nu) 2\mathrm{i}\mathrm{Im}\, G_c^R(\varepsilon) G_f(\mathrm{i}\omega + \mathrm{i}\nu - \varepsilon) \\ &\quad + n_F(-\varepsilon) \Gamma(\mathrm{i}\omega, \mathrm{i}\omega + \mathrm{i}\nu - \varepsilon, \mathrm{i}\nu) G_c(\mathrm{i}\omega + \mathrm{i}\nu - \varepsilon) (-2\mathrm{i}\mathrm{Im}\, G_f^R(\varepsilon)) \Big\} \\ &= -\frac{1}{2\pi} \int_{-D}^{+D} \mathrm{d}\varepsilon \Big\{ n_F(\varepsilon) \Gamma(\mathrm{i}\omega, \varepsilon, \mathrm{i}\nu) 2\mathrm{Im}\, G_c^R(\varepsilon) G_f(\mathrm{i}\omega + \mathrm{i}\nu - \varepsilon) \\ &\quad + n_F(-\varepsilon) \Gamma(\mathrm{i}\omega, \mathrm{i}\omega + \mathrm{i}\nu - \varepsilon, \mathrm{i}\nu) G_c(\mathrm{i}\omega + \mathrm{i}\nu - \varepsilon) (-2\mathrm{Im}\, G_f^R(\varepsilon)) \Big\} \\ &= \frac{1}{2\pi} \int_{-D}^{+D} \mathrm{d}\varepsilon \Big\{ n_F(\varepsilon) \Gamma(\mathrm{i}\omega, \varepsilon, \mathrm{i}\nu) A_c(\varepsilon) G_f(\mathrm{i}\omega + \mathrm{i}\nu - \varepsilon) \\ &\quad - n_F(-\varepsilon) \Gamma(\mathrm{i}\omega, \mathrm{i}\omega + \mathrm{i}\nu - \varepsilon, \mathrm{i}\nu) G_c(\mathrm{i}\omega + \mathrm{i}\nu - \varepsilon) A_f(\varepsilon) \Big\} \;. \end{aligned} \tag{3.185}$$

The 'retarded branch'[13] is obtained via the transformations

$$\begin{aligned} \mathrm{i}\omega &\mapsto \omega + \mathrm{i}\eta^+ \ , \\ \mathrm{i}\nu &\mapsto \nu + \mathrm{i}\eta^+ \ , \\ \mathrm{i}\Omega &\mapsto \Omega + \mathrm{i}\eta^+ \ , \end{aligned} \tag{3.186}$$

as

$$\begin{aligned} \mathcal{K}^R_{dir,1} = \frac{1}{2\pi}\int_{-D}^{+D} \mathrm{d}\varepsilon \Big\{ & n_F(\varepsilon)\Gamma^R(\omega,\varepsilon,\nu)A_c(\varepsilon)G^R_f(\omega+\nu-\varepsilon) \\ & - n_F(-\varepsilon)\Gamma^R(\omega,\omega+\nu-\varepsilon,\nu)G^R_c(\omega+\nu-\varepsilon)A_f(\varepsilon)\Big\} \ . \end{aligned} \tag{3.187}$$

Using the mapping for $\nu \mapsto \nu + \lambda$ for Abrikosov's pseudo-fermions (Appendix C), one obtains

$$\begin{aligned} \hat{\mathcal{K}}^R_{dir,1} = \frac{1}{2\pi}\int_{-D}^{+D} \mathrm{d}\varepsilon \Big\{ & n_F(\varepsilon)\Gamma^R(\omega,\varepsilon,\nu+\lambda)A_c(\varepsilon) \underbrace{G^R_f(\omega+\nu+\lambda-\varepsilon)}_{=\hat{G}^R_f(\omega+\nu-\varepsilon)} \\ & - n_F(-\varepsilon)\Gamma^R(\omega,\omega+\nu+\lambda-\varepsilon,\nu+\lambda)G^R_c(\omega+\nu+\lambda-\varepsilon)A_f(\varepsilon)\Big\} \ . \end{aligned} \tag{3.188}$$

Finally, applying the transformation $\varepsilon \mapsto \varepsilon + \lambda$ in the second term, the expression yields

$$\begin{aligned} \hat{\mathcal{K}}^R_{dir,1} &= \frac{1}{2\pi}\int_{-D}^{+D} \mathrm{d}\varepsilon \Big\{ n_F(\varepsilon)\Gamma^R(\omega,\varepsilon,\varepsilon+\lambda)A_c(\varepsilon)\hat{G}^R_f(\omega+\nu-\varepsilon) \\ &\quad - n_F(-(\varepsilon+\lambda))\Gamma^R(\omega,\omega+\nu-\varepsilon,\nu+\lambda)G^R_c(\omega+\nu-\varepsilon)\hat{A}_f(\varepsilon)\Big\} \\ &= \frac{1}{2\pi}\int_{-D}^{+D} \mathrm{d}\varepsilon \Big\{ n_F(\varepsilon)\hat{\Gamma}^R(\omega,\varepsilon,\nu)A_c(\varepsilon)\hat{G}^R_f(\omega+\nu-\varepsilon) \\ &\quad - \hat{\Gamma}^R(\omega,\omega+\nu-\varepsilon,\nu)G^R_c(\omega+\nu-\varepsilon)\hat{A}_f(\varepsilon)\Big\} \ . \end{aligned} \tag{3.189}$$

Second direct contribution The second contribution (up to $\mathcal{O}(y)$) to the direct term is shown in Fig. 3.10

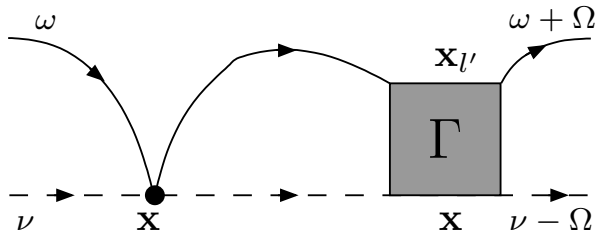

Figure 3.10: Second direct contribution (up to $\mathcal{O}(y)$) to the one-loop RG.

and corresponds to the expression,

[13] For a detailed discussion of the analytical properties of the vertices, consult Ref. [120].

$$\mathcal{K}_{dir,2} = \frac{1}{\beta}\sum_{\mathrm{i}\Omega_n} G_c(\mathbf{x}_{l'}-\mathbf{x},\mathrm{i}\Omega_n)G_f(\mathbf{x}-\mathbf{x},\mathrm{i}\nu_n)\Gamma(\mathbf{x}_{l'},\mathrm{i}\Omega_n;\mathrm{i}\omega+\mathrm{i}\Omega;\mathbf{x},\mathrm{i}\nu_n) \tag{3.190}$$

The Matsubara sum over the frequencies is performed taking into account the branch-cuts. The contour integral over the large contour C is

$$0 = \frac{1}{2\pi\mathrm{i}}\oint_C \mathrm{d}z\, n_F(z)G_c(z)G_f(\mathrm{i}\omega+\mathrm{i}\nu-z)\Gamma(z,\mathrm{i}\omega+\mathrm{i}\nu-z,\mathrm{i}\omega+\mathrm{i}\Omega) \tag{3.191}$$

with branch-cuts at

$$\begin{aligned} z &= \varepsilon \in \mathbb{R}\ , \\ z &= \mathrm{i}\omega+\mathrm{i}\nu-\varepsilon\ . \end{aligned} \tag{3.192}$$

Therefore,

$$\begin{aligned} &\frac{1}{2\pi\mathrm{i}}\int_{-D}^{+D}\mathrm{d}\varepsilon\, n_F(\varepsilon)[G_c(\varepsilon+\mathrm{i}\eta^+)-G_c(\varepsilon-\mathrm{i}\eta^+)]G_f(\mathrm{i}\omega+\mathrm{i}\nu-\varepsilon)\Gamma(\varepsilon,\mathrm{i}\omega+\mathrm{i}\Omega,\mathrm{i}\omega+\mathrm{i}\nu-\varepsilon) \\ &+\frac{1}{2\pi\mathrm{i}}\int_{-D}^{+D}\mathrm{d}\varepsilon\, n_F(\underbrace{\mathrm{i}\omega+\mathrm{i}\nu-\varepsilon}_{\text{bosonic}})G_c(\mathrm{i}\omega+\mathrm{i}\nu-\varepsilon)[G_f(\varepsilon-\mathrm{i}\eta^+)-G_f(\varepsilon+\mathrm{i}\eta^+)]\Gamma(\mathrm{i}\omega+\mathrm{i}\nu-\varepsilon,\mathrm{i}\omega+\mathrm{i}\Omega,\varepsilon) \\ &-\frac{1}{2\pi\mathrm{i}}\oint_{C_F}\mathrm{d}z\, n_F(z)G_c(z)G_f(\mathrm{i}\omega+\mathrm{i}\nu-z)\Gamma(z,\mathrm{i}\omega+\mathrm{i}\Omega,\mathrm{i}\omega+\mathrm{i}\nu-z)=0\ . \end{aligned} \tag{3.193}$$

Hence,

$$\begin{aligned} \mathcal{K}^R_{dir,1} &= -\frac{1}{2\pi\mathrm{i}}\int_{-D}^{+D}\mathrm{d}\varepsilon\Big\{n_F(\varepsilon)[2\mathrm{i}\mathrm{Im}\,G^R_c(\varepsilon)]G_f(\mathrm{i}\omega+\mathrm{i}\nu-\varepsilon)\Gamma(\varepsilon,\mathrm{i}\omega+\mathrm{i}\Omega,\mathrm{i}\omega+\mathrm{i}\nu-\varepsilon) \\ &\quad + n_F(-\varepsilon)[-2\mathrm{i}\mathrm{Im}\,G^R_f(\varepsilon)]\Gamma(\mathrm{i}\omega+\mathrm{i}\nu-\varepsilon,\mathrm{i}\omega+\mathrm{i}\Omega,\varepsilon)G_c(\mathrm{i}\omega+\mathrm{i}\nu-\varepsilon)\Big\} \\ &= \frac{1}{2\pi}\int_{-D}^{+D}\mathrm{d}\varepsilon\Big\{n_F(\varepsilon)A_c(\varepsilon)G_f(\mathrm{i}\omega+\mathrm{i}\nu-\varepsilon)\Gamma(\varepsilon,\mathrm{i}\omega+\mathrm{i}\Omega,\mathrm{i}\omega+\mathrm{i}\nu-\varepsilon) \\ &\quad - n_F(-\varepsilon)A_f(\varepsilon)\Gamma(\mathrm{i}\omega+\mathrm{i}\nu-\varepsilon,\mathrm{i}\omega+\mathrm{i}\Omega,\varepsilon)G_C(\mathrm{i}\omega+\mathrm{i}\nu-\varepsilon)\Big\} \\ &= \frac{1}{2\pi}\int_{-D}^{+D}\mathrm{d}\varepsilon\Big\{n_F(\varepsilon)A_c(\varepsilon)G_f(\mathrm{i}\omega+\mathrm{i}\nu-\varepsilon)\Gamma(\varepsilon,\mathrm{i}\omega+\mathrm{i}\Omega,\mathrm{i}\omega+\mathrm{i}\nu-\varepsilon) \\ &\quad - n_F(-\varepsilon)A_f(\varepsilon)\Gamma(\mathrm{i}\omega+\mathrm{i}\nu-\varepsilon,\mathrm{i}\omega+\mathrm{i}\Omega,\varepsilon)G_c(\mathrm{i}\omega+\mathrm{i}\nu-\varepsilon)\Big\}\ . \end{aligned} \tag{3.194}$$

As in the previous case, the 'retarded branch'[14] is obtained via the transformations

$$\begin{aligned} \mathrm{i}\omega &\mapsto \omega+\mathrm{i}\eta^+\ , \\ \mathrm{i}\Omega &\mapsto \Omega+\mathrm{i}\eta^+\ , \\ \mathrm{i}\nu &\mapsto \nu+\mathrm{i}\eta^+\ , \end{aligned} \tag{3.195}$$

[14] For a detailed discussion of the analytical properties of the vertices, consult Ref. [120].

and using the transformation $\nu \mapsto \nu + \lambda$ for the pseudo-fermions (Appendix C),

$$\begin{aligned}
\mathcal{K}^R_{dir,2}(\omega, \omega+\Omega, \nu+\lambda) &= \frac{1}{2\pi}\int_{-D}^{+D} \mathrm{d}\varepsilon \Big\{ n_F(\varepsilon) A_c(\varepsilon) G^R_f(\omega+\nu-\varepsilon+\lambda)\Gamma^R(\varepsilon, \omega+\Omega, \omega+\nu-\varepsilon+\lambda) \\
&\quad - n_F(-\varepsilon) A_f(\varepsilon)\Gamma^R(\omega+\nu-\varepsilon+\lambda, \omega+\Omega, \varepsilon) G^R_c(\omega+\nu-\varepsilon+\lambda)\Big\} \\
&= \frac{1}{2\pi}\int_{-D}^{+D} \mathrm{d}\varepsilon \Big\{ n_F(\varepsilon) A_c(\varepsilon) \hat{G}^R_f(\omega+\nu-\varepsilon)\hat{\Gamma}^R(\varepsilon, \omega+\Omega, \omega+\nu-\varepsilon) \\
&\quad - n_F(-(\varepsilon+\lambda)) A_f(\varepsilon+\lambda)\Gamma^R(\omega+\nu-\varepsilon, \omega+\Omega, \varepsilon+\lambda) G^R_c(\omega+\nu-\varepsilon)\Big\} \\
&= \frac{1}{2\pi}\int_{-D}^{+D} \mathrm{d}\varepsilon \Big\{ n_F(\varepsilon) A_c(\varepsilon) \hat{G}^R_f(\omega+\nu-\varepsilon)\hat{\Gamma}^R(\varepsilon, \omega+\Omega, \omega+\nu-\varepsilon) \\
&\quad - \hat{A}_f(\varepsilon)\hat{\Gamma}^R(\omega+\nu-\varepsilon, \omega+\Omega, \varepsilon) G^R_c(\omega+\nu-\varepsilon)\Big\} \ , \qquad (3.196)
\end{aligned}$$

where we have used

$$\lim_{\lambda\to+\infty} n_F\left(-(\varepsilon+\lambda)\right) = 1 \ .$$

3.4.2 Exchange RG diagram

The exchange diagram contribution to the one-loop RG flow equation (Fig. 3.11) is obtained along the same way as the contribution of the direct diagram. The are also two exchange contributions.

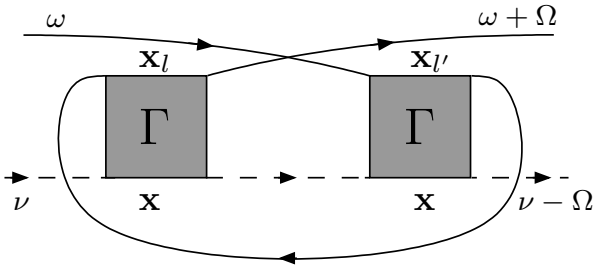

Figure 3.11: Exchange contribution to the one-loop RG.

First exchange contribution The first contribution (up to $\mathcal{O}(y)$) to the exchange term is shown in Fig. 3.12

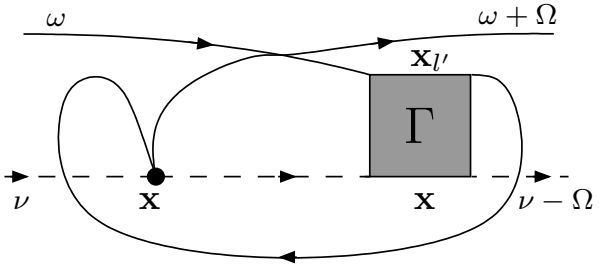

Figure 3.12: First exchange contribution (up to $\mathcal{O}(y)$) to the RG.

and yields the expression,

$$\mathcal{K}_{ex,1} = \frac{1}{\beta}\sum_{\mathrm{i}\Omega_n}\sum_{\mathbf{x}_{l''}} \Gamma(\mathbf{x}_{l'}, \mathrm{i}\Omega; \mathrm{i}(\omega+\Omega); \mathbf{x}, \mathrm{i}\nu) G_f(\mathbf{x}-\mathbf{x}, \mathrm{i}\nu_n) G_c(\mathbf{x}-\mathbf{x}_{l'}, \mathrm{i}\Omega_n) \tag{3.197}$$

The Matsubara summation over the frequencies is obtained via a contour integration,

$$0 = \frac{1}{2\pi\mathrm{i}}\oint_C \mathrm{d}z\, n_F(z)\Gamma(z, \mathrm{i}\omega+\mathrm{i}\Omega, \mathrm{i}\nu) G_f(z+\mathrm{i}\nu-\mathrm{i}(\omega+\Omega)) G_c(z)\ , \tag{3.198}$$

with the branch-cuts at

$$\begin{aligned} z &= \varepsilon \in \mathbb{R}\ , \\ z &= \varepsilon + \mathrm{i}(\omega+\Omega) - \mathrm{i}\nu\ ; \end{aligned}$$

therefore,

$$\begin{aligned} &\frac{1}{2\pi\mathrm{i}}\int_{-D}^{+D} \mathrm{d}\varepsilon\, n_F(\varepsilon)\Gamma(\varepsilon, \mathrm{i}\omega+\mathrm{i}\Omega, \mathrm{i}\nu) G_f(\varepsilon+\mathrm{i}\nu-\mathrm{i}(\omega+\Omega))[G_c(\varepsilon+\mathrm{i}\eta^+) - G_c(\varepsilon-\mathrm{i}\eta^+)] \\ &+ \frac{1}{2\pi\mathrm{i}}\int_{-D}^{+D} \mathrm{d}\varepsilon\, n_F(\underbrace{\varepsilon+\mathrm{i}(\omega+\Omega)-\mathrm{i}\nu}_{\text{bosonic}})\Gamma(\varepsilon+\mathrm{i}(\omega+\Omega)-\mathrm{i}\nu, \mathrm{i}\omega+\mathrm{i}\Omega, \mathrm{i}\nu) \\ &\quad\times [G_f(\varepsilon+\mathrm{i}\eta^+) - G_f(\varepsilon-\mathrm{i}\eta^+)] G_c(\varepsilon+\mathrm{i}(\omega+\Omega)-\mathrm{i}\nu) \\ &- \frac{1}{2\pi\mathrm{i}}\oint_{C_F} \mathrm{d}z\, n_F(z)\Gamma(z, \mathrm{i}\omega+\mathrm{i}\Omega, \mathrm{i}\nu) G_f(z+\mathrm{i}\nu-\mathrm{i}(\omega+\Omega)) G_c(z) = 0\ . \end{aligned} \tag{3.199}$$

Hence,

$$\begin{aligned} \mathcal{K}_{ex,1} &= -\frac{1}{2\pi\mathrm{i}}\int_{-D}^{+D} \mathrm{d}\varepsilon\, n_F(\varepsilon)\Gamma(\varepsilon, \mathrm{i}(\omega+\Omega), \mathrm{i}\nu) G_f(\varepsilon+\mathrm{i}\nu-\mathrm{i}(\omega+\Omega))[2\mathrm{i}\,\mathrm{Im}\, G_c^R(\varepsilon)] \\ &\quad - \frac{1}{2\pi\mathrm{i}}\int_{-D}^{+D} \mathrm{d}\varepsilon\, n_F(\varepsilon)\Gamma(\varepsilon+\mathrm{i}(\omega+\Omega)-\mathrm{i}\nu, \mathrm{i}(\omega+\Omega), \mathrm{i}\nu)[2\mathrm{i}\,\mathrm{Im}\, G_f^R(\varepsilon)] G_c(\varepsilon+\mathrm{i}(\omega+\Omega)-\mathrm{i}\nu) \\ &= \frac{1}{2\pi}\int_{-D}^{+D} \mathrm{d}\varepsilon\, n_F(\varepsilon)\Gamma(\varepsilon, \mathrm{i}(\omega+\Omega), \mathrm{i}\nu) G_f(\varepsilon+\mathrm{i}\nu-\mathrm{i}(\omega+\Omega)) A_c(\varepsilon) \\ &\quad + \frac{1}{2\pi}\int_{-D}^{+D} \mathrm{d}\varepsilon\, n_F(\varepsilon)\Gamma(\varepsilon+\mathrm{i}(\omega+\Omega)-\mathrm{i}\nu, \mathrm{i}\omega+\Omega), \mathrm{i}\nu) A_f(\varepsilon) G_c(\varepsilon+\mathrm{i}(\omega+\Omega)-\mathrm{i}\nu)\ . \end{aligned} \tag{3.200}$$

Using the transformations

$$\begin{aligned} \mathrm{i}\omega &\mapsto \omega + \mathrm{i}\eta^+\ , \\ \mathrm{i}\Omega &\mapsto \Omega + \mathrm{i}\eta^+\ , \\ \mathrm{i}\nu &\mapsto \nu + \mathrm{i}\eta^+\ , \end{aligned} \tag{3.201}$$

one obtains

$$\mathcal{K}^R_{ex,1} = \frac{1}{2\pi}\int_{-D}^{+D} \mathrm{d}\varepsilon\, n_F(\varepsilon)\Gamma(\varepsilon,\omega+\Omega,\nu)G^A_f(\varepsilon+\nu-(\omega+\Omega))A_c(\varepsilon) + \frac{1}{2\pi}\int_{-D}^{+D} \mathrm{d}\varepsilon\, n_F(\varepsilon)\Gamma(\varepsilon+\omega+\Omega-\nu,\omega+\Omega,\nu)A_f(\varepsilon)G^R_c(\varepsilon+\omega+\Omega-\nu) \tag{3.202}$$

With the transformation $\nu \mapsto \nu+\lambda$ for pseudo-fermions (Appendix C),

$$\begin{aligned}\hat{\mathcal{K}}^R_{ex,1} &= \frac{1}{2\pi}\int_{-D}^{+D} \mathrm{d}\varepsilon\, n_F(\varepsilon)\Gamma(\varepsilon,\omega+\Omega,\nu+\lambda)G^A_f(\varepsilon+\nu+\lambda-(\omega+\Omega))A_c(\varepsilon)\\ &\quad+\frac{1}{2\pi}\int_{-D}^{+D} \mathrm{d}\varepsilon\, n_F(\varepsilon)\Gamma(\varepsilon+\omega+\Omega-(\nu+\lambda),\omega+\Omega,\nu+\lambda)A_f(\varepsilon)G^R_c(\varepsilon+\omega+\Omega-(\nu+\lambda))\\ &= \frac{1}{2\pi}\int_{-D}^{+D} \mathrm{d}\varepsilon\, n_F(\varepsilon)\hat{\Gamma}(\varepsilon,\omega+\Omega,\nu)\hat{G}^A_f(\varepsilon+\nu-(\omega+\Omega))A_c(\varepsilon)\\ &\quad+\frac{1}{2\pi}\int_{-D}^{+D} \mathrm{d}\varepsilon\, \underbrace{n_F(\varepsilon+\lambda)}_{\to 0}\hat{\Gamma}(\varepsilon+\omega+\Omega-\nu,\omega+\Omega,\nu)\hat{A}_f(\varepsilon)G^R_c(\varepsilon+\omega+\Omega-\nu)\\ &= \frac{1}{2\pi}\int_{-D}^{+D} \mathrm{d}\varepsilon\, n_F(\varepsilon)\hat{\Gamma}(\varepsilon,\omega+\Omega,\nu)\hat{G}^A_f(\varepsilon+\nu-(\omega+\Omega))A_c(\varepsilon)\ ,\end{aligned} \tag{3.203}$$

where we have used

$$\lim_{\lambda\to\infty} n_F(\varepsilon+\lambda) = e^{-\beta\lambda} \to 0\ .$$

Second exchange contribution The second contribution (up to $\mathcal{O}(y)$) to the exchange term is shown in Fig. 3.13

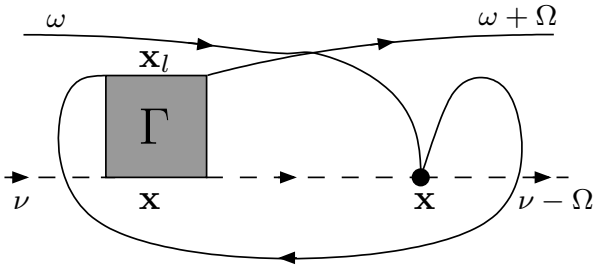

Figure 3.13: Second exchange contribution (up to $\mathcal{O}(y)$) to the one-loop RG.

and yields the expression,

$$\mathcal{K}_{ex,2} = \frac{1}{\beta}\sum_{\mathrm{i}\Omega_n} G_f(\mathbf{x}-\mathbf{x},\mathrm{i}\nu_n)G_c(\mathbf{x}_l-\mathbf{x},\mathrm{i}\Omega_n)\Gamma(\mathbf{x}_l,\mathrm{i}\omega;\mathrm{i}\Omega_n;\mathbf{x},\mathrm{i}\nu_n) \tag{3.204}$$

The Matsubara sum can be obtained by a contour integration,

$$0 = \frac{1}{2\pi\mathrm{i}}\oint_C \mathrm{d}z\, n_F(z)G_f(z+\mathrm{i}\nu-\mathrm{i}(\omega+\Omega))G_c(z)\Gamma(\mathrm{i}\omega;z;z+\mathrm{i}\nu-\mathrm{i}(\omega+\Omega))\ , \tag{3.205}$$

with the branch-cuts at

$$\begin{aligned} z &= \varepsilon \in \mathbb{R} \ , \\ z &= \varepsilon + \mathrm{i}(\omega + \Omega) - \mathrm{i}\nu \ . \end{aligned} \tag{3.206}$$

Therefore,

$$\begin{aligned} &\frac{1}{2\pi\mathrm{i}} \int_{-D}^{+D} \mathrm{d}\varepsilon \, n_F(\varepsilon) G_f(\varepsilon + \mathrm{i}\nu - \mathrm{i}(\omega + \Omega))[G_c(\varepsilon + \mathrm{i}\eta^+) - G_c(\varepsilon - \mathrm{i}\eta^+)]\Gamma(\mathrm{i}\omega, \varepsilon, \varepsilon + \mathrm{i}\nu - \mathrm{i}(\omega + \Omega)) \\ &+ \frac{1}{2\pi\mathrm{i}} \int_{-D}^{+D} \mathrm{d}\varepsilon \, n_F(\varepsilon + \underbrace{\mathrm{i}(\omega + \Omega) - \mathrm{i}\nu}_{\text{bosonic}})[G_f(\varepsilon + \mathrm{i}\eta^+) - G_f(\varepsilon - \mathrm{i}\eta^+)]G_c(\varepsilon + \mathrm{i}(\omega + \Omega) - \mathrm{i}\nu)\Gamma(\mathrm{i}\omega, \varepsilon + \mathrm{i}(\omega + \Omega) - \mathrm{i}\nu \\ &- \frac{1}{2\pi\mathrm{i}} \oint_{C_F} \mathrm{d}z \, n_F(z) G_f(z + \mathrm{i}\nu - \mathrm{i}(\omega + \Omega)) A_C(\varepsilon)\Gamma(\mathrm{i}\omega, \varepsilon, \varepsilon + \mathrm{i}\nu - \mathrm{i}(\omega + \Omega)) = 0 \ . \end{aligned} \tag{3.207}$$

Hence,

$$\begin{aligned} \mathcal{K}_{ex,2} = &\frac{1}{2\pi} \int_{-D}^{+D} \mathrm{d}\varepsilon \, n_F(\varepsilon) G_f(\varepsilon + \mathrm{i}\nu - \mathrm{i}(\omega + \Omega)) A_c(\varepsilon)\Gamma(\mathrm{i}\omega, \varepsilon, \varepsilon + \mathrm{i}\nu - \mathrm{i}(\omega + \Omega)) \\ &+ \frac{1}{2\pi} \int_{-D}^{+D} \mathrm{d}\varepsilon \, n_F(\varepsilon) A_f(\varepsilon) G_c(\varepsilon + \mathrm{i}(\omega + \Omega) - \mathrm{i}\nu)\Gamma(\mathrm{i}\omega, \varepsilon + \mathrm{i}(\omega + \Omega) - \mathrm{i}\nu, \varepsilon) \ . \end{aligned} \tag{3.208}$$

The 'retarded branch'[15] is obtained via the transformations

$$\begin{aligned} \mathrm{i}\omega &\mapsto \omega + \mathrm{i}\eta^+ \ , \\ \mathrm{i}\Omega &\mapsto \Omega + \mathrm{i}\eta^+ \ , \\ \mathrm{i}\nu &\mapsto \nu + \mathrm{i}\eta^+ \ , \end{aligned} \tag{3.209}$$

which obtain

$$\begin{aligned} \mathcal{K}_{ex,2} = &\frac{1}{2\pi} \int_{-D}^{+D} \mathrm{d}\varepsilon \, n_F(\varepsilon) G_f^A(\varepsilon + \nu - (\omega + \Omega)) A_c(\varepsilon)\Gamma(\omega, \varepsilon, \varepsilon + \nu - (\omega + \Omega)) \\ &- \frac{1}{2\pi} \int_{-D}^{+D} \mathrm{d}\varepsilon \, n_F(\varepsilon) A_f(\varepsilon) G_c^R(\varepsilon + (\omega + \Omega) - \nu)\Gamma(\omega, \varepsilon + (\omega + \Omega) - \nu, \varepsilon) \end{aligned} \tag{3.210}$$

Using the transformation $\nu \mapsto \nu + \lambda$ for pseudo-fermions (Appendix C),

$$\begin{aligned} \mathcal{K}_{ex,2}^R = &\frac{1}{2\pi} \int_{-D}^{+D} \mathrm{d}\varepsilon \, n_F(\varepsilon) G_f^A(\varepsilon + \nu + \lambda - (\omega + \Omega)) A_C(\varepsilon)\Gamma(\omega, \varepsilon, \varepsilon + \nu + \lambda - (\omega + \Omega)) \\ &+ \frac{1}{2\pi} \int_{-D}^{+D} \mathrm{d}\varepsilon \, n_F(\varepsilon) A_f(\varepsilon) G_c^R(\varepsilon + (\omega + \Omega) - \nu - \lambda)\Gamma(\omega, \varepsilon + (\omega + \Omega) - \nu - \lambda, \varepsilon) \ , \end{aligned} \tag{3.211}$$

[15] For a detailed discussion of the analytical properties of the vertices, consult Ref. [120].

and

$$\hat{\mathcal{K}}_{ex,2} = \frac{1}{2\pi}\int_{-D}^{+D} \mathrm{d}\varepsilon\, n_F(\varepsilon) G_f^A(\varepsilon+\nu-(\omega+\Omega)) A_c(\varepsilon)\hat{\Gamma}(\omega,\varepsilon,\varepsilon+\nu-(\omega+\Omega)) + \frac{1}{2\pi}\int_{-D}^{+D} \mathrm{d}\varepsilon\, n_F(\varepsilon+\lambda)\hat{A}_f(\varepsilon)\hat{G}_c(\varepsilon+(\omega+\Omega)-\nu,\varepsilon)\hat{\Gamma}(\omega,\varepsilon+(\omega+\Omega)-\nu,\varepsilon)\ . \quad (3.212)$$

Notice that

$$\lim_{\lambda\to+\infty} n_F(\varepsilon+\lambda) \to e^{-\beta\lambda} = 0\ ;$$

therefore,

$$\hat{\mathcal{K}}^R_{ex,2} = \frac{1}{2\pi}\int_{-D}^{+D} \mathrm{d}\varepsilon\, n_F(\varepsilon) G_f^A(\varepsilon+\nu-(\omega+\Omega)) A_c(\varepsilon)\hat{\Gamma}(\omega,\varepsilon,\varepsilon+\nu-(\omega+\Omega)) \quad (3.213)$$

3.4.2.1 Reproducing the single-impurity results

The previously derived equations for the RKKY-corrected vertex can be verified by reproducing the results obtained for the single-impurity case by using the bare Kondo vertex,

$$\Gamma^0(\mathbf{x}_l, \mathrm{i}\omega; \mathrm{i}\omega+\mathrm{i}\Omega; \mathbf{x}, \mathrm{i}\nu) \stackrel{!}{=} J\delta(\mathbf{x}-\mathbf{x}_l)\ . \quad (3.214)$$

Then

$$\hat{\mathcal{K}}^R_{dir,1} = \frac{1}{2\pi}\int_{-D}^{+D} \mathrm{d}\varepsilon \left\{ n_F(\varepsilon) A_c(\varepsilon)\hat{G}_f^R(\omega+\nu-\varepsilon) - G_c^R(\omega+\nu-\varepsilon)\hat{A}_f(\varepsilon)\right\}, \quad (3.215)$$

where all spectral and Green functions are 'local'.

$$\hat{\mathcal{K}}^R_{dir,2} = \frac{1}{2\pi}\int_{-D}^{+D} \mathrm{d}\varepsilon \left\{ n_F(\varepsilon) A_c(\varepsilon)\hat{G}_f^R(\omega+\nu-\varepsilon) - \hat{A}_f(\varepsilon) G_c^R(\omega+\nu-\varepsilon)\right\}. \quad (3.216)$$

The exchange contributions are

$$\hat{\mathcal{K}}^R_{ex,1} = \frac{1}{2\pi}\int_{-D}^{+D} \mathrm{d}\varepsilon \left\{ n_F(\varepsilon)\hat{G}_f^R(\varepsilon+\nu-(\omega+\Omega)) A_c(\varepsilon)\right\}$$
$$\hat{\mathcal{K}}^R_{ex,2} = \frac{1}{2\pi}\int_{-D}^{+D} \mathrm{d}\varepsilon \left\{ n_F(\varepsilon)\hat{G}_f^R(\varepsilon+\nu-(\omega+\Omega)) A_c(\varepsilon)\right\}. \quad (3.217)$$

The above relations correctly reproduce the single-impurity results (section 2.6).

3.4.3 Renormalization group in presence of the RKKY interaction

To obtain the flow equation, one has to differentiate the calculated vertices, $\mathcal{K}_{dir}$ and $\mathcal{K}_{ex}$, with respect to the running energy scale, $\ln D$.

3.4.3.1 Contribution of the direct RG diagram

First direct RG diagram The first direct RG diagram

$$\mathcal{K}_{dir,1} = \int_{-D}^{D} \mathrm{d}\varepsilon\, F(\varepsilon, D) \ ,$$
$$F(\varepsilon, D) := n_F(\varepsilon)\hat{\Gamma}^R(\omega, \varepsilon, \nu)\frac{A_c(\varepsilon)}{2\pi}\hat{G}_f^R(\omega + \nu - \varepsilon)$$
$$- \hat{\Gamma}^R(\omega, \omega + \nu - \varepsilon, \nu)G_c^R(\omega + \nu - \varepsilon)\frac{\hat{A}_f(\varepsilon)}{2\pi} \ . \tag{3.218}$$

Differentiating with respect to $\ln D$ and using the Leibniz integral rule (Appendix H), yields

$$\frac{\partial \mathcal{K}^d}{\partial \ln D} = D\frac{\partial}{\partial D}\mathcal{K}^d \ ;$$

in explicit terms,

$$\begin{aligned}
\frac{\partial \mathcal{K}_{dir,1}}{\partial D} &= \frac{\partial}{\partial D}\left[\int_{-D}^{D} \mathrm{d}\varepsilon\, F(\varepsilon, D)\right] \\
&= F(\varepsilon = D, D) + F(\varepsilon = -D, D) + \int_{-D}^{D} \mathrm{d}\varepsilon\, \frac{\partial}{\partial D}F(\varepsilon, D) \\
&= n_F(D)\hat{\Gamma}^R(\omega, \varepsilon = D, \nu)\frac{\hat{A}_c(D)}{2\pi}\hat{G}_f^R(\omega + \nu - D) \\
&\quad - \hat{\Gamma}^R(\omega, \omega + \nu - D, \nu)G_c^R(\omega + \nu - D)\frac{\hat{A}_f(D)}{2\pi} \\
&\quad + n_F(-D)\hat{\Gamma}^R(\omega, \varepsilon = -D, \nu)\frac{A_c(-D)}{2\pi}\hat{G}_f^R(\omega + \nu + D) \\
&\quad - \hat{\Gamma}^R(\omega, \omega + \nu + D, \nu)G_c^R(\omega + \nu + D)\frac{\hat{A}_f(-D)}{2\pi} \\
&\quad + \int_{-D}^{D} \mathrm{d}\varepsilon\, \frac{\partial}{\partial D}F(\varepsilon, D) \ .
\end{aligned} \tag{3.219}$$

Remind that

$$n_F(D) \overset{\beta D \gg 1}{=} e^{-\beta D} \to 0 \quad , \quad n_F(-D) \overset{\beta D \gg 1}{=} 1 \ ; \tag{3.220}$$

Moreover, since

$$\frac{\hat{A}_f(\varepsilon)}{2\pi} \approx \delta(\varepsilon - \xi_d) \ , \tag{3.221}$$

then,

$$\begin{aligned}
\frac{\hat{A}_f(\varepsilon = D)}{2\pi} &\approx \delta(D - \xi_d) = 0 \ , \\
\frac{\hat{A}_f(\varepsilon = -D)}{2\pi} &\approx \delta(-D - \xi_d) = 0 \ ,
\end{aligned} \tag{3.222}$$

due to the fact that $\xi_d \ll D$. Thus,

$$\mathrm{Im}\,\hat{G}_f(\varepsilon = \pm D) = 0\ . \tag{3.223}$$

Letting $\omega \stackrel{!}{=} 0$ corresponding to the c-electrons on the Fermi surface, we obtain

$$\begin{aligned}\frac{\partial \mathcal{K}_{dir,1}}{\partial D} &= \hat{\Gamma}^R(\omega = 0; \varepsilon = -D; \nu)\frac{A_c(-D)}{2\pi}\hat{G}_f^{R\prime}(\nu + D) \\ &\quad + \int_{-D}^{D} \mathrm{d}\varepsilon\, \frac{\partial}{\partial D} F(\varepsilon, D)\ .\end{aligned} \tag{3.224}$$

The explicit form of the (non-interacting) pseudo-fermion Green function is

$$\hat{G}_f^{R\prime}(\varepsilon) = \frac{1}{\varepsilon - \xi_d} \Rightarrow \hat{G}_f^{R\prime}(\nu + D) = \frac{1}{\nu + D - \xi_d}\ . \tag{3.225}$$

Therefore,

$$\hat{\Gamma}_{d,R}(\mathbf{x}_l, \omega = 0; \mathbf{x}_l{}', -D; \mathbf{x}, \nu) = 4JJ_0^2\chi_f(-D)\chi_c(\mathbf{x} - \mathbf{x}_l, -D)\ . \tag{3.226}$$

Notice that the imaginary part of the susceptibilities can be ignored when $\Omega \sim \mathcal{O}(T_K) \ll D$, since

$$\begin{aligned}|\frac{\chi_c''(\mathbf{x}, \Omega)}{\chi_c'(\mathbf{x}, \Omega)}| &\sim \frac{\Omega}{D} \to 0, \\ |\frac{\chi_f''(\mathbf{x}, \Omega)}{\chi_f'(\mathbf{x}, \Omega)}| &\sim \frac{\Omega}{D} \to 0\ .\end{aligned} \tag{3.227}$$

The last term in Eq. (3.224), $\int_{-D}^{D} \mathrm{d}\varepsilon\, \frac{\partial F(\varepsilon, D)}{\partial D}$, can be neglected because it is an integration over the whole bandwidth which cannot produce a critical contribution. The previous results, lead to

$$\begin{aligned}\frac{\partial \mathcal{K}_{dir,1}}{\partial D} &= \hat{\Gamma}_{dir}(\omega = 0; \varepsilon = -D; \nu)\frac{A_c(-D)}{2\pi}\frac{1}{D(1 + \frac{\nu - \xi_d}{D})} \\ \Rightarrow D\frac{\partial \mathcal{K}_{dir,1}}{\partial D} &= \hat{\Gamma}_{dir}(\omega = 0; \varepsilon = -D; \nu)\frac{A_c(-D)}{2\pi}\frac{1}{1 + \frac{\nu - \xi_d}{D}}\ .\end{aligned} \tag{3.228}$$

Remind that (see Fig. 3.9)

$$\Gamma_{dir}(\mathbf{x}_l, \omega; \varepsilon; \mathbf{x}, \nu) = 4JJ_0^2\chi_f'(\varepsilon - D)\,\chi_c'(\mathbf{x} - \mathbf{x}_l, \varepsilon - D) \tag{3.229}$$

and

$$\begin{aligned}\Gamma_{dir}(\mathbf{x}_l, \omega = 0; \varepsilon = -D; \mathbf{x}, \nu) &= 4JJ_0^2\chi_f'(-D)\,\chi_c'(\mathbf{x} - \mathbf{x}_l, -D) \\ &= 4JJ_0^2\chi_f'(-D)\,\chi_c'(\mathbf{x} - \mathbf{x}_l, -D) \\ &= 4JJ_0^2\chi_f'(D)\,\chi_c'(\mathbf{x} - \mathbf{x}_l, -D)\ ,\end{aligned} \tag{3.230}$$

where in the last line, we have used

$$\chi_f'(-\varepsilon) = \chi_f'(\varepsilon) \ . \tag{3.231}$$

Thus,

$$\frac{\partial \mathcal{K}_{dir,1}}{\partial \ln D} \equiv D\frac{\partial K_{dir,1}}{\partial D} = 4J^2 J_0^2 \chi_f'(D) \left[\sum_{\mathbf{x}_l} \frac{A_c(\mathbf{x}-\mathbf{x}_l,-D)}{2\pi}\chi_c'(\mathbf{x}-\mathbf{x}_l,-D)\right] \ . \tag{3.232}$$

Second direct RG diagram The second contribution to the direct diagram can be obtained similar to the first one.

$$\begin{aligned}
\mathcal{K}_{dir,2} &=: \int_{-D}^{D} \mathrm{d}\varepsilon \, F(\varepsilon, D) \\
F(\varepsilon, D) &:= n_F(\varepsilon)\frac{A_c(\varepsilon)}{2\pi}\hat{G}_f^R(\omega+\nu-\varepsilon)\hat{\Gamma}^R(\varepsilon;\omega+\Omega;\omega+\nu-\varepsilon) \\
&\quad - \frac{\hat{A}_f(\varepsilon)}{2\pi}\hat{\Gamma}^R(\omega+\nu-\varepsilon;\omega+\Omega;\varepsilon)G_c^R(\omega+\nu-\varepsilon) \ ;
\end{aligned} \tag{3.233}$$

therefore,

$$\begin{aligned}
\frac{\partial}{\partial D}\mathcal{K}_{dir,2} &= \frac{\partial}{\partial D}\left(\int_{-D}^{D} \mathrm{d}\varepsilon \, F(\varepsilon, D)\right) \\
&= F(\varepsilon = D, D) + F(\varepsilon = -D, D) + \int_{-D}^{D} \mathrm{d}\varepsilon \, \frac{\partial}{\partial D} F(\varepsilon, D) \\
&= n_F(D)\frac{A_c(D)}{2\pi}\hat{G}_f^R(\omega+\nu-D)\hat{\Gamma}^R(D;\omega+\Omega;\omega+\nu-D) \\
&\quad - \frac{\hat{A}_f(D)}{2\pi}\hat{\Gamma}^R(\omega+\nu-D;\omega+\Omega;D)G_c^R(\omega+\nu-D) \\
&\quad + n_F(-D)\frac{A_c(-D)}{2\pi}G_f^R(\omega+\nu+D)\hat{\Gamma}^R(-D;\omega+\Omega;\omega+\nu+D) \\
&\quad - \frac{\hat{A}_f(-D)}{2\pi}\hat{\Gamma}^R(\omega+\nu+D;\omega+\Omega;-D)G_c^R(\omega+\nu+D) \\
&\quad + \int_{-D}^{D} \mathrm{d}\varepsilon \, \frac{\partial}{\partial D} F(\varepsilon, D) \ .
\end{aligned} \tag{3.234}$$

The same considerations as for $K_{dir,1}$ yields

$$\begin{aligned}
\frac{\partial}{\partial D}\mathcal{K}_{dir,2} &= \frac{A_c(-D)}{2\pi}G_f^R(\omega+\nu+D)\Gamma^R(-D;\omega+\Omega;\omega+\nu+D) \\
&\overset{\omega\overset{!}{=}0}{=\!=} \frac{A_c(-D)}{2\pi}G_f^{R\prime}(\nu+D)\Gamma^R(-D;\Omega;\nu+D)
\end{aligned} \tag{3.235}$$

Note that (see Fig. 3.9)

$$\Gamma^R(-D;\Omega;\nu+D) = 4JJ_0^2\chi_f'(D)\chi_c'(\mathbf{x}-\mathbf{x}_l,D) \ . \tag{3.236}$$

Furthermore,

$$G_f(\nu + D) = \frac{1}{\nu + D - \xi_d} = \frac{1}{D(1 + \frac{\nu - \xi_d}{D})} \ , \tag{3.237}$$

and

$$\frac{\partial \mathcal{K}_{dir,2}}{\partial \ln D} \equiv D \frac{\partial \mathcal{K}_{dir,2}}{\partial D} = 4J^2 J_0^2 \chi_f'(D) \left[\sum_{\mathbf{x}_l \neq \mathbf{x}} \frac{A_c(\mathbf{x} - \mathbf{x}_l, -D)}{2\pi} \chi_c'(\mathbf{x} - \mathbf{x}_l, D) \right] \tag{3.238}$$

3.4.3.2 Contribution of the exchange RG diagram

First exchange RG diagram The contributions to the first exchange diagram can be obtained following the same steps as for the direct diagram.

$$\begin{aligned} \mathcal{K}_{ex,1} &=: \int_{-D}^{D} F(\varepsilon, D) \ , \\ F(\varepsilon, D) &= n_F(\varepsilon) \hat{\Gamma}(\varepsilon; \omega + \Omega; \nu) \hat{G}_f^A(\varepsilon + \nu - (\omega + \Omega)) A_c(\varepsilon) \ . \end{aligned} \tag{3.239}$$

Therefore,

$$\begin{aligned} \frac{\partial \mathcal{K}_{ex,1}}{\partial D} &= F(\varepsilon = D, D) + F(\varepsilon = -D, D) + \int_{-D}^{D} \mathrm{d}\varepsilon \, \frac{\partial}{\partial D} F(\varepsilon, D) \\ &= n_F(D) \Gamma(D; \omega + \Omega; \nu) G_f^A(D + \nu - (\omega + \Omega)) A_c(D) \\ &+ n_F(-D) \Gamma(-D; \omega + \Omega; \nu) G_f^A(-D + \nu - (\omega + \Omega)) A_c(-D) \\ &+ \int_{-D}^{D} \mathrm{d}\varepsilon \, \frac{\partial}{\partial D} F(\varepsilon, D) \ . \end{aligned} \tag{3.240}$$

Letting $\omega \stackrel{!}{=} 0$, and using

$$n_F(D) \to 0 \quad , \quad n_F(-D) \to 1, \quad \text{for } D \gg 1 \tag{3.241}$$

and

$$\begin{aligned} \operatorname{Im} G_f^A(-D + \nu - (\omega + \Omega)) &= \pi \delta(-D + \nu - (\omega + \Omega) - \xi_d) \\ &\stackrel{\omega \stackrel{!}{=} 0}{=\!=} \pi \delta(-D + \nu - \xi_d - \Omega) = 0 \ , \end{aligned} \tag{3.242}$$

one obtains

$$\begin{aligned} \frac{\partial \mathcal{K}_{ex,1}}{\partial D} &= \Gamma(-D; \Omega; \nu) G_f^{A\prime}(-D + \nu - \Omega) A_c(-D) \\ &+ \int_{-D}^{D} \mathrm{d}\varepsilon \, \frac{\partial}{\partial D} F(\varepsilon, D) \ . \end{aligned} \tag{3.243}$$

The vertex Γ_{ex} reads (see Fig. 3.9)

$$\begin{aligned}\Gamma_{ex}(\mathbf{x}_l,-D;\Omega;\mathbf{x},\nu) &= 4JJ_0^2\chi_f(D+\Omega)\chi_c(\mathbf{x}-\mathbf{x}_l,D+\Omega)\\ &= 4JJ_0^2\chi_f(D)\chi_c(\mathbf{x}-\mathbf{x}_l,D)+\mathcal{O}(\frac{\Omega}{D})\ .\end{aligned} \tag{3.244}$$

By neglecting the imaginary parts of the susceptibilities with respect to the real parts, one obtains

$$\Gamma(\mathbf{x}_l,-D;\Omega;\mathbf{x},\nu) = 4JJ_0^2\chi_f'(D)\chi_c(\mathbf{x}-\mathbf{x}_l,D)+\mathcal{O}(\frac{\Omega}{D})\ . \tag{3.245}$$

The last term, the integration over ε can be neglected as explained before. Hence,

$$\begin{aligned}\frac{\partial\mathcal{K}_{ex,1}}{\partial D} &= 4J^2J_0^2\chi_f'(D)\sum_{\mathbf{x}_l\neq\mathbf{x}}\chi_c'(D)\frac{1}{-D+\nu-\xi_d-\Omega}A_c(-D)\\ &= 4J^2J_0^2\chi_f'(D)\sum_{\mathbf{x}_l\neq\mathbf{x}}\chi_c'(D)\frac{1}{-D(1+\frac{-\nu-\Omega-\xi_d}{D})}A_c(-D)\ ,\end{aligned} \tag{3.246}$$

Therefore,

$$\begin{aligned}\frac{\partial\mathcal{K}_{ex,1}}{\partial\ln D} &= D\frac{\partial\mathcal{K}_{ex,1}}{\partial D}\\ &= -4J^2J_0^2\chi_f'(D)\left[\sum_{\mathbf{x}_l\neq\mathbf{x}}A_c(\mathbf{x}-\mathbf{x}_l,-D)\,\chi_c'(\mathbf{x}-\mathbf{x}_l,D)\right]+\mathcal{O}(\frac{1}{D})\ .\end{aligned} \tag{3.247}$$

Second exchange RG diagram The second contribution to the exchange diagram can be obtained along the similar lines followed for the first exchange contribution:

$$\begin{aligned}\mathcal{K}_{ex,2} &= \int_{-D}^{D}\mathrm{d}\varepsilon\,F(\varepsilon,D)\ ,\\ F(\varepsilon,D) &:= n_F(\varepsilon)G_f^A(\varepsilon+\nu-(\omega+\Omega))\frac{A_c(\varepsilon)}{2\pi}\hat{\Gamma}(\omega;\varepsilon;\varepsilon+\nu-(\omega+\Omega))\ .\end{aligned} \tag{3.248}$$

Using the Leibniz integral rule (Appendix H),

$$\begin{aligned}\frac{\partial}{\partial D}\mathcal{K}_{ex,2} &= F(D,D)+F(-D,D)+\int_{-D}^{D}\mathrm{d}\varepsilon\,\frac{\partial}{\partial D}F(\varepsilon,D)\\ &= n_F(D)G_f^A(D+\nu-(\omega+\Omega))\frac{A_c(D)}{2\pi}\hat{\Gamma}(\omega;D;D+\nu-(\omega+\Omega))\\ &+ n_F(-D)G_f^A(-D+\nu-(\omega+\Omega))\frac{A_c(-D)}{2\pi}\hat{\Gamma}(\omega;-D;-D+\nu-(\omega+\Omega))\\ &+\int_{-D}^{D}\mathrm{d}\varepsilon\,\frac{\partial}{\partial D}F(\varepsilon,D)\ .\end{aligned} \tag{3.249}$$

Noting that

$$n_F(D)\to 0\quad,\quad n_F(-D)\to 1$$

and

$$\begin{aligned}\operatorname{Im} G_f^A(-D+\nu-(\omega+\Omega)) &= \pi\delta(-D+\nu-(\omega+\Omega)-\xi_d)\\ &\overset{\omega\overset{!}{=}0}{=\!=\!=} \pi\delta(-D+\nu-\Omega-\xi_d)=0\ ,\end{aligned} \tag{3.250}$$

one obtains

$$\begin{aligned}\frac{\mathcal{K}_{ex,2}}{\partial D} &= G_f^{A\prime}(-D+\nu-\Omega)\frac{A_c(-D)}{2\pi}\hat{\Gamma}(\omega=0;-D;-D+\nu-\Omega)\\ &\quad+\int_{-D}^{D}\mathrm{d}\varepsilon\,\frac{\partial}{\partial D}F(\varepsilon,D)\ .\end{aligned} \tag{3.251}$$

The last term can be neglected as explained before. Therefore (see Fig. 3.9),

$$\Gamma_{dir}(\omega=0;-D;-D+\nu-\Omega)=4JJ_0^2\chi_f(-D)\chi_c(\mathbf{x}-\mathbf{x}_l,-D)\ . \tag{3.252}$$

Neglecting the imaginary parts of the susceptibilities justified as before, one obtains

$$\begin{aligned}\Gamma_{dir}(\omega=0;-D;-D+\nu-\Omega) &= 4JJ_0^2\underbrace{\chi_f'(-D)}_{=\chi_f'(D)}\chi_c'(\mathbf{x}-\mathbf{x}_l,-D)\\ &= 4JJ_0^2\chi_f'(D)\chi_c'(\mathbf{x}-\mathbf{x}_l,-D)\ .\end{aligned} \tag{3.253}$$

Therefore,

$$\begin{aligned}\frac{\partial}{\partial D}\mathcal{K}_{ex,2} &= \frac{1}{-D+\nu-\Omega-\xi_d}4JJ_0^2\chi_f'(D)\sum_{\mathbf{x}_l\neq\mathbf{x}}\frac{A_c(\mathbf{x}-\mathbf{x}_l,-D)}{2\pi}\chi_c'(\mathbf{x}-\mathbf{x}_l,-D)\\ &= \frac{1}{-D(1-\frac{\nu-\Omega-\xi_d}{D})}4JJ_0^2\chi_f'(D)\sum_{\mathbf{x}_l\neq\mathbf{x}}\frac{A_c(\mathbf{x}-\mathbf{x}_l,-D)}{2\pi}\chi_c'(\mathbf{x}-\mathbf{x}_l,-D)\ ,\end{aligned} \tag{3.254}$$

and finally,

$$\frac{\partial}{\partial\ln D}\mathcal{K}_{ex,2}\equiv D\frac{\partial}{\partial D}\mathcal{K}_{ex,2}=-4JJ_0^2\chi_f'(D)\sum_{\mathbf{x}_l\neq\mathbf{x}}\frac{A_c(\mathbf{x}-\mathbf{x}_l,-D)}{2\pi}\chi_c'(\mathbf{x}-\mathbf{x}_l,-D)\ . \tag{3.255}$$

3.4.4 RG flow equation for the multi-impurity Kondo problem

Now, one can re-assemble all the previous results to obtain the change in the Kondo coupling due to the reduction of the bandwidth:

$$\begin{aligned}\delta J &= \delta J_{dir}+\delta J_{ex}\\ &= \underbrace{(-2)}_{\substack{\text{spin algebra}\\ \text{for}\\ \text{direct diag.}}}(\mathcal{K}_{dir,1}+\mathcal{K}_{dir,2})+\underbrace{(+2)}_{\substack{\text{spin algebra}\\ \text{for}\\ \text{exchange diag.}}}(\mathcal{K}_{ex,1}+\mathcal{K}_{ex,2})\ .\end{aligned} \tag{3.256}$$

Therefore, in explicit form,

$$\begin{aligned}\frac{\partial J}{\partial \ln D} &= (-2)(2)4J^2J_0^2\chi_f'(D)\sum_{\mathbf{x}_l\neq\mathbf{x}}\frac{A_c(\mathbf{x}-\mathbf{x}_l,-D)}{2\pi}\chi_c'(\mathbf{x}-\mathbf{x}_l,D)\\ &+ (+2)(2)(-4)J^2J_0^2\chi_f'(D)\sum_{\mathbf{x}_l\neq\mathbf{x}}\frac{A_c(\mathbf{x}-\mathbf{x}_l,-D)}{2\pi}\chi_c'(\mathbf{x}-\mathbf{x}_l,D)\\ &= -16J^2J_0^2\chi_f'(D)\sum_{\mathbf{x}_l\neq\mathbf{x}}\frac{A_c(\mathbf{x}-\mathbf{x}_l,-D)}{2\pi}\chi_c'(\mathbf{x}-\mathbf{x}_l,D)\end{aligned} \tag{3.257}$$

It is crucial to notice that the functions under the sum are slowly varying functions of energy/frequency on the Kondo scale $\Delta\varepsilon \sim \mathcal{O}(T_K) \ll D_0$. They change on a much higher scale, the Fermi scale, $\varepsilon_F \sim D_0$. By these considerations, one finally obtains the RG flow equation as

$$\begin{aligned}\frac{\partial J}{\partial \ln D} &= -2\mathcal{N}(\varepsilon_F)J^2 - 16J^2J_0^2\chi_f^{R\prime}(D)\,\mathcal{R}(r)\\ &= -2\mathcal{N}(\varepsilon_F)J^2\left(1+\frac{1}{\mathcal{N}(\varepsilon_F)}\,8J_0^2\chi_f'(R)\,\mathcal{R}(r)\right)\end{aligned} \tag{3.258}$$

where $\mathcal{R}(r)$ is a 'static' (approximately energy/frequency -independent) function of distance r. Using the explicit form of the local f-susceptibility,

$$\chi_f^{R\prime}(D) = \frac{a'}{T_K}\frac{1}{\sqrt{1+(D/T_k)^2}} \quad ; \quad a' \sim \mathcal{O}(1)\ , \tag{3.259}$$

and introducing the dimensionless coupling,

$$J \mapsto \mathcal{N}(\varepsilon_F)J\ , \tag{3.260}$$

one can re-write the flow equation as

$$\frac{\partial J}{\partial \ln D} = -2J^2\Big(1+J_0^2\frac{D_0}{T_K}\frac{1}{\sqrt{1+(D/T_K)^2}}\underbrace{\Big(\frac{8a'}{D_0\mathcal{N}(\varepsilon_F)^3}\,\mathcal{R}(r)\Big)}_{=-y}\Big)\ , \tag{3.261}$$

where we have defined the dimensionless parametre y as[16]

$$y := \text{const.}\,\frac{-1}{D_0\mathcal{N}(\varepsilon_F)^3}\frac{1}{V^2}\sum_{\mathbf{x}_l\neq\mathbf{x}}\frac{A_c(\mathbf{x}-\mathbf{x}_l)}{2\pi}\chi_c(\mathbf{x}-\mathbf{x}_l)\ , \tag{3.263}$$

[16] This can be observed by the following dimensional relations,

$$\begin{aligned}[\![A_c]\!] = \frac{1}{E} \quad &, \quad [\![\chi_c]\!] = \frac{1}{E}\\ [\![D_0]\!] = E \quad &, \quad [\![\mathcal{N}(\varepsilon_F)]\!] = \frac{1}{E}\\ \Rightarrow [\![y]\!] \quad &= \quad \frac{1}{E}\frac{1}{\frac{1}{E^2}}\frac{1}{E^2} = 1\ .\end{aligned} \tag{3.262}$$

where the constant coefficient is positive definite and of order $\mathcal{O}(1)$; moreover, we have dropped the energy dependence of the conduction electron susceptibility and spectral function, since in effect, they change only at a higher energy scale of Fermi energy, $\varepsilon_F \gg T_K$. Notice that since

$$\chi_c \sim -\mathcal{N}(\varepsilon_F) < 0 \quad \text{and} \quad A_c > 0 \ , \tag{3.264}$$

the presence of the minus sign in the definition of y ensures its positivity. For a lattice with discrete translational symmetry, using the mapping $\mathbf{x}_l \mapsto \mathbf{x}_l + \mathbf{x}$, one can re-write y as

$$y \propto \sum_{\mathbf{k}} A_c^0(\mathbf{k})\chi_c(\mathbf{k}) \ . \tag{3.265}$$

Note that

$$A_c^0(k, \omega \to 0) \sim \frac{1}{\mathcal{N}(\varepsilon_F)} \quad , \quad \chi_c(k, \omega \to 0) \approx \chi_c(k = 0, \omega \to 0) \ . \tag{3.266}$$

Thus, the parametre y is essentially an average of the strength of the RKKY interaction over the set of impurities.

Therefore, finally, we arrive at the expected RG equation for a multi-impurity Kondo system,

$$\frac{\partial J(D)}{\partial \ln(D)} = -2J^2 \left(1 - yJ_0^2 \frac{D_0}{T_K} \frac{1}{\sqrt{1 + (D/T_K)^2}}\right) \ . \tag{3.267}$$

Finally, note that the presence of $\frac{1}{T_K}$ in the RKKY-modification to the RG β-function leads to a feedback mechanism in the RG flow; that is, as the RKKY interaction reduces the Kondo temperature, its effect becomes stronger due to the proportionality of the RKKY-correction to $\frac{1}{T_K}$.

3.4.5 Solution of the RKKY-modified RG flow equation

In the previous section, the RG equation was obtained as

$$\frac{\partial J(D)}{\partial \ln D} = -2J^2(D) \left(1 - yJ_0^2 \frac{D_0}{T_K} \frac{1}{\sqrt{1 + (D/T_K)^2}}\right) \ . \tag{3.268}$$

Remind that here, $T_K = T_K(y)$, where y depends on the properties of itinerant conduction electrons; furthermore, y is directly proportional to the strength of the carrier-mediated RKKY interaction.

Similar to the single-impurity case, integrating the differential equation yields

$$-\int_{J(D_0)}^{J(T_K(y))} \mathrm{d}J \, \frac{1}{2J^2} = \int_{D_0}^{T_K(y)} \frac{\mathrm{d}D}{D} \left(1 - yJ_0^2 \frac{D_0}{T_K} \frac{1}{\sqrt{1 + (D/T_K)^2}}\right) \ . \tag{3.269}$$

Hence, on the LHS,

$$\frac{1}{2J}\Big|_{J(D_0)}^{J(T_K(y))} = \frac{1}{2}\left(\frac{1}{J(T_K)} - \frac{1}{J(D_0)}\right) = \frac{1}{2}\left(0 - \frac{1}{J(D_0)}\right) = -\frac{1}{2J_0} \ , \tag{3.270}$$

where in the third equality, we have used

$$\lim_{\varepsilon \to T_K} J(\varepsilon) \to +\infty \ ;$$

that is, the coupling diverges at the Kondo temperature (energy scale) indicating a flow towards the strong-coupling fixed point. Notice that at the full band-width D_0,

$$\begin{aligned} J(D_0) &= J_0 + \mathcal{N}(\varepsilon_F)\Gamma_{dir}(D_0) = J_0 + \mathcal{O}(\frac{1}{D_0^2}) \\ \Gamma_{dir}(D_0) &\equiv \Gamma_{dir}(\omega = 0; \varepsilon = D_0; \nu) \propto \chi_f^{R'}(D_0) \\ &\sim \frac{1}{T_K} \frac{1}{\sqrt{1 + (D_0/T_K)^2}} \sim \mathcal{O}(\frac{1}{D_0}) \to 0 \ , \end{aligned} \tag{3.271}$$

meaning that at the full bandwidth, RKKY modifications are absent. Furthermore, $T_K^0 \equiv T_K(y = 0)$, the Kondo temperature in absence of RKKY correlations, satisfies

$$\frac{T_K(y=0)}{D_0} = \frac{T_K^0}{D_0} = \exp[-\frac{1}{2J_0}] \Rightarrow -\frac{1}{2J_0} = \ln(\frac{T_K^0}{D_0}) \ , \tag{3.272}$$

which is essentially, the *single-impurity* result. In order to solve the differential equation, Eq. (3.268), the following integrals are needed:

$$\begin{aligned} \int \frac{\mathrm{d}\omega}{\omega} &= \ln|\omega| \ , \\ \int \frac{\mathrm{d}\omega}{\omega} \frac{1}{\sqrt{1+\omega^2}} &= \int \frac{\mathrm{d}u}{u^2-1} = \frac{1}{2}\int \mathrm{d}u \left[\frac{1}{u-1} - \frac{1}{u+1}\right] \\ &= \frac{1}{2}\ln|\frac{u-1}{u+1}| = \frac{1}{2}\ln|\frac{\sqrt{1+\omega^2}-1}{\sqrt{1+\omega^2}+1}| \ , \end{aligned} \tag{3.273}$$

where a change of variable is performed for the second integral as

$$\begin{aligned} u &:= \sqrt{1+\omega^2} \quad \equiv \quad \omega^2 = u^2 - 1 \ , \\ \mathrm{d}u &= \frac{\omega \mathrm{d}\omega}{\sqrt{1+\omega^2}} \ . \end{aligned} \tag{3.274}$$

With these, one can integrate the RHS of Eq. (3.269) as

$$\begin{aligned}\int_{D_0/T_K}^{1}\frac{\mathrm{d}\omega}{\omega}\left(1-yJ_0^2\frac{D_0}{T_K}\frac{1}{\sqrt{1+\omega^2}}\right) &= \ln|\omega| - \frac{1}{2}yJ_0^2\frac{D_0}{T_K}\underbrace{\ln\left|\frac{1-\sqrt{1+\omega^2}}{1+\sqrt{1+\omega^2}}\right|}_{\approx 2}\Big|_{D_0/T_K}^{1}\\ &= \underbrace{\ln(1)}_{=0} - \ln(\frac{D_0}{T_K})\\ &\quad - \frac{1}{2}yJ_0^2\frac{D_0}{T_K}\left(\ln\left|\frac{1-\sqrt{2}}{1+\sqrt{2}}\right| - \ln\left|\frac{1-\sqrt{1+(D_0/T_K)^2}}{1+\sqrt{1+(D_0/T_K)^2}}\right|\right)\\ &\overset{D_0/T_K\gg 1}{=\!=} -\ln(\frac{D_0}{T_K}) - \frac{1}{2}yJ_0^2\frac{D_0}{T_K}\Big(-2-\underbrace{\ln\left|\frac{-D_0/T_K}{D_0/T_K}\right|}_{=\ln(1)=0}\Big)\\ &= -\ln(\frac{D_0}{T_K}) + yJ_0^2\frac{D_0}{T_K}\ .\end{aligned} \tag{3.275}$$

Therefore, Eq. (3.269) reduces to an equation for the RKKY-modified Kondo temperature, $T_K(y)$,

$$\begin{aligned}-\frac{1}{2J_0} &= -\ln(\frac{D_0}{T_K}) + yJ_0^2\frac{D_0}{T_K}\\ \Rightarrow \ln(\frac{T_K^0}{D_0}) &= -\ln(\frac{D_0}{T_K}) + yJ_0^2\frac{D_0}{T_K}\\ \Rightarrow \ln(\frac{T_K^0}{T_K}) &= +yJ_0^2\frac{D_0}{T_K}\\ \Rightarrow \ln(\frac{T_K}{T_K^0}) &= -yJ_0^2\frac{D_0}{T_K} = -yJ_0^2\frac{D_0}{T_K^0}\frac{T_K^0}{T_K}\\ \Rightarrow \frac{T_K(y)}{T_K(0)} &= \exp\left[-yJ_0^2\frac{D_0}{T_K(0)}\frac{T_K(0)}{T_K(y)}\right]\ .\end{aligned} \tag{3.276}$$

Defining a rescaled Kondo temperature,

$$\tau(y) := \frac{T_K(y)}{T_K(0)} \equiv \frac{T_K(y)}{T_K^0}\ , \tag{3.277}$$

and a bare parametre,

$$\gamma_0 := J_0^2\frac{D_0}{T_K(0)} = \frac{1}{4}\frac{1}{\left(\ln(D_0/T_K^0)\right)^2}\frac{D_0}{T_K^0} = J_0^2\ \exp[\frac{1}{2\mathcal{N}(\varepsilon_F)J_0}]\ , \tag{3.278}$$

leads to a notational simplification,

$$\tau(y) = \exp\left[-y\frac{\gamma_0}{\tau(y)}\right]\ . \tag{3.279}$$

Again, note that at $y = 0$ (vanishing RKKY-interaction), one recovers the single-impurity result,

$$\frac{T_K(y)}{T_K(0)} = 1 \Rightarrow T_K(y) = T_K(0) \equiv T_K^0 \ . \tag{3.280}$$

To obtain an analytical solution to the equation Eq. (3.279), one can define

$$\begin{aligned} x &:= \frac{\tau}{y\gamma_0} \ , \\ \mathsf{y} &:= y\gamma_0 \ , \end{aligned} \tag{3.281}$$

to re-write the equation simply as

$$\mathsf{y}x = e^{-\frac{1}{x}} \ . \tag{3.282}$$

The exact solution to this equation will be obtained below; however, even without the exact solution at hand, the behaviour of the solutions to this equation can be understood via a 'geometric scheme' as shown in Fig. 3.14.

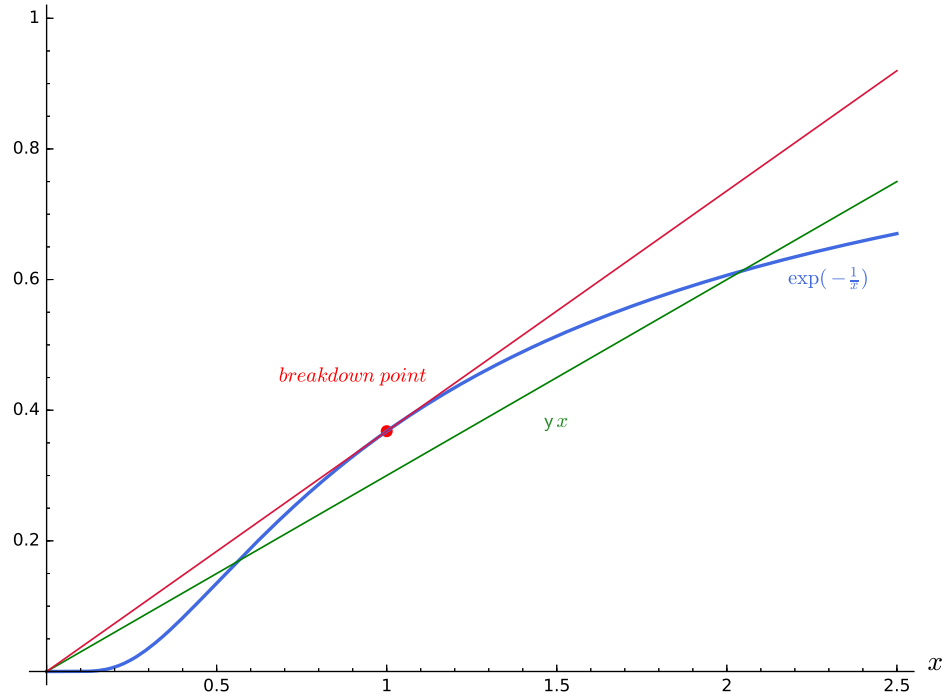

Figure 3.14: Solution(s) to the equation for the RKKY-modified Kondo temperature as the intersection of two curves: the line $\mathsf{y}x$ and the exponential curve $e^{-\frac{1}{x}}$. When two solutions exist, the higher temperature will be the physical solution. The Kondo breakdown happens when the line becomes a tangent to the exponential curve, allowing only one solution.

The solution to the equation is the points of the intersection of the two curves: the line, $\mathsf{y}x$, and the exponential curve, $e^{-\frac{1}{x}}$. For a certain range of y values, there are two solutions, but remarkably, by increasing y, we arrive at a point beyond which there is no solution. This point corresponds to the breakdown of Kondo screening, since beyond that there is no divergence of

the Kondo coupling which was the hallmark of the perturbative RG for the Kondo problem. This means that beyond this point, the fixed point is no longer a strong-coupling one, and only partial Kondo screening can exist[17]. Exactly at this point, there is only one solution and this can be obtained due to the fact that at the point, the value of the two curves as well as their derivatives coincide; that is,

$$\begin{cases} \mathsf{y}_{max}\, x_{max} &= e^{-\frac{1}{x_{max}}} \\ \mathsf{y}_{max} &= \frac{1}{x_{max}^2}\, e^{-\frac{1}{x_{max}}} \end{cases} , \tag{3.283}$$

Using the fact that $x_{max} \neq 0$ (since $\tau \neq 0$), one obtains

$$\begin{aligned} \frac{\mathsf{y}_{max}\, x_{max}^2}{\mathsf{y}_{max}\, x_{max}} &= \frac{e^{-\frac{1}{x_{max}}}}{e^{-\frac{1}{x_{max}}}} \equiv 1 \\ &\Rightarrow x_{max} = 1 \ . \end{aligned} \tag{3.284}$$

From this relation, one readily finds a relation for y_{max} in terms of the bare parameters of the system,

$$\begin{aligned} \mathsf{y}_{max} = \frac{1}{e} \Rightarrow y_{max} &= \frac{4}{e}\, \frac{T_K^0}{D_0} \left(\ln(\frac{T_K^0}{D_0}) \right)^2 \\ &= \frac{1}{e} \frac{\exp[-\frac{1}{2\mathcal{N}(\varepsilon_F)\, J_0}]}{(\mathcal{N}(\varepsilon_F)\, J_0)^2} \end{aligned} \tag{3.285}$$

where e is the Euler's number ≈ 2.7 (see Fig. 3.15). Notice that with the typical values of T_K^0/D_0, this breakdown happens *inside* the *perturbative* range of y values, $0 \leq y \ll 1$ where a perturbative RG is reliable.

y-dependence of the Kondo temperature near breakdown Near the breakdown point, one can find the y-dependence of the Kondo temperature. Suppose that

$$\begin{cases} x &= x_{max} + \delta x \\ \mathsf{y} &= \mathsf{y}_{max} + \delta \mathsf{y} \end{cases} , \tag{3.286}$$

[17] Notice that the existence of this breakdown point indicates that in a multi-impurity (or dense) system of Kondo ions (e.g., a Kondo lattice), complete Kondo screening ceases to exist above a maximum RKKY coupling strength, *regardless* of occurrence of magnetic ordering. Possibility of magnetic instability is discussed in chapter 5.

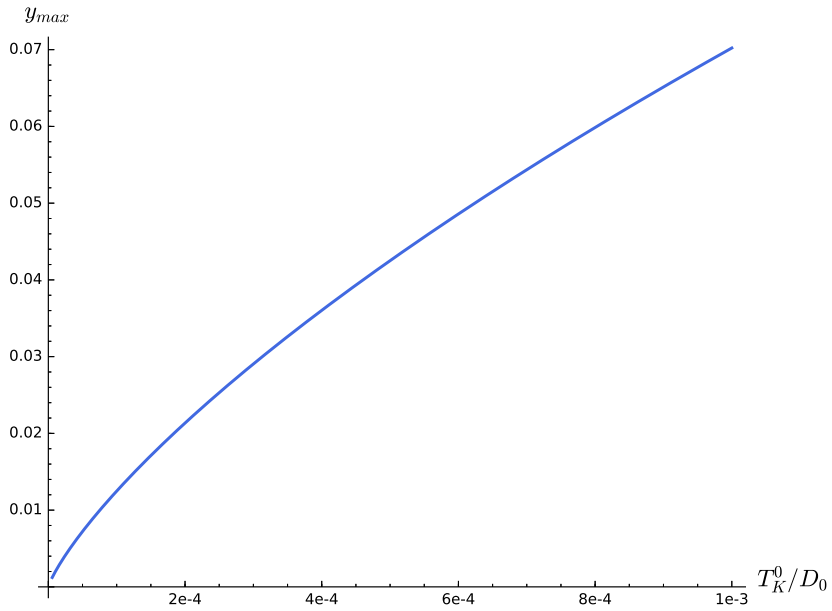

Figure 3.15: The maximal RKKY strength, y_{max}, as a function of the *bare* Kondo temperature.

with $|\delta x| \ll |x|$ and $|\delta \mathsf{y}| \ll |\mathsf{y}|$, so that

$$
\begin{aligned}
&(\mathsf{y}_{max} + \delta\mathsf{y})\ (x_{max} + \delta x) = \exp[-\frac{1}{x_{max} + \delta x}] \\
&\Rightarrow \mathsf{y}_{max}\ x_{max} + \mathsf{y}_{max}\ \delta x + x_{max}\ \delta\mathsf{y} + \delta x\ \delta\mathsf{y} \\
&\quad = \underbrace{e^{-\frac{1}{x_{max}}}}_{=\mathsf{y}_{max}\ x_{max}} + \delta x\ \underbrace{\frac{e^{-\frac{1}{x_{max}}}}{x_{max}^2}}_{=\mathsf{y}_{max}} + \frac{1}{2!}\delta x^2\ \frac{e^{-\frac{1}{x_{max}}}}{x_{max}^4}(1 - 2x_{max}) + \mathcal{O}(\delta x^3) \\
&\Rightarrow (x_{max} + \delta x)\ \delta\mathsf{y} = \frac{1}{2!}\delta x^2\ \frac{e^{-\frac{1}{x_{max}}}}{x_{max}^4}\ (1 - 2x_{max}) + \mathcal{O}(\delta x^3) \\
&\quad = \frac{1}{2!}\delta x^2\ \underbrace{\frac{e^{-\frac{1}{x_{max}}}}{x_{max}^2}}_{=\mathsf{y}_{max}}\ \frac{(1 - 2x_{max})}{x_{max}^2} + \mathcal{O}(\delta x^3)\ .
\end{aligned}
\tag{3.287}
$$

Thus,

$$
\begin{aligned}
x\delta\mathsf{y} &= \frac{1}{2!}\mathsf{y}_{max}\ \frac{1 - 2x_{max}}{x_{max}^2}\ \delta x^2 + \mathcal{O}(\delta x^3) \\
\rightarrow \delta x^2 &= \frac{2}{\mathsf{y}_{max}}\ \frac{x_{max}^2}{1 - 2x_{max}}\ x\ \delta\mathsf{y} = \frac{2}{\mathsf{y}_{max}}\ \frac{x_{max}^2}{1 - 2x_{max}}\ x_{max}\ \delta\mathsf{y} \\
\rightarrow \delta x^2 &= -2e\ \delta\mathsf{y} = 2e\ (\mathsf{y}_{max} - \mathsf{y}) \\
&= \frac{2e}{\mathsf{y}_{max}}\ (1 - \frac{\mathsf{y}}{\mathsf{y}_{max}})\ ,
\end{aligned}
\tag{3.288}
$$

where we have used the known values from Eq. (3.284) and Eq. (3.285),

$$x_{max} = 1 \quad , \quad \mathsf{y}_{max} = \frac{1}{e} \ . \tag{3.289}$$

Therefore, as $\mathsf{y} \to \mathsf{y}^{-}_{max}$,

$$\begin{aligned} \delta x = \ & \sqrt{2}\, e \, (1 - \frac{\mathsf{y}}{\mathsf{y}_{max}})^{\frac{1}{2}} \\ \Rightarrow \ & \frac{1}{y_m \, \gamma_0} \, \delta\tau = \sqrt{2}\, e \, (1 - \frac{y}{y_m})^{\frac{1}{2}} \\ \Rightarrow \ & \delta\tau = \sqrt{2} \, (1 - \frac{y}{y_m})^{\frac{1}{2}} \ . \end{aligned} \tag{3.290}$$

Using Eq. (3.281), one obtains

$$\begin{aligned} \frac{\mathsf{y}}{\mathsf{y}_{max}} &= \frac{y}{y_m} \ , \\ x = \frac{\tau}{y\gamma_0} &\Rightarrow \delta x = \frac{1}{y\gamma_0}\delta\tau \ , \end{aligned} \tag{3.291}$$

and finally,

$$\tau - \tau_m \propto (y - y_m)^{1/2} \ . \tag{3.292}$$

Exact analytical solution The exact analytical solution for the whole range of y can be also found in terms of the *Lambert W function*[18] which is the solution to the equation

$$z = W(z)\, e^{W(z)} \ . \tag{3.293}$$

In our case,

$$\begin{aligned} \mathsf{y}x = e^{-\frac{1}{x}} &\Rightarrow y = \frac{1}{x} e^{-\frac{1}{x}} \\ \Rightarrow -\mathsf{y} = \underbrace{-\frac{1}{x}}_{\equiv W} & e^{-\frac{1}{x}} \\ \Rightarrow -\frac{1}{x} &= W(-\mathsf{y}) \\ \Rightarrow x &= \frac{-1}{W(-\mathsf{y})} \ . \end{aligned} \tag{3.294}$$

Therefore, finally,

$$\tau(\mathsf{y}) = \frac{-\mathsf{y}}{W(-\mathsf{y})} \ . \tag{3.295}$$

The universal curve for the solution is depicted in Fig. 3.16 along with the (universal) breakdown point for the Kondo screening.

[18] Indeed, the first branch of the Lambert function, W_0, is the solution. More information can be found in Refs. [126, 127].

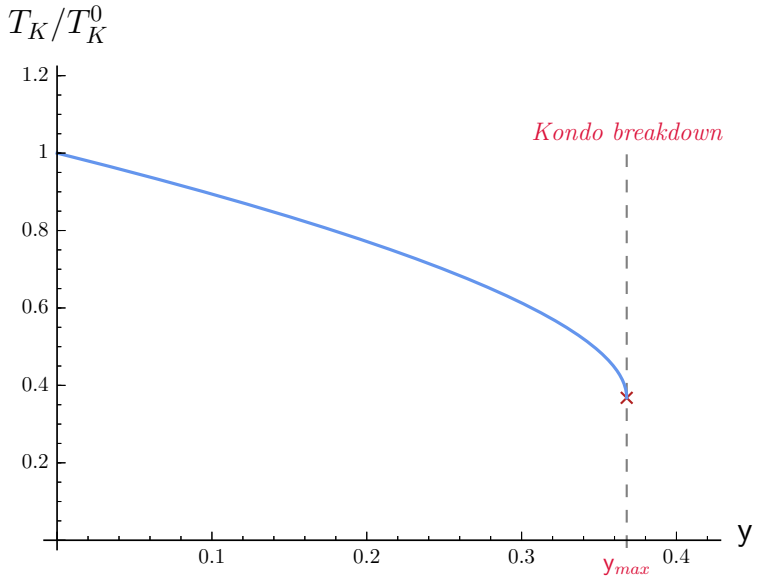

Figure 3.16: RKKY-corrected Kondo temperature as a function of the RKKY strength, y. Note that the breakdown of Kondo screening occurs at $T_K/T_K^0 = 1/e$ where e is the Euler's number.

3.5 'Symmetric' two-impurity setting with scanning tunneling spectroscopy

3.5.1 Scanning tunneling spectroscopy as a probe of Kondo effect

The scanning tunneling microscopy (STM) technique was introduced by Binnig and coworkers [128] in early 1980s, basically to measure the atomic-scale topography of surfaces with sub-Ångstrom resolution. This is performed by approaching the surface by a metallic tip (in proximity of $\sim \mathcal{O}(1\text{–}10)$ Å) and applying a bias voltage to the tip (with respect to the sample) (see Fig. 3.17)[19]. A tiny current ($\sim$ nA) would then flow through the tip via the quantum tunneling of electrons of the sample across the potential barrier due to to the gap between the tip and the sample (the "tunneling junction"). This implicates that if there is an overlap between the electronic wavefunctions of the tip and the surface states of the sample, then there will be a measurable tunneling current (see, e.g., Ref. [123] for a concise description). When scanning with the tip laterally across the surface area, the resulting current can be used to measure the "height" of the surface, or its atomic topography.

The same device can be used for scanning tunneling spectroscopy (STS) to measure the local density-of-states (LDOS) as a probe of the electronic structure of the sample. This can be performed by fixing the tip position and varying the bias voltage which yields a differential conductance (dI/dV) curve that is related to the LDOS and the spectral density [123, 130].

Besides the measuring techniques, it is possible to use the STM tip to manipulate single atoms or molecules on a surface [130].

The first theoretical description of the STM (neglecting strong correlations) was provided by the Tersoff-Hamann model [130–133].

[19] The bias voltage V_{bias} should be much smaller than the work function of the sample material.

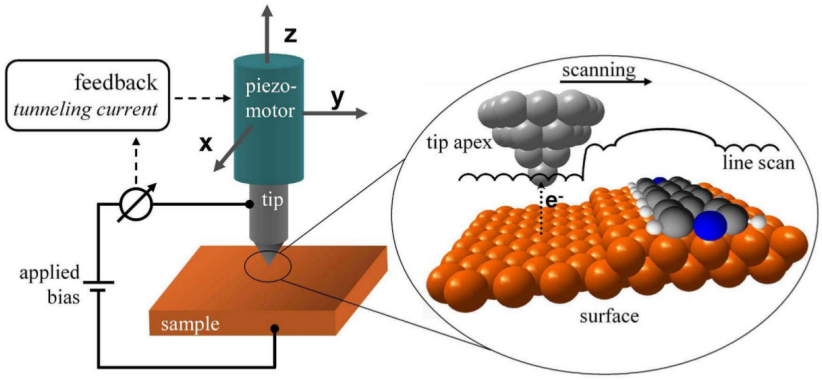

Figure 3.17: Schematic depiction of the constant-current operation of an STM (adopted from Ref. [129]).

3.5.1.1 Kondo effect in STS

Since STS can measure the LDOS and the spectral density of electrons, it provides another (very precise) way to observe the Kondo resonance (see, e.g., Refs. [67, 68, 134, 135]). In such an experiment, the tip is positioned over an impurity (a single atom, dimer, or larger molecules) on the surface of a non-magnetic substrate and the bias voltage is varied near the zero-bias limit ($V_{bias} = 0$). If the impurity possesses a localized d- or f- level which can hybridize with the delocalized states on the metallic substrate, then it will exhibit the Kondo effect at low enough temperature $\sim \mathcal{O}(1)$ K (see Fig. 3.18).[20]

The electrons of the tip can tunnel into the Fermi sea of the substrate embedding the impurity. It should be reminded that due the locality of the d- or f- levels of the impurity and their closeness to the atomic core, the direct tunneling of the electrons into these localized levels is negligible when they are sufficiently separated (the 'tunneling' regime) [136–138]. The tunneling process can be described qualitatively by a (non-interacting) Fano resonance and anti-resonance [139], where the Fano effect occurs due to the interference between two scattering channels (a resonant and a non-resonant channel). Depending on the phase shift between the two channels, the interference can be either constructive (Fano resonance), or destructive (Fano anti-resonance) [140, 141] (see Ref. [142] for an extensive discussion of the Fano effect). The Fano regime is characterized by strong coupling to the leads, therefore, the description of the zero-bias splitting in terms of a Fano anti-resonance is suitable for *high* inter-dot hopping. When the electrons are strongly localized in the dots (as in the Kondo regime) the explanation in terms of the RKKY interaction is more appropriate [143].

The Kondo resonance has been observed for Co atoms on different metallic surfaces [134] and for different atoms, such as, e.g., Ti, Co, and Ni on gold surface [144]. When Kondo resonance is detected, the Kondo scale can be extracted from the width of the the peak ($\sim 2T_K$).

[20] STM experiments rely on the fact that magnetic impurities (e.g., Co or Ce) which produce a Kondo effect in the bulk of a metallic host, will produce almost the same effect when placed on the surface of the host. The spectroscopy results show that the Kondo temperature is lower than that of the bulk. Furthermore, one assumes that due to the weakness of the coupling, the STM tip does not significantly perturb the local electronic properties of the host and that a dI/dV measurement provides information on the Kondo impurity in equilibrium with the Fermi sea of the host metal [70]. When the tip gets too close to the surface, in the "point-contact regime", besides mechanical instabilites, an direct coupling could be established between the impurity spin and the conduction electrons of the tip itself, which will change the physics of the system away from single-impurity Kondo physics in equilibrium.

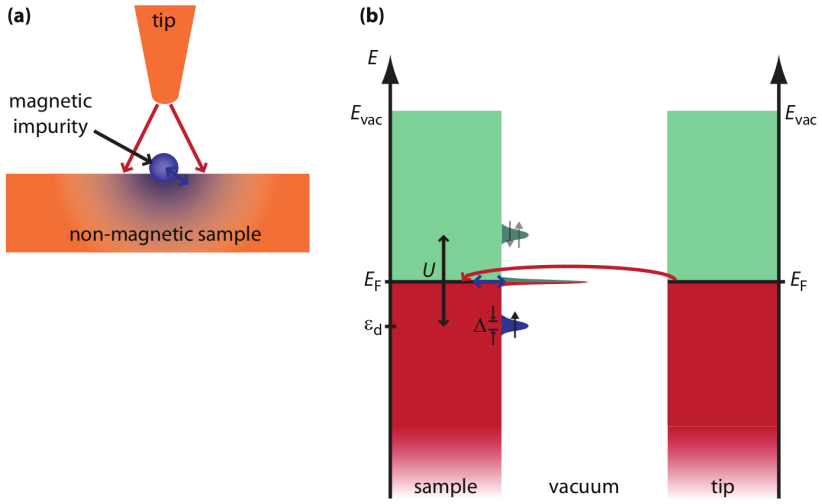

Figure 3.18: (a) A single magnetic impurity on a metallic surface. Electrons from the tip tunnel into the substrate surrounding the magnetic impurity where they scatter from the magnetic moment of the impurity (with spin flipping), creating a Kondo resonance as depicted in (b). (b) Schematic energy diagram of a d-state impurity Kondo system with Coulomb repulsion U and hybridization Δ (adopted from Ref. [129]).

3.5.1.2 Strongly-interacting theory of STS for a single impurity on a metallic surface

Schiller and Hershfield [145] have proposed a theoretical description of the STS of a single magnetic adatom on a metallic host. Their approach is based on the Anderson model and uses a self-consistent perturbation theory to obtain the Green's functions and density-of-states in the limit of infinite Coulomb repulsion for the impurity electrons. It predicts the Fano lineshape in the differential conductance at the position of the magnetic impurity. Újsághy *et al.* [136] have also showed that the Kondo effect is the origin of a narrow Fano lineshape by using a local spin density approximation (LSDA) and a non-crossing approximation (NCA) method. They obtain the dependence of the lineshape on the distance of the tip from the impurity by using bulk and surface state Green's functions. They obtain also a weakly energy-dependent Friedel oscillation superimposed on the Fano lineshape which is induced by potential scattering off the local level. Furthermore, Lin *et al.* [146] have developed a theory of Kondo resonance in an STM experiment using an Anderson model for the sample. They calculate the hybridization energies for the Anderson Hamiltonian of a magnetic impurity interacting with surface and bulk states and show that, for an impurity on the surface, the hybridization matrix elements are strongly momentum-dependent near the Fermi surface, and Kondo effect can occur with equal strength between bulk and surface states.

3.5.2 Scanning tunneling spectroscopy of a tunable two-impurity Kondo system

Bork *et al.* [129, 147] have realized a tunable two-impurity Kondo problem via a scanning tunneling microscopy of two Kondo atoms. In this experiment, a magnetic Cobalt (Co) atom is attached to the tip of a scanning tunneling microscope and another Co atom is placed on a

metallic gold surface, Au(111).[21] Together, these two magnetic atoms constitute a two-impurity Kondo system. The distance between the two magnetic moments can be varied (with picometer precision) by changing the tip-sample distance, and in this way, the strength of the RKKY interaction between the moments can be tuned continuously with high precision. This is of crucial importance for comparison with theoretical results.
A single Co atom is attached to the STM tip by positioning the tip on top of an adatom and applying a voltage pulse. A successful attachment of a Co atom is confirmed by obtaining the spectrum taken over a clean region of the sample, which shows a resonance similar to the one found for Co adatoms on the surface.[22] The STM tip is made of tungsten, but its apex is covered with gold. The latter facts suggest that the atom attached to the tip has an environment similar to that on the surface.
When the Co atom attached to the tip is positioned on top of the Co adatom on the surface, the tunneling spectrum exhibits a "superposition" of the Kondo resonances of tip and sample. In the tunneling regime, the spectra shows a resonance similar to the one found for a single cobalt atom in the junction.
The shape of spectra changes very little for relatively large tip-sample distances (distance > 2Å). Within the distance of 2Å, the width of the resonance is reduced which implies a reduction of the Kondo temperature. At a certain distance between the two Co atoms, the junction makes a transition from the tunneling to the "point-contact" regime in which a direct magnetic inter-moment interaction wins over the indirect RKKY interaction. At the transition point, mechanical relaxation effects of tip and sample become strong and reduce the quality of the experimental results. Near the transition to the point-contact regime, the resonance changes its shape from a dip to a peak of similar width, and closer to the sample, the peak splits into two resonances at almost symmetric positions with respect to zero bias. The reduction of the width of the Kondo resonance in the tunneling regime is a consequence of the exchange interaction between the two Kondo atoms, since for a single Co atom, no reduction is observed.

3.5.3 RKKY-modified RG applied to the two-impurity STS experiment

We can apply the method developed for multi-impurity Kondo systems to this situation. Since the two Kondo impurities are similar and they have approximately same environment, the RG flow equation obtained in Eq. (3.268) should be able to describe the results for the Kondo temperature.
It turns out that the agreement of the theoretical predictions with experimental results is very good. Interestingly, the predicted Kondo break-down happens inside the point-contact regime. In these experiments, the coupling of the two impurities to the electronic reservoir was approximately the same (a 'symmetric' coupling). In the next chapter, we extend the RG method to an 'asymmetric' case where the couplings of the impurities to the reservoir are not the same. We will see that such an asymmetry will have a drastic effect on the Kondo temperatures, which is utterly different from the symmetric case.

[21] The single-impurity Kondo temperature of a cobalt adatom on Au(111) has been determined to be approximately 75 K [147].
[22] They found Kondo temperatures ranging between 100 and 230 K for tip-attached atoms.

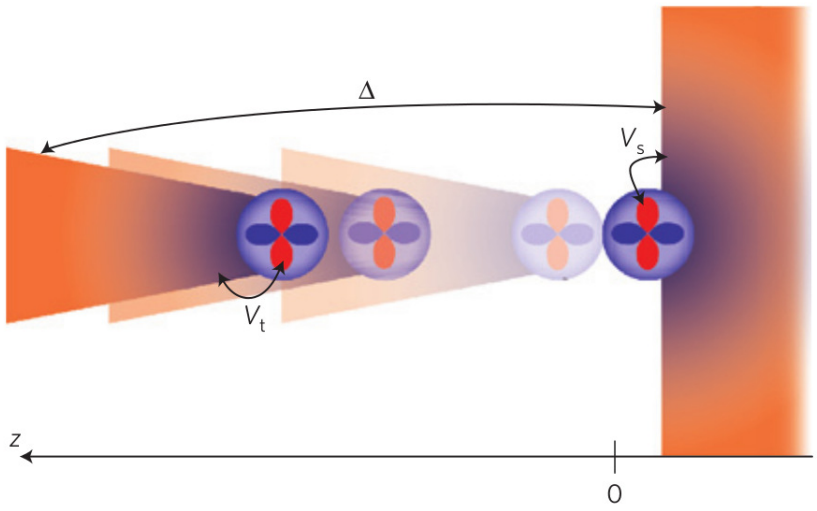

Figure 3.19: The measurement setup with one cobalt atom on the tip and one on the surface. The hybridizations, V_s and V_t, between the cobalt atoms and their respective electrodes leads to Kondo screening of the spins of the cobalt atoms. The coupling between tip and sample results in an antiferromagnetic interaction between the two spins. The strength of the interaction is varied by changing the tip–sample distance (adopted from Ref. [147]).

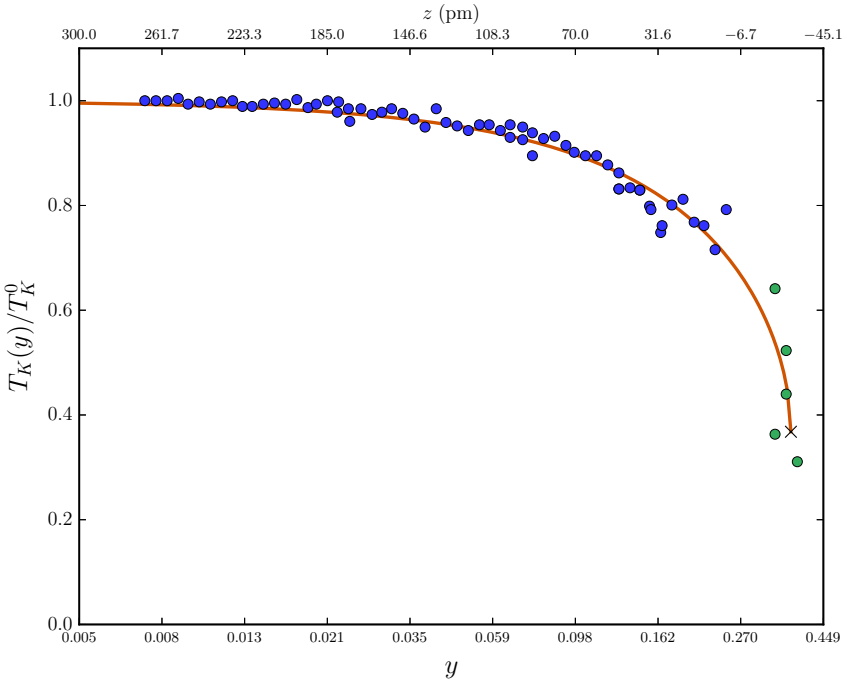

Figure 3.20: Comparison of the experimental results for the Kondo temperature from Ref. [147] with those from the RKKY-modified RG method. z denotes the tip–sample distance and y represents the strength of the RKKY interaction (calculated according to the *Supplementary information* to Ref. [147]). The blue circles are measured in the 'tunneling' regime and green circles near the transition to the 'point-contact' regime.

CHAPTER 4

Two Asymmetrically-coupled Kondo Impurities

As mentioned before, when the number of impurities increases merely to two, the Kondo problem becomes much more complicated and indeed, more interesting, since new phases arise in such a system which compete with the Kondo screening. This further complication is due to the presence of a carrier-mediated indirect exchange coupling, the RKKY interaction (see section 6.1 for more details), between the impurities, which originates from the *same* Kondo Hamiltonian. RKKY interaction strength is $I_{\mathrm{RKKY}} \sim \mathcal{N}(\varepsilon_F)J^2$ (with J being the Kondo coupling) and it has an oscillatory behaviour (with sign-change) as a function of position (with the wavelength $\sim 2k_F$) due to the presence of the Fermi surface. In its most general form, the RKKY interaction appears in a second-order perturbative expansion in terms of the Kondo coupling J and decays as $\cos(k_F R)/(k_F R)^3$ for a large impurity separation, R. This exchange interaction is 'carried' by the conduction electrons and prefers to 'freeze' the local moments in a certain direction (parallel or anti-parallel), and hence, competes with the Kondo effect which entails continuous flipping of the local moments by the conduction electrons. Therefore, the RKKY interaction and the Kondo effect 'struggle' against each other to determine the ground-state of the system to be either a 'molecular' spin-singlet (a 'dimer') made of the two impurity moments (due to RKKY), or a paramagnetic spin-singlet ground-state made of the spins of the conduction electrons and each impurity ('Kondo singlets').

Theoretical investigations of the two-impurity Kondo effect appeared much earlier than its experimental realizations. The earliest "thermodynamic scaling" (perturbative scaling) studies of the problem [148] found a two-stage Kondo effect for the ferromagnetic case, and a mutually exclusive competition between RKKY and Kondo effect for the antiferromagnetic case (see below). Later, the NRG solution to the problem [149–151] revealed three distinct low-temperature fixed points (or ground-states) for a two-impurity Kondo system described by the following Hamiltonian [8][1]:

$$H = \sum_{\mathbf{k}\sigma} \varepsilon_{\mathbf{k}\sigma}\, c^{\dagger}_{\mathbf{k}\sigma} c_{\mathbf{k}\sigma} + \underbrace{J_0 \left(\mathbf{s}(\mathbf{x}_1)\cdot\mathbf{S}(\mathbf{x}_1) + \mathbf{s}(\mathbf{x}_2)\cdot\mathbf{S}(\mathbf{x}_2)\right)}_{\text{Kondo interaction}} + \underbrace{I\,\mathbf{S}(\mathbf{x}_1)\cdot\mathbf{S}(\mathbf{x}_2)}_{\text{exchange interaction}} \,, \tag{4.1}$$

where $\mathbf{S}(\mathbf{x}_i)(\mathbf{s}(\mathbf{x}_i))$ denote the spin of the impurity (conduction electron) at position $\mathbf{x}_i$. Notice

[1] Note that mirror symmetry about the midpoint of the two impurities leads to conservation of parity for the conduction electrons. The two spin flavors of the conduction electrons (up and down) provide two scattering channels. Therefore, totally there exits four channels of conduction electrons (parity plus spin) [8].

that the RKKY interaction is *added* to the Hamiltonian as a *direct* interaction, although it should be, in principle, generated by the Kondo interaction itself. This addition is performed to simplify the NRG calculations, since it turns out to be very intricate to include the full energy-dependence of the indirect RKKY interaction in the actual numerical computations (see, e.g., Ref. [152]). It should be emphasized that this is a non-trivial issue since this direct coupling proportional to I is a relevant term in the renormalization-group (RG) sense, which alters the structure of the fixed points.
In any case, the three phases obtained from an NRG calculation for the Hamiltonian given in Eq. (4.1) are:

(i) When particle-hole symmetry is present, Kondo effect occurs for all values of the strength of the RKKY interaction from moderately antiferromagnetic ($I/T_K > -2.2$) to all ferromagnetic values of the RKKY interaction ($I > 0$). For larger values of the ferromagnetic RKKY, there is a two-stage Kondo effect happening separately in the even and odd channels (the larger coupling will have the higher Kondo temperature).[2] The ground-state will be a Kondo singlet.

(ii) For larger antiferromagnetic RKKY strengths, $I/T_K < -2.2$, the impurity moments form a 'molecular' singlet (a 'dimer'), and no Kondo effect occurs. The nature of the ground-state is not trivial (see, e.g., Ref. [153]) although it is a Fermi liquid.

(iii) At the critical value of $I/T_K \approx -2.2$, there is an unstable non-Fermi liquid (nFL) fixed point. This leads to a second-order quantum phase transition (see below). In the nFL phase, the linear coefficients of specific heat and magnetic susceptibility grow to very large numerical values (i.e., they diverge), while the staggered susceptibility remains finite with a possible discontinuity.

In the two-impurity Kondo model, Wilson ratio is no longer universal [81]; namely, it goes to the Kondo value of 2 and above for the ferromagnetic region of the RKKY interaction. For the antiferromagnetic region, the Wilson ratio is always less than 2 and approaches zero at the unstable nFL fixed point [8]. For a large antiferromagnetic coupling, the Wilson ratio goes to the free-electron value of 1.
The quintessential upshot of the NRG results is that universality of the single-impurity Kondo problem is lost; i.e., there is no single scaling parameter.
If particle-hole symmetry is absent (e.g., due to additional potential scattering), the divergences in susceptibility and specific heat coefficients are reduced to peaks, the unstable nFL fixed point and the quantum phase transition disappear, and all the ground-states are Fermi liquids [154].[3]
Another important observation is that for the larger part of the phase diagram, Kondo and RKKY effect (either ferromagnetic or antiferromagnetic) are present together and are *not* mutually exclusive. The non-Fermi liquid behaviour at the critical point is extremely difficult to access experimentally since it is necessary to maintain stringent conditions (e.g., equivalence of the two Kondo couplings) in the experimental device.

[2] For the ferromagnetic case, both local moments have to be screened by the two screening channels (even and odd combinations) of the conduction electrons. Since these two channels have generically different Kondo couplings and hence, different Kondo temperatures, then upon lowering temperature, these two impurities will be screened at two distinct temperatures.

[3] One should not readily conclude that the particle-hole symmetry plays the role of the critical parameter, since it turns out that additional *parity-conserving* potential scattering terms which break particle-hole symmetry, still yield a line of nFL fixed points [8].

Two-impurity Anderson model Since the two-impurity Kondo model can be obtained from the two-impurity Anderson model via the Schrieffer-Wolff transformation (see section 4.6 for more details), the latter model is also a very important model for strongly-correlated systems, especially, quantum impurity models.
The first NRG study of the particle-hole symmetric/asymmetric two-impurity Anderson model [155, 156] found that the above picture of two local moments Kondo-coupled to conduction electrons persists in a large part of the phase space (at low temperatures and when Coulomb interaction is greater than the hybridization strength). When the Coulomb interaction does not overcome the hybridization, the impurity remains essentially free at high temperatures, and when the temperature drops below the strength of the Coulomb interaction, the Hamiltonian flows towards strong-coupling regime at low temperatures and develops a moment [8].

4.1 Experimental realizations of the two-impurity Anderson/Kondo model

Realization of the two-impurity Anderson or Kondo model has become possible due to the advancements in precise manufacture and control of nano-structures like semiconductor quantum dots [81, 157, 158], graphene sheets [159] and molecular nano-devices [77].

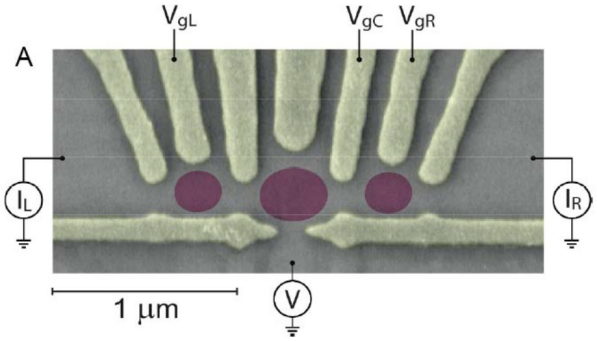

Figure 4.1: Scanning electron micrograph of the RKKY-coupled parallel double quantum dot device used by Craig *et al.* [157] to study the two-impurity Kondo model. The RKKY interaction between the left and right dots is mediated through the third large dot in the middle.

The first realization of a two-impurity system was performed by Chen *et al.* [160] via a scanning tunneling spectroscopy of a pair of magnetic cobalt (Co) atoms on a non-magnetic metallic gold (Au) surface. They observed an abrupt disappearance of the Kondo resonance when the distance between the adatoms goes below a certain limit (≤ 6 Å). Jeong *et al.* [161] produced a two-impurity system with two GaAs/AlGaAs quantum dots coupled in series. They observed an absence of Kondo effect (where it was expected), but it was not possible to modify (or 'tune') the strength of the inter-dot exchange interaction to observe the transition, apparently due to the *direct* coupling of the quantum dots. Later, Craig *et al.* [157] produced a more tunable device with two semiconductor quantum dots coupled through a relatively larger electron reservoir in the middle (Fig. 4.1). With this configuration, it was possible to control the number of electrons in each dot and the inter-dot coupling. In the absence of inter-dot coupling, both dots could be tuned to a Kondo valley, showing a Kondo resonance in the differential conductance (dI/dV) measurements. When one of the dots in a Kondo valley was coupled to another dot with an *even*

number of electrons (with no Kondo resonance), there was no change in the Kondo resonance of the first dot. But, if both dots were in a Kondo valley, introduction of an inter-dot coupling via the middle reservoir, led to suppression of the Kondo resonance in one of the dots (for a comprehensive review, consult Ref. [81]).
In the next section, we discuss the basic physics of quantum dot systems.

4.2 Semiconductor quantum dots as tunable Kondo impurities

Semiconductor quantum dots (QDs) are made by confining a 2-dimensional gas of electrons (2DEG) in a restricted region of nanometer dimensions, by controllable electrostatic gates. The dimensions of the confinement region is of the order of the Fermi wavelength. The typical dimensions of QDs are in the range of nanometers to a few microns [162, 163], so that the system behaves as a zero-dimensional quantum well with a discrete energy spectrum. The 2DEG resides at the interface of a semiconductor heterostructure (e.g., GaAs/AlGaAs), located tens to hundreds of nanometers below the surface [11]. Such a confinement is performed by a local depletion of the 2DEG, via etching techniques or metal gate electrodes. The final structure is weakly coupled to source and drain electrical contacts by tunneling barriers [164].
Due to the latter properties, these structures can be likened to atoms (hence, they are sometimes called 'artificial atoms' [162, 163, 165], but with a greater possibility of detailed control and manipulation (via contact leads and electrostatic gates) compared to the natural atoms.
A current or voltage can be applied to the dots via metallic leads which act as electron reservoirs (relatively-extended sections of 2DEG). The discrete energy levels and the number of electrons on the QDs can be tuned by applying a voltage via 'plunger' gates.
Furthermore, in case of multiple dots, inter-dot couplings can also be varied by changing the distances, or electro-static gates which control the tunneling between the dots. Both equilibrium and nonequilibrium situations can be realized and investigated. Such nano-structures can be built from GaAs/AlGaAs heterostructures [72–74], carbon nano-tubes [166], and organo-metallic molecules [167, 168].[4]
The most flexible and controllable devices are semiconductor heterostuctures; therefore such devices play a significant role in physics of strongly-correlated electrons.[5]

4.2.1 Quantum phase transition in quantum dot settings

Quantum dot (QD) systems provide a suitable controllable setting for realization of quantum phase transitions (QPTs). A quantum phase transition is a change of the phase of the system solely due to *quantum* fluctuations, in contrast to thermal fluctuations which produce classical phase transitions (see section 5.1). The transition is between competing ground-states with starkly different characteristics. In QD devices, the transition is driven by external control parameters like external fields (e.g., magnetic field or bias voltage) or changing voltages of the electrostatic gates which tune the coupling strengths [169]. QPTs happen, in principle, at (the

[4] As an estimate, the maximal Kondo temperature is in the range of 0.1–1 K for typical semiconductor QDs and up to 10 K in carbon nano-tube-based devices. To compare, notice that Kondo scales higher than 500 K has been observed for atomic impurities in bulk metals [11].

[5] In summary, the advantages of nano-structures over bulk systems are [11]: 1. Single-site measurements, rather than a statistical average over many sites; 2. Well-defined and tailored microscopic states of the system compared to bulk systems; 3. Precise control over and measurement of the important parameters of the system; 4. Possibility of investigations out of equilibrium and in regimes that are inaccessible in other contexts.

experimentally inaccessible) zero temperature; however the existence of a quantum critical point has a significant effect on the physical properties of the system in a broad range near QCP. This has encouraged a tremendous activity for theoretical and experimental investigations of QPTs. Due to a comparatively high degree of tunability of the QD systems, they provide a fertile ground to tailor and investigate QPTs of various kinds, and the corresponding exotic phases at the critical point.

4.2.2 Transport in quantum dots

The starting point to model a QD system is the electrostatic circuit models where the QDs and leads are considered as a electrical circuit of capacitors and resistors under the potential of the gates [170, 171].

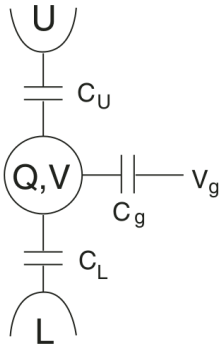

Figure 4.2: A circuit model of a single quantum dot, Q, coupled to two leads (U and L); the circuit includes only capacitors and voltages (adopted from Ref. [81]).

A more accurate description is obtained by the considering the energy spectrum and the cost of the Coulomb interaction in the dots via the 'constant interaction' model [123]. These considerations provide the basic transport properties of the QD systems: charge quantization on the dot. When the coupling to the leads are small enough compared to the Coulomb interaction scale, the number of electrons on a dot will be an integer[6]. The tunneling between the dots, or between a dot and the leads can merely changes this integer, corresponding to a transfer of a single electron.
Accumulation of charge in a QD leads to an increase in the intra-dot Coulomb interaction, or the 'charging energy'. At a temperature below the charging energy, the effects of the Coulomb interaction become significant and can be observed in transport properties, even, in linear response regime where the applied voltage (as the external field) is smaller than the thermal energy scale, $\mu_S - \mu_D \ll T$, meaning that the bias is relatively weak, $\mu_S \approx \mu_D$ [172].

4.2.2.1 Coulomb blockade

Existence of relatively large energy cost for adding a charge to the quantum dot (the charging energy) leads to significant effects in the transport properties. In the simplest consideration, one can model the quantum dot as a capacitor ('constant interaction' model), where the energy

[6] QDs typically contain zero to several thousands electrons [164].

stored in the capacitor due the presence of N electrons is given by [123]

$$E(N) = E_C\, N^2 - e\, V_g\, N \ ,$$

where E_C is the 'charging energy' of a capacitor C by a single electron, $E_C = e^2/2C$, and V_g is the gate voltage[7]. The energy minimum will occur for an optimal number of electrons, $N_{opt} = e\, V_g/2E_C$; in fact, this value is not guaranteed to be an integer. However, if N_{opt} is an integer, then adding/removing a single electron ($N \mapsto N \pm 1$) will incur an energy cost of E_C and at low energies, the transport is blocked. This is called a 'Coulomb blockade'. If N_{opt} is a half-integer, then $N_{opt} + \frac{1}{2}$ and $N_{opt} - \frac{1}{2}$ will be an integer, and the states corresponding to these two occupation numbers will have the same energy, $\frac{1}{4}E_C$; that is, adding an electron does not incur an energy cost; hence, single-electron transport becomes possible near these charge degeneracy points. Therefore, a periodic behaviour will be observed if the gate voltage sweeps a large range of potentials, and this leads to the a diamond-like pattern in the differential conductance trace ('Coulomb diamonds') [123, 164, 173, 174].
However, so far, we have considered the QD system quasi-classically; namely, the constant interaction model does not include the full quantum nature of the Coulomb interaction. The Coulomb blockade is only a first-order result of sequential tunnelings of electrons between the dots and leads. Higher-order processes involving "cotunneling" (or 'simultaneous' tunneling) of more electrons, can affect the transport properties significantly at low temperatures. Such cotunneling processes can be elastic (conserving the kinetic energy and possible at zero bias) or inelastic (energy non-conserving and happening at non-zero bias). The Kondo effect in QDs is an example of elastic cotunneling.

4.2.2.2 Kondo effect in quantum dots

If the number of electrons on the QD is an odd integer, the total spin of the dot will be a half-integer, the smallest value being $S = 1/2$. In late 1980s, it was theoretically predicted that the Kondo effect should be observable in a system made of a single QD (with odd occupation and a net spin) coupled to two metallic leads [175, 176]. A decade later, the Kondo effect was observed in single-QD systems [72–74, 177].
In should be noted that directly varying the Kondo energy scale is a challenging experimentall task. However, the large number of tunable parameters available in the case of a quantum dot system makes that possible in such a system. Since the Kondo conductance depends exponentially on the tunnel coupling to the leads, one way to tune the Kondo temperature is by changing the position of the dot level with respect to the Fermi level in the leads using a plunger gate.
In a QD setting, the Kondo interaction opens a new channel for electron transfer and therefore, a higher conductance, ultimately eliminating the Coulomb blockade. This is in contrast to the Kondo effect in the real metals in which the formation of the Kondo screening cloud leads to a resonant scattering of (otherwise, freely moving) electrons from the impurity and hence, a higher resistance. This is due to the fact that transport in QD systems is dominated by tunneling through the QD states, and an increase in scattering (through hopping) leads to an increase in conductance, since a new mechanism for transport is available. Therefore, in the Kondo regime, the conductance is enhanced in a 'Coulomb valley' (with an odd number of dot electrons) where

[7] In a real experiment, V_g is a combination of the source, drain and the plunger gate voltages including their mutual capacitances.

conductance was suppressed due to the Coulomb blockade, while in the valleys with an even number of electrons the conductance decreases since the thermal energy required to overcome the potential barrier due to the charging energy is not available. When the temperature is below the Kondo scale, $T \ll T_K$, the conductance can reach its maximum value, or the 'unitary limit', of $G_{max} = 2e^2/\hbar$ for a spin-degenerate channel [171, 178]. This leads to a a perfect transmission through the dot. This enhancement is due to the fact that in the QDs, the Kondo screening of the local moment occurs through electron exchange with the leads; therefore, as the screening emerges, the transport through the dot is enhanced.

The differential conductance of the QD as a function of source-drain bias voltage, $G(V_{sd})$ is a measure of its density-of-states, and therefore the emergence of a Kondo resonance in the density-of-states at the Fermi level, will cause a sharp zero-bias peak in conductance. Therefore, the Kondo resonance manifests itself at the zero-bias (when the voltage difference applied to the leads is very small) as a sharp peak, called the 'zero-bias anomaly' (ZBA) in the conductance. This peak is suppressed by increasing the bias voltage. At a finite bias, the resonance splits into two peaks placed at the Fermi levels of the leads [179]. The Kondo scale can be determined experimentally from the width of the resonance [22]:

$$T_K \approx \frac{\pi\, w}{4k_B}\, \Delta \ , \tag{4.2}$$

where $w \approx 0.4128$ is the Wilson number, and Δ is the half-width at half maximum (HWHM) of the Kondo zero-bias anomaly [22].[8]

Because of decoherence effects due to the application of source-drain voltage, the width of the ZBA does not yield a very accurate measure of the Kondo scale. Another approach is concerned with the temperature dependence of the zero bias conductance, since another characteristic of the Kondo state is its high sensitivity to temperature variations, because the conductance shows a logarithmic decrease as the temperature is increased.

In the Kondo effect in quantum dots, by lowering the temperature, a $\ln(T)$ increase in conductance is observed which is saturated to $g_0 - cT^2$ below the Kondo scale. Numerical results for the whole ranges of temperature has been provide by Costi *et al.* [30] via an NRG approach from which a fitting formula was obtained to compare with experimental results [73, 180],

$$g(T) = g_0 \left(\frac{T_K'^2}{T^2 + T_K'^2} \right)^s \ , \tag{4.3}$$

where $T_K' := \frac{T_K}{\sqrt{2^{1/s}-1}}$.

Applying an external magnetic field will remove the initial degeneracy of the spin states, and hence, tend to suppress the Kondo effect. At field strengths below the Kondo scale, $B < T_K$, the Kondo peak begins to split into two peaks separated by the Zeeman energy, positioned at $\pm g\mu_B B$ where g is the gyromagnetic ratio, μ_B is the Bohr magneton, and B is the applied field [72, 74, 171, 174]. The peak-to-peak distance is thus related to the Zeeman energy as $E_Z = e\,\Delta V_{sd} = 2\mu_B\, g^*\, B$ where g is the effective electron Landé factor [181].

At a finite magnetic field, the Kondo effect can be recovered by application of a bias voltage of

[8] Note that this does not provide a very accurate measure of the Kondo scale. Instead, temperature dependence of the zero-bias conductance is often the preferred manner [180].

the scale of the Zeeman energy [11].[9]

4.3 Highly tunable seminconductor double quantum dot device

To observe and manipulate the Kondo and RKKY effects, Haug's group in the University of Hannover have produced a highly tunable double-quantum-dot device [181, 186]. The setup is made of two QDs (labeled QD1 and QD2) located at a distance of *ca.* 600 Å apart, so that *direct* inter-dot tunneling be absent. The dots are connected to the source (S) via a large reservoir and to separate drains. Six in-plane gates, G1 – G6, coupled capacitively to the QDs act as plunger gates to control the energy spectrum and occupation of the dots, and to vary the coupling of the dots to the leads. The middle reservoir between the dots is decoupled from the source via a 1D constriction between this region and the source (Fig. 4.3).[10] Although in this setting, the two QDs are *not* coupled directly, their coupling to the middle reservoir provides an *indirect* way of inter-dot interaction. This is essentially the RKKY interaction mediated by the conduction electrons of the middle reservoir (see the schematic depiction in Fig. 4.4).

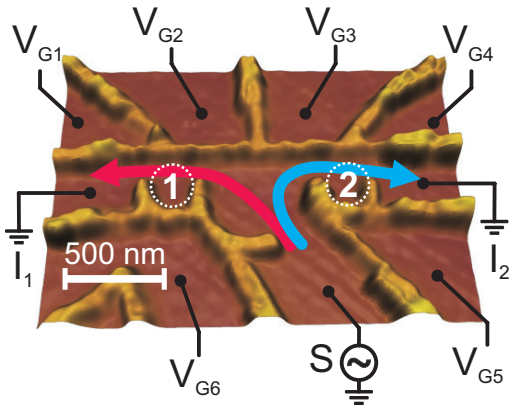

Figure 4.3: AFM image of the double quantum dot device used in Ref. [186]. Quantum dots, 1 and 2 (separated by *ca.* 600 Å), are connected to a common source S, and each to individual drains, I_1 and I_2. Six in-plane gates, G1 to G6, control the potentials of the dots and their coupling to the leads. The arrows mark the measured transport paths.

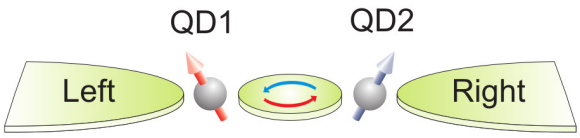

Figure 4.4: Schematic depiction of a double quantum dot system as two Kondo impurities (adopted from Ref. [181]).

[9] A microwave radiation can also decohere the Kondo effect due to the photon-induced inelastic scatterings [182, 183]. Yet, the effect of photons is non-trivial in presence of other external fields (e.g., a magnetic field), since it leads to a photon-assisted tunneling [184, 185].

[10] In this setup, the gates G1 and G4 are maintained at a fixed voltage. The voltages of the gates G2 and G3 are varied to control the couplings of the dots to the middle reservoir, and the voltages of G5 and G6 are used as plunger gates controlling the dot occupations.

The electrostatic gates provide the possibility of tuning of the coupling of the dots to the leads and the middle reservoir and thus, indirectly, the Kondo couplings which depend on the Coulomb interaction and hybridization strengths. However, the actual experimental tuning of the system parameters is a challenging task since, due to the proximity of the gates and leads, changing the potential on one of the them will alter the others inevitably.
The two QDs can be separately tuned (via the gates G1 – G6) into the Kondo regime, and the individual Kondo scale of a dot can be measured by tuning the dot to exhibit a Kondo resonance while keeping the other dot inside a non-Kondo valley (with an even number of dot electrons).[11] The Kondo temperatures are measured from the width of the zero-bias peak in the differential conductance, and the strength of the RKKY interaction from the Zeeman splitting of the shoulders in the differential conductance for the quantum dot for which the Kondo resonance is suppressed (see below).

4.3.1 Symmetric Kondo couplings

When the couplings of the dots to the middle reservoir is approximately equal, *both* dots can be simultaneously tuned into their Kondo regime (Fig. 4.5). The Kondo scales can be extracted from the widths of the resonances and are roughly the same for the two dots. The main effect of the RKKY interaction in this case is a reduction of the Kondo temperatures for *both* dots.

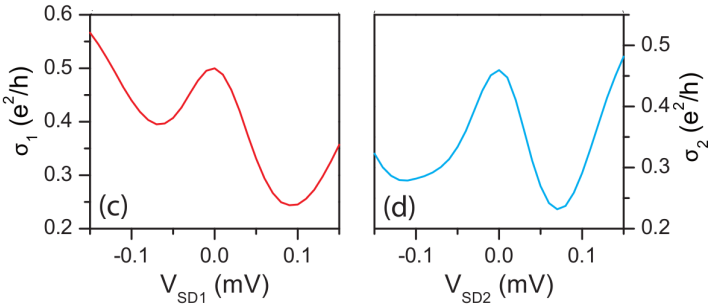

Figure 4.5: Measured differential conductance for the two quantum dots in the case of *symmetric* couplings (only slight asymmetry), showing the zero-bias anomaly in *both* dots (adopted from Ref. [181]).

4.3.2 Asymmetric Kondo couplings

When couplings of the dots to the middle reservoir differ significantly, the observations change substantially. In this case, when both dots are tuned into the middle of their respective (individual) Kondo valleys, one observes in one of the dots (say QD1), a slight *suppression* of the Kondo resonance compared to the case where inter-dot coupling is absent. The other dot (QD2) exhibits a more drastic change where the Kondo resonance is *completely absent* (Fig. 4.6). This is interpreted as a consequence of the competition between the Kondo effect and the RKKY interaction between the QDs.

[11] Inelastic cotunneling currents are also present in this setup, but in comparison with elastic cotunneling via a Kondo state, inelastic cotunneling currents are much smaller due to the relaxation time of the excited electron [181].

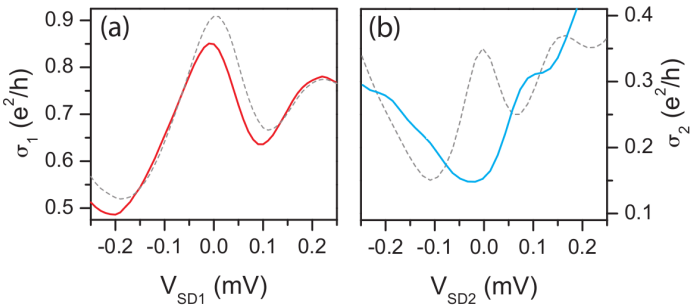

Figure 4.6: Measured differential conductance for the two quantum dots in the case of *asymmetric* couplings, showing the slightly-suppressed Kondo resonance in QD1, and absence of the Kondo resonance in QD2 (adopted from Ref. [181]). Dashed lines mark the situation in the absence of the RKKY interaction.

4.4 Anderson model for the double quantum dot system

As explained before, Anderson model can describe the full quantum behaviour of the QD systems. In this model, usually, one assumes a single (spin-degenerate) level for the quantum dot(s) with an energy well below the chemical potentials of the leads. The metallic leads are represented by free conduction electrons which can tunnel through the dot(s) via hybridization terms.
Therefore, the double quantum dot device discussed in section 4.3, can be modelled by an Anderson Hamiltonian with two dots and three leads (see the schema in Fig. 4.7):

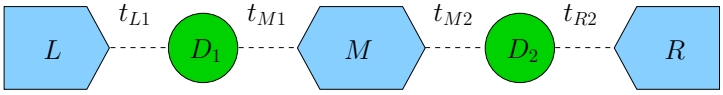

Figure 4.7: Schematic depiction of the Anderson model with 2 dots (D_1, D_2) and 3 leads (L, M, R). A dashed line denotes a dot–lead hybridization with the strength t, given above.

$$
\begin{aligned}
H_{2QD} &= H_{\text{dots}} + H_{\text{leads}} + H_{\text{dot-lead}} \ ; \\
H_{\text{dots}} &= \sum_{i=1,2} \sum_{\sigma=\uparrow,\downarrow} \varepsilon_{di}\, d^{\dagger}_{i\sigma} d_{i\sigma} + U_i \hat{n}_{i\uparrow} \hat{n}_{i\downarrow} \ , \\
H_{\text{leads}} &= \sum_{\alpha=L,M,R} \sum_{\nu_\alpha \sigma} \varepsilon_{\nu_\alpha \sigma}\, c^{\dagger}_{\nu_\alpha \sigma} c_{\nu_\alpha \sigma} \ , \\
H_{\text{dot-lead}} &= \sum_{\nu_L \sigma} t_{\nu_L 1}\, c^{\dagger}_{\nu\sigma} d_{1\sigma} + \sum_{\nu_M \sigma} t_{\nu_M 1}\, c^{\dagger}_{\nu_M \sigma} d_{1\sigma} \\
&\quad + \sum_{\nu_M \sigma} t_{\nu_M 2}\, c^{\dagger}_{\nu_M \sigma} d_{2\sigma} + \sum_{\nu_R \sigma} t_{\nu_R 2}\, c^{\dagger}_{\nu_R \sigma} d_{2\sigma} + h.c. \ ,
\end{aligned}
\tag{4.4}
$$

where ε_{di} represents the local level for each dot, U denotes the on-site Coulomb repulsion, $\varepsilon_{\nu_\alpha \sigma}$ are the energy levels of the metallic leads, and $t_{\nu_\alpha \sigma}$ are the hybridization strengths. This is a highly non-trivial Anderson model due to the presence of two dots and their coupling to three leads. However, at low temperatures, it can be mapped to a simpler Anderson model and ultimately, treated by the RKKY-modified RG method as demonstrated in the following

sections.

4.5 Glazman-Raikh transformations

The presence of two (or more) leads in a QD setting might lead to the conclusion that there are two separate channels of conduction electrons interacting with the impurity, which would result in an over-screened moment and non-Fermi liquid behaviour [59]. However, as shown by Glazman and Raikh [175] for a single quantum dot (or impurity), the lead degrees-of-freedom can be 'rotated' by an $SU(2)$ canonical transformation which produces a superposition of the electronic states of the two leads, leaving a single effective reservoir connected to the dot (which produces a Kondo effect), and another decoupled from the rest of the system. So, the effective number of conduction electron channels is one, and the ground-state of the system will be a Fermi liquid. Therefore, simply coupling additional leads to the quantum dot merely modifies the Kondo effect, since the leads behave as a single effective reservoir as long as the dots can freely exchange electrons between each pair of reservoirs.
For the current case of two quantum dots and three leads, it can be demonstrated that it is *not* possible to reduce the number of leads to a single one via a general $SU(3)$ Glazman-Raikh transformation (details of the proof is given in Appendix E).
We will apply a slight generalization of Glazman-Raikh transformation for two dots to the current system. For the current system of double quantum dots with 3 leads, the tunneling part of the Hamiltonian which mixes quantum-dot and lead levels can be written concisely as

$$\begin{aligned} H_T &=: H_{T_1} + H_{T_2} \ , \\ H_{T_1} &:= (t_L^* c_L^\dagger + t_{M1}^* c_M^\dagger) d_1 + d_1^\dagger (t_L c_L + t_{M1} c_M) \ , \\ H_{T_2} &:= (t_R^* c_R^\dagger + t_{M2}^* c_M^\dagger) d_2 + d_2^\dagger (t_R c_R + t_{M2} c_M) \ ; \end{aligned} \tag{4.5}$$

therefore, the structure of the dot-lead sector of the Hamiltonian can be represented by a matrix as

$$\begin{array}{c} \\ D_1 \\ L \\ M \\ R \\ D_2 \end{array} \begin{array}{c} \begin{array}{ccccc} D_1 & L & M & R & D_2 \end{array} \\ \begin{pmatrix} \varepsilon_{d_1} & t_{L1}^* & t_{M1}^* & 0 & 0 \\ t_{L1} & \varepsilon_L & 0 & 0 & 0 \\ t_{M1} & 0 & \varepsilon_M & 0 & t_{M2} \\ 0 & 0 & 0 & \varepsilon_R & t_{R2} \\ 0 & 0 & t_{M2}^* & t_{R2}^* & \varepsilon_{d_2} \end{pmatrix} \end{array} . \tag{4.6}$$

First Glazman-Raikh transformation The first transformation introduces two new channels[12], $\hat{\psi}_1$ and $\hat{\psi}_2$, which are mixtures (quantum superpositions) of the left and the middle conduction channels, c_L and c_M; that is,

$$\begin{pmatrix} c_L \\ c_M \end{pmatrix} = U \begin{pmatrix} \hat{\psi}_1 \\ \hat{\psi}_2 \end{pmatrix} \ , \tag{4.7}$$

[12] We will denote the operators corresponding to the new channels by a hat to prevent confusion with the angular variables of the transformations.

where U is a general $SU(2)$ transformation which preserves the canonical anti-commutation relations and is parameterized in terms of real angles φ and θ as

$$U := \begin{pmatrix} u_{11} & u_{12} \\ u_{21} & u_{22} \end{pmatrix} \doteq \begin{pmatrix} \cos\theta & e^{i\varphi}\sin\theta \\ -e^{-\mathrm{i}\varphi}\sin\theta & \cos\theta \end{pmatrix} \in SU(2) \ . \tag{4.8}$$

Upon this transformation, c_L and c_M channels transform to linear combinations of $\hat{\psi}_1$ and $\hat{\psi}_2$,

$$\begin{cases} c_L &= \cos\theta\hat{\psi}_1 + e^{\mathrm{i}\varphi}\sin\theta\hat{\psi}_2 \\ c_M &= -e^{-\mathrm{i}\varphi}\sin\theta\hat{\psi}_1 + \cos\theta\hat{\psi}_2 \end{cases} , \tag{4.9}$$

and thereupon,

$$\begin{aligned} H_{T_1} &= d_1^\dagger \left[t_L \underbrace{(\cos\theta\hat{\psi}_1 + e^{\mathrm{i}\varphi}\sin\theta\hat{\psi}_2)}_{c_L} + t_{M1} \underbrace{(-e^{-\mathrm{i}\varphi}\sin\theta\hat{\psi}_1 + \cos\theta\hat{\psi}_2)}_{c_M} \right] \\ &= d_1^\dagger \left[\underbrace{\left(t_L\cos\theta - t_{M1}e^{-\mathrm{i}\varphi}\sin\theta\right)}_{\stackrel{!}{=}0} \hat{\psi}_1 + \left(t_L e^{\mathrm{i}\varphi}\sin\theta + t_{M1}\cos\theta\right)\hat{\psi}_2 \right] \ . \end{aligned} \tag{4.10}$$

In order to decouple a channel, say $\hat{\psi}_1$, one has to impose the condition

$$\begin{aligned} t_L\cos\theta - t_{M1}e^{-\mathrm{i}\varphi}\sin\theta \stackrel{!}{=} 0 \stackrel{\div t_L \neq 0}{\Longrightarrow} \cos\theta - \underbrace{\frac{t_{M1}}{t_L}}_{=:t_1} e^{-\mathrm{i}\varphi}\sin\theta = 0 \\ \Rightarrow \cos\theta = t_1 e^{-\mathrm{i}\varphi}\sin\theta \ , \end{aligned} \tag{4.11}$$

from which one can also re-write the coefficient of $\hat{\psi}_2$ in Eq. (4.10) as

$$\begin{aligned} t_L e^{\mathrm{i}\varphi}\sin\theta + t_{M1}\cos\theta &= t_L e^{\mathrm{i}\varphi}\sin\theta + t_{M1}t_1 e^{-\mathrm{i}\varphi}\sin\theta \\ &= t_L \sin\theta e^{\mathrm{i}\varphi}(1 + (t_1 e^{-\mathrm{i}\varphi})^2) \ . \end{aligned} \tag{4.12}$$

Upon the $SU(2)$ transformation, Eq. (4.8), the sector of the Hamiltonian for the left and middle leads is transformed as

$$\begin{aligned} H_L^0 + H_M^0 &= \sum_\nu \varepsilon_\nu^L c_{L\nu}^\dagger c_{L\nu} + \sum_\nu \varepsilon_\nu^M c_{M\nu}^\dagger c_{M\nu} \quad ; \quad \nu : \text{quantum numbers } (\mathbf{k}, \sigma) \\ &\doteq \mathsf{c}_\nu^\dagger \mathsf{H}_\nu^0 \mathsf{c}_\nu \quad : \quad \text{matrix form, diagonal in } \nu \qquad (4.13) \\ &= \hat{\psi}_\nu^\dagger \underbrace{\mathsf{U}^\dagger \mathsf{H}_\nu^0 \mathsf{U}}_{=:\tilde{\mathsf{H}}_\nu^0} \hat{\psi}_\nu =: \hat{\psi}_\nu^\dagger \tilde{\mathsf{H}}_\nu^0 \hat{\psi}_\nu \ , \qquad (4.14) \end{aligned}$$

where

$$\mathsf{c}_\nu = \begin{pmatrix} c_{L\nu} \\ c_{M\nu} \end{pmatrix} \quad , \quad \mathsf{c}_\nu^\dagger = \begin{pmatrix} c_{L\nu}^\dagger & c_{M\nu}^\dagger \end{pmatrix} \quad , \quad \mathsf{H}_\nu^0 = \begin{pmatrix} \varepsilon_\nu^L & 0 \\ 0 & \varepsilon_\nu^M \end{pmatrix} \ , \tag{4.15}$$

and the new channels satisfy

$$\mathsf{c}_\nu = \mathsf{U}\hat{\psi}_\nu \quad , \quad \mathsf{c}_\nu^\dagger = \hat{\psi}_\nu^\dagger \mathsf{U}^\dagger \ . \tag{4.16}$$

Using the explicit representation of U in terms of its matrix elements (Eq. (4.8)), the transformed Hamiltonian, $\tilde{\mathsf{H}}_\nu^0$, becomes

$$\begin{aligned}
\tilde{\mathsf{H}}_\nu^0 &= \mathsf{U}^\dagger \mathsf{H}_\nu^0 \mathsf{U} \\
&= \begin{pmatrix} \varepsilon_\nu^L \cos^2\theta + \varepsilon_\nu^M \sin^2\theta & (\varepsilon_\nu^L - \varepsilon_\nu^M) e^{\mathrm{i}\varphi} \sin\theta\cos\theta \\ (\varepsilon_\nu^L - \varepsilon_\nu^M) e^{-\mathrm{i}\varphi} \sin\theta\cos\theta & \varepsilon_\nu^L \sin^2\theta + \varepsilon_\nu^M \cos^2\theta \end{pmatrix} \\
&\underline{\underline{\quad \varepsilon_\nu^L \overset{!}{=} \varepsilon_\nu^M =: \varepsilon_\nu \quad}} \begin{pmatrix} \varepsilon_\nu & 0 \\ 0 & \varepsilon_\nu \end{pmatrix} \ ,
\end{aligned} \tag{4.17}$$

where in the last equality, we have assumed that the quantum levels of the left and right leads are approximately the same. From Eq. (4.11), the parameters θ and φ of the $SU(2)$ transformation, Eq. (4.8), can be obtained in terms of the mixing (hopping) amplitudes, $t_1 = t_{M1}/t_L$, as

$$\begin{aligned}
\cos\theta = t_1 e^{-\mathrm{i}\varphi} \sin\theta \Rightarrow \cos^2\theta = |t_1|^2 \sin^2\theta \Rightarrow (1 + |t_1|^2) \sin^2\theta = 1 \\
\Rightarrow \sin^2\theta = \frac{1}{1+|t_1|^2} \\
\Rightarrow \sin\theta = \frac{1}{\sqrt{1+|t_1|^2}} \quad , \quad \theta \in [0, \frac{\pi}{2}] \\
\cos\theta = \frac{|t_1|}{\sqrt{1+|t_1|^2}} \ .
\end{aligned} \tag{4.18}$$

Note that, we have restricted θ to be in the first quadrant, without loss of generality. Moreover, one can easily show that the phase of t_1 must be equal to ϕ: suppose that

$$t_1 := |t_1| e^{\mathrm{i}\gamma_1} \quad \text{with} \quad \gamma_1 := \arg(t_1) \ ; \tag{4.19}$$

then, from the previous relation, Eq. (4.18), and the reality of $\cos\theta$, one concludes

$$\begin{aligned}
\underbrace{\cos\theta}_{\in\mathbb{R}} = \underbrace{|t_1|}_{\in\mathbb{R}} e^{\mathrm{i}\gamma_1} e^{-\mathrm{i}\varphi} \underbrace{\sin\theta}_{\in\mathbb{R}} \\
\Rightarrow e^{\mathrm{i}(\gamma_1 - \varphi)} = 1 \Rightarrow \gamma_1 = \varphi \\
\Rightarrow t_1 = |t_1| e^{\mathrm{i}\varphi} \quad ; \quad \varphi = \arg(t_1) = \gamma_1 \ .
\end{aligned} \tag{4.20}$$

Hence, Eq. (4.12) simplifies to

$$\begin{aligned} t_L \sin\theta e^{i\varphi}(1+(\underbrace{t_1 e^{-i\varphi}}_{=|t_1|})^2) &= t_L e^{i\varphi}\frac{1}{\sqrt{1+|t_1|^2}}(1+|t_1|^2) \\ &= t_L e^{i\varphi}\sqrt{1+|t_1|^2} \\ &= t_L \underbrace{|t_1|e^{i\varphi}}_{=t_1}\sqrt{1+\frac{1}{|t_1|^2}} \\ &= t_L \frac{t_{M1}}{t_L}\sqrt{1+|\frac{t_L}{t_{M1}}|^2} \\ &= t_{M1}\sqrt{1+|\frac{t_L}{t_{M1}}|^2}\ , \end{aligned} \tag{4.21}$$

and

$$\begin{aligned} H_{T_1} &= d_1^\dagger\left(t_{M1}\sqrt{1+|\frac{t_L}{t_{M1}}|^2}\ \hat{\psi}_2\right)+h.c. \\ &= d_1^\dagger\Big(\underbrace{\frac{t_{M1}}{|t_{M1}|}}_{\text{phase factor}}\sqrt{|t_{M1}|^2+|t_L|^2}\ \hat{\psi}_2\Big)+h.c.\ . \end{aligned} \tag{4.22}$$

Note that only $\hat{\psi}_2$-channel couples to QD1. From Eq. (4.18) above, the dispersion relations for the new channels, $\hat{\psi}_{1,2}$, in Eq. (4.17) are also obtained as

$$\begin{aligned} \varepsilon_{\nu,\psi_1} &:= \varepsilon_\nu^L\cos^2\theta+\varepsilon_\nu^M\sin^2\theta = \varepsilon_\nu^L(|t_1|^2\sin^2\theta)+\varepsilon_\nu^M\sin^2\theta = \sin^2\theta(\varepsilon_\nu^L|t_1|^2+\varepsilon_\nu^M)\ , \\ \varepsilon_{\nu,\psi_2} &:= \varepsilon_\nu^L\sin^2\theta+\varepsilon_\nu^M\cos^2\theta = \varepsilon_\nu^L\sin^2\theta+(|t_1|^2\sin^2\theta)\varepsilon_\nu^M = \sin^2\theta(\varepsilon_\nu^L+|t_1|^2\varepsilon_\nu^M)\ . \end{aligned} \tag{4.23}$$

Furthermore, from Eq. (4.18),

$$\sin^2\theta = \frac{1}{1+|t_1|^2}\quad,\quad \cos^2\theta = \frac{|t_1|^2}{1+|t_1|^2}\ , \tag{4.24}$$

one obtains the off-diagonal elements of Eq. (4.17):

$$\begin{aligned} \underbrace{e^{-i\varphi}\sin\theta}_{=\frac{1}{t_1}\cos\theta}\cos\theta &= \frac{\cos^2\theta}{t_1} = \frac{|t_1|}{t_1}\frac{|t_1|}{1+|t_1|^2} = e^{-i\varphi}\frac{|t_1|}{1+|t_1|^2}\ ; \\ &\overset{(4.20)}{\rightarrow} \frac{|t_1|}{t_1} = \frac{|t_1|}{|t_1|e^{i\varphi}} = e^{-i\varphi}\ ; \end{aligned} \tag{4.25}$$

Thus, Eq. (4.17) yields

$$\begin{aligned}\tilde{\mathsf{H}}^0_\nu &= \begin{pmatrix} \sin^2\theta(\varepsilon^L_\nu|t_1|^2+\varepsilon^M_\nu) & (\varepsilon^L_\nu-\varepsilon^M_\nu)\frac{\cos^2\theta}{t_1^*} \\ \frac{\cos^2\theta}{t_1}(\varepsilon^L_\nu-\varepsilon^M_\nu) & \sin^2\theta(\varepsilon^L_\nu+|t_1|^2\varepsilon^M_\nu)\end{pmatrix} \\ &= \frac{1}{\sin^2\theta}\begin{pmatrix} \varepsilon^L_\nu|t_1|^2+\varepsilon^M_\nu & \frac{\cot^2\theta}{t_1^*}(\varepsilon^L_\nu-\varepsilon^M_\nu) \\ \frac{\cot^2\theta}{t_1}(\varepsilon^L_\nu-\varepsilon^M_\nu) & \varepsilon^L_\nu+|t_1|^2\varepsilon^M_\nu\end{pmatrix} .\end{aligned} \tag{4.26}$$

Note that from Eq. (4.18),

$$\cot^2\theta = \frac{\cos^2\theta}{\sin^2\theta} = |t_1|^2 \; ; \tag{4.27}$$

hence,

$$\tilde{\mathsf{H}}^0_\nu = \frac{1}{1+|t_1|^2}\begin{pmatrix} \varepsilon^L_\nu|t_1|^2+\varepsilon^M_\nu & \frac{|t_1|^2}{t_1^*}(\varepsilon^L_\nu-\varepsilon^M_\nu) \\ \frac{|t_1|^2}{t_1}(\varepsilon^L_\nu-\varepsilon^M_\nu) & \varepsilon^L_\nu+|t_1|^2\varepsilon^M_\nu\end{pmatrix} \tag{4.28}$$

and, finally, the dispersion relations for the $\hat{\psi}_1$- and $\hat{\psi}_2$-channels read

$$\begin{aligned}\varepsilon_{\nu,\psi_1} &= \frac{\varepsilon^L_\nu|t_1|^2+\varepsilon^M_\nu}{1+|t_1|^2} \\ \varepsilon_{\nu,\psi_2} &= \frac{\varepsilon^L_\nu+|t_1|^2\varepsilon^M_\nu}{1+|t_1|^2} \quad ; \quad t_1 := \frac{t_{M1}}{t_L} .\end{aligned} \tag{4.29}$$

Second Glazman-Raikh transformation The first Glazman-Raikh transformation, Eq. (4.8),

$$\begin{pmatrix} c_L \\ c_M\end{pmatrix} = U\begin{pmatrix}\hat{\psi}_1 \\ \hat{\psi}_2\end{pmatrix} \tag{4.30}$$

affects also the tunneling part for QD2,

$$H_{T_2} = d_2^\dagger\,(t_R c_R + t_{M2} c_M) + h.c. \; , \tag{4.31}$$

since QD2 is also coupled to the middle reservoir, c_M. This implies that upon the first Glazman-Raikh transformation, H_{T_2} is transformed as

$$H_{T_2} = d_2^\dagger\left(t_R c_R + t_{M2}\underbrace{(-e^{-\mathrm{i}\varphi}\sin\theta\hat{\psi}_1+\cos\theta\hat{\psi}_2)}_{=c_M}\right) . \tag{4.32}$$

Now, one can further transform the right reservoir, c_R, and the channel $\hat{\psi}_1$ by a second $SU(2)$ Glazman-Raikh transformation so that only one shared channel remains ($\hat{\psi}_2$ is left unchanged):

$$H_{T_2} = d_2^\dagger(t_R c_R \underbrace{-t_{M2}e^{-\mathrm{i}\varphi}\sin\theta}_{:=\tau_{M2}}\hat{\psi}_1 + t_{M2}\cos\theta\,\hat{\psi}_2) + h.c. \; , \tag{4.33}$$

where we have defined

$$\tau_{M2} := -t_{M2}\, e^{-\mathrm{i}\varphi} \sin\theta \ . \tag{4.34}$$

Then, two new channels, $\hat{\phi}_1$ and $\hat{\phi}_2$, are obtained by an $SU(2)$ transformation as

$$\begin{pmatrix} c_R \\ \hat{\psi}_1 \end{pmatrix} = U \begin{pmatrix} \hat{\phi}_1 \\ \hat{\phi}_2 \end{pmatrix} \ . \tag{4.35}$$

An analogous procedure as in the first Glazman-Raikh transformation leads to

$$H_{T_2} = d_2^\dagger \Big(\underbrace{\frac{\tau_{M2}}{|\tau_{M2}|}}_{\text{phase factor}} \sqrt{|\tau_{M2}|^2 + |t_R|^2}\ \hat{\phi}_2 + t_{M2} \cos\theta\ \hat{\psi}_2 \Big) + h.c. \ , \tag{4.36}$$

where the channel $\hat{\phi}_1$ is decoupled from QD2.[13] The dispersion relations for $\phi_{1,2}$-channels read (analogous to Eq. (4.29))

$$\begin{aligned} \varepsilon_{\nu,\phi_1} &= \frac{\varepsilon_\nu^R |\tau_2|^2 + \varepsilon_{\nu,\psi_1}}{1+|\tau_2|^2} \quad ; \quad \tau_2 := \frac{\tau_{M2}}{t_R} \ , \\ \varepsilon_{\nu,\phi_2} &= \frac{\varepsilon_\nu^R + |\tau_2|^2 \varepsilon_{\nu,\psi_1}}{1+|\tau_2|^2} \ . \end{aligned} \tag{4.38}$$

Furthermore,

$$\begin{aligned} \tau_{M2} &= -e^{-\mathrm{i}\varphi} \sin\theta\, t_{M2} \\ &\Rightarrow |\tau_{M2}|^2 = \sin^2\theta\, |t_{M2}|^2 \ , \end{aligned} \tag{4.39}$$

and from Eq. (4.38),

$$|\tau_2|^2 = \frac{|\tau_{M2}|^2}{|t_R|^2} = \sin^2\theta \frac{|t_{M2}|^2}{|t_R|^2} \quad ; \quad \sin^2\theta \overset{(4.18)}{=} \frac{1}{1+|t_1|^2} \ . \tag{4.40}$$

[13] If we define $t_{M2}/|t_{M2}| = e^{\mathrm{i}\varphi_{M2}}$, and use Eq. (4.20),

$$\frac{t_1}{|t_1|} = e^{\mathrm{i}\varphi} \ ,$$

we obtain an explicit expression for the phase factor,

$$\begin{aligned} \frac{\tau_{M2}}{|\tau_{M2}|} \equiv -e^{\mathrm{i}(\varphi_{M2}-\varphi)} &= -\frac{t_{M2}}{|t_{M2}|}\frac{|t_1|}{t_1} = -\frac{t_{M2}}{|t_{M2}|}\frac{|t_{M1}/t_L|}{t_{M1}/t_L} \\ &= -\frac{t_{M2}}{|t_{M2}|}\frac{t_{M1}}{|t_{M1}|}\frac{t_L}{|t_L|} \\ &\equiv -\frac{t_{M2}/t_{M1}}{|t_{M2}/t_{M1}|}\frac{t_L}{|t_L|} \ . \end{aligned} \tag{4.37}$$

From Eq. (4.26), Eq. (4.38), and Eq. (4.40),

$$\begin{aligned}
\varepsilon_{\nu,\phi_1} &= \frac{\varepsilon_\nu^R \sin^2\theta|\frac{t_{M2}}{t_R}|^2 + \sin^2\theta(\varepsilon_\nu^L|t_1|^2+\varepsilon_\nu^M)}{1+\sin^2\theta|\frac{t_{M2}}{t_R}|^2} = \frac{\varepsilon_\nu^R|\frac{t_{M2}}{t_R}|^2 + \varepsilon_\nu^L|\frac{t_{M1}}{t_L}|^2+\varepsilon_\nu^M}{\frac{1}{\sin^2\theta}+|\frac{t_{M2}}{t_R}|^2} \ , \\
\varepsilon_{\nu,\phi_2} &= \frac{\varepsilon_\nu^R + \sin^2\theta|\frac{t_{M2}}{t_R}|^2\left(\sin^2\theta(\varepsilon_\nu^L|t_1|^2+\varepsilon_\nu^M)\right)}{1+\sin^2\theta|\frac{t_{M2}}{t_R}|^2} = \frac{\frac{1}{\sin^2\theta}\varepsilon_\nu^R + |\frac{t_{M2}}{t_R}|^2\sin^2\theta\left(\varepsilon_\nu^L|t_1|^2+\varepsilon_\nu^M\right)}{\frac{1}{\sin^2\theta}+|\frac{t_{M2}}{t_R}|^2} \ .
\end{aligned} \tag{4.41}$$

Thus, from Eq. (4.18), and using a simplified notation,

$$\begin{aligned}
t_1 &:= \frac{t_{M1}}{t_L} \ , \\
t_2 &:= \frac{t_{M2}}{t_R} \ ,
\end{aligned} \tag{4.42}$$

one can re-write the dispersions as

$$\begin{aligned}
\varepsilon_{\nu,\phi_1} &= \frac{\varepsilon_\nu^R|t_2|^2+\varepsilon_\nu^L|t_1|^2+\varepsilon_\nu^M}{1+|t_1|^2+|t_2|^2} \quad : \text{ decoupled from QD2} \ , \\
\varepsilon_{\nu,\phi_2} &= \frac{\varepsilon_\nu^R(1+|t_1|^2)+|t_2|^2\frac{\varepsilon_\nu^L|t_1|^2+\varepsilon_\nu^M}{1+|t_1|^2}}{1+|t_1|^2+|t_2|^2} \ .
\end{aligned} \tag{4.43}$$

Then, Eq. (4.33) becomes

$$H_{T_2} = d_2^\dagger\left(\frac{\tau_{M2}}{|\tau_{M2}|}\sqrt{|\tau_{M2}|^2+|t_R|^2}\ \hat{\phi}_2 + t_{M2}\frac{|t_1|}{\sqrt{1+|t_1|^2}}\ \hat{\psi}_2\right) + h.c. \ . \tag{4.44}$$

Note that only $\hat{\phi}_2$ couples to QD2. Furthermore, $\frac{\tau_{M2}}{|\tau_{M2}|}$ is only a phase factor, $e^{i\vartheta}$, and from Eq. (4.39),

$$|\tau_{M2}|^2 = \sin^2\theta|t_{M2}|^2 \ . \tag{4.45}$$

Therefore,

$$\begin{aligned}
H_{T_2} &= d_2^\dagger(e^{i\vartheta}\sqrt{\sin^2\theta|t_{M2}|^2+|t_R|^2}\ \hat{\phi}_2 + t_{M2}\frac{|t_1|}{\sqrt{1+|t_1|^2}}\ \hat{\psi}_2) + h.c. \\
&\overset{(4.18)}{=} d_2^\dagger(e^{i\vartheta}|t_R|\sqrt{1+\frac{|t_2|^2}{1+|t_1|^2}}\ \hat{\phi}_2 + t_{M2}\frac{|t_1|}{\sqrt{1+|t_1|^2}}\ \hat{\psi}_2) + h.c. \\
&\overset{(4.42)}{=} d_2^\dagger(e^{i\vartheta}\frac{|t_R|}{\sqrt{1+|t_1|^2}}\sqrt{1+|t_1|^2+|t_2|^2}\ \hat{\phi}_2 + \frac{t_{M2}}{|t_{M1}|}\frac{|t_L|}{\sqrt{1+|t_1|^2}}\ \hat{\psi}_2) + h.c. \\
&= d_2^\dagger(e^{i\vartheta}\frac{|t_R|}{\sqrt{1+|t_1|^2}}\sqrt{1+|t_1|^2+|t_2|^2}\ \hat{\psi}_2 + \frac{|t_L|}{\sqrt{1+|t_1|^2}}\frac{t_{M2}}{|t_{M1}|}\ \hat{\psi}_2) + h.c. \ .
\end{aligned} \tag{4.46}$$

Putting Eq. (4.22) and Eq. (4.46) together, one obtains

$$\begin{aligned} H_T &= H_{T_1} + H_{T_2} \\ &= d_1^\dagger (e^{\mathrm{i}\varphi_{M1}} \sqrt{|t_{M1}|^2 + |t_L|^2}\ \hat{\psi}_2) + h.c. \\ &\quad + d_2^\dagger (e^{\mathrm{i}\vartheta} \frac{|t_R|}{\sqrt{1+|t_1|^2}} \sqrt{1+|t_1|^2+|t_2|^2}\ \hat{\phi}_2 + \frac{t_L}{\sqrt{1+|t_1|^2}} \frac{t_{M2}}{|t_{M1}|}\ \hat{\psi}_2) + h.c.\ , \end{aligned} \tag{4.47}$$

which can be also re-written as

$$\begin{aligned} H_T &= d_1^\dagger (e^{\mathrm{i}\varphi_{M1}} |t_L| \sqrt{1+|t_1|^2}\ \hat{\psi}_2) + h.c. \\ &= d_1^\dagger \left(|t_L| \sqrt{1+|t_1|^2}\ \hat{\psi}_2 \right) + h.c. \\ &\quad + d_2^\dagger \Big(\underbrace{\frac{t_L}{\sqrt{1+|t_1|^2}} \frac{t_{M2}}{|t_{M1}|}}_{=: t_{\hat{\psi}}}\ \hat{\psi}_2 + \underbrace{\frac{|t_R|}{1+|t_1|^2} \sqrt{1+|t_1|^2+|t_2|^2}}_{=: t_{\hat{\phi}}}\ \hat{\phi}_2 \Big) + h.c.\ . \end{aligned} \tag{4.48}$$

As usual, the complex $U(1)$ phases in the hybridizations do not play a substantial role at low temperatures, and therefore, can be neglected.

Dispersion relations For later reference, the dispersion relations for the new channels are given below

$$\begin{cases} \varepsilon_{\nu,\psi_1} &= \frac{\varepsilon_\nu^L |t_1|^2 + \varepsilon_\nu^M}{1+|t_1|^2} \\ \varepsilon_{\nu,\psi_2} &= \frac{\varepsilon_\nu^L + |t_1|^2 \varepsilon_\nu^M}{1+|t_1|^2} \end{cases} \\ \begin{cases} \varepsilon_{\nu,\phi_1} &= \frac{\varepsilon_\nu^R |t_2|^2 + \varepsilon_\nu^L |t_1|^2 + \varepsilon_\nu^M}{1+|t_1|^2+|t_2|^2} \\ \varepsilon_{\nu,\phi_2} &= \frac{\varepsilon_\nu^R (1+|t_1|^2) + |t_2|^2 \frac{\varepsilon_\nu^L |t_1|^2 + \varepsilon_\nu^M}{1+|t_1|^2}}{1+|t_1|^2+|t_2|^2} \end{cases} \tag{4.49}$$

where $t_1 = t_{M1}/t_L$ and $t_2 = t_{M2}/t_R$. Henceforth, we will suppose that the quantum levels of the metallic leads are the same; that is, $\varepsilon_\nu^L \approx \varepsilon_\nu^R \approx \varepsilon_\nu^M =: \varepsilon_\nu$.

4.5.1 Single effective lead at low temperatures

To have only a single remaining shared lead between the two dots, we have to impose the following condition on Eq. (4.48)

$$\frac{|t_{\hat{\phi}}|}{|t_{\hat{\psi}}|} < 1\ , \tag{4.50}$$

so that at low temperatures, the coupling to to the shared lead $\hat{\psi}_2$ wins over the coupling to $\hat{\phi}_2$.[14] This condition leads to

$$\begin{aligned}
&\frac{|t_\phi|}{|t_\psi|} < 1 \Rightarrow \frac{|t_\phi|^2}{|t_\psi|^2} < 1 \\
&\Rightarrow \frac{|t_R|^2(1+|t_1|^2+|t_2|^2)}{|t_L|^2\frac{|t_{M2}|^2}{|t_{M1}|^2}} < 1 \\
&\Rightarrow |\frac{t_R}{t_L}|^2|\frac{t_{M1}}{t_{M2}}|^2(1+|t_1|^2+|t_2|^2) < 1 \\
&\Rightarrow |\frac{t_{M1}}{t_L}|^2\frac{1}{|t_{M2}/t_R|^2}(1+|t_1|^2+|t_2|^2) < 1 \\
&\Rightarrow |t_1|^2\frac{1}{|t_2|^2}(1+|t_1|^2+|t_2|^2) < 1 \\
&\Rightarrow |\frac{t_1}{t_2}|^2(1+|t_1|^2+|t_2|^2) < 1 \ ;
\end{aligned} \tag{4.51}$$

therefore, the mixing strengths should satisfy

$$\frac{|t_1|^2}{|t_2|^2}(1+|t_1|^2+|t_2|^2) < 1 \ . \tag{4.52}$$

By defining

$$\begin{aligned}
x &:= |t_1|^2 > 0 \ , \\
y &:= |t_2|^2 > 0 \ ,
\end{aligned} \tag{4.53}$$

one can re-write the previous inequality as

$$\begin{aligned}
\frac{x}{y}(1+x+y) < 1 \Rightarrow x(1+x+y) &< y \\
\Rightarrow x^2+xy+x &< y \\
\Rightarrow x^2+xy+x-y &< 0 \\
\Rightarrow x^2+y(x-1)+x &< 0 \ .
\end{aligned} \tag{4.54}$$

[14] The case where all the hybridizations are the same is rarely accessible in the experiments since it needs a exigent control on the system. Usually, such a case leads to non-Fermi liquid behaviour [187].

To find the solution boundary, one should solve[15]

$$x^2 + x + y(x-1) = 0 \Rightarrow y(1-x) = x^2 + x \Rightarrow y = \frac{x^2+x}{1-x} \ . \tag{4.57}$$

The solution is depicted in Fig. 4.8.

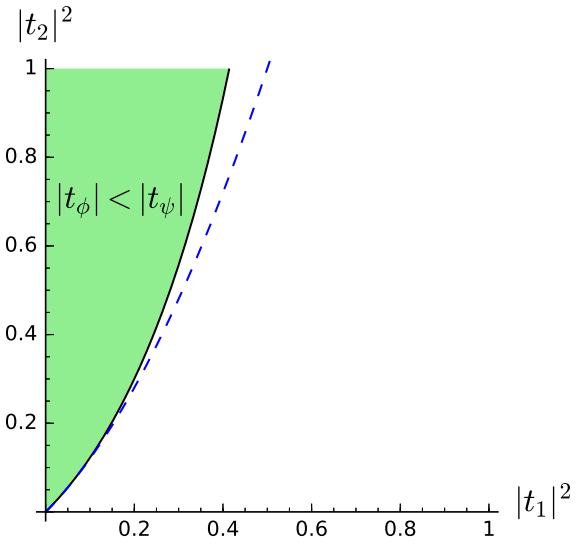

Figure 4.8: The solution to the inequality $\frac{|t_\phi|}{|t_\psi|} < 1$ is depicted by the filled region (green). The approximate condition, Eq. (4.55), results in the region which is confined by the dashed line. Note that in this region, $\hat{\phi}$-channel is decoupled from the rest of the system, leaving utterly a 2-impurity Anderson model coupled to a shared effective lead, $\hat{\psi}$.

4.5.2 Low-energy effective Hamiltonian

The final conclusion is that, at low energies, provided that the condition in Eq. (4.50) or Eq. (4.52) is satisfied, the original system is mapped to an Anderson model in which the two dots are coupled to a *single* effective lead. The important point is that the coupling to the lead is different for each dot ('asymmetric' couplings). With a Schrieffer-Wolff transformation on this effective Anderson model with a single lead (see section 4.6 for explicit derivation of the Schrieffer-Wolff transformation), one obtains a 2-impurity Kondo model as the low-energy sector

[15] Note that, approximately,

$$y(x) = \frac{x^2+x}{1-x}\Big|_{x=0} = x + 2x^2 + \mathcal{O}(x^3) \ , \tag{4.55}$$

and hence, the approximate inequality,

$$|t_2| > |t_1| \Rightarrow |\frac{t_{M2}}{t_R}| > |\frac{t_{M1}}{t_L}| \ , \tag{4.56}$$

is a necessary (but insufficient) condition for having $|t_\psi| > |t_\phi|$ (see Fig. 4.8). Taking $|t_R| \approx |t_L|$ (which is often the case in quantum dot settings), this condition implies that $|t_{M2}| > |t_{M1}|$; in other words, the couplings of the dots to the central reservoir should be different, which is usually the case in the experiments considered here.

for the double quantum dot system:

$$H_{2QD} = \sum_{\nu} \varepsilon_\nu c^\dagger_{\nu\sigma} c_{\nu\sigma} + J_{01}\, \mathbf{S}(\mathbf{x}_1) \cdot \mathbf{s}(\mathbf{x}_1) + J_{02}\, \mathbf{S}(\mathbf{x}_2) \cdot \mathbf{s}(\mathbf{x}_2) \ , \tag{4.58}$$

where the two dots are coupled to a shared effective bath, c_ν, with unequal (or 'asymmetric') Kondo couplings, J_{0i}, which are related to the parameters of the original Anderson model; i.e., $J_0 \sim |t|^2/U$. This model can be treated by the RKKY-modified RG method which was developed in chapter 3.

4.6 Schrieffer-Wolff transformation for double quantum dots

4.6.1 General Anderson model for two quantum dots and three leads

Consider a system quantum dots described by the Hamiltonian

$$H = H_D + H_{lead} + H_T \ , \tag{4.59}$$

where H_D is the Hamiltonian for the dots

$$\begin{aligned} H_D &= H_{D_1} + H_{D_2} \\ H_{D_j} &= H^0_{D_j} + \hat{U}_j \quad ; \quad j = 1, 2 \\ H^0_{D_j} &= \sum_\sigma \xi_j d^\dagger_{j\sigma} d_{j\sigma} \\ \hat{U}_j &= U_j \hat{n}_{j\uparrow} \hat{n}_{j\downarrow} \quad : \text{Coulomb repulsion for each dot} \ , \end{aligned} \tag{4.60}$$

and the leads are described by

$$\begin{aligned} H^0_{lead} \equiv H^0_l &= \sum_{\alpha=L,R} \sum_{\nu_\alpha \sigma} \xi_{\nu_\alpha} c^\dagger_{\nu_\alpha \sigma} c_{\nu_\alpha \sigma} \quad ; \ \nu_\alpha : \text{quantum numbers of the lead } \alpha \\ H_m &= \sum_{\substack{\nu_R, \nu_L \\ \sigma}} (t_m c^\dagger_{\nu_R \sigma} c_{\nu_L \sigma} + h.c.) \quad : \text{inter-lead mixing} \\ H_{lead} = H^0_l + H_m &=: \sum_{\alpha, \alpha' = L,R} \sum_{\substack{\nu_\alpha \nu_{\alpha'} \\ \sigma}} (\tau_{\alpha\alpha'} c^\dagger_{\nu_\alpha \sigma} c_{\nu_{\alpha'} \sigma} + h.c.) \\ \tau_{\alpha\alpha} &= \frac{1}{2} \xi_{\nu_\alpha} \quad ; \quad \tau_{\substack{\alpha\alpha' \\ \alpha \neq \alpha'}} = \tau^*_{\alpha'\alpha} = \frac{1}{2} t_m \ . \end{aligned} \tag{4.61}$$

Finally, the dot-lead hopping (mixing) is included as

$$\begin{aligned} H_T &= \sum_{j=1,2} \sum_{\alpha=L,R} \sum_{\nu_\alpha \sigma} (t_{j\alpha} c^\dagger_{\nu_\alpha \sigma} d_{j\sigma} + h.c.) =: H^-_T + H^+_T \ ; \\ H^+_T &= (H^-_T)^\dagger \ . \end{aligned} \tag{4.62}$$

4.6.2 Elimination of the lead-mixing terms

In case there is a mixing between L and R sectors (leads), the lead part of the Hamiltonian will be

$$\begin{aligned} H_{lead} = H_l^0 + H_m &= \sum_{\alpha=L,R}\sum_{\nu_\alpha\sigma} \xi_{\nu_\alpha} c^\dagger_{\nu_\alpha\sigma} c_{\nu_\alpha\sigma} + \sum_{\nu_R\nu_L,\sigma} (t_m c^\dagger_{\nu_R\sigma} c_{\nu_L\sigma} + h.c.) \\ &= \sum_\sigma \Big\{ \sum_{\nu_R} \xi_{\nu_R} c^\dagger_{\nu_R\sigma} c_{\nu_R\sigma} + \sum_{\nu_L} \xi_{\nu_L} c^\dagger_{\nu_L\sigma} c_{\nu_L\sigma} \\ &\quad + \sum_{\nu_R\nu_L} (t_m c^\dagger_{\nu_R\sigma} c_{\nu_L\sigma} + h.c.) \Big\} \\ &= \sum_{\nu_R\nu_L,\sigma} \underbrace{\begin{pmatrix} c^\dagger_{\nu_R\sigma} & c^\dagger_{\nu_L\sigma} \end{pmatrix}}_{=:\mathsf{c}^\dagger} \underbrace{\begin{array}{c} \\ R \\ L \end{array} \begin{array}{c} \begin{array}{cc} R & L \end{array} \\ \begin{pmatrix} \xi_{\nu_R} & t_m \\ t_m^* & \xi_{\nu_L} \end{pmatrix} \end{array}}_{=:\mathsf{h}} \underbrace{\begin{pmatrix} c_{\nu_R\sigma} \\ c_{\nu_L\sigma} \end{pmatrix}}_{=:\mathsf{c}} . \end{aligned} \tag{4.63}$$

Let us define $\tilde{\mathsf{c}}$ so that

$$\begin{aligned} \mathsf{c} &= \mathsf{U}\tilde{\mathsf{c}}^\dagger , \\ \mathsf{c}^\dagger &= \tilde{\mathsf{c}}^\dagger \mathsf{U}^\dagger , \end{aligned} \tag{4.64}$$

where U is a unitary transformation, $\mathsf{U}\mathsf{U}^\dagger = \mathbb{1}$. Therefore,

$$\mathsf{c}^\dagger \mathsf{h} \mathsf{c} = \tilde{\mathsf{c}}^\dagger \underbrace{\mathsf{U}^\dagger \mathsf{h} \mathsf{U}}_{=:\tilde{\mathsf{h}}} \tilde{\mathsf{c}} , \tag{4.65}$$

where we demand that $\tilde{\mathsf{h}}$ is a diagonal matrix,

$$\tilde{\mathsf{h}} =: \mathrm{diag}(\tilde{\xi}_R, \tilde{\xi}_L) . \tag{4.66}$$

Diagonalization of h yields the eigenvalues and eigenvectors[16]

$$\begin{aligned} \tilde{\xi}_R &= \frac{1}{2}(\xi_R + \xi_L) + \sqrt{(\frac{\xi_R - \xi_L}{2})^2 + |t|^2} , \\ \tilde{\mathsf{v}}_R &= \begin{pmatrix} \left(\frac{1}{2}(\xi_R - \xi_L) + \sqrt{(\frac{\xi_R - \xi_L}{2})^2 + |t|^2} \right) / t^* \\ 1 \end{pmatrix} , \end{aligned} \tag{4.67}$$

and

$$\begin{aligned} \tilde{\xi}_L &= \frac{1}{2}(\xi_R + \xi_L) - \sqrt{(\frac{\xi_R - \xi_L}{2})^2 + |t|^2} , \\ \tilde{\mathsf{v}}_L &= \begin{pmatrix} \left(\frac{1}{2}(\xi_R - \xi_L) - \sqrt{(\frac{\xi_R - \xi_L}{2})^2 + |t|^2} \right) / t^* \\ 1 \end{pmatrix} . \end{aligned} \tag{4.68}$$

[16] Note that the eigenvectors are *not* normalized.

Hence, the transformation U will be concisely,

$$\mathsf{U} = \begin{pmatrix} \frac{1}{\mathcal{N}_R}\tilde{\mathsf{v}}_R & \frac{1}{\mathcal{N}_L}\tilde{\mathsf{v}}_L \end{pmatrix} \quad ; \quad \mathcal{N}_\alpha := \|\tilde{\mathsf{v}}_\alpha\|,\ \alpha = L, R\ , \tag{4.69}$$

where the normalized eigenvectors $\frac{1}{\mathcal{N}_\alpha}\tilde{\mathsf{v}}_\alpha$ comprise the columns of U. Finally, we can write the transformed $\tilde{\mathsf{c}}, \tilde{\mathsf{c}}^\dagger$ operators in terms of the original $\mathsf{c}, \mathsf{c}^\dagger$:

$$\begin{aligned} \mathsf{c} = \mathsf{U}\tilde{\mathsf{c}} \Rightarrow c_\alpha = u_{\alpha\alpha'}\tilde{c}_{\alpha'} \quad ; \quad u_{\alpha\alpha'} = (\mathsf{U})_{\alpha\alpha'}\ ; \alpha, \alpha' = L, R \\ \mathsf{c}^\dagger = \tilde{\mathsf{c}}^\dagger\mathsf{U}^\dagger \Rightarrow c^\dagger_\alpha = \tilde{c}^\dagger_{\alpha'}(\mathsf{U}^\dagger)_{\alpha'\alpha} = \tilde{c}^\dagger_{\alpha'}(u_{\alpha\alpha'})^*\ . \end{aligned} \tag{4.70}$$

Then, in this new basis $(\tilde{\mathsf{c}}, \tilde{\mathsf{c}}^\dagger)$, the lead Hamiltonian will be composed of two *decoupled* sectors[17], L and R:

$$H_{lead} = \sum_{\alpha=L,R}\sum_{\nu_\alpha\sigma} \tilde{\xi}_{\nu_\alpha}\tilde{c}^\dagger_{\nu_\alpha\sigma}\tilde{c}_{\nu_\alpha\sigma}\ , \tag{4.71}$$

with

$$\begin{aligned} \tilde{\xi}_R &= \frac{1}{2}(\xi_R + \xi_L) + \sqrt{(\frac{\xi_R - \xi_L}{2})^2 + |t_m|^2}\ , \\ \tilde{\xi}_L &= \frac{1}{2}(\xi_R + \xi_L) - \sqrt{(\frac{\xi_R - \xi_L}{2})^2 + |t_m|^2}\ . \end{aligned} \tag{4.72}$$

Furthermore, H_T can be also re-written as

$$\begin{aligned} H_T = \sum_{\substack{j\alpha \\ \nu_\alpha\sigma \\ \alpha=L,R}} (t_{j\alpha}c^\dagger_{\nu_\alpha\sigma}d_{j\sigma} + h.c.) = \sum_{\substack{j\alpha' \\ \nu_{\alpha'}\sigma}} (\tilde{t}_{j\alpha'}\tilde{c}^\dagger_{\nu'_\alpha}d_{j\sigma} + h.c.) \\ \overset{\alpha'\mapsto\alpha}{=\!=\!=} \sum_{\substack{j\alpha \\ \nu_\alpha\sigma}} (\tilde{t}_{j\alpha}\tilde{c}^\dagger_{\nu\alpha}d_{j\sigma} + h.c.)\ , \end{aligned} \tag{4.73}$$

with

$$\begin{aligned} \tilde{t}_{j\alpha'} &:= \sum_\alpha t_{j\alpha}u^*_{\alpha\alpha'}\ , \\ \tilde{t}_{j\alpha} &= \sum_{\alpha'} t_{j\alpha'}u^*_{\alpha'\alpha}\ , \\ u^*_{\alpha'\alpha} \equiv (u_{\alpha'\alpha})^* &= (\mathsf{U}^\dagger)_{\alpha\alpha'}\ . \end{aligned} \tag{4.74}$$

Thus, in the rest of the calculation, one can neglect the inter-lead mixing, H_m, and merely change $t_{j\alpha}$ to $\tilde{t}_{j\alpha}$.

[17] More precisely, they should be labeled as $\tilde{L}, \tilde{R}$.

4.6.3 Schrieffer-Wolff transformation

The Schrieffer-Wolff transformation [18, 188] is a unitary transformation which yields the low-energy sector, $\tilde{H}$, of an Anderson Hamiltonian, H as

$$\tilde{H} = e^{\mathrm{i}S} H e^{-\mathrm{i}S}. \tag{4.75}$$

Using

$$e^{A} B e^{-A} = \sum_{m=0}^{\infty} \frac{1}{m!} [A,B]_m \equiv B + [A,B] + \frac{1}{2!}[A,[A,B]] + \cdots \ , \tag{4.76}$$

one obtains

$$e^{\mathrm{i}S} H e^{-\mathrm{i}S} = H + [\mathrm{i}S, H] + \frac{1}{2!}[\mathrm{i}S, [\mathrm{i}S, H]] + \cdots \ . \tag{4.77}$$

The goal is to eliminate the dot-lead mixing term H_T up to the *linear* order in t (note that $S \sim \mathcal{O}(t)$):

$$e^{\mathrm{i}S} H e^{-\mathrm{i}S} = H_D + H_l + \underbrace{H_T}_{\sim\mathcal{O}(t)} + \mathrm{i}\underbrace{[S,H]}_{\sim\mathcal{O}(t)} + \frac{1}{2!}\underbrace{[\mathrm{i}S,[\mathrm{i}S,H]]}_{\sim\mathcal{O}(t^2)} + \cdots \ . \tag{4.78}$$

Therefore,

$$\begin{aligned} [S,H] &= [S, H_D + H_l + H_T] = \underbrace{[S, H_D + H_l]}_{\sim\mathcal{O}(t)} + \underbrace{[S,H_T]}_{\sim\mathcal{O}(t^2)} \\ &= [S, H_D + H_l] + \mathcal{O}(t^2) \ . \end{aligned} \tag{4.79}$$

To eliminate H_T in the linear order in t, S has to be found such that

$$H_T + [\mathrm{i}S, [H_D + H_l]] = 0 \Rightarrow [\mathrm{i}S, H_D + H_l] = -H_T \ . \tag{4.80}$$

If such an operator S is found, then

$$\begin{aligned} \tilde{H} = e^{\mathrm{i}S} H e^{-\mathrm{i}S} &= H_D + H_l + \underbrace{H_T + [\mathrm{i}S, H_D + H_l]}_{=0} \\ &\quad + \mathrm{i}\underbrace{[S,H_T]}_{\sim\mathcal{O}(t^2)} + \frac{1}{2!}\underbrace{[\mathrm{i}S,[\mathrm{i}S,H_D+H_l]]}_{\sim\mathcal{O}(t^2)} + \mathcal{O}(t^3) \\ &= H_D + H_l + \mathrm{i}[S,H_T] + \frac{1}{2!}[\mathrm{i}S, \underbrace{[\mathrm{i}S, H_D + H_l]}_{=-H_T}] + \mathcal{O}(t^3) \\ &= H_D + H_l + \underbrace{\frac{\mathrm{i}}{2}[S,H_T]}_{=:H_S^{(2)}} + \mathcal{O}(t^3) \ . \end{aligned} \tag{4.81}$$

4.6.3.1 Generator of the Schrieffer-Wolff transformation

The essential problem is to find a suitable operator S as the generator of the Schrieffer-Wolff transformation. Without loss of generality, one can decompose the generator as

$$S = S^{-} + (S^{-})^{\dagger} \ , \tag{4.82}$$

so that $S^{\dagger} = S$. The general observation is that the operator S^{-} is essentially proportional to the 'current', $\mathcal{J}_{c-d}$, out of the d-sector into the c-sector of the Hamiltonian:

$$S^{-} \propto \mathcal{J}_{c-d} P_d \ , \tag{4.83}$$

where P_d projects onto the d-sector of the Hilbert space. The Schrieffer-Wolff transformation is essentially a perturbative expansion in powers of H_T, the mixing term of the Hamiltonian, which 'connects' (and mixes) different sectors of the Hilbert space.

Therefore, for the current multi-quantum-dot setting,

$$S^{-} = -\mathrm{i} \sum_{j\nu} \lambda_{j\nu} H_T P_{\nu}^{(j)} \ , \tag{4.84}$$

where j is the index labeling different dots, ν indexes the many-body states of the quantum dot j, $\lambda_{j\nu}$ is a c-number coefficient, H_T is the mixing (or tunneling) between quantum dots and leads which mixes different sectors of the full Hilbert space, and $P_{\nu}^{(j)}$ is the projection operator onto the state ν of the quantum dot j. The projection operator P_{ν} should be constructed from the many-body (Fock-space) operators; e.g., the projection to a many-body state with $|0, 0, \underbrace{1}_{s}, 0, \cdots\rangle \equiv d_s^{\dagger}|vac\rangle$ where s is one of the single-particle states (which form the basis of the Fock-space), is obtained by noting that the operator,

$$\hat{n}_s = d_s^{\dagger} d_s \ ,$$

projects onto the states with *at least one* s-state occupied and the operator,

$$d_s^{\dagger} d_s^{\dagger} d_s d_s \ ,$$

projects onto the states with s-state *at least doubly* occupied, and so on. Then[18]

$$(\mathbb{1} - d_s^{\dagger} d_s^{\dagger} d_s d_s)\hat{n}_s$$

projects onto a state in which the s-state is *singly* occupied.

Projection operators for the single-level quantum dot

The many-body states of a single-level quantum dot are

$$|\sigma = \uparrow, \downarrow\rangle \quad , \quad |\uparrow\downarrow\rangle \ ; \tag{4.85}$$

[18] Note that $\mathbb{1}$ is the identity operator in the Fock space.

that is, the single occupation of a state $\sigma =\uparrow,\downarrow$, and double occupation where $\uparrow$ and $\downarrow$ are both occupied. Therefore, the projection operators are

$$P_\uparrow = (\mathbb{1} - d_\downarrow^\dagger d_\downarrow) d_\uparrow^\dagger d_\uparrow = (\mathbb{1} - \hat{n}_\downarrow)\hat{n}_\uparrow \quad \text{for } \mathcal{N}_\uparrow = 1, \mathcal{N}_\downarrow = 0 \ , \tag{4.86}$$

and

$$P_\downarrow = (\mathbb{1} - d_\uparrow^\dagger d_\uparrow) d_\downarrow^\dagger d_\downarrow = (\mathbb{1} - \hat{n}_\uparrow)\hat{n}_\downarrow \quad \text{for } \mathcal{N}_\uparrow = 0, \mathcal{N}_\downarrow = 1 \ ; \tag{4.87}$$

therefore,

$$P_{\sigma=\uparrow,\downarrow} = (\mathbb{1} - \hat{n}_{\bar{\sigma}})\hat{n}_\sigma \ . \tag{4.88}$$

For the doubly-occupied state,

$$P_{\uparrow\downarrow} = d_\uparrow^\dagger d_\uparrow d_\downarrow^\dagger d_\downarrow = \hat{n}_\uparrow \hat{n}_\downarrow \quad \text{for } \mathcal{N}_\uparrow = 1, \mathcal{N}_\downarrow = 1 \ . \tag{4.89}$$

In fact, such a heuristic construction of the many-body projection operators is simple for *fermions* since their occupation number is restricted to either 1 or 0. Moreover, another simplification occurs for *fermions*:

$$d_\nu \hat{n}_\nu = d_\nu (d_\nu^\dagger d_\nu) = (-d_\nu^\dagger d_\nu + \mathbb{1}) d_\nu = -d_\nu^\dagger \underbrace{d_\nu d_\nu}_{=0} + d_\nu = d_\nu \ ; \tag{4.90}$$

that is, for fermions,

$$d_\nu \hat{n}_\nu \equiv d_\nu \ . \tag{4.91}$$

In the current case where

$$H_T \propto c_\alpha^\dagger d_\nu \ ,$$

we have

$$c_\alpha^\dagger d_\nu \hat{n}_\nu \equiv c_\alpha^\dagger d_\nu \ . \tag{4.92}$$

In the following, we explicitly construct the generator of the Schrieffer-Wolff transformation.

Ansatz for the generator of the transformation

Let us first decompose the generator, S, of the Schrieffer-Wolff transformation as

$$S =: S^+ + S^- = (S^-)^\dagger + S^- \ . \tag{4.93}$$

The following ansatz is a possible operator for S:

$$S^- = -\mathrm{i} \sum_{j\sigma} \sum_{\nu_\alpha \alpha} (\zeta^1_{j\nu_\alpha\alpha}\ \hat{n}_{j\bar{\sigma}} c^\dagger_{\nu_\alpha\sigma} d_{j\sigma} + \zeta^2_{j\nu_\alpha\alpha}\ (1 - \hat{n}_{j\bar{\sigma}}) c^\dagger_{\nu_\alpha\sigma} d_{j\sigma}) \ . \tag{4.94}$$

One can explicitly verify $[\mathrm{i}S, H_D + H_l] = -H_T$ by using

$$\begin{aligned}
[\hat{n}_{j\bar{\sigma}} c^\dagger_{\nu_\alpha} d_{j\sigma}, \hat{n}_{j'\sigma'}] &= \hat{n}_{j\bar{\sigma}} c^\dagger_{\nu_\alpha\sigma}[d_{j\sigma}, \hat{n}_{j'\sigma'}] = \hat{n}_{j\bar{\sigma}} c^\dagger_{\nu_\alpha\sigma} d_{j\sigma}\delta_{jj'}\delta_{\sigma\sigma'} \\
[\hat{n}_{j\bar{\sigma}} c^\dagger_{\nu_\alpha} d_{j\sigma}, \hat{n}_{j'\uparrow}\hat{n}_{j\downarrow}] &= \hat{n}_{j\bar{\sigma}} c^\dagger_{\nu_\alpha\sigma}[d_{j\sigma}, \hat{n}_{j'\uparrow}\hat{n}_{j'\downarrow}] = \hat{n}_{j\bar{\sigma}} c^\dagger_{\nu_\alpha\sigma}([d_{j\sigma}, \hat{n}_{j'\uparrow}]\hat{n}_{j'\downarrow} + \hat{n}_{j'\uparrow}[d_{j\sigma}, \hat{n}_{j'\downarrow}]) \\
&= \hat{n}_{j\bar{\sigma}} c^\dagger_{\nu_\alpha\sigma}(\delta_{\sigma\uparrow} d_{j\sigma}\hat{n}_{j\downarrow} + \delta_{\sigma\downarrow} d_{j\sigma}\hat{n}_{j\uparrow})\delta_{jj'} \\
&= \hat{n}_{j\bar{\sigma}} c^\dagger_{\nu_\alpha\sigma} d_{j\sigma}(\delta_{\sigma\uparrow}\hat{n}_{j\bar{\sigma}} + \delta_{\sigma\downarrow}\hat{n}_{j\bar{\sigma}})\delta_{jj'} \\
&= (\hat{n}_{j\bar{\sigma}})^2 c^\dagger_{\nu_\alpha\sigma} d_{j\sigma}(\delta_{\sigma\uparrow} + \delta_{\sigma\downarrow})\delta_{jj'} \\
&= \hat{n}_{j\bar{\sigma}} c^\dagger_{\nu_\alpha\sigma} d_{j\sigma}(\delta_{\sigma\uparrow} + \delta_{\sigma\downarrow})\delta_{jj'} \ , \qquad (4.95)
\end{aligned}$$

where for the last equality, we have used the following identities for *fermions*

$$\begin{aligned}
\hat{n}^2_{j\sigma} &= \hat{n}_{j\sigma} \ , \\
(1 - \hat{n}_{j\sigma})\hat{n}_{j\sigma} \equiv \hat{n}_{j\sigma} - \hat{n}^2_{j\sigma} &= \hat{n}_{j\sigma} - \hat{n}_{j\sigma} = 0 \ . \qquad (4.96)
\end{aligned}$$

Similarly,

$$\begin{aligned}
[(1 - \hat{n}_{j\bar{\sigma}}) c^\dagger_{\nu_\alpha} d_{j\sigma}, \hat{n}_{j'\sigma'}] &= (1 - \hat{n}_{j\bar{\sigma}}) c^\dagger_{\nu_\alpha\sigma} d_{j\sigma}\delta_{jj'}\delta_{\sigma\sigma'} \ , \\
[(1 - \hat{n}_{j\bar{\sigma}}) c^\dagger_{\nu_\alpha} d_{j\sigma}, \hat{n}_{j'\uparrow}\hat{n}_{j'\downarrow}] &= (1 - \hat{n}_{j\bar{\sigma}}) c^\dagger_{\nu_\alpha\sigma} d_{j\sigma}(\delta_{\sigma\uparrow}\hat{n}_{j\bar{\sigma}} + \delta_{\sigma\downarrow}\hat{n}_{j\bar{\sigma}})\delta_{jj'} \\
&= \underbrace{(1 - \hat{n}_{j\bar{\sigma}})\hat{n}_{j\bar{\sigma}}}_{=0} c^\dagger_{\nu_\alpha\sigma} d_{j\sigma}(\delta_{\sigma\uparrow} + \delta_{\sigma\downarrow})\delta_{jj'} \\
&= 0 \ , \qquad (4.97)
\end{aligned}$$

$$\begin{aligned}
[\hat{n}_{j\bar{\sigma}} c^\dagger_{\nu_\alpha} d_{j\sigma}, c^\dagger_{\nu_{\alpha'}\sigma'} c_{\nu_{\alpha'}\sigma'}] &= -\hat{n}_{j\bar{\sigma}} d_{j\sigma}[c^\dagger_{\nu_\alpha\sigma}, c^\dagger_{\nu_{\alpha'}\sigma'} c_{\nu_{\alpha'}\sigma'}] \\
&= \hat{n}_{j\bar{\sigma}} d_{j\sigma} c^\dagger_{\nu_\alpha\sigma}\delta_{\nu_\alpha\nu_{\alpha'}}\delta_{\sigma\sigma'} \ , \qquad (4.98) \\
[(1 - \hat{n}_{j\bar{\sigma}}) c^\dagger_{\nu_\alpha} d_{j\sigma}, c^\dagger_{\nu_{\alpha'}\sigma'} c_{\nu_{\alpha'}\sigma'}] &= (1 - \hat{n}_{j\bar{\sigma}}) d_{j\sigma} c^\dagger_{\nu_\alpha\sigma}\delta_{\nu_\alpha\nu_{\alpha'}}\delta_{\sigma\sigma'} \ , \\
[\hat{n}_{j\bar{\sigma}} c^\dagger_{\nu_\alpha\sigma} d_{j\sigma}, c^\dagger_{\nu_\gamma\sigma'} c_{\nu_{\gamma'}\sigma'}] &= -\hat{n}_{j\bar{\sigma}} d_{j\sigma}[c^\dagger_{\nu_\alpha\sigma}, c^\dagger_{\nu_\gamma\sigma'} c_{\nu_{\gamma'}\sigma'}] \\
&= \hat{n}_{j\bar{\sigma}} d_{j\sigma} c^\dagger_{\nu_\gamma\sigma}\delta_{\nu_\alpha\nu_{\gamma'}}\delta_{\sigma\sigma'} \\
&= -\hat{n}_{j\bar{\sigma}} c^\dagger_{\nu_\gamma\sigma} d_{j\sigma}\delta_{\nu_\alpha\nu_{\gamma'}}\delta_{\sigma\sigma'} \ , \\
[(1 - \hat{n}_{j\bar{\sigma}}) c^\dagger_{\nu_\alpha} d_{j\sigma}, c^\dagger_{\nu_{\gamma\sigma'}} c_{\nu_{\gamma'}\sigma'}] &= -(1 - \hat{n}_{j\bar{\sigma}}) c^\dagger_{\nu_\gamma} d_{j\sigma}\delta_{\nu_\alpha\nu_{\gamma'}}\delta_{\sigma\sigma'} \ . \qquad (4.99)
\end{aligned}$$

Therefore, using the relations above, one obtains

$$\begin{aligned}
[\mathrm{i}S^-, H_D] = \sum_{j\sigma}\sum_{\alpha,\nu_\alpha} \Big\{ &\left(\zeta^1_{j\alpha}\hat{n}_{j\bar{\sigma}} + \zeta^2_{j\alpha}(1 - \hat{n}_{j\bar{\sigma}})\right) \xi^d_j c^\dagger_{\nu_\alpha\sigma} d_{j\sigma} \\
&+ U_j \left(\zeta^1_{j\alpha}\hat{n}_{j\bar{\sigma}} + \zeta^2_{j\alpha}\underbrace{\hat{n}_{j\bar{\sigma}}(1 - \hat{n}_{j\bar{\sigma}})}_{=0 \text{ for fermions}}\right) c^\dagger_{\nu_\alpha\sigma} d_{j\sigma} \Big\} \ , \qquad (4.100)
\end{aligned}$$

and

$$\begin{aligned}
[\mathrm{i}S^-, H_l] &= [\mathrm{i}S^-, \sum_{\alpha_1\alpha_1'}\sum_{\nu_{\alpha_1}\nu_{\alpha_1'}}\sum_{\sigma'}(\tau_{\alpha_1\alpha_1'}c^\dagger_{\nu_{\alpha_1}\sigma'}c_{\nu_{\alpha_1'}\sigma'} + h.c.)] \\
&= \sum_{j\sigma}\sum_{\alpha\nu_\alpha}\sum_{\alpha_1\alpha_1'}\sum_{\nu_{\alpha_1}\nu_{\alpha_1'}}\sum_{\sigma'}\Big(-\tau_{\alpha_1\alpha_1'}\left(\zeta^1_{j\alpha}\hat{n}_{j\bar{\sigma}} + \zeta^2_{j\alpha}(1-\hat{n}_{j\bar{\sigma}})\right) c^\dagger_{\nu_{\alpha_1}\sigma}d_{j\sigma}\delta_{\sigma\sigma'}\delta_{\nu_{\alpha_1}\nu_\alpha}\delta_{\alpha\alpha_1'} \\
&\quad - \tau^*_{\alpha_1\alpha_1'}\left(\zeta^1_{j\alpha}\hat{n}_{j\bar{\sigma}} + \zeta^2_{j\alpha}(1-\hat{n}_{j\bar{\sigma}})\right) c^\dagger_{\nu_{\alpha_1'}\sigma}d_{j\sigma}\delta_{\sigma\sigma'}\delta_{\nu_{\alpha_1}\nu_\alpha}\delta_{\alpha\alpha_1}\Big) \\
&= \sum_{j\sigma}\sum_{\alpha\nu_\alpha}\sum_{\alpha_1\nu_{\alpha_1}}\Big(-\tau_{\alpha_1\alpha}\left(\zeta^1_{j\alpha}\hat{n}_{j\bar{\sigma}} + \zeta^2_{j\alpha}(1-\hat{n}_{j\bar{\sigma}})\right) c^\dagger_{\nu_{\alpha_1}\sigma}d_{j\sigma} \\
&\quad - \underbrace{\tau^*_{\alpha\alpha_1}}_{\tau_{\alpha_1,\alpha}}\left(\zeta^1_{j\alpha}\hat{n}_{j\bar{\sigma}} + \zeta^2_{j\alpha}(1-\hat{n}_{j\bar{\sigma}})\right) c^\dagger_{\nu_{\alpha_1}\sigma}d_{j\sigma}\Big) \\
&= -2\sum_{j\sigma}\sum_{\alpha\nu_\alpha}\sum_{\alpha_1\nu_{\alpha_1}}\tau_{\alpha_1\alpha}\left(\zeta^1_{j\alpha}\hat{n}_{j\bar{\sigma}} + \zeta^2_{j\alpha}(1-\hat{n}_{j\bar{\sigma}})\right) c^\dagger_{\nu_{\alpha_1}\sigma}d_{j\sigma}\ . \qquad (4.101)
\end{aligned}$$

Thus,

$$\begin{aligned}
[\mathrm{i}S^-, H_D + H_l] &= \sum_{j\sigma}\sum_{\alpha\nu_\alpha}\Big\{\xi^d_j\left(\zeta^1_{j\alpha}\hat{n}_{j\bar{\sigma}} + \zeta^2_{j\alpha}(1-\hat{n}_{j\bar{\sigma}})\right) c^\dagger_{\nu_\alpha\sigma}d_{j\sigma} \\
&\quad + U_j(\zeta^1_{j\alpha}\hat{n}_{j\bar{\sigma}})c^\dagger_{\nu_\alpha\sigma}d_{j\sigma} \\
&\quad - \sum_{\substack{\gamma\nu_\gamma \\ \gamma=L,R}} 2\tau_{\gamma\alpha}\left(\zeta^1_{j\alpha}\hat{n}_{j\bar{\sigma}} + \zeta^2_{j\alpha}(1-\hat{n}_{j\bar{\sigma}})\right) c^\dagger_{\nu_\gamma\sigma}d_{j\sigma}\Big\} \\
&= \sum_{j\sigma}\sum_{\alpha\nu_\alpha}\Big\{\left(\zeta^1_{j\alpha}\hat{n}_{j\bar{\sigma}} + \zeta^2_{j\alpha}(1-\hat{n}_{j\bar{\sigma}})\right)\sum_{\gamma\nu_\gamma}((\xi^d_j + U_j)\delta_{\gamma\alpha} - 2\tau_{\gamma\alpha})c^\dagger_{\nu_\gamma\sigma}d_{j\sigma}\Big\}\ . \qquad (4.102)
\end{aligned}$$

Note that

$$\begin{aligned}
([S,H])^\dagger &= H^\dagger S^\dagger - S^\dagger H^\dagger = [H^\dagger, S^\dagger] \\
&\overset{H\overset{!}{=}H^\dagger}{=\!=\!=} [H, S^\dagger] = -[S^\dagger, H]\ ; \qquad (4.103)
\end{aligned}$$

hence,

$$[S^+, H_D + H_l] \overset{(S^+)^\dagger = S^-}{=\!=\!=} -([S^-, H_D + H_l])^\dagger\ , \qquad (4.104)$$

and

$$[\mathrm{i}S^+, H_D + H_l] = -\mathrm{i}([S^-, H_D + H_l])^\dagger = -\mathrm{i}([\mathrm{i}S^-, H_D + H_l])^\dagger = ([\mathrm{i}S^-, H_D + H_l])^\dagger\ ; \qquad (4.105)$$

therefore,

$$\begin{aligned}
[\mathrm{i}S, H_D + H_l] \equiv [\mathrm{i}(S^- + S^+), H_D + H_l] &= [\mathrm{i}S^-, H_D + H_l] + ([\mathrm{i}S^-, H_D + H_l])^\dagger \\
&\overset{!}{=} -H_T \equiv -\sum_{j\sigma}\sum_{\alpha\nu_\alpha}\left(t_{j\alpha}c^\dagger_{\nu_\alpha\sigma}d_{j\sigma} + t^*_{j\sigma}d^\dagger_{j\sigma}c_{\nu_\alpha\sigma}\right)\ . \qquad (4.106)
\end{aligned}$$

Thus,

$$\begin{aligned}
[\mathrm{i}S, H_D + H_l] &= \sum_{j\sigma}\sum_{\alpha\nu_\alpha}\sum_{\gamma\nu_\gamma}\Big\{\Big[\Big(\xi_j^d\delta_{\alpha\gamma} - 2\tau_{\gamma\alpha}\Big)\Big(\zeta_{j\alpha}^1\hat{n}_{j\bar{\sigma}} + \zeta_{j\alpha}^2(1-\hat{n}_{j\bar{\sigma}})\Big) \\
&\quad + U_j\delta_{\alpha\gamma}\zeta_{j\alpha}^1\hat{n}_{j\bar{\sigma}}\Big]\, c_{\nu_\gamma\sigma}^\dagger d_{j\sigma} + h.c.\Big\} \\
&= \sum_{j\sigma}\sum_{\alpha\nu_\alpha}\sum_{\gamma\nu_\gamma}\Big\{\Big(\Big((\xi_j^d + U_j)\delta_{\alpha\gamma} - 2\tau_{\gamma\alpha}\Big)\zeta_{j\alpha}^1\hat{n}_{j\bar{\sigma}} \\
&+ \Big(\xi_j^d\delta_{\alpha\gamma} - 2\tau_{\gamma\alpha}\Big)\zeta_{j\alpha}^2(1-\hat{n}_{j\bar{\sigma}})\Big)\, c_{\nu_\gamma\sigma}^\dagger d_{j\sigma} + h.c.\Big\} \\
&\stackrel{!}{=} -\sum_{j\sigma}\sum_{\alpha\nu_\alpha}(t_{j\alpha}c_{\nu_\alpha\sigma}^\dagger d_{j\sigma} + h.c.)\ .
\end{aligned} \tag{4.107}$$

Therefore, one concludes

$$\begin{aligned}
\Big(\Big((\xi_j^d + U_j)\delta_{\alpha\gamma} - 2\tau_{\gamma\alpha}\Big)\zeta_{j\alpha}^1\hat{n}_{j\bar{\sigma}} + (\xi_j^d\delta_{\alpha\gamma} - 2\tau_{\gamma\alpha})\zeta_{j\alpha}^2(1-\hat{n}_{j\bar{\sigma}})\Big) &= -t_{j\alpha}\delta_{\alpha\gamma} \quad ; \\
\text{for all } \gamma,\nu_\gamma,\alpha,\nu_\alpha,j,\sigma \quad &: \text{matrix equation}\ .
\end{aligned} \tag{4.108}$$

If $\tau_{\alpha\gamma} = \tau_{\alpha\alpha}\delta_{\alpha\gamma}$ (no inter-lead mixing), then, in the sector of the Hilbert space where $n_{j\bar{\sigma}} = 1$ or $1 - n_{j\bar{\sigma}} = 0$,

$$\begin{aligned}
\Big((\zeta_j^d + U_j) - 2\tau_{\alpha\alpha}\Big)\zeta_{j\alpha}^1 &= -t_{j\alpha} \\
\Rightarrow \zeta_{j\alpha}^1 &= \frac{-t_{j\alpha}}{(\xi_j^d + U_j) - 2\tau_{\alpha\alpha}} \\
&\stackrel{\tau_{\alpha\alpha}=\frac{1}{2}\xi_\alpha}{=\!=\!=} \frac{-t_{j\alpha}}{\xi_j^d + U_j - \xi_d} \\
\Rightarrow \zeta_{j\alpha}^1 &= \frac{t_{j\alpha}}{\xi_\alpha - (E_j^{(2)} - E_j^{(1)})}\ ,
\end{aligned} \tag{4.109}$$

where, $E_j^{(n)}$ is the energy of a state with n particles on dot j.

In the sector of the Hilbert space where $1 - n_{j\bar{\sigma}} = 0$ ($n_{j\bar{\sigma}} = 0$),

$$\begin{aligned}
(\xi_j^d - 2\tau_{\alpha\alpha})\zeta_{j\alpha}^2 &= -t_{j\alpha} \\
\Rightarrow \zeta_{j\alpha}^2 &= \frac{-t_{j\alpha}}{\xi_j^d - 2\tau_{\alpha\alpha}} \\
&= \frac{t_{j\alpha}}{\xi_d - \xi_j^d} \\
\Rightarrow \zeta_{j\alpha}^2 &= \frac{t_{j\alpha}}{\xi_\alpha - (E_j^{(1)} - E_j^{(0)})}\ .
\end{aligned} \tag{4.110}$$

Therefore,

$$S^{-} = -\mathrm{i}\sum_{j\sigma}\sum_{\alpha\nu_\alpha}\Big(\frac{t_{j\alpha}}{\xi_\alpha - (E_j^{(2)} - E_j^{(1)})}\hat{n}_{j\bar{\sigma}}c^\dagger_{\nu_\alpha\sigma}d_{j\sigma} + \frac{t_{j\alpha}}{\xi_\alpha - (E_j^{(1)} - E_j^{(0)})}(1-\hat{n}_{j\bar{\sigma}})c^\dagger_{\nu_\alpha}d_{j\sigma}\Big) \ . \tag{4.111}$$

4.6.3.2 Higher-order commutators

As it is clear from Eq. (4.81), higher order commutators are also needed to obtain the low-energy sector of the Anderson Hamiltonian; namely, one needs $H_S^{(2)} = \frac{\mathrm{i}}{2}[S, H_T]$, where

$$[S, H_T] = [S, H_T^- + H_T^+] \ , \tag{4.112}$$

with

$$H_T^- = \sum_{j\nu\alpha} t_{j\alpha\nu}c^\dagger_\alpha d_{j\nu} \quad ; \quad H_T^+ = (H_T^-)^\dagger = \sum_{j\nu\alpha} t^*_{j\alpha\nu}d^\dagger_\nu c_\alpha \ . \tag{4.113}$$

Note that H_T^- (H_T^+) removes (adds) one electron from (to) a quantum dot; similarly, S^- (S^+) removes (adds) one electron from (to) a quantum dot.
The commutator $[S^-, H_T^-]$ involves

$$[\hat{n}_{\bar{\sigma}}, c^\dagger_\alpha d_\sigma c^\dagger_{\alpha'}d_{\sigma'}] = [\hat{n}_{\bar{\sigma}}, c^\dagger_{\alpha'}d_{\sigma'}]c^\dagger_\alpha d_\sigma = c^\dagger_{\alpha'}[\hat{n}_{\bar{\sigma}}, d_{\sigma'}]c^\dagger_\alpha d_\sigma \ , \tag{4.114}$$

where we have used

$$\begin{aligned} [c^\dagger_\alpha, c^\dagger_{\alpha'}d_{\sigma'}] = 0 = [d_\sigma, c^\dagger_{\alpha'}d_{\sigma'}] \ , \\ [c^\dagger_\alpha, \hat{n}_\sigma] = 0 \ , \\ -c^\dagger_{\alpha'}d_{\bar{\sigma}}\delta_{\bar{\sigma}\sigma'}c^\dagger_\alpha d_\sigma = +\delta_{\bar{\sigma}\sigma'}c^\dagger_{\alpha'}c^\dagger_\alpha d_{\bar{\sigma}}d_\sigma \ . \end{aligned} \tag{4.115}$$

Note that[19]

$$[S^+, H_T^+] = -[S^-, H_T^-] \propto d^\dagger_\sigma d^\dagger_{\bar{\sigma}}c_\alpha c_{\alpha'} \ . \tag{4.117}$$

That means $[S^-, H_T^-]$ and $[S^+, H_T^+]$ are related to processes which increase or decrease the dot occupation number by two. Such processes take out the system from its ground-state manifold; i.e., the states in which the quantum dot is singly-occupied. This can be specified formally by defining a projector P_G onto the singly-occupied ground-state manifold and enforcing the following condition on the low-energy Hamiltonian $\tilde{H}$:

$$(\mathbb{1} - P_G)\tilde{H}P_G \stackrel{!}{=} 0 \ ; \tag{4.118}$$

Therefore, the contribution of $[S^-, H_T^-]$ and $[S^+, H_T^+]$ vanishes. To obtain the commutators

[19] The following relation is used

$$([A, B])^\dagger = -[A^\dagger, B^\dagger] \Leftrightarrow [A^\dagger, B^\dagger] = -[A, B]^\dagger \ . \tag{4.116}$$

$[S^-, H_T^+]$ and $[S^+, H_T^-] = -[S^-, H_T^+]$ [20], we need the commutation relations

$$\begin{aligned}
[c_\alpha^\dagger d_\sigma, d_{\sigma'}^\dagger c_{\alpha'}] &= [c_\alpha^\dagger, d_{\sigma'}^\dagger c_{\alpha'}] d_\sigma + c_\alpha^\dagger [d_\sigma, d_{\sigma'}^\dagger c_{\alpha'}] \\
&= -d_{\sigma'}^\dagger d_\sigma \delta_{\alpha\alpha'} + c_\alpha^\dagger c_{\alpha'} \delta_{\sigma\sigma'} \ , \qquad (4.119) \\
[\hat{n}_{\bar\sigma} c_\alpha^\dagger d_\sigma, d_{\sigma'}^\dagger c_{\alpha'}] &= [\hat{n}_{\bar\sigma}, d_{\sigma'}^\dagger c_{\alpha'}] c_\alpha^\dagger d_\sigma + \hat{n}_{\bar\sigma} [c_\alpha^\dagger d_\sigma, d_{\sigma'}^\dagger c_{\alpha'}] \\
&= \delta_{\bar\sigma\sigma'} d_{\bar\sigma}^\dagger c_{\alpha'} c_\alpha^\dagger d_\sigma + \hat{n}_{\bar\sigma} (-\delta_{\alpha\alpha'} d_{\sigma'}^\dagger d_\sigma + \delta_{\sigma\sigma'} c_\alpha^\dagger c_{\alpha'}) \\
&= \delta_{\bar\sigma\sigma'} c_{\alpha'} c_\alpha^\dagger d_{\bar\sigma}^\dagger d_\sigma + \hat{n}_{\bar\sigma} \\
&= \delta_{\bar\sigma\sigma'} d_{\bar\sigma}^\dagger c_{\alpha'} c_\alpha^\dagger d_\sigma + \hat{n}_{\bar\sigma} (-\delta_{\alpha\alpha'} d_{\sigma'}^\dagger d_\sigma + \delta_{\sigma\sigma'} c_\alpha^\dagger c_{\alpha'}) \\
&= \delta_{\bar\sigma\sigma'} c_{\alpha'} c_\alpha^\dagger d_{\bar\sigma}^\dagger d_\sigma + \hat{n}_{\bar\sigma} (\delta_{\sigma\sigma'} c_\alpha^\dagger c_{\alpha'} - \delta_{\alpha\alpha'} d_{\sigma'}^\dagger d_\sigma) \ , \qquad (4.120)
\end{aligned}$$

where we have used

$$\begin{aligned}
[\hat{n}_{\bar\sigma}, d_{\sigma'}^\dagger c_{\alpha'}] = [\hat{n}_{\bar\sigma}, d_{\sigma'}^\dagger] c_{\alpha'} = d_{\bar\sigma}^\dagger c_{\alpha'} \delta_{\bar\sigma,\sigma'} \ , \\
[\hat{n}_{\bar\sigma}, c_{\alpha'}] = 0 \ . \qquad (4.121)
\end{aligned}$$

Therefore,

$$\begin{aligned}
[S^-, H_T^+] &= -\mathrm{i} \sum_{j\sigma} \sum_{\alpha} \Big\{ \lambda_{j\alpha}^{(2)} [\hat{n}_{j\bar\sigma} c_{\alpha\sigma}^\dagger d_{j\sigma}, \sum_{j'\sigma'\alpha'} t_{j'\alpha'}^* c_{\alpha'\sigma'}^\dagger d_{j'\sigma'}] \\
&\quad + \lambda_{j\alpha}^{(1)} [(\mathbb{1} - \hat{n}_{j\bar\sigma}) c_{\alpha\sigma}^\dagger d_{j\sigma}, \sum_{j'\sigma'\alpha'} t_{j'\alpha'}^* c_{\alpha'\sigma'}^\dagger d_{j'\sigma'}] \Big\} \\
&= -\mathrm{i} \sum_{j\sigma} \sum_{\alpha} \Big\{ (\lambda_{j\alpha}^{(2)} - \lambda_{j\alpha}^{(1)}) \sum_{j'\sigma'\alpha'} t_{j'\alpha'}^* \delta_{jj'} \Big(\delta_{\bar\sigma\sigma'} c_{\alpha'\bar\sigma} c_{\alpha\sigma}^\dagger d_{\bar\sigma}^\dagger d_\sigma + \hat{n}_{\bar\sigma} (\delta_{\sigma\sigma'} c_{\alpha\sigma}^\dagger c_{\alpha'\sigma} - \delta_{\alpha\alpha'} d_\sigma^\dagger d_\sigma) \Big) \\
&\quad + \lambda_{j\alpha}^{(1)} \sum_{j'\sigma'\alpha'} t_{j'\alpha'}^* (\delta_{\sigma\sigma'} c_\alpha^\dagger c_{\alpha'} - \delta_{\alpha\alpha'} d_{\sigma'}^\dagger d_\sigma) \delta_{jj'} \Big\} \\
&= -\mathrm{i} \sum_{j\sigma} \sum_{\alpha} \Big\{ (\lambda_{j\alpha}^{(2)} - \lambda_{j\alpha}^{(1)}) \left(\sum_{\alpha'} t_{j\alpha'}^* c_{\alpha'\bar\sigma} c_{\alpha\sigma}^\dagger d_{\bar\sigma}^\dagger d_\sigma + \sum_{\alpha'} t_{j\alpha'}^* \hat{n}_{\bar\sigma} c_{\alpha\sigma}^\dagger c_{\alpha'\sigma} - t_{j\alpha} \hat{n}_{\bar\sigma} d_{\bar\sigma}^\dagger d_\sigma \right) \\
&\quad + \lambda_{j\alpha}^{(1)} \left(\sum_{\alpha'} t_{j\alpha'}^* c_{\alpha\sigma}^\dagger c_{\alpha'\sigma} - t_{j\alpha}^* d_\sigma^\dagger d_\sigma \right) \Big\} \\
&= -\mathrm{i} \sum_{j\sigma} \sum_{\alpha} \Big\{ (\lambda_{j\alpha}^{(2)} - \lambda_{j\alpha}^{(1)}) \left(\sum_{\alpha'} t_{j\alpha'}^* [c_{\alpha'\bar\sigma} c_{\alpha\sigma}^\dagger d_{\bar\sigma}^\dagger d_\sigma + \hat{n}_{\bar\sigma} c_{\alpha\sigma}^\dagger c_{\alpha'\sigma}] - t_{j\alpha}^* \hat{n}_{\bar\sigma} \hat{n}_\sigma \right) \Big\} \\
&= -\mathrm{i} \sum_{j\sigma} \sum_{\alpha} \Big\{ (\lambda_{j\alpha}^{(2)} - \lambda_{j\alpha}^{(1)}) \left(\sum_{\alpha'} t_{j\alpha'}^* [c_{\alpha'\bar\sigma} c_{\alpha\sigma}^\dagger d_{\bar\sigma}^\dagger d_\sigma + \hat{n}_{\bar\sigma} c_{\alpha\sigma}^\dagger c_{\alpha'\sigma}] - t_{j\alpha}^* \hat{n}_{\bar\sigma} \hat{n}_\sigma \right) \\
&\quad + \lambda_{j\alpha}^{(1)} \sum_{\alpha'} (t_{j\alpha'}^* c_{\alpha\sigma}^\dagger c_{\alpha'\sigma} - t_{j\alpha}^* \hat{n}_\sigma) \Big\} \ . \qquad (4.122)
\end{aligned}$$

Furthermore,

$$[S^+, H_T^-] = -([S^-, H_T^+])^\dagger \ , \qquad (4.123)$$

[20] Note that $([A, B]_{\zeta=\pm 1})^\dagger = -\zeta [A^\dagger, B^\dagger]$.

so that

$$[S^-, H_T^+] + [S^+, H_T^-] = [S^-, H_T^+] - [S^-, H_T^+]^\dagger \ . \tag{4.124}$$

4.6.4 Low-energy sector of the Anderson Hamiltonian

Since we are interested only in the low-energy/temperature behaviour (near the ground-state with single occupation, $\sum_\sigma \hat{n}_\sigma = \mathbb{1}$), then

$$\hat{n}_{\bar{\sigma}} \hat{n}_\sigma \stackrel{!}{=} 0 \ , \tag{4.125}$$

and therefore,

$$\begin{aligned}
[S^-, H_T^+] = &-\mathrm{i} \sum_{j\sigma} \sum_{\alpha} \Big\{ (\lambda_{j\alpha}^{(2)} - \lambda_{j\alpha}^{(1)}) \sum_{\alpha'} t_{j\alpha'}^* \left(c_{\alpha'\bar{\sigma}} c_{\alpha\sigma}^\dagger d_{\bar{\sigma}}^\dagger d_\sigma + \hat{n}_{\bar{\sigma}} c_{\alpha\sigma}^\dagger c_{\alpha'\sigma} \right) \\
&+ \lambda_{j\alpha}^{(1)} \left(\sum_{\alpha'} t_{j\alpha'}^* c_{\alpha\sigma}^\dagger c_{\alpha'\sigma} - \underbrace{t_{j\alpha}^* \hat{n}_\sigma}_{\text{c-number}} \right) \Big\} \\
= &-\mathrm{i} \sum_{j\sigma} \sum_{\alpha} \Big\{ (\lambda_{j\alpha}^{(2)} - \lambda_{j\alpha}^{(1)}) \sum_{\alpha'} t_{j\alpha'}^* \left(-c_{\alpha\sigma}^\dagger c_{\alpha'\bar{\sigma}} d_{\bar{\sigma}}^\dagger d_\sigma + \hat{n}_{\bar{\sigma}} c_{\alpha\sigma}^\dagger c_{\alpha'\sigma} \right) \\
&+ \lambda_{j\alpha}^{(1)} \sum_{\alpha'} t_{j\alpha'}^* c_{\alpha\sigma}^\dagger c_{\alpha'\sigma} \Big\} \\
= &-\mathrm{i} \sum_{j\sigma} \sum_{\alpha} \Big\{ (\lambda_{j\alpha}^{(2)} - \lambda_{j\alpha}^{(1)}) \sum_{\alpha'} t_{j\alpha'}^* \left(-c_{\alpha\sigma}^\dagger c_{\alpha'\bar{\sigma}} d_{\bar{\sigma}}^\dagger d_\sigma + \hat{n}_{\bar{\sigma}} c_{\alpha\sigma}^\dagger c_{\alpha'\sigma} \right) \\
&+ \lambda_{j\alpha}^{(1)} \sum_{\alpha'} t_{j\alpha'}^* c_{\alpha\sigma}^\dagger c_{\alpha'\sigma} \Big\} \ .
\end{aligned} \tag{4.126}$$

Since there is a fixed number of electrons on the quantum dots in the ground-state, one can express the effective Hamiltonian in terms of difference between spin-up and down occupation numbers:

$$n_\sigma = \frac{1}{2} (\underbrace{n_\sigma + n_{\bar{\sigma}}}_{\stackrel{!}{=}1} + n_\sigma - n_{\bar{\sigma}}) = \frac{1}{2} + \frac{1}{2}(n_\sigma - n_{\bar{\sigma}}) \quad ; \quad n_{\bar{\sigma}} = \frac{1}{2} + \frac{1}{2}(n_{\bar{\sigma}} - n_\sigma) \ ; \tag{4.127}$$

hence,

$$
\begin{aligned}
[S^-, H_T^+] &= -\mathrm{i}\sum_{j\sigma}\sum_{\alpha}\Big\{(\lambda_{j\alpha}^{(2)}-\lambda_{j\alpha}^{(1)})\sum_{\alpha'}t_{j\alpha'}^*\left(\frac{1}{2}c_{\alpha\sigma}^\dagger c_{\alpha'\sigma}+\frac{1}{2}(\hat{n}_{\bar\sigma}-\hat{n}_\sigma)c_{\alpha\sigma}^\dagger c_{\alpha'\sigma}-c_{\alpha\sigma}^\dagger c_{\alpha'\bar\sigma}d_{\bar\sigma}^\dagger d_\sigma\right)\\
&\quad+\lambda_{j\alpha}^{(1)}\sum_{\alpha'}t_{j\alpha'}^*c_{\alpha\sigma}^\dagger c_{\alpha'\sigma}\Big\}\\
&= -\mathrm{i}\sum_{j\sigma}\sum_{\alpha}\Big\{(\lambda_{j\alpha}^{(2)}-\lambda_{j\alpha}^{(1)})\sum_{\alpha'}t_{j\alpha'}^*\left(\frac{1}{2}(\hat{n}_{\bar\sigma}-\hat{n}_\sigma)c_{\alpha\sigma}^\dagger c_{\alpha'\sigma}-c_{\alpha\sigma}^\dagger c_{\alpha'\bar\sigma}-c_{\alpha\sigma}^\dagger c_{\alpha'\bar\sigma}d_{\bar\sigma}^\dagger d_\sigma\right)\\
&\quad+(\lambda_{j\alpha}^{(2)}-\lambda_{j\alpha}^{(1)})\sum_{\alpha'}\frac{1}{2}t_{j\alpha'}^*c_{\alpha\sigma}^\dagger c_{\alpha'\sigma}+\lambda_{j\alpha}^{(1)}\sum_{\alpha'}t_{j\alpha'}^*c_{\alpha\sigma}^\dagger c_{\alpha'\sigma}\Big\}\\
&= -\frac{\mathrm{i}}{2}\sum_{j}\sum_{\alpha\alpha'}(\lambda_{j\alpha}^{(2)}-\lambda_{j\alpha}^{(1)})t_{j\alpha'}^*\sum_{\sigma}\left((\hat{n}_{\bar\sigma}-\hat{n}_\sigma)c_{\alpha\sigma}^\dagger c_{\alpha'\sigma}-2c_{\alpha\sigma}^\dagger c_{\alpha'\bar\sigma}d_{\bar\sigma}^\dagger d_\sigma\right)\\
&\quad-\frac{\mathrm{i}}{2}\sum_{j}\sum_{\alpha\alpha'}\left((\lambda_{j\alpha}^{(2)}-\lambda_{j\alpha}^{(1)})t_{j\alpha'}^*c_{\alpha\sigma}^\dagger c_{\alpha'\sigma}+2\lambda_{j\alpha}^{(1)}t_{j\alpha'}^*c_{\alpha\sigma}^\dagger c_{\alpha'\sigma}\right)\ .
\end{aligned}
\tag{4.128}
$$

The last summand can be re-written as

$$
\begin{aligned}
(\lambda_{j\alpha}^{(2)}-\lambda_{j\alpha}^{(1)})t_{j\alpha'}^*c_{\alpha\sigma}^\dagger c_{\alpha'\sigma}+2\lambda_{j\alpha}^{(1)}t_{j\alpha'}^*c_{\alpha\sigma}^\dagger c_{\alpha'\sigma} &= \left((\lambda_{j\alpha}^{(2)}-\lambda_{j\alpha}^{(1)})t_{j\alpha'}^*+2\lambda_{j\alpha}^{(1)}t_{j\alpha'}^*\right)c_{\alpha\sigma}^\dagger c_{\alpha'\sigma}\\
&= (\lambda_{j\alpha}^{(2)}+\lambda_{j\alpha}^{(1)})t_{j\alpha'}^*c_{\alpha\sigma}^\dagger c_{\alpha'\sigma}\ .
\end{aligned}
\tag{4.129}
$$

Comparing the expression for $[S^-, H_T^+]$ with a spin-spin interaction (Appendix B),

$$
\begin{aligned}
\mathbf{S}_d\cdot\mathbf{s}_{\alpha\alpha'} &= \frac{1}{4}\sum_{\gamma=x,y,z}\sum_{\substack{\nu\nu'\eta\eta'\\(\text{spin})}}(d_\nu^\dagger\sigma_{\nu\nu'}^\gamma d_{\nu'})(c_{\alpha\eta}^\dagger\sigma_{\eta\eta'}^\gamma c_{\alpha'\eta'})\\
&= \frac{1}{2}\sum_{\sigma}\underbrace{d_{\bar\sigma}^\dagger d_\sigma c_{\alpha\sigma}^\dagger c_{\alpha'\bar\sigma}}_{\text{spin-flip}}+\frac{1}{4}\sum_{\sigma}\underbrace{(\hat{n}_\sigma-\hat{n}_{\bar\sigma})c_{\alpha\sigma}^\dagger c_{\alpha'\sigma}}_{\text{no spin-flip}}\ ,
\end{aligned}
\tag{4.130}
$$

one observes

$$
\begin{aligned}
[S^-, H_T^+] &= -\frac{\mathrm{i}}{2}\sum_{j}\sum_{\alpha\alpha'}(\lambda_{j\alpha}^{(2)}-\lambda_{j\alpha}^{(1)})t_{j\alpha'}^*(-4)(\mathbf{S}_d\cdot\mathbf{s}_{\alpha\alpha'})\\
&\quad-\frac{\mathrm{i}}{2}\sum_{j}\sum_{\alpha\alpha'}(\lambda_{j\alpha}^{(2)}+\lambda_{j\alpha}^{(1)})t_{j\alpha'}^*c_{\alpha\sigma}^\dagger c_{\alpha'\sigma}\\
&= 2\mathrm{i}\sum_{j}\sum_{\alpha\alpha'}(\lambda_{j\alpha}^{(2)}-\lambda_{j\alpha}^{(1)})t_{j\alpha'}^*(\mathbf{S}_d\cdot\mathbf{s}_{\alpha\alpha'}) \quad : \quad \text{spin-spin interaction}\\
&\quad-\frac{\mathrm{i}}{2}\sum_{j}\sum_{\alpha\alpha'}(\lambda_{j\alpha}^{(2)}+\lambda_{j\alpha}^{(1)})t_{j\alpha'}^*c_{\alpha\sigma}^\dagger c_{\alpha'\sigma} \quad : \quad \text{potential scattering}
\end{aligned}
\tag{4.131}
$$

Plugging in the λ_j's (near Fermi surface, $\xi_\alpha \approx 0$),

$$\begin{aligned}\lambda_j^{(1)} &= \frac{t_{j\alpha}}{\xi_\alpha - (E_j^{(1)} - E_j^{(0)})} \approx \frac{-t_{j\alpha}}{E_j^{(1)} - E_j^{(0)}} \ , \\ \lambda_j^{(2)} &= \frac{t_{j\alpha}}{\xi_\alpha - (E_j^{(2)} - E_j^{(1)})} \approx \frac{-t_{j\alpha}}{E_j^{(2)} - E_j^{(1)}} \ ,\end{aligned} \tag{4.132}$$

the commutator becomes,

$$\begin{aligned}[S^-, H_T^+] &\approx -2\mathrm{i} \sum_j \sum_{\alpha\alpha'} \left(\frac{t_{j\alpha} t_{j\alpha'}^*}{E_j^{(2)} - E_j^{(1)}} - \frac{t_{j\alpha} t_{j\alpha'}^*}{E_j^{(1)} - E_j^{(0)}} \right) \mathbf{S}_{jd} \cdot \mathbf{s}_{\alpha\alpha'} \\ &\quad + \frac{\mathrm{i}}{2} \sum_j \sum_{\alpha\alpha'} \left(\frac{t_{j\alpha} t_{j\alpha'}^*}{E_j^{(2)} - E_j^{(1)}} + \frac{t_{j\alpha} t_{j\alpha'}^*}{E_j^{(1)} - E_j^{(0)}} \right) c_{\alpha\sigma}^\dagger c_{\alpha'\sigma} \\ &= -\mathrm{i} \sum_j \sum_{\alpha\alpha'} \underbrace{2 t_{j\alpha} t_{j\alpha'}^* \left(\frac{1}{E_j^{(2)} - E_j^{(1)}} - \frac{1}{E_j^{(1)} - E_j^{(0)}} \right)}_{:= J_{j,\alpha\alpha'}} \mathbf{S}_{jd} \cdot \mathbf{s}_{\alpha\alpha'} \\ &\quad - \mathrm{i} \sum_j \sum_{\alpha\alpha'} \underbrace{(-\frac{1}{2} t_{j\alpha} t_{j\alpha'}^*) \left(\frac{1}{E_j^{(2)} - E_j^{(1)}} + \frac{1}{E_j^{(1)} - E_j^{(0)}} \right)}_{:= W_{j\alpha\alpha'}} c_{\alpha\sigma}^\dagger c_{\alpha'\sigma} \\ &=: -\mathrm{i} \sum_j \sum_{\alpha\alpha'} J_{j\alpha\alpha'} \mathbf{S}_{jd} \cdot \mathbf{s}_{\alpha\alpha'} - \mathrm{i} \sum_j \sum_{\alpha\alpha'} W_{j\alpha\alpha'} c_{\alpha\sigma}^\dagger c_{\alpha'\sigma} \ .\end{aligned} \tag{4.133}$$

Using the relation

$$[S^+, H_T^-] = -[S^-, H_T^+] \ ,$$

one obtains

$$\begin{aligned}[S^+, H_T^-] &= -\mathrm{i} \sum_j \sum_{\alpha\alpha'} J_{j\alpha\alpha'}^* \mathbf{S}_{jd} \cdot \mathbf{s}_{\alpha\alpha'} - \mathrm{i} \sum_j \sum_{\alpha\alpha'} W_{j\alpha\alpha'}^* c_{\alpha'\sigma}^\dagger c_{\alpha\sigma} \\ &\overset{\alpha \leftrightarrow \alpha'}{=} -\mathrm{i} \sum_j \sum_{\alpha\alpha'} J_{j\alpha'\alpha}^* \mathbf{S}_{jd} \cdot \mathbf{s}_{\alpha'\alpha} - \mathrm{i} \sum_j \sum_{\alpha'\alpha} W_{j\alpha\alpha'}^* c_{\alpha\sigma}^\dagger c_{\alpha'\sigma} \ .\end{aligned} \tag{4.134}$$

Therefore,

$$\begin{aligned}[S^-, H_T^+] + [S^+, H_T^-] &= \sum_j \sum_{\alpha\alpha'} (-\mathrm{i} J_{j\alpha\alpha'} - \mathrm{i} J_{j\alpha'\alpha}^*) \mathbf{S}_{jd} \cdot \mathbf{s}_{\alpha\alpha'} \\ &\quad + \sum_j \sum_{\alpha\alpha'} (-\mathrm{i} W_{j\alpha\alpha'} - \mathrm{i} W_{j\alpha'\alpha}^*) c_{\alpha\sigma}^\dagger c_{\alpha'\sigma} \ ,\end{aligned} \tag{4.135}$$

where

$$
\begin{aligned}
J_{j\alpha\alpha'} &= 2t_{j\alpha}t^*_{j\alpha'}\left(\frac{1}{E_j^{(2)}-E_j^{(1)}}-\frac{1}{E_j^{(1)}-E_j^{(0)}}\right)\ , \\
J^*_{j\alpha\alpha'} &= 2t^*_{j\alpha'}t_{j\alpha}\left(\frac{1}{E_j^{(2)}-E_j^{(1)}}-\frac{1}{E_j^{(1)}-E_j^{(0)}}\right)\equiv J_{j\alpha\alpha'}\ , \\
W^*_{j\alpha'\alpha} &= W_{j\alpha\alpha'}\ .
\end{aligned}
\tag{4.136}
$$

Finally,

$$
\begin{aligned}
[S^-,H_T^+]+[S^+,H_T^-] = &-2\mathrm{i}\sum_j\sum_{\alpha\alpha'}J_{j\alpha\alpha'}\mathbf{S}_{jd}\cdot\mathbf{s}_{\alpha\alpha'} \\
&-2\mathrm{i}\sum_j\sum_{\alpha\alpha'}W_{j\alpha\alpha'}c^\dagger_{\alpha\sigma}c_{\alpha'\sigma}\ .
\end{aligned}
\tag{4.137}
$$

Therefore,

$$
\begin{aligned}
H^{(2)} &= \frac{\mathrm{i}}{2}([S^-,H_T^+]+[S^+,H_T^-]) \\
&\approx \sum_j\sum_{\alpha\alpha'}J_{j\alpha\alpha'}\mathbf{S}_{jd}\cdot\mathbf{s}_{\alpha\alpha'}+\sum_j\sum_{\alpha\alpha'}W_{j\alpha\alpha'}c^\dagger_{\alpha\sigma}c_{\alpha'\sigma}\ .
\end{aligned}
\tag{4.138}
$$

Thus, we have shown that a two-impurity Kondo Hamiltonian, Eq. (4.58), can be obtained via a Schrieffer-Wolff transformation on the effective single-lead Anderson model.

4.7 Renormalization group analysis for the asymmetrically-coupled Kondo impurities

In previous sections we demonstrated in detail that the original Anderson Hamiltonian, Eq. (4.4), can be mapped at low temperatures to an effective two-impurity Kondo model given by the Hamiltonian (Eq. (4.58)),

$$H_{2QD} = \sum_{\nu} \varepsilon_{\nu} c^{\dagger}_{\nu\sigma} c_{\nu\sigma} + J_{01}\, \mathbf{S}(\mathbf{x}_1) \cdot \mathbf{s}(\mathbf{x}_1) + J_{02}\, \mathbf{S}(\mathbf{x}_2) \cdot \mathbf{s}(\mathbf{x}_2)\ .$$

In this system, an RKKY interaction is present between the impurities, which is mediated by the conduction electrons. This implies that, after a Kondo interaction with the first impurity, the itinerant conduction electrons can travel to the second impurity and locally interact with that one, while carrying the 'information' about the spin-flip scattering at the first impurity. Such a process will lead to an RKKY-modified Kondo vertex depicted (for the first impurity as instance) in Fig. 4.9. The important point is that the RKKY-modifications of each vertex (say, for QD1) depends on the local Kondo scale of the other dot (QD2) through the local impurity susceptibility, χ_{f2}.

Having the RKKY-modified Kondo vertices for the two impurities, the RG equations for the asymmetric quantum dots can be obtained by the same procedure developed in detail in chapter 3; namely, we consider the variation in the conduction electron–impurity vertex (Kondo vertex) under the RG flow. The only difference is that in this 2-impurity case, the RG flow equations for the Kondo coulings are coupled to each other.

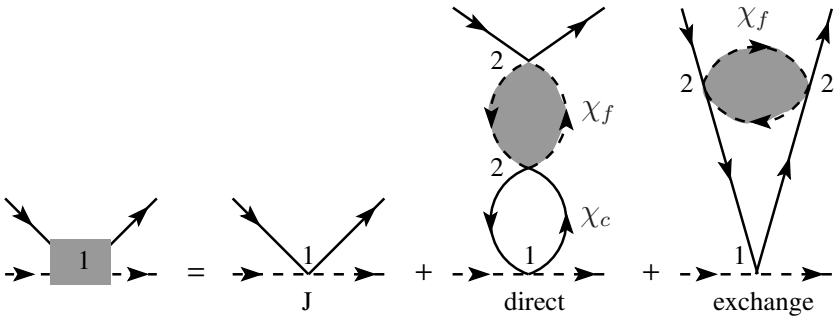

Figure 4.9: RKKY vertex corrections for the first impurity in the two-impurity Kondo system (or double quantum dot). The solid (dashed) lines represent conduction electrons (impurities). $\chi_c(\chi_f)$ is the conduction electron (impurity) susceptibility. Note that the itinerant conduction electrons can travel from one impurity to the other after an spin-flip scattering.

4.7.1 RG flow equations for the asymmetrically-coupled Kondo impurities

Using the RKKY-modified vertices for the two impurities, Fig. 4.9, in terms of the conduction-electron and local impurity susceptibilities, and following the same path as in chapter 3, the RG equations for the two Kondo couplings as a function of the reduced conduction bandwidth, D,

are obtained as

$$\frac{\partial J_1}{\partial \ln D} = -2J_1(D)^2 \left(1 - y_{12}\, J_{20}^2 \frac{D_0}{T_{K2}} \frac{1}{\sqrt{1+(\frac{D}{T_{K2}})^2}}\right) ,$$
$$\frac{\partial J_2}{\partial \ln D} = -2J_2(D)^2 \left(1 - y_{21}\, J_{10}^2 \frac{D_0}{T_{K1}} \frac{1}{\sqrt{1+(\frac{D}{T_{K1}})^2}}\right) , \tag{4.139}$$

where (as before) D_0 is the full bandwidth of the conduction electrons, J_{0i} are the bare Kondo couplings, T_{Ki} are the RKKY-modified Kondo scales (to be determined), and y is a dimensionless RKKY strength parameter,

$$\begin{aligned} y_{ij} &= -\frac{4(g\mu_B)^2}{\pi} \frac{1}{D_0 \mathcal{N}(\varepsilon_F)^3}\, A_c(\mathbf{x}_i - \mathbf{x}_j)\, \chi_c^{R\prime}(\mathbf{x}_i - \mathbf{x}_j) \quad ; \quad j \neq i \\ &= \underbrace{\text{const.}}_{>0}\, A_c(\mathbf{x}_i - \mathbf{x}_j)\, I_{\text{RKKY}}(\mathbf{x}_i - \mathbf{x}_j) \ . \end{aligned} \tag{4.140}$$

To obtain the RKKY-modified Kondo temperatures, one should integrate the RG equation for the coupling J_i up to the Kondo temperature, T_{Ki}, and use the fact that as the running energy scale, D, reaches the Kondo temperature, the Kondo coupling will diverge, indicating that RG flows to the strong-coupling fixed point corresponding to the full Kondo screening. Considering this and integrating the RG equation for J_1 up to the Kondo temperature, T_{K1}, one finds

$$\begin{aligned} \int_{J_1(D_0)}^{J(T_{K1}(y))} \frac{\mathrm{d}J_1}{-2J_1^2} &= \int_{D_0}^{T_{K1}(y)} \frac{\mathrm{d}D}{D} \left(1 - y_{12} J_{20}^2 \frac{D_0}{T_{K2}} \frac{1}{\sqrt{1+(D/T_{K2})^2}}\right) \\ \Rightarrow \frac{1}{2J_1}\Big|_{J_1(D_0)}^{J_1(T_{K1})} &= \int_{D_0/T_{K1}}^{1} \frac{\mathrm{d}\omega}{\omega} \left(1 - y_{12} J_{20}^2 \frac{D_0}{T_{K2}} \frac{1}{\sqrt{1+(\frac{T_{K1}}{T_{K2}}\omega)^2}}\right) , \end{aligned} \tag{4.141}$$

where the dimensionless variable $\omega := \frac{D}{T_{K1}}$ is introduced. The integration can be performed as

$$\begin{aligned} \int_{D_0/T_{K1}}^{1} \frac{\mathrm{d}\omega}{\omega} \frac{1}{\sqrt{1+(\omega r)^2}} &= \ln|\omega| - \ln|1 + \sqrt{1+(\omega r)^2}|\Big|_{\omega = D_0/T_{K1}}^{1} \quad ; \quad \text{with } r := T_{K1}/T_{K2} \\ &= \ln\Big|\frac{\omega}{1+\sqrt{1+(\omega r)^2}}\Big|\Big|_{\omega = D_0/T_{K1}}^{1} \\ &= \ln\Big|\frac{1}{1+\sqrt{1+r^2}}\Big| - \ln\Big|\frac{D_0/T_{K1}}{1+\sqrt{1+(\frac{D_0}{T_{K1}}r)^2}}\Big| \\ &\xrightarrow{\frac{D_0}{T_{K1}} r = \frac{D_0}{T_{K2}} \gg 1} - \ln|1+\sqrt{1+r^2}| - \ln\Big|\frac{1}{r}\Big| \\ &= \ln\Big|\frac{r}{1+\sqrt{1+r^2}}\Big| \ . \end{aligned} \tag{4.142}$$

Therefore,

$$\ln\Big|\frac{T_{K1}}{T_{K1}^0}\Big| = y_{12} J_{20}^2 \frac{D_0}{T_{K2}} \ln\Big|\frac{r}{1+\sqrt{1+r^2}}\Big| \ . \tag{4.143}$$

Remember that in the absence of the RKKY interaction, the bare Kondo couplings for the impurities (quantum dots),

$$J_{i0} \equiv J_i(D_0) \quad ; \quad i = 1, 2 \ ,$$

satisfy

$$-\frac{1}{2J_{i0}} = \ln(\frac{T^0_{Ki}}{D_0}) \quad ; \quad i = 1, 2 \ . \tag{4.144}$$

By defining the rescaled Kondo temperatures,

$$\tau_i := \frac{T_{Ki}}{T^0_{Ki}} \ , \tag{4.145}$$

and a measure of asymmetry,

$$R_K := \frac{T^0_{K1}}{T^0_{K2}} \ , \tag{4.146}$$

and integrating the RG equation for QD2 in an analogous manner, one obtains

$$\begin{aligned} \ln \tau_1 &= y_{12}\, J^2_{20}\, \frac{D_0}{T^0_{K2}} \frac{1}{\tau_2} \ln\left(\frac{R_K \tau_1/\tau_2}{1 + \sqrt{1 + (R_K \tau_1/\tau_2)^2}} \right) \\ \ln \tau_2 &= y_{21}\, J^2_{10}\, \frac{D_0}{T^0_{K1}} \frac{1}{\tau_1} \ln\left(\frac{\tau_2/(R_K \tau_1)}{1 + \sqrt{1 + (\tau_2/(R_K \tau_1))^2}} \right) \ . \end{aligned} \tag{4.147}$$

Using the logarithmic representation of the arcsinh function[21], and the fact that the RKKY strength satisfy

$$y_{ij} = y_{ji} =: y \ , \tag{4.148}$$

one can re-write the equations concisely as

$$\begin{aligned} \ln \tau_1 &= -y \frac{\gamma_2}{\tau_2} \mathrm{arcsinh}(\frac{1}{R_K} \frac{\tau_2}{\tau_1}) \ , \\ \ln \tau_2 &= -y \frac{\gamma_1}{\tau_1} \mathrm{arcsinh}(R_K \frac{\tau_1}{\tau_2}) \ , \end{aligned} \tag{4.149}$$

with the bare parametre,

$$\gamma_i := \frac{J^2_{0i}}{T^0_{Ki}} = \frac{1}{4(\ln(T^0_{Ki}/D_0))^2} \frac{1}{T^0_{Ki}/D_0} \ . \tag{4.150}$$

[21] Note that

$$\begin{aligned} &\mathrm{arcsinh}(x) \equiv \ln(x + \sqrt{1 + x^2}) \\ \Rightarrow\ &\mathrm{arcsinh}(\frac{1}{x}) \equiv \ln(\frac{1}{x} + \sqrt{1 + (\frac{1}{x})^2}) \ . \end{aligned}$$

These are coupled non-linear equations which cannot be solved analytically.

4.7.2 General properties of the solution to the equations for Kondo scales

In this section, before providing the solution to the non-linear equations, Eq. (4.149), we consider the general properties of the possible solutions. Throughout this section, we use dimensionless quantities, $T_{Ki} \equiv T_{Ki}/D_0$ and $J_i \equiv \mathcal{N}(\varepsilon_F)J_i$, to simplify the notation, and assume, without loss of generality, that $T^0_{K1} > T^0_{K2}$ or equivalently, $R_K > 1$.

i) At $y = 0$ (vanishing RKKY interaction), the solutions will be the bare Kondo temperatures, $T^0_{Ki} = \exp(-\frac{1}{2J_{0i}})$; $\quad i = 1, 2$.

ii) When $J_{01} = J_{02}$, a single solution is obtained for T_{K1} and T_{K2} which is indeed the solution for the symmetric case, as in the previous chapter (section 3.4).

iii) There is no solution set in which τ_1 or τ_2 vanishes; that is

$$\tau_1 \neq 0 \quad \text{and} \quad \tau_2 \neq 0 \quad \text{for all } y \ , \tag{4.151}$$

simply because Eq. (4.149) are *not* well-defined for $\tau_1 = 0$ or $\tau_2 = 0$. This implies that the Kondo energy scales never vanish, although they can become very small.

iv) Calculating the differentials of both sides yields

$$\frac{\delta\tau_1}{\tau_1} = -\gamma_2\,\delta y\,\delta\left(\frac{1}{\tau_2}\text{arcsinh}(\frac{1}{R_K}\frac{\tau_2}{\tau_1})\right) = -\underbrace{\frac{\gamma_2}{\tau_2}\,\text{arcsinh}(\frac{1}{R_K}\frac{\tau_2}{\tau_1})}_{>0}\,\delta y + \mathcal{O}\left((\delta y)^2\right) \tag{4.152}$$

If $\delta y > 0$, then $\delta\tau_1 < 0$ which implies that τ_1 is a *monotonically decreasing* function of y. By the same token, τ_2 is also a *monotonically decreasing* function of y.

v) The rate of decrease of $\tau_2(y)$ is greater than that of $\tau_1(y)$ as a function of y. To see this note that a Taylor expansion around $y = 0$ yields the behaviour of the solutions when the RKKY-strength is very small:

$$\tau_1 = \exp\left[-y\frac{\gamma_2}{\tau_2}\text{arcsinh}(\frac{1}{R_K}\frac{\tau_2}{\tau_1})\right] = 1 - y\,\gamma_2\,\text{arcsinh}(\frac{1}{R_K}) + \mathcal{O}(y^2) \ , \tag{4.153}$$

where we have used

$$\begin{aligned} \tau_i &= 1 + \mathcal{O}(y) \quad ; \quad i = 1, 2 \ , \\ \text{arcsinh}(1 + y) &= 1 + \frac{y}{\sqrt{2}} + \mathcal{O}(y^2) \ . \end{aligned} \tag{4.154}$$

Similarly,

$$\tau_2 = \exp\left[-y\frac{\gamma_1}{\tau_1}\text{arcsinh}(R_K\frac{\tau_1}{\tau_2})\right] = 1 - y\,\gamma_1\,\text{arcsinh}(R_K) + \mathcal{O}(y^2) \ . \tag{4.155}$$

Note that

$$\frac{\gamma_1}{\gamma_2} = \frac{J_{01}^2/T_{K1}^0}{J_{02}^2/T_{K2}^0} = \frac{J_{01}^2}{J_{02}^2}\frac{1}{R_K} = \left(\frac{\ln T_{K2}^0}{\ln T_{K1}^0}\right)^2 \frac{1}{R_K} \; ; \tag{4.156}$$

thus,

$$\frac{\gamma_1}{\gamma_2}\frac{\operatorname{arcsinh}(R_K)}{\operatorname{arcsinh}(1/R_K)} \overset{T_{K2}^0 = T_{K1}^0/R_K}{=\!=\!=} \left(\frac{\ln(T_{K1}^0/R_K)}{\ln T_{K1}^0}\right)^2 \frac{1}{R_K}\frac{\operatorname{arcsinh}(R_K)}{\operatorname{arcsinh}(1/R_K)} \; . \tag{4.157}$$

One can show that for

$$R_K > 1 \quad \text{and} \quad T_{K1}^0, T_{K2}^0 < 1 \; , \tag{4.158}$$

which is the case here, the following inequality holds true:

$$\frac{\gamma_1}{\gamma_2}\frac{\operatorname{arcsinh}(R_K)}{\operatorname{arcsinh}(1/R_K)} > 1 \; , \tag{4.159}$$

which implies that the rate of decrease of $\tau_2(y)$ is greater than that of $\tau_1(y)$ as a function of y. To prove the inequality Eq. (4.159), firstly,

$$|\ln(\frac{T_{K1}^0}{R_K})| = |\ln T_{K1}^0 - \ln R_K| \overset{R_K>1, T_{K1}^0<1}{=\!=\!=} \ln R_K - \ln T_{K1}^0 \; , \tag{4.160}$$

since $T_{K1}^0 < 1$, and $|\ln T_{K1}^0| = -\ln T_{K1}^0$. Then, because $R_K > 1 \Rightarrow \ln R_K > 0$,

$$|\ln(\frac{T_{K1}^0}{R_K})| = \ln R_K - \ln T_{K1}^0 > -\ln T_{K1}^0 = |\ln T_{K1}^0| \; . \tag{4.161}$$

Thus, one concludes that

$$\frac{|\ln(T_{K1}^0/R_K)|}{|\ln T_{K1}^0|} > 1 \; . \tag{4.162}$$

Now, consider the function

$$f(R) := \frac{1}{R}\frac{\operatorname{arcsinh}(R)}{\operatorname{arcsinh}(1/R)}$$

For $R > 1$, we observe that $f(R) > 1$; see Fig. 4.10.

Hence, for $R > 1$,

$$\begin{aligned} \left(\frac{\ln(T_{K1}^0/R)}{\ln T_{K1}^0}\right)^2 &> 1 \; , \\ f(R) = \frac{1}{R}\frac{\operatorname{arcsinh}(R)}{\operatorname{arcsinh}(1/R)} &> 1 \; , \end{aligned} \tag{4.163}$$

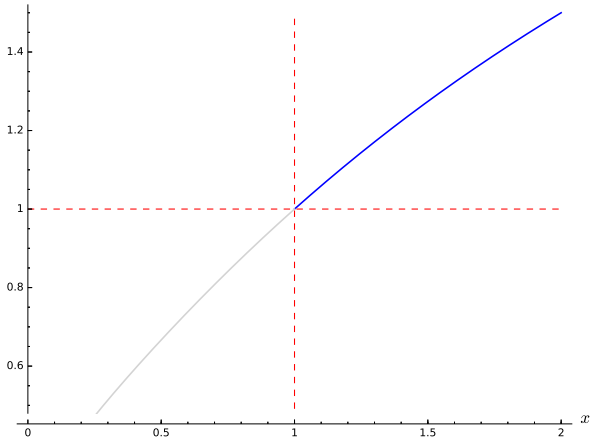

Figure 4.10: The function $f(R) = \frac{1}{R}\frac{\operatorname{arcsinh}(R)}{\operatorname{arcsinh}(1/R)}$. Note that $f(R) > 1$ for $R > 1$.

which leads to

$$\left(\frac{\ln(T_{K1}^0/R_K)}{\ln T_{K1}^0}\right)^2 \frac{1}{R_K}\frac{\operatorname{arcsinh}(R_K)}{\operatorname{arcsinh}(1/R_K)} > 1 \quad \text{for } R_K > 1 \ , \tag{4.164}$$

which is the inequality mentioned above, Eq. (4.159) .

vi) There is no non-zero value of y for which $\tau_1(y) = \tau_2(y)$, unless $T_{K1}^0 = T_{K2}^0$ or equivalently, $R_K = 1$. This implies that, in the asymmetric case, the curves for $\tau_1(y)$ and $\tau_2(y)$ do *not* coincide for $y > 0$.

Proof If for some $y > 0$, $\tau_1(y) = \tau_2(y)$, then, from the set of equations, Eq. (4.149), one deduces that

$$\begin{aligned} -y\frac{\gamma_2}{\tau_2}\operatorname{arcsinh}(\frac{1}{R_K}\frac{\tau_2}{\tau_1}) &= -y\frac{\gamma_1}{\tau_1}\operatorname{arcsinh}(R_K\frac{\tau_1}{\tau_2}) \\ \Rightarrow \gamma_2 \operatorname{arcsinh}(\frac{1}{R_K}) &= \gamma_1 \operatorname{arcsinh}(R_K) \\ \Rightarrow \frac{\gamma_1}{\gamma_2} &= \frac{\operatorname{arcsinh}(1/R_K)}{\operatorname{arcsinh}(R_K)} \ . \end{aligned} \tag{4.165}$$

Notice that $R_K \geq 1$ and $\frac{\gamma_1}{\gamma_2} \leq 1$, since $T_{K1}^0 \geq T_{K2}^0$ by assumption. If $R_K = 1$,

$$\begin{aligned} \frac{\gamma_1}{\gamma_2} &= \frac{\operatorname{arcsinh}(1)}{\operatorname{arcsinh}(1)} = 1 \\ \Rightarrow \gamma_1 = \gamma_2 &\Rightarrow T_{K1}^0 = T_{K2}^0 \ , \end{aligned} \tag{4.166}$$

which means that the bare Kondo temperatures and the Kondo couplings must be the same.

If $R_K > 1$, according to Eq. (4.165), we have to see if the following relation can be satisfied:

$$\left(\frac{\ln T^0_{K2}}{\ln T^0_{K1}}\right)^2 = R_K \frac{\operatorname{arcsinh}(1/R_K)}{\operatorname{arcsinh}(R_K)} \ . \tag{4.167}$$

Using the relation $T^0_{K2} = T^0_{K1}/R_K$, we obtain

$$\begin{aligned}
(\frac{\ln(T^0_{K1}/R_K)}{\ln T^0_{K1}})^2 &= \underbrace{R_K \frac{\operatorname{arcsinh}(1/R_K)}{\operatorname{arcsinh}(R_K)}}_{=:\alpha^2>0} \\
\Rightarrow |\frac{\ln(T^0_{K1}/R_K)}{\ln T^0_{K1}}| &= \alpha \Rightarrow |\ln(\frac{T^0_{K1}}{R_K})| = \alpha |\ln T^0_{K1}| \\
\Rightarrow |\underbrace{\ln T^0_{K1} - \ln R_K}_{<0}| &= \alpha |\ln T^0_{K1}| \overset{R_K>1, T^0_{K1}<1}{=\!=\!=} -\ln T^0_{K1} + \ln R_K = -\alpha \ln T^0_{K1} \\
\Rightarrow (1-\alpha) \ln T^0_{K1} &= \ln R_K \Rightarrow \ln T^0_{K1} = \frac{1}{1-\alpha} \ln R_K \\
\Rightarrow T^0_{K1} &= (R_K)^{\frac{1}{(1-\alpha)}} \ .
\end{aligned} \tag{4.168}$$

Since $\alpha > 0$,

$$1 - \alpha < 1 \ . \tag{4.169}$$

One can further show that $0 < \alpha < 1$ as follows:

Firstly, we note that

$$0 < \alpha < 1 \Leftrightarrow 0 < \alpha^2 < 1 \ . \tag{4.170}$$

So it suffices to prove $\alpha^2 < 1$; in other words, one should show that

$$f(R) = R \frac{\operatorname{arcsinh}(1/R)}{\operatorname{arcsinh}(R)} < 1 \quad \text{for } R > 1 \ ; \tag{4.171}$$

but this is obvious by considering the function $f(R)$ depicted in Fig. 4.11.

Therefore,

$$0 < \alpha < 1 \ . \tag{4.172}$$

From this, one concludes

$$\begin{aligned}
0 < 1 - \alpha < 1 \Rightarrow \frac{1}{1-\alpha} &> 1 \\
\Rightarrow \quad T^0_{K1} = (R_K)^{\frac{1}{1-\alpha}} &> R_K \\
\Rightarrow \quad T^0_{K1} > R_K &> 1 \ ,
\end{aligned} \tag{4.173}$$

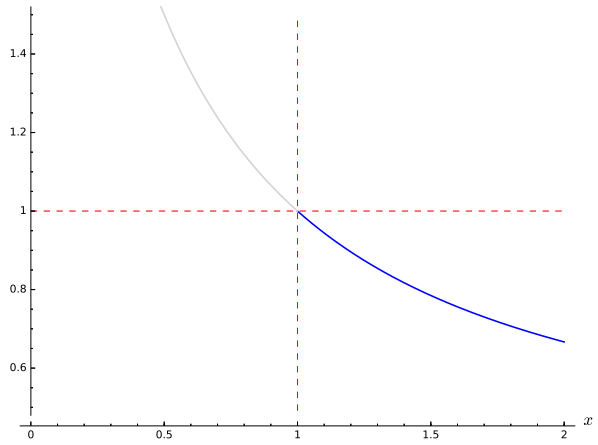

Figure 4.11: The function $f(R) = R\frac{\text{arcsinh}(1/R)}{\text{arcsinh}(R)}$. Note that $f(R) < 1$ for $R > 1$.

which is a contradiction since we know

$$T_{K1}^0 \ll 1 \ . \tag{4.174}$$

Hence, we have finally proven that when $R_K > 1$, $\tau_1(y)$ and $\tau_2(y)$ never coincide for $y > 0$.

4.7.3 Approximate solution to the equations for Kondo scales

One can find an approximate analytic solution for the strongly-asymmetric case where $R_K \gg 1$. In this case, since $\tau_1(y) \geq \tau_2(y)$ for all y, one concludes that

$$R_K \frac{\tau_1}{\tau_2} \gg 1 \ ;$$

hence using the Taylor expansion for $x \ll 1$,

$$\text{arcsinh}(x)\Big|_{x=0} = x + \mathcal{O}(x^2) \ ,$$

the equation for τ_1, Eq. (4.149), becomes

$$\ln \tau_1 \approx -y\frac{\gamma_2}{\tau_2}(\frac{1}{R_K}\frac{\tau_2}{\tau_1}) = -y\frac{\gamma_2}{R_K}\frac{1}{\tau_1} \ . \tag{4.175}$$

The equation for τ_2 will be obtained by using the asymptotic form of arcsinh for $x \gg 1$,

$$\text{arcsinh}(x)\Big|_{x\gg 1} = \ln x \ ;$$

therefore,

$$\begin{aligned} \ln \tau_2 &\approx -y\frac{\gamma_1}{\tau_1} \ \ln(R_K \frac{\tau_1}{\tau_2}) \\ \Rightarrow \ln \tau_2 &\approx \frac{y\ \gamma_1}{y\ \gamma_1 - \tau_1} \ \ln(R_K\, \tau_1) \ . \end{aligned} \tag{4.176}$$

Thus[22],

$$\begin{cases} \tau_1(y) & \approx \exp\left[-y\ \frac{\gamma_2}{R_K}\ \frac{1}{\tau_1}\right] \Rightarrow \tau_1 \approx \frac{-y\,\gamma_2/R_K}{W(-y\,\gamma_2/R_K)} \\ \tau_2(y) & \approx \exp\left[\frac{y\,\gamma_1}{y\,\gamma_1-\tau_1}\ \ln(R_K\,\tau_1)\right] \end{cases} .$$

4.7.4 "Matthew effect" in asymmetrically-coupled double quantum dots

By considering the numerical solutions to the equations for T_{Ki}, Eq. (4.149), one can observe that the essential behaviour is summarily the following: There is a strong suppression of the Kondo temperature for the 'weaker' quantum dot (the dot which has a smaller bare Kondo coupling) as the asymmetry is increased, while the stronger quantum dot remains much less affected by the inter-dot coupling via the RKKY interaction (see below). As in the symmetric case (section 3.4.4), there exists always a certain maximal value y_{max} of the RKKY strength parameter beyond which there is no solution to the equations, Eq. (4.149), indicating that the strong-coupling fixed point is absent from the RG flow and Kondo screening has broken down for *both* dots. This happens in the perturbative range of y, $0 < y \ll 1$, where a perturbative RG is reliable.

In Figs. 4.12, 4.13, 4.14, and 4.15, the rescaled Kondo temperatures, $\tau_i \equiv T_{Ki}(y)/T^0_{Ki}$, are depicted as a function of the RKKY strength parameter, y. It turns out that for a slightly-asymmetric case (Fig. 4.12, $R_K = 1.2$), both Kondo temperatures are suppressed upon increasing the RKKY interaction. However, as we slightly increase the asymmetry ratio, R_K (Fig. 4.13, $R_K = 1.5$), the Kondo temperature for the weaker dot is exponentially suppressed to very small values (close to zero). This exponential suppression is much more evident for the strongly asymmetric case (Fig. 4.14, $R_K = 10$), for which we have also provided a logarithmic plot in Fig. 4.15.

Finally, one can fix the strength of the RKKY interaction to a value away from the breakdown point ($y < y_{max}$) and consider the effect of the asymmetricity of the Kondo couplings on the Kondo temperatures (Fig. 4.16). One observes that as the asymmetry of the couplings is increased, the suppressive effect of the RKKY interaction becomes more intense for the weaker quantum dot, while the stronger quantum dot becomes lesser affected by the same strength of the RKKY interaction. This is, in fact, an instance of the "Matthew effect"[23] where "the strong becomes stronger, while the weak becomes weaker".

These results are in qualitative agreement with the experimental observations given in section 4.3. To provide a quantitative comparsion, one requires access to the detailed experimental data (hitherto, unavailable).

[22] Note that to find a solution for $\tau_1(y)$, we have used the property of the Lambert function $W(x)$ [126, 127],

$$\exp[W(x)] = \frac{x}{W(x)} .$$

[23] The term, "Matthew effect", was first coined by the sociologist Robert K. Merton [189] in the context of sociology of science, and is adopted from a verse in the *Gospel of Matthew*: "For unto every one that hath shall be given, and he shall have abundance: but from him that hath not shall be taken even that which he hath." (Matthew 25:29, King James version)

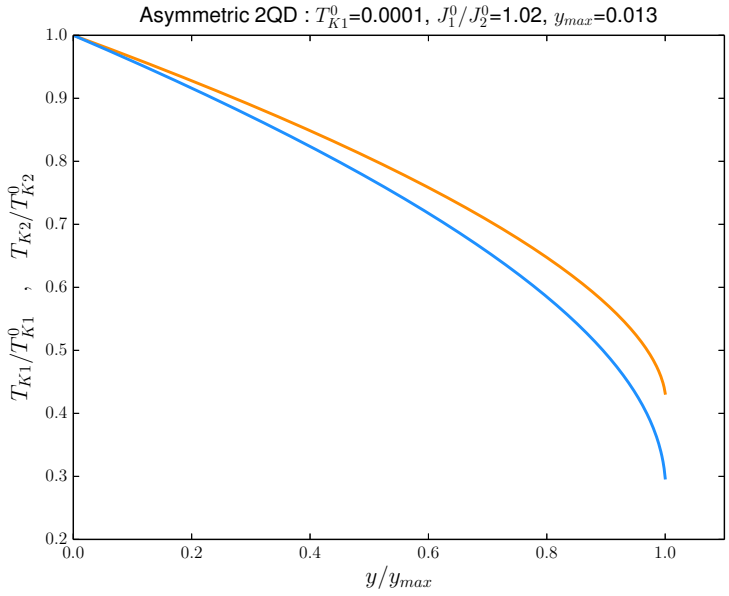

Figure 4.12: Rescaled Kondo temperatures for the two dots; $R_K = 1.2$ (slightly-asymmetric case). The orange (blue) curve belongs to the stronger (weaker) dot.

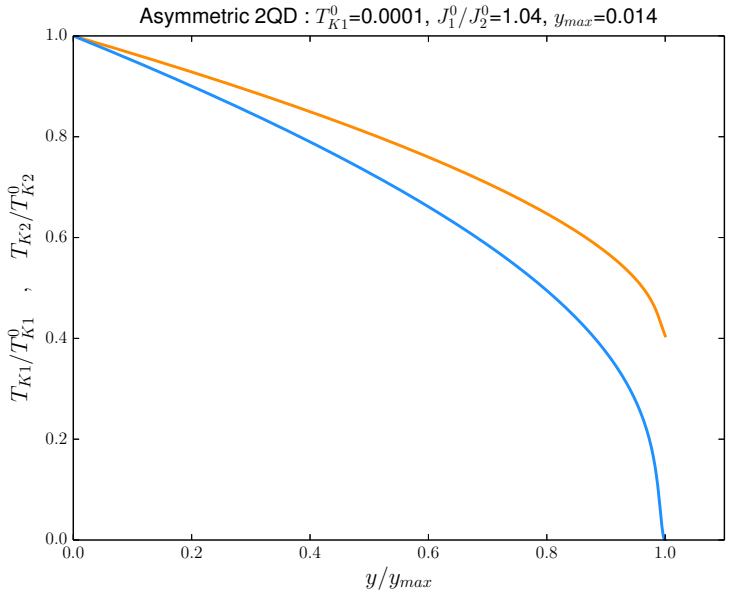

Figure 4.13: Rescaled Kondo temperatures for the two dots; $R_K = 1.5$. The orange (blue) curve belongs to the stronger (weaker) dot.

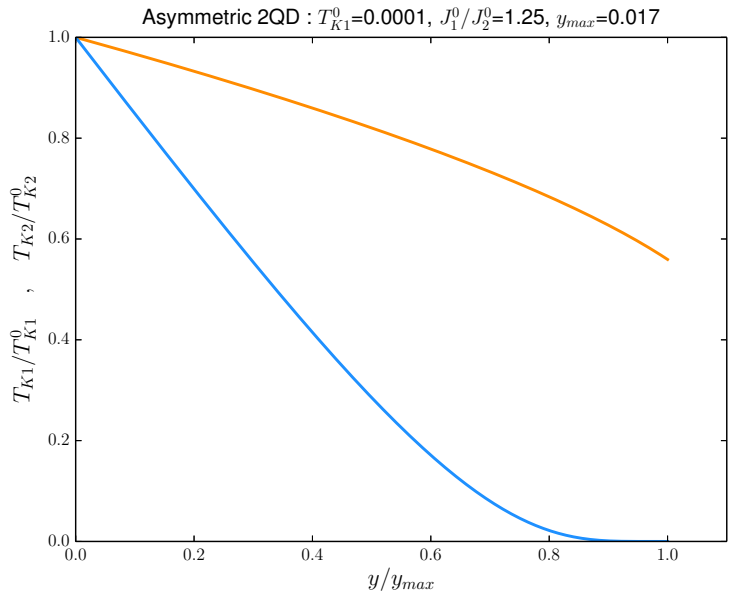

Figure 4.14: Rescaled Kondo temperatures for the two dots; $R_K = 10$ (strongly-asymmetric case). The orange (blue) curve belongs to the stronger (weaker) dot. Notice the suppression of the Kondo temperature for the weaker dot compared to the stronger dot.

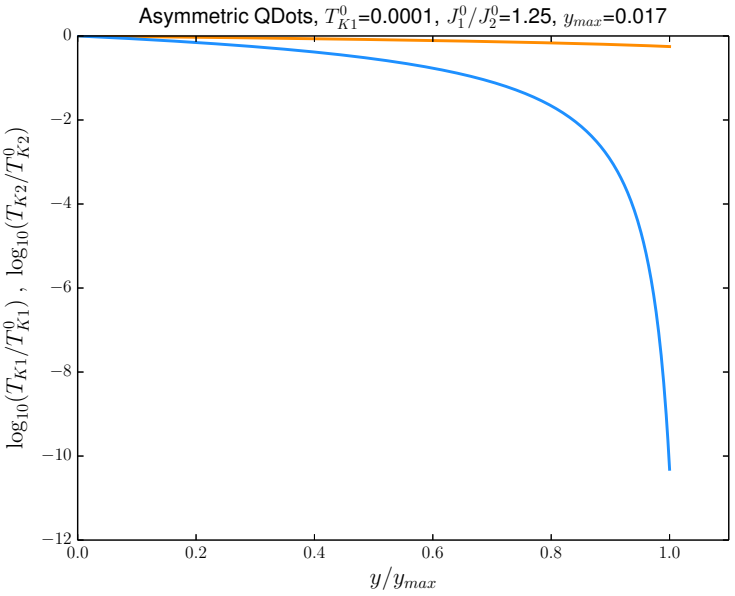

Figure 4.15: Rescaled Kondo temperatures for the two dots; $R_K = 10$ (strongly-asymmetric case). The orange (blue) curve belongs to the stronger (weaker) dot. Notice the exponential suppression of the Kondo temperature for the weaker quatum dot.

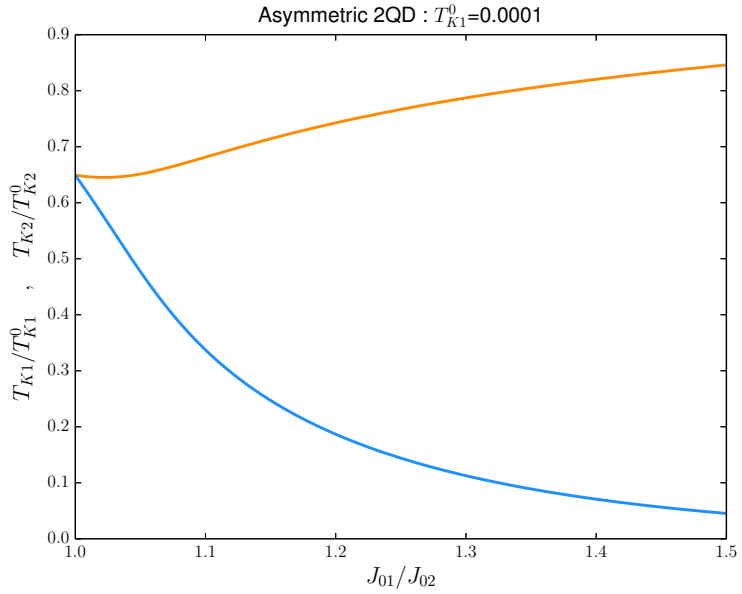

Figure 4.16: Rescaled Kondo temperatures for the two dots at a fixed RKKY interaction strength, $y = \frac{9}{10}\, y_{max}$, away from the Kondo breakdown point. The orange (blue) curve belongs to the stronger (weaker) dot. Notice that the weaker quantum dot is much more affected by the RKKY interaction as the asymmetry of the Kondo couplings is increased.

CHAPTER 5

Magnetic Instability in the Kondo Lattice

5.1 Quantum phase transitions

Many-body quantum systems can exhibit a novel type of phase transition in which the system undergoes a phase change at *zero* temperature upon varying a *non-thermal* external parameter like chemical doping, hydrostatic pressure, or an external field (e.g., magnetic field) [169, 190–193]. Upon crossing the transition point, or the quantum critical point (QCP), an ordered phase is destroyed or established solely due to *quantum* fluctuations which are rooted in the operator nature of quantum mechanics and the Heisenberg's uncertainty principle. The nature of the quantum critical state is different from the asymptotic phases on both sides, and its physical properties are expected to be universal. On the two sides of the quantum phase transition (QPT), two (or more) essentially-different states (e.g., paramagnetic against magnetic) are competing to determine the ground-state of the system. This competition leads to emergence of a continuum of excitations and 'anomalous' behaviour (e.g., nontrivial power-laws or nFLs) at the critical point. Although, the exact QPT happens at zero temperature, mere existence of a QCP affects a relatively extended part of the phase diagram around the point, with significant changes in the experimentally observable thermodynamic and transport properties.[1]

Analogous to the classical phase transitions, QPTs can also be divided into two major types according to the Ehrenfest's classification[2] : discontinuous (first-order) and continuous (higher-order) phase transitions. A first-order transition is a simple "level crossing" or a jump discontinuity in the free energy due to presence of two minima in the free energy landscape. The finite-temperature properties of the system are a thermodynamic mixture of the two phases. A more interesting situation happens with continuous QPTs where the transition between the two phases is smooth.

Quantum impurity systems (like an Anderson or a Kondo system) can exhibit different kinds of QPTs, either continuous or discontinuous [192]. In this work, we are interested only in the continuous QPTs in such systems.

For continuous QPTs, the temporal fluctuations of the critical degrees-of-freedom are of equal importance or even sometimes dominant compared to the spatial fluctuations. Due to the

[1] Of course, measurements can never be performed at exact zero temperature; the current understanding of QPT is obtained by going to very low temperatures ($\mathcal{O}$(mK)) which are accessible.

[2] In Eherenfest's classification, one considers the continuity of the nth derivative of the free energy to distinguish phase transitions. When the first derivative is singular at the transition point, the transition will be first-order or discontinuous; if higher-order derivatives are singular, the transition is continuous.

strong interactions at QCP, the emergent low-energy excitations are highly collective. The most fundamental issue in quantum criticality is the nature of such low-energy excitations near QCP.

5.1.1 Quantum criticality in heavy-fermionic systems

When a metal undergoes a continuous quantum phase transition, non-Fermi liquid behaviour arises near the critical point, which is observed in transport and thermodynamic measurements. In a clean metal, a Fermi liquid phase expresses itself with characteristic physical properties such as a quadratic temperature (T) dependence, T^2, of electrical resistivity due to the scattering of quasi-particles from each other, and a linear temperature dependence of the electronic specific heat (see section 5.1.2). Digression from such a Fermi liquid behaviour is generally denoted as "non-Fermi liquid" (nFL) behaviour. Typical nFL behaviour at QCP is a logarithmic divergence in Sommerfeld coefficient, $C/T \propto -\ln T$, and power-law dependence of electrical resistivity, T^α with $\alpha < 2$. Several quantum critical compounds even exhibit unconventional superconductivity around the QCP [194]. In such an unconventional superconductivity, spin fluctuations play a substantial role in formation of Cooper pairs.
Heavy-fermionic (HF) systems provide a proper test bed for quantum criticality of metals. HFs are usually inter-metallic compounds containing a dense periodic array of rare-earth or actinide ions (see section 5.1.2). The effective mass of charge carriers in these compounds is sometimes up to 10^3 times larger than the mass of a free electron. Such massive charge carriers are called "heavy fermions/electrons". Many HF compounds can be tuned with a non-thermal parameter like pressure, doping or an external field, so that their antiferromagnetic ordering temperature is driven continuously down to zero, leading to a QCP [14, 21, 195]. Around the QCP, at a finite temperature, nFL behaviour is observed over a wide range of the phase diagram. In some compounds, near the QCP, there is also a tendency to form a superconducting phase [194, 195].

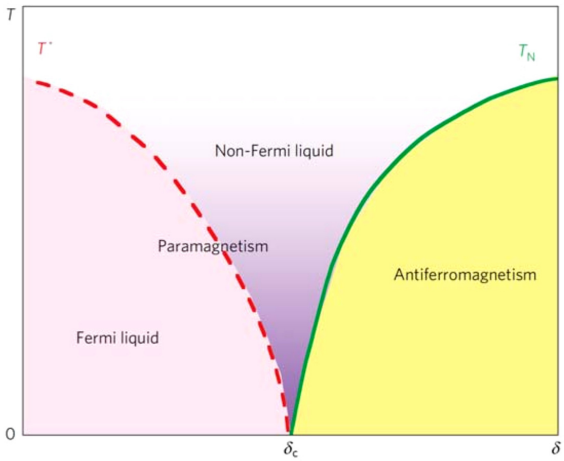

Figure 5.1: Schematic phase diagram for quantum criticality in a heavy-fermionic system (adopted from Ref. [196]).

The existence of such a QCP in HFs brings up some fundamental questions about the nature of the QPT; namely, how it happens microscopically, which degrees-of-freedom become critical and what the critical excitations are. Furthermore, since the Anderson and Kondo physics are understood to be behind the heavy-fermionic behaviour, quantum criticality of HFs points also

to the question about the fate of the heavy fermionic quasi-particles and Kondo screening; that is, whether the quasi-particles break down or the Kondo screening is destroyed.

In the following chapters we introduce the concept of fermionic quasi-particles and Fermi liquids, and afterwards, we consider the fate of such quasi-particles across a continuous QPT.

5.1.2 Landau's Fermi liquid theory and heavy quasi-particles

The theory of simple metals relies on the Bloch theorem and a non-interacting band-structure theory for the single-particle spectrum which can successfully predict the behaviour of a normal metallic state in those systems. However, the validity of such a theory can be questioned from a fundamental perspective, since there exists a strong Coulomb interaction between the electrons floating in the metal. Indeed, one can resort to Hartree–Fock or RPA approximation to account for the effect of the interaction when the share of the Coulomb interaction in total energy of the system is relatively smaller than that of the kinetic energy. Based on this nontrivial assumption, one can take a perturbative approach to the interacting electronic systems. This is the heart of the Landau's theory of interacting fermionic liquids.

Landau's theory of Fermi liquid (originally aimed at describing ^{3}He) [197–199] provides an economic description of the low-energy excitations of an interacting system of electrons as a weakly interacting gas of quasi-particles with fermionic character. The main reason for the success of this approximation is the Pauli principle and the spontaneous screening of the Coulomb interaction. A fundamental assumption is the 'adiabatic continuity', meaning that if we start from the ground-state of the non-interacting fermionic system and switch on the interaction strength very slowly ('adiabatically'), then the ground-state of the interacting system will be reached after sufficient time. Validity of this assumption is vital for the applicability of perturbation theory (Gell-Mann–Low theorem [119, 200]). It is further assumed that there is a one-to-one correspondence between the states of the non-interacting system and those of the interacting one. In this way, the quantum numbers of the non-interacting system will be still 'good' quantum numbers to label the states of the interacting system.

If the interaction is amenable to a perturbative treatment, then Luttinger theorem states that, even in presence of the interaction, the Fermi surface survives (although the discontinuity of the occupation number at the Fermi level is reduced), and the 'volume' enclosed by the Fermi surface remains the same as that of the non-interacting system [201].

The properties of the quasi-particles (like the effective mass) are renormalized by the interaction since they are 'dressed' by a 'cloud' of electron-hole pairs. Such a quasi-particle picture is useful only when the life-time of the quasi-particle states is long enough. This leads to the restriction of the Fermi liquid picture to low temperatures and near the Fermi surface.

At low energies compared to the Fermi energy, when the number of the excited fermionic quasi-particles is small, the weakly-interacting quasi-particle gas can be described by a free energy which depends on the number of excited quasi-particles. From this free energy, one can obtain the thermodynamic properties of the system; transport equations can also be obtained via a semi-classical Boltzmann approach. In this way, the physical properties of a Fermi liquid can be derived in terms of a set of parameters known as 'Fermi-liquid parameters' or 'Landau parameters' to be determined experimentally. For example, the heat capacity per unit volume of the Fermi liquid is given by a linear temperature-dependence [202],

$$c_V(T) = \frac{\pi^2}{3}\mathcal{N}(\varepsilon_F)\,T\ , \tag{5.1}$$

where $\mathcal{N}(\varepsilon_F)$ is the density-of-states of quasi-particles, which is itself proportional to their effective mass — this provides also an experimental way to determine the effective mass. The magnetic susceptibility of a Fermi liquid is given by a weakly temperature-dependent relation [202],

$$\chi = \frac{1}{2}(g\mu_B)^2\,\mathcal{N}(\varepsilon_F)\frac{1}{1+F_0^a}\ , \tag{5.2}$$

where F_0^a is a Landau parameter that is negative for a repulsive interaction between quasi-particles of opposite spin. Therefore, the factor $1/(1+F_0^a)$ leads to an enhancement of the susceptibility (like the Stoner factor [92, 123]). This also yields a stability criterion, since the Fermi liquid is stable as long as $1+F_0^a > 0$. When the denominator vanishes, the interaction between the fermions of opposite spin paves the way for a magnetic ordering. The general stability conditions for a Fermi liquid are given in terms of the Landau parameters as [203]

$$F_l^a > -(2l+1) \quad , \quad F_l^s > -(2l+1) \quad , \ l = 0, 1, \cdots\ , \tag{5.3}$$

which correspond to a positive effective mass, a positive magnetic susceptibility and a positive compressibility. A violation of these conditions lead to "Pomeranchuk instabilities" and a continuous or discontinuous transition into a new phase [204].
It should be emphasized that Landau's theory of fermionic liquids is a phenomenological theory. The microscopic justification for the theory and its region of validity can provided with the methods of quantum many-body theory [199].
As stated before, Landau's theory has been successful in describing the low-energy properties of most normal metals. Yet, a crucial and valid question is about the extent that this picture persists in real systems. When the energy scales of the bandwidth and the Coulomb potential are comparable, one can no longer neglect the interaction and the electronic correlations produced by it; namely, the independent (or weakly-interacting) single-particle picture breaks down. Indeed, one often encounters physical systems in which the Landau's theory does not apply since the ground-state and the excitations of the interacting system are utterly different from the non-interacting ones. So, there is no adiabatic continuity between the two (interacting and non-interacting) ground-states. In fact, by introducing the interaction, the spectral weight of the quasi-particles is gradually lost to the 'incoherent' part of the spectrum, so that at some point, the quasi-particle picture breaks downs with the vanishing of the spectral weight. The simplest instance of this can be found in superconductors, or magnetically-ordered electronic systems. This scenario is particularly true in the inter-metallic compounds which include lanthanide (rare-earth) ions with localized $4f$ orbitals or actinides with incomplete $5f$ shells.
Heavy-fermion systems are inter-metallic compounds containing a dense periodic array of rare-earth (such as Ce) or actinide ions (such as U). Due to the spatial localization of the $4f$ and $5f$ orbitals, there can be hardly an overlap between nearest neighbors, and it is the intra-atomic Coulomb interaction that plays the central role in the behaviour of such systems. The mixing of these f orbitals with the s and p orbitals of conduction electrons, provides the possibility

of formation of delocalized bands which are mixtures of $s-p$ and f orbitals. This leads to a novel type of behaviour and appearance of heavy quasi-particles. The essential physics of these systems can be described by Anderson or Kondo lattice models, where the ions containing the localized orbitals (the 'impurities') are arranged as a regular lattice (see section 5.3).

Heavy-fermion systems provide an astounding stance of Fermi liquid picture persisting despite considerable interactions and strong correlations. The cost is, of course, more complicated quasi-particles living at the brink of destruction [205–209]. Deviations from the Fermi liquid theory predictions are generally called non-Fermi liquid (nFL) behavior and manifest themselves as, e.g., a logarithmic temperature dependence ($\ln(T)$) in the specific heat over T, C/T, a low-temperature singularity of the susceptibility, and a power-law temperature-dependence of resistivity which is different from T^2 [203].

Heavy-fermion compounds can have various phases: a paramagnetic (heavy) Fermi liquid phase, antiferromagnetic or ferromagnetic long-range order, superconductivity and other exotic states such as "hidden" order in URu_2Si_2 [194].

The first instances of HFs were found in 1980s [194], attracting the attention of the researchers due to their unconventional superconductivity. The major finding was that these materials showed a Fermi liquid behaviour (e.g., low-temperature specific heat being linear in temperature) but with an effective electronic mass much higher (even 10^3 times) than simple metals (hence the name). Since many Fermi liquid properties (like susceptibility or specific heat) are related to the density-of-states at the Fermi level, such relatively high values for the coefficients (like the coefficient of specific heat) could be explained with an extremely large density-of-states at the Fermi level. Another important property of these materials was Curie-like susceptibility at high temperatures which indicated the presence of unquenched localized magnetic moments. However, these magnetic moments seemingly disappeared at low enough temperatures with emergence of a temperature-independent Pauli susceptibility. This was the clue to a theoretical description of HF systems by a Kondo screening mechanism. Hence, thermodynamic properties of HF compounds is expected to have similarities to Kondo impurities; more importantly, they should have a characteristic energy scale, the Kondo temperature T_K — which indeed differs from the single-impurity case. However, this is not the only energy scale in the HFs systems, since several other effects are apparently present in these systems. For example, there is a 'lattice coherence' temperature, T_{coh}, defined as the temperature below which Fermi liquid behaviour appears in the physical properties, like resistivity. Usually, this temperature is below T_K and the ratio between T_{coh} and T_K is non-universal [195, 210] (cf. [211]).

Examples of HF compounds are $CeAl_3$, $CeCu_6$, $CeCu_2Si_2$, $YbRh_2Si_2$, UPt_3 , and UBe_{13}. The Fermi liquid behaviour is exhibited also in the Wilson ratio defined as [202],

$$R_W = \frac{\chi}{\gamma} \frac{\pi^2}{(g_J \mu_B)^2 \, J(J+1)} \ , \tag{5.4}$$

where g_J is the Landé factor and J is the total angular momentum of the ions, or in comparing the Sommerfeld coefficient γ of the linear term in the specific heat with the coefficient A of the T^2 term of the resistivity ($\rho = \rho_0 + A\,T^2$). For a Fermi liquid, the specific heat is proportional to the effective mass m^*, while $A \propto (m^*)^2$, and hence, the ratio A/γ has to be universal [202]. This is the Kadowaki-Woods relation,

$$R_{KW} = A/\gamma^2 \approx \text{const.} \,, \tag{5.5}$$

which is satisfied for a large number of HF systems at low temperatures [14].
The presence of localized magnetic moments in HFs provides the possibility of magnetic (usually antiferromagnetic) ordering at low temperatures. Furthermore, as a surprise, some of these materials become superconducting at low temperatures. Since the superconductivity neighbors magnetically ordered phase, it is postulated that the magnetic fluctuations are the origin of such an unconventional superconductivity.

5.1.2.1 Cerium (Ce) and Ytterbium (Yb) compounds

HF compounds based on Ce and Yb are among the most studied HF systems. Here we briefly summarize their behaviour near and across their quantum phase transition (for details, consult Refs. [194, 195]).

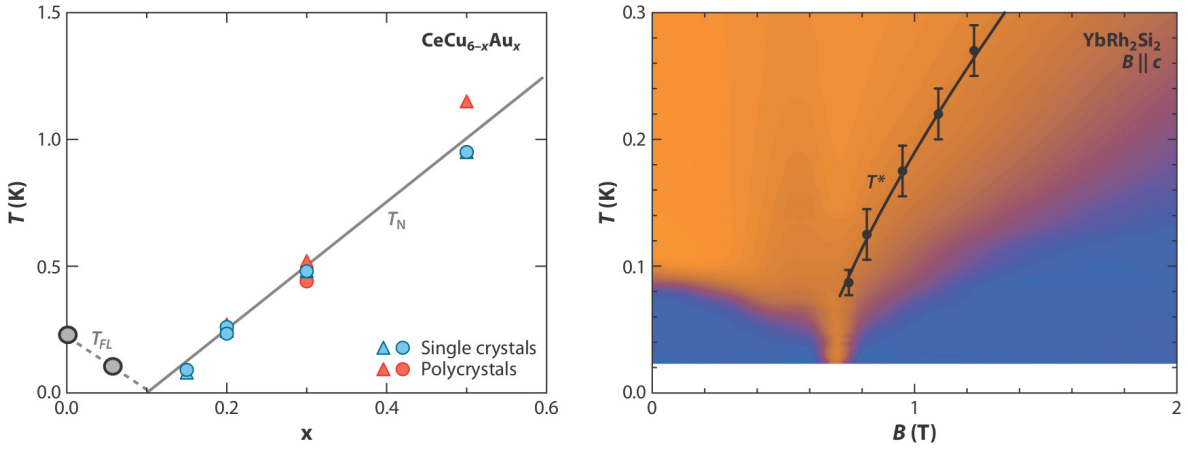

Figure 5.2: Magnetic quantum phase transitions in (a) $CeCu_{6-x}Au_x$ and (b) $YbRh_2Si_2$ as instances of heavy-fermionic systems (adopted from Ref. [194]). Left: Linear variation of the Néel temperature, T_N, with Au concentration x in $CeCu_{6-x}Au_x$, above the quantum critical point at $x = x_c \approx 0.1$. For $x < x_c$, Fermi liquid behavior is found below T_{FL}. Right: Magnetic-field driven quantum criticality in $YbRh_2Si_2$. Blue color denotes the Fermi liquid behavior observed in electrical resistivity ($\Delta R \propto T^2$), the orange color marks the non-Fermi liquid behavior with a resistivity linear in temperature, T. The data points and the solid line indicate the T^*-line, which marks the crossover regime where the Kondo effect breaks down.

Ce^{3+} of total angular momentum $j = 5/2$ and Yb^{3+} of $j = 7/2$ are Kramers ions[3]in which crystalline electric fields have a significant role. For a crystal-field splitting much larger than T_K, the situation reduces to that of an $S = 1/2$ Kondo model. However, in general, the degeneracy of the angular momentum multiplets needs to be taken into account. For Yb^{3+}, one has to consider holes in the f-shell instead of electrons [203].

[3] Kramers degeneracy theorem states that in a time-reversal-invariant system with an *odd* number of fermions, all the energy levels must be doubly degenerate; that is, for an eigenstate $\psi_{n\mathbf{k}\sigma}$ of the Hamiltonian, there must be another time-reversed state, $\psi^*_{n,-\mathbf{k},-\sigma} \equiv \mathcal{T}\psi_{n\mathbf{k}\sigma}$ which has the same energy ($\mathcal{T}$ is the time-reversal operator). This holds true especially for a 'Kramers ion', an ion with an odd number of electrons (hence, a half-integral spin) [117].

The energy scale for the singlet formation, T_K, sets the scale below which a coherent Fermi liquid (Kondo liquid) is formed which is signaled by a maximum in electrical resistivity. The lattice Kondo scale (sometimes denoted by T^*) differs indeed from the single-ion Kondo temperature in dilute magnetic alloys, due to presence of a lattice. The Kondo temperature is experimentally determined via fitting the specific heat or magnetic susceptibility to the known single-impurity results. Typically, $T_K \sim$ 10–100 K, which is much smaller compared to the Fermi temperature, $T_F \sim 10^4 - 10^5$ K. At sufficiently low temperatures, $T \ll T_K$, deep inside the Fermi liquid regime, a large effective mass m^* for charge carriers is obtained from the huge linear specific-heat coefficient $\gamma = C/T$ and a large Pauli susceptibility, both being weakly dependent on the temperature.

The parent compound, $CeCu_6$, is a prototypical HF system with a Kondo temperature $T_K \approx 6$ K. Magnetic ordering happens around 5 mK. Inelastic neutron scattering reveals antiferromagnetic fluctuations in the dynamic structure factor with a peak with large width corresponding to correlation lengths extending only to the nearest Ce neighbors. Alloying the $CeCu_6$ with Au into $CeCu_{6-x}Au_x$ leads to an expansion of the lattice and a decrease in hybridization between Ce $4f$-electrons and the itinerant conduction electrons. Finally, at a critical Au concentration, $x_c \approx 0.1$, an incommensurate antiferromagnetic order sets in. For $0.1 \leq x \leq 1.0$, the Néel temperature T_N varies linearly with x. Beyond $x = 1.0$, T_N decreases due to a change in lattice structure. For $x = x_c$, nFL behaviour is observed as a logarithmic divergence in the coefficient of the specific heat $C/T \propto \ln(T_0/T)$ over a broad range of temperature. No magnetic ordering is observed at $x = x_c$ (with the detection limit being $\mu < 10^{-3}\mu_B$). A temperature scale $T_{1/2}$ is defined as the temperature where the entropy[4] reaches $\frac{1}{2}R\ln(2)$ per Ce atom, where R is the ideal gas constant.[5] This is used as a measure of the Kondo temperature below which the moments are screened. This temperature scale decreases when approaching critical point, but does *not* vanish at that point, $x = x_c$. Neutron scattering experiments on this compound shows that a fractional exponent ($\alpha < 1$) appears in the frequency and temperature dependence of the dynamical spin susceptibility at generic wave-vectors, over essentially the entire Brillouin zone [212]. Moreover, the dynamical spin susceptibility exhibits ω/T scaling [212].

The formation of the heavy quasi-particles in $CeCu_{6-x}Au_x$ and their breakdown at the QCP have been also investigated by ultraviolet and X-ray photo-emission spectroscopy at temperatures $T \geq 15K \gg T_K$, above the lattice coherence temperature [124, 213, 214]. The results show that the single-ion Kondo temperature T_K decreases sharply for higher Au concentrations, giving a direct high-temperature indication for a potential breakup of the heavy quasi-particles at the QCP.

It is possible also to produce a quantum criticality in $CeCu_{6-x}Au_x$ by applying either hydrostatic pressure or magnetic field [215]. In fact, hydrostatic pressure opposes the effect of Au doping by reducing the volume of the unit cell. Hence, under pressure, for $x > x_c$, the Néel temperature is successively driven to zero, leading to a QCP.

$YbRh_2Si_2$ was the first Yb compound which showed a pronounced nFL behaviour, at low temperatures, near the magnetic ordering transition. At high temperatures, $T > 200$ K, an anisotropic Curie-Weiss susceptibility is observed with $\mu_{eff} = 4.5\ \mu_B$ per Yb atom. Well above the magnetic ordering temperature, specific heat shows a logarithmic divergence $C/T \propto \ln(T_0/T)$. The electrical resistivity shows a linear temperature dependence, and coefficient of T^2-dependence of the resistivity appear to diverge, suggesting a divergence of the quasi-particle effective mass,

[4] Entropy is obtained by integrating the specific heat data over temperature.
[5] Note that $R\ln(2)$ corresponds to the entropy of a free spin-1/2 moment.

and breakdown of the Fermi liquid picture. Unfortunately, so far, elastic or inelastic neutron-scattering data have not been provided in order to identify the nature of the critical magnetic fluctuations beyond controversy.
For $YbRh_2Si_{2-x}Ge_x$, the specific heat coefficient develops a $1/T^{1/3}$ divergence at low temperatures [14]. Near the QCP, a pronounced non-Fermi liquid behaviour is observed, and the linear coefficient of the specific heat and the quadratic coefficient of the resistivity appear to diverge [216, 217], suggesting a divergence of the quasi-particle effective mass, and breakdown of the Fermi liquid picture.
A key characteristic of both $CeCu_{5.9}Au_{0.1}$ and $YbRh_2Si_2$ is a drastic enhancement of the effective charge-carrier mass at the QCP; that is, the coefficient of the T-linear electronic specific-heat (Sommerfeld coefficient) shows a logarithmic divergence. This diverging effective mass is associated with the destruction of Kondo quasi-particles due to vanishing quasi-particle weight everywhere on the Fermi surface.
The Hall effect and de Haas-van Alphen (dHvA) measurements in these HFs, suggest a sudden change of the Fermi surface at the QCP (a collapse of the large Fermi surface into a small one), as if a large number of charge carriers of the non-magnetic phase are suddenly lost as the system enters QCP [218].

5.1.3 Doniach's picture of heavy-fermionic systems

Doniach's picture [66] has provided the essential ingredients to describe the physics of HF systems. He considered the competition of the Kondo effect and the RKKY interaction [48, 62–65] to explain the appearance of the antiferromagnetic and Kondo liquid phases in these compounds. This picture is essentially based on a comparison of energy scales corresponding to the Kondo singlet formation, $T_K/D_0 \sim \exp[-\frac{1}{\mathcal{N}(\varepsilon_F)J_0}]$, and antiferromagnetic ordering via the RKKY interaction, $J_{\mathrm{RKKY}} \sim \mathcal{N}(\varepsilon_F)J_0^2$. For a small exchange coupling, the RKKY interaction dominates and an antiferromagnetic ground-state is preferred below the ordering temperature, T_c; above the transition temperature, the system is in a paramagnetic phase with local moments. With increasing the exchange coupling J, the Kondo screening becomes stronger, eventually winning over the RKKY interaction, and the system enters the Kondo liquid (or 'local' Fermi liquid) regime; at temperatures higher than T_{coh}, the system is a paramagnet with local moments. In between the two phases, when the two energy scales are comparable, there is a QCP, around which a cross-over to nFL behaviour is expected. The exchange interaction can be tuned by applying pressure, or chemical doping or by application of a magnetic field.[6]
Such a magnetically-tuned quantum criticality (QC) is observed for $YbRh_2Si_2$ [217][7], pressure-induced QC is found for $CeIn_3$ and $CePd_2Si_2$ [221], and QC by chemical doping is induced, e.g., for $YbRh_2Ge_xSi_{2-x}$ ($x \approx 0.05$) [220], and $CeCu_{2-x}Au_x$ ($x \approx 0.1$) [205][8].
Although Doniach phase diagram indicates the general mechanisms and the competing effects in HFs, it does not provide a clue for how the transition actually happens. There are several

[6] For Ce and Yb systems, alloying is changes the hybridization matrix element (and sometimes the density of conduction electrons), while hydrostatic pressure increases (decreases) the hybridization in Ce (Yb) compounds [203].

[7] YbRh2Si2 orders antiferromagnetically at $T_N = 70$ mK [219]. The antiferromagnetic order is driven to $T_N \approx 0$ by magnetic fields or alternatively via chemical pressure by replacing 5% of Si by Ge [220].

[8] The parent compound, $CeCu_6$, is susceptible to magnetic long-range order if tuned via chemical pressure. $CeCu_{6-x}M_x$ orders magnetically for M = Au if $x \geq x_c = 0.1$. The Néel temperature T_N decreases with hydrostatic pressure, so that quantum criticality can also be pressure-tuned for $x > x_c$. The compound $CeCu_{5.8}Au_{0.2}$ has also been pressure-tuned and magnetic-field tuned to a QCP [195, 222].

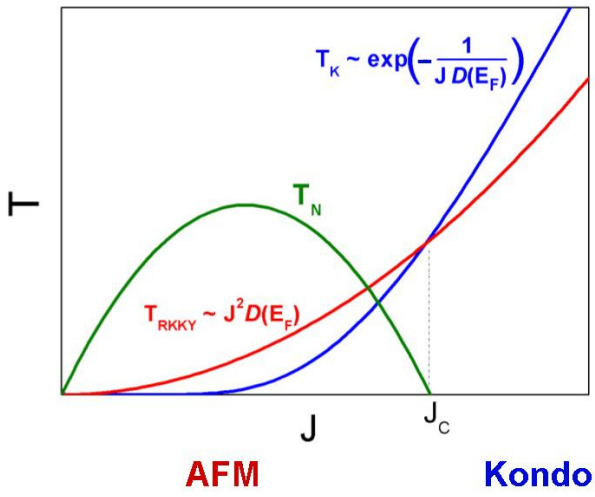

Figure 5.3: Doniach's phase diagram illustrating a qualitative scenario for quantum criticality in heavy-fermionic systems. The antiferromagnetic regime extends where $T_K < T_{\mathrm{RKKY}}$ and the heavy-fermionic regime begins when $T_K > T_{\mathrm{RKKY}}$. Since the nature of the two asymptotic phases are different, a quantum critical point is expected in between the two phases (at $J = J_c$).

theories which aim at describing the nature of the quantum criticality in heavy fermions.

5.1.4 Fate of the fermionic quasi-particles

To describe the microscopic origins of the QPTs and the nature of the quantum criticality, several approaches have been proposed, each of which can account for a certain aspect of the criticality and matches the experimental observations for a certain material. In this section, we briefly overview the main scenarios for QC in HF systems. For an overview of other scenarios, consult Refs. [14, 203].

Very broadly, two distinct major scenarios can occur for the QPT in HFs. In the first scenario, a spin density wave (SDW) instability can occur in the parent heavy Fermi liquid leading to a magnetic ordering, while the Kondo screening of local moments is left (almost) intact; the (delocalized) local moments contribute to a Fermi sea with a 'large' Fermi surface. The Kondo temperature does not change considerably across the QCP. This is called a "SDW metal" [195]. A second major scenario involves a drastic change in the Fermi surface due to the suppression and/or breakdown of Kondo screening and heavy quasi-particles due to magnetic fluctuations. The local moments do not participate in the Fermi sea which leads to a sharp change of the 'large' Fermi surface to a 'small' one (composed solely of Bloch electrons); the moments can order due to a long-range RKKY interaction mediated by the itinerant conduction electrons. The Kondo temperature is considerably reduced and might vanish at QCP. This is called a "local-moment magnetic metal" [195]. Therefore, there exist additional quantum critical degrees-of-freedom corresponding to the Kondo effect. In the latter scenario, it is also possible that the breakdown of Kondo screening does *not* coincide with the formation of long-range magnetic ordering, separated with an 'exotic' phase in between.

5.2 Scenarios for quantum criticality in heavy-fermionic systems

5.2.1 Hertz-Millis-Moriya scenario or spin density wave criticality

The Hertz-Millis quantum renormalization group analysis and Moriya's self-consistent renormalization (SCR) theory of spin-fluctuations [223] are the pioneering theoretical descriptions of QC in metallic compounds and their nFL behaviour at QCP. This Hertz-Millis (HM) theory assumes that the only critical degrees-of-freedom are long-wavelength fluctuations of the order parameter (spin density) [223–225]. For a magnetic QCP, such long-wavelength fluctuations are usually called "paramagnons", or spin-density waves in the parent Fermi liquid. The HM theory is based on the classical theory of finite-temperature phase transitions à la Landau, Ginzburg and Wilson. The Ginzburg-Landau action is then written purely in terms of the frequency-dependent spin density (magnetization) at wave-vectors close to the ordering wave-vector. The fermionic degrees-of-freedom of the parent Fermi liquid are integrated out; therefore, they act as a bath with fixed properties. The resulting action is finally purely bosonic representing over-damped spin waves,

$$\begin{aligned} S[\phi] &= S_2 + S_4 + \cdots \ , \\ S_2 &= \frac{1}{\beta V} \sum_{\mathbf{k},\mathrm{i}\omega} \epsilon_0 \left(\delta_0 + \xi_0^2 k^2 + \frac{|\omega|}{\gamma k} \right) \phi(\mathbf{k},\omega) \cdot \phi(-\mathbf{k},-\omega) \ , \\ S_4 &= u_0 \int \mathrm{d}\tau \int \mathrm{d}^d x |\phi(x,\tau)|^4 \ , \end{aligned} \tag{5.6}$$

where ϵ_0, δ_0, ξ_0 are model dependent parameters, and u_0 is the strength of the quartic interaction between density modes (simplified to a constant). The term $|\omega|/\gamma(k)$ accounts for the damping of the spin density modes by the Landau damping process via particle-hole excitations. Notice that the coefficient of ϕ^2 in S_2 is essentially the inverse of the dynamical susceptibility of the electrons which appears due to elimination of fermionic degrees-of-freedom by 'integrating them out'. The damping term is therefore derived upon an assumption of Fermi-liquid behaviour which can be justified only *a posteriori*. Obviously, such a form of the action does not apply in the magnetically-ordered phase (a detailed discussion is provided in Ref. [195, 226]).

In this way, the standard ϕ^4 theory for a classical phase transition is extended by including the quantum fluctuations of the order parameter in time direction. The correlation time, τ, is related to the correlation length, ξ, as $\tau \propto \xi^z$, where z is the 'dynamical exponent'. For a 3-dimensional antiferromagnetic metal, for instance, $z = 2$. These temporal fluctuations effectively add an extra z dimensions to the system, so that the effective dimensionality of the system becomes $d_{\mathit{eff}} = d + z$ instead of d spatial dimensions. In many cases of interest, this effective dimensionality d_{eff} is above the upper critical dimension, so that the fluctuations are essentially non-interacting and the fixed point corresponds to a Gaussian or quadratic action with parameters renormalized by the interactions in the original (bare) action.

An itinerant antiferromagnet is microscopically described in terms of a spontaneous spatial modulation of the spins of the charge carriers, or a spin-density wave, and quantum criticality is therefore, a spin-density-wave QCP.

Some important consequences follow from the Hertz-Millis-Moriya scenario: First, the dynamical spin susceptibility at generic wave-vectors (wave-vectors far or even close to the antiferromagnetic ordering wave-vector), has the usual Fermi-liquid form; i.e., it is linear in frequency and second,

the so-called ω/T scaling is violated [212]. The spin-density wave which arises from this scenario has a large Fermi surface [227]. Furthermore, the vanishing of quasi-particle spectral weight occurs only near the 'hot spots', the portions of the Fermi surface that are connected by the antiferromagnetic wave-vector. For a 3-dimensional spin-density-wave QCP, the Fermi-surface-averaged effective mass remains finite [218].
This scenario predicts that, in a three-dimensional metal, the quantum spin density wave fluctuations give rise to a weak $\sqrt{T}$ singularity in the low-temperature behavior of the specific heat coefficient [14].
Examples of such behavior is observed in $CeNi_2Ge_2$, chemically doped $Ce_{2-x}La_xRu_2Si_2$ and 'A'-type antiferromagnetic phases of $CeCu_2Si_2$ at a pressure-tuned QCP [14].
While this scenario provides a good description for some metallic and non-metallic systems, for certain metallic systems experimental observations cast strong doubts on the validity or adequacy of this scenario, and raise the possibility that the QPT includes suppression of the Kondo effect and destruction of Kondo singlets, and emergence of a (weak) magnetic metallic state where the local moments do *not* participate in the Fermi surface. Such a behavior occurs, for instance, in the chemically tuned QCP in $CeCu_{6-x}Au_x$ [205, 228–230], $YbRh_2Si_{2-x}Ge_x$ [220, 231] and the field-tuned QCP of $YbRh_2Si_2$ [217].

5.2.2 Local quantum criticality

Experimental studies indicate that in a compound such as $CeCu_{6-x}Au_x$, the scale-invariant component of the dynamical spin susceptibility appears to be a *momentum-independent* anomalous power-law, suggesting that the critical behavior involves 'local' degrees-of-freedom [229, 230]. Such an observation has led to the introduction of a 'local' scenario of quantum criticality which includes the critical breakdown of the Kondo effect in a lattice due to magnetic fluctuations. The theory has been developed by Smith, Si, Rabello, and Ingersent [212, 232, 233].
In this theory, the Kondo lattice model, Eq. (5.7), is used as the microscopic model in which a local moment at each lattice site interacts via an exchange coupling J_K with the spin of a conduction electron at the same site. An average occupancy of less than one conduction electron per lattice site is assumed to restrict all phases to be metallic.

$$H_{KLM} = \sum_{ij,\sigma} t_{ij} c^\dagger_{i\sigma} c_{j\sigma} + \sum_i J_K \mathbf{S}_i \cdot \mathbf{s}_i + \sum_{ij} I_{ij} \mathbf{S}_i \cdot \mathbf{S}_j \ . \tag{5.7}$$

The applied method is the 'extended dynamical mean-field theory' (EDMFT). As in the standard dynamical mean-field theory [234, 235], the correlation functions of the lattice problem in the EDMFT are calculated via mapping the lattice problem to an effective single-impurity Kondo problem in which the local moment is coupled to *two* dissipative baths (compared to a single fermionic bath in the standard DMFT): A fermionic bath which accounts for all temporal fluctuations arising from hopping of electrons between the local site and the rest of the lattice, and a bosonic bath represents the fluctuating magnetic field generated by the local moments at all other sites [212]:

$$H_{loc} = J_K \, \mathbf{S} \cdot \mathbf{s} + \sum_{\mathbf{k}\sigma} \varepsilon_{\mathbf{k}} \, c^\dagger_{\mathbf{k}\sigma} c_{\mathbf{k}\sigma} + g \sum_{\mathbf{k}} \mathbf{S} \cdot (\phi_{\mathbf{k}} + \phi^\dagger_{-\mathbf{k}}) + \sum_{\mathbf{k}} w_{\mathbf{k}} \, \phi^\dagger_{\mathbf{k}} \phi_{\mathbf{k}} \ , \tag{5.8}$$

where $c_{\mathbf{k}\sigma}$ amd $\phi_{\mathbf{k}}$ denote the fermionic and bosonic dissipative baths, respectively.

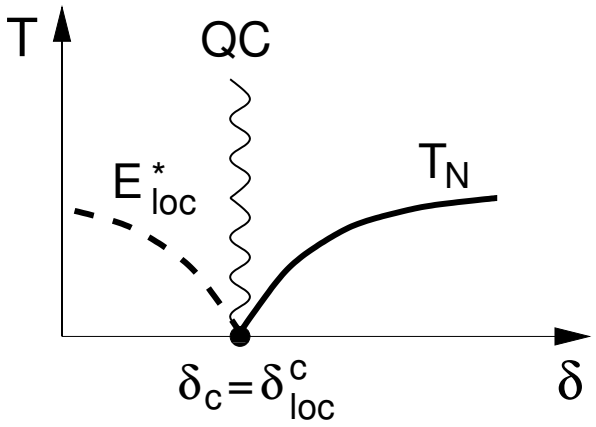

Figure 5.4: Schematic phase diagram for a local quantum criticality in Kondo lattices (adopted from Ref. [212]). Notice that the local energy scale, E^*_{loc}, vanishes at the quantum critical point. See the text for a description of notation.

In this way, the quantum criticality of the lattice model in mapped onto the criticality of the effective single-impurity model.[9] The predicted QPT happens with tuning a parameter $\delta = g/T_K$, where g is the coupling to the bosonic bath and T_K is the Kondo scale related to the coupling J_K to the fermionic bath. At a certain ratio of the couplings $\delta = \delta^c_{loc}$, the dynamically fluctuating magnetic field overcomes the screening of the local moment by the fermionic bath, and thus, yields a singular *local* susceptibility. This critical point is also marked by the vanishing of a "local" energy scale E^*_{loc} which denotes a scale below which a heavy (or 'local') Fermi liquid is formed. So, in this scenario, the magnetic ordering of the local moments in the lattice and the collapse of the Fermi liquid (and the screening) happen precisely at the same point. At this QCP, two kinds of critical degrees-of-freedom coexist: long-wavelength fluctuations of the magnetic order parameter, and *local* (momentum-independent) fluctuations of the Kondo quasi-particles. At QCP, magnetic fluctuations can decohere and destroy Kondo effect; therefore, the transition is also 'locally critical' (hence the name).[10] This type of QCP is found when spin fluctuations are two-dimensional. However, in order for the ordering temperature T_N to be nonzero for $\delta > \delta_c$, it is necessary to have an infinitesimal RKKY coupling in the third dimension [212].[11] Thus, for such a local quantum criticality, the Ginzburg-Landau action with a *single* (time-dependent) magnetic order parameter (as the ϕ^4 term in the Hertz-Millis-Moriya scenario) is not sufficient to describe the critical behaviour at the QCP. The other independent quantum critical modes which should be included in the Ginzburg-Landau action, correspond to the continuous transition that causes the destruction of Kondo screening as QPC is approached from the paramagnetic side. They have a spatially-local character since Kondo screening is a

[9] The Bose-Fermi single-impurity Kondo model is known to have a QCP.

[10] There are also other cases: a) when δ_c goes to zero at a finite value of E^*_{loc}; this corresponds to a conventional spin-density wave instability of the parent heavy Fermi liquid. b) when E^*_{loc} line terminates at a point different from δ_c which implies a finite range of phase space in which the local moments are neither Kondo screened nor magnetically ordered; this can happen especially if the lattice of local moments is highly frustrated.

[11] To determine the universal low-energy behaviour, the density-of-states of the fermionic bath near the Fermi energy is taken to be a non-zero constant, and the spectral function of the fluctuating magnetic field to have a power-law dependence on frequency for frequencies below some cut-off scale [212] (see a critique of this point in Ref. [14]).

local phenomenon happening at each lattice site.

5.2.3 Fractionalization, spin-charge separation and quantum criticality

A starkly different approach to QC in HFs by Senthil, Vojta and Sachdev [227], leaves out the assumptions about spatial locality or any magnetic order, and uses the notion of fractionalization known from low-dimensional systems to describe the breakdown of the heavy Fermi liquid. This scenario is based mainly on the known facts of destruction of large Fermi surface, and the weak-moment magnetism in heavy-fermion materials [227].

The major transition in heavy-fermion QC is considered to be the destruction of the large Fermi surface which can happen even without magnetic ordering. Magnetic ordering could potentially be a low-energy instability of the resulting non-magnetic translation-invariant (liquid-like) state in which the local moments are not participating in the Fermi volume (hence, a small Fermi surface); this state is denoted as FL*. A metallic magnetic state (denoted by SDW*) then can develop out of such FL* states via a spin-density wave instability in the small Fermi surface with, possibly, weak ordered local moments. The local moments are in a state which is adiabatically connected to a spin-liquid state with emergent gauge excitations.

A 3-dimensional 'fractionalized Fermi liquid' with a *small* spinon Fermi surface and a U(1) gauge structure, is assumed to be produced by the destruction of the large Fermi surface of the heavy Fermi liquid. It is shown that a direct second-order transition (with a jump in the electron Fermi-surface volume) from this state to the conventional Fermi liquid is possible. The critical point displays non-Fermi liquid behavior. The FL coherence temperature vanishes as the transition is approached from the FL side. The specific heat acquires a singular contribution from gauge-field fluctuations with $C/T \sim \ln(1/T)$ in 3 dimensions, resembling the experimental result for $CeCu_{6-x}Au_x$ [195], however the predicted transport properties are not consistent with experimental observations.

This fractionalized phase, FL*, might have a spin-density wave instability of the spinon Fermi surface leading to a magnetically-ordered phase. This exotic magnetic metal may have a weak ordered moment, but the local moments do not participate in the Fermi surface. In this scenario, the weakness of the ordered magnetic moments are justified by strong quantum fluctuations of the spins in 3-dimensional systems which reduce the moments, even when Kondo screening is *absent*. The initial *assumption* is that the Kondo effect becomes suppressed on approaching the magnetic state.

The heavy fermion (FL) and fractionalized Fermi liquid (FL*) phases are studied by a 'slave boson' mean-field theory (with large-N expansion). In this method, the condensation of the slave boson marks the onset of Kondo coherence that characterizes the heavy Fermi-liquid phase, while in the FL* phase, the slave boson is not condensed indicating absence of Kondo effect. Fluctuations about this mean-field description lead to the critical theory of the transition involving a propagating boson coupled to a compact $U(1)$ gauge field, in presence of damping from fermionic excitations [227]. In this method, breakdown of the Kondo screening is possible only upon including frustrating inter-moment exchange interactions.

Another scenario for the breakdown of Kondo screening based on spin-charge separation has been proposed by Pépin [236] which is based on the idea that the heavy quasiparticle fractionalizes into a spinon and a spinless fermion at the QCP [237], plus some phenomenological assumptions about the dynamics of the fermionic field. A major problem is that the heavy Fermi liquid phase does not arise in this theory since the fermionic field cannot condense [195].

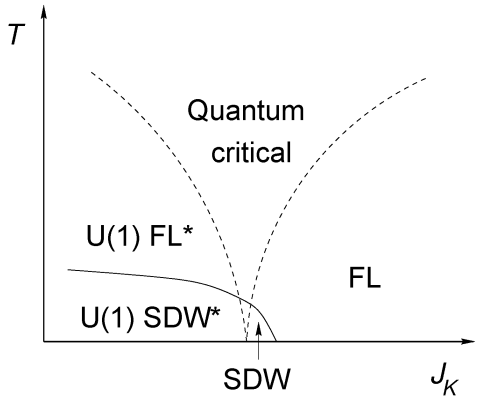

Figure 5.5: Schematic phase diagram for the fractional Fermi liquid scenario for quantum criticality in heavy-fermionic systems. The figure illustrates the possible transition from an FL* or SDW* to the conventional Fermi liquid phase upon increasing the Kondo coupling, J_K (adopted from Ref. [227]). See the text for a description of notation.

5.2.4 Critical Landau quasi-particles

Most recently, Wölfle and Abrahams [238–240] have proposed a semi-phenomenological scenario of critical quasi-particles for QC in HF systems. They present a self-consistent theory of the frequency-dependent effective mass enhancement m^*/m of Landau quasi-particles coupled to 3-dimensional antiferromagnetic spin fluctuations. Their crucial argument is that even *inside* the *non-Fermi liquid* regime, the width of the fermionic quasi-particles does not exceed the quasi-particle energy; in other words, the metallic quasi-particle is stable despite relatively large spectral weight of incoherent excitations.

The quasi-particles arise from an Anderson lattice model in the heavy Fermi liquid regime, in the limit of large on-site Coulomb interaction and close to half-filling ($n_f \lesssim 1$ electrons per site), where the quasi-particle weight $Z \ll 1$; this implies an enhancement of the effective quasi-particle mass ratio, since $Z^{-1} = m^*/m$.

Near an antiferromagnetic QCP, the 3-dimensional antiferromagnetic quantum critical fluctuations (which finally lead to the ordering of local moments in the antiferromagnetic state) renormalize the quasi-particle spectrum, and this in turn, ultimately leads to a critical behavior of the effective mass. A one-loop perturbative expansion for the quasi-particle self-energy[12] leads to a self-consistent equation for the quasi-particle weight. Furthermore, they assume a power-law frequency-dependence for the quasi-particle weight, $Z = Z(\omega) \propto \omega^\alpha$, with $\omega \sim E$ where E is the relevant energy scale, e.g., the temperature or Zeeman splitting due to a magnetic field. A "strong-coupling" (non-Gaussian) solution is obtained only if the initial value of $Z^{-1}(T)$, when one enters the 3-dimensional antiferromagnetic fluctuation regime, is sufficiently large. They argue that for $YbRh_2Si_2$ in which quasi-2-dimensional antiferromagnetic and/or 3-dimensional ferromagnetic Gaussian fluctuations leads to a logarithmic increase in the effective mass m^*, this scenario is valid and the system is driven into the 3-dimensional "strong-coupling regime". They find critical exponents of the temperature dependence of the specific heat coefficient $\gamma \propto T^{-\frac{1}{4}}$ and of the resistivity $\rho(T) = \rho_0 + A\,T^{\frac{3}{4}}$ in agreement with experiments on $YbRh_2Si_2$ in the temperature range $T < 0.3$ K.

[12] The self-energy is assumed to have weak momentum dependence so that the renormalized quasi-particle effective mass will be approximately uniform over the Fermi surface.

This scenario depends crucially on the detailed nature of spin fluctuations in the system. For instance, 3-dimensional antiferromagnetic fluctuations will fit within a *non-interacting* Gaussian theory if the effective mass ratio is not large enough in the beginning. Yet the authors argue that, e.g., in $YbRh_2Si_2$ one has a wide region of quasi-2-dimensional antiferromagnetic or 3-dimensional ferromagnetic fluctuations which enhance the effective mass sufficiently to drive the system into a "strong-coupling regime" of 3-dimensional antiferromagnetic fluctuations [238]. The ordered state, in this scenario, is an itinerant heavy-quasi-particle SDW state near the QCP with a small ordered magnetic moment. The Kondo effect is only weakly suppressed [238, 240]. A significant point is that this scenario does *not* invoke the Kondo effect at all; that is, a sufficiently large effective mass and coupling to certain magnetic fluctuations is enough to produce the results.

5.3 Magnetic instability of the Kondo lattice

As explained in detail in the previous sections, the major effect which competes with the Kondo screening is the magnetic instability in form of an spin density wave in the Kondo lattice. Therefore, to see the effect of a magnetic instability we should include the possibility of such an instability in the RKKY-modified RG method which we developed previously in chapter 3. As it was discussed in section 5.2, the major scenarios for the critical breakdown of the Kondo screening, are based on certain strong assumptions, especially on the form of the susceptibility, to predict a breakdown. Here, we will relax such assumptions altogether to see the possibility of collapse of the Kondo quasi-particles as the magnetic fluctuations increase, without adding further intricacies to the system.
It is important to remind that the interaction between the local moments is mediated by the conduction electrons (particle-hole excitations near the Fermi surface); this means that there is no *direct* interaction whatsoever between the local moments. Diagrammatically, the indirect carrier-mediated interaction between the local moments is depicted as in Fig. 5.6 which is essentially the conduction electron susceptibility.

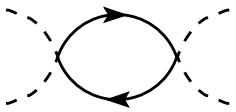

χ_c

Figure 5.6: The interaction between the f-impurities (denoted by dashed lines) is mediated by the conduction electrons (particles-hole excitations) in terms of the conduction electron susceptibility, χ_c.

So far, we have only considered a non-interacting (bare) susceptibility for the conduction electrons which cannot lead to a critical term at low energies. In this section, we dress the conduction electron susceptibility, χ_c by the local Kondo interaction via an RPA resummation; namely, we will obtain the renormalized susceptibility of conduction electrons, $\tilde{\chi}_c$ as

$$\tilde{\chi}_c = \frac{\chi_c}{1 - J^2\,\chi_c\,\chi_f}\ , \tag{5.9}$$

which is diagrammatically represented as in Fig. 5.7 where χ_f stands for the local impurity susceptibility and J_0 for the bare Kondo coupling.

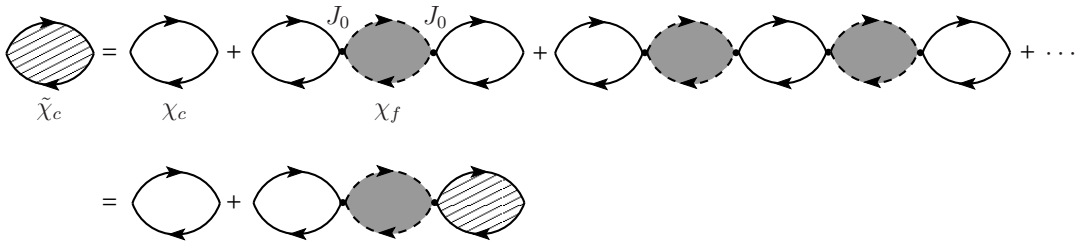

Figure 5.7: The conduction electron susceptibility is renormalized by the local contributions from the Kondo interaction with the impurities.

This RPA resummation can be inferred readily from the Feynman diagrams; yet we provide a detailed derivation via a Hubbard-Stratonovich transformation in the next section.

Finally, with this dressed conduction electron susceptibility, we will find a condition for magnetic instability in the Kondo lattice. We will obtain the RG flow equations including this spin density wave (SDW) instability and therefrom, the RKKY-modified Kondo temperature for the lattice. The goal is to see whether this SDW instability changes the result for the lattice Kondo temperature as compared to the previous case in chapter 3 where SDW instability was absent from the RG formalism.

5.3.1 Decoupling spin densities via the Hubbard-Stratonovich transformation

A Hubbard-Stratonovich transformation [241, 242][13] is needed to decouple the interaction in density-density (or more accurately, f-density–c-density) channel in the Kondo lattice model. Hubbard-Stratonovich transformation is performed in the functional formalism and on the action. The action for the Kondo lattice model (KLM) reads

$$\begin{aligned} S_{\mathrm{KLM}}(\beta) &= S_c^0 + S_f^0 + S_{int} \\ S_c^0 &= \int_0^\beta \mathrm{d}\tau \sum_{\mathbf{k}\sigma} c^\dagger_{\mathbf{k}\sigma}(\partial_\tau + \xi_{\mathbf{k}}) c_{\mathbf{k}\sigma}(\tau) \\ S_f^0 &= \int_0^\beta \mathrm{d}\tau \sum_{\mathbf{x}_l\sigma} f^\dagger_{l\sigma}(\tau)(\partial_\tau + \xi_d) f_{l\sigma}(\tau) \\ S_{int} &= \frac{J}{2}\int_0^\beta \mathrm{d}\tau \sum_{\mathbf{x}_l} \mathbf{S}_f(\mathbf{x}_l)\cdot \mathbf{s}_c(\mathbf{x}_l) = \frac{J}{2}\int_0^\beta \mathrm{d}\tau \sum_{\mathbf{x}_l}\sum_{\alpha=x,y,z} S_f^\alpha(\mathbf{x}_l) s_c^\alpha(\mathbf{x}_l) \ , \end{aligned} \tag{5.10}$$

where[14]

$$\begin{aligned} S_f^\dagger &\equiv (S_f)^* = S_f \ , \\ s_c^\dagger &\equiv (s_c)^* = s_c \ , \end{aligned} \tag{5.11}$$

[13] A detailed description of the Hubbard-Stratonovich transformation for the case of interacting electronic gas can be found, e.g., in Ref. [243].

[14] Note that we have used the complex conjugation (f^*) and Hermitian conjugate ($f^\dagger$) interchangeably.

are real-valued fields in the functional-integral formalism. The partition function will be

$$Z(\beta) = \int \mathcal{D}c\mathcal{D}c^{\dagger}\mathcal{D}f\mathcal{D}f^{\dagger}\exp[-S(\beta)] \ . \tag{5.12}$$

If we define

$$e^{-S_K} := e^{-S_{int}} = \exp\left[-\frac{J}{2}\int_0^{\beta} \mathrm{d}\tau \sum_{\mathbf{x}_l}\sum_{\alpha=x,y,z} S_f^{\alpha}(\mathbf{x}_l,\tau)s_c^{\alpha}(\mathbf{x}_l,\tau)\right] \ , \tag{5.13}$$

then, for each l, α and τ, we can write

$$\exp\left[-\frac{J}{2}S_f^{\alpha}(\mathbf{x}_l,\tau)s_c^{\alpha}(\mathbf{x}_l,\tau)\right] =: e^{-\frac{uv}{a}} \ , \tag{5.14}$$

with

$$\begin{aligned} u &:= -\mathrm{i}\frac{\sqrt{J}}{2}S_f^{\alpha}(\mathbf{x}_l) \ , \\ v &:= -\mathrm{i}\frac{\sqrt{J}}{2}s_c^{\alpha}(\mathbf{x}_l) \ , \\ a &:= 1 \ , \end{aligned} \tag{5.15}$$

and using the Gaussian integral (Appendix F),

$$e^{\frac{uv}{a}} = \frac{a}{\pi}\int_{\mathbb{C}} \frac{\mathrm{d}z\,\mathrm{d}\bar{z}}{2\mathrm{i}} e^{-\bar{z}az+uz+\bar{z}v} \quad ; u,v \in \mathbb{C}; a > 0 \tag{5.16}$$

we can decouple the action in the spin-density channel by introducing the auxiliary fields, φ and $\bar{\varphi}$; that is,

$$\begin{aligned} \exp[-\frac{J}{2}S_f^{\alpha}(\mathbf{x}_l)s_c^{\alpha}(\mathbf{x}_l)] = \mathcal{N}\int \mathcal{D}\bar{\varphi}^{\alpha}(\mathbf{x}_l)\mathcal{D}\varphi^{\alpha}(\mathbf{x}_l) \\ \times \exp[-\bar{\varphi}^{\alpha}(\mathbf{x}_l)\varphi^{\alpha}(\mathbf{x}_l) - \mathrm{i}\sqrt{\frac{J}{2}}S_f^{\alpha}(\mathbf{x}_l)\varphi^{\alpha}(\mathbf{x}_l) - \mathrm{i}\sqrt{\frac{J}{2}}\bar{\varphi}^{\alpha}(\mathbf{x}_l)s_c^{\alpha}(\mathbf{x}_l)] \ , \end{aligned} \tag{5.17}$$

where $\mathcal{N}$ is a normalization constant,

$$\mathcal{N}^{-1} := \int \mathcal{D}\bar{\varphi}^{\alpha}(\mathbf{x}_l)\mathcal{D}\varphi^{\alpha}(\mathbf{x}_l)\exp[-\bar{\varphi}^{\alpha}(\mathbf{x}_l)\varphi^{\alpha}(\mathbf{x}_l)] \ , \tag{5.18}$$

and τ-dependence is dropped for brevity. The auxiliary fields φ, $\bar{\varphi}$ are the conjugate fields to S_f and s_c respectively. Therefore, the Kondo interaction part, including the auxiliary fields, reads

$$\begin{aligned} e^{-S_K} = \mathcal{N} \int \mathcal{D}\bar{\varphi}^\alpha(\mathbf{x}_l,\tau)\mathcal{D}\varphi^\alpha(\mathbf{x}_l,\tau) \\ \times \exp\Big[-\int_0^\beta \mathrm{d}\tau \sum_{\mathbf{x}_l} \bar{\varphi}^\alpha(\mathbf{x}_l,\tau)\varphi^\alpha(\mathbf{x}_l,\tau) \\ - \mathrm{i}\sqrt{\frac{J}{2}} \int_0^\beta \mathrm{d}\tau \sum_{\mathbf{x}_l} S_f^\alpha(\mathbf{x}_l,\tau)\varphi^\alpha(\mathbf{x}_l,\tau) - \mathrm{i}\sqrt{\frac{J}{2}} \int_0^\beta \mathrm{d}\tau \sum_{\mathbf{x}_l} \bar{\varphi}^\alpha(\mathbf{x}_l,\tau) s_c^\alpha(\mathbf{x}_l,\tau)\Big] , \end{aligned} \tag{5.19}$$

and the full partition function will be

$$\begin{aligned} Z = \int \mathcal{D}c^\dagger \mathcal{D}c \mathcal{D}f^\dagger \mathcal{D}f \mathcal{D}\varphi^\dagger \mathcal{D}\varphi \\ \times \exp\Big[-\int_0^\beta \mathrm{d}\tau \sum_{\mathbf{k},\sigma} c^\dagger_{\mathbf{k}\sigma}(\tau)(\partial_\tau + \xi_{\mathbf{k}}) c_{\mathbf{k}\sigma}(\tau) - \int_0^\beta \mathrm{d}\tau \sum_{\mathbf{x}_l\sigma} f^\dagger_{l\sigma}(\tau)(\partial_\tau + \xi_d) f_{l\sigma}(\tau) \\ - \int_0^\beta \mathrm{d}\tau \sum_{\mathbf{x}_l} \bar{\varphi}^\alpha(\mathbf{x}_l,\tau)\varphi^\alpha(\mathbf{x}_l,\tau) \\ - \mathrm{i}\sqrt{\frac{J}{2}} \int_0^\beta \mathrm{d}\tau \sum_{\mathbf{x}_l} S_f^\alpha(\mathbf{x}_l,\tau)\varphi^\alpha(\mathbf{x}_l,\tau) - \mathrm{i}\sqrt{\frac{J}{2}} \int_0^\beta \mathrm{d}\tau \sum_{\mathbf{x}_l} \bar{\varphi}^\alpha(\mathbf{x}_l,\tau) s_c^\alpha(\mathbf{x}_l,\tau)\Big] . \end{aligned} \tag{5.20}$$

Using a pseudo-fermionic representation of the spin operator (Appendix C), one can re-write the parts including the spins as

$$\begin{aligned} S_f^\alpha(\mathbf{x}_l)\varphi^\alpha(\mathbf{x}_l) &= \sum_{\nu'\nu} f^\dagger_{l\nu'} \sigma^\alpha_{\nu'\nu} f_{l\nu}\ \varphi^\alpha_l \\ \bar{\varphi}^\alpha(\mathbf{x}_l) s^\alpha(\mathbf{x}_l) &= \sum_{\mu'\mu} \bar{\varphi}^\alpha_l\ c^\dagger_{l\mu'} \sigma^\alpha_{\mu'\mu} c_{l\mu} \end{aligned} \tag{5.21}$$

where $\varphi_l \equiv \varphi(\mathbf{x}_l)$ and $c_l \equiv c(\mathbf{x}_l)$, $c_l^\dagger \equiv c^\dagger(\mathbf{x}_l)$. The partition function Eq. (5.20) can be factorized into two parts, the c-electron and f-electron parts.

conduction electrons

The conduction-electron part of the partition function reads

$$Z_c := \int \mathcal{D}c^\dagger \mathcal{D}c \exp\Big[-\int_0^\beta \mathrm{d}\tau \sum_{\mathbf{k},\sigma} c^\dagger_{\mathbf{k}\sigma}(\tau)(\partial_\tau + \xi_{\mathbf{k}}) c_{\mathbf{k}\sigma}(\tau) - \mathrm{i}\sqrt{\frac{J}{2}} \int_0^\beta \mathrm{d}\tau \sum_{\mathbf{x}_l} \bar{\varphi}^\alpha(\mathbf{x}_l,\tau) s_c^\alpha(\mathbf{x}_l,\tau)\Big] . \tag{5.22}$$

Using the momentum-frequency representation of fields,

$$\begin{aligned} \psi_\sigma(\mathbf{x},\tau) &= \sum_{\mathbf{k},\mathrm{i}\omega} e^{\mathrm{i}\mathbf{k}\cdot\mathbf{x} - \mathrm{i}\omega\tau} \psi_\sigma(\mathbf{k},\mathrm{i}\omega) \equiv \sum_k e^{\mathrm{i}kx} \psi_\sigma(k) \\ \psi^\dagger_\sigma(\mathbf{x},\tau) &= \sum_{\mathbf{k},\mathrm{i}\omega} e^{-\mathrm{i}\mathbf{k}\cdot\mathbf{x} + \mathrm{i}\omega\tau} \psi^\dagger_\sigma(\mathbf{k},\mathrm{i}\omega) \equiv \sum_k e^{-\mathrm{i}kx} \psi^\dagger_\sigma(k) , \end{aligned} \tag{5.23}$$

where we have used the 4-vector notation,

$$\begin{aligned} k &:= (\mathbf{k}, \mathrm{i}\omega) \ , \\ x &:= (\mathbf{x}, \tau) \ , \\ kx &:= \mathbf{k}\cdot\mathbf{x} - \omega\tau \ , \end{aligned} \tag{5.24}$$

one obtains

$$\int_0^\beta \mathrm{d}\tau \sum_{\mathbf{k}\sigma} c^\dagger_{\mathbf{k}\sigma}(\partial_\tau + \xi_{\mathbf{k}}) c_{\mathbf{k}\sigma} = \sum_{\mathbf{k}\omega\sigma} c^\dagger_{\mathbf{k}\sigma}(\mathrm{i}\omega)(-\mathrm{i}\omega + \xi_{\mathbf{k}}) c_{\mathbf{k}\sigma}(\mathrm{i}\omega) \ ; \tag{5.25}$$

and

$$\begin{aligned} \int_0^\beta \mathrm{d}\tau \sum_{\mathbf{x}_l} \bar\varphi^\alpha_l s^\alpha_c(\mathbf{x}_l) &= \sum_\alpha \sum_{\mathbf{k},\mathbf{q}} \sum_{\nu',\nu} \bar\varphi^\alpha(\mathbf{p}-\mathbf{q})\ c^\dagger_{\mathbf{q}\nu'} \sigma^\alpha_{\nu'\nu} c_{\mathbf{p}\nu} \\ &= \sum_\alpha \sum_{\substack{\mathbf{p},\mathbf{q} \\ \mathrm{i}\omega,\mathrm{i}\Omega}} \sum_{\nu',\nu} \bar\varphi^\alpha(\mathbf{p}-\mathbf{q}, \mathrm{i}\omega - \mathrm{i}\Omega)\ c^\dagger_{\mathbf{q}\nu'}(\mathrm{i}\omega) \sigma^\alpha_{\nu'\nu} c_{\mathbf{p}\nu}(\mathrm{i}\Omega) \end{aligned} \tag{5.26}$$

where $\mathrm{i}\omega$ and $\mathrm{i}\Omega$ are fermionic Matsubara frequencies. Therefore,

$$\begin{aligned} S_c &= \sum_{\substack{\mathbf{k}\nu \\ \mathrm{i}\omega}} c^\dagger_{\mathbf{k}\nu}(\mathrm{i}\omega)(-\mathrm{i}\omega + \xi_{\mathbf{k}}) c_{\mathbf{k}\nu}(\mathrm{i}\omega) \\ &\quad + \mathrm{i}\sqrt{\frac{J}{2}} \sum_\alpha \sum_{\substack{\mathbf{k}\mathbf{q} \\ \mathrm{i}\omega,\mathrm{i}\Omega}} \bar\varphi^\alpha(\mathbf{k}-\mathbf{q}, \mathrm{i}\omega - \mathrm{i}\Omega) \sum_{\nu'\nu} c^\dagger_{\mathbf{q}\nu'}(\mathrm{i}\omega) \sigma^\alpha_{\nu'\nu} c_{\mathbf{k}\nu}(\mathrm{i}\Omega) \\ &= \sum_{\substack{\mathbf{k},\mathbf{q} \\ \mathrm{i}\omega,\mathrm{i}\Omega \\ \nu'\nu}} c^\dagger_{\mathbf{k}\nu'} \Big[(-\mathrm{i}\omega + \xi_{\mathbf{k}}) \delta_{\mathbf{k}\mathbf{q}} \delta(\Omega - \omega) \delta_{\nu'\nu} + \sqrt{\frac{J}{2}} \sum_\alpha \bar\varphi^\alpha(\mathbf{k}-\mathbf{q}, \mathrm{i}\omega - \mathrm{i}\Omega) \sigma^\alpha_{\nu'\nu} \Big] c_{\mathbf{k}\nu}(\mathrm{i}\Omega) \\ &\equiv \sum_{\substack{kq \\ \nu'\nu}} c^\dagger_{\nu'}(k) \Big[(-\mathrm{i}\omega + \xi_{\mathbf{k}}) \delta_{kq} \delta_{\nu'\nu} + \mathrm{i}\sqrt{\frac{J}{2}} \sum_\alpha \bar\varphi^\alpha(k-q) \sigma^\alpha_{\nu'\nu} \Big] c_\nu(k) \ . \end{aligned} \tag{5.27}$$

f-pseudo-fermions

Analogously, the part of the action corresponding to the f-pseudo-fermions reads

$$\begin{aligned}
S_f^0 &= \int_0^\beta \mathrm{d}\tau \sum_{\mathbf{x}_l,\nu} \left\{ f_\nu^\dagger(\mathbf{x}_l,\tau)\partial_\tau f_\nu(\mathbf{x}_l,\tau) + \xi_d f_\nu^\dagger(\mathbf{x}_l,\tau) f_\nu(\mathbf{x}_l,\tau) \right\} \ ; \\
S_f &= S_f^0 + \mathrm{i}\sqrt{\frac{J}{2}} \int_0^\beta \mathrm{d}\tau \sum_{\mathbf{x}_l,\alpha} S_f^\alpha(\mathbf{x}_l,\tau)\varphi^\alpha(\mathbf{x}_l,\tau) \\
&= \int_0^\beta \mathrm{d}\tau \sum_{\mathbf{x}_l,\nu} \left\{ f_{l\nu}^\dagger(\tau)\partial_\tau f_{l\nu}(\tau) + \xi_d f_{l\nu}^\dagger(\tau) f_{l\nu}(\tau) \right\} \\
&+ \mathrm{i}\sqrt{\frac{J}{2}} \int_0^\beta \mathrm{d}\tau \sum_{\substack{\mathbf{x}_l\alpha \\ \nu'\nu}} f_{l\nu'}^\dagger(\tau)\sigma_{\nu'\nu}^\alpha f_{l\nu}(\tau)\ \varphi^\alpha(\mathbf{x}_l) \\
&= \int_0^\beta \mathrm{d}\tau \sum_{\substack{\mathbf{x}_l\alpha \\ \nu'\nu}} f_{l\nu'}^\dagger \left((\partial_\tau + \xi_d)\delta_{\nu'\nu} + \mathrm{i}\sqrt{\frac{J}{2}} \sum_\alpha \varphi^\alpha(\mathbf{x}_l)\sigma_{\nu'\nu}^\alpha \right) f_{l\nu} \\
&= \sum_{\substack{\mathbf{x}_l \\ \mathrm{i}\omega,\mathrm{i}\Omega}} \sum_{\nu'\nu} f_{l\nu'}^\dagger(\mathrm{i}\omega) \left((-\mathrm{i}\omega + \xi_d)\delta_{\nu'\nu}\delta(\omega-\Omega) + \mathrm{i}\sqrt{\frac{J}{2}} \sum_\alpha \varphi^\alpha(\mathbf{x}_l, \mathrm{i}\omega - \mathrm{i}\Omega)\sigma_{\nu'\nu}^\alpha \right) f_{l\nu'}(\mathrm{i}\Omega) \ .
\end{aligned} \tag{5.28}$$

where $\mathrm{i}\omega$ and $\mathrm{i}\Omega$ are fermionic Matsubara frequencies.

To obtain an action in terms of the auxiliary fields only, we have to eliminate the conduction electrons and the f-pseudo-fermions.

5.3.1.1 Integrating-out conduction electrons

For fermionic (Grassmann) variables, ψ, ψ^*, and symmetric matrix (bilinear operator), A,

$$\int \mathcal{D}(\psi^*,\psi) e^{-\psi^* A \psi} = \mathrm{Det} A \ . \tag{5.29}$$

Thus, for conduction electrons,

$$\begin{aligned}
Z_c &= \underbrace{(Z_c^0)^{-1}}_{\text{normalization factor}} \int \mathcal{D}(c^*,c) e^{-S_c} \\
&= \mathrm{Det}\left[(-\mathrm{i}\omega + \xi_{\mathbf{k}})\delta_{kq}\delta_{\nu'\nu} + \mathrm{i}\sqrt{\frac{J}{2}} \sum_\alpha \bar{\varphi}^\alpha(k-q)\sigma_{\nu'\nu}^\alpha \right] \ ,
\end{aligned} \tag{5.30}$$

where the determinant is in (k,ν)-space. Note that the spin degrees-of-freedom, $\sigma =\uparrow,\downarrow$, are *not* decoupled due to the presence of $\sigma_{\nu'\nu}$. Therefore[15],

$$Z_c = \mathrm{Det}A = \exp[\mathrm{Tr}\ln A] = \exp\Big\{\mathrm{Tr}\ln[-G_c^{0,-1}(k'\nu',k\nu) + \underbrace{\mathrm{i}\sqrt{\frac{J}{2}}\sum_\alpha \bar{\varphi}^\alpha(k'-k)\sigma^\alpha_{\nu'\nu}}_{=:M}]\Big\} \ . \quad (5.31)$$

We use the relations

$$\mathrm{Tr}\ln[-G_c^{0,-1}+M] = \mathrm{Tr}\ln[-G_c^{0,-1}(1-G_c^0M)] = \underbrace{\mathrm{Tr}\ln[-G_c^{0,-1}]}_{=Z_c^0} + \mathrm{Tr}\ln[1-G_c^0M] \ , \quad (5.32)$$

where

$$\begin{aligned} \ln(1-X) &= -\sum_{n=1}^{\infty}\frac{X^n}{n} \ , \\ \rightarrow \ln(1-G_c^0M) &= -\sum_{n=1}^{\infty}\frac{(G_c^0M)^n}{n} \ , \end{aligned} \quad (5.33)$$

so that

$$Z_c = Z_c^0\exp\left\{-\sum_{n=1}^{\infty}\frac{1}{n}\mathrm{Tr}[(G_c^0M)^n]\right\} = Z_c^0\exp\left\{-\mathrm{Tr}[G_c^0M] - \frac{1}{2}\mathrm{Tr}[(G_c^0M)^2] + \cdots\right\} \ . \quad (5.34)$$

5.3.1.2 Random-phase approximation (RPA)

In the random-phase approximation (RPA), one truncates the above expression, Eq. (5.34), at the quadratic order $\sim \mathcal{O}(M^2)$.

More explicitly,

$$\mathrm{Tr}[G^0M] = \sum_{p'p} G^0_{pp'}M_{p'p}; \quad p\text{: set of quantum numbers} \ , \quad (5.35)$$

and since

$$G^0_{pp'} = G^0_p\delta_{pp'} \ , \quad (5.36)$$

then

$$\mathrm{Tr}[G^0M] = \sum_p G^0_pM_{pp} \ , \quad (5.37)$$

[15] Note that Tr denotes a functional trace.

and

$$\begin{aligned}\mathrm{Tr}[(G^0M)^2] = \mathrm{Tr}[G^0MG^0M] &= \sum_{\substack{pp'\\qq'}} G^0_{pp'}M_{p'q}G^0_{qq'}M_{q'p} \\ &= \sum_{pp'} G^0_p M_{pp'}G^0_{p'}M_{p'p}\ . \end{aligned} \tag{5.38}$$

In a *paramagnetic* phase (which is the case here), the odd powers in $\ln(1 - G_0M)$ should vanish due to the symmetry of the action under $\varphi \mapsto -\varphi$ (Z_2- or $O(N)$-symmetry).

Furthermore,

$$\begin{aligned} \frac{1}{V}\int_V \mathrm{d}x^3\, M(\mathbf{x},t) &= 0 \\ \Rightarrow \frac{1}{V}\int_V \mathrm{d}x^3 \sum_{\mathbf{k}} e^{\mathrm{i}\mathbf{k}\cdot\mathbf{x}} M_{\mathbf{k}}(t) &= 0 \\ \Rightarrow \sum_{\mathbf{k}} M_{\mathbf{k}}(t)\delta_{\mathbf{k},0} &= 0 \\ \Rightarrow M(\mathbf{k}=0,t) &= 0\ , \end{aligned} \tag{5.39}$$

which, due to the fact that $M \propto \varphi$ (Eq. (5.31)) implies

$$\varphi_{\mathbf{k}=0} = 0\ . \tag{5.40}$$

Therefore, in a paramagnetic phase, the linear term G_0M vanishes, and only the even orders in M remain, and hence, in RPA, one has to calculate only $\mathrm{Tr}[(G_0M)^2]$. With

$$\begin{aligned} M(k'\nu', k\nu) &= \mathrm{i}\sqrt{\frac{J}{2}} \sum_{\alpha=x,y,z} \bar{\varphi}^\alpha(k'-k)\sigma^\alpha_{\nu'\nu}\ , \\ G^0_c(k'\nu', k\nu) &= \frac{1}{\mathrm{i}\omega - \xi_{\mathbf{k}}}\delta_{k'k}\delta_{\nu'\nu}\ , \end{aligned} \tag{5.41}$$

one obtains[16]

$$\begin{aligned} S_c &= \sum_{\substack{k'\nu'\\k\nu}} G^0_k \underbrace{\left(\mathrm{i}\sqrt{\frac{J}{2}}\sum_\alpha \bar{\varphi}^\alpha(k-k')\sigma^\alpha_{\nu\nu'}\right)}_{=M(k\nu,k'\nu')} G^0_{k'} \underbrace{\left(\mathrm{i}\sqrt{\frac{J}{2}}\sum_{\alpha'} \bar{\varphi}^{\alpha'}(k'-k)\sigma^\alpha_{\nu'\nu}\right)}_{=M(k'\nu',k\nu)} \\ &= -\frac{J}{2}\sum_{\substack{k'\nu'\\k\nu}} G^0_k \sum_\alpha \bar{\varphi}^\alpha(k-k')\sigma^\alpha_{\nu\nu'} \sum_{\alpha'} \bar{\varphi}^{\alpha'}(k'-k)\sigma^\alpha_{\nu'\nu}\, G^0_{k'} \\ &= -\frac{J}{2}\sum_{k'k} G^0_k\, G^0_{k'} \sum_{\alpha,\alpha'} \bar{\varphi}^\alpha(k-k')\ \bar{\varphi}^{\alpha'}(k'-k) \sum_{\nu\nu'} \sigma^\alpha_{\nu\nu'}\sigma^{\alpha'}_{\nu'\nu}\ . \end{aligned} \tag{5.42}$$

[16] Note that the frequency component of k is bosonic, and that of q is fermionic.

Using Pauli spin algebra (Appendix A),

$$\sum_{\nu\nu'} \sigma^{\alpha}_{\nu\nu'}\sigma^{\alpha'}_{\nu'\nu} = \mathrm{Tr}[\sigma^{\alpha}\sigma^{\alpha'}] = 2\delta_{\alpha\alpha'} \ ; \tag{5.43}$$

thus,

$$\begin{aligned} S_c &= -J\sum_{k'k} G^0_k G^0_{k'} \sum_{\alpha} \ \bar{\varphi}^{\alpha}(k-k')\bar{\varphi}^{\alpha}(k'-k) \\ &\equiv -J\sum_{kk'} G^0_k G^0_{k'} \bar{\varphi}(k-k')\cdot\bar{\varphi}(k'-k) \\ &\overset{k-k'\mapsto k}{=\!=\!=} -J\sum_{kq} G^0_{k+q}G^0_q \ \bar{\varphi}(k)\cdot\bar{\varphi}(-k) \ . \end{aligned} \tag{5.44}$$

Moreover,

$$\frac{1}{\beta}\sum_{q} G^0_{k+q}G^0_q = \frac{1}{\beta}\sum_{\mathbf{q},\mathrm{i}\Omega} G^0_c(\mathbf{k}+\mathbf{q},\mathrm{i}\omega+\mathrm{i}\Omega)G^0_c(\mathbf{q},\mathrm{i}\Omega) = \chi_c(\mathbf{k},\mathrm{i}\omega) \ , \tag{5.45}$$

where $\mathrm{i}\Omega$ is fermionic and $\mathrm{i}\omega$ is bosonic.

5.3.1.3 Integrating-out f-pseudo-fermions

The part of the action corresponding to the f-pseudo-fermions reads

$$S_f = \sum_{\mathrm{i}\omega,\mathrm{i}\Omega}\sum_{\mathbf{x}_l}\sum_{\nu\nu'} f^{\dagger}_{l\nu'}(\mathrm{i}\omega)\left[(-\mathrm{i}\omega+\xi_d)\delta_{\nu'\nu}\delta(\omega-\Omega) + \mathrm{i}\sqrt{\frac{J}{2}}\sum_{\alpha}\varphi^{\alpha}(\mathbf{x}_l,\mathrm{i}\omega-\mathrm{i}\Omega)\sigma^{\alpha}_{\nu'\nu}\right] f_{l\nu}(\mathrm{i}\Omega) \ , \tag{5.46}$$

and the corresponding partition function is

$$Z_f = \mathrm{Det}A = \exp(\mathrm{Tr}\ln A) = \exp\Big\{\mathrm{Tr}\ln\Big[-G^{0,-1}_f + \underbrace{\mathrm{i}\sqrt{\frac{J}{2}}\sum_{\alpha}\varphi^{\alpha}(\mathbf{x}_l,\mathrm{i}\omega-\mathrm{i}\Omega)\sigma^{\alpha}_{\nu'\nu}}_{=:M}\Big]\Big\} \ . \tag{5.47}$$

Note that, as before,

$$\mathrm{Tr}\ln[-G^{0,-1}_f + M] = \mathrm{Tr}\ln[-G^{0,-1}_f(1-G^0_f M)] = \underbrace{\mathrm{Tr}\ln[-G^{0,-1}_f]}_{=\beta F^0_f} + \mathrm{Tr}\ln[1-G^0_f M] \ , \tag{5.48}$$

and

$$\begin{aligned} \mathrm{Tr}\ln[1-G^0_f M] &= -\sum_{n=1}^{\infty}\frac{1}{n}\mathrm{Tr}[(G^0_f M)^n] \\ &= -\mathrm{Tr}[G^0_f M] - \frac{1}{2}\mathrm{Tr}[(G^0_f M)^2] + \cdots \ . \end{aligned} \tag{5.49}$$

Using the fact that in the *paramagnetic* phase, the *odd* powers of M vanish due to the symmetry, $\varphi \mapsto -\varphi$, only the quadratic power remains in RPA:

$$\mathrm{Tr}[(G_f^0 M)^2] = \sum_{\mathbf{x}_l} \sum_{\substack{\mathrm{i}\omega,\mathrm{i}\Omega \\ \nu'\nu}} G_f^0(\mathbf{x}_l, \mathrm{i}\omega) \left(\mathrm{i}\sqrt{\frac{J}{2}} \sum_{\alpha} \varphi_l^{\alpha}(\mathrm{i}\omega - \mathrm{i}\Omega)\sigma_{\nu\nu'}^{\alpha} \right) G_f^0(\mathbf{x}_l, \mathrm{i}\Omega) \\ \times \left(\mathrm{i}\sqrt{\frac{J}{2}} \sum_{\alpha'} \varphi_l^{\alpha'}(\mathrm{i}\Omega - \mathrm{i}\omega)\sigma_{\nu'\nu}^{\alpha'} \right) \ . \tag{5.50}$$

Since M is local (diagonal) in $\mathbf{x}_l$ (position index),

$$\begin{aligned} \mathrm{Tr}[(G_f^0 M)^2] &= -\frac{J}{2} \sum_{\mathbf{x}_l} \sum_{\mathrm{i}\omega,\mathrm{i}\Omega} G_f^0(\mathbf{x}_l, \mathrm{i}\omega) G_f^0(\mathbf{x}_l, \mathrm{i}\Omega) \sum_{\alpha,\alpha'} \varphi_l^{\alpha}(\mathrm{i}\omega - \mathrm{i}\Omega)\varphi_l^{\alpha}(\mathrm{i}\Omega - \mathrm{i}\omega) \underbrace{\sum_{\nu'\nu} \sigma_{\nu\nu'}^{\alpha}\sigma_{\nu'\nu}^{\alpha'}}_{=\mathrm{Tr}(\sigma^{\alpha}\sigma^{\alpha'})=2\delta_{\alpha,\alpha}} \\ &= -J \sum_{\mathbf{x}_l} \sum_{\mathrm{i}\omega,\mathrm{i}\Omega} G_f^0(\mathbf{x}_l, \mathrm{i}\omega) G_f^0(\mathbf{x}_l, \mathrm{i}\omega - \mathrm{i}\Omega) \sum_{\alpha} \varphi_l^{\alpha}(\mathrm{i}\Omega)\varphi_l^{\alpha}(-\mathrm{i}\Omega) \\ &= -J \sum_{\mathbf{x}_l} \sum_{\mathrm{i}\omega} \varphi_l(\mathrm{i}\omega)\varphi_l(-\mathrm{i}\omega) \sum_{\mathrm{i}\Omega} G_f^0(\mathbf{x}_l, \mathrm{i}\Omega) G_f^0(\mathbf{x}_l, \mathrm{i}\Omega - \mathrm{i}\omega) \\ &= -J \sum_{\mathbf{x}_l} \sum_{\mathrm{i}\omega} \varphi_l(\mathrm{i}\omega) \cdot \varphi_l(-\mathrm{i}\omega)\ \chi_f(\mathbf{x}_l, \mathrm{i}\omega) \ . \end{aligned} \tag{5.51}$$

where $\mathrm{i}\omega$ is bosonic.

5.3.1.4 Effective RPA action

After integrating out c- and f- fields, the full action can be formally written as

$$\begin{aligned} Z &= \exp[\mathrm{Tr}\ln A] = \exp\{\mathrm{Tr}\ln[-G_0^{-1}(1 - G_0 M)]\} \\ &= \exp\{\mathrm{Tr}\ln[-G_0^{-1}] + \mathrm{Tr}\ln[1 - G_0 M]\} \\ &= \underbrace{\exp[\beta F_0]}_{=Z_0} \exp\{\mathrm{Tr}\ln[1 - G_0 M]\} = Z_0 \exp\{\mathrm{Tr}\ln[1 - G_0 M]\} \\ &= Z_0 \exp\{-\mathrm{Tr}\ln[G_0 M] - \frac{1}{2}\mathrm{Tr}\ln[(G_0 M)^2] + \cdots\} \\ &= Z_0 \exp\{-\frac{1}{2}\mathrm{Tr}\ln[(G_0 M)^2] + \cdots\} \ . \end{aligned} \tag{5.52}$$

Therefore, the RPA correction to the action will be

$$\delta S_{\mathrm{RPA}} = \frac{1}{2}\mathrm{Tr}\ln[(G_0 M)^2] \ . \tag{5.53}$$

From the integration over the conduction electrons, we obtained

$$\delta S_{\mathrm{RPA}}^{c} = J \sum_{k} \chi_c(k)\ \bar{\varphi}(k) \cdot \bar{\varphi}(-k) \quad ; k = (\mathbf{k}, \mathrm{i}\omega) \ , \tag{5.54}$$

where iω is bosonic. The integration over the f-fermions resulted in

$$\delta S^f_{\rm RPA} = J \sum_{\mathbf{x}_l} \sum_{\mathrm{i}\omega} \chi_f(\mathbf{x}_l, \mathrm{i}\omega)\ \varphi(\mathbf{x}_l, \mathrm{i}\omega) \cdot \varphi(\mathbf{x}_l, -\mathrm{i}\omega)\ . \tag{5.55}$$

where iω is bosonic.

Action in terms of auxiliary fields Putting the above results together, the action for auxiliary fields, $\bar{\varphi}, \varphi$, will be

$$\begin{aligned} -S[\bar{\varphi}, \varphi] = &- \int_0^\beta \mathrm{d}\tau \sum_{\mathbf{x}_l} \bar{\varphi}(\mathbf{x}_l, \tau) \cdot \varphi(\mathbf{x}_l, \tau) \quad : S^0[\bar{\varphi}, \varphi] \\ &- J \sum_{\mathbf{k}, \mathrm{i}\omega} \chi_c(\mathbf{k}, \mathrm{i}\omega)\ \bar{\varphi}(\mathbf{k}, \mathrm{i}\omega) \cdot \bar{\varphi}(-\mathbf{k}, -\mathrm{i}\omega) \quad : \delta S^c_{\rm RPA}[\bar{\varphi}, \varphi] \\ &- J \sum_{\mathbf{x}_l} \sum_{\mathrm{i}\omega} \chi_f(\mathbf{x}_l, \mathrm{i}\omega)\ \varphi(\mathbf{x}_l, \mathrm{i}\omega) \cdot \varphi(\mathbf{x}_l, -\mathrm{i}\omega) \quad : \delta S^f_{\rm RPA}[\bar{\varphi}, \varphi]\ . \end{aligned} \tag{5.56}$$

We have

$$\begin{aligned} S^0[\bar{\varphi}, \varphi] &= \int_0^\beta \mathrm{d}\tau \sum_{\mathbf{x}_l} \bar{\varphi}(\mathbf{x}_l, \tau) \cdot \varphi(\mathbf{x}_l, \tau)\ , \\ \delta S^c_{\rm RPA}[\bar{\varphi}, \varphi] &= J \int_0^\beta \mathrm{d}\tau \int_0^\beta \mathrm{d}\tau' \sum_{\mathbf{x}_l, \mathbf{x}_l{}'} \chi_c(\mathbf{x}_l - \mathbf{x}_l{}', \tau - \tau')\ \bar{\varphi}(\mathbf{x}_l, \tau) \cdot \bar{\varphi}(\mathbf{x}_l{}', \tau')\ , \\ \delta S^f_{\rm RPA}[\bar{\varphi}, \varphi] &= J \sum_{\mathbf{x}_l} \int_0^\beta \mathrm{d}\tau\, \mathrm{d}\tau'\, \chi_f(\mathbf{x}_l, \tau - \tau')\ \varphi(\mathbf{x}_l, \tau) \cdot \bar{\varphi}(\mathbf{x}_l, \tau')\ , \end{aligned} \tag{5.57}$$

and in frequency-momentum representation,

$$\begin{aligned} S[\bar{\varphi}, \varphi] = &\sum_{\mathbf{k}, \mathrm{i}\omega} \bar{\varphi}(\mathbf{k}, \mathrm{i}\omega) \cdot \varphi(-\mathbf{k}, -\mathrm{i}\omega) \\ &+ J \sum_{\mathbf{k}, \mathrm{i}\omega} \chi_c(\mathbf{k}, \mathrm{i}\omega)\ \bar{\varphi}(\mathbf{k}, \mathrm{i}\omega) \cdot \bar{\varphi}(-\mathbf{k}, -\mathrm{i}\omega) \\ &+ J \sum_{\mathbf{k}, \mathrm{i}\omega} \chi_f(\mathrm{i}\omega)\ \varphi(\mathbf{k}, \mathrm{i}\omega) \cdot \left(\sum_{\mathbf{q}} \varphi(-\mathbf{q}, -\mathrm{i}\omega) \right)\ . \end{aligned} \tag{5.58}$$

Note that in a lattice with discrete translational symmetry, the f-susceptibility is *local*, i.e.,

$$\chi_f(\mathbf{x}) = \sum_{\mathbf{x}_l} \chi_f(\mathbf{x} = 0) \delta(\mathbf{x} - \mathbf{x}_l)\ , \tag{5.59}$$

and it has only frequency dependence. This fact leads to the third term which mixes all momenta ($\mathbf{q}$), but *not* frequencies.

5.3.1.5 Spin-spin correlation function

The action $S[\bar{\varphi},\varphi]$ can be written compactly as

$$S[\bar{\varphi},\varphi] = \bar{\varphi}\varphi + J\bar{\varphi}\chi_c\bar{\varphi} + J\varphi\chi_f\varphi \ , \tag{5.60}$$

and the corresponding partition function will be

$$Z = \int \mathcal{D}(\bar{\varphi},\varphi) e^{-\bar{\varphi}\varphi - J\bar{\varphi}\chi_c\bar{\varphi} - J\varphi\chi_f\varphi} \ . \tag{5.61}$$

The spin-spin correlation function can be obtained from the auxiliary field correlation functions as[17]

$$\begin{aligned}\langle\varphi^\alpha(\mathbf{x}_l,\tau)\varphi^\alpha(\mathbf{x}_l{}',\tau')\rangle &= \frac{1}{Z}\frac{\partial Z}{\partial\bar{\varphi}^\alpha(\mathbf{x}_l,\tau)\bar{\varphi}^\alpha(\mathbf{x}_l{}',\tau')} \\ &= \frac{J}{2}\langle s^\alpha(\mathbf{x}_l,\tau)s^\alpha(\mathbf{x}_l{}',\tau')\rangle \quad \text{for} \quad \alpha = x,y,z. \end{aligned} \tag{5.62}$$

We define

$$D(\mathbf{x}t;\mathbf{x}'t') = -\langle T\varphi(\mathbf{x},t)\varphi(\mathbf{x},t')\rangle \equiv -\langle T\varphi\varphi\rangle \ ,$$

and use the 4-vector notation, $x \equiv (\mathbf{x},\tau)$, for notational simplification,

$$D(x,x') := -\langle T\varphi(x)\varphi(x')\rangle \ , \tag{5.63}$$

$$\begin{aligned} G_{\bar{\varphi}\varphi}(x,x') &:= -\langle T\bar{\varphi}(x)\varphi(x')\rangle_0 \ , \\ G_{\varphi\bar{\varphi}}(x,x') &:= -\langle T\varphi(x)\bar{\varphi}(x')\rangle_0 \ , \end{aligned} \tag{5.64}$$

with

$$\langle\cdots\rangle_0 \equiv \langle\cdots\rangle\Big|_{J=0} \ . \tag{5.65}$$

Note that the action is composed of a 'free part', $\bar{\varphi}\varphi$, plus two 'potential scattering' terms, $J\bar{\varphi}\chi_c\bar{\varphi}+J\varphi\chi_f\varphi$. So, it is straightforward to obtain a perturbative series for the dressed/renormalized $\tilde{D}$, which ultimately gives the dressed spin-spin correlation,

$$\begin{aligned}\tilde{D} &= J\,G_{\varphi\bar{\varphi}}\,\chi_c\,G_{\bar{\varphi}\varphi} + J^3\,G_{\varphi\bar{\varphi}}\,\chi_c\,G_{\bar{\varphi}\varphi}\,\chi_c\,G_{\bar{\varphi}\varphi} \\ &\quad + J^5\,G_{\varphi\bar{\varphi}}\,\chi_c\,G_{\bar{\varphi}\varphi}\,\chi_f\,G_{\varphi\bar{\varphi}}\,\chi_c\,G_{\bar{\varphi}\varphi}\,\chi_f\,G_{\varphi\bar{\varphi}}\,\chi_c\,G_{\bar{\varphi}\varphi} + \cdots \\ &= J\,G_{\varphi\bar{\varphi}}\,\chi_c\,G_{\bar{\varphi}\varphi} + J^2\,G_{\varphi\bar{\varphi}}\,\chi_c\,G_{\bar{\varphi}\varphi}\,\chi_f\left(J\,G_{\varphi\bar{\varphi}}\,\chi_c\,G_{\bar{\varphi}\varphi} + J^3\,G_{\varphi\bar{\varphi}}\,\chi_c\,G_{\bar{\varphi}\varphi}\,\chi_f\,G_{\varphi\bar{\varphi}}\,\chi_c\,G_{\bar{\varphi}\varphi} + \cdots\right) \\ &= J\,G_{\varphi\bar{\varphi}}\,\chi_c\,G_{\bar{\varphi}\varphi} + J^2\,G_{\varphi\bar{\varphi}}\,\chi_c\,G_{\bar{\varphi}\varphi}\,\chi_f\,\tilde{D} \ , \end{aligned} \tag{5.66}$$

[17] In general, any m-point correlation function for the auxiliary fields corresponds to a $(n = 2m)$-point correlation function for the original degrees-of-freedom (here, conduction electrons and f-pseudo-fermions). The converse is not true: Not all n-point and fermionic correlation functions can be written as m-point correlation functions for the auxiliary fields [243].

or equivalently,

$$\begin{aligned}\tilde{D} &= J\, G_{\varphi\bar{\varphi}} \left(\chi_c + J^2\, \chi_c\, G_{\bar{\varphi}\varphi}\, \chi_f\, G_{\varphi\bar{\varphi}}\, \chi_c + J^4\, \chi_c\, G_{\bar{\varphi}\varphi}\, \chi_f\, G_{\varphi\bar{\varphi}}\, \chi_c\, G_{\bar{\varphi}\varphi}\, \chi_f\, G_{\varphi\bar{\varphi}}\, \chi_c + \cdots\right) G_{\bar{\varphi}\varphi} \\ &= J\, G_{\varphi\bar{\varphi}}\, \tilde{\chi}_c\, G_{\bar{\varphi}\varphi}\ . \end{aligned} \tag{5.67}$$

Then,

$$\begin{aligned}\tilde{\chi}_c = \chi_c &+ J^2\, \chi_c\, G_{\bar{\varphi}\varphi}\, \chi_f\, G_{\varphi\bar{\varphi}}\, \chi_c \\ &+ J^4\, \chi_c\, G_{\bar{\varphi}\varphi}\, \chi_f\, G_{\varphi\bar{\varphi}}\, \chi_c + \cdots\ ,\end{aligned} \tag{5.68}$$

which is the expected RPA resummation for the conduction electron susceptibility. Plugging in the definitions for $G_{\varphi\bar{\varphi}}$, etc., yields[18]

$$\begin{aligned}\chi_c\, G_{\bar{\varphi}\varphi}\, \chi_f\, G_{\varphi\bar{\varphi}}\, \chi_c &\equiv \int \mathrm{d}x_1 x_2 x_3 x_4\ \chi_c(x - x_1)\, G_{\bar{\varphi}\varphi}(x_1 - x_2)\, \chi_f(x_2 - x_3)\, G_{\varphi\bar{\varphi}}(x_3 - x_4)\, \chi_c(x_4 - x') \\ &= \int \mathrm{d}x_1 x_2 x_3 x_4\ \chi_c(x - x_1)\, \delta(x_1 - x_2)\, \chi_f(x_2 - x_3)\, \delta(x_3 - x_4)\, \chi_c(x_4 - x') \\ &= \int \mathrm{d}x_1\, \mathrm{d}x_3\ \chi_c(x - x_1)\, \chi_f(x_1 - x_3)\, \chi_c(x_3 - x')\ . \end{aligned} \tag{5.71}$$

Since χ_f is local (in position representation),

$$\chi_f(x_1 - x_3) = \chi_f(x_1)\ ,$$

one obtains,

$$\begin{aligned}\chi_c\, G_{\bar{\varphi}\varphi}\, \chi_f\, G_{\varphi\bar{\varphi}}\, \chi_c &= \int \mathrm{d}x_1\ \chi_c(x - x_1)\, \chi_f(x_1)\, \chi_c(x_1 - x') \\ &=: \chi_c\ \chi_f\ \chi_c\ . \end{aligned} \tag{5.72}$$

Hence,

$$\begin{aligned}\tilde{\chi}_c &= \chi_c + J^2\, \chi_c\, \chi_f\, \chi_c + J^4\, \chi_c\, \chi_f\, \chi_c\, \chi_f\, \chi_c + \cdots \\ &= \chi_c + J^2\, \chi_c\, \chi_f \left(\chi_c + J^2\, \chi_c\, \chi_f\, \chi_c + \cdots\right) \\ &= \chi_c + J^2\, \chi_c\, \chi_f\, \tilde{\chi}_c\ . \end{aligned} \tag{5.73}$$

[18] Note that the 'free' Green's functions are

$$G_{\bar{\varphi}\varphi}(x_1, x_2) = \delta(x_1 - x_2)\ , \tag{5.69}$$

$$G_{\varphi\bar{\varphi}}(x_1, x_2) = \delta(x_1 - x_2)\ . \tag{5.70}$$

Therefore[19],

$$\begin{aligned}\left(1 - J^2 \chi_c \chi_f\right)\ \tilde{\chi}_c &= \chi_c \\ \tilde{\chi}_c &= \left(1 - J^2\, \chi_c\, \chi_f\right)^{-1}\, \chi_c \\ &\equiv \frac{\chi_c}{1 - J^2\, \chi_c\, \chi_f}\ . \end{aligned} \tag{5.77}$$

Thus, diagrammatically, the effective interaction between the localized spins is represented as in Fig. 5.8 in terms of the conduction electron susceptibility.

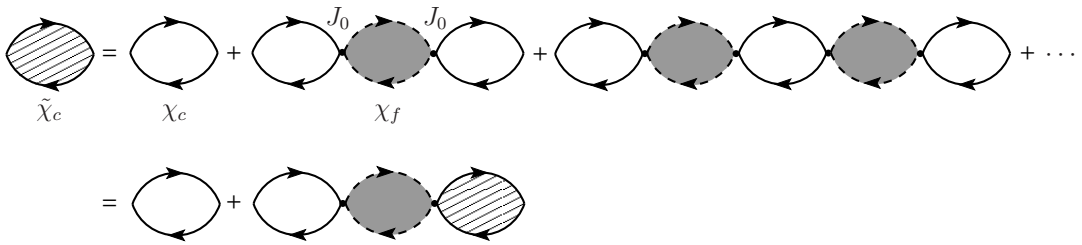

Figure 5.8: The susceptibility of the condition electrons is dressed by the local Kondo interaction.

Thus, the retarded susceptibility will be explicitly given by

$$\tilde{\chi}_c^R(\mathbf{q}, \omega) = \frac{\chi_c^{0,R}(\mathbf{q}, \mathrm{i}\omega)}{1 - J^2\, \chi_c^{0,R}(\mathbf{q}, \mathrm{i}\omega)\, \chi_f^{0,R}(\omega)}\ . \tag{5.78}$$

At low energies, the imaginary parts of the susceptibilities can be neglected[20], so that

$$\mathrm{Re}\, \chi_c^R(\mathbf{q}, \omega) = \frac{\mathrm{Re}\, \chi_c^{0,R}(\mathbf{q}, \omega)}{1 - J_0^2\ \mathrm{Re}\, \chi_c^{0,R}(\mathbf{q}, \omega)\ \mathrm{Re}\, \chi_f^R(\omega)}\ , \tag{5.79}$$

[19] More explicitly,

$$\tilde{\chi}_c(x - x') = \chi_c(x - x') + J^2 \int \mathrm{d}y\, \mathrm{d}y'\, \chi_c(x - y)\, \chi_f(y - y')\, \tilde{\chi}_c(y' - x') \tag{5.74}$$

where 4-vector notation is used:

$$\begin{aligned} x &\equiv (\mathbf{x}, t)\ , \\ q &\equiv (\mathbf{q}, \omega)\ . \end{aligned} \tag{5.75}$$

Therefore,

$$\tilde{\chi}_c(q) = \chi_c(q) + J^2 \chi_c(q) \chi_f(q) \tilde{\chi}_c(q)\ ; \tag{5.76}$$

Notice that χ_f is 'local' in position representation; that is, it has no momentum dependence.

[20] Dissipation which is proportional to the imaginary part of the susceptibility vanishes linearly near the Fermi surface [244])

with

$$\begin{aligned}\mathrm{Re}\,\chi_f(\omega) &= \frac{a'}{T_K}\frac{1}{\sqrt{1+(\omega/T_K)^2}} \quad ; a' \sim \mathcal{O}(1) \\ &= a' D_0 \frac{1}{T_K/D_0}\frac{1}{\sqrt{1+(\frac{D_0}{T_K}\,\frac{\omega}{D_0})}} \ . \end{aligned} \tag{5.80}$$

given in section 3.2.

5.3.2 Criterion for magnetic instability

The effective interaction between the local moments was obtained in Eq. (5.79) in terms of the dressed conduction electron susceptibility, $\tilde{\chi}_c$. A spin density wave (magnetic) instability occurs when [245]

$$1 - J_0^2\ \chi_c^{0,R\prime}(\mathbf{q},\omega)\ \chi_f^{R\prime}(\omega) = 0 \ . \tag{5.81}$$

In the low-frequency, long-wavelength limit, the divergence happens at a certain momentum $\mathbf{Q}$, and ω, which depend on the band-structure of the conduction electrons and the properties of the impurity lattice.[21] Before the transition, this leads to an enhancement factor in Eq. (5.79). Note

[21] For instance, for an electronic system with a tight-binding dispersion and 'perfect nesting property',

$$\begin{aligned}\varepsilon(\mathbf{k}) &= \varepsilon_0 + \gamma\sum_{i=1} 3\cos(k_i a) \ , \\ \varepsilon(\mathbf{k}+\mathbf{Q}) &= -\varepsilon(\mathbf{k}) \quad , \quad \mathbf{Q} = \pi(\pm1,\pm1,\pm1) : \text{nesting order} \ , \end{aligned} \tag{5.82}$$

the susceptibility is

$$\begin{aligned}\chi_c(\mathbf{q}=\mathbf{Q},\omega\to0) &= \frac{1}{V}\sum_{\mathbf{p}}\frac{n_F(\xi_{\mathbf{p}})-n_F(\xi_{\mathbf{p}+\mathbf{Q}})}{\xi_{\mathbf{p}+\mathbf{Q}}-\xi_{\mathbf{p}}} \overset{\mu=0}{=\!=} \frac{1}{V}\sum_{\mathbf{p}}\frac{n_F(\varepsilon_{\mathbf{p}})-n_F(\varepsilon_{\mathbf{p}+\mathbf{Q}})}{\varepsilon_{\mathbf{p}+\mathbf{Q}}-\varepsilon_{\mathbf{p}}} \\ &\overset{\text{nesting}}{=\!=} \frac{1}{V}\sum_{\mathbf{p}}\frac{n_F(\varepsilon_{\mathbf{p}})-n_F(-\varepsilon_{\mathbf{p}})}{-\varepsilon_{\mathbf{p}}-\varepsilon_{\mathbf{p}}} = -\frac{1}{V}\sum_{\mathbf{p}}\frac{n_F(\varepsilon_{\mathbf{p}})-n_F(-\varepsilon_{\mathbf{p}})}{-\varepsilon_{\mathbf{p}}-\varepsilon_{\mathbf{p}}} \\ &= \frac{1}{V}\sum_{\mathbf{p}}\frac{1-2n_F(\varepsilon_{\mathbf{p}})}{2\varepsilon_{\mathbf{p}}} = \int \mathrm{d}\xi\,\mathcal{N}(\xi)\frac{1-2n_F(\xi)}{2\xi} \\ &= \int \mathrm{d}\xi\,\mathcal{N}(\xi)\frac{\tanh(\frac{\beta\xi}{2})}{2\xi} \approx \mathcal{N}(\varepsilon_F)\int_{-D}^{+D}\mathrm{d}\xi\,\frac{\tanh(\frac{\beta\xi}{2})}{2\xi} \ . \end{aligned} \tag{5.83}$$

Expanding the tanh function in different regions,

$$\tanh(\frac{\beta\xi}{2}) = \begin{cases} -1, & \xi < -2T \\ \beta\frac{\xi}{2}, & -2T \le \xi \le 2T \\ +1, & \xi > 2T \end{cases} \quad ,$$

one obtains

$$\begin{aligned}\chi_c(\mathbf{q}=\mathbf{Q},\omega\to0) &= \mathcal{N}(\varepsilon_F)\left(\int_{-D}^{-2T}\mathrm{d}\xi\,\frac{-1}{2\xi} + \int_{-2T}^{2T}\mathrm{d}\xi\,\frac{\beta}{2} + \int_{2T}^{+D}\mathrm{d}\xi\,\frac{1}{2\xi}\right) \\ &= \mathcal{N}(\varepsilon_F)\left(-\frac{1}{2}\ln|\frac{2T}{D}| + 2 + \frac{1}{2}\ln|\frac{D}{2T}|\right) \\ &= \mathcal{N}(\varepsilon_F)\left(\ln|\frac{D}{2T}| + 2\right) \ , \end{aligned} \tag{5.84}$$

that $\chi_c(\mathbf{x},\omega)$ is a slowly-varying function of ω at low frequencies, $\omega \sim \mathcal{O}(T_K) \ll D_0$. Therefore, the enhancement factor of the susceptibility will be well-approximated by

$$\frac{1}{1 - J_0^2 \chi_f(\omega)\chi_c(\mathbf{q}=\mathbf{Q},\omega=0)} \ , \tag{5.85}$$

where $\chi_c(\mathbf{q}=\mathbf{Q},\omega=0)$ is the critical mode in χ_c; the maximum (or divergence) of χ_c occurs at a certain momentum, $\mathbf{Q}$ (at $\omega \to 0$) which in turn determines the critical value of the coupling, J_c, at which the system becomes unstable towards a magnetically-ordered phase; e.g., antiferromagnetic ordering, spin density waves, etc. Therefore, at low energies,

$$\tilde{\chi}_c(\mathbf{q},\omega) = \frac{1}{1 - J_0^2\, \chi_f(\omega)\, \chi_c(q=Q,\omega=0)}\ \chi_c(q,\omega) \tag{5.86}$$

from which a Fourier transformation to the position representation gives

$$\tilde{\chi}_c(\mathbf{x},\omega) = \frac{1}{1 - J_0^2\, \chi_f(\omega)\, \chi_c(q=Q,\omega=0)}\ \chi_c(\mathbf{x},\omega) \ . \tag{5.87}$$

From the definition of the RKKY strength parameter, as in Eq. (3.177),

$$y \propto \sum_{\mathbf{x}_l} A_c^0(\mathbf{x}_l)\ \chi_c(\mathbf{x}_l) \ , \tag{5.88}$$

it is clear that y is an average of the strength of the RKKY interaction over the lattice, and here, it is dominated by the maximum value of χ_c which occurs at $\mathbf{q}=\mathbf{Q}$. Essentially, y should be considered as an average value which is dependent on the density of impurities (through the sum $\sum_{\mathbf{x}_l}$), the band-structure of the conduction electrons, and their response function χ_c; that is, non-universal properties of the conduction band. With this parametre, one can re-write the renormalized conduction electron susceptibility as

$$\tilde{\chi}_c(\mathbf{x},\omega) \approx \chi_c(\mathbf{x},\omega) \Big/ \left(1 - g_0^2 y \frac{1}{T_K/D_0} \frac{1}{\sqrt{1+(\omega/T_K)^2}}\right) \quad ; \quad g_0 := \mathcal{N}(\varepsilon_F) J \ . \tag{5.89}$$

5.3.3 RG flow including the possibility of magnetic instability

Having this renormalized susceptibility and following an analogous procedure as in chapter 3, the RKKY-modified RG equation will be obtained as

$$\frac{\mathrm{d}g}{\mathrm{d}\ln D} = -g^2 \left(1 - g_0^2 y \frac{1}{T_K/D_0} \frac{1}{\sqrt{1+(D/T_K)^2}} \frac{1}{1 - g_0^2 y \frac{1}{T_K/D_0} \frac{1}{\sqrt{1+(D/T_K)^2}}}\right) \ . \tag{5.90}$$

which leads to a low-temperature *logarithmic* divergence at $\mathbf{q}=\mathbf{Q}$ (see Ref. [246]).

Therefore, integrating the differential equation, one finds

$$-\frac{\mathrm{d}g}{g^2}\Big|_{g=g_0}^{g(T_K)\to\infty} = \int_{D_0}^{T_K} \frac{\mathrm{d}D}{D} \left(1 - g_0^2 y \frac{1}{T_K/D_0} \frac{1}{\sqrt{1+(D/T_K)^2}} \frac{1}{1 - g_0^2 y \frac{1}{T_K/D_0} \frac{1}{\sqrt{1+(D/T_K)^2}}} \right) , \tag{5.91}$$

where the LHS is simply,

$$-\frac{\mathrm{d}g}{g^2}\Big|_{g=g_0}^{g(T_K)\to\infty} = -\frac{1}{2g_0} = \ln(T_K^0/D_0) \ . \tag{5.92}$$

To solve the RG equation, we have to perform the integral on the RHS,

$$I := \int_{\omega=\frac{D_0}{T_K}}^{1} \frac{\mathrm{d}\omega}{\omega} \Big(1 - g_0^2 y \frac{1}{T_K/D_0} \frac{1}{\sqrt{1+\omega^2}} \frac{1}{1 - \underbrace{g_0^2 y \frac{1}{T_K/D_0}}_{=:\aleph} \frac{1}{\sqrt{1+\omega^2}}} \Big) \ . \tag{5.93}$$

The indefinite integral

$$I := \int \frac{\mathrm{d}\omega}{\omega} \frac{1}{\sqrt{1+\omega^2}} \frac{1}{1 - \aleph \frac{1}{\sqrt{1+\omega^2}}} \quad ; \quad \aleph > 0 \tag{5.94}$$

can be performed analytically with a change of variable

$$\begin{aligned} z &:= \sqrt{1+\omega^2} \\ \Rightarrow z^2 &= 1+\omega^2 \Rightarrow z\mathrm{d}z = \omega\mathrm{d}\omega \\ \Rightarrow \mathrm{d}\omega &= \frac{z}{\omega}\mathrm{d}z \ , \end{aligned} \tag{5.95}$$

so that

$$\begin{aligned} I &= \int \mathrm{d}z \, \frac{z}{\omega^2} \frac{1}{z} \frac{1}{1-\aleph/z} = \int \mathrm{d}z \, \frac{1}{z^2-1} \frac{1}{1-\aleph/z} \\ &= \int \mathrm{d}z \, \frac{z}{(z^2-1)(z-\aleph)} \ . \end{aligned} \tag{5.96}$$

Partial fraction decomposition yields

$$\frac{z}{(z^2-1)(z-\aleph)} = \frac{1}{2(1-\aleph)(z-1)} - \frac{1}{2(1+\aleph)(z+1)} + \frac{\aleph}{(\aleph-1)(\aleph+1)(z-\aleph)} \ ; \tag{5.97}$$

therefore,

$$
\begin{aligned}
I &= \frac{1}{2(1-\aleph)}\ln|z-1| + \frac{1}{2(1+\aleph)}\ln|z+1| - \frac{\aleph}{(1-\aleph)(1+\aleph)}\ln|z-\aleph| \\
&= \frac{1}{2(1-\aleph)(1+\aleph)}\left[(1+\aleph)\ln|z-1| - (1-\aleph)\ln|z+1| - 2\aleph\ln|z-\aleph|\right] \\
&= \frac{1}{2(1-\aleph)(1+\aleph)}\left[\ln|\frac{z-1}{z+1}| + \aleph\ln|z^2-1| - 2\aleph\ln|z-\aleph|\right] \\
&= \frac{1}{2(1-\aleph^2)}\left[\ln|\frac{1-\sqrt{1+\omega^2}}{1+\sqrt{1+\omega^2}}| + \aleph\ln|\omega^2| - 2\aleph\ln|\sqrt{1+\omega^2}-\aleph|\right] \\
&= \frac{1}{2(1-\aleph^2)}\left[\ln|\frac{1-\sqrt{1+\omega^2}}{1+\sqrt{1+\omega^2}}| - 2\aleph\ln|\frac{\sqrt{1+\omega^2}-\aleph}{\omega}|\right] \\
&= \frac{1}{2(\aleph^2-1)}\left[\aleph\ln|\frac{\sqrt{1+\omega^2}-\aleph}{\omega}| + \frac{1}{2}\ln|\frac{1+\sqrt{1+\omega^2}}{1-\sqrt{1+\omega^2}}|\right] \quad . \qquad (5.98)
\end{aligned}
$$

Then, the result of the definite integral, Eq. (5.93), is

$$
\begin{aligned}
I\Big|_{\omega=D_0/T_K}^{1} &= \ln(1) - \frac{\aleph}{(\aleph^2-1)}\left[\aleph\ln|\frac{\sqrt{2}-\aleph}{1}| + \frac{1}{2}\ln|\frac{1+\sqrt{2}}{1-\sqrt{2}}|\right] \\
&\quad - \ln|\frac{D_0}{T_K}| + \frac{\aleph}{\aleph^2+1}\left[\aleph\ln|\frac{\sqrt{1+(D_0/T_K)^2}-\aleph}{D_0/T_K}| + \frac{1}{2}\ln|\frac{1+\sqrt{1+(D_0/T_K)^2}}{1-\sqrt{1+(D_0/T_K)^2}}|\right] \\
&\overset{D_0/T_K\gg 1}{=\!=\!=} -\frac{\aleph}{\aleph^2-1}\Big[\aleph\ln|\aleph-\sqrt{2}| + \frac{1}{2}\ln|\underbrace{\frac{1+\sqrt{2}}{1-\sqrt{2}}}_{\approx 0.881\approx 1.0}|\Big] \\
&\quad + \ln(\frac{T_K}{D_0}) + \frac{\aleph}{\aleph^2-1}\Big[\underbrace{\aleph\ln(1) + \frac{1}{2}\ln(1)}_{=0}\Big] \\
&= \ln(\frac{T_K}{D_0}) - \frac{\aleph}{\aleph^2-1}\left[\aleph\ln|\aleph-\sqrt{2}| + 1\right] \quad . \qquad (5.99)
\end{aligned}
$$

Thus, the RG equation Eq. (5.91) yields the following equation for the RKKY-modified Kondo temperature, T_K:

$$
\begin{aligned}
\ln(\frac{T_K^0}{D_0}) &= \ln(\frac{T_K}{D_0}) - \frac{\aleph}{\aleph^2-1}\left[\aleph\ln|\aleph-\sqrt{2}| + 1\right] \\
&\Rightarrow \ln(\frac{T_K}{T_K^0}) = \frac{\aleph}{\aleph^2-1}\left[1 + \aleph\ln|\aleph-\sqrt{2}|\right] \\
&\Rightarrow \frac{T_K}{T_K^0} = \exp\left[\frac{\aleph}{\aleph^2-1}(1+\aleph\ln|\aleph-\sqrt{2}|)\right] \quad . \qquad (5.100)
\end{aligned}
$$

Using the following definitions for the rescaled Kondo temperature, τ, and y,

$$\begin{aligned}\tau &:= \frac{T_K}{T_K^0} \ , \\ \aleph &= g_0^2\, y\, \frac{1}{T_K/D_0} = \underbrace{g_0^2 \frac{y}{T_K^0/D_0}}_{:=\mathsf{y}} \frac{1}{T_K/T_K^0} \equiv \mathsf{y}\frac{1}{T_K/T_K^0} \equiv \mathsf{y}/\tau \ , \\ \mathsf{y} &:= g_0^2\, \frac{y}{T_K^0/D_0}\end{aligned} \tag{5.101}$$

one can re-write the above equation for $T_K(y)$ as

$$\tau(\mathsf{y}) = \exp\left[\frac{\mathsf{y}/\tau}{(\mathsf{y}/\tau)^2 - 1}\left(1 + \frac{\mathsf{y}}{\tau}\ln|\frac{\mathsf{y}}{\tau} - \sqrt{2}|\right)\right] \ . \tag{5.102}$$

Furthermore, the instability criterion, Eq. (5.81), can be re-written as

$$\begin{aligned} g_0^2 y \frac{1}{T_K/D_0}\frac{1}{\sqrt{1+(\omega/T_K)^2}} &= 1 \\ \Rightarrow g_0^2 \frac{y}{T_K^0/D_0}\frac{1}{T_K/T_K^0}\frac{1}{\sqrt{1+(\omega/T_K)^2}} &= 1 \\ \Rightarrow \frac{\mathsf{y}}{\tau}\frac{1}{\sqrt{1+(\omega/T_K)^2}} &= 1 \\ \overset{\omega\lesssim T_K}{\Longrightarrow} \frac{\mathsf{y}}{\tau} &\approx 1 \end{aligned} \tag{5.103}$$

Note that the last line is exact when $\omega \to 0$, i.e., the static limit. Furthermore, before the onset of instability, y and τ satisfy

$$1 - \frac{\mathsf{y}}{\tau} \geq 0 \Rightarrow \frac{\mathsf{y}}{\tau} \leq 1 \ . \tag{5.104}$$

To solve the equation for $\tau(\mathsf{y})$, Eq. (5.102), it is useful to define

$$x := \frac{\tau}{\mathsf{y}} > 0 \ ; \tag{5.105}$$

therefore, Eq. (5.102) becomes[22]

[22] Notice that the function $\mathcal{F}(x)$ has singularities (apart from $x = 0$) at

$$\begin{aligned} x &= 1 \ , \\ x &= \frac{1}{\sqrt{2}} \approx 0.7 < 1 \quad : \text{logarithmic singularity} \ . \end{aligned} \tag{5.106}$$

$$
\begin{aligned}
\mathsf{y}x &= \exp\left[-\frac{1}{x}\left(\frac{1}{1-\frac{1}{x^2}}(1+\frac{1}{x}\ln|\frac{1}{x}-\sqrt{2}|)\right)\right] \\
&= \exp\left[-\frac{1}{x}\left(\frac{x^2}{x^2-1}(1+\frac{1}{x}\ln|\frac{1}{x}-\sqrt{2}|)\right)\right] \\
&= \exp\Big[\underbrace{-\frac{1}{x}\left(\frac{x^2+x\ln|\frac{1}{x}-\sqrt{2}|}{x^2-1}\right)}_{:=\mathcal{F}(x)}\Big] \,.
\end{aligned}
\tag{5.107}
$$

Again, as in chapter 3, one can obtain the solution 'geometrically' as the point(s) of intersection of two curves: a line, $\mathsf{y}x$, and a curve, $e^{\mathcal{F}(x)}$ (see Fig. 5.9). We have to look for the solution away from the magnetic instability region.

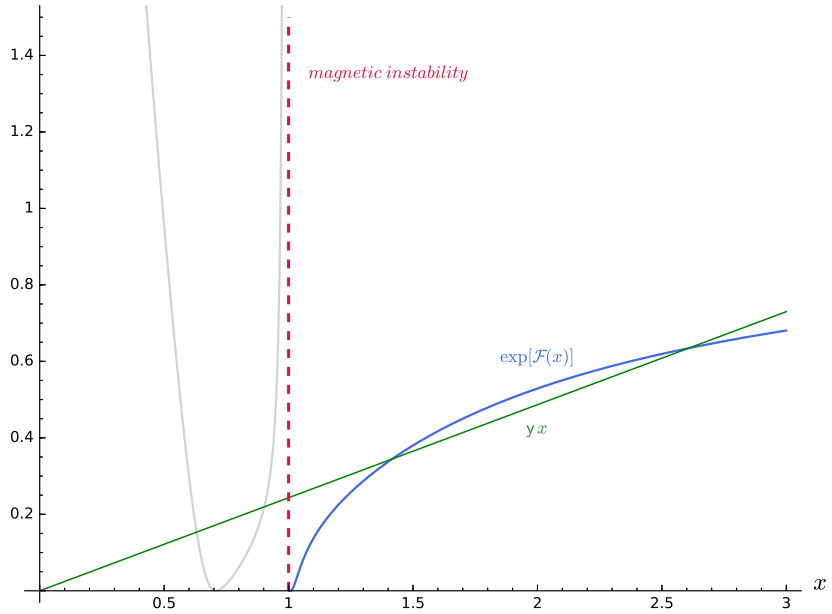

Figure 5.9: The function $\exp[\mathcal{F}(x)]$ (blue and gray curve). The region $x \leq 1$ corresponds to the magnetically-ordered region, separated by a dashed red line (denoting magnetic instability threshold) from the rest of the x-axis. The green line represents $\mathsf{y}x$.

Notice that, as in Eq. (5.104), the magnetic singularity occurs for $x \leq 1$. The breakdown of local Kondo screening happens at $\mathsf{y} = \mathsf{y}_{max}$, where the values and slopes of the right and left-hand-side of Eq. (5.107) coincide:

$$
\begin{cases}
\mathsf{y}_{max}\, x_{max} &= \exp[\mathcal{F}(x_{max})] \\
\mathsf{y}_{max} &= \left.\frac{\partial\mathcal{F}(x)}{\partial x}\right|_{x=x_{max}} \cdot \exp[\mathcal{F}(x_{max})]
\end{cases} .
$$

Then, the equation that determines x_{max} will be

$$\frac{1}{x_{max}} = \frac{\partial \mathcal{F}(x)}{\partial x}\Big|_{x=x_{max}} , \tag{5.108}$$

and

$$\mathsf{y}_{max} = \frac{1}{x_{max}} \exp[\mathcal{F}(x)]\Big|_{x=x_{max}} . \tag{5.109}$$

The numerical solution to this equation is found to be

$$\begin{aligned} & x_{max} \approx 1.832 \ , \\ \rightarrow \mathsf{y}_{max}\ & x_{max} \equiv \tau_m \equiv \frac{T_K(\mathsf{y}_{max})}{T_K(0)} = \exp[\mathcal{F}(x_{max})] \approx 0.488 > \frac{1}{e} \approx 0.368 \ , \\ \rightarrow & \ \mathsf{y}_{max} = \frac{1}{x_{max}} \exp[\mathcal{F}(x_{max})] \approx 0.266 < \frac{1}{e} \ . \end{aligned} \tag{5.110}$$

The full variation of the RKKY-modified Kondo temperature upon increasing RKKY strength parameter is shown in Fig. 5.10.

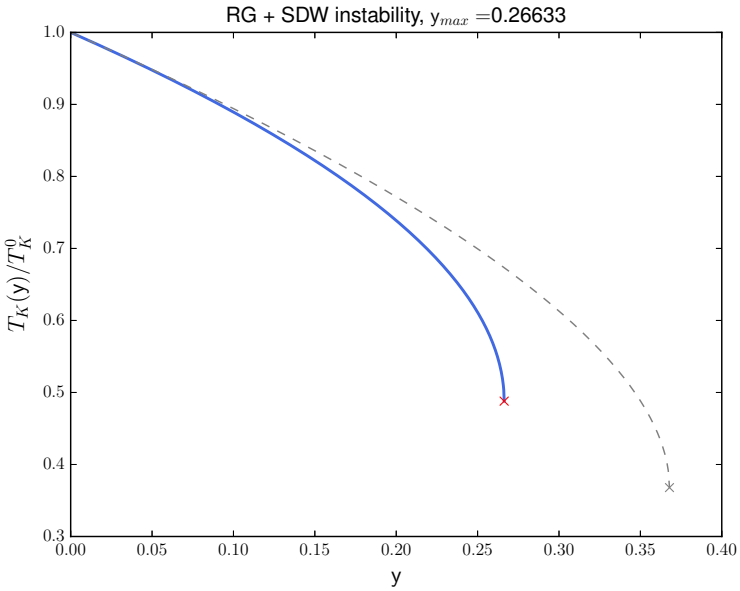

Figure 5.10: Universal curve for the RKKY-modified Kondo temperature including the SDW instability (blue curve) as a function of the RKKY strength parameter, y; the curve ends at the breakdown point at $\mathsf{y}_{max} \approx 0.266$ where $T_K/T_K^0 \approx 0.488$. The gray dashed curve corresponding to the RKKY-modified Kondo temperature obtained without inclusion of magnetic instability, is given for comparison. Note that, even with inclusion of the SDW instability, the Kondo temperature does *not* vanish at the breakdown point.

Notice that compared to the previous case in section 3.4, where the conduction electron susceptibility, χ_c, was not dressed by the local interaction, the breakdown of the local Kondo screening happens *earlier*; that is, with a *smaller* value of the RKKY-strength (for the 'non-

renormalized' case, $y_{max} = \frac{1}{e} \approx 0.368$) (see also Fig. 5.12). Furthermore, the onset of magnetic instability occurs *later* than (not simultaneously with) the breakdown of Kondo screening, when $x = 1 < x_{max} \approx 1.8$. This is qualitatively consistent with the experimental observations obtained, e.g., for quantum criticality in $CeCu_{6-x}Au_x$ [124] (see Fig. 5.11).[23]

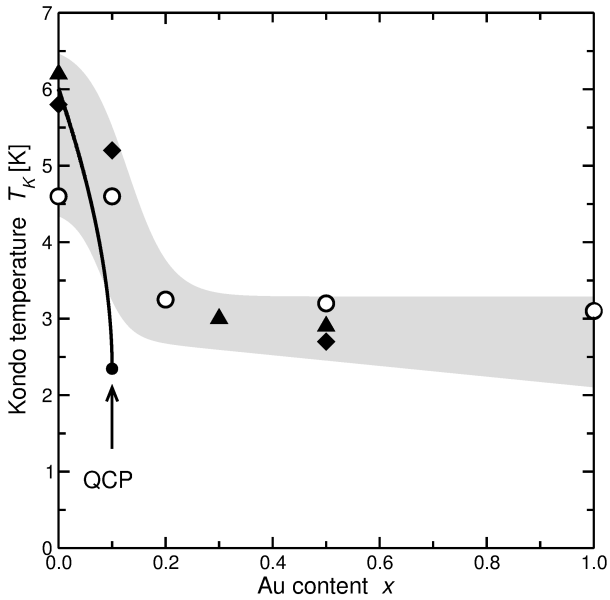

Figure 5.11: Variation of the Kondo temperature of the heavy-fermionic compound $CeCu_{6-x}Au_x$ with the Au content, x, as determined by UPS (open circles), specific heat (triangles) and neutron scattering (diamonds) (adopted from Ref. [124]). Notice that the Kondo temperature does *not* drop to zero at the quantum critical point.

In this intermediate region, full Kondo screening ceases; hence the local moments are only *partially-screened* while there is *no* magnetic order. In this phase, the conduction electrons and local moments are only weakly interacting, since the strong-coupling fixed point (corresponding to full Kondo screening) is absent. This is a very interesting phase in itself, since it can exhibit various interesting (perhaps, exotic) properties (like glassy behaviour) depending on the non-universal details of the system. The next chapter is devoted to this partially-screened disordered phase.

[23] Notice that the relation of the RKKY strength parameter, y, to the concentration of Au in $CeCu_{6-x}Au_x$ compound is not easily to determie since this depends on the details of the change in band-structure of the compound upon varying x.

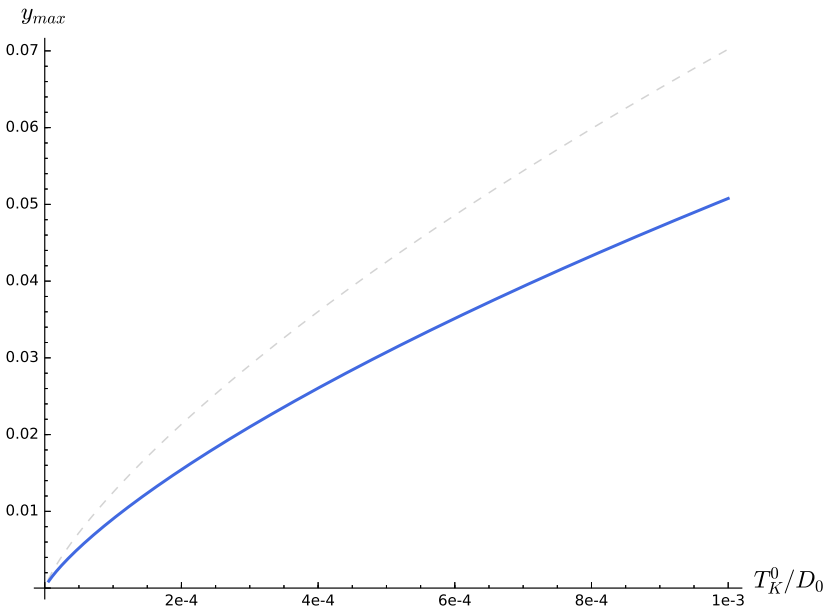

Figure 5.12: The maximal RKKY strength, y_{max}, as a function of the *bare* Kondo temperature. The gray dashed curve corresponding to the maximal RKKY strength without inclusion of magnetic instability, is given for comparison.

CHAPTER 6

Partially-Screened Moments in a Disordered Phase

In the previous chapter on the Kondo screening and magnetic instability in a Kondo lattice, we found a phase in which Kondo screening has collapsed while the local moments are not ordered. In this phase, RG flow does not diverge anymore, meaning that the strong-coupling fixed point (corresponding to the formation of Kondo singlets) is absent. This implies that as we decrease the temperature, the Kondo coupling increases but it does not diverge. Hence, there is only partial Kondo screening for the local moments.

Inside this regime, the system can be described by a Heisenberg model in which the Heisenberg coupling is renormalized by the 'Kondo fluctuations'. The partial screening of the local moments can be included as a modified magentic moment through a renormalized Heisenberg exchange coupling or Landé factor.

In this chapter, we begin by a detailed derivation of the RKKY interaction from the Kondo model. Afterwards, we apply a random-phase approximation (RPA) [103, 246–248] to the Heisenberg model with renormalized Kondo couplings in order to find the possible magnetic instability of this phase.

6.1 Effective RKKY interaction

In this section, we explicitly derive the expression for the RKKY interaction via a canonical transformation on the Heisenberg model [202, 246].

Consider the Kondo lattice Hamiltonian

$$H = \sum_{\mathbf{k}\sigma} c^\dagger_{\mathbf{k}\sigma} c_{\mathbf{k}\sigma} + H_1 \ , \tag{6.1}$$

where

$$H_1 = J \sum_l \mathbf{S}(\mathbf{x}_l) \cdot \mathbf{s}(\mathbf{x}_l) = \frac{J}{2} \sum_{l,\mu\mu'} \mathbf{S}(\mathbf{x}_l) \cdot c^\dagger_{\mu'}(\mathbf{x}_l)\, \sigma_{\mu'\mu}\, c_\mu(\mathbf{x}_l) \ , \tag{6.2}$$

with

$$c_\mu(\mathbf{x}_l) = \frac{1}{\sqrt{V}} \sum_{\mathbf{k}} e^{\mathrm{i}\mathbf{k}\cdot\mathbf{x}_l} c_\mu(\mathbf{k}) \quad , \quad c^\dagger_\mu(\mathbf{x}_l) = \frac{1}{\sqrt{V}} \sum_{\mathbf{k}} e^{-\mathrm{i}\mathbf{k}\cdot\mathbf{x}_l} c^\dagger_\mu(\mathbf{k})$$
$$H_1 = \frac{J}{2}\frac{1}{V} \sum_l \sum_{\mathbf{k}'\mathbf{k},\mu'\mu} \mathbf{S}(\mathbf{x}_l)\cdot\sigma_{\mu'\mu}\, e^{-\mathrm{i}\mathbf{x}_l\cdot(\mathbf{k}'-\mathbf{k})} c^\dagger_{\mathbf{k}'\mu'} c_{\mathbf{k}_\mu} \ . \tag{6.3}$$

The effective interaction between the local moments (spins) can be obtained via a unitary transformation on the Hamiltonian, which eliminates the conduction electrons, leaving out a spin-spin interaction between the local moments:

$$H_{\mathit{eff}} = e^{\mathrm{i}A} H e^{-\mathrm{i}A} = H + [\mathrm{i}A, H] + \frac{1}{2}[\mathrm{i}A, [\mathrm{i}A, H]] + \textit{higher orders} \ , \tag{6.4}$$

where the operator A, generator of transformation, is a function of the coupling J. If one demands that (to the linear order in J),

$$[\mathrm{i}A, H_0] = -H_1 \ , \tag{6.5}$$

then, to the second order in J,

$$H_{\mathrm{eff}} = H_0 + \frac{1}{2}[\mathrm{i}A, H_1] \ . \tag{6.6}$$

For the Kondo Hamiltonian the generator of the transformation can be chosen as

$$\mathrm{i}A = \frac{J}{2}\frac{1}{V} \sum_l \sum_{\mathbf{k}\mathbf{k}'} \sum_{\nu\nu'} e^{\mathrm{i}(\mathbf{k}-\mathbf{k}')\cdot\mathbf{x}_l} \frac{1}{\varepsilon_{\mathbf{k}'} - \varepsilon_{\mathbf{k}}} \mathbf{S}(\mathbf{x}_l)\cdot c^\dagger_{\mathbf{k}'\nu'}\, \sigma_{\nu'\nu}\, c_{\mathbf{k}\nu} \ . \tag{6.7}$$

Note that

$$\begin{aligned}
[\mathrm{i}A, H_0] &= \frac{J}{2}\frac{1}{V} \sum_l \sum_{\mathbf{k}'\mathbf{k},\nu'\nu} e^{\mathrm{i}(\mathbf{k}-\mathbf{k}')\cdot\mathbf{x}_l} \frac{1}{\varepsilon_{\mathbf{k}'} - \varepsilon_{\mathbf{k}}} \sum_{\mathbf{q}\mu} \varepsilon_{\mathbf{q}} \underbrace{[\mathbf{S}_l \cdot c^\dagger_{\mathbf{k}'\nu'}\sigma_{\nu'\nu}c_{\mathbf{k}\nu}, c^\dagger_{\mathbf{q}\mu}c_{\mathbf{q}\mu}]}_{=(\mathbf{S}_l\cdot\sigma_{\nu'\nu})(c^\dagger_{\mathbf{k}'\nu'}c_{\mathbf{q}\mu}\delta_{\mathbf{k}\mathbf{q}}\delta_{\mu\nu} - c^\dagger_{\mathbf{q}\mu}c_{\mathbf{k}\nu}\delta_{\mathbf{q}\mathbf{k}'}\delta_{\nu'\mu})} \\
&= \frac{J}{2}\frac{1}{V} \sum_l \sum_{\mathbf{k}\mathbf{k}',\nu'\nu} e^{\mathrm{i}(\mathbf{k}-\mathbf{k}')\cdot\mathbf{x}_l} \frac{1}{\varepsilon_{\mathbf{k}'} - \varepsilon_{\mathbf{k}}} (\mathbf{S}_l\cdot\sigma_{\nu'\nu}) \underbrace{(\varepsilon_{\mathbf{k}} c^\dagger_{\mathbf{k}'\nu'}c_{\mathbf{k}\nu} - \varepsilon_{\mathbf{k}'} c^\dagger_{\mathbf{k}'\nu'}c_{\mathbf{k}\nu})}_{=(\varepsilon_{\mathbf{k}}-\varepsilon_{\mathbf{k}'})c^\dagger_{\mathbf{k}'\nu'}c_{\mathbf{k}\nu}} \\
&= -\frac{J}{2}\frac{1}{V} \sum_l \sum_{\mathbf{k}\mathbf{k}',\nu'\nu} e^{\mathrm{i}(\mathbf{k}-\mathbf{k}')\cdot\mathbf{x}_l} \mathbf{S}_l\cdot\sigma_{\nu'\nu} c^\dagger_{\mathbf{k}'\nu'}c_{\mathbf{k}\nu} = -H_1 \ .
\end{aligned} \tag{6.8}$$

So, the operator A above satisfies the necessary equation, Eq. (6.5). To find the effective Hamiltonian, one has to obtain

$$\begin{aligned}
[\mathrm{i}A, H_1] = (\frac{J}{2V})^2 \sum_l \sum_{\mathbf{k}\mathbf{k}',\nu\nu'} e^{\mathrm{i}(\mathbf{k}-\mathbf{k}')\cdot\mathbf{x}_l} \frac{1}{\varepsilon_{\mathbf{k}'} - \varepsilon_{\mathbf{k}}} \\
\times \sum_{l'} \sum_{\mathbf{q}'\mathbf{q},\mu'\mu} e^{-\mathrm{i}(\mathbf{q}'-\mathbf{q})\cdot\mathbf{x}_{l'}} [\mathbf{S}_l\cdot\sigma_{\nu'\nu}c^\dagger_{\mathbf{k}'\nu'}c_{\mathbf{k}\nu}, \mathbf{S}_{l'}\cdot\sigma_{\mu'\mu}c^\dagger_{\mathbf{q}'\mu'}c_{\mathbf{q}\mu}] \ .
\end{aligned} \tag{6.9}$$

The commutator under the sum is obtained as

$$[\mathbf{S}_l \cdot \sigma_{\nu'\nu} c^\dagger_{\mathbf{k}'\nu'} c_{\mathbf{k}\nu}, \mathbf{S}_{l'} \cdot \sigma_{\mu'\mu} c^\dagger_{\mathbf{q}'\mu'} c_{\mathbf{q}\mu}] = (\mathbf{S}_l \cdot \sigma_{\nu'\nu})(\mathbf{S}_{l'} \cdot \sigma_{\mu'\mu})[c^\dagger_{\mathbf{k}'\nu'} c_{\mathbf{k}\nu}, c^\dagger_{\mathbf{q}'\mu'} c_{\mathbf{q}\mu}], \quad \text{for } l \neq l' \ . \tag{6.10}$$

Note that the contribution of $l = l'$ is proportional to $S_l^2 = S(S+1)$; this contribution is neglected in the following. Furthermore, the commutator on the RHS is obtained as

$$\begin{aligned}[c^\dagger_{\mathbf{k}'\nu'} c_{\mathbf{k}\nu}, c^\dagger_{\mathbf{q}'\mu'} c_{\mathbf{q}\mu}] &= c^\dagger_{\mathbf{k}'\nu'}(\delta_{\mathbf{k}\mathbf{q}'}\delta_{\nu\mu'} c_{\mathbf{q}\mu}) + (-c^\dagger_{\mathbf{q}'\mu'}\delta_{\mathbf{k}'\mathbf{q}}\delta_{\mu\nu'}) c_{\mathbf{k}\nu} \\ &= \delta_{\mathbf{k}\mathbf{q}}\delta_{\nu\mu'} c^\dagger_{\mathbf{k}'\nu'} c_{\mathbf{q}\mu} - \delta_{\mathbf{k}'\mathbf{q}}\delta_{\mu\nu'} c^\dagger_{\mathbf{q}'\mu'} c_{\mathbf{k}\nu} \ . \end{aligned} \tag{6.11}$$

Therefore, Eq. (6.10) yields

$$(\mathbf{S}_l \cdot \sigma_{\nu'\nu})(\mathbf{S}_{l'} \cdot \sigma_{\nu\mu})\delta_{\mathbf{k}\mathbf{q}'}\delta_{\nu\mu'} c^\dagger_{\mathbf{k}'\nu'} c_{\mathbf{q}\mu} - (\mathbf{S}_l \cdot \sigma_{\nu'\nu})(\mathbf{S}_{l'} \cdot \sigma_{\mu'\nu'})\delta_{\mathbf{k}'\mathbf{q}}\delta_{\mu\nu'} c^\dagger_{\mathbf{q}'\mu'} c_{\mathbf{k}\nu} \ . \tag{6.12}$$

Thus,

$$\begin{aligned}[\mathrm{i}A, H_1] = &(\frac{J}{2V})^2 \sum_{l,l'} \sum_{\substack{\mathbf{k}\mathbf{k}',\nu' \\ \mathbf{q}\mathbf{q}',\mu}} e^{\mathrm{i}(\mathbf{k}-\mathbf{k}')\cdot\mathbf{x}_l} \frac{1}{\varepsilon_{\mathbf{k}'} - \varepsilon_{\mathbf{k}}} e^{-\mathrm{i}(\mathbf{q}'-\mathbf{q})\cdot\mathbf{x}_{l'}} \sum_{ab} (\mathbf{S}_l^a S_{l'}^b)(\sigma^a\sigma^b)_{\nu'\mu} c^\dagger_{\mathbf{k}'\nu'} c_{\mathbf{q}\mu}\delta_{\mathbf{k}\mathbf{q}'} \\ &- (\frac{J}{2V})^2 \sum_{l,l'} \sum_{\substack{\mathbf{k}\mathbf{k}'\nu \\ \mathbf{q}\mathbf{q}'\mu'}} e^{\mathrm{i}(\mathbf{k}-\mathbf{k}')\cdot\mathbf{x}_l} \frac{1}{\varepsilon_{\mathbf{k}\prime} - \varepsilon_{\mathbf{k}}} e^{-\mathrm{i}(\mathbf{q}'-\mathbf{q})\cdot\mathbf{x}_{l'}} \sum_{ab} (S_l^a S_{l'}^b)(\sigma^b\sigma^a)_{\mu'\nu} c^\dagger_{\mathbf{q}'\mu'} c_{\mathbf{k}\nu}\delta_{\mathbf{k}'\mathbf{q}} \ , \end{aligned} \tag{6.13}$$

and,

$$
\begin{aligned}
[\mathrm{i}A, H] &= (\frac{J}{2V})^2 \sum_{ll'} \sum_{\substack{\mathbf{k}\mathbf{k}'\nu' \\ \mathbf{q}\mu}} \frac{1}{\varepsilon_{\mathbf{k}'} - \varepsilon_{\mathbf{k}}} e^{\mathrm{i}\mathbf{k}\cdot(\mathbf{x}_l - \mathbf{x}_{l'})} e^{\mathrm{i}\mathbf{k}\cdot\mathbf{x}_l} e^{-\mathrm{i}\mathbf{q}'\cdot\mathbf{x}_{l'}} \sum_{ab} (S_l^a S_{l'}^b)(\sigma^b\sigma^a)_{\mu'\nu} c^\dagger_{\mathbf{q}'\mu'} c_{\mathbf{k}\nu} \\
&\quad - (\frac{J}{2V})^2 \sum_{ll'} \sum_{\substack{\mathbf{k}\mathbf{k}'\nu' \\ \mathbf{q}\mu}} \frac{1}{\varepsilon_{\mathbf{k}'} - \varepsilon_{\mathbf{k}}} e^{\mathrm{i}\mathbf{k}'\cdot(\mathbf{x}_{l'} - \mathbf{x}_l)} e^{\mathrm{i}\mathbf{k}\cdot\mathbf{x}_l} e^{-\mathrm{i}\mathbf{q}'\cdot\mathbf{x}_{l'}} \sum_{ab} (S_l^a S_{l'}^b)(\sigma^b\sigma^a)_{\mu'\nu} c^\dagger_{\mathbf{q}'\mu'} c_{\mathbf{k}\nu} \\
&= (\frac{J}{2V})^2 \sum_{ll'} \sum_{\substack{\mathbf{k}\mathbf{k}'\nu' \\ \mathbf{q}\mu}} \frac{1}{\varepsilon_{\mathbf{k}'} - \varepsilon_{\mathbf{k}}} e^{\mathrm{i}\mathbf{k}'\cdot(\mathbf{x}_{l'} - \mathbf{x}_l)} e^{\mathrm{i}\mathbf{k}'\cdot\mathbf{x}_l} e^{-\mathrm{i}\mathbf{q}'\cdot\mathbf{x}_{l'}} c^\dagger_{\mathbf{k}'\nu'} c_{\mathbf{q}\mu} \sum_{ab} S_l^a S_{l'}^b (\delta_{ab}\delta_{\nu'\mu} + \mathrm{i}\sum_c \epsilon_{abc}\sigma^c_{\nu'\mu}) \\
&\quad - (\frac{J}{2V})^2 \sum_{ll'} \sum_{\substack{\mathbf{k}\mathbf{k}'\nu' \\ \mathbf{q}'\mu'}} \frac{1}{\varepsilon_{\mathbf{k}'} - \varepsilon_{\mathbf{k}}} e^{\mathrm{i}\mathbf{k}'\cdot(\mathbf{x}_{l'} - \mathbf{x}_l)} e^{\mathrm{i}\mathbf{k}\cdot\mathbf{x}_l} e^{-\mathrm{i}\mathbf{q}'\cdot\mathbf{x}_{l'}} c^\dagger_{\mathbf{q}'\mu'} c_{\mathbf{k}\nu} \sum_{ab} S_l^a S_{l'}^b (\delta_{ab}\delta_{\mu'\nu} - \mathrm{i}\sum_c \epsilon_{abc}\sigma^c_{\mu'\nu}) \\
&= (\frac{J}{2V})^2 \sum_{ll'} \sum_{\substack{\mathbf{k}\mathbf{k}'\nu' \\ \mathbf{q}}} \frac{e^{\mathrm{i}\mathbf{k}\cdot(\mathbf{x}_l - \mathbf{x}_{l'})}}{\varepsilon_{\mathbf{k}'} - \varepsilon_{\mathbf{k}}} e^{-\mathrm{i}\mathbf{k}'\cdot\mathbf{x}_l} e^{\mathrm{i}\mathbf{q}\cdot\mathbf{x}_{l'}} c^\dagger_{\mathbf{k}'\nu'} c_{\mathbf{q}\nu'} \, (\mathbf{S}_l \cdot \mathbf{S}_{l'}) \\
&\quad + (\frac{J}{2V})^2 \sum_{ll'} \sum_{\substack{\mathbf{k}\mathbf{k}'\nu' \\ \mathbf{q}\mu'}} \frac{e^{\mathrm{i}\mathbf{k}\cdot(\mathbf{x}_l - \mathbf{x}_{l'})}}{\varepsilon_{\mathbf{k}'} - \varepsilon_{\mathbf{k}}} e^{-\mathrm{i}\mathbf{k}'\cdot\mathbf{x}_l} e^{-\mathrm{i}\mathbf{q}\cdot\mathbf{x}_{l'}} c^\dagger_{\mathbf{k}'\nu'} c_{\mathbf{q}\mu} \, (\mathrm{i}\sum_{abc} \epsilon_{abc} S_l^a S_{l'}^b \sigma^c_{\nu'\mu}) \\
&\quad - (\frac{J}{2V})^2 \sum_{ll'} \sum_{\substack{\mathbf{k}\mathbf{k}'\nu \\ \mathbf{q}'}} \frac{e^{\mathrm{i}\mathbf{k}'\cdot(\mathbf{x}_{l'} - \mathbf{x}_l)}}{\varepsilon_{\mathbf{k}'} - \varepsilon_{\mathbf{k}}} e^{-\mathrm{i}\mathbf{k}\cdot\mathbf{x}_l} e^{-\mathrm{i}\mathbf{q}'\cdot\mathbf{x}_{l'}} c^\dagger_{\mathbf{q}'\nu} c_{\mathbf{k}\nu} \, (\mathbf{S}_l \cdot \mathbf{S}_{l'}) \\
&\quad + (\frac{J}{2V})^2 \sum_{ll'} \sum_{\substack{\mathbf{k}\mathbf{k}'\nu \\ \mathbf{q}'\mu'}} \frac{e^{\mathrm{i}\mathbf{k}'\cdot(\mathbf{x}_l - \mathbf{x}_{l'})}}{\varepsilon_{\mathbf{k}'} - \varepsilon_{\mathbf{k}}} e^{-\mathrm{i}\mathbf{k}\cdot\mathbf{x}_l} e^{-\mathrm{i}\mathbf{q}'\cdot\mathbf{x}_{l'}} c^\dagger_{\mathbf{q}'\nu'} c_{\mathbf{k}\nu} \, (\mathrm{i}\sum_{abc} \epsilon_{abc} S_l^a S_{l'}^b \sigma^c_{\mu'\nu}) \; . \qquad (6.14)
\end{aligned}
$$

If we restrict the resulting Hamiltonian to the *pairwise* interaction of local spins and consider the ground-state of the conduction electrons, the operator products, $c^\dagger_{\mathbf{k}\mu} c_{\mathbf{q}\nu}$, reduce to

$$
c^\dagger_{\mathbf{k}\mu} c_{\mathbf{q}\nu} = \langle c^\dagger_{\mathbf{k}\mu} c_{\mathbf{q}\nu} \rangle_0 = \langle c^\dagger_{\mathbf{k}\mu} c_{\mathbf{k}\mu} \rangle_0 \, \delta_{\mathbf{k}\mathbf{q}} \delta_{\mu\nu} \; , \qquad (6.15)
$$

and thereupon, we can further simplify the effective Hamiltonian. Note that this entails the assumption that the Fermi sea of the electrons remains in the ground-state and is unpolarized (i.e., energy levels, $\varepsilon_{\mathbf{k}}$, remain spin-independent). Notice also that by this assumption, the terms involving the Levi-Civita tensors, ϵ_{abc}, vanish, since, e.g., $\nu' = \mu$ and using the spin algebra (Appendix A),

$$
\sum_c \sigma^c_{\nu\nu} = \mathrm{Tr}[\sigma^c] = 0 \; . \qquad (6.16)
$$

Hence,

$$
\begin{aligned}
[\mathrm{i}A, H] &= (\frac{J}{2V})^2 \sum_{ll'} \sum_{\mathbf{k}\mathbf{k}'\nu'} e^{\mathrm{i}\mathbf{k}\cdot(\mathbf{x}_l - \mathbf{x}_{l'})} \varepsilon_{\mathbf{k}'} - \varepsilon_{\mathbf{k}} \langle c^\dagger_{\mathbf{k}'\nu'} c_{\mathbf{k}'\nu'} \rangle_0 \, \mathbf{S}_l \cdot \mathbf{S}_{l'} \\
&\quad - (\frac{J}{2V})^2 \sum_{ll'} \sum_{\mathbf{k}\mathbf{k}'\nu} e^{\mathrm{i}\mathbf{k}'\cdot(\mathbf{x}_{l'} - \mathbf{x}_l)} \varepsilon_{\mathbf{k}'} - \varepsilon_{\mathbf{k}} e^{\mathrm{i}\mathbf{k}\cdot(\mathbf{x}_l - \mathbf{x}_{l'})} \langle c^\dagger_{\mathbf{k}\nu} c_{\mathbf{k}\nu} \rangle_0 \, \mathbf{S}_l \cdot \mathbf{S}_{l'} \\
&= (\frac{J}{2V})^2 \sum_{ll'} \sum_{\mathbf{k}\mathbf{k}'\nu'} e^{\mathrm{i}\mathbf{k}\cdot(\mathbf{x}_l - \mathbf{x}_{l'})} \Big(\frac{e^{-\mathrm{i}\mathbf{k}'\cdot(\mathbf{x}_l - \mathbf{x}_{l'})}}{\varepsilon_{\mathbf{k}'} - \varepsilon_{kk}} n_F(\varepsilon_{\mathbf{k}'}) - \frac{e^{+\mathrm{i}\mathbf{k}'\cdot(\mathbf{x}_{l'} - \mathbf{x}_l)}}{\varepsilon_{\mathbf{k}'} - \varepsilon_{\mathbf{k}}} n_F(\varepsilon_{\mathbf{k}}) \Big) \, \mathbf{S}_l \cdot \mathbf{S}_{l'} \\
&= \underbrace{2}_{\text{sum over spin index } \nu} (\frac{J}{2V})^2 \sum_{ll',\mathbf{k}} e^{\mathrm{i}\mathbf{k}\cdot(\mathbf{x}_l - \mathbf{x}_{l'})} \, \mathbf{S}_l \cdot \mathbf{S}_{l'} \, \left(\sum_{\mathbf{k}'} \frac{e^{\mathrm{i}\mathbf{k}'\cdot(\mathbf{x}_{l'} - \mathbf{x}_l)}}{\varepsilon_{\mathbf{k}\prime} - \varepsilon_{\mathbf{k}}} [n_F(\varepsilon_{\mathbf{k}'}) - n_F(\varepsilon_{\mathbf{k}})] \right) \\
&= (\frac{J}{2V})^2 \sum_{ll',\mathbf{k}} e^{\mathrm{i}\mathbf{k}\cdot(\mathbf{x}_l - \mathbf{x}_{l'})} \, \mathbf{S}_l \cdot \mathbf{S}_{l'} \, \left(\frac{2}{V} \sum_{\mathbf{k}'} e^{\mathrm{i}\mathbf{k}'\cdot(\mathbf{x}_{l'} - \mathbf{x}_l)} \frac{n_F(\varepsilon_{\mathbf{k}'}) - n_F(\varepsilon_{\mathbf{k}})}{\varepsilon_{\mathbf{k}'} - \varepsilon_{\mathbf{k}}} \right) \\
&= (\frac{J}{2})^2 \sum_{ll'} \mathbf{S}_l \cdot \mathbf{S}_{l'} \, \frac{2}{V} \sum_{\mathbf{k}\mathbf{k}'} e^{\mathrm{i}(\mathbf{k}-\mathbf{k}')\cdot(\mathbf{x}_l - \mathbf{x}_{l'})} \frac{n_F(\varepsilon_{\mathbf{k}'}) - n_F(\varepsilon_{\mathbf{k}})}{\varepsilon_{\mathbf{k}'} - \varepsilon_{\mathbf{k}}} \\
&= \frac{1}{2} \sum_{ll'} I(\mathbf{x}_l - \mathbf{x}_{l'}) \, \mathbf{S}_l \cdot \mathbf{S}_{l'} \ , \qquad (6.17)
\end{aligned}
$$

where the RKKY interaction is defined (for $l \neq l'$) as

$$
I_{\mathrm{RKKY}}(\mathbf{x}_l - \mathbf{x}_{l'}) := (\frac{J}{V})^2 \sum_{\mathbf{k}\mathbf{k}'} e^{\mathrm{i}(\mathbf{k}-\mathbf{k}')\cdot(\mathbf{x}_l - \mathbf{x}_{l'})} \, \frac{n_F(\varepsilon_{\mathbf{k}'}) - n_F(\varepsilon_{\mathbf{k}})}{\varepsilon_{\mathbf{k}'} - \varepsilon_{\mathbf{k}}} \ . \qquad (6.18)
$$

Thus,

$$
\begin{aligned}
I_{\mathrm{RKKY}}(\mathbf{R}) &= (\frac{J}{V})^2 \sum_{\mathbf{k}\mathbf{q}} e^{\mathrm{i}\mathbf{q}\cdot\mathbf{R}} \, \frac{n_F(\varepsilon_{\mathbf{k}-\mathbf{q}}) - n_F(\varepsilon_{\mathbf{k}})}{\varepsilon_{\mathbf{k}-\mathbf{q}} - \varepsilon_{\mathbf{k}}} \\
&= (\frac{J}{V})^2 \sum_{\mathbf{k}\mathbf{q}} e^{\mathrm{i}\mathbf{q}\cdot\mathbf{R}} \, \frac{n_F(\varepsilon_{\mathbf{k}}) - n_F(\varepsilon_{\mathbf{k}-\mathbf{q}})}{\varepsilon_{\mathbf{k}} - \varepsilon_{\mathbf{k}-\mathbf{q}}} \\
&= J^2 \frac{1}{V} \sum_{\mathbf{q}} e^{\mathrm{i}\mathbf{q}\cdot\mathbf{R}} \, \chi^0_c(\mathbf{q}, \omega = 0) \ , \qquad (6.19)
\end{aligned}
$$

where

$$
\chi^0_c(\mathbf{q}, \omega = 0) = \frac{1}{V} \sum_{\mathbf{k}} \frac{n_F(\varepsilon_{\mathbf{k}}) - n_F(\varepsilon_{\mathbf{k}-\mathbf{q}})}{\varepsilon_{\mathbf{k}} - \varepsilon_{\mathbf{k}-\mathbf{q}}} = \frac{1}{V} \sum_{\mathbf{k}} \frac{n_F(\varepsilon_{\mathbf{k}+\mathbf{q}}) - n_F(\varepsilon_{\mathbf{k}})}{\varepsilon_{\mathbf{k}+\mathbf{q}} - \varepsilon_{\mathbf{k}}} \ , \qquad (6.20)
$$

is the susceptibility of the non-interacting conduction electrons. We can further obtain the

momentum representation of the RKKY interaction as

$$\begin{aligned} I_{\mathrm{RKKY}}(\mathbf{R}) &= (\frac{J}{V})^2 \sum_{\mathbf{k}\mathbf{k}'} e^{\mathrm{i}(\mathbf{k}-\mathbf{k}')\cdot\mathbf{R}} \frac{n_F(\varepsilon_{\mathbf{k}'}) - n_F(\varepsilon_{\mathbf{k}})}{\varepsilon_{\mathbf{k}'} - \varepsilon_{\mathbf{k}}} \\ &\equiv \frac{J^2}{V} \sum_{\mathbf{q}} e^{\mathrm{i}\mathbf{q}\cdot\mathbf{R}} \frac{1}{V} \sum_{\mathbf{k}} \frac{n_F(\varepsilon_{\mathbf{k}+\mathbf{q}}) - n_F(\varepsilon_{\mathbf{k}})}{\varepsilon_{\mathbf{k}+\mathbf{q}} - \varepsilon_{\mathbf{k}}} = \frac{J^2}{V} \sum_{\mathbf{q}} e^{\mathrm{i}\mathbf{q}\cdot\mathbf{R}} \chi_c^0(\mathbf{q}, \omega = 0) \\ &\Rightarrow I(\mathbf{q}) = J^2 \chi_c^0(\mathbf{q}, \omega = 0) \ . \end{aligned} \tag{6.21}$$

Position representation of the RKKY interaction in 3 dimensions One can obtain the position-representation of the RKKY interaction in 3-dimensions as follows:

$$I(\mathbf{x}) = J^2 \frac{1}{V} \sum_{\mathbf{q}} e^{\mathrm{i}\mathbf{q}\cdot\mathbf{x}} \chi_c^0(\mathbf{q}, \omega = 0) \ . \tag{6.22}$$

This is essentially the position representation of the Lindhard function (see e.g., Ref. [123]). The Fermi-Dirac distribution function can be re-written as

$$\begin{aligned} n_F(\varepsilon_{\mathbf{k}'}) - n_F(\varepsilon_{\mathbf{k}}) &= n_F(\varepsilon_{\mathbf{k}'}) - n_F(\varepsilon_{\mathbf{k}}) + n_F(\varepsilon_{\mathbf{k}'}) n_F(\varepsilon_{\mathbf{k}}) - n_F(\varepsilon_{\mathbf{k}'}) n_F(\varepsilon_{\mathbf{k}}) \\ &= n_F(\varepsilon_{\mathbf{k}'}) \Big(1 - n_F(\varepsilon_{\mathbf{k}})\Big) - n_F(\varepsilon_{\mathbf{k}}) \Big(1 - n_F(\varepsilon_{\mathbf{k}'})\Big) \ , \end{aligned} \tag{6.23}$$

so that

$$\begin{aligned} I(\mathbf{x}) &= (\frac{J}{V})^2 \sum_{\mathbf{k}\mathbf{k}'} e^{\mathrm{i}(\mathbf{k}-\mathbf{k}')\cdot\mathbf{x}} \left[\frac{n_F(\varepsilon_{\mathbf{k}'})(1 - n_F(\varepsilon_{\mathbf{k}}))}{\varepsilon_{\mathbf{k}'} - \varepsilon_{\mathbf{k}}} - \frac{n_F(\varepsilon_{\mathbf{k}})(1 - n_F(\varepsilon_{\mathbf{k}'}))}{\varepsilon_{\mathbf{k}'} - \varepsilon_{\mathbf{k}}} \right] \\ &= -(\frac{J}{V})^2 \sum_{\mathbf{k}\mathbf{k}'} e^{\mathrm{i}(\mathbf{k}-\mathbf{k}')\cdot\mathbf{x}} \left[\frac{n_F(\varepsilon_{\mathbf{k}'})(1 - n_F(\varepsilon_{\mathbf{k}}))}{\varepsilon_{\mathbf{k}'} - \varepsilon_{\mathbf{k}}} + \frac{n_F(\varepsilon_{\mathbf{k}})(1 - n_F(\varepsilon_{\mathbf{k}'}))}{\varepsilon_{\mathbf{k}'} - \varepsilon_{\mathbf{k}}} \right] \\ &= -(\frac{J}{V})^2 \sum_{\mathbf{k}\mathbf{k}'} e^{\mathrm{i}(\mathbf{k}-\mathbf{k}')\cdot\mathbf{x}} \frac{n_F(\varepsilon_{\mathbf{k}'})(1 - n_F(\varepsilon_{\mathbf{k}}))}{\varepsilon_{\mathbf{k}} - \varepsilon_{\mathbf{k}'}} \\ &\quad - (\frac{J}{V})^2 \sum_{\mathbf{k}\mathbf{k}'} e^{\mathrm{i}(\mathbf{k}-\mathbf{k}')\cdot\mathbf{x}} \frac{n_F(\varepsilon_{\mathbf{k}})(1 - n_F(\varepsilon_{\mathbf{k}'}))}{\varepsilon_{\mathbf{k}'} - \varepsilon_{\mathbf{k}}} \\ &= -(\frac{J}{V})^2 \sum_{\mathbf{k}\mathbf{k}'} e^{\mathrm{i}(\mathbf{k}'-\mathbf{k})\cdot\mathbf{x}} \frac{n_F(\varepsilon_{\mathbf{k}})(1 - n_F(\varepsilon_{\mathbf{k}'}))}{\varepsilon_{\mathbf{k}'} - \varepsilon_{\mathbf{k}}} \\ &\quad - (\frac{J}{V})^2 \sum_{\mathbf{k}\mathbf{k}'} e^{\mathrm{i}(\mathbf{k}-\mathbf{k}')\cdot\mathbf{x}} \frac{n_F(\varepsilon_{\mathbf{k}})(1 - n_F(\varepsilon_{\mathbf{k}'}))}{\varepsilon_{\mathbf{k}'} - \varepsilon_{\mathbf{k}}} \ . \end{aligned} \tag{6.24}$$

If we define

$$\mathcal{I}(x) := \frac{1}{V^2} \sum_{\mathbf{k}\mathbf{k}'} e^{\mathrm{i}(\mathbf{k}'-\mathbf{k})\cdot\mathbf{x}} \frac{n_F(\varepsilon_{\mathbf{k}})(1 - n_F(\varepsilon_{\mathbf{k}'}))}{\varepsilon_{\mathbf{k}'} - \varepsilon_{\mathbf{k}}} \ , \tag{6.25}$$

then

$$I(\mathbf{x}) = -J^2 \left(\mathcal{I}(x) + \mathcal{I}(-x) \right) \ . \tag{6.26}$$

Therefore, we have to obtain the integral, $\mathcal{I}$ (see Appendix G):

$$\begin{aligned}\mathcal{I}(\mathbf{x}) &= \int_{|\mathbf{k}|\leq k_F} \frac{\mathrm{d}^3 k}{(2\pi)^3} \int_{|\mathbf{k}'|\geq k_F} \frac{\mathrm{d}^3 k'}{(2\pi)^3} e^{\mathrm{i}(\mathbf{k}'-\mathbf{k})\cdot\mathbf{x}} \frac{1}{\varepsilon_{\mathbf{k}'} - \varepsilon_{\mathbf{k}}} \\ &= \frac{4m{k_F}^4}{(2\pi)^3} F(2k_F r) \quad ; \quad r = |\mathbf{x}| \ , \end{aligned} \tag{6.27}$$

where

$$F(x) := \frac{\sin x - x\cos x}{x^4} = \frac{1}{x^2}\, j_1(x) \ , \tag{6.28}$$

and j_1 is the spherical Bessel function. Therefore,

$$I(x) = -\frac{m{k_F}^4}{\pi^3}\, J^2\, F(2k_F r) \ . \tag{6.29}$$

The momentum representation of $\mathcal{I}$ reads (see, e.g., Ref. [123])

$$\begin{aligned}\mathcal{I}(\mathbf{q}) &= J^2\, \chi_c^0(\mathbf{q}, \omega = 0) = J^2\, \mathrm{Re}\, \chi_c^{0,R}(\mathbf{q}, \omega = 0) \quad : \text{Lindhard function} \\ &= -\frac{J^2}{2}\, \mathcal{N}(\varepsilon_F)\, (1 + \frac{1-p^2}{2p} \ln|\frac{1+p}{1-p}|) \quad ; \quad p = \frac{q}{2k_F} \ . \end{aligned} \tag{6.30}$$

For a parabolic dispersion relation, the density-of-states (per spin per volume) is $\mathcal{N}(\epsilon)$:

$$\begin{aligned}\nu(\epsilon) &= \frac{1}{2\pi^2} mk[\epsilon] \Rightarrow \mathcal{N}(\varepsilon_F) = \frac{1}{2\pi^2} mk_F \ , \\ k(\epsilon) &= \sqrt{2m\epsilon} \ . \end{aligned} \tag{6.31}$$

Hence,

$$\mathcal{I} = -\frac{2}{\pi}\, \mathcal{N}(\varepsilon_F)\, (k_F)^3\, J^2\, F(2k_F r) \ . \tag{6.32}$$

For a parabolic dispersion relation and a cubic lattice with $k_F \sim \frac{\pi}{a}$, the RKKY interaction is always *ferromagnetic* between nearest neighbors.

6.2 RPA/Tyablikov decoupling for the Heisenberg Hamiltonian ($s = \frac{1}{2}$)

The effective Heisenberg Hamiltonian can be studied with the RPA/Tyablikov decoupling method.[1] In general, the Hamiltonian of the Heisenberg model reads

$$H = -\sum_{ij} J_{ij}(S_i^+ S_j^- + S_i^z S_j^z) - g\mu_B B_0 \sum_i S_i^z \ , \tag{6.33}$$

where translational invariance is assumed; i.e.,

$$\begin{aligned} J_{ij} &= J(\mathbf{R}_i - \mathbf{R}_j) = J_{ji} \ , \\ J_{ii} &= 0 \ . \end{aligned} \tag{6.34}$$

Furthermore, note that

$$\begin{aligned} S^2 &= S_z^2 + S_x^2 + S_y^2 = S_z^2 + \frac{1}{2}(S^+S^- + S^-S^+) \\ &= S_z^2 + \frac{1}{2}(2S^+S^- + \underbrace{[S^-, S^+]}_{=-2S_z}) = S_z^2 + S^+S^- - S_z \\ &\Rightarrow S^+S^- = S^2 - S_z^2 + S_z \ ; \end{aligned} \tag{6.35}$$

so for spin $s = \frac{1}{2}$,

$$(S^z)^2 = \frac{1}{4}\mathbb{1} \ , \tag{6.36}$$

and thereupon,

$$\langle S^+S^- \rangle = \langle S^2 \rangle - \langle S_z^2 \rangle + \langle S_z \rangle \overset{s=\frac{1}{2}}{=\!=\!=} S(S+1) - \frac{1}{4} + \langle S_z \rangle = \frac{1}{2} + \langle S_z \rangle \ . \tag{6.37}$$

To investigate magnetic instabilities, one can consider the correlation function

$$\chi^{+-,ret}(\mathbf{x}_i - \mathbf{x}_j, t) =: \chi_{ij}^{+-,ret}(t) =: \chi_{ij}^{+-}(t) \quad : \text{for brevity} \ . \tag{6.38}$$

The Heisenberg equation of motion for $\chi_{ij}^{+-}(t)$ reads

$$\chi_{ij}^{+-}(t) = -\mathrm{i}\Theta(t)\langle [S_i^+(t), S_j^-(t=0)] \rangle =: \langle\!\langle S_i^+(t); S_j^-(t=0) \rangle\!\rangle_{ret} \ . \tag{6.39}$$

Using

$$\begin{aligned} \chi_{ij}^{+}(t) &= \int_{-\infty}^{+\infty} \frac{\mathrm{d}\omega}{2\pi} e^{-\mathrm{i}\omega t} \chi_{ij}^{+-}(\omega) \ , \\ \chi_{ij}^{+}(\omega) &= \int_{-\infty}^{+\infty} \mathrm{d}t \, e^{\mathrm{i}\omega t} \chi_{ij}^{+-}(t) \ , \end{aligned} \tag{6.40}$$

[1] The method is originally due to N. N. Bogoliubov and S. V. Tyablikov, and is based on a decoupling of the hierarchy of equations-of-motion for the magnetic susceptibility. For further details, consult Refs. [247, 248].

one obtains

$$\omega\chi_{ij}^{+-}(\omega) = \langle[S_i^+, S_j^-]\rangle + \langle\langle[S_i^+, H]_-; S_j^-\rangle\rangle^{ret}|_\omega \ . \tag{6.41}$$

Note that

$$\begin{aligned}
[S_i^+, S_j^-] &= 2\delta_{ij}S_i^z \ , \\
[S_i^z, S_j^+] &= \delta_{ij}S_i^+ \ , \\
[S_i^z, S_j^-] &= \delta_{ij}S_i^-;
\end{aligned} \tag{6.42}$$

therefore,

$$[S_i^+, H] = -2\sum_{il} J_{il}(S_l^+S_i^z - S_i^+S_l^z) + g\mu_B B_0 S_i^+ \tag{6.43}$$

where we have used $J_{ii} = 0, \forall i$. Hence,

$$\begin{aligned}
\omega\chi_{ij}^{+-}(\omega) &= 2\delta_{ij}\langle S_i^z\rangle - 2\sum_l J_{il}(\langle\langle S_l^+S_i^z(t); S_j^-(t=0)\rangle\rangle^{ret}|_\omega \\
&\quad - \langle\langle S_i^+S_l^z(t); S_j^-(t=0)\rangle\rangle^{ret}|_\omega) \\
\Rightarrow (\omega - g\mu_B B_0)\chi_{ij}^{+}(\omega) &= 2\delta_{ij}\langle S_i^z\rangle - 2\sum_l J_{il}(\langle\langle S_l^+S_i^z(t); Sj^-(t=0)\rangle\rangle^{ret}|_\omega \\
&\quad - \langle\langle S_i^+S_l^z(t); Sj^-(t=0)\rangle\rangle^{ret}|_\omega) \ .
\end{aligned} \tag{6.44}$$

The RPA/Tyablikov decoupling is the application of the following approximations,

$$\begin{aligned}
\langle\langle S_l^+S_i^z(t); S_j^-(t=0)\rangle\rangle^{ret}|_\omega &\approx \langle S_i^z\rangle\langle\langle S_l^+(t); S_j^-(t=0)\rangle\rangle^{ret}|_\omega \ , \\
\langle\langle S_i^+S_l^z(t); S_j^-(t=0)\rangle\rangle^{ret}|_\omega &\approx \langle S_l^z\rangle\langle\langle S_i^+(t); S_j^-(t=0)\rangle\rangle^{ret}|_\omega \ ;
\end{aligned} \tag{6.45}$$

which will yield

$$\begin{aligned}
(\omega - g\mu_B B_0)\chi_{ij}^{+-}(\omega) &\overset{\text{RPA}}{\approx} 2\delta_{ij}\langle S_i^z\rangle \\
&\quad - 2\sum_l J_{il}\langle S_i^z\rangle\langle\langle S_l^+(t); S_j^-(t=0)\rangle\rangle^{ret}|_\omega \\
&\quad + 2\sum_l J_{il}\langle S_l^z\rangle\langle\langle S_i^+(t); S_j^-(t=0)\rangle\rangle^{ret}|_\omega \\
&= 2\delta_{ij}\langle S_i^z\rangle - 2\langle S_i^z\rangle\sum_l J_{il}\langle\langle S_i^+(t); S_j^-(t=0)\rangle\rangle^{ret}|_\omega \\
&\quad + 2(\sum_l J_{il}\langle S_l^z\rangle\langle\langle S_i^+(t); S_j^-(t=0)\rangle\rangle^{ret}|_\omega \ .
\end{aligned} \tag{6.46}$$

The translational symmetry and inversion symmetry of the lattice lead to

$$\begin{aligned}
J_{ij} = J(\mathbf{R}_i - \mathbf{R}_j) &= \frac{1}{V}\sum_{\mathbf{q}} e^{i\mathbf{q}\cdot(\mathbf{R}_i - \mathbf{R}_j)}J(\mathbf{q}) \\
&= J(\mathbf{R}_j - \mathbf{R}_i) = \frac{1}{V}\sum_{\mathbf{q}} e^{i\mathbf{q}\cdot(\mathbf{R}_j - \mathbf{R}_i)}J(\mathbf{q}) \ .
\end{aligned} \tag{6.47}$$

Therefore,

$$J(\mathbf{q}) = J(-\mathbf{q}) \ . \tag{6.48}$$

From the reality of the coupling one obtains

$$J_{ij}^* = J_{ij} = J_{ji} \ , \tag{6.49}$$

and thence,

$$\begin{aligned} \frac{1}{V}\sum_{\mathbf{q}} e^{-\mathrm{i}\mathbf{q}\cdot(\mathbf{R}_i-\mathbf{R}_j)} J^*(\mathbf{q}) &= \frac{1}{V}\sum_{\mathbf{q}} e^{\mathrm{i}\mathbf{q}\cdot(\mathbf{R}_i-\mathbf{R}_j)} J(\mathbf{q}) \\ \Rightarrow J^*(-\mathbf{q}) = J(\mathbf{q}) &\Rightarrow J^*(\mathbf{q}) = J(-\mathbf{q}) \\ \Rightarrow J(\mathbf{q}) = J(-\mathbf{q}) &= J^*(\mathbf{q}) \ . \end{aligned} \tag{6.50}$$

Therefore,

$$\chi_{ij}^{+-}(\omega) = \chi^{+-}(\mathbf{R}_i - \mathbf{R}_j, \omega) = \frac{1}{V}\sum_{\mathbf{q}} e^{\mathrm{i}\mathbf{q}\cdot(\mathbf{R}_i-\mathbf{R}_j)} \chi^{+-}(\mathbf{q},\omega) \ . \tag{6.51}$$

The RPA/Tyablikov decoupling results in the following equations:

$$\begin{aligned} (\omega - g\mu_B B_0)\chi_{ij}^{+-}(\omega) &= 2\delta_{ij}\langle S_i^z\rangle - 2\sum_l J_{il}\langle S_i^z\rangle \chi_{lj}^{+-}(\omega) + 2\sum_l J_{il}\langle S_l^z\rangle \chi_{ij}^{+-}(\omega) \ , \\ (\omega - g\mu_B B_0 - 2\sum_l J_{il}\langle S_l^z\rangle)\chi_{ij}^{+-}(\omega) &= 2\delta_{ij}\langle S_i^z\rangle - 2\langle S_i^z\rangle \sum_l J_{il}\chi_{lj}^{+-}(\omega) \ . \end{aligned} \tag{6.52}$$

As a warm-up example, we begin with the simplest case:

Ferromagnetic case For ferromagnetic case,

$$\langle S_l^z\rangle = \langle S^z\rangle \ ; \tag{6.53}$$

therefore,

$$(\omega - g\mu_B B_0 - 2\langle S^z\rangle \underbrace{\sum_l J_{il}}_{=:\bar{J}_0}) = 2\delta_{ij}\langle S^z\rangle - 2\langle S^z\rangle \sum_l J_{il}\chi_{lj}^{+-}(\omega) \ , \tag{6.54}$$

and in momentum representation,

$$\begin{aligned} \chi_{ij}^{+-} \equiv \chi^{+-}(\mathbf{R}_i - \mathbf{R}_j) = \frac{1}{V}\sum_{\mathbf{k}} e^{\mathrm{i}\mathbf{k}\cdot(\mathbf{R}_i-\mathbf{R}_j)}\chi^{+-}(\mathbf{k}) \quad ; \quad \delta_{ij} = \frac{1}{V}\sum_{\mathbf{k}} e^{\mathrm{i}\mathbf{k}\cdot(\mathbf{R}_i-\mathbf{R}_j)} \ , \\ J_{ij} = J(\mathbf{R}_i - \mathbf{R}_j) = \frac{1}{V}\sum_{\mathbf{k}} e^{\mathrm{i}\mathbf{k}\cdot(\mathbf{R}_i-\mathbf{R}_j)} J(\mathbf{k}) \ , \end{aligned} \tag{6.55}$$

which lead to a set of algebraic equations

$$\begin{aligned}(\omega - g\mu_B B_0 - 2\langle S^z\rangle \bar{J}_0)\chi^{+-}(\mathbf{k},\omega) &= 2\langle S^z\rangle - 2\langle S^z\rangle J(\mathbf{k})\chi^{+-}(\mathbf{k},\omega) \ , \\ (\omega - g\mu_B B_0 - 2\langle S^z\rangle \bar{J}_0 + 2\langle S^z\rangle J(\mathbf{k}))\chi^{+-}(\mathbf{k},\omega) &= 2\langle S^z\rangle \ , \end{aligned} \tag{6.56}$$

which yields

$$\chi^{+-}(\mathbf{k},\omega) = \frac{2\langle S^z\rangle}{\omega - g\mu_B B_0 - 2\langle S^z\rangle(\bar{J}_0 - J(\mathbf{k}))} \ . \tag{6.57}$$

Therefore,

$$\begin{aligned}\chi^{+-,ret}(\mathbf{k},\omega) &= \frac{2\langle S^z\rangle}{\omega - g\mu_B B_0 - 2\langle S^z\rangle(\bar{J}_0 - J(\mathbf{k})) + \mathrm{i}\eta^+} \\ &= \frac{2\langle S^z\rangle}{\omega - g\mu_B B_0 - E(\mathbf{k}) + \mathrm{i}\eta^+} \ , \end{aligned} \tag{6.58}$$

with

$$E(\mathbf{k}) = 2\langle S^z\rangle(\bar{J}_0 - J(\mathbf{k})) \ , \tag{6.59}$$

where $E(\mathbf{k})$ is the energy of spin waves.

Another equation for $\langle S^z\rangle$ is needed to produce a self-consistent equation. From the spectral representation, one obtains a relation for the *static* correlation function as

$$\begin{aligned}\langle S_j^- S_i^+\rangle &= \int_{-\infty}^{+\infty} \mathrm{d}\varepsilon \, \frac{-\frac{1}{\pi}\mathrm{Im}\,\chi_{ij}^{+-,ret}(\varepsilon)}{e^{\beta\varepsilon} - 1} \\ &= \frac{1}{V}\sum_{\mathbf{q}} e^{\mathrm{i}\mathbf{q}\cdot(\mathbf{R}_i - \mathbf{R}_j)} \int_{-\infty}^{+\infty} \mathrm{d}\varepsilon \, \frac{-\frac{1}{\pi}\mathrm{Im}\,\chi^{+-,ret}(\mathbf{q},\varepsilon)}{e^{\beta\varepsilon} - 1} \ . \end{aligned} \tag{6.60}$$

Notice that for *bosons*,

$$\begin{aligned}&G_\nu^<(t) = -\mathrm{i}\langle a_\nu^\dagger(t) a_\nu(t=0)\rangle \ , \\ &G_\nu^<(t) = \int_{-\infty}^{+\infty} \frac{\mathrm{d}\omega}{2\pi} e^{-\mathrm{i}\omega t} G_\nu^<(\omega) \Rightarrow G_\nu^<(t=0) = \int_{-\infty}^{+\infty} \frac{\mathrm{d}\omega}{2\pi} G_\nu^<(\omega) \ . \end{aligned} \tag{6.61}$$

From the spectral representation, for bosons, we have

$$\mathrm{i}G_\nu^<(\omega) = A_\nu(\omega) n_B(\omega) \ ; \tag{6.62}$$

thus,

$$\begin{aligned}\langle a_\nu^\dagger a_\nu\rangle = \mathrm{i}G_\nu^<(t) &= \mathrm{i}\int_{-\infty}^{+\infty} \frac{\mathrm{d}\omega}{2\pi} G_\nu^<(\omega) = \int_{-\infty}^{+\infty} \frac{\mathrm{d}\omega}{2\pi} A_\nu(\omega) n_B(\omega) \\ &= \int_{-\infty}^{+\infty} \frac{\mathrm{d}\omega}{2\pi} (-2\mathrm{Im}\, G_\nu^{ret}(\omega)) n_B(\omega) \ , \end{aligned} \tag{6.63}$$

where

$$G_\nu^{ret}(t) = -\mathrm{i}\Theta(t)\langle[c_\nu(t), c_\nu^\dagger(t=0)]\rangle \ . \tag{6.64}$$

In the same way, the correlation function $\langle S_j^- S_i^+\rangle$ satisfies

$$\langle S_j^- S_i^+\rangle = \int_{-\infty}^{+\infty} \mathrm{d}\varepsilon \, \frac{-\frac{1}{\pi}\mathrm{Im}\,\chi_{ij}^{+-,ret}(\varepsilon)}{e^{\beta\varepsilon}-1} \ . \tag{6.65}$$

If $i = j$, then for $S = \frac{1}{2}$,

$$\begin{aligned} \langle S_i^- S_i^+\rangle &= \frac{1}{2} - \langle S_i^z\rangle \\ \overset{\langle S_i^z\rangle \overset{!}{=} \langle S^z\rangle}{\Rightarrow} \langle S_i^- S_i^+\rangle &= \frac{1}{2} \langle S_i^z\rangle \\ &= \frac{1}{V}\sum_{\mathbf{k}} \int_{-\infty}^{+\infty} \mathrm{d}\varepsilon \, \frac{-\frac{1}{\pi}\mathrm{Im}\,\chi^{+-,ret}(\mathbf{q},\varepsilon)}{e^{\beta\varepsilon}-1} \end{aligned} \tag{6.66}$$

where we have used the the relation for the ferromagnetic ordered phase,

$$\langle S_i^z\rangle \overset{!}{=} \langle S^z\rangle \ .$$

The imaginary part of the susceptibility is

$$\mathrm{Im}\,\chi^{+-,ret}(\mathbf{k},\omega) = -2\pi\langle S^z\rangle\delta(\omega - \omega_0 - E_{\mathbf{k}}) \ , \tag{6.67}$$

with the Zeeman energy,

$$\omega_0 = g\mu_B B_0 \ , \tag{6.68}$$

and the spin-wave dispersion,

$$E_{\mathbf{k}} = 2\langle S_i^z\rangle(\bar{J}_0 - J(\mathbf{k})) =: 2\langle S_i^z\rangle\gamma_{\mathbf{k}} \ . \tag{6.69}$$

Then,

$$\begin{aligned} &\frac{1}{2} - \langle S^z\rangle = 2\langle S^z\rangle \frac{1}{V}\sum_{\mathbf{k}} n_B(\omega_0 + E_{\mathbf{k}}) \\ &\Rightarrow 2\langle S^z\rangle(1 + 2\frac{1}{V}\sum_{\mathbf{k}} n_B(\omega_0 + E_{\mathbf{k}})) = 1 \end{aligned} \tag{6.70}$$

From the equation above, one can obtain the critical temperature for the onset of ferromagnetic order. Just slightly below the transition to the disordered state,

$$B_0 \to 0^+ \quad , \quad T \to T_C^- \quad , \quad \langle S^z\rangle \to 0^+ \ , \tag{6.71}$$

so that

$$n_B(\omega_0+E_{\mathbf{k}}) = \frac{1}{e^{\beta_C(\omega_0+E_{\mathbf{k}})}-1} \overset{\omega_0\to 0^+}{=} \frac{1}{e^{\beta_C E_{\mathbf{k}}}-1} \overset{E_{\mathbf{k}}\propto\langle S^z\rangle\to 0^+}{=\!=\!=\!=\!=\!=\!=\!=} \frac{1}{1+\beta_C E_{\mathbf{k}}-1} = \frac{1}{\beta_C E_{\mathbf{k}}} \ . \tag{6.72}$$

Hence,

$$\begin{aligned} & 2\langle S_i^z\rangle(1+\frac{1}{\beta_C}\sum_{\mathbf{k}}\frac{2}{2\langle S_i^z\rangle\gamma_{\mathbf{k}}}) = 1 \\ & \Rightarrow 2\langle S_i^z\rangle + 2T_C\frac{1}{V}\sum_{\mathbf{k}}\frac{1}{\gamma_{\mathbf{k}}} = 1 \\ & \overset{\langle S_i^z\rangle\to 0^+}{\Rightarrow} 2T_C\sum_{\mathbf{k}}\frac{1}{\gamma_{\mathbf{k}}} = 1 \\ & \Rightarrow T_C = (\frac{2}{V}\sum_{\mathbf{k}}\frac{1}{\gamma_{\mathbf{k}}})^{-1} \equiv (\frac{2}{V}\sum_{\mathbf{k}}\frac{1}{\bar{J}_0 - J(\mathbf{k})})^{-1} \end{aligned} \tag{6.73}$$

In this way, the transition temperature (Curie-Weiss temperature) for a *ferromagnetic* order is obtained.

6.3 Isotropic antiferromagnetic order

One can consider also an isotropic ferromagnetic order. First, note that

$$\begin{aligned} H &= -\sum_{ij} J_{ij}\mathbf{S}_i\cdot\mathbf{S}_j \quad ; J_{ij} = J_{ji} = J(\mathbf{R}_i - \mathbf{R}_j) \\ &= -\sum_{ij}(S_i^+S_j^- + S_i^zS_j^z) \ . \end{aligned} \tag{6.74}$$

We will require the following commutators in the course of the calculations:

$$\begin{aligned} [S_n^+, H] &= -\sum_{ij} J_{ij}([S_n^+, S_i^+S_j^-] + [S_n^+, S_i^zS_j^z]) \ , \\ [S_n^+, S_i^+S_j^-] &= S_i^+[S_n^+, S_j^-] = 2\delta_{nj}S_i^+S_n^z \ , \\ [S_n^+, S_i^zS_j^z] &= [S_n^+, S_i^z]S_j^z + S_i^z[S_n^+, S_j^z] = -\delta_{nj}S_n^+S_j^z - \delta_{jn}S_i^zS_n^+ \ , \\ [S_n^+, H] &= -2\sum_i J_{in}S_n^zS_i^+ + 2\sum_i J_{in}S_i^zS_n^+ \quad ; \quad J_{ij} = J_{ji} \ . \end{aligned} \tag{6.75}$$

The antiferromagnetically-ordered state is described by dividing the original lattice into two sub-lattices A and B:

Then, the equations for the transverse susceptibility will be

$$\begin{aligned}\chi_{AA}^{+-,ret}(a,a';t) &= -\mathrm{i}\Theta(t)\langle[S_a^+(t),S_{a'}^-(t=0)]\rangle \\ &\equiv \langle\!\langle S_a^+(t);S_{a'}^-(t=0)\rangle\!\rangle \quad ; \quad a,a'\in A\ , \end{aligned} \tag{6.76}$$

$$\begin{aligned}\chi_{BA}^{+-,ret}(b,a;t) &= -\mathrm{i}\Theta(t)\langle[S_b^+(t),S_a^-(t=0)]\rangle \\ &\equiv \langle\!\langle S_a^+(t);S_{a'}^-(t=0)\rangle\!\rangle \quad ; \quad a\in A, b\in B\ . \end{aligned} \tag{6.77}$$

The frequency-representation of the equations will be

$$\omega\chi_{AA}^{+-,ret}(a,a';\omega) = \langle[S_a^+,S_{a'}^-]\rangle + \langle\!\langle[S_a^+,H];S_{a'}^-\rangle\!\rangle\ , \tag{6.78}$$

$$\omega\chi_{BA}^{+-,ret}(b,a;\omega) = \underbrace{\langle[S_b^+,S_a^-]\rangle}_{=0} + \langle\!\langle[S_b^+,H];S_a^-\rangle\!\rangle\ , \tag{6.79}$$

where in the second line, we have used the fact that $b\neq a$ since they belong to different sub-lattices. Therefore,

$$\begin{aligned}\omega\chi_{AA}^{+-}(a,a';\omega) &= 2\delta_{aa'}\langle S_a^z\rangle - 2\sum_{l\in L}J_{la}\langle\!\langle S_a^zS_l^+;S_{a'}^-\rangle\!\rangle_\omega\ , \\ &\quad + 2\sum_{l\in L}J_{la}\langle\!\langle S_l^zS_a^+;S_{a'}^-\rangle\!\rangle_\omega \end{aligned} \tag{6.80}$$

$$\omega\chi_{BA}^{+-}(b,a;\omega) = -2\sum_{l\in L}J_{lb}\langle\!\langle S_b^zS_l^+;S_a^-\rangle\!\rangle_\omega + 2\sum_{l\in L}J_{lb}\langle\!\langle S_l^zS_b^+;S_a^-\rangle\!\rangle_\omega \tag{6.81}$$

where $L\equiv A\cup B$ is the whole lattice. Note that the sum on l goes over the whole lattice, i.e. both sub-lattices A and B; that is, the sum can be decomposed as

$$\sum_{l\in L} = \sum_{a\in A} + \sum_{b\in B}\ ;$$

therefore,

$$\begin{aligned}\omega\chi_{AA}(a,a') &= 2\delta_{aa'}\langle S_a^z\rangle - 2\sum_{a''\in A}J_{aa''}\langle\!\langle S_a^zS_{a''}^+;S_{a'}^-\rangle\!\rangle \\ &\quad - 2\sum_{b''\in B}J_{ab''}\langle\!\langle S_a^zS_{a''}^+;S_{a'}^-\rangle\!\rangle \\ &\quad + 2\sum_{a''\in A}J_{aa''}\langle\!\langle S_{a''}^zS_a^+;S_{a'}^-\rangle\!\rangle \\ &\quad + 2\sum_{b''\in B}J_{ab''}\langle\!\langle S_{b''}^zS_a^+;S_{a'}^-\rangle\!\rangle\ . \end{aligned} \tag{6.82}$$

Note that $J_{ij}=J_{ji}$, and

$$\begin{aligned}\omega\chi_{BA}(b,a) &= -2\sum_{a''\in A}J_{ba''}\langle\!\langle S_b^zS_{a''}^+;S_a^-\rangle\!\rangle - 2\sum_{b''\in B}J_{bb''}\langle\!\langle S_b^zS_{b''}^+;S_a^-\rangle\!\rangle \\ &\quad + 2\sum_{a''\in A}J_{ba''}\langle\!\langle S_{a''}^zS_b^+;S_a^-\rangle\!\rangle + 2\sum_{b''\in B}J_{bb''}\langle\!\langle S_{b''}^zS_b^+;S_a^-\rangle\!\rangle\ . \end{aligned} \tag{6.83}$$

The Tyablikov decoupling is equivalent to

$$\langle\langle S_l^z S_i^+; S_j^- \rangle\rangle \approx \langle S_l^z \rangle \langle\langle S_i^+; S_j^- \rangle\rangle \ . \tag{6.84}$$

Therefore,

$$\begin{aligned}\omega\chi_{AA}(a,a') = {} & 2\delta_{aa'}\langle S_{a'}^z\rangle \\ & - 2\sum_{a''\in A} J_{aa''}\langle S_a^z\rangle \chi_{AA}(a'',a') - 2\sum_{b''\in B} J_{ab''}\langle S_a^z\rangle \chi_{BA}(b'',a') \\ & + 2\sum_{a''\in A} J_{aa''}\langle S_{a''}^z\rangle \chi_{AA}(a,a') + 2\sum_{b''\in B} J_{ab''}\langle S_{b''}^z\rangle \chi_{AA}(a,a') \ ,\end{aligned} \tag{6.85}$$

and

$$\begin{aligned}\omega\chi_{BA}(b,a) = {} & -2\sum_{a''\in A} J_{a''b}\langle S_b^z\rangle \chi_{AA}(a'',a) - 2\sum_{b''\in B} J_{b''b}\langle S_b^z\rangle \chi_{BA}(b'',a) \\ & + 2\sum_{a''\in A} J_{a''b}\langle S_{a''}^z\rangle \chi_{BA}(b,a) + 2\sum_{b''\in B} J_{b''b}\langle S_{b''}^z\rangle \chi_{BA}(b,a) \ .\end{aligned} \tag{6.86}$$

For the isotropic AFM order, the sub-lattice magnetization, M, is

$$\begin{aligned} M &:= \langle S_a^z\rangle \ , \\ -M &= \langle S_b^z\rangle \ . \end{aligned} \tag{6.87}$$

Thus, for this type of magnetic order,

$$\begin{aligned}\omega\chi_{AA}(a,a') = {} & 2\delta_{aa'}M - 2M\sum_{a''\in A} J_{aa''}\chi_{AA}(a'',a') - 2M\sum_{b''\in B} J_{ab''}\chi_{BA}(b'',a') \\ & + 2M[\sum_{a''\in A} J_{aa''}]\chi_{AA}(a,a') - 2M[\sum_{b''\in B} J_{ab''}]\chi_{AA}(a,a') \ ,\end{aligned} \tag{6.88}$$

$$\begin{aligned}\omega\chi_{BA}(b,a) = {} & 2M\sum_{a''\in A} J_{a''b}\chi_{AA}(a'',a) + 2M\sum_{b''\in B} J_{b''b}\chi_{BA}(b'',a) \\ & 2M[\sum_{a''\in A} J_{a''b}]\chi_{BA}(b,a) - 2M[\sum_{b''\in B} J_{b''b}]\chi_{BA}(b,a) \ .\end{aligned} \tag{6.89}$$

Re-arranging terms, one obtains

$$\begin{aligned}[\omega - 2M(\sum_{a''\in A} J_{aa''} - \sum_{b''\in B} J_{ab''})]\chi_{AA}(a,a') = {} & 2\delta_{aa'}M - 2M\sum_{a''\in A} J_{aa''}\chi_{AA}(a'',a') \\ & - 2M\sum_{b''\in B} J_{ab''}\chi_{BA}(b'',a') \ ,\end{aligned} \tag{6.90}$$

$$\begin{aligned}[\omega + 2M(\sum_{b''\in B} J_{b''b} - \sum_{a''\in A} J_{a''b})\chi_{BA}(b,a) = {} & 2M\sum_{a''\in A} J_{a''b}\chi_{a'',a} \\ & + 2M\sum_{b''\in B} J_{b''b}\chi_{BA}(b'',a) \ .\end{aligned} \tag{6.91}$$

To simplify the notation, we define

$$J_{0A} := -\sum_{a''\in A} J_{aa''} + \sum_{b''\in B} Jab'' \ ,$$
$$J_{0B} := +\sum_{a''\in A} J_{a''b} - \sum_{b''\in B} J_{b''b} \ . \tag{6.92}$$

Due to the translational symmetry of the original lattice L, and the inversion symmetry ($J_{ij} = J_{ji}$), one concludes

$$J_{0A} = J_{0B} =: J_0 = -\sum_{a''\in A} J_{aa''} - \sum_{b''\in B} J_{ab''} \ . \tag{6.93}$$

In momentum representation,

$$\chi_{AA}(a,a') = \frac{1}{V}\sum_{\mathbf{k}\in 1\mathrm{BZ}} e^{\mathrm{i}\mathbf{k}\cdot(\mathbf{R}_a-\mathbf{R}_{a'})}\chi_{AA}(\mathbf{k}) \ ,$$
$$\chi_{BA}(b,a) = \frac{1}{V}\sum_{\mathbf{k}\in 1\mathrm{BZ}} e^{\mathrm{i}\mathbf{k}\cdot(\mathbf{R}_b-\mathbf{R}_a)}\chi_{BA}(\mathbf{k}) \ ,$$
$$J_{ij} \equiv J(\mathbf{R}_i-\mathbf{R}_j) = \frac{1}{V}\sum_{\mathbf{k}\in 1\mathrm{BZ}} e^{\mathrm{i}\mathbf{k}\cdot(\mathbf{R}_i-\mathbf{R}_j)}J(\mathbf{k}) \ ,$$
$$\sum_{j\in L} e^{\mathrm{i}\mathbf{R}_j\cdot(\mathbf{k}-\mathbf{q})} = \delta_{\mathbf{k},\mathbf{q}} \quad ; \quad \mathbf{k},\mathbf{q}\in 1\mathrm{BZ} \ . \tag{6.94}$$

Thus,

$$\begin{aligned}[\omega - 2MJ_0]\frac{1}{V}\sum_{\mathbf{k}} e^{\mathrm{i}\mathbf{k}\cdot(\mathbf{R}_a-\mathbf{R}_{a'})}\chi_{AA}(\mathbf{k}) &= 2M\frac{1}{V}\sum_{\mathbf{k}} e^{\mathrm{i}\mathbf{k}\cdot(\mathbf{R}_a-\mathbf{R}_{a'})} \\ &\quad - 2M\sum_{a''\in A}\frac{1}{V}\sum_{\mathbf{k}} e^{\mathrm{i}\mathbf{k}\cdot(\mathbf{R}_a-\mathbf{R}_{a''})}J(\mathbf{k})\ \frac{1}{V}\sum_{\mathbf{q}} e^{\mathrm{i}\mathbf{q}\cdot(\mathbf{R}_{a''}-\mathbf{R}_{a'})}\chi_{AA}(\mathbf{q}) \\ &\quad - 2M\sum_{b''\in B}\frac{1}{V}\sum_{\mathbf{k}} e^{\mathrm{i}\mathbf{k}\cdot(\mathbf{R}_a-\mathbf{R}_{b''})}J(\mathbf{k})\ \frac{1}{V}\sum_{\mathbf{q}} e^{\mathrm{i}\mathbf{q}\cdot(\mathbf{R}_{b''}-\mathbf{R}_{a'})}\chi_{BA}(\mathbf{q}) \ ,\end{aligned} \tag{6.95}$$

$$\begin{aligned}[\omega + 2MJ_0]\frac{1}{V}\sum_{\mathbf{k}} e^{\mathrm{i}\mathbf{k}\cdot(\mathbf{R}_b-\mathbf{R}_a)}\chi_{BA}(\mathbf{k}) &= 2M\sum_{a''\in A}\frac{1}{V}\sum_{\mathbf{k}} e^{\mathrm{i}\mathbf{k}\cdot(\mathbf{R}_{a''}-\mathbf{R}_b)}J(\mathbf{k})\ \frac{1}{V}\sum_{\mathbf{q}} e^{\mathrm{i}\mathbf{q}\cdot(\mathbf{R}_{a''}-\mathbf{R}_a)}\chi_{AA}(\mathbf{q}) \\ &\quad + 2M\sum_{b''\in B}\frac{1}{V}\sum_{\mathbf{k}} e^{\mathrm{i}\mathbf{k}\cdot(\mathbf{R}_{b''}-\mathbf{R}_b)}J(\mathbf{k})\ \frac{1}{V}\sum_{\mathbf{q}} e^{\mathrm{i}\mathbf{q}\cdot(\mathbf{R}_{b''}-\mathbf{R}_a)}\chi_{BA}(\mathbf{q}) \ .\end{aligned} \tag{6.96}$$

Note that, the sum over the sub-lattice sites (half of the original lattice) yields (see Appendix I)

$$\begin{aligned}\sum_{a''\in A} e^{\mathrm{i}\mathbf{k}\cdot\mathbf{R}_{a''}} &= \frac{V}{2}\delta(\mathbf{k}) = \sum_{b''\in B} e^{\mathrm{i}\mathbf{k}\cdot\mathbf{R}_{b''}} \\ &\equiv \frac{1}{2}\sum_{l\in L} e^{\mathrm{i}\mathbf{k}\cdot\mathbf{R}_l} \ .\end{aligned} \tag{6.97}$$

Then,

$$[\omega - 2MJ_0]\frac{1}{V}\sum_{\mathbf{k}} e^{i\mathbf{k}\cdot(\mathbf{R}_a-\mathbf{R}_{a'})}\chi_{AA}(\mathbf{k}) = 2M\frac{1}{V}\sum_{\mathbf{k}} e^{i\mathbf{k}\cdot(\mathbf{R}_a-\mathbf{R}_{a'})} - 2M\frac{1}{2V}\sum_{\mathbf{k}} e^{i\mathbf{k}\cdot(\mathbf{R}_a-\mathbf{R}_{a'})}J(\mathbf{k})\chi_{AA}(\mathbf{k}) - 2M\frac{1}{2V}\sum_{\mathbf{k}} e^{i\mathbf{k}\cdot(\mathbf{R}_a-\mathbf{R}_{a'})}J(\mathbf{k})\chi_{BA}(\mathbf{k}) \ , \tag{6.98}$$

$$[\omega + 2MJ_0]\frac{1}{V}\sum_{\mathbf{k}} e^{i\mathbf{k}\cdot(\mathbf{R}_b-\mathbf{R}_a)}\chi_{BA}(\mathbf{k}) = 2M\frac{1}{2V}\sum_{\mathbf{k}} e^{i\mathbf{k}\cdot(\mathbf{R}_b-\mathbf{R}_a)}J(\mathbf{k})\chi_{AA}(\mathbf{k}) + 2M\frac{1}{2V}\sum_{\mathbf{k}} e^{i\mathbf{k}\cdot(\mathbf{R}_b-\mathbf{R}_a)}J(\mathbf{k})\chi_{BA}(\mathbf{k}) \ , \tag{6.99}$$

where we have used

$$J(\mathbf{k}) = J(-\mathbf{k}) \ .$$

Therefore, one finally obtains

$$\begin{aligned} [\omega + M(2J_0 + J_{\mathbf{k}})]\,\chi_{AA}(\mathbf{k}) &= 2M - MJ_{\mathbf{k}}\,\chi_{BA}(\mathbf{k}) \ , \\ [\omega - M(2J_0 + J_{\mathbf{k}})]\,\chi_{BA}(\mathbf{k}) &= J_{\mathbf{k}}\,\chi_{AA}(\mathbf{k}) \ , \end{aligned} \tag{6.100}$$

with

$$J_0 = \sum_{b''\in B} J_{ab''} - \sum_{a''\in A} J_{aa''} \ . \tag{6.101}$$

This is an algebraic equation to be solved.

Solution of the algebraic equation To simplify the notation, we define

$$\begin{aligned} x &:= 2MJ_0 \ , \\ y &:= MJ_{\mathbf{k}} \ , \end{aligned} \tag{6.102}$$

so that the set of the equations above becomes

$$\begin{aligned} (\omega + x + y)\chi_{AA} &= 2M - y\,\chi_{BA} \ , \\ (\omega - x - y)\chi_{BA} &= y\,\chi_{AA} \ , \end{aligned} \tag{6.103}$$

with the solution

$$\begin{aligned} \chi_{AA} &= 2M\frac{\omega - x - y}{\omega^2 - x^2 - 2xy} \\ &= \frac{M}{\varepsilon}\left(\frac{\varepsilon - (x+y)}{\omega - \varepsilon} + \frac{\varepsilon + (x+y)}{\omega + \varepsilon}\right) \ , \end{aligned} \tag{6.104}$$

and

$$\varepsilon^2 := x^2 + 2xy \ , \tag{6.105}$$

where a fraction decomposition is performed to obtain the simple poles of the correlation function χ_{AA}.[2] Hence, the retarded susceptibility will be

$$\chi^{R}_{AA}(\mathbf{k},\omega) = \frac{M}{\varepsilon}\left(\frac{\varepsilon-(x+y)}{\omega-\varepsilon+\mathrm{i}\eta^{+}} + \frac{\varepsilon+(x+y)}{\omega+\varepsilon+\mathrm{i}\eta^{+}}\right) , \tag{6.113}$$

and

$$-\frac{1}{\pi}\mathrm{Im}\,\chi^{+-,ret}_{AA}(\mathbf{k},\omega) = \frac{M}{\varepsilon}\left[(\varepsilon-(x+y))\,\delta(\omega-\varepsilon) + (\varepsilon+(x+y))\,\delta(\omega+\varepsilon)\right] . \tag{6.114}$$

Notice that $\varepsilon = \varepsilon(\mathbf{q}) \equiv \varepsilon_{\mathbf{q}}$ is momentum dependent. Now, one can use the self-consistent equation for $M = \langle S^{z}_{a}\rangle$ for $a \in A$:

$$\langle S^{-}_{a'} S^{+}_{a}\rangle = \frac{1}{V}\sum_{\mathbf{q}} e^{\mathrm{i}\mathbf{k}\cdot(\mathbf{R}_{a}-\mathbf{R}_{a'})}\int_{-\infty}^{+\infty}\mathrm{d}\varepsilon\,\frac{-\frac{1}{\pi}\mathrm{Im}\,\chi^{+-,ret}_{AA}(\mathbf{q},\varepsilon)}{e^{\beta\varepsilon}-1} . \tag{6.115}$$

---

[2] The fraction decomposition can be performed as follows:

$$\frac{\omega-x-y}{\omega^2-x^2-2xy} =: \frac{A}{\omega-\varepsilon_1} + \frac{B}{\omega-\varepsilon_1} , \tag{6.106}$$

with A, B and $\varepsilon_{1,2}$ being parameters to be determined. Matching the RHS and LHS in the equation, i.e.,

$$\frac{\omega-x-y}{\omega^2-x^2-2xy} = \frac{(A+B)\omega-(A\varepsilon_2+B\varepsilon_1)}{\omega^2-(\varepsilon_1+\varepsilon_2)\omega+\varepsilon_1\varepsilon_2} , \tag{6.107}$$

yields

$$\begin{aligned} A+B=1 \Rightarrow B=1-A\ , \\ \varepsilon_1+\varepsilon_2=0 \Rightarrow \varepsilon_1=-\varepsilon_2=:\varepsilon\ . \end{aligned} \tag{6.108}$$

Hence

$$\begin{aligned} A\varepsilon_2+B\varepsilon_1=(1-2A)\varepsilon=x+y\ , \\ \varepsilon_1\varepsilon_2=-\varepsilon^2=-x^2-2xy \Rightarrow \varepsilon^2=x^2+2xy \overset{!}{\geq} 0\ . \end{aligned} \tag{6.109}$$

Finally,

$$\begin{aligned} A=\frac{\varepsilon-(x+y)}{2\varepsilon}\ , \\ B=\frac{\varepsilon+(x+y)}{2\varepsilon}\ . \end{aligned} \tag{6.110}$$

Notice that, as a necessary condition,

$$\varepsilon^2 = x^2+2xy = (2MJ_0)^2 + 2(2MJ_0)(MJ_{\mathbf{k}}) = (2MJ_0)^2\left(1+\frac{J_{\mathbf{k}}}{J_0}\right) \tag{6.111}$$

should *not* be less than zero; therefore,

$$1+\frac{J_{\mathbf{k}}}{J_0} \geq 0\ , \tag{6.112}$$

which is certainly satisfied when $\frac{J_{\mathbf{k}}}{J_0} \geq 0$. If $\frac{J_{\mathbf{k}}}{J_0} < 0$, then one must explicitly ensure that the inequality holds true.

For $a' = a$ ($S = \frac{1}{2}$),

$$\begin{aligned}\langle S_a^- S_a^+ \rangle &= \frac{1}{2} - \langle S_a^z \rangle = \frac{1}{2} - M \\ &= \frac{1}{V} \sum_{\mathbf{q}} \int_{-\infty}^{+\infty} \mathrm{d}\varepsilon \, \frac{-\frac{1}{\pi} \mathrm{Im}\, \chi_{AA}^{+-,ret}(\mathbf{q}, \varepsilon)}{e^{\beta\varepsilon} - 1} \; ; \end{aligned} \tag{6.116}$$

hence

$$\begin{aligned}\frac{1}{2} - M &= \frac{1}{V} \sum_{\mathbf{q}} \int_{-\infty}^{+\infty} \mathrm{d}\omega \, n_B(\varepsilon_{\mathbf{q}}) \frac{M}{\varepsilon_{\mathbf{q}}} [(\varepsilon_{\mathbf{q}} - (x+y))\delta(x - \varepsilon_{\mathbf{q}}) + (\varepsilon_{\mathbf{q}} + (x+y))\delta(x + \varepsilon_{\mathbf{q}})] \\ &= \frac{1}{V} \sum_{\mathbf{q}} \frac{M}{\varepsilon_{\mathbf{q}}} [(\varepsilon_{\mathbf{q}} - (x+y)) n_B(\varepsilon_{\mathbf{q}}) + (\varepsilon_{\mathbf{q}} + (x+y)) n_B(-\varepsilon_{\mathbf{q}})] \; . \end{aligned} \tag{6.117}$$

One can obtain the critical temperature T_C for the AFM order, by using the limit

$$T \to T_C^- \quad (\beta \to \beta_C^+) \; , \tag{6.118}$$

for which

$$M \to 0^+ \; , \tag{6.119}$$

and

$$\varepsilon_{\mathbf{q}} = 2M \sqrt{J_0^2 + J_0 J_{\mathbf{k}}} \overset{M \to 0^+}{\to} 0^+ \; . \tag{6.120}$$

Therefore,

$$\begin{aligned} n_B(\varepsilon_{\mathbf{q}}) &= \frac{1}{e^{\beta\varepsilon_{\mathbf{q}}} - 1} \overset{\beta \to \beta_C^+, \varepsilon_{\mathbf{q}} \to 0^+}{=\!=\!=} \frac{1}{1 + \beta_C \varepsilon_{\mathbf{q}} - 1} = \frac{1}{\beta_C \varepsilon_{\mathbf{q}}} \; , \\ n_B(-\varepsilon_{\mathbf{q}}) &\overset{\beta \to \beta_C^+, \varepsilon_{\mathbf{q}} \to 0^+}{=\!=\!=} \frac{-1}{\beta\varepsilon_{\mathbf{q}}} \; , \end{aligned} \tag{6.121}$$

so that

$$\begin{aligned}\frac{1}{2} - M &= \frac{1}{V} \sum_{\mathbf{q}} \frac{M}{\varepsilon_{\mathbf{q}}} [(\varepsilon_{\mathbf{q}} - (x+y)) \frac{1}{\beta_C \varepsilon_{\mathbf{q}}} + (\varepsilon_{\mathbf{q}} + (x+y)) \frac{-1}{\beta\varepsilon_{\mathbf{q}}}] \\ &= \frac{1}{V} \sum_{\mathbf{q}} \frac{M}{\beta_C \varepsilon_{\mathbf{q}}^2} [\varepsilon_{\mathbf{q}} - (x+y) - \varepsilon_{\mathbf{q}} - (x+y)] = \frac{-2}{V} \sum_{\mathbf{q}} \frac{M}{\beta_C \varepsilon_{\mathbf{q}}^2} (x+y) \\ &= \frac{-1}{\beta_C V} \sum_{\mathbf{k}} \frac{2M}{(2M)^2} \frac{1}{J_0^2 + J_0 J_{\mathbf{k}}} (2M J_0 + M J_{\mathbf{k}}) \\ &= -\frac{1}{\beta_C V} \sum_{\mathbf{k}} \frac{J_0 + \frac{1}{2} J_{\mathbf{k}}}{J_0^2 + J_0 J_{\mathbf{k}}} \; . \end{aligned} \tag{6.122}$$

As $M \to 0^+$,

$$\begin{aligned} \frac{1}{2} &= -\frac{J_0 + \frac{1}{2}J_{\mathbf{k}}}{J_0^2 + J_0 J_{\mathbf{k}}} \\ \Rightarrow \beta_C &= -\frac{1}{V}\sum_{\mathbf{k}} \frac{2J_0 + J_{\mathbf{k}}}{J_0^2 + J_0 J_{\mathbf{k}}} \\ \Rightarrow T_C &= [-\frac{1}{V}\sum_{\mathbf{k}} \frac{2J_0 + J_{\mathbf{k}}}{J_0^2 + J_0 J_{\mathbf{k}}}]^{-1} \ . \end{aligned} \tag{6.123}$$

The RKKY-interaction was obtained as

$$I_{\mathrm{RKKY}}(\mathbf{x}) = -\gamma_0 J^2 F(2k_F r) \quad ; \quad \gamma_0 := \frac{2}{\pi}\mathcal{N}(\varepsilon_F){k_F}^3 > 0, r := |\mathbf{x}| \ , \tag{6.124}$$

with the momentum representation

$$I_{\mathrm{RKKY}}(\mathbf{q}) = -\gamma_1 J^2 \mathcal{L}(q) \quad ; \quad \gamma_1 := \frac{1}{2}\mathcal{N}(\varepsilon_F) > 0, q := |\mathbf{q}| \ . \tag{6.125}$$

For the isotropic AFM order, the band structure and therefore the spatial variation of the RKKY-interaction should be such that it is antiferromagnetic for the nearest-neighbors and ferromagnetic for the next-nearest-neighbors. Therefore, the RKKY-interaction can be approximated by

$$\begin{aligned} I_{\mathrm{RKKY}}(r = a) &= -I_1 \quad ; \quad I_1 > I_2 > 0 \\ I_{\mathrm{RKKY}}(r = 2a) &= I_2 \ . \end{aligned} \tag{6.126}$$

Hence,

$$\begin{aligned} T_C^{AFM} &= [-\frac{1}{V}\sum_{\mathbf{q}} \frac{2J_0 + J_{\mathbf{q}}}{J_0^2 + J_0 J_{\mathbf{q}}}]^{-1} \\ &= [-\frac{1}{V}\frac{2}{J_0}\sum_{\mathbf{q}} \frac{1 + J_{\mathbf{q}}/(2J_0)}{1 + J_{\mathbf{q}}}]^{-1} \\ &= -\frac{J_0}{2}[\frac{1}{V}\sum_{\mathbf{q}} \frac{1 + \frac{1}{2}J_{\mathbf{q}}/J_0}{1 + J_{\mathbf{q}}/J_0}]^{-1} \ . \end{aligned} \tag{6.127}$$

We have to obtain

$$J_0 = \sum_{b'' \in B} J_{ab''} - \sum_{a'' \in A} J_{aa''} \ , \tag{6.128}$$

so we consider only the z nearest-neighbors in the A and B sub-lattices:

$$\begin{aligned} J_0 &= z(-I_2) - z(+I_1) \\ &= -z(I_1 + I_2) \ , \end{aligned} \tag{6.129}$$

where z is the coordination number and for a cubic lattice in 3d, $z = 6$. The coupling J in the formula for the RKKY-interaction will be the renormalized Kondo coupling $J_K \equiv J_K(y, T)$.

Then

$$\begin{cases} I_1 & \approx \gamma_0 J_K^2 \frac{1}{a^3} \\ I_2 & \approx \gamma_0 J_K^2 \frac{1}{(2a)^3} \end{cases} \Rightarrow I_1 + I_2 = \frac{9}{8}\gamma_0 J_K^2 \ .$$

The Kondo coupling can be written as

$$J_K = J_K^0 f_K(y,T) \ , \tag{6.130}$$

where f_K includes the effect of Kondo screening. Therefore,

$$T_C^{AFM} \approx \frac{1}{2} z \frac{9}{8} \gamma_0 J_K^2 \underbrace{[\frac{1}{V}\sum_{\mathbf{q}} \frac{1 + \frac{1}{2}\frac{\gamma_1}{\frac{9}{8}z\gamma_0}\mathcal{L}(q)}{1 + \frac{\gamma_1}{\frac{9}{8}z\gamma_0}\mathcal{L}(q)}]^{-1}}_{:=\zeta_0} \ ,$$

$$\frac{\gamma_1}{\gamma_0} = \frac{\frac{1}{2}\mathcal{N}(\varepsilon_F)}{\frac{2}{\pi}\mathcal{N}(\varepsilon_F)} \sim 1 \ , \tag{6.131}$$

where $\mathcal{L}(q)$ is the static Lindhard function and ζ_0 has no temperature dependence. Therefore,

$$\begin{aligned} T_C^{AFM} &\approx \frac{9z}{16} 2\pi \mathcal{N}(\varepsilon_F)\zeta_0 J_K^2 \\ &= \frac{9\pi}{8} z\zeta_0 \frac{1}{\mathcal{N}(\varepsilon_F)} (\mathcal{N}(\varepsilon_F) J_{\mathbf{k}})^2 \\ &= \frac{9\pi}{8} z\zeta_0 \frac{1}{\mathcal{N}(\varepsilon_F)} \underbrace{(\mathcal{N}(\varepsilon_F) J_K^0)^2}_{\approx y} f_K^2(y,T) \\ \Rightarrow \mathcal{N}(\varepsilon_F)\, T_C^{AFM} &= \frac{T_C^{AFM}}{D_0} = \frac{9\pi}{8} z\, \zeta_0 y\, f_K^2(y,T) \end{aligned} \tag{6.132}$$

The numerical value of $\zeta_0(z)$ can be computed depending on details of the lattice structure; yet, for a cubic lattice in 3d, with $z = 6$,

$$\zeta_0^{-1} \approx 0.541 \approx \frac{1}{2} \Rightarrow \zeta_0 \approx 2.0 \tag{6.133}$$

The equations determining $f_K(y,T)$ can be obtained by integrating the RG equation up a temperature T (see section 5.3):

$$\frac{1}{g}|_{g_0}^{g(T)} = \ln|\omega| - \frac{\mathsf{y}}{\mathsf{y}^2 - 1}[\mathsf{y}\ln|\frac{\sqrt{1+\omega^2} - \mathsf{y}}{\omega}| + \frac{1}{2}\ln|\frac{1 + \sqrt{1+\omega^2}}{1 - \sqrt{1+\omega^2}}|]|_{\omega = D_0/T}^1 \tag{6.134}$$

with

$$\mathsf{y} = y\, g_0^2 \frac{1}{T_K/D_0} \overset{T_K \approx T_K^0}{=\!=\!=} y\, g_0^2 \frac{1}{T_K^0/D_0} \ , \tag{6.135}$$

where we have used the bare Kondo temperature T_K^0 for the renormalized Kondo scale $T_K(y)$. The bare Kondo temperature satisfies

$$-\frac{1}{2g_0} = \ln(\frac{T_K^0}{D_0}) \ , \tag{6.136}$$

so that,

$$\mathsf{y} \approx y \ \frac{1}{4\frac{T_K^0}{D_0}(\ln(\frac{T_K^0}{D_0}))^2} \ . \tag{6.137}$$

Thus,

$$\begin{aligned}\frac{1}{g(T)} - \frac{1}{g_0} = &\underbrace{\ln(1)}_{=0} + \frac{\mathsf{y}}{1-\mathsf{y}^2}[\mathsf{y}\ln|\sqrt{2}-\mathsf{y}| + \underbrace{\frac{1}{2}\ln|\frac{1+\sqrt{2}}{1-\sqrt{2}}|}_{\approx 0.881}] \\ &- (\ln|\frac{D_0}{T}| + \frac{\mathsf{y}}{1-\mathsf{y}^2}[\mathsf{y}\ln|\frac{\sqrt{1+(D_0/T)^2}-\mathsf{y}}{D_0/T}| + \frac{1}{2}\ln|\frac{1+\sqrt{1+(D_0/T)^2}}{1-\sqrt{1+(D_0/T)^2}}|]) \ .\end{aligned} \tag{6.138}$$

Defining

$$\tau := \frac{T}{D_0} \ ,$$

one obtains

$$\begin{aligned}\frac{1}{g(T)} &= \frac{1}{g_0} + \frac{\mathsf{y}}{1-\mathsf{y}^2}[\mathsf{y}\ln|\sqrt{2}-\mathsf{y}| + 0.881] + \ln|\tau| \\ &\quad - \frac{\mathsf{y}}{1-\mathsf{y}^2}[\mathsf{y}\ln|\frac{\sqrt{1+1/\tau^2}-\mathsf{y}}{1/\tau}| + \frac{1}{2}\ln|\frac{1+\sqrt{1+1/\tau^2}}{1-\sqrt{1+1/\tau^2}}|] \\ &= \frac{1}{g_0} + \ln|\tau| + \frac{\mathsf{y}}{1-\mathsf{y}^2}[\mathsf{y}\ln|\frac{(\sqrt{2}-\mathsf{y})/\tau}{\sqrt{1+1/\tau^2}-\mathsf{y}}| + \frac{1}{2}\ln|\frac{(1+\sqrt{2})(1-\sqrt{1+1/\tau^2})}{(1-\sqrt{2})(1+\sqrt{1+1/\tau^2})}| \\ &= \frac{1}{g_0}(1 + g_0\ln|\tau| + \frac{g_0\mathsf{y}}{1-\mathsf{y}^2}[\mathsf{y}\ln|\frac{(\sqrt{2}-\mathsf{y})/\tau}{\sqrt{1+1/\tau^2}-\mathsf{y}}| + \frac{1}{2}\ln|\frac{(1+\sqrt{2})(1-\sqrt{1+1/\tau^2})}{(1-\sqrt{2})(1+\sqrt{1+1/\tau^2})}|] \\ &\equiv \frac{1}{g_0}\frac{1}{f_K} \ .\end{aligned} \tag{6.139}$$

By introducing a dimensionless AFM critical temperature, τ_C^{AFM}, as

$$\tau_C := \tau_C^{AFM} := \frac{T_C^{AFM}}{D_0} \ , \tag{6.140}$$

the equation for T_C^{AFM} becomes

$$\frac{T_C^{AFM}}{D_0} = c_0\, y\, f_K^2(y,T)|_{T=T_C^{AFM}} \quad ; \quad c_0 \sim \mathcal{O}(1) \ , \tag{6.141}$$

so that,

$$\tau_C = c_0\, y\, f_K^2(y, \tau_C)\ . \tag{6.142}$$

This equation should be solved numerically.

Numerical solution For the numerical solution, we re-formulate the equations as follows:

$$\begin{aligned} \frac{1}{\tau_C} &= \frac{1}{c_0}\frac{1}{y}\frac{1}{f_K^2} \\ \Rightarrow c_0 &= \frac{\tau_C}{y}\frac{1}{f_K^2(y, \tau = \tau_C)} \\ &\Rightarrow \frac{\tau_C}{y}\frac{1}{f_K^2(y, \tau = \tau_C)} - c_0 = 0\ . \end{aligned} \tag{6.143}$$

Therefore,

$$\begin{aligned} \frac{1}{f_K} = 1 + g_0 \ln(\tau) + \frac{g_0 \mathsf{y}}{1-\mathsf{y}^2}[\mathsf{y}\ln|\frac{(\sqrt{2}-\mathsf{y})/\tau}{\sqrt{1+1/\tau^2}-\mathsf{y}}| \\ + \frac{1}{2}\ln|\frac{(1+\sqrt{2})(1-\sqrt{1+1/\tau^2})}{(1-\sqrt{2})(1+\sqrt{1+1/\tau^2})}|]\ . \end{aligned} \tag{6.144}$$

Define

$$x := \frac{1}{\tau}\ ,$$

such that

$$\begin{aligned} \frac{1}{f_K} = 1 - g_0 \ln|x| \\ + \frac{g_0 \mathsf{y}}{1-\mathsf{y}^2}[\mathsf{y}\ln|\frac{(\sqrt{2}-\mathsf{y})x}{\sqrt{1+x^2}-\mathsf{y}}| + \frac{1}{2}\ln|\frac{(1+\sqrt{2})(1-\sqrt{1+x^2})}{(1-\sqrt{2})(1+\sqrt{1+x^2})}|]\ . \end{aligned} \tag{6.145}$$

We should look for a solution for T_C where the following conditions are satisfied

$$\begin{aligned} T_C < D_0 \equiv \tau_C < 1\ , \\ \mathsf{y} < 1\ , \\ y_{max} < y \leq 1\ . \end{aligned} \tag{6.146}$$

From previous calculations for lattice case, at the Kondo break-down point (see chapter 3),

$$\mathsf{y}_{max} \approx 0.266 \approx 0.3\ . \tag{6.147}$$

From this we can obtain y_{max}; for example, for $\frac{T_K^0}{D_0} \sim 10^{-3}$; therefore,

$$\mathsf{y} \sim 10^2\, y \Rightarrow y_{max} \sim 10^{-3}\ . \tag{6.148}$$

The upper bound for y is obtained by $\mathsf{y} = 1$ (where the expression for f_K diverges); hence, $\sup[y] \sim 10^{-2}$.

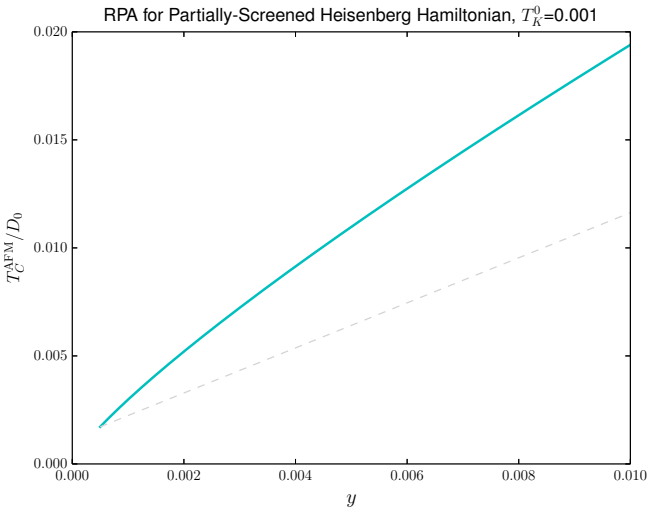

Figure 6.1: AFM critical temperature, T_C^{AFM}, as a function of the RKKY strength parameter, y. The bare Kondo scale is $T_K^0/D_0 = 10^{-3}$. The curve can be fitted to a sublinear relation, $T_C^{AFM} \approx \text{const.} + c_0(y-y_0)^p$ where $c_0 = 1.0$ and $p = 0.88$. The linear relation is denoted by a gray dashed line as guide for the eye.

As an example, for bare $T_K^0/D_0 = 10^{-3}$, the results are shown in Fig. 6.1. The approximate relation (obtained by fitting) between the AFM critical temperature, T_C^{AFM}, and the RKKY strength parameter, y, is found to be roughly $T_C^{AFM} \propto y^p$ where, e.g., $p \sim 0.8$ for $T_K^0/D_0 = 10^{-3}$. The behaviour does not change for other bare values of T_K, although the power p varies between 0.7 and 0.9, i.e., $p < 1.0$; namely, it remains *sublinear* for the appropriate values of the bare Kondo temperature.

CHAPTER 7

Afterword

In this work, we developed in detail, a perturbative renormalization group method for multi-impurity Kondo systems (e.g., a two-impurity system or an impurity lattice) by incorporating the dynamic effect of the indirect carrier-mediated RKKY exchange interaction between the impurities as a modification to the original bare Kondo vertex (RKKY vertex corrections).

We observed in the case of 'symmetrically'- or 'asymmetrically'-coupled systems, that increasing the RKKY magnetic fluctuations results in a suppression of the Kondo screened phase, which is signaled by a strong reduction of the Kondo energy scale/temperature, T_K, and ultimately, a complete breakdown of the phase, in a *universal* manner. The upshot was that the system cannot maintain a Kondo liquid phase and 'yields' ultimately, via a cross-over, to a phase in which Kondo screening is broken and Kondo (heavy) quasi-particles have collapsed, and one is left with partially-screened unordered moments in presence of Kondo fluctuations. We found out that even a possibility of magnetic instability cannot change this scenario qualitatively, in the sense that it cannot preclude neither the collapse of the Kondo-screened phase, nor leads to a simultaneous magnetic ordering with Kondo breakdown. This has profound consequences for the microscopic scenarios for quantum phase transitions in heavy-fermionic systems. Thus, we could show that, without any extraneous assumptions about the interactions or phases, merely a relatively small amount of magnetic fluctuations suffice to break the Kondo liquid phase. We also made a bird's eye view into the nature of the partially-screened phase using an RG-corrected random-phase approximation to the impurity lattice. The main observation there was that the Kondo fluctuations would lead to nonlinear behaviour in the critical temperature for magnetic ordering as a function of the strength of the RKKY interaction. This can provide some clear-cut experimental signatures to examine in heavy-fermionic systems.

All this being said, there is still large room for extensions and improvements of the current theory in various directions. First, one can include other instabilities, such as Cooper-pairing instability, in the RG method to study such instabilites in Kondo lattice systems (heavy fermions) and their competition with the Kondo effect. Secondly, these results, indeed, need to be compared and confirmed, whenever possible, with those which can be obtained from other methods, like numerical RG, functional RG (fRG), conformal field theory, or exact-diagonalization methods. Moreover, our coupling-constant RG method — despite its remarkable results — can only deliver the renormalized cross-over or phase-transition scales, but cannot yield any correlation function directly; hence, there is a need for RG methods which can access correlation functions and transport properties in a rigorous framework which ensures consistency and averts bias.

The final and most important point is that this RG theory clearly hints at a possibility of

constructing a Kadanoff-Baym conserving approximation for Kondo lattices, which includes possible instabilites in several channels. That would be the 'holy grail' in the domain of Kondo physics and heavy fermions, since such a theory could provide equilibrium and nonequilibrium results for the strongly-correlated Kondo phase and describe its breakdown in microscopic detail. This could be much more interesting regarding the recent developments in considering the non-trivial topological phases of the Kondo insulators. Hence, this would open up a very exciting avenue of research in the physics of strongly-correlated electronic systems.

APPENDIX A

Pauli-matrix algebra

Throughout the calculation of spin expression, we use the following identities for the Pauli matrices ($i, j \in \{x, y, z\}$)[1]:

$$\begin{aligned}
\sigma_i^2 &= \mathbb{1}, \\
\{\sigma_i, \sigma_j\} &\equiv \sigma_i\sigma_j + \sigma_j\sigma_i = 2\delta_{ij}, \\
[\sigma_i, \sigma_j] &= 2\mathrm{i}\epsilon_{ijk}\sigma_k, \\
\sigma_i\sigma_j &= \delta_{ij}\mathbb{1} + \mathrm{i}\sum_c \epsilon_{abc}\sigma_c, \\
\sigma^{\pm} &\equiv \sigma^{+} \pm \mathrm{i}\sigma^{-}, \\
(\sigma^{\pm})^2 &= (\sigma_x \pm \mathrm{i}\sigma_y)^2 = \sigma_x^2 - \sigma_y^2 \pm \mathrm{i}\{\sigma_x, \sigma_y\} = 0\,, \\
\sigma^{-}\sigma^{+} &= \sigma_x^2 + \sigma_y^2 + \mathrm{i}[\sigma_x, \sigma_y] = 2(\mathbb{1} - \sigma_z), \\
\sigma^{+}\sigma^{-} &= \sigma_x^2 + \sigma_y^2 - \mathrm{i}[\sigma_x, \sigma_y] = 2(\mathbb{1} + \sigma_z), \\
\sigma_z\sigma^{-} &= -\sigma^{-}, \\
\sigma_z\sigma^{+} &= \sigma^{+}, \\
\sigma^{-}\sigma_z &= \sigma^{-}, \\
\sigma^{+}\sigma_z &= -\sigma^{+}.
\end{aligned} \tag{A.1}$$

Furthermore,

$$\begin{aligned}
S^{\pm} &= S_x \pm \mathrm{i}S_y\ , \\
[S^z, S^{\pm}] &= \pm S^{\pm}\ , \\
[S^{+}, S^{-}] &= 2S^z\ .
\end{aligned} \tag{A.2}$$

[1] The symbol ϵ_{ijk} denotes the Levi-Civita tensor.

APPENDIX B

Spin-spin interaction

A spin-spin interaction is generally of the form

$$\mathbf{S}_{jd} \cdot \mathbf{s}_{\alpha\alpha'} = \frac{1}{4} \sum_{i=x,y,z} \sum_{\sigma\sigma'\eta\eta'} (d^\dagger_\sigma \sigma^i_{\sigma\sigma'} d_{\sigma'})(c^\dagger_{\alpha\eta} \sigma^i_{\eta\eta'} c_{\alpha'\eta'}) \ . \tag{B.1}$$

Hence, using the relations,

$$\begin{aligned} \sigma^\pm &= \sigma^x \pm \mathrm{i}\sigma^y \ , \\ S^\pm &= S^x \pm \mathrm{i}S^y \ , \end{aligned} \tag{B.2}$$

one can decompose a spin interaction as

$$\begin{aligned} \mathbf{S}_1 \cdot \mathbf{S}_2 &= \sum_{i=x,y,z} S^i_1 S^i_2 = S^z_1 S^z_2 + S^x_1 S^x_2 + S^y_1 S^y_2 \\ &= S^z_1 S^z_2 + \frac{1}{4}(S^+_1 + S^-_1)(S^+_2 + S^-_2) - \frac{1}{4}(S^+_1 - S^-_1)(S^+_2 - S^-_2) \\ &= S^z_1 S^z_2 + \frac{1}{2}(S^+_1 S^-_2 + S^-_1 S^+_2) \ . \end{aligned} \tag{B.3}$$

For spin $s = \frac{1}{2}$, $\mathbf{S} = \frac{1}{2}\boldsymbol{\sigma}$, and

$$\boldsymbol{\sigma} \cdot \boldsymbol{\sigma} = \sigma^z \sigma^z + \frac{1}{2}(\sigma^+ \sigma^- + \sigma^- \sigma^+) \ . \tag{B.4}$$

Therefore,

$$\begin{aligned} \mathbf{S}_{jd} \cdot \mathbf{s}_{\alpha\alpha'} &= \frac{1}{4} \sum_{\sigma\sigma'\eta\eta'} d^\dagger_\sigma d_{\sigma'} (\sum_i \sigma^i_{\sigma\sigma'} \sigma^i_{\eta\eta'}) c^\dagger_{\alpha\eta} c_{\alpha'\eta'} \ , \\ \sum_i \sigma^i_{\sigma\sigma'} \sigma^i_{\eta\eta'} &= \sigma^z_{\sigma\sigma'} \sigma^z_{\eta\eta'} + \frac{1}{2}(\sigma^+_{\sigma\sigma'} \sigma^-_{\eta\eta'} + \sigma^-_{\sigma\sigma'} \sigma^+_{\eta\eta'}) \ , \end{aligned} \tag{B.5}$$

and

$$\sigma^z_{\sigma\sigma'} = \delta_{\sigma\uparrow}\delta_{\sigma'\downarrow} - \delta_{\sigma\downarrow}\delta_{\sigma'\downarrow} \quad ; \quad \sigma^+_{\sigma\sigma'} = 2\delta_{\sigma\uparrow}\delta_{\sigma'\downarrow} \quad ; \quad \bar{\sigma}_{\sigma\sigma'} = 2\delta_{\sigma\downarrow}\delta_{\sigma'\uparrow} \ . \tag{B.6}$$

- The part proportional $\sigma^z\sigma^z$ is

$$\begin{aligned}\sum_{\sigma\sigma'\eta\eta'} d^\dagger_\sigma d_{\sigma'}(\sigma^z_{\sigma\sigma'}\sigma^z_{\eta\eta'})c^\dagger_\eta c_{\eta'} &= \sum_{\sigma\sigma'\eta\eta'}(\delta_{\sigma\uparrow}\delta_{\sigma'\uparrow}-\delta_{\sigma\downarrow}\delta_{\sigma'\downarrow})(\delta_{\eta\uparrow}\delta_{\eta'\uparrow}-\delta_{\eta\downarrow}\delta_{\eta'\downarrow})c^\dagger_\eta c_{\eta'}\\ &= (d^\dagger_\uparrow d_\uparrow - d^\dagger_\downarrow d_\downarrow)(c^\dagger_\uparrow c_\uparrow - c^\dagger_\downarrow c_\downarrow)\\ &= (\hat{n}_{d\uparrow}-\hat{n}_{d\downarrow})(c^\dagger_\uparrow c_\uparrow - c^\dagger_\downarrow c_\downarrow)\\ &= \sum_\sigma(\hat{n}_{d\sigma}-\hat{n}_{d\bar{\sigma}})\hat{n}_{c\sigma}\ . \end{aligned} \tag{B.7}$$

- The part proportional to $\sigma^+\sigma^-$ is

$$4\sum_{\sigma\sigma'\eta\eta'} d^\dagger_\sigma d_{\sigma'}(\delta_{\sigma\uparrow}\delta_{\sigma'\downarrow}\delta_{\eta\downarrow}\delta_{\eta'\uparrow})c^\dagger_\sigma c_{\bar{\sigma}} = 4d^\dagger_\uparrow d_\downarrow c^\dagger_\downarrow c_\uparrow\ . \tag{B.8}$$

- The part proportional to $\sigma^-\sigma^+$ is

$$4\sum_{\sigma\sigma'\eta\eta'} d^\dagger_\sigma d_{\sigma'}(\delta_{\sigma\downarrow}\delta_{\sigma'\uparrow}\delta_{\eta\uparrow}\delta_{\eta'\downarrow})c^\dagger_\eta c_{\eta} = 4d^\dagger_\downarrow d_\uparrow c^\dagger_\uparrow c_\downarrow\ . \tag{B.9}$$

Therefore, $\mathbf{S}_{jd}\cdot\mathbf{s}_{\alpha\alpha'}$ entails

$$\begin{aligned}\frac{1}{4}\left(\sigma^z\sigma^z+\frac{1}{2}(\sigma^+\sigma^-+\sigma^-\sigma^+)\right) &= \frac{1}{4}\left(\sum_\sigma(\hat{n}_{d\sigma}-\hat{n}_{d\bar{\sigma}})c^\dagger_{\alpha\sigma}c_{\alpha'\sigma}+\frac{4}{2}(d^\dagger_\uparrow d_\downarrow c^\dagger_\downarrow c_\uparrow + d^\dagger_\downarrow d_\uparrow c^\dagger_\uparrow c_\downarrow)\right)\\ &= \frac{1}{4}\left(\sum_\sigma(\hat{n}_{d\sigma}-\hat{n}_{d\bar{\sigma}})c^\dagger_{\alpha\sigma}c_{\alpha'\sigma}+2(\sum_\sigma d^\dagger_\sigma d_{\bar{\sigma}}c^\dagger_{\alpha\bar{\sigma}}c_{\alpha'\sigma})\right)\\ &= \frac{1}{4}\sum_\sigma\left(\underbrace{(\hat{n}_{d\sigma}-\hat{n}_{d\bar{\sigma}})c^\dagger_{\alpha\sigma}c_{\alpha'\sigma}}_{\text{no spin-flip}}+2\underbrace{d^\dagger_\sigma d_{\bar{\sigma}}c^\dagger_{\alpha\bar{\sigma}}c_{\alpha'\sigma}}_{\text{spin-flip}}\right)\ . \end{aligned} \tag{B.10}$$

APPENDIX C

Abrikosov's pseudo-particle representation

In order to perform the usual diagrammatic perturbation calculations for spin operators, Abrikosov [42] introduced a faithful representation of the spin in terms of pseudo-fermions. In this representation, $2S+1$ pseudo-fermions are introduced corresponding to the $2S+1$ states of the impurity spin S with the z-component, $m_S = S, S-1, \cdots, -S$. The pseudo-fermions are considered as quantum states which can be created or annihilated by their corresponding operators in the Fock space. An arbitrary spin operator, $\hat{S}$, is represented by pseudo-fermions as

$$\hat{S} \doteq \sum_{m_S, m_{S'}} f^{\dagger}_{m_{S'}} \langle m_{S'}|\hat{S}|m_S\rangle f_{m_S} \equiv \sum_{m_S, m_{S'}} f^{\dagger}_{m'_S} S_{m_{S'}, m_S} f_{m_S} \tag{C.1}$$

where $\langle m_{S'}|\hat{S}|m_S\rangle \equiv S_{m_{S'},m_S}$ denote the matrix elements of the spin operator, $\hat{S}$ [7]. For the simplest case of $S = \frac{1}{2}$, the representation will be

$$\mathbf{S} = \frac{1}{2} \sum_{\nu\nu'} f^{\dagger}_{\nu'} \boldsymbol{\sigma}_{\nu'\nu} f_{\nu} \ , \tag{C.2}$$

where $\boldsymbol{\sigma}$ denotes the Pauli matrix. Usually, in the diagrams, the full lines represent electrons and broken lines represent pseudo-fermions.

A major difficulty which arises with this representation is that the *physical* spin states correspond to pseudo-fermionic states with *single* occupation; thus, the sector of the Hilbert space in which no pseudo-fermionic state or more than a single pseudo-fermionic state is occupied, is unphysical and should be eliminated. The unphysical doubly-occupied states are 'projected out' by assuming a large energy, λ, for the pseudo-fermions. In this manner, the expectation values must be normalized to the probability of single occupation $(2S+1)\exp(-\lambda/T)$ with $\lambda \to +\infty$. Furthermore, one notices that the pseudo-fermionic vacuum, with no pseudo-fermionic states occupied, gives no contribution to the actual calculations [7, 45].

Keiter [87] put forward a criticism of Abrikosov's pseudo-fermionic representation, showing that the *linked-cluster theorem*[1] cannot be applied in this representation. The problem was removed by a generalization of Abrikosov's representation by Zawadowski and Fazekas [44] (see a review in Ref. [88]). In this work, we use the latter representation.

In general, to use the pseudo-particle representation, one adds a term to the Hamiltonian,

[1] For an extended discussion of the linked-cluster theorem, consult Refs. [119, 249].

corresponding to the number of pseudo-particles; that is,

$$H \mapsto \mathcal{H}_\lambda := H + \lambda \hat{Q} \ , \tag{C.3}$$

where λ is a constant and $\hat{Q}$ is the pseudo-particle counting operator,

$$\hat{Q} := \sum_f \hat{n}_f \ . \tag{C.4}$$

The *physical* expectation value for an observable $\hat{A}$, can be obtained as

$$\langle \hat{A} \rangle_{phys} = \lim_{\lambda \to +\infty} \frac{\langle \hat{A}\, \hat{Q} \rangle_\lambda}{\langle \hat{Q} \rangle_\lambda} \ , \tag{C.5}$$

where $\langle \hat{Q} \rangle_\lambda$ is the expectation value of the pseudo-particle counting operator, $\hat{Q}$, defined as

$$\langle \hat{Q} \rangle_\lambda = \frac{\mathrm{tr}\{e^{-\beta \mathcal{H}_\lambda} \hat{Q}\}}{\mathrm{tr}\{e^{-\beta \mathcal{H}_\lambda}\}} \ , \tag{C.6}$$

and the subscript λ denotes a quantity in the pseudo-particle representation with all pseudo-particle states (singly-occupied, doubly-occupied, or unoccupied) included. Notice that the limit[2], $\lambda \to +\infty$, projects out the doubly-occupied pseudo-particle states with a large energy punishment, and the operator $\hat{Q}$ in the numerator of RHS of Eq. (C.5) eliminates the contribution of the fictitious pseudo-particle vacuum, $|vac\rangle \equiv |Q = 0\rangle$. If further,

$$\hat{A}|Q = 0\rangle \equiv \hat{A}|vac\rangle = 0 \ , \tag{C.7}$$

that is, if $\hat{A}$ annihilates the pseudo-particle vacuum[3], then the relation above, Eq. (C.5), simplifies to

$$\langle \hat{A} \rangle_{phys} = \lim_{\lambda \to +\infty} \frac{\langle \hat{A} \rangle_\lambda}{\langle \hat{Q} \rangle_\lambda} \ , \tag{C.8}$$

since the operator $\hat{Q}$ in the numerator of RHS of Eq. (C.5) is there merely to project out the fictitious vacuum, $|Q = 0\rangle$.

Due to Eq. (C.3), the pseudo-particle energies will depend linearly on λ which ultimately tends to infinity; for instance, the non-interacting Green's function of pseudo-fermions will be

$$G_f^0(\omega) = \frac{1}{\omega - (\xi_d + \lambda) \pm \mathrm{i}\eta^+} \ . \tag{C.9}$$

To prevent a trivial divergence of the spectrum and vanishing of the Green's functions due to this infinite parametre, in the actual calculations, we shift the frequencies as

$$\omega \mapsto \omega + \lambda \ , \tag{C.10}$$

[2] The limit, $\lambda \to +\infty$, should only be taken at the end of the calculations.
[3] This is particularly true for spin operators.

to obtain the frequency-shifted quantities like

$$\begin{aligned} \hat{G}_f^0(\omega) &:= G_f^0(\omega + \lambda) = \frac{1}{\omega - \xi_d \pm \mathrm{i}\eta^+} \ , \\ \hat{A}_f^0(\omega) &:= A_f^0(\omega + \lambda) = \delta(\omega - \xi_d) \ , \end{aligned} \tag{C.11}$$

which we mark by a hat. In general, we define

$$\hat{\mathcal{F}}(z) := \mathcal{F}(z + \lambda) \ . \tag{C.12}$$

A detailed discussion of Abrikosov's representation can be found in Refs. [7, 45, 88].

APPENDIX D

T-matrix renormalization

The idea of renormalization is to successively reduce the bandwidth, D, of the conduction electrons and include the effect of the eliminated higher energy states (or 'modes') in the couplings. This will result in a 'flow' of the couplings which would have some fixed points (where couplings do not change anymore). The fixed points describe the properties of the system at low energies.

The simplest way to obtain the RG flow for the single-impurity Kondo problem is to use the T-matrix renormalization, which Anderson has called "poor man's scaling". In this method, one considers the Kondo interaction as a scattering of itinerant conduction electrons and the localized impurity, and investigates the change in the scattering amplitude upon elimination of high-energy modes of the conduction electrons.

For a general scattering potential V, the T-matrix is defined as [28, 202]

$$T(z) = V + V\,G(z)\,T(z)\ ,\ z \in \mathbb{C} \tag{D.1}$$

where $G(z)$ is the *non-interacting* Green's function *operator* ('resolvent') for the conduction electrons,

$$G(z) \equiv G^0(z) = \frac{1}{z - H_0}\ . \tag{D.2}$$

Let us define P as the projection operator onto the high-energy modes (near the band edge of the conduction electron) with an energy (with respect to the Fermi level) $\xi \in [-D, -D + \delta D] \cup [D - \delta D, D]$. Then,

$$[P, H_0] = 0 \Rightarrow [P, G] = 0\ ; \tag{D.3}$$

furthermore, the unity operator $\mathbb{1}$ can be written in terms of P as

$$\mathbb{1} = P + \mathbb{1} - P\ . \tag{D.4}$$

Therefore,

$$\begin{aligned} T &= V + V\mathbb{1}GT \\ &= V + V(\mathbb{1} - P)GT + VPGT\ . \end{aligned} \tag{D.5}$$

Iterating the last term on the RHS, one obtains an infinite series,

$$\begin{aligned}
T &= V + V(\mathbb{1}-P)GT + VPG\,(V + V(\mathbb{1}-P)GT + VPGT) \\
&\equiv V + VPGV + (V + VPGV)(\mathbb{1}-P)GT + VPGVPGT \\
&= V + VPGV + (V + VPGV)(\mathbb{1}-P)GT + \\
&\quad VPGVPG\,(V + VPGV + (V + VPGV)(\mathbb{1}-P)GT + VPGVPGT) \\
&\equiv V + VPGV + VPGVPGV + VPGVPGVPGV \\
&\quad + (V + VPGV + VPGVPGV + VPGVPGVPGV)\,(\mathbb{1}-P)GT \\
&\quad + VPGVPGVPGVPGT\ ,
\end{aligned} \tag{D.6}$$

which reveals the repetitive structure of the series in terms of the combination VPG. The last term of the series expansion will be of arbitrary high order of the interaction V, and therefore, can be neglected in a perturbative analysis. Hence, one obtains

$$\begin{aligned}
T &= (V + VPGV + VPGVPGV + \cdots) \\
&\quad + (V + VPGV + VPGVPGV + \cdots)(1-P)GT
\end{aligned} \tag{D.7}$$

The *reduced* T-matrix, T', in the low-energy sector of the Hilbert space is defined as

$$\begin{aligned}
T' &:= (\mathbb{1}-P)T(\mathbb{1}-P) \\
&= (\mathbb{1}-P)(V + VPGV + \cdots)(\mathbb{1}-P) \\
&\quad + (\mathbb{1}-P)(V + VPGV + \cdots)(\mathbb{1}-P)G(\mathbb{1}-P)T(\mathbb{1}-P)\ ,
\end{aligned} \tag{D.8}$$

where we have used the fact that since P and $\mathbb{1}-P$ are projection operators,

$$(\mathbb{1}-P)^2 = \mathbb{1}-P\ , \tag{D.9}$$

and due to Eq. (D.3),

$$[P, G] = 0\ . \tag{D.10}$$

Therefore,

$$T' = V' + V'GT'\ , \tag{D.11}$$

where the renormalized interaction V' is given by

$$V' = (\mathbb{1}-P)(V + VPGV + \cdots)(\mathbb{1}-P)\ , \tag{D.12}$$

which can obtained up to a deliberate order in interaction strength.

For the anisotropic single-impurity Kondo Hamiltonian,

$$V = \sum_{\mathbf{k},\mathbf{k}',\alpha\beta} \left\{ J_\pm \left(S^+\sigma^-_{\alpha\beta} + S^-\sigma^+_{\alpha\beta} \right) + J_z S^z \sigma^z_{\alpha\beta} \right\} c^\dagger_{\mathbf{k}'\alpha} c_{\mathbf{k}\beta}\ , \tag{D.13}$$

in which

$$S^+ = S_x + \mathrm{i}S_y \ ,$$
$$S^- = (S^+)^\dagger = S_x - \mathrm{i}S_y \ , \tag{D.14}$$

σ denotes the Pauli matrices, and the impurity is assumed to be at $\mathbf{x} = 0$ (without loss of generality). The above 'T-matrix scaling' leads to a renormalization of the potential,

$$V' = V + \delta V \ , \tag{D.15}$$

where (up to the second order in the couplings J),

$$\begin{aligned}\delta V &= (\mathbb{1} - P)VPGV(\mathbb{1} - P) \\ &= (\mathbb{1} - P)\Big[\sum_{\mathbf{k}_1,\mathbf{k}_2,\alpha\beta} \{J_\pm \left(S^+\sigma^-_{\alpha\beta} + S^-\sigma^+_{\alpha\beta}\right) + J_z S^z \sigma^z_{\alpha\beta}\} c^\dagger_{\mathbf{k}_1\alpha} c_{\mathbf{k}_2\beta} \\ &\times P\frac{1}{z - H_0} \sum_{\mathbf{k}_3,\mathbf{k}_4,\gamma\delta} \{J_\pm \left(S^+\sigma^-_{\gamma\delta} + S^-\sigma^+_{\gamma\delta}\right) + J_z S^z \sigma^z_{\gamma\delta}\} c^\dagger_{\mathbf{k}_3\gamma} c_{\mathbf{k}_4\delta}\Big](\mathbb{1} - P) \ .\end{aligned} \tag{D.16}$$

It turns out that at the second order, two processes contribute to the renormalization[1]:

i) The 'direct' process in which an electron scatters from the impurity into a high-energy state near the band edge, along with a spin flip of the impurity and the electron (Fig. D.1),

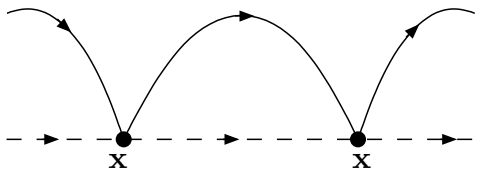

Figure D.1: Direct process.

$$\begin{aligned} \xi_{\mathbf{k}_1}, \xi_{\mathbf{k}_4} &\in [-D + \delta D, D - \delta D] \quad : \text{reduced band} \ , \\ \mathbf{k}_3 = \mathbf{k}_2 \to \xi_{\mathbf{k}_3} = \xi_{\mathbf{k}_2} &\in [D - \delta D, D] \quad : \text{upper band-edge} \ . \end{aligned}$$

ii) The 'exchange' process in which a hole excitation is produced due to the scattering, which is finally absorbed to return to the ground-state of the Fermi sea (Fig. D.2):

$$\begin{aligned} \xi_{\mathbf{k}_2}, \xi_{\mathbf{k}_3} &\in [-D + \delta D, D - \delta D] \quad : \text{reduced band} \ , \\ \mathbf{k}_1 = \mathbf{k}_4 \to \xi_{\mathbf{k}_1} = \xi_{\mathbf{k}_4} &\in [-D, -D + \delta D] \quad : \text{lower band-edge} \ . \end{aligned}$$

[1] We neglect processes which involve two particles (or holes) or more.

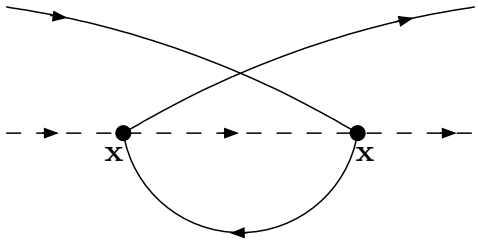

Figure D.2: Exchange process.

D.1 Direct process

The direct process leads to

$$\delta V_{dir} = (\mathbb{1}-P)\Big[\sum_{\mathbf{k}_1,\mathbf{k}_2,\mathbf{k}_4,\alpha\beta\delta}\{J_\pm\left(S^+\sigma^-_{\alpha\beta}+S^-\sigma^+_{\alpha\beta}\right)+J_zS^z\sigma^z_{\alpha\beta}\}c^\dagger_{\mathbf{k}_1\alpha}c_{\mathbf{k}_2\beta}$$
$$P\times\frac{1}{z-H_0}\left[J_\pm\left(S^+\sigma^-_{\beta\delta}+S^-\sigma^+_{\beta\delta}\right)+J_zS^z\sigma^z_{\beta\delta}\}c^\dagger_{\mathbf{k}_2\beta}c_{\mathbf{k}_4\delta}\right](\mathbb{1}-P)\ . \tag{D.17}$$

Note that the projection operator P in between (in PG) of Eq. (D.17) constrains the intermediate states to be of high energy, so that $\xi_{\mathbf{k}_2}\in[D-\delta D,D]$ and

$$\frac{1}{z-H_0}=\frac{1}{z-(\xi_{\mathbf{k}_2}-\xi_{\mathbf{k}_4})}\overset{\xi_{\mathbf{k}_2}\approx D}{\approx}\frac{1}{z-D+\xi_{\mathbf{k}_4}}\overset{\xi_{\mathbf{k}_4}\ll D}{\approx}\frac{1}{z-D}\ , \tag{D.18}$$

where the approximation is valid since $\delta D\ll D$ and $\mathbf{k}_4$ belongs to the low-energy part of the band-with, away from the edges, $\xi_{\mathbf{k}_4}\ll D$. Hence,

$$\delta V_{dir} = (\mathbb{1}-P)\Big[\sum_{\mathbf{k}_1,\mathbf{k}_4,\alpha\delta\beta}\mathrm{Spin}(\alpha,\beta)\,c^\dagger_{\mathbf{k}_1\alpha}c_{\mathbf{k}_2\beta}$$
$$\times\frac{1}{z-D}\,\mathrm{Spin}(\beta,\delta)\,c^\dagger_{\mathbf{k}_2\beta}c_{\mathbf{k}_4\delta}\Big](\mathbb{1}-P)\ , \tag{D.19}$$

where the Pauli spin parts are denoted concisely to avoid clutter and will be considered later. The combination $c_{\mathbf{k}_2\beta}c^\dagger_{\mathbf{k}_2\beta}$ is equal to the number of holes (empty states) in $[D-\delta D,D]$; therefore, at a low-energy state (due to $\mathbb{1}-P$) $\mathbf{k}_2$-state is certainly unoccupied and $c_{\mathbf{k}_2\beta}c^\dagger_{\mathbf{k}_2\beta}=1$. Thus,

$$\delta V_{dir} = (\mathbb{1}-P)\sum_{\mathbf{k}_1,\mathbf{k}_4,\alpha\delta}\sum_{\xi_{\mathbf{k}_2},\beta}\mathrm{Spin}(\alpha,\beta)\,\mathrm{Spin}(\beta,\delta)\,\frac{1}{z-D}\,c^\dagger_{\mathbf{k}_1\alpha}c_{\mathbf{k}_4\delta}(\mathbb{1}-P)\ . \tag{D.20}$$

Notice that the momentum sum over $\mathbf{k}_2$ yields[2]

$$\sum_{\xi_{\mathbf{k}_2}\in[D-\delta D,D]}\approx\mathcal{N}(\varepsilon_F)\,\delta D\ , \tag{D.21}$$

[2] We have used the relation

$$\sum_{\mathbf{k}}=\int\mathrm{d}\varepsilon\,\mathcal{N}(\varepsilon)\ .$$

where $\mathcal{N}$ is the density-of-states of the conduction electrons assumed to be constant ('wide-band limit').

Spin part The spin part is

$$\begin{aligned}\mathrm{Spin}_{dir} &= \sum_{\beta} \mathrm{Spin}(\alpha,\beta)\,\mathrm{Spin}(\beta,\delta) \\ &= \sum_{\beta} \left\{ J_{\pm}\left(S^{+}\sigma^{-}_{\alpha\beta} + S^{-}\sigma^{+}_{\alpha\beta}\right) + J_z S^z \sigma^z_{\alpha\beta} \right\} \left\{ J_{\pm}\left(S^{+}\sigma^{-}_{\beta\delta} + S^{-}\sigma^{+}_{\beta\delta}\right) + J_z S^z \sigma^z_{\beta\delta} \right\} \end{aligned} \tag{D.22}$$

The spin sum includes three parts for which we have to use the identities for the Pauli matrices (Appendix A):

i) The part proportional to $J_{\pm}^2$ is

$$\begin{aligned}&\sum_{\beta}\left(S^{+}\sigma^{-}_{\alpha\beta} + S^{-}\sigma^{+}_{\alpha\beta}\right)\left(S^{+}\sigma^{-}_{\beta\delta} + S^{-}\sigma^{+}_{\beta\delta}\right) \\ &= \sum_{\beta}\Big(S^{+}S^{+}\sigma^{-}_{\alpha\beta}\sigma^{-}_{\beta\delta} + S^{-}S^{-}\sigma^{+}_{\alpha\beta}\sigma^{+}_{\beta\delta} \\ &+ \; S^{+}S^{-}\sigma^{-}_{\alpha\beta}\sigma^{+}_{\beta\delta} + S^{-}S^{+}\sigma^{+}_{\alpha\beta}\sigma^{-}_{\beta\delta}\Big) \\ &= \sum_{\beta}\Big(2S^{+}S^{-}(\delta_{\alpha\delta} - \sigma^z_{\alpha\delta}) + 2S^{-}S^{+}(\delta_{\alpha\delta} + \sigma^z_{\alpha\delta})\Big)\ . \end{aligned} \tag{D.23}$$

ii) The part proportional to J_z^2 is

$$\sum_{\beta} S^z S^z \sigma^z_{\alpha\beta}\sigma^z_{\beta\delta} = S^z S^z \delta_{\alpha\delta}\ . \tag{D.24}$$

iii) The part proportional to $J_z J_{\pm}$ is

$$\begin{aligned}&\sum_{\beta} S^z\sigma^z_{\alpha\beta}(S^{+}\sigma^{-}_{\beta\delta} + S^{-}\sigma^{+}_{\beta\delta}) + (S^{+}\sigma^{-}_{\beta\delta} + S^{-}\sigma^{+}_{\beta\delta})S^z\sigma^z_{\beta\delta} \\ &= -S^z S^{+}\sigma^{-}_{\alpha\delta} + S^z S^{-}\sigma^{+}_{\alpha\delta} + S^{+}S^z\sigma^{-}_{\alpha\delta} - S^{-}S^z\sigma^{+}_{\alpha\delta}\ . \end{aligned} \tag{D.25}$$

Finally, the spin sum for the direct process yields

$$\begin{aligned}\mathrm{Spin}_{dir} &= 2J_{\pm}^2\left(S^{+}S^{-}(\delta_{\alpha\delta} - \sigma^z_{\alpha\delta}) + S^{-}S^{+}(\delta_{\alpha\delta} + \sigma^z_{\alpha\delta})\right) \\ &- J_{\pm}J_z\left(S^z S^{+}\sigma^{-}_{\alpha\delta} + S^{-}S^z\sigma^{+}_{\alpha\delta} - S^z S^{-}\sigma^{+}_{\alpha\delta} - S^{+}S^z\sigma^{-}_{\alpha\delta}\right) \\ &+ J_z^2 S^z S^z \delta_{\alpha\delta}\ . \end{aligned} \tag{D.26}$$

Therefore,

$$\begin{aligned}\delta V_{dir} = (\mathbb{1}-P)\sum_{\mathbf{k}_1,\mathbf{k}_4,\alpha\delta}\frac{\mathcal{N}(\varepsilon_F)\delta D}{z-D}\,c^\dagger_{\mathbf{k}_1\alpha}c_{\mathbf{k}_4\delta}\\ \times\Big\{2J_\pm^2\left(S^+S^-(\delta_{\alpha\delta}-\sigma^z_{\alpha\delta})+S^-S^+(\delta_{\alpha\delta}+\sigma^z_{\alpha\delta})\right)\\ -J_\pm J_z\left(S^zS^+\sigma^-_{\alpha\delta}+S^-S^z\sigma^+_{\alpha\delta}-S^zS^-\sigma^+_{\alpha\delta}-S^+S^z\sigma^-_{\alpha\delta}\right)\\ +J_z^2S^zS^z\delta_{\alpha\delta}\Big\}(\mathbb{1}-P)\ .\end{aligned}\tag{D.27}$$

D.2 Exchange process

The exchange process leads to δV_{ex}

$$\begin{aligned}\delta V_{ex} = (\mathbb{1}-P)\Big[\sum_{\mathbf{k}_1,\mathbf{k}_2,\mathbf{k}_3,\alpha\beta\gamma}\{J_\pm\left(S^+\sigma^-_{\alpha\beta}+S^-\sigma^+_{\alpha\beta}\right)+J_zS^z\sigma^z_{\alpha\beta}\}\,c^\dagger_{\mathbf{k}_1\alpha}c_{\mathbf{k}_2\beta}\\ P\times\frac{1}{z-H_0}\{J_\pm\left(S^+\sigma^-_{\gamma\alpha}+S^-\sigma^+_{\gamma\alpha}\right)+J_zS^z\sigma^z_{\gamma\alpha}\}\,c^\dagger_{\mathbf{k}_3\gamma}c_{\mathbf{k}_1\alpha}\Big](\mathbb{1}-P)\ .\end{aligned}\tag{D.28}$$

Note that the projection operator P in the middle of Eq. (D.28) (in PG) constrains the intermediate states to be of high energy so that $\xi_{\mathbf{k}_1}=\xi_{\mathbf{k}_4}\in[-D,D+\delta D]$ and

$$\frac{1}{z-H_0}=\frac{1}{z-\xi_{\mathbf{k}_3}+\xi_{\mathbf{k}_1}}\overset{\xi_{\mathbf{k}_1}\approx-D}{\approx}\frac{1}{z-D-\xi_{\mathbf{k}_3}}\approx\frac{1}{z-D}\ ,\tag{D.29}$$

where the approximation is valid since $\delta D\ll D$ and $\mathbf{k}_3$ belongs to the low-energy part of the band-with, away from the edges, $|\xi_{\mathbf{k}_3}|\ll D$. Hence,

$$\delta V_{ex}=(\mathbb{1}-P)\left[\sum_{\mathbf{k}_2,\mathbf{k}_3,\alpha\beta\gamma}\mathrm{Spin}(\alpha,\beta)\,c_{\mathbf{k}_2\beta}c^\dagger_{\mathbf{k}_3\gamma}\times\frac{1}{z-D}\,\mathrm{Spin}(\gamma,\alpha)\,c^\dagger_{\mathbf{k}_1\alpha}c_{\mathbf{k}_1\alpha}\right](\mathbb{1}-P)\ ,\tag{D.30}$$

where the spin parts are denoted concisely to avoid clutter and will be considered below. The combination $c^\dagger_{\mathbf{k}_1\alpha}c_{\mathbf{k}_1\alpha}$ is equal to the number of electrons (occupied states) in $[-D,-D+\delta D]$; therefore, $c^\dagger_{\mathbf{k}_1\alpha}c_{\mathbf{k}_1\beta}=1$, and

$$\delta V_{ex}=(\mathbb{1}-P)\Big[\sum_{\mathbf{k}_2,\mathbf{k}_3,\beta\gamma}\sum_{\mathbf{k}_1,\alpha}\mathrm{Spin}(\alpha,\beta)\,\mathrm{Spin}(\gamma,\alpha)\,\frac{1}{z-D}\,c^\dagger_{\mathbf{k}_2\beta}c_{\mathbf{k}_3\gamma}\Big](\mathbb{1}-P)\tag{D.31}$$

Notice that the momentum sum over $\mathbf{k}_1$ is

$$\sum_{\xi_{\mathbf{k}_1}\in[-D,-D+\delta D]}\approx\mathcal{N}(\varepsilon_F)\,\delta D\ ,\tag{D.32}$$

where $\mathcal{N}(\varepsilon_F)$ is the density-of-states of the conduction electrons assumed to be constant ('wide-band limit').

Spin part The spin part is

$$\begin{aligned}\mathrm{Spin}_{ex} &= \sum_{\alpha} \mathrm{Spin}(\alpha,\beta)\,\mathrm{Spin}(\gamma,\alpha) \\ &= \sum_{\alpha} \left(J_{\pm}\left(S^{+}\sigma^{-}_{\alpha\beta} + S^{-}\sigma^{+}_{\alpha\beta}\right) + J_z S^z \sigma^z_{\alpha\beta}\right)\left(J_{\pm}\left(S^{+}\sigma^{-}_{\gamma\alpha} + S^{-}\sigma^{+}_{\gamma\alpha}\right) + J_z S^z \sigma^z_{\gamma\alpha}\right) \end{aligned} \tag{D.33}$$

This spin sum comprises of three parts for which we have to use the identities for the Pauli matrices (Appendix A):

i) The part proportional to $J_{\pm}^2$ is

$$\begin{aligned}&\sum_{\alpha}\left(S^{+}\sigma^{-}_{\alpha\beta} + S^{-}\sigma^{+}_{\alpha\beta}\right)\left(S^{+}\sigma^{-}_{\gamma\alpha} + S^{-}\sigma^{+}_{\gamma\alpha}\right) \\ &= 2S^{+}S^{-}(\mathbb{1}+\sigma^z)_{\gamma\beta} + 2S^{-}S^{+}(\mathbb{1}-\sigma^z)_{\gamma\beta}\ .\end{aligned} \tag{D.34}$$

ii) The part proportional to J_z^2 is

$$\sum_{\alpha} S^z S^z \sigma^z_{\alpha\beta}\sigma^z_{\gamma\alpha} = S^z S^z (\sigma^z)^2_{\gamma\beta} = S^z S^z \delta_{\gamma\beta}\ . \tag{D.35}$$

iii) The part proportional to $J_z J_{\pm}$ is

$$\begin{aligned}&\sum_{\alpha} S^z \sigma^z_{\alpha\beta}(S^{+}\sigma^{-}_{\gamma\alpha} + S^{-}\sigma^{+}_{\gamma\alpha}) + (S^{+}\sigma^{-}_{\alpha\beta} + S^{-}\sigma^{+}_{\alpha\beta})S^z\sigma^z_{\gamma\alpha} \\ &= S^z S^{+}\sigma^{-}_{\gamma\beta} - S^z S^{-}\sigma^{+}_{\gamma\beta} - S^{+}S^z\sigma^{-}_{\gamma\beta} + S^{-}S^z\sigma^{+}_{\gamma\beta}\ .\end{aligned} \tag{D.36}$$

Finally, the spin sum for the exchange process yields

$$\begin{aligned}\mathrm{Spin}_{ex} = {}& 2J_{\pm}^2\left(S^{+}S^{-}(\delta_{\gamma\beta}+\sigma^z_{\gamma\beta}) + S^{-}S^{+}(\delta_{\gamma\beta}-\sigma^z_{\gamma\beta})\right) \\ &- J_{\pm}J_z\left(S^{+}S^z\sigma^{-}_{\gamma\beta} - S^{-}S^z\sigma^{+}_{\gamma\beta} - S^z S^{+}\sigma^{-}_{\gamma\beta} + S^z S^{-}\sigma^{+}_{\gamma\beta}\right) \\ &+ J_z^2 S^z S^z \delta_{\gamma\beta}\ .\end{aligned} \tag{D.37}$$

Therefore,

$$\begin{aligned}\delta V_{ex} = {}& (\mathbb{1}-P)\sum_{\mathbf{k}_2,\mathbf{k}_3,\beta\gamma}\frac{\mathcal{N}(\varepsilon_F)\delta D}{z-D}\,c_{\mathbf{k}_2\beta}c^{\dagger}_{\mathbf{k}_3\gamma} \\ &\times\Big\{2J_{\pm}^2\left(S^{+}S^{-}(\delta_{\gamma\beta}+\sigma^z_{\gamma\beta}) + S^{-}S^{+}(\delta_{\gamma\beta}-\sigma^z_{\gamma\beta})\right) \\ &- J_{\pm}J_z\left(S^{+}S^z\sigma^{-}_{\gamma\beta} - S^{-}S^z\sigma^{+}_{\gamma\beta} - S^z S^{+}\sigma^{-}_{\gamma\beta} + S^z S^{-}\sigma^{+}_{\gamma\beta}\right) \\ &+ J_z^2 S^z S^z \delta_{\gamma\beta}\Big\}(\mathbb{1}-P)\ .\end{aligned} \tag{D.38}$$

D.3 'Scaling' of the Kondo interaction

From the results for the direct and exchange processes obtained above, one can calculate the renormalization of the Kondo interaction up to the second order in the couplings[3],

$$\delta V = \delta V_{dir} + \delta V_{ex} = (\mathbb{1} - P) \sum_{\mathbf{k},\mathbf{k}',\alpha\beta} \frac{\mathcal{N}(\varepsilon_F)\delta D}{z - D} c^\dagger_{\mathbf{k}'\alpha} c_{\mathbf{k}\beta} \times \Big\{ -2J_\pm^2 S^z \sigma^z_{\alpha\beta} - 2J_\pm J_z (S^+ \sigma^-_{\alpha\beta} + S^- \sigma^+_{\alpha\beta}) \Big\} (\mathbb{1} - P) \ . \tag{D.39}$$

By comparing this with the Kondo interaction, Eq. (D.13), one obtains the change in the couplings due to elimination of high-energy modes ('scaling'):

$$\begin{aligned} \delta J_z &= -2 \frac{\mathcal{N}(\varepsilon_F)\delta D}{z - D} J_\pm^2 \ , \\ \delta J_\pm &= -2 \frac{\mathcal{N}(\varepsilon_F)\delta D}{z - D} J_\pm J_z \ . \end{aligned} \tag{D.40}$$

By neglecting the energy/frequency z compared to D (which is the largest energy scale in the problem) in the previous equation, it will be further simplified to

$$\begin{aligned} \delta J_z &= 2\mathcal{N}(\varepsilon_F) \frac{\delta D}{D} J_\pm^2 \ , \\ \delta J_\pm &= 2\mathcal{N}(\varepsilon_F) \frac{\delta D}{D} J_\pm J_z \ . \end{aligned} \tag{D.41}$$

Since $\delta D > 0$, then $\mathrm{d}D = -\delta D$, and one obtains a differential equation[4],

$$\begin{aligned} \frac{\mathrm{d}J_z}{\mathrm{d}\ln D} &= -2\mathcal{N}(\varepsilon_F)\, J_\pm^2 \ , \\ \frac{\mathrm{d}J_\pm}{\mathrm{d}\ln D} &= -2\mathcal{N}(\varepsilon_F)\, J_\pm J_z \ , \end{aligned} \tag{D.42}$$

which is the RG flow equation. This equation can be solved by noting that

$$\begin{aligned} J_z\, \mathrm{d}J_z \ &= -2\mathcal{N}(\varepsilon_F)\, J_\pm^2 J_z = J_\pm \mathrm{d}J_\pm \\ \rightarrow J_z^2 - J_z(0)^2 &= J_\pm^2 - J_\pm(0)^2 \ . \end{aligned} \tag{D.43}$$

[3] Notice the -1 sign due to anti-commuting $c_{\mathbf{k}_2\beta}\, c_{\mathbf{k}_3\gamma}$ in Eq. (D.28).
[4] Note that $\mathrm{d}\ln D \equiv \frac{\mathrm{d}D}{D}$.

For the isotropic case, $J_z = J_\pm$, the RG flow equations reduce to

$$\begin{aligned} \frac{\mathrm{d}J(D)}{\mathrm{dln}\, D} &= -2\mathcal{N}(\varepsilon_F)J(D)^2 \\ \rightarrow -\frac{1}{J}\Big|_{J_0\equiv J(D_0)}^{J(T)} &= -2\mathcal{N}(\varepsilon_F)\ \ln(D)\Big|_{D_0}^{T} \\ \rightarrow \frac{1}{J(T)} - \frac{1}{J(D_0)} &= +2\mathcal{N}(\varepsilon_F)\ \ln(\frac{T}{D_0}) \\ \rightarrow J(T) &= J_0/\left(1 + 2\mathcal{N}(\varepsilon_F)\, J_0\ \ln(\frac{T}{D_0})\right)\ . \end{aligned} \tag{D.44}$$

In the ferromagnetic case, $J_0 < 0$, the coupling decreases as the temperature or energy scale, T, goes to zero. In contrast, in the antiferromagnetic case, $J_0 > 0$, there is a pole at $T = T_K$,

$$\begin{aligned} 1 + 2\,\mathcal{N}(\varepsilon_F)\, J_0\ \ln(\frac{T_K}{D_0}) &= 0 \\ \rightarrow \frac{T_K}{D_0} &= \exp\left[-\frac{1}{2\mathcal{N}(\varepsilon_F)J_0}\right]\ . \end{aligned} \tag{D.45}$$

At this energy/temperature, the coupling diverges; this is essentially the strong-coupling fixed point. This energy scale is called the Kondo temperature.

APPENDIX E

$SU(3)$ Glazman-Raikh transformation

For the double-quantum-dot setting described in section 4.4, the tunneling part of the Hamiltonian is

$$\begin{aligned} H_T = & t_L c_L^\dagger d_1 + t_{M1} c_M^\dagger d_1 \\ & + t_R c_R^\dagger d_2 + t_{M2} c_M^\dagger d_2 + h.c. \, . \end{aligned} \tag{E.1}$$

To decouple two channels and keep a single channel, let us use an $SU(3)$ transformation,

$$U = \begin{pmatrix} u_{11} & u_{12} & u_{13} \\ u_{21} & u_{22} & u_{23} \\ u_{31} & u_{32} & u_{33} \end{pmatrix} \tag{E.2}$$

to rotate the lead operators as

$$\begin{pmatrix} c_L^\dagger \\ c_M^\dagger \\ c_R^\dagger \end{pmatrix} = U \begin{pmatrix} \psi_1^\dagger \\ \psi_2^\dagger \\ \psi_3^\dagger \end{pmatrix} \, . \tag{E.3}$$

Thereupon, H_T maps to

$$\begin{aligned}
H_T &= (t_L c_L^\dagger + t_{M1} c_M^\dagger) d_1 + h.c. \\
&= (t_R c_R^\dagger + t_{M2} c_M^\dagger) d_2 + h.c. \\
&= \left(t_L \underbrace{(u_{11}\psi_1^\dagger + u_{12}\psi_2^\dagger + u_{13}\psi_3^\dagger)}_{=c_L^\dagger} + t_{M1} \underbrace{(u_{21}\psi_1^\dagger + u_{22}\psi_2^\dagger + u_{23}\psi_3^\dagger)}_{=c_M^\dagger} \right) d_1 + h.c. \\
&\quad + \left(t_R \underbrace{(u_{31}\psi_1^\dagger + u_{32}\psi_2^\dagger + u_{33}\psi_3^\dagger)}_{=c_R^\dagger} + t_{M2} (u_{21}\psi_1^\dagger + u_{22}\psi_2^\dagger + u_{23}\psi_3^\dagger) \right) d_2 + h.c. \\
&= \left((t_L u_{11} + t_{M1} u_{21})\psi_1^\dagger + (t_L u_{12} + t_{M1} u_{22})\psi_2^\dagger + (t_L u_{13} + t_{M1} u_{23})\psi_3^\dagger \right) d_1 + h.c. \\
&\quad + \left((t_R u_{31} + t_{M2} u_{21})\psi_1^\dagger + (t_R u_{32} + t_{M2} u_{22})\psi_2^\dagger + (t_R u_{33} + t_{M2} u_{23})\psi_3^\dagger \right) d_2 + h.c. \\
&\quad + (L \mapsto R \ , \ M1 \mapsto M2) \ . \qquad \text{(E.4)}
\end{aligned}$$

We want to decouple two channels, resulting in a single channel of conduction electrons (say, ψ_1) coupled to two quantum dots; therefore, we have to impose

$$\begin{aligned}
t_L u_{12} + t_{M1} u_{22} &\stackrel{!}{=} 0 \ , \\
t_L u_{13} + t_{M1} u_{23} &\stackrel{!}{=} 0 \ , \\
t_R u_{32} + t_{M2} u_{22} &\stackrel{!}{=} 0 \ , \\
t_R u_{33} + t_{M2} u_{23} &\stackrel{!}{=} 0 \ . \qquad \text{(E.5)}
\end{aligned}$$

By defining

$$\tau_L := \frac{t_{M1}}{t_L} \quad \tau_R := \frac{t_{M2}}{t_R} \ , \qquad \text{(E.6)}$$

we can re-write the previous equations as

$$\begin{aligned}
u_{12} + \tau_L u_{22} &= 0 \ , \qquad \text{(E.7)} \\
u_{13} + \tau_L u_{23} &= 0 \ , \qquad \text{(E.8)} \\
u_{32} + \tau_R u_{22} &= 0 \ , \qquad \text{(E.9)} \\
u_{33} + \tau_R u_{23} &= 0 \ . \qquad \text{(E.10)}
\end{aligned}$$

An algebraic re-arrangement gives

$$\begin{aligned}
\tau_R u_{12} - \tau_L u_{32} &= 0 \ , \\
\tau_R u_{13} - \tau_L u_{33} &= 0 \ . \qquad \text{(E.11)}
\end{aligned}$$

Thus,

$$u_{12} = \frac{\tau_L}{\tau_R} u_{32} \ , \tag{E.12}$$

$$u_{13} = \frac{\tau_L}{\tau_R} u_{33} \ . \tag{E.13}$$

To simplify the notation, we define

$$t := \frac{\tau_L}{\tau_R} \ . \tag{E.14}$$

Using the explicit form of an explicit parametrization of the $SU(3)$ transformation [250], in terms of eight parameters, one obtains

$$\begin{aligned} &E.12 : \sin\theta_1 e^{\mathrm{i}\phi_3} = t \cos\theta_1 \sin\theta_3 e^{\mathrm{i}\phi_5} \\ &E.13 : \cos\theta_1 \sin\theta_2 e^{\mathrm{i}\phi_4} = t \cos\theta_2 \cos\theta_3 e^{-\mathrm{i}(\phi_1+\phi_2)} - t \sin\theta_1 \sin\theta_2 \sin\theta_3 e^{\mathrm{i}(\phi_4+\phi_5-\phi_3)} \ ; \end{aligned} \tag{E.15}$$

hence,

$$\begin{aligned} &E.12 : \sin\theta_1 = t \cos\theta_1 \sin\theta_3 e^{\mathrm{i}(\phi_5-\phi_3)} \ , \\ &E.13 : \cos\theta_1 \sin\theta_2 = t \cos\theta_2 \cos\theta_3 e^{-\mathrm{i}(\phi_1+\phi_2+\phi_4)} - t \sin\theta_1 \sin\theta_2 \sin\theta_3 e^{\mathrm{i}(\phi_5-\phi_3)} \ . \end{aligned} \tag{E.16}$$

Then,

$$\sin\theta_1 e^{\mathrm{i}\phi_3} + \tau_L \cos\theta_1 \cos\theta_3 e^{\mathrm{i}\phi_2} = 0 \ , \tag{E.17}$$

$$\cos\theta_1 \sin\theta_3 e^{\mathrm{i}\phi_5} + \tau_R \cos\theta_1 \cos\theta_3 e^{\mathrm{i}\phi_2} = 0 \ , \tag{E.18}$$

$$\cos\theta_1 \sin\theta_2 e^{\mathrm{i}\phi_4} + \tau_L \left(- \cos\theta_2 \sin\theta_3 e^{-\mathrm{i}(\phi_1+\phi_5)} - \sin\theta_1 \sin\theta_2 \cos\theta_3 e^{\mathrm{i}(\phi_2-\phi_3+\phi_4)} \right) = 0 \ , \tag{E.19}$$

$$\begin{aligned} &\cos\theta_2 \cos\theta_3 e^{-\mathrm{i}(\phi_1+\phi_2)} - \sin\theta_1 \sin\theta_2 \sin\theta_3 e^{\mathrm{i}(\phi_4+\phi_5-\phi_3)} \\ &\quad + \tau_R \left(- \cos\theta_2 \sin\theta_3 e^{-\mathrm{i}(\phi_1+\phi_5)} - \sin\theta_1 \sin\theta_2 \cos\theta_3 e^{\mathrm{i}(\phi_2-\phi_3+\phi_4)} \right) = 0 \ , \end{aligned} \tag{E.20}$$

or equivalently,

$$\begin{aligned} &E.17 : \sin\theta_1 + \tau_L \cos\theta_1 \cos\theta_3 e^{\mathrm{i}(\phi_2-\phi_3)} = 0 \ , \\ &E.18 : \cos\theta_1 \sin\theta_3 + \tau_R \cos\theta_1 \cos\theta_3 e^{\mathrm{i}(\phi_2-\phi_5)} = 0 \ , \\ &E.19 : \cos\theta_1 \sin\theta_2 - \tau_L \left(\cos\theta_2 \sin\theta_3 e^{-\mathrm{i}(\phi_1+\phi_4+\phi_5)} + \sin\theta_1 \sin\theta_2 \cos\theta_3 e^{\mathrm{i}(\phi_2-\phi_3)} \right) = 0 \ , \\ &E.20 : \cos\theta_2 \cos\theta_3 - \sin\theta_1 \sin\theta_2 \sin\theta_3 e^{\mathrm{i}(\phi_1+\phi_2+\phi_4+\phi_5-\phi_3)} \\ &\qquad - \tau_R \left(\cos\theta_2 \sin\theta_3 e^{\mathrm{i}(\phi_2-\phi_5)} + \sin\theta_1 \sin\theta_2 \cos\theta_3 e^{\mathrm{i}(\phi_1+\phi_2+\phi_2-\phi_3+\phi_4)} \right) = 0 \ . \end{aligned} \tag{E.21}$$

To simplify notation, let us define the phases factors,

$$\begin{aligned} \phi_{23} := \phi_2 - \phi_3 \quad ; \quad \phi_{25} := \phi_2 - \phi_5 \quad ; \quad \phi_{145} := \phi_1 + \phi_4 + \phi_5 \ , \\ \phi_1 + \phi_2 + \phi_4 + \phi_5 - \phi_3 = \phi_1 + \phi_4 + \phi_5 + \phi_2 - \phi_3 = \phi_{145} + \phi_{23} \ , \\ \phi_1 + \phi_4 + \phi_5 - \phi_5 + \phi_2 - \phi_3 + \phi_2 = \phi_{145} + \phi_{25} + \phi_{23} \ . \end{aligned} \tag{E.22}$$

Therefore,

$$\begin{aligned}
&E.17 : \sin\theta_1 + \tau_L \cos\theta_1 \cos\theta_3 e^{\mathrm{i}\phi_{23}} = 0 \ , \\
&E.18 : \cos\theta_1 \sin\theta_3 + \tau_R \cos\theta_1 \cos\theta_3 e^{\mathrm{i}\phi_{25}} = 0 \ , \\
&E.19 : \cos\theta_1 \sin\theta_2 - \tau_L \left(\cos\theta_2 \sin\theta_3 e^{-\mathrm{i}\phi_{145}} + \sin\theta_1 \sin\theta_2 \cos\theta_3 e^{\mathrm{i}\phi_{23}}\right) = 0 \ , \\
&E.20 : \cos\theta_2 \cos\theta_3 - \sin\theta_1 \sin\theta_2 \sin\theta_3 e^{\mathrm{i}(\phi_{145}+\phi_{23})} \\
&\qquad - \tau_R \left(\cos\theta_2 \sin\theta_3 e^{\mathrm{i}\phi_{25}} + \sin\theta_1 \sin\theta_2 \cos\theta_3 e^{\mathrm{i}(\phi_{145}+\phi_{25}+\phi_{23})}\right) = 0 \ .
\end{aligned} \tag{E.23}$$

The last equation can be re-written as

$$\begin{aligned}
&\cos\theta_1 \cos\theta_3 - \sin\theta_1 \sin\theta_2 \sin\theta_3 e^{\mathrm{i}(\phi_{145}+\phi_{23})} \\
&- \tau_R e^{\mathrm{i}(\phi_{145}+\phi_{25}+\phi_{23})} \left(\cos\theta_2 \sin\theta_3 e^{-\mathrm{i}(\phi_{145}+\phi_{23})} + \sin\theta_1 \sin\theta_2 \cos\theta_3\right) = 0 \ .
\end{aligned} \tag{E.24}$$

By defining

$$\tilde{t}_R := \tau_R e^{\mathrm{i}\phi_{25}} \quad ; \quad \tilde{t}_L := \tau_L e^{\mathrm{i}\phi_{23}} \tag{E.25}$$

to absorb phase factors and

$$\phi := \phi_{23} + \phi_{145} \ , \tag{E.26}$$

one obtains

$$\begin{aligned}
&E.17 : \sin\theta_1 + \tilde{t}_L \cos\theta_1 \cos\theta_3 = 0 \ , \\
&E.18 : \cos\theta_1 \sin\theta_3 + \tilde{t}_R \cos\theta_1 \cos\theta_3 = 0 \ , \\
&E.19 : \cos\theta_1 \sin\theta_2 - \tilde{t}_L \left(\cos\theta_2 \sin\theta_3 e^{-\mathrm{i}\phi} + \sin\theta_1 \sin\theta_2 \cos\theta_3\right) = 0 \ , \\
&E.20 : \cos\theta_2 \cos\theta_3 - \sin\theta_1 \sin\theta_2 \sin\theta_3 e^{\mathrm{i}\phi} - \tilde{t}_R \left(\cos\theta_2 \sin\theta_3 + \sin\theta_1 \sin\theta_2 \cos\theta_3 e^{\mathrm{i}\phi}\right) = 0 \ ,
\end{aligned} \tag{E.27}$$

which is 4 equations with 4 unknowns. We observe that

$$\cos\theta_1 \neq 0 \ , \tag{E.28}$$

since if $\cos\theta_1 = 0 \overset{E.17}{\rightarrow} \sin\theta_1 = 0$ which is not possible. Dividing Eq. (E.18) by $\cos\theta_1$, one obtains

$$\sin\theta_3 + \tilde{t}_R \cos\theta_3 = 0 \ ; \tag{E.29}$$

therefore,

$$\begin{aligned}
&\cos\theta_3 \neq 0 \ , \\
&\sin\theta_3 \neq 0 \ ,
\end{aligned} \tag{E.30}$$

since otherwise both must vanish simultaneously. From Eq. (E.29) and Eq. (E.20), we obtain

$$\begin{aligned}
&\cos\theta_2\cos\theta_3 + \sin\theta_1\sin\theta_2\tilde{t}_R\cos\theta_3 e^{\mathrm{i}\phi} - \tilde{t}_R\left(-\cos\theta_2\tilde{t}_R\cos\theta_3 + \sin\theta_1\sin\theta_2\cos\theta_3 e^{\mathrm{i}\phi}\right) = 0\ , \\
&\overset{\div\cos\theta_3\neq 0}{\Longrightarrow} \cos\theta_2 + \sin\theta_1\sin\theta_2\tilde{t}_R e^{\mathrm{i}\phi} + \tilde{t}_R\left(\cos\theta_2\tilde{t}_R - \sin\theta_1\sin\theta_2 e^{\mathrm{i}\phi}\right) = 0 \qquad \text{(E.31)} \\
&\Rightarrow \cos\theta_2 + \sin\theta_1\sin\theta_2\tilde{t}_R e^{\mathrm{i}\phi} - \sin\theta_1\sin\theta_2\tilde{t}_R e^{\mathrm{i}\phi} + \tilde{t}_R^2\cos\theta_2 = 0 \\
&\Rightarrow (1+\tilde{t}_R^2)\cos\theta_2 = 0 \\
&\Rightarrow \cos\theta_2 = 0\ . \qquad \text{(E.32)}
\end{aligned}$$

From Eq. (E.29) and Eq. (E.19), we obtain

$$\begin{aligned}
&\cos\theta_1\sin\theta_2 - \tilde{t}_L\left(-\tilde{t}_R\cos\theta_2\cos\theta_3 e^{-\mathrm{i}\phi} + \sin\theta_1\sin\theta_2\cos\theta_3\right) = 0 \\
&\Rightarrow \cos\theta_1\sin\theta_2 + \tilde{t}_L\cos\theta_3\left(\tilde{t}_R\cos\theta_2 e^{-\mathrm{i}\phi} - \sin\theta_1\sin\theta_2\right) = 0 \qquad \text{(E.33)} \\
&\Rightarrow \cos\theta_1\sin\theta_2 + \tilde{t}_L\tilde{t}_R\cos\theta_3\cos\theta_2 e^{-\mathrm{i}\phi} - \tilde{t}_L\cos\theta_3\sin\theta_1\sin\theta_2 = 0 \qquad \text{(E.34)} \\
&\overset{E.32}{\Rightarrow} \cos\theta_1\sin\theta_2 - \tilde{t}_L\sin\theta_1\sin\theta_2\cos\theta_3 = 0\ . \qquad \text{(E.35)}
\end{aligned}$$

The relation $\cos\theta_2 = 0$ ensures that $\sin\theta_2 \neq 0$; then dividing the last relation by $\sin\theta_2$, one obtains

$$\begin{aligned}
&\cos\theta_1 - \tilde{t}_L\sin\theta_1\cos\theta_3 = 0 \qquad \text{(E.36)} \\
&\overset{E.17}{\Rightarrow} \cos\theta_1 + \tilde{t}_L\cos\theta_3(\tilde{t}_L\cos\theta_1\cos\theta_3) = 0\ . \qquad \text{(E.37)}
\end{aligned}$$

Since $\cos\theta_1 \neq 0$, one can divide by $\cos\theta_1$ to obtain

$$1 + (\tilde{t}_L\cos\theta_3)^2 = 0\ . \qquad \text{(E.38)}$$

Therefore, one can summarize the relations obtained so far as

$$\begin{aligned}
&E.17 : \sin\theta_1 + \tilde{t}_L\cos\theta_1\cos\theta_3 = 0 \quad (\cos\theta_1 \neq 0) \\
&E.29 : \sin\theta_3 + \tilde{t}_R\cos\theta_3 = 0 \quad (\sin\theta_3 \neq 0, \cos\theta_3 \neq 0) \\
&E.32 : \cos\theta_2 = 0 \quad (\sin\theta_2 \neq 0) \\
&E.38 : (\tilde{t}_L\cos\theta_3)^2 + 1 = 0\ . \qquad \text{(E.39)}
\end{aligned}$$

Note that

$$\begin{aligned}
\tilde{t}_R &= \tau_R e^{\mathrm{i}\phi_{25}} \quad , \quad \tau_R = \frac{t_{M2}}{t_R}\ , \\
\tilde{t}_L &= \tau_L e^{\mathrm{i}\phi_{23}} \quad , \quad \tau_L = \frac{t_{M1}}{t_L}\ . \qquad \text{(E.40)}
\end{aligned}$$

From Eq. (E.38), one obtains

$$\begin{aligned}(\tilde{t}_L \cos\theta_3)^2 = -1 \Rightarrow \tilde{t}_L \cos\theta_3 &= \pm \mathrm{i} \\ \rightarrow \tau_L e^{\mathrm{i}\phi_{23}} \cos\theta_3 &= \pm \mathrm{i} \\ \rightarrow \tau_L \cos\theta_3 &= \pm \mathrm{i} e^{-\mathrm{i}\phi_{23}} \\ \rightarrow \cos\theta_3 &= \pm \mathrm{i} e^{-\mathrm{i}\phi_{23}} \frac{1}{\tau_L} = \pm \mathrm{i} e^{-\mathrm{i}\phi_{23}} \frac{t_L}{t_{M1}} \\ \rightarrow \cos\theta_3 &= \pm \mathrm{i} e^{-\mathrm{i}\phi_{23}} |\frac{t_L}{t_{M1}}| e^{\mathrm{i}\phi_L} \\ \Rightarrow \pm \mathrm{i} e^{\mathrm{i}(\phi_L - \phi_{23})} &= \pm 1 \quad , \quad \text{since } \cos\theta_3 \in \mathbb{R} \ .\end{aligned} \tag{E.41}$$

Using $\mathrm{i} = e^{\mathrm{i}\frac{\pi}{2}}$, one obtains

$$e^{\mathrm{i}(\phi_L - \phi_{23} + \frac{\pi}{2})} = 1 \ ; \tag{E.42}$$

therefore,

$$\begin{aligned}\phi_L - \phi_{23} + \frac{\pi}{2} &= 2\pi\mathbb{Z} \\ \Rightarrow \phi_{23} &= \phi_L + \frac{\pi}{2} + 2\pi\mathbb{Z} \ ;\end{aligned} \tag{E.43}$$

so that, e.g.,

$$\phi_{23} = \phi_L + \frac{\pi}{2} \ , \tag{E.44}$$

and

$$|\frac{t_L}{t_{M1}}| \leq 1 \ . \tag{E.45}$$

From Eq. (E.29), one obtains

$$\begin{aligned}&\sin\theta_3 + \tilde{t}_R \cos\theta_3 = 0 \\ &\rightarrow \tilde{t}_R \cos\theta_3 = -\sin\theta_3 \\ &\rightarrow \tilde{t}_L \cos\theta_3 = -\frac{\tilde{t}_L}{\tilde{t}_R} \sin\theta_3 \\ &\rightarrow (\tilde{t}_L \cos\theta_3)^2 = (\frac{\tilde{t}_L}{\tilde{t}_R} \sin\theta_3)^2 \overset{E.38}{=} -1 \\ &\Rightarrow (\sin\theta_3)^2 = -(\frac{\tilde{t}_R}{\tilde{t}_L})^2 \ .\end{aligned} \tag{E.46}$$

Thus,

$$
\begin{aligned}
(\sin\theta_3)^2 + (\cos\theta_3)^2 &= -(\frac{\tilde{t}_R}{\tilde{t}_L})^2 - (\frac{1}{\tilde{t}_L})^2 = 1 \\
\Rightarrow \frac{\tilde{t}_R^2 + 1}{\tilde{t}_L^2} &= -1 \\
\Rightarrow 1 + \tilde{t}_R^2 &= -\tilde{t}_L^2 \ .
\end{aligned} \tag{E.47}
$$

From Eq. (E.32), one concludes

$$
\cos\theta_2 = 0 \Rightarrow \theta_2 = \frac{\pi}{2} \Rightarrow \sin\theta_2 = 1 \ , \tag{E.48}
$$

and from Eq. (E.17), one obtains

$$
\begin{aligned}
&\sin\theta_1 + \cos\theta_1 \tilde{t}_L \cos\theta_3 = 0 \\
&\rightarrow \cos\theta_1 \tilde{t}_L \cos\theta_3 = -\sin\theta_1 \\
&\rightarrow (\cos\theta_1)^2 (\tilde{t}_L \cos\theta_3)^2 = (\sin\theta_1)^2 \\
&\overset{E.38}{\Rightarrow} (\cos\theta_1)^2 (-1) = (\sin\theta_1)^2 \\
&\Rightarrow -(\cos\theta_1)^2 = (\sin\theta_1)^2 \ .
\end{aligned} \tag{E.49}
$$

The last line is a contradiction. Therefore, we conclude finally that it is *not* possible to reduce the original three-lead system (given in section 4.4) via a unitary $SU(3)$ transformation, to a system in which the quantum dots are coupled only to a *single* effective lead or channel.

APPENDIX F

Gaussian integrals

The Gaussian integral

$$\int_{-\infty}^{+\infty} e^{-ax^2+\mathrm{i}bx} = \frac{\pi}{a} e^{-\frac{b^2}{4a}} \quad ; a > 0, b \in \mathbb{R} \tag{F.1}$$

can be proved by a contour integration [251]. There are some corollaries to this integral which we explicitly derive below.

Corollaries

i) First corollary: Consider the integral

$$I = \int_{-\infty}^{+\infty} \mathrm{d}x\, e^{-ax^2+zx} = \int_{-\infty}^{+\infty} \mathrm{d}x\, e^{-ax^2+z'x+\mathrm{i}z''x} \quad ; z \in \mathbb{C}, a > 0 \tag{F.2}$$

where

$$z =: z' + \mathrm{i}z'' \quad ; z', z'' \in \mathbb{R}\ .$$

This can be shown by 'completing the square',

$$\begin{aligned} -ax^2 + z'x &= -a(x^2 - \frac{z'}{a}x) = -a(x^2 - \frac{z'}{a}x + (\frac{z'}{2a})^2 - (\frac{z'}{2a})^2) \\ &= -a(x - \frac{z'}{2a})^2 - a(-(\frac{z'}{2a})^2) = -a(x - \frac{z'}{2a})^2 + \frac{(z')^2}{4a}\ , \end{aligned} \tag{F.3}$$

and using the transformation $x \mapsto x + \frac{z'}{2a}$, so that

$$\begin{aligned} I &= \int_{-\infty}^{+\infty} \mathrm{d}x\, \exp[-ax^2 + \frac{(z')^2}{4a} + \mathrm{i}z''(x + \frac{z'}{2a})] \\ I &= e^{+\frac{(z')^2}{4a}} \int_{-\infty}^{+\infty} \mathrm{d}x\, \exp[-ax^2 + \mathrm{i}z''x + \mathrm{i}\frac{z'z''}{2a}] = e^{+\frac{(z')^2}{4a}} e^{+\mathrm{i}\frac{z'z''}{2a}} \sqrt{\frac{\pi}{a}}\, e^{-\frac{(z'')^2}{4a}} \\ &= \sqrt{\frac{\pi}{a}}\, \exp[\frac{(z')^2}{4a} - \frac{(z'')^2}{4a} + \mathrm{i}\frac{z'z''}{4a}] = \sqrt{\frac{\pi}{a}}\, \exp[\frac{1}{4a}(z' + \mathrm{i}z'')^2] \\ &= \sqrt{\frac{\pi}{a}}\, \exp[\frac{1}{4a}z^2]\ . \end{aligned} \tag{F.4}$$

Therefore,

$$I = \int_{-\infty}^{+\infty} \mathrm{d}x\, e^{-ax^2+zx} = \sqrt{\frac{\pi}{a}}\, e^{\frac{z^2}{4a}} \quad ; z \in \mathbb{C}, a > 0 \ . \tag{F.5}$$

ii) Second corollary:

$$I = \int_{\mathbb{R}^2} \mathrm{dRe}\, z \ \mathrm{dIm}\, z \ e^{-\bar{z}az+uz+\bar{z}v} \quad ; u, v \in \mathbb{C}, a > 0 \ . \tag{F.6}$$

This can be shown by using the definitions

$$\begin{aligned} z &=: x + \mathrm{i}y \quad ; x, y \in \mathbb{R} \\ \bar{z} &=: x - \mathrm{i}y \ ; \end{aligned} \tag{F.7}$$

to re-write the exponent as

$$\begin{aligned} \bar{z}az &= (x - \mathrm{i}y)a(x + \mathrm{i}y) = xax + yay \ , \\ uz &= ux + \mathrm{i}yu \ , \\ \bar{z}v &= vx - \mathrm{i}yv \ . \end{aligned} \tag{F.8}$$

So the exponent will be $-xax + x(u + v) - yay + \mathrm{i}y(u - v)$, so that

$$I = \int_{-\infty}^{+\infty} \mathrm{d}x\, e^{-xax+x(u+v)} \int_{-\infty}^{+\infty} \mathrm{d}y\, e^{-yay+\mathrm{i}y(u-v)} \ . \tag{F.9}$$

From the previous corollary, Eq. (F.5), and taking $z = u + v \in \mathbb{C}$, or $z = \mathrm{i}(u - v) \in \mathbb{C}$, one obtains

$$\begin{aligned} I &= \sqrt{\frac{\pi}{a}} \exp[\frac{(u+v)^2}{4a}] \sqrt{\frac{\pi}{a}} \exp[-\frac{(u-v)^2}{4a}] \\ &= \frac{\pi}{a} \exp[\frac{4uv}{4a}] = \frac{\pi}{a} e^{\frac{uv}{a}} \quad \text{for } a > 0;\ u, v \in \mathbb{C} \ . \end{aligned} \tag{F.10}$$

Thus,

$$\int_{\mathbb{R}^2} \mathrm{dRe}\, z \ \mathrm{dIm}\, z \ \exp[-\bar{z}az + uz + \bar{z}v] = \frac{\pi}{a} e^{\frac{uv}{a}} \quad \text{for } a > 0; u, v \in \mathbb{C} \ .$$

Using the complex measure,

$$\mathrm{dRe}\, z \ \mathrm{dIm}\, z \equiv \frac{\mathrm{d}z\, \mathrm{d}\bar{z}}{2\mathrm{i}} \ ,$$

the previous integral can be re-written as

$$\int_{\mathbb{C}} \frac{\mathrm{d}z\, \mathrm{d}\bar{z}}{2\mathrm{i}} e^{-\bar{z}az+uz+\bar{z}v} = \frac{\pi}{a}\, e^{\frac{uv}{a}} \ . \tag{F.11}$$

For a more general Gaussian integral, see Ref. [252].

APPENDIX G

RKKY interaction: static susceptibility in position representation

To obtain the position representation of the susceptibility of the conduction electrons in section 6.1, one has to calculate

$$\mathcal{I} = \frac{1}{V^2} \sum_{\mathbf{k},\mathbf{k}'} \frac{n_F(\varepsilon_{\mathbf{k}})(1 - n_F(\varepsilon_{\mathbf{k}'}))}{\varepsilon_{\mathbf{k}'} - \varepsilon_{\mathbf{k}}} \, e^{-\mathrm{i}(\mathbf{k}-\mathbf{k}')\cdot\mathbf{r}} \ . \tag{G.1}$$

At low temperatures, $T \to 0^+$,

$$\begin{aligned} n_F(\varepsilon_{\mathbf{k}}) &\approx \Theta(-\varepsilon_{\mathbf{k}}) \ , \\ 1 - n_F(\varepsilon_{\mathbf{k}}) &\approx 1 - \Theta(-\varepsilon_{\mathbf{k}}) = \Theta(\varepsilon_{\mathbf{k}}) \ , \end{aligned} \tag{G.2}$$

where we have used

$$\Theta(-x) = 1 - \Theta(x) \quad ; \quad \Theta(x=0) = \frac{1}{2} \ . \tag{G.3}$$

Therefore,

$$\mathcal{I} = \frac{1}{(2\pi)^6} \int_{|\mathbf{k}|\le k_F} \mathrm{d}\mathbf{k} \int_{|\mathbf{k}'|\ge k_F} \mathrm{d}\mathbf{k}' \, \frac{e^{-\mathrm{i}(\mathbf{k}-\mathbf{k}')\cdot\mathbf{r}}}{\varepsilon_{\mathbf{k}'} - \varepsilon_{\mathbf{k}}} \ . \tag{G.4}$$

In 3-dimensions, and for a parabolic dispersion relation, $\varepsilon_{\mathbf{k}} = \frac{k^2}{2m}$, using spherical coordinates with z-axis taken to be parallel to $\mathbf{r}$, with the standard notation,

$$\mathrm{d}\mathbf{k} \ = \mathrm{d}k \, k^2 \sin\theta \mathrm{d}\theta \, \mathrm{d}\phi \ , \tag{G.5}$$

the integral will become

$$\mathcal{I} = \frac{1}{(2\pi)^6} \underbrace{\int_0^{2\pi} \mathrm{d}\phi \int_0^{2\pi} \mathrm{d}\phi'}_{=(2\pi)^2} \int_0^{k_F} \mathrm{d}k \, k^2 \int_{k_F}^{+\infty} \mathrm{d}k' \, k'^2 \frac{1}{\varepsilon_{\mathbf{k}'} - \varepsilon_{\mathbf{k}}} \int_0^{\pi} \mathrm{d}\theta \, \sin\theta \int_0^{\pi} \mathrm{d}\theta' \, \sin\theta' e^{-\mathrm{i}(\mathbf{k}-\mathbf{k}')\cdot\mathbf{r}} \ . \tag{G.6}$$

By defining $\lambda := \cos\theta \in [-1, 1]$,

$$\begin{aligned} \mathrm{d}\theta\, \sin\theta = \mathrm{d}\cos\theta\, &= \mathrm{d}\lambda\ , \\ \mathbf{k}\cdot\mathbf{r} = kr\cos\theta &= kr\lambda\ , \end{aligned} \tag{G.7}$$

one obtains

$$\begin{aligned} \int_0^\pi \mathrm{d}\theta\, \sin\theta e^{-\mathrm{i}\mathbf{k}\cdot\mathbf{r}} &= \int_{-1}^1 \mathrm{d}\lambda\, e^{-\mathrm{i}kr\lambda} = \frac{-1}{\mathrm{i}kr} e^{-\mathrm{i}kr}|_{\lambda=-1}^1 = \frac{-1}{\mathrm{i}kr}\left(e^{-\mathrm{i}kr} - e^{\mathrm{i}kr}\right) = \frac{2}{kr}\sin(kr)\ , \\ \int_0^\pi \mathrm{d}\theta'\, \sin\theta' e^{-\mathrm{i}\mathbf{k}'\cdot\mathbf{r}} &= \int_{-1}^1 \mathrm{d}\lambda\, e^{-\mathrm{i}k'r\lambda} = \frac{1}{\mathrm{i}k'r} e^{\mathrm{i}k'r}\Big|_{\lambda=-1}^1 \\ &= \frac{1}{\mathrm{i}k'r}\left(e^{\mathrm{i}k'r} - e^{-\mathrm{i}k'r}\right) = \frac{2}{k'r}\sin(k'r)\ , \end{aligned} \tag{G.8}$$

with a similar expression for the integration on θ'. Using the parabolic dispersion relation, the integral then reduces to

$$\mathcal{I} = 4\frac{(2\pi)^2}{(2\pi)^6}(2m)\int_0^{k_F} \mathrm{d}k \int_{k_F}^\infty \mathrm{d}k'\, \frac{k^2 k'^2}{k'^2 - k^2}\frac{\sin(kr)}{kr}\frac{\sin(k'r)}{k'r}\ . \tag{G.9}$$

By defining the dimensionless variables,

$$\kappa := kr \to k = \frac{\kappa}{r} \quad , \quad \mathrm{d}k\, = \frac{\mathrm{d}\kappa}{r}\ , \tag{G.10}$$

and analogous definition for κ', one can re-write the integral as

$$\mathcal{I} = 4\frac{(2\pi)^2}{(2\pi)^6}2m\frac{1}{r^4}\int_0^{k_F r} \mathrm{d}\kappa \int_{k_F r}^\infty \mathrm{d}\kappa'\, \frac{\kappa\sin\kappa\cdot\kappa'\sin\kappa'}{\kappa'^2 - \kappa^2}\ . \tag{G.11}$$

Notice that

$$I' := \int_0^{k_F r} \mathrm{d}\kappa \int_0^{k_F r} \mathrm{d}\kappa'\, \frac{\kappa\sin\kappa\kappa'\sin\kappa'}{\kappa'^2 - \kappa^2} \tag{G.12}$$

is *antisymmetric* with respect to the variable interchange $\kappa \leftrightarrow \kappa'$; therefore, it vanishes since κ and κ' are dummy variables and

$$I' = I'(\kappa \leftrightarrow \kappa') = -I' \Rightarrow I' = 0\ . \tag{G.13}$$

Therefore, the limits of the κ'-integration in $\mathcal{I}$ reduce to

$$\mathcal{I} = 4\frac{(2\pi)^2}{(2\pi)^6}2m\frac{1}{r^4}\int_0^{k_F r} \mathrm{d}\kappa \int_0^\infty \mathrm{d}\kappa'\, \frac{\kappa\sin\kappa\cdot\kappa'\sin\kappa'}{\kappa'^2 - \kappa^2}\ . \tag{G.14}$$

Then, we have to calculate

$$\begin{aligned} I &:= \int_0^\infty \mathrm{d}\kappa'\, \frac{\kappa'\sin\kappa'}{\kappa'^2 - \kappa^2} \\ &= \frac{1}{2}\mathrm{pv}\int_{-\infty}^\infty \mathrm{d}\kappa'\, \frac{\kappa'\sin\kappa'}{\kappa'^2 - \kappa^2} \end{aligned} \tag{G.15}$$

where, in the second step, Cauchy principal-value (pv) appears since $\frac{\kappa' \sin \kappa'}{\kappa'^2 - \kappa^2}$ is an *even* function of κ'. This integration can be performed by transforming it to a contour integration via $\kappa' \sin \kappa' = \mathrm{Im}\left(\kappa' e^{\mathrm{i}\kappa'}\right)$,

$$\begin{aligned} I &= \frac{1}{2}\mathrm{pv}\int_{-\infty}^{\infty} \mathrm{d}\kappa' \, \frac{\kappa' \sin \kappa'}{\kappa'^2 - \kappa^2} \\ &= \frac{1}{2}\mathrm{Im}\left\{\mathrm{pv}\int_{-\infty}^{\infty} \mathrm{d}\kappa' \, \frac{\kappa' e^{\mathrm{i}\kappa'}}{\kappa'^2 - \kappa^2}\right\} \ . \end{aligned} \tag{G.16}$$

We have to consider the contour integral I_C, where the contour encompasses the upper-half plane,

$$I_C := \oint_{C_{\mathrm{UHP}}} \mathrm{d}z \, \frac{z e^{iz}}{z^2 - \kappa^2} \ . \tag{G.17}$$

The poles are on the real axis: $z_{\mathrm{poles}} = \pm\kappa$ (Fig. G.1).

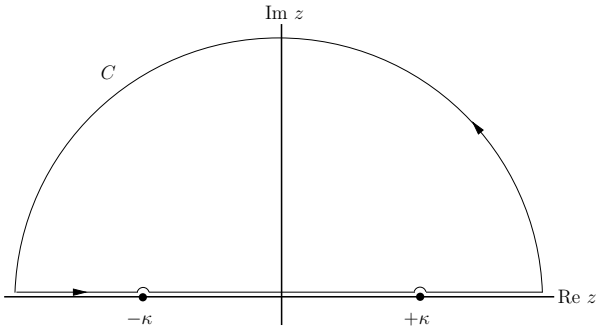

Figure G.1: Complex contour in the upper-half plane with poles at $\pm\kappa$.

The residue theorem yields

$$\begin{aligned} I_C = \underbrace{\mathrm{i}\frac{\pi}{2}e^{-\mathrm{i}\kappa}}_{\text{residue at } z=-\kappa} + \underbrace{\mathrm{i}\frac{\pi}{2}e^{\mathrm{i}\kappa}}_{\text{residue at } z=\kappa} &= \mathrm{i}\frac{\pi}{2}\left(e^{-\mathrm{i}\kappa} + e^{\mathrm{i}\kappa}\right) = \mathrm{i}\pi\cos\kappa \\ &= \frac{1}{2}\mathrm{Im}\left\{\mathrm{i}\pi\cos\kappa\right\} = \frac{\pi}{2}\cos\kappa \ . \end{aligned} \tag{G.18}$$

Thus,

$$\mathcal{I} = 4\frac{(2\pi)^2}{(2\pi)^6}2m\frac{1}{r^4}\int_0^{k_F r} \mathrm{d}\kappa \, \sin\kappa \cdot (\frac{\pi}{2})\cos\kappa \ . \tag{G.19}$$

Note that

$$\int \mathrm{d}\kappa \, \sin\kappa\cos\kappa = \frac{1}{2}\int \mathrm{d}\kappa \, \kappa \sin(2\kappa) \overset{x:=2\kappa}{=\!=\!=} \frac{1}{2}\frac{1}{4}\int \mathrm{d}x \, x \sin x \ , \tag{G.20}$$

and

$$\begin{aligned}\int \mathrm{d}x\, x \sin(x) &= -\frac{\partial}{\partial\alpha}\Big|_{\alpha=1} \int \mathrm{d}x\, \cos(\alpha x) = -\frac{\partial}{\partial\alpha}\Big|_{\alpha=1} \left(\frac{1}{\alpha}\sin(\alpha x)\right) \\ &= -\left(\frac{x}{\alpha}\cos(\alpha x) - \frac{1}{\alpha^2}\sin(\alpha x)\right)\Big|_{\alpha=1} = \sin x - x\cos x \ . \end{aligned} \tag{G.21}$$

Finally,

$$\int \mathrm{d}\kappa\, \kappa \sin\kappa\cos\kappa = \frac{1}{8}\left(\sin(2\kappa) - 2\kappa\cos(2\kappa)\right) \ . \tag{G.22}$$

Therefore,

$$\begin{aligned}\mathcal{I} &= 4\frac{(2\pi)^2}{(2\pi)^6} 2m \frac{1}{r^4}\frac{\pi}{2}\frac{1}{8}\left(\sin(2\kappa) - 2\kappa\cos(2\kappa)\right)\Big|_{\kappa=0}^{k_F r} \\ &= 4\frac{(2\pi)^2}{(2\pi)^6} 2m \frac{\pi}{2}\frac{1}{8}(2k_F)^4 \underbrace{\left(\frac{\sin(2k_F r) - 2k_F r\cos(2k_F r)}{(2k_F r)^4}\right)}_{:=F(2k_F r)} \ , \end{aligned} \tag{G.23}$$

where,

$$F(x) := \frac{\sin x - x\cos x}{x^4} \tag{G.24}$$

and concisely,

$$\mathcal{I} = \frac{4m{k_F}^4}{(2\pi)^3} F(2k_F r) \ . \tag{G.25}$$

The zeros of $F(x)$ are the solutions to $\tan(x) = x$.
For further details (especially, the full dynamical susceptibility), consult Refs. [253–255].

APPENDIX H

Leibniz integral rule

The Leibniz integral rule is obtained as below:

$$
\begin{aligned}
&\frac{\partial}{\partial D}\left\{\int_{-D}^{+D} f(x,D)\right\} = \lim_{\varepsilon\to 0}\frac{\int_{-D-\varepsilon}^{+D}\mathrm{d}x\, f(x,D+\varepsilon) - \int_{-D}^{D}\mathrm{d}x\, f(x,D)}{\varepsilon}\\
&= \lim_{\varepsilon\to 0}\frac{\int^{D+\varepsilon}\mathrm{d}x\, f(x,D+\varepsilon) - \int^{-D-\varepsilon}\mathrm{d}x\, f(x,D+\varepsilon) - \int_{-D}^{+D}\mathrm{d}x\, f(x,D)}{\varepsilon}\\
&= \lim_{\varepsilon\to 0}\frac{1}{\varepsilon}\Big(\int^{+D}\mathrm{d}x\, f(x,D+\varepsilon) + \int_{D}^{D+\varepsilon}\mathrm{d}x\, f(x,D+\varepsilon) - \int^{-D}\mathrm{d}x\, f(x,D+\varepsilon)\\
&\quad - \int_{-D}^{-D-\varepsilon}\mathrm{d}x\, f(x,D+\varepsilon) - \int_{-D}^{+D}\mathrm{d}x\, f(x,D)\Big)\\
&= \lim_{\varepsilon\to 0}\frac{\int_{-D}^{+D}\mathrm{d}x\, f(x,D+\varepsilon) + \int_{D}^{D+\varepsilon}\mathrm{d}x\, f(x,D+\varepsilon) - \int_{-D}^{-D-\varepsilon}\mathrm{d}x\, f(x,D+\varepsilon) - \int_{-D}^{D}\mathrm{d}x\, f(x,D)}{\varepsilon}\\
&= \lim_{\varepsilon\to 0}\frac{\int_{-D}^{+D}\mathrm{d}x\, f(x,D) + \varepsilon\int_{-D}^{D}\mathrm{d}x\,\frac{\partial f(x,D)}{\partial D} + \varepsilon f(D,D) - (-\varepsilon)f(-D,D) - \int_{-D}^{D}\mathrm{d}f\,(x,D) + \mathcal{O}(\varepsilon^2)}{\varepsilon}\\
&= \int_{-D}^{D}\mathrm{d}x\,\frac{\partial f(x,D)}{\partial D} + f(x=D,D) + f(x=-D,D)\ . \qquad \text{(H.1)}
\end{aligned}
$$

More generally [256],

$$
\frac{\mathrm{d}}{\mathrm{d}\theta}\left[\int_{a(\theta)}^{b(\theta)}\mathrm{d}x\, f(x,\theta)\right] = \int_{a(\theta)}^{b(\theta)}\mathrm{d}x\,\partial_\theta f(x,\theta) + f\left(b(\theta),\theta\right)\frac{\mathrm{d}\,b(\theta)}{\mathrm{d}\theta} - f\left(a(\theta),\theta\right)\frac{\mathrm{d}\,a(\theta)}{\mathrm{d}\theta}\ . \qquad \text{(H.2)}
$$

APPENDIX I

Fourier expansion for the half-lattice

The Fourier expansion rests on the completeness relation (for the set of periodic functions for which $f(x+L)=f(x)$),

$$\frac{1}{L}\sum_{n=-\infty}^{n=+\infty} e^{\mathrm{i}\frac{2\pi x}{L}n} = \delta(x)\ , \tag{I.1}$$

where the infinite sum is defined as

$$\sum_{n=-\infty}^{+\infty} := \lim_{N\to\infty}\sum_{n=-N}^{n=N}\ , \tag{I.2}$$

and in the discrete case, $L=2N+1$. The $N\to\infty$ limit should be taken *after* all other limits. The completeness relation can be proved as follows:

$$\begin{aligned}\sum_{n=-N}^{N} e^{\mathrm{i}n\theta} &= 1+\sum_{n=1}^{N} e^{\mathrm{i}n\theta}+\sum_{n=-1}^{-N} e^{\mathrm{i}n\theta}\\ &= 1+\sum_{n=1}^{N} e^{\mathrm{i}n\theta}+\sum_{n=1}^{N} e^{-\mathrm{i}n\theta}\ ;\end{aligned} \tag{I.3}$$

furthermore,

$$\sum_{n=1}^{N} e^{\mathrm{i}n\theta} = \sum_{n=0}^{N} e^{\mathrm{i}n\theta} - 1 = \frac{e^{\mathrm{i}(N+1)\theta}-1}{e^{\mathrm{i}\theta}-1} - 1 = \frac{e^{\mathrm{i}(N+1)\theta}-1-e^{\mathrm{i}\theta}+1}{e^{\mathrm{i}\theta}-1}\ . \tag{I.4}$$

Note that

$$\sum_{k=0}^{N} a\, r^k = a\,\frac{r^{N+1}-1}{r-1}\ , \tag{I.5}$$

therefore,

$$\sum_{n=1}^{N} e^{\mathrm{i}n\theta} = e^{\mathrm{i}\theta}\frac{e^{\mathrm{i}N\theta}-1}{e^{\mathrm{i}\theta}-1} = e^{\mathrm{i}\theta}\,\frac{e^{\mathrm{i}\frac{N}{2}\theta}}{e^{\mathrm{i}\frac{\theta}{2}}}\,\frac{e^{\mathrm{i}\frac{N}{2}\theta}-e^{-\mathrm{i}\frac{N}{2}\theta}}{e^{\mathrm{i}\frac{\theta}{2}}-e^{-\mathrm{i}\frac{\theta}{2}}} = e^{\mathrm{i}(N+1)\frac{\theta}{2}}\,\frac{\sin(\frac{N}{2}\theta)}{\sin(\frac{\theta}{2})}\ . \tag{I.6}$$

Analogously,

$$\sum_{n=1}^{N} e^{-in\theta} = \sum_{n=1}^{N} e^{in\theta}|_{\theta\to-\theta} = e^{-i(N+1)\frac{\theta}{2}} \frac{\sin(\frac{N}{2}\theta)}{\sin(\frac{\theta}{2})} \ , \tag{I.7}$$

so that

$$\begin{aligned}\sum_{n=-N}^{N} e^{in\theta} &= \frac{\sin(\frac{N}{2}\theta)}{\sin(\frac{\theta}{2})}[e^{i(N+1)\frac{\theta}{2}} + e^{-i(N+1)\frac{\theta}{2}}] + 1 \\ &= 2\cos((N+1)\frac{\theta}{2}) \frac{\sin(\frac{N}{2}\theta)}{\sin(\frac{\theta}{2})} + 1 \ .\end{aligned} \tag{I.8}$$

Using

$$2\cos\alpha\sin\beta = \sin(\alpha+\beta) - \sin(\alpha-\beta) \ ,$$

one obtains

$$\sum_{n=-N}^{N} e^{in\theta} = \frac{\sin(\frac{\theta}{2}(2N+1)) - \sin(\frac{\theta}{2})}{\sin(\frac{\theta}{2})} + 1 = \frac{\sin(\frac{\theta}{2}(2N+1))}{\sin(\frac{\theta}{2})} \ . \tag{I.9}$$

If $\theta = 0$, then

$$\sum_{n=-N}^{N} e^{in\theta}|_{\theta=0} = \sum_{n=-N}^{N} 1 = 2N+1 \ , \tag{I.10}$$

therefore,

$$\lim_{N\to\infty} \sum_{n=-N}^{N} e^{in\theta} = \lim_{N\to\infty} \frac{\sin(\frac{\theta}{2}(2N+1))}{\sin(\frac{\theta}{2})} = (2N+1)\,\delta(\theta) \equiv L\,\delta(\theta) \ . \tag{I.11}$$

Now, if we sum only over even n's (assume N is even)

$$\begin{aligned}\sum_{\substack{n=-N \\ n:\,\text{even}}}^{N} e^{in\theta} &= \sum_{n=-\frac{N}{2}}^{\frac{N}{2}} e^{2in\theta} \overset{\frac{N}{2}=:M\in\mathbb{N}}{=\!=\!=} \sum_{n=-M}^{M} e^{2in\theta} \\ &= \frac{\sin(\frac{2\theta}{2}(2M+1))}{\sin(\frac{\theta}{2})} = \frac{\sin(\theta(2M+1))}{\sin(\theta)} \ .\end{aligned} \tag{I.12}$$

If $\theta = 0$,

$$\sum_{n=-M}^{M} e^{2in\theta}|_{\theta=0} = 2M+1 \equiv 2\frac{N}{2} + 1 = N+1 \ ; \tag{I.13}$$

therefore,

$$\lim_{N\to\infty} \sum_{\substack{n=-N \\ n:\,\text{even}}}^{N} e^{\mathrm{i}n\theta} e^{\mathrm{i}n\theta} = L'\,\delta(\theta) \quad ; \quad L' = N+1 \;, \tag{I.14}$$

since

$$\lim_{N\to\infty} \frac{L'}{L} = \lim_{N\to\infty} \frac{N+1}{2N+1} = \frac{1}{2} \;. \tag{I.15}$$

Hence,

$$\lim_{N\to\infty} \frac{1}{L} \sum_{\substack{n=-N \\ n:\,\text{even}}}^{N} e^{\mathrm{i}n\theta} = \lim_{N\to\infty} \frac{L'}{L}\,\delta(x) = \frac{1}{2}\,\delta(x) \;. \tag{I.16}$$

This demonstrates how to sum over the half-lattice.

References

[1] P. Nozières,
"The Kondo problem: Fancy mathematical techniques versus simple physical ideas",
Low Temperature Physics Conference Proceedings – LT14,
ed. by M. Krusius and M. Vuorio, vol. 5, North-Holland, 1975 339–374
(cit. on pp. 1, 3, 14, 15).

[2] Y. Matsushita et al., *Evidence for charge Kondo effect in superconducting Tl-doped PbTe*,
Physical Review Letters **94**.15 (2005) 157002 (cit. on p. 1).

[3] U. Wilhelm et al., *Experimental evidence for spinless Kondo effect in two electrostatically coupled quantum dot systems*, Physica E **14**.4 (2002) 385–390
(cit. on p. 1).

[4] S. Sasaki et al.,
Enhanced Kondo effect via tuned orbital degeneracy in a spin 1/2 artificial atom,
Physical Review Letters **93**.1 (2004) 017205 (cit. on p. 1).

[5] P. Jarillo-Herrero et al., *Orbital Kondo effect in carbon nanotubes*,
Nature **434**.7032 (2005) 484–488 (cit. on pp. 1, 5).

[6] D. L. Cox and A. Zawadowski, *Exotic Kondo effects in metals: magnetic ions in a crystalline electric field and tunnelling centres*, Advances in Physics **47**.5 (1998) 599–942,
arXiv: cond-mat/9704103 (cit. on pp. 1, 4).

[7] G. Grüner and A. Zawadowski, *Magnetic impurities in non-magnetic metals*,
Reports on Progress in Physics **37**.12 (1974) 1497
(cit. on pp. 1–3, 7, 9–11, 17, 18, 213, 215).

[8] B. A. Jones, "Handbook of magnetism and advanced magnetic materials",
ed. by H. Kronmüller et al., Wiley, 2007, chap. The Kondo effect
(cit. on pp. 1, 2, 16, 97–99).

[9] G. Grüner and A. Zawadowski, *Low temperature properties of Kondo alloys*,
Reports on Progress in Physics **7B** (1978) 591–647 (cit. on pp. 1, 2, 7, 9, 18).

[10] W. Meissner and B. Voigt, *Messungen mit Hilfe von flüssigem Helium XI Widerstand der reinen Metalle in tiefen Temperaturen*, Annalen der Physik **399**.8 (1930) 892–936
(cit. on p. 1).

[11] M. Grobis et al., "Handbook of magnetism and advanced magnetic materials",
ed. by H. Kronmüller et al., Wiley, 2007,
chap. The Kondo effect in mesoscopic quantum dots (cit. on pp. 1, 5, 14, 15, 100, 104).

[12] W. J. de Haas, J. de Boer and G. J. van den Berg,
The electrical resistance of gold, copper and lead at low temperatures,
Physica **1**.7-12 (1934) 1115–1124 (cit. on pp. 1, 8).

[13] J. P. Franck, F. D. Manchester and D. L. Martin,
The specific heat of pure copper and of some dilute copper+iron alloys showing a minimum in the electrical resistance at low temperatures, **263**.1315 (1961) 494–507
(cit. on p. 2).

[14] P. Coleman, "Handbook of magnetism and advanced magnetic materials", ed. by H. Kronmüller et al., Wiley, 2007, chap. Heavy fermions: Electrons at the edge of magnetism (cit. on pp. 2–4, 7, 8, 18, 146, 150, 152, 153, 155, 156).

[15] J. Kondo, *Resistance minimum in dilute magnetic alloys*, Progress of Theoretical Physics **32**.1 (1964) 37–49 (cit. on pp. 2, 7).

[16] J. Kondo, *Sticking to my bush*, Journal of the Physical Society of Japan **74**.1 (2005) 1–3 (cit. on p. 2).

[17] C. Zener, *Interaction between the d shells in the transition metals*, Physical Review **81**.3 (1951) 440 (cit. on pp. 2, 7).

[18] J. R. Schrieffer and P. A. Wolff, *Relation between the Anderson and Kondo hamiltonians*, Physical Review **149**.2 (1966) 491 (cit. on pp. 2, 12, 121).

[19] J. Kondo, *Theory of dilute magnetic alloys*, Solid State Physics **23** (1970) 183–281 (cit. on p. 2).

[20] A. J. Heeger, *Localized moments and nonmoments in metals: the Kondo effect*, Solid State Physics **23** (1970) 283–411 (cit. on p. 2).

[21] P. Coleman, *Heavy fermions and the Kondo lattice: A 21st century perspective* (2015), arXiv: 1509.05769 (cit. on pp. 2, 4, 146).

[22] A. C. Hewson, *The Kondo problem to heavy fermions*, Cambridge University Press, 1997 (cit. on pp. 2, 4, 8, 9, 12, 13, 37, 103).

[23] R. Bulla, T. A. Costi and T. Pruschke, *Numerical renormalization group method for quantum impurity systems*, Reviews of Modern Physics **80**.2 (2008) 395 (cit. on pp. 2, 3, 14).

[24] P. W. Anderson, *Basic notions of condensed matter physics*, Benjamin/Cummings, 1984 (cit. on pp. 2, 11).

[25] A. A. Abrikosov, *Magnetic impurities in nonmagnetic metals*, Physics-Uspekhi **12**.2 (1969) 168–181 (cit. on pp. 2, 10).

[26] P. W. Anderson and G. Yuval, *Exact results in the Kondo problem: equivalence to a classical one-dimensional Coulomb gas*, Physical Review Letters **23**.2 (1969) 89 (cit. on pp. 2, 11).

[27] P. W. Anderson, G. Yuval and D. R. Hamann, *Exact results in the Kondo problem. II. Scaling theory, qualitatively correct solution, and some new results on one-dimensional classical statistical models*, Physical Review B **1**.11 (1970) 4464 (cit. on pp. 2, 11).

[28] P. W. Anderson, *A poor man's derivation of scaling laws for the Kondo problem*, Journal of Physics C: Solid State Physics **3**.12 (1970) 2436 (cit. on pp. 2, 11, 217).

[29] K. G. Wilson, *The renormalization group: Critical phenomena and the Kondo problem*, Reviews of Modern Physics **47**.4 (1975) 773 (cit. on p. 3).

[30] T. A. Costi, A. C. Hewson and V. Zlatic, *Transport coefficients of the Anderson model via the numerical renormalization group*, Journal of Physics: Condensed Matter **6**.13 (1994) 2519 (cit. on pp. 3, 103).

[31] N. Andrei, K. Furuya and J. H. Lowenstein, *Solution of the Kondo problem*, Reviews of Modern Physics **55**.2 (1983) 331 (cit. on pp. 3, 40, 41).

[32] N. Andrei and C. Destri, *Solution of the multichannel Kondo problem*, Physical Review Letters **52**.5 (1984) 364 (cit. on pp. 3, 4).

[33] A. M. Tsvelick and P. B. Wiegmann, *Exact solution of the multichannel Kondo problem, scaling, and integrability*, Journal of Statistical Physics **38**.1-2 (1985) 125–147 (cit. on p. 3).

[34] A. C. Hewson, *A general derivation of Wiegmann's solution of the s-d exchange (Kondo) model*, Journal of Physics C **15**.20 (1982) L611 (cit. on p. 3).

[35] P. Nozières, *A "Fermi-liquid" description of the Kondo problem at low temperatures*, Journal of Low Temperature Physics **17**.1-2 (1974) 31–42 (cit. on pp. 3, 15).

[36] Y. Nagaoka, *Self-consistent treatment of Kondo's effect in dilute alloys*, Physical Review **138**.4A (1965) A1112 (cit. on p. 3).

[37] Y. Nagaoka, *Effect of the potential scattering on the low-temperature anomalies due to the s-d interaction*, Progress of Theoretical Physics **39**.2 (1968) 533–535 (cit. on p. 3).

[38] K. Fischer, *Self-consistent treatment of the Kondo effect*, Physical Review **158**.3 (1967) 613 (cit. on p. 3).

[39] J. Zittartz and E. Müller-Hartmann, *Green's function theory of the Kondo effect in dilute magnetic alloys*, Zeitschrift für Physik **212**.4 (1968) 380–407 (cit. on p. 3).

[40] H. Suhl, *Paramagnetic impurities in metals at finite temperatures*, Physics **2**.1 (1965) 39–59 (cit. on p. 3).

[41] H. Suhl, *Dispersion theory of the Kondo effect*, Physical Review **138**.2A (1965) A515 (cit. on pp. 3, 11, 18).

[42] A. A. Abrikosov, *Electron scattering on magnetic impurities in metals and anomalous resistivity effects*, Physics **2**.1 (1965) 5–20 (cit. on pp. 3, 9, 11, 18, 213).

[43] W. Brenig and W. Götze, *On Suhl's approach to the Kondo problem*, Zeitschrift für Physik **217**.2 (1968) 188–212 (cit. on pp. 3, 9).

[44] A. Zawadowski and P. Fazekas, *Dynamics of impurity spin above the Kondo temperature*, Zeitschrift für Physik **226**.3 (1969) 235–265 (cit. on pp. 3, 9, 213).

[45] S. D. Silverstein and C. B. Duke, *Theory of s-d scattering in dilute magnetic alloys. I. Perturbation theory and the derivation of the Low equation*, Physical Review **161**.2 (1967) 456 (cit. on pp. 3, 213, 215).

[46] C. B. Duke and S. D. Silverstein, *Theory of s-d scattering in dilute magnetic alloys. II. Derivation and solution of linear vertex equations*, Physical Review **161**.2 (1967) 470 (cit. on p. 3).

[47] K. Yosida and A. Yoshimori, "The ground state of the *s-d* model", *Magnetism*, ed. by G. T. Rado and H. Suhl, vol. 1973, Academic Press, 1973 253–286 (cit. on p. 3).

[48] K. Yosida, *Theory of magnetism*, vol. 122, 1996 (cit. on pp. 3, 4, 37, 152).

[49] N. E. Bickers, *Review of techniques in the large-N expansion for dilute magnetic alloys*, Reviews of Modern Physics **59**.4 (1987) 845 (cit. on p. 3).

[50] O. Parcollet et al., *Overscreened multichannel $SU(N)$ Kondo model: Large-N solution and conformal field theory*, Physical Review B **58**.7 (1998) 3794 (cit. on p. 4).

[51] B. A. Jones, B. G. Kotliar and A. J. Millis, *Mean-field analysis of two antiferromagnetically coupled Anderson impurities*, Physical Review B **39**.5 (1989) 3415 (cit. on p. 4).

[52] A. J. Millis, B. G. Kotliar and B. A. Jones, "Antiferromagnetic phase instability in the two-impurity Kondo problem", *Field theories in condensed matter physics: A workshop*, ed. by Z. Tešanović, Addison-Wesley, 1990 (cit. on p. 4).

[53] P. Simon, R. López and Y. Oreg, *Ruderman-Kittel-Kasuya-Yosida and magnetic-field interactions in coupled Kondo quantum dots*, Physical Review Letters **94**.8 (2005) 086602 (cit. on p. 4).

[54] P. Simon, *Kondo screening cloud in a double quantum dot system*, Physical Review B **71**.15 (2005) 155319 (cit. on p. 4).

[55] P. Schlottmann, *Some exact results for dilute mixed-valent and heavy-fermion systems*, Physics Reports **181**.1 (1989) 1–119 (cit. on p. 4).

[56] A. W. W. Ludwig and I. Affleck, *Exact conformal-field-theory results on the multi-channel Kondo effect: Asymptotic three-dimensional space-and time-dependent multi-point and many-particle Green's functions*, Nuclear Physics B **428**.3 (1994) 545–611 (cit. on p. 4).

[57] I. Affleck and A. W. W. Ludwig, *Exact conformal-field-theory results on the multichannel Kondo effect: Single-fermion Green's function, self-energy, and resistivity*, Physical Review B **48**.10 (1993) 7297 (cit. on p. 4).

[58] I. Affleck, *Conformal field theory approach to the Kondo effect*, Acta Physica Polonica B **26** (1995) 1869–1932, arXiv: cond-mat/9512099 (cit. on p. 4).

[59] P. Nozières and A. Blandin, *Kondo effect in real metals*, Journal de Physique **41**.3 (1980) 193–211 (cit. on pp. 4, 15, 107).

[60] H. B. Pang and D. L. Cox, *Stability of the fixed point of the two-channel Kondo Hamiltonian*, Physical Review B **44**.17 (1991) 9454 (cit. on p. 4).

[61] D. L. Cox and A. E. Ruckenstein, *Spin-flavor separation and non-Fermi-liquid behavior in the multichannel Kondo problem: A large-N approach*, Physical Review Letters **71**.10 (1993) 1613 (cit. on p. 4).

[62] M. A. Ruderman and C. Kittel, *Indirect exchange coupling of nuclear magnetic moments by conduction electrons*, Physical Review **96**.1 (1954) 99 (cit. on pp. 4, 37, 152).

[63] T. Kasuya, *A theory of metallic ferro- and antiferromagnetism on Zener's model*, Progress of Theoretical Physics **16**.1 (1956) 45–57 (cit. on pp. 4, 37, 152).

[64] K. Yosida, *Magnetic properties of Cu-Mn alloys*, Physical Review **106**.5 (1957) 893 (cit. on pp. 4, 37, 152).

[65] J. H. van Vleck,
Note on the interactions between the spins of magnetic ions or nuclei in metals,
Reviews of Modern Physics **34**.4 (1962) 681 (cit. on pp. 4, 37, 152).

[66] S. Doniach, *The Kondo lattice and weak antiferromagnetism*,
Physica B+C **91** (1977) 231–234 (cit. on pp. 5, 152).

[67] V. Madhavan et al.,
Tunneling into a single magnetic atom: spectroscopic evidence of the Kondo resonance,
Science **280**.5363 (1998) 567–569 (cit. on pp. 5, 93).

[68] J. Li et al., *Kondo scattering observed at a single magnetic impurity*,
Physical Review Letters **80**.13 (1998) 2893 (cit. on pp. 5, 93).

[69] R. C. Ashoori, *Electrons in artificial atoms*, Nature **379** (1996) 413–419 (cit. on p. 5).

[70] S. de Franceschi and W. G. van der Wiel,
"Handbook of nanophysics: Nanoparticles and quantum dots", ed. by K. D. Sattler,
CRC Press, 2010, chap. Kondo effect in quantum dots (cit. on pp. 5, 14, 93).

[71] D. Ferry and S. M. Goodnick, *Transport in nanostructures*,
Cambridge University Press, 1997 (cit. on p. 5).

[72] D. Goldhaber-Gordon et al., *Kondo effect in a single-electron transistor*,
Nature **391**.6663 (1998) 156–159 (cit. on pp. 5, 100, 102, 103).

[73] D. Goldhaber-Gordon et al.,
From the Kondo regime to the mixed-valence regime in a single-electron transistor,
Physical Review Letters **81**.23 (1998) 5225 (cit. on pp. 5, 100, 102, 103).

[74] S. M. Cronenwett, T. H. Oosterkamp and L. P. Kouwenhoven,
A tunable Kondo effect in quantum dots, Science **281**.5376 (1998) 540–544
(cit. on pp. 5, 100, 102, 103).

[75] J. Schmid et al., *A quantum dot in the limit of strong coupling to reservoirs*,
Physica B **256** (1998) 182–185 (cit. on p. 5).

[76] L. P. Kouwenhoven and L. I. Glazman, *Revival of the Kondo effect*,
Physics World **14**.1 (2001) 33, arXiv: cond-mat/0104100 (cit. on p. 5).

[77] G. D. Scott and D. Natelson, *Kondo resonances in molecular devices*,
ACS Nano **4**.7 (2010) 3560–3579 (cit. on pp. 5, 99).

[78] D. Loss and D. P. DiVincenzo, *Quantum computation with quantum dots*,
Physical Review A **57**.1 (1998) 120 (cit. on p. 5).

[79] W. A. Coish and D. Loss, "Handbook of magnetism and advanced magnetic materials",
ed. by H. Kronmüller et al., Wiley, 2007, chap. Quantum computing with spins in solids,
arXiv: cond-mat/0606550 (cit. on p. 5).

[80] A. M. J. Schakel,
Boulevard of broken symmetries: Effective field theories of condensed matter,
World Scientific, 2008 (cit. on p. 6).

[81] A. M. Chang and J. C. Chen, *The Kondo effect in coupled-quantum dots*,
Reports on Progress in Physics **72**.9 (2009) 096501 (cit. on pp. 6, 8, 98–101).

[82] G. D. Mahan, *Many-particle Physics*, Plenum Press, 1981 (cit. on pp. 8, 10).

[83] A. M. Tsvelik, *Quantum field theory in condensed matter physics*, Cambridge University Press, 2007 (cit. on p. 9).

[84] S. Gluzman and V. I. Yukalov, *Unified approach to crossover phenomena*, Physical Review E **58**.4 (1998) 4197 (cit. on p. 9).

[85] H. Nishimori and G. Ortiz, *Elements of phase transitions and critical phenomena*, Oxford University Press, 2010 (cit. on p. 9).

[86] H. J. Spencer, *Theory of s-d scattering in dilute magnetic alloys with spin-1/2 impurities*, Physical Review **171**.2 (1968) 515 (cit. on p. 9).

[87] H. Keiter, *Green's function perturbation technique for the Kondo system. I. Linked diagram expansion technique for the one electron Green's function*, Zeitschrift für Physik **214**.1 (1968) 22–41 (cit. on pp. 9, 213).

[88] R. Frésard, J. Kroha and P. Wölfle, "Strongly correlated systems: Theoretical methods", ed. by A. Avella and F. Mancini, Springer, 2012, chap. The pseudoparticle approach to strongly correlated electron systems (cit. on pp. 9, 213, 215).

[89] C. B. Duke and S. D. Silverstein, *Does logarithmic accuracy uniquely define the low-temperature properties of dilute magnetic alloy systems?*, Journal of Applied Physics **39**.2 (1968) 708–709 (cit. on p. 10).

[90] V. V. Sudakov, *Meson-Meson Scattering in Meson Field Theory*, Soviet Physics Doklady **1** (1957) 662–665 (cit. on p. 10).

[91] V. V. Sudakov, *Vertex parts at very high energies in quantum electrodynamics*, Sov.Phys. JETP **3** (1956) 65–71 (cit. on p. 10).

[92] S. Doniach and E. H. Sondheimer, *Green's functions for solid state physicists*, Imperial College Press, 1998 (cit. on pp. 10, 18, 148).

[93] B. Roulet, J. Gavoret and P. Nozières, *Singularities in the X-ray absorption and emission of metals. I. First-order parquet calculation*, Physical Review **178**.3 (1969) 1072 (cit. on p. 10).

[94] P. Nozières, J. Gavoret and B. Roulet, *Singularities in the X-ray absorption and emission of metals. II. Self-consistent treatment of divergences*, Physical Review **178**.3 (1969) 1084 (cit. on p. 10).

[95] J. Solyom, *Renormalization and scaling in the X-ray absorption and Kondo problems*, Journal of Physics F: Metal Physics **4**.12 (1974) 2269 (cit. on p. 10).

[96] K. K. Murata, *Potential and correlation effects in dilute localized moment systems*, PhD Thesis: Cornell University, 1971 (cit. on p. 11).

[97] K. Fukushima, *Extended parquet theory for s-d system*, Progress of Theoretical Physics **46**.5 (1971) 1307–1322 (cit. on p. 11).

[98] C. Y. Cheung and R. D. Mattuck, *Removing the divergence at the Kondo temperature by means of self-consistent perturbation theory*, Physical Review B **2**.7 (1970) 2735 (cit. on p. 11).

[99] R. D. Mattuck, *A guide to Feynman diagrams in the many-body problem*, 2nd ed., McGraw-Hill, 1976 (cit. on p. 11).

[100] A. H. Nevidomskyy, "Many-body physics: From Kondo to Hubbard", ed. by E. Pavarini, E. Koch and C. P., Forschungszentrum Jüulich, 2015, chap. The Kondo Model and Poor Man's Scaling (cit. on p. 11).

[101] P. Coleman, *Local moment physics in heavy electron systems* (2002), arXiv: cond-mat/0206003 (cit. on p. 12).

[102] J. Cardy, *Scaling and renormalization in statistical physics*, Cambridge University Press, 1996 (cit. on p. 13).

[103] R. M. White and B. Bayne, *Quantum theory of magnetism*, vol. 1, Springer, 1983 (cit. on pp. 13, 183).

[104] M. Fowler and A. Zawadowski, *Scaling and the renormalization group in the Kondo effect*, Solid State Communications **9**.8 (1971) 471–476 (cit. on p. 14).

[105] A. A. Abrikosov and A. A. Migdal, *On the theory of the Kondo effect*, Journal of Low Temperature Physics **3**.5 (1970) 519–536 (cit. on p. 14).

[106] Y. A. Izyumov and Y. N. Skryabin, *Statistical mechanics of magnetically ordered systems*, Springer, 1988 (cit. on p. 14).

[107] P. W. Anderson, *Infrared catastrophe in Fermi gases with local scattering potentials*, Physical Review Letters **18**.24 (1967) 1049 (cit. on p. 14).

[108] V. Barzykin and I. Affleck, *The Kondo screening cloud: What can we learn from perturbation theory?*, Physical Review Letters **76**.26 (1996) 4959 (cit. on p. 14).

[109] E. S. Sørensen and I. Affleck, *Scaling theory of the Kondo screening cloud*, Physical Review B **53**.14 (1996) 9153 (cit. on p. 14).

[110] I. Affleck, *The Kondo screening cloud: what it is and how to observe it* (2009), arXiv: 0911.2209 (cit. on p. 14).

[111] J. Park et al., *How to directly measure a Kondo cloud's length*, Physical Review Letters **110**.24 (2013) 246603 (cit. on p. 14).

[112] J. Friedel, *The distribution of electrons round impurities in monovalent metals*, Philosophical Magazine **43**.337 (1952) 153–189 (cit. on p. 17).

[113] J. Friedel, *On some electrical and magnetic properties of metallic solid solutions*, Canadian Journal of Physics **34**.12A (1956) 1190–1211 (cit. on p. 17).

[114] J. Friedel, *Metallic alloys*, Il Nuovo Cimento **7** (1958) 287–311 (cit. on p. 17).

[115] P. W. Anderson, *Localized magnetic states in metals*, Physical Review **124**.1 (1961) 41 (cit. on p. 17).

[116] A. Blandin and J. Friedel, *Propriétés magnétiques des alliages dilués. Interactions magnétiques et antiferromagnétisme dans les alliages du type métal noble-métal de transition*, Journal de Physique et Le Radium **20**.2-3 (1959) 160–168 (cit. on p. 17).

[117] C. P. Poole Jr, *Encyclopedic dictionary of condensed matter physics*, Academic Press, 2004 (cit. on pp. 17, 150).

[118] F. J. Wegner and A. Houghton, *Renormalization group equation for critical phenomena*, Physical Review A **8**.1 (1973) 401 (cit. on p. 20).

[119] G. Stefanucci and R. van Leeuwen, *Nonequilibrium many-body theory of quantum systems: A modern introduction*, Cambridge University Press, 2013 (cit. on pp. 20, 147, 213).

[120] G. M. Eliashberg, *Transport equation for a degenerate system of Fermi particles*, Sov. Phys. JETP **14** (1962) 886–892 (cit. on pp. 24, 26, 71, 72, 76).

[121] N. Dupuis, "Notes on the many-body problem", 2011 (accessed Mar, 2016), URL: http://www.lptmc.jussieu.fr/users/dupuis (cit. on p. 40).

[122] A. L. Fetter and J. D. Walecka, *Quantum theory of many-particle systems*, McGraw-Hill, 1983 (cit. on pp. 54, 66).

[123] H. Bruus and K. Flensberg, *Many-body quantum theory in condensed matter physics: An introduction*, 2nd ed., Oxford University Press, 2004 (cit. on pp. 54, 66, 92, 101, 102, 148, 188, 189).

[124] M. Klein et al., *Signature of quantum criticality in photoemission spectroscopy*, Physical Review Letters **101**.26 (2008) 266404 (cit. on pp. 68, 151, 180).

[125] D. N. Aristov, *Indirect RKKY interaction in any dimensionality*, Physical Review B **55**.13 (1997) 8064 (cit. on p. 68).

[126] S. R. Valluri, D. J. Jeffrey and R. M. Corless, *Some applications of the Lambert W function to physics*, Canadian Journal of Physics **78**.9 (2000) 823–831 (cit. on pp. 91, 141).

[127] D. Veberič, *Lambert W function for applications in physics*, Computer Physics Communications **183**.12 (2012) 2622–2628 (cit. on pp. 91, 141).

[128] G. Binnig et al., *Surface studies by scanning tunneling microscopy*, Physical Review Letters **49**.1 (1982) 57 (cit. on p. 92).

[129] J. Bork, *Probing nanoscale electronic and magnetic interaction with scanning tunneling spectroscopy*, PhD Thesis: Aalborg University, 2010 (cit. on pp. 93, 94).

[130] C. J. Chen, *Introduction to scanning tunneling microscopy*, Oxford University Press, 1993 (cit. on p. 92).

[131] P. K. Hansma and J. Tersoff, *Scanning tunneling microscopy*, Journal of Applied Physics **61**.2 (1987) R1–R24 (cit. on p. 92).

[132] J. Tersoff and D. R. Hamann, *Theory and application for the scanning tunneling microscope*, Physical Review Letters **50**.25 (1983) 1998 (cit. on p. 92).

[133] J. Tersoff and D. R. Hamann, *Theory and application for the scanning tunneling microscope*, Physical Review B **31** (1985) 805–813 (cit. on p. 92).

[134] P. Wahl et al., *Kondo temperature of magnetic impurities at surfaces*, Physical Review Letters **93**.17 (2004) 176603 (cit. on p. 93).

[135] A. Yamasaki et al., *Direct observation of the single-domain limit of Fe nanomagnets by spin-polarized scanning tunneling spectroscopy*, Physical Review Letters **91**.12 (2003) 127201 (cit. on p. 93).

[136] O. Újsághy et al., *Theory of the Fano resonance in the STM tunneling density of states due to a single Kondo impurity*, Physical Review Letters **85**.12 (2000) 2557 (cit. on pp. 93, 94).

[137] P. Lucignano et al., *Kondo conductance in an atomic nanocontact from first principles*, Nature Materials **8**.7 (2009) 563–567 (cit. on p. 93).

[138] M. Maltseva, M. Dzero and P. Coleman, *Electron cotunneling into a Kondo lattice*, Physical Review Letters **103**.20 (2009) 206402 (cit. on p. 93).

[139] U. Fano, *Effects of configuration interaction on intensities and phase shifts*, Physical Review **124**.6 (1961) 1866 (cit. on p. 93).

[140] G. B. Martins et al., *Transport properties of strongly correlated electrons in quantum dots studied with a simple circuit model*, Physical Review Letters **96**.6 (2006) 066802 (cit. on p. 93).

[141] C. Fühner, *Magneto-Transport Investigation on Multi-Electron Quantum Dots: Coulomb Blockade, Kondo Effect, and Fano Regime*, PhD Thesis: University of Hannover, 2002 (cit. on p. 93).

[142] M. Plihal and J. W. Gadzuk, *Nonequilibrium theory of scanning tunneling spectroscopy via adsorbate resonances: Nonmagnetic and Kondo impurities*, Physical Review B **63**.8 (2001) 085404 (cit. on p. 93).

[143] R. Žitko, *Fano-Kondo effect in side-coupled double quantum dots at finite temperatures and the importance of two-stage Kondo screening*, Physical Review B **81**.11 (2010) 115316 (cit. on p. 93).

[144] T. Jamneala et al., *Scanning tunneling spectroscopy of transition-metal impurities at the surface of gold*, Physical Review B **61**.15 (2000) 9990 (cit. on p. 93).

[145] A. Schiller and S. Hershfield, *Theory of scanning tunneling spectroscopy of a magnetic adatom on a metallic surface*, Physical Review B **61**.13 (2000) 9036 (cit. on p. 94).

[146] C.-Y. Lin, A. H. Castro Neto and B. A. Jones, *Microscopic theory of the single impurity surface Kondo resonance*, Physical Review B **71**.3 (2005) 035417 (cit. on p. 94).

[147] J. Bork et al., *A tunable two-impurity Kondo system in an atomic point contact*, Nature Physics **7**.11 (2011) 901–906 (cit. on pp. 94–96).

[148] C. Jayaprakash, H. R. Krishna-Murthy and J. W. Wilkins, *Two-impurity Kondo problem*, Physical Review Letters **47**.10 (1981) 737 (cit. on p. 97).

[149] B. A. Jones and C. M. Varma, *Study of two magnetic impurities in a Fermi gas*, Physical Review Letters **58**.9 (1987) 843 (cit. on p. 97).

[150] B. A. Jones, C. M. Varma and J. W. Wilkins, *Low-temperature properties of the two-impurity Kondo Hamiltonian*, Physical Review Letters **61**.1 (1988) 125 (cit. on p. 97).

[151] B. A. Jones and C. M. Varma, *Critical point in the solution of the two magnetic impurity problem*, Physical Review B **40**.1 (1989) 324 (cit. on p. 97).

[152] B. Lechtenberg,
Equilibrium and nonequilibrium dynamics close to impurity quantum phase transitions,
PhD Thesis: Technische Universität Dortmund, 2016 (cit. on p. 98).

[153] P. Mehta et al.,
Regular and singular Fermi-liquid fixed points in quantum impurity models,
Physical Review B **72**.1 (2005) 014430 (cit. on p. 98).

[154] B. A. Jones, *Pair correlation effects in heavy fermions*,
Physica B: Condensed Matter **171**.1 (1991) 53–60 (cit. on p. 98).

[155] H. R. Krishna-Murthy, J. W. Wilkins and K. G. Wilson,
Renormalization-group approach to the Anderson model of dilute magnetic alloys. I. Static properties for the symmetric case, Physical Review B **21**.3 (1980) 1003
(cit. on p. 99).

[156] H. R. Krishna-Murthy, J. W. Wilkins and K. G. Wilson,
Renormalization-group approach to the Anderson model of dilute magnetic alloys. II. Static properties for the asymmetric case, Physical Review B **21**.3 (1980) 1044
(cit. on p. 99).

[157] N. J. Craig et al., *Tunable nonlocal spin control in a coupled-quantum dot system*,
Science **304**.5670 (2004) 565–567 (cit. on p. 99).

[158] S. Sasaki et al., *Nonlocal control of the Kondo effect in a double quantum dot–quantum wire coupled system*, Physical Review B **73**.16 (2006) 161303(R) (cit. on p. 99).

[159] J.-H. Chen et al., *Tunable Kondo effect in graphene with defects*,
Nature Physics **7**.7 (2011) 535–538 (cit. on p. 99).

[160] W. Chen et al.,
Disappearance of the Kondo resonance for atomically fabricated cobalt dimers,
Physical Review B **60**.12 (1999) R8529 (cit. on p. 99).

[161] H. Jeong, A. M. Chang and M. R. Melloch,
The Kondo effect in an artificial quantum dot molecule,
Science **293**.5538 (2001) 2221–2223 (cit. on p. 99).

[162] L. P. Kouwenhoven, D. G. Austing and S. Tarucha, *Few-electron quantum dots*,
Reports on Progress in Physics **64**.6 (2001) 701 (cit. on p. 100).

[163] L. L. Sohn, L. P. Kouwenhoven and G. Schön, eds., *Mesoscopic electron transport*,
vol. 345, Nato Science Series E, Springer, 1997 (cit. on p. 100).

[164] W. G. van der Wiel et al., *Electron transport through double quantum dots*,
Reviews of Modern Physics **75**.1 (2002) 1 (cit. on pp. 100–102).

[165] M. A. Kastner, *The single-electron transistor*,
Reviews of Modern Physics **64**.3 (1992) 849 (cit. on p. 100).

[166] J. Nygård, D. H. Cobden and P. E. Lindelof, *Kondo physics in carbon nanotubes*,
Nature **408**.6810 (2000) 342–346 (cit. on p. 100).

[167] J. Park et al., *Coulomb blockade and the Kondo effect in single-atom transistors*,
Nature **417**.6890 (2002) 722–725 (cit. on p. 100).

[168] W. Liang et al., *Kondo resonance in a single-molecule transistor*,
Nature **417**.6890 (2002) 725–729 (cit. on p. 100).

[169] S. L. Sondhi et al., *Continuous quantum phase transitions*, Reviews of Modern Physics **69**.1 (1997) 315 (cit. on pp. 100, 145).

[170] C. W. J. Beenakker and H. van Houten, *Quantum transport in semiconductor nanostructures*, Solid State Physics **44**.1 (1991) 228 (cit. on p. 101).

[171] M. Pustilnik and L. I. Glazman, *Kondo effect in quantum dots*, Journal of Physics: Condensed Matter **16**.16 (2004) R513 (cit. on pp. 101, 103).

[172] S. Datta, *Electronic transport in mesoscopic systems*, Cambridge University Press, 1997 (cit. on p. 101).

[173] D. V. Averin and K. K. Likharev, *Coulomb blockade of single-electron tunneling, and coherent oscillations in small tunnel junctions*, Journal of Low Temperature Physics **62**.3-4 (1986) 345–373 (cit. on p. 102).

[174] L. I. Glazman and M. Pustilnik, "Coulomb blockade and Kondo effect in quantum dots", *New directions in mesoscopic physics*, Springer, 2003 93–115 (cit. on pp. 102, 103).

[175] L. I. Glazman and M. E. Raikh, *Resonant Kondo transparency of a barrier with quasilocal impurity states*, JETP Letters **47**.8 (1988) 452–455 (cit. on pp. 102, 107).

[176] T. K. Ng and P. A. Lee, *On-site Coulomb repulsion and resonant tunneling*, Physical Review Letters **61**.15 (1988) 1768 (cit. on p. 102).

[177] F. Simmel et al., *Anomalous Kondo effect in a quantum dot at nonzero bias*, Physical Review Letters **83**.4 (1999) 804 (cit. on p. 102).

[178] W. G. van der Wiel et al., *The Kondo effect in the unitary limit*, Science **289**.5487 (2000) 2105–2108 (cit. on p. 103).

[179] Y. Meir, N. S. Wingreen and P. A. Lee, *Low-temperature transport through a quantum dot: The Anderson model out of equilibrium*, Physical Review Letters **70**.17 (1993) 2601 (cit. on p. 103).

[180] R. M. Potok, *Probing many-body effects in semiconductor nanostructures*, PhD Thesis: Harvard University, 2006 (cit. on p. 103).

[181] D. Tutuc, *Electron correlation effects in lateral quantum dots*, PhD Thesis: University of Hannover, 2011 (cit. on pp. 103–106).

[182] A. Kaminski, Y. V. Nazarov and L. I. Glazman, *Suppression of the Kondo effect in a quantum dot by external irradiation*, Physical Review Letters **83**.2 (1999) 384 (cit. on p. 104).

[183] J. M. Elzerman et al., *Suppression of the Kondo effect in a quantum dot by microwave radiation*, Journal of Low Temperature Physics **118**.5-6 (2000) 375–389 (cit. on p. 104).

[184] B. Hemingway et al., *Dynamic response of a spin-1/2 Kondo singlet*, Physical Review B **90**.12 (2014) 125151 (cit. on p. 104).

[185] A. Khedri, A. Nejati and J. Kroha, "Non-equilibrium renormalization group for Kondo qdots in a microwave photon field", 2016 (cit. on p. 104).

[186] D. Tutuc et al., *Tunable nonlocal coupling between Kondo impurities*, Physical Review B **83**.24 (2011) 241308 (cit. on p. 104).

[187] R. M. Potok et al., *Observation of the two-channel Kondo effect*, Nature **446**.7132 (2007) 167–171 (cit. on p. 115).

[188] S. Bravyi, D. P. DiVincenzo and D. Loss, *Schrieffer–Wolff transformation for quantum many-body systems*, Annals of Physics **326**.10 (2011) 2793–2826 (cit. on p. 121).

[189] R. K. Merton, *The Matthew effect in science*, Science **159**.3810 (1968) 56–63 (cit. on p. 141).

[190] L. Carr, ed., *Understanding quantum phase transitions*, CRC Press, 2011 (cit. on p. 145).

[191] S. Sachdev, *Quantum phase transitions*, Cambridge University Press, 1999 (cit. on p. 145).

[192] M. Vojta, *Impurity quantum phase transitions*, Philosophical Magazine **86**.13-14 (2006) 1807–1846 (cit. on p. 145).

[193] M. Vojta, *Quantum phase transitions*, Reports on Progress in Physics **66**.12 (2003) 2069 (cit. on p. 145).

[194] O. Stockert and F. Steglich, *Unconventional quantum criticality in heavy-fermion compounds*, Annual Review of Condensed Matter Physics **2**.1 (2011) 79–99 (cit. on pp. 146, 149, 150).

[195] H. von Löhneysen et al., *Fermi-liquid instabilities at magnetic quantum phase transitions*, Reviews of Modern Physics **79**.3 (2007) 1015 (cit. on pp. 146, 149, 150, 152–154, 157).

[196] W. Knafo et al., *Antiferromagnetic criticality at a heavy-fermion quantum phase transition*, Nature Physics **5**.10 (2009) 753–757 (cit. on p. 146).

[197] L. D. Landau, *The theory of a Fermi liquid*, Soviet Physics JETP **3**.6 (1957) 920–925 (cit. on p. 147).

[198] P. Nozières and D. Pines, *The theory of quantum liquids*, Perseus, 1999 (cit. on p. 147).

[199] A. A. Abrikosov, L. P. Gorkov and I. E. Dzialoshinskii, *Quantum field theoretical methods in statistical physics* (1965) (cit. on pp. 147, 148).

[200] L. G. Molinari, *Another proof of Gell-Mann and Low's theorem*, Journal of Mathematical Physics **48**.5 (2007) 052113 (cit. on p. 147).

[201] J. M. Luttinger, *Fermi surface and some simple equilibrium properties of a system of interacting fermions*, Physical Review **119**.4 (1960) 1153 (cit. on p. 147).

[202] J. Solyom, *Fundamentals of the physics of solids: Normal, broken-symmetry, and correlated systems*, vol. 3, Springer, 2014 (cit. on pp. 147–149, 183, 217).

[203] S. P., "Handbook of magnetic materials", ed. by K. H. J. Buschow, Elsevier, 2003, chap. Non-Fermi liquid behavior in heavy fermion systems (cit. on pp. 148–150, 152, 153).

[204] I. Y. Pomeranchuk, *Stability of a Fermi liquid*, Soviet Physics JETP **8** (1959) 361 (cit. on p. 148).

[205] H. von Löhneysen et al., *Non-Fermi-liquid behavior in a heavy-fermion alloy at a magnetic instability*, Physical Review Letters **72**.20 (1994) 3262 (cit. on pp. 149, 152, 155).

[206] H. von Löhneysen, *Non-Fermi-liquid behavior in heavy-fermion systems*, Physica B: Condensed Matter **206** (1995) 101–107 (cit. on p. 149).

[207] M. B. Maple et al., *Non Fermi liquid behavior in strongly correlated f-electron materials*, Journal of Low Temperature Physics **95**.1-2 (1994) 225–243 (cit. on p. 149).

[208] G. R. Stewart, *Non-Fermi-liquid behavior in d-and f-electron metals*, Reviews of Modern Physics **73**.4 (2001) 797 (cit. on p. 149).

[209] G. R. Stewart, *Addendum: Non-Fermi-liquid behavior in d-and f-electron metals*, Reviews of Modern Physics **78**.3 (2006) 743 (cit. on p. 149).

[210] S. Burdin, A. Georges and D. R. Grempel, *Coherence scale of the Kondo lattice*, Physical Review Letters **85**.5 (2000) 1048 (cit. on p. 149).

[211] Y.-F. Yang et al., *Scaling the Kondo lattice*, Nature **454**.7204 (2008) 611–613 (cit. on p. 149).

[212] Q. Si et al., *Locally critical quantum phase transitions in strongly correlated metals*, Nature **413**.6858 (2001) 804–808 (cit. on pp. 151, 155, 156).

[213] M. Klein et al., *Echo of the quantum phase transition of $CeCu_{6-x}Au_x$ in XPS: Breakdown of Kondo screening*, Physical Review B **79**.7 (2009) 075111 (cit. on p. 151).

[214] J. Kroha et al., *High-temperature signatures of quantum criticality in heavy-fermion systems*, Journal of Physics: Condensed Matter **22**.16 (2010) 164203 (cit. on p. 151).

[215] H. V. Löhneysen, C. Pfleiderer and A. Schroder, *Antiferromagnetic order, magnetic instability and non-Fermi-liquid behavior in $CeCu_{6-x}Au_x$: Tuning by Au concentration, hydrostatic pressure and magnetic field*, Journal of the Physical Society of Japan **69** (2000) 63–70 (cit. on p. 151).

[216] P. Estrela et al., *Resistivity of non-Fermi liquid U_2Pt_2In under pressure*, Physica B **312**.313 (2002) 482 (cit. on p. 152).

[217] O. Trovarelli et al., *$YbRh_2Si_2$: Pronounced non-Fermi-liquid effects above a low-lying magnetic phase transition*, Physical Review Letters **85**.3 (2000) 626 (cit. on pp. 152, 155).

[218] P. Gegenwart, Q. Si and F. Steglich, *Quantum criticality in heavy-fermion metals*, Nature Physics **4**.3 (2008) 186–197 (cit. on pp. 152, 155).

[219] P. Gegenwart et al., *Magnetic-field induced quantum critical point in $YbRh_2Si_2$*, Physical Review Letters **89**.5 (2002) 056402 (cit. on p. 152).

[220] J. Custers et al., *The break-up of heavy electrons at a quantum critical point*, Nature **424**.6948 (2003) 524–527 (cit. on pp. 152, 155).

[221] N. D. Mathur et al., *Magnetically mediated superconductivity in heavy fermion compounds*, Nature **394**.6688 (1998) 39–43 (cit. on p. 152).

[222] H. von Löhneysen et al.,
Pressure versus magnetic-field tuning of a magnetic quantum phase transition,
Physical Review B **63**.13 (2001) 134411 (cit. on p. 152).

[223] T. Moriya, *Spin fluctuations in itinerant electron magnetism*, Springer, 1985
(cit. on p. 154).

[224] J. A. Hertz, *Quantum critical phenomena*, Physical Review B **14**.3 (1976) 1165
(cit. on p. 154).

[225] A. P. Young,
Quantum effects in the renormalization group approach to phase transitions,
Journal of Physics C: Solid State Physics **8**.15 (1975) L309 (cit. on p. 154).

[226] M. L. Lawley, *Aspects of quantum criticality in itinerant electron ferromagnetic systems*,
PhD Thesis: University of Birmingham, 2010 (cit. on p. 154).

[227] T. Senthil, M. Vojta and S. Sachdev,
Weak magnetism and non-Fermi liquids near heavy-fermion critical points,
Physical Review B **69**.3 (2004) 035111 (cit. on pp. 155, 157, 158).

[228] H. von Löhneysen, *Non-fermi-liquid behaviour in the heavy-fermion system* $CeCu_{6-x}Au_x$,
Journal of Physics: Condensed Matter **8**.48 (1996) 9689 (cit. on p. 155).

[229] A. Schröder et al., *Scaling of magnetic fluctuations near a quantum phase transition*,
Physical Review Letters **80**.25 (1998) 5623 (cit. on p. 155).

[230] A. Schröder et al., *Onset of antiferromagnetism in heavy-fermion metals*,
Nature **407**.6802 (2000) 351–355 (cit. on p. 155).

[231] P. Gegenwart et al.,
Ferromagnetic quantum critical fluctuations in $YbRh_2(Si_{0.95}\ Ge_{0.05})_2$,
Physical Review Letters **94**.7 (2005) 076402 (cit. on p. 155).

[232] J. L. Smith and Q. Si, *Spatial correlations in dynamical mean-field theory*,
Physical Review B **61**.8 (2000) 5184 (cit. on p. 155).

[233] Q. Si et al., *Local fluctuations in quantum critical metals*,
Physical Review B **68**.11 (2003) 115103 (cit. on p. 155).

[234] A. Georges et al., *Dynamical mean-field theory of strongly correlated fermion systems and the limit of infinite dimensions*, Reviews of Modern Physics **68**.1 (1996) 13
(cit. on p. 155).

[235] A. Georges and Y. Meir,
Electronic correlations in transport through coupled quantum dots,
Physical Review Letters **82**.17 (1999) 3508 (cit. on p. 155).

[236] C. Pépin, *Fractionalization and fermi-surface volume in heavy-fermion compounds: The case of* $YbRh_2Si_2$, Physical Review Letters **94**.6 (2005) 066402 (cit. on p. 157).

[237] P. Coleman et al., *How do Fermi liquids get heavy and die?*,
Journal of Physics: Condensed Matter **13**.35 (2001) R723 (cit. on p. 157).

[238] P. Wölfle and E. Abrahams,
Quasiparticles beyond the Fermi liquid and heavy fermion criticality,
Physical Review B **84**.4 (2011) 041101 (cit. on pp. 158, 159).

[239] E. Abrahams and P. Wölfle, *Critical quasiparticle theory applied to heavy fermion metals near an antiferromagnetic quantum phase transition*, Proceedings of the National Academy of Sciences **109**.9 (2012) 3238–3242 (cit. on p. 158).

[240] E. Abrahams, J. Schmalian and P. Wölfle, *Strong-coupling theory of heavy-fermion criticality*, Physical Review B **90**.4 (2014) 045105 (cit. on pp. 158, 159).

[241] R. L. Stratonovich, *On a method of calculating quantum distribution functions*, Soviet Physics Doklady **2** (1957) 416 (cit. on p. 160).

[242] J. Hubbard, *Calculation of partition functions*, Physical Review Letters **3** (1959) 77–78 (cit. on p. 160).

[243] C. Mudry, *Lecture notes on field theory in condensed matter physics*, World Scientific, 2014 (cit. on pp. 160, 170).

[244] R. A. Jishi, *Feynman diagram techniques in condensed matter physics*, Cambridge University Press, 2013 (cit. on p. 172).

[245] G. Grüner, *Density waves in solids*, Westview Press, 2000 (cit. on p. 173).

[246] P. Fazekas, *Lecture notes on electron correlation and magnetism*, World Scientific, 1999 (cit. on pp. 174, 183).

[247] S. V. Tyablikov, *Methods in the quantum theory of magnetism*, Plenum Press, 1967 (cit. on pp. 183, 190).

[248] D. A. Yablonskiy, *Tyablikov approximation in the theory of low-dimensional quantum Heisenberg ferromagnets and antiferromagnets*, Physical Review B **44**.9 (1991) 4467 (cit. on pp. 183, 190).

[249] M. Salmhofer, *Renormalization: An introduction*, Springer, 1999 (cit. on p. 213).

[250] J. B. Bronzan, *Parametrization of $SU(3)$*, Physical Review D **38**.6 (1988) 1994 (cit. on p. 229).

[251] S. Hassani, *Mathematical physics: A modern introduction to its foundations*, Springer, 2013 (cit. on p. 235).

[252] D. Desbrow, *On Evaluating $\int_{-\infty}^{+\infty} e^{ax(x-2b)}dx$ by contour integration round a parallelogram*, American Mathematical Monthly **105**.8 (1998) 726–731 (cit. on p. 236).

[253] P. Apell, *The dynamical versus static asymptotic behaviour of the spatial fourier transform of the Lindhard dielectric function*, Physica Scripta **23**.3 (1981) 284 (cit. on p. 240).

[254] F. C. Khanna and H. R. Glyde, *Dynamic susceptibility of Fermi liquids at finite temperature*, Canadian Journal of Physics **54**.6 (1976) 648–654 (cit. on p. 240).

[255] B. Mihaila, *Lindhard function of a d-dimensional Fermi gas* (1995), arXiv: 1111.5337 (cit. on p. 240).

[256] H. Flanders, *Differentiation under the integral sign*, American Mathematical Monthly **80**.6 (1973) 615–627 (cit. on p. 241).

List of Figures